Investigating the Cell Biology of Novel Protein Hydroxylases Implicated in Human Developmental Disorders

By Charlotte Hall

A thesis submitted to The University of Birmingham,

College of Medical and Dental sciences, for the degree of

DOCTOR OF PHILOSOPHY

Institute of Cancer and Genomic Sciences

College of Medical and Dental Sciences

University of Birmingham

September 2019

UNIVERSITY OF BIRMINGHAM

University of Birmingham Research Archive

e-theses repository

Abstract

The 2-oxyglutarate oxygenase family of enzymes catalyse post-translational hydroxylation of substrates associated with fundamental cellular processes and are often implicated in disease. The focus of this thesis was two poorly characterised 2-oxyglutarate oxygenases, JMJD7 and JMJD5.

JMJD7 was recently assigned as a novel lysyl hydroxylase that targets two substrates, Developmentally Regulated GTPases (DRG) 1 and 2. Although the molecular function of DRG hydroxylation is unclear, the JMJD7-DRG pathway may play a role in neurodevelopment due to the association of JMJD7 and DRG mutations with Autism Spectrum Disorder (ASD) and intellectual disability. Here we begin to address the potential role of this novel pathway in neuronal differentiation and ASD. We successfully characterise key stages of cortical neuron differentiation and develop JMJD7 loss of function models in neuronal-like SHSY5Y cell lines. On the basis of this work we hypothesise how dysregulation of the JMJD7 pathway might contribute to neurodevelopmental disorders and propose future areas for investigation.

The second enzyme investigated was JMJD5, a JMJD7-related oxygenase whose catalytic activity remains controversial. Here we characterise JMJD5 mutations identified in patients with a novel human developmental disorder, which we demonstrate is associated with DNA replication stress. We propose two novel candidate hydroxylation substrates of JMJD5, minichromosome maintenance (MCM) subunits 3 and 5, which form part of the essential DNA helicase required for replication. Future investigation will aim to decipher the molecular mechanism of JMJD5-associated replication stress and whether this is mediated by hydroxylation of MCM3/5.

Overall, our work highlights the importance of protein hydroxylation in fundamental cellular processes and human development and demonstrates the benefit that studies of human disorders can provide in elucidating the function of poorly characterised 2-oxyglutarate oxygenases.

Acknowledgments

Firstly, I would like to say a huge thank you to my supervisor Mat who has offered continued support and advice throughout the last four years. Thanks to all members of the Tumour Oxygenase Group both past and present. In particular Char, Christian, Tristan, Regina and the TOG Harriers (Sally and Eline) for your help in the lab, always being available bang on 12 for lunch and the random conversations and crazy antics that made long lab hours fly by. Thanks also to Uncaar for your help cloning and endless support in the lab.

Thank you so much to Sally, who has been my running partner, J5 teammate, honorary lab supervisor and a voice of reason.

An enormous thanks to Martin for teaching me fibres and foci techniques and being a continued help with all things replication stress. In addition thanks to Grant for your help in culturing patient fibroblasts and for your sound advice throughout my replication stress endeavours.

Thank you to Mirella and Gio for giving me the opportunity to work in your lab in Melbourne and for welcoming me into your families. Thanks also to everyone at the 'Centre for Neural Engineering' and the 'JetBoilers' for making my time inside and outside the lab unforgettable.

Thanks to Andy and all the staff at Boulder Central for providing a space for me to write up, the endless cups of tea and words of encouragement- you made writing up bearable!

Thank you doesn't quite cover how much I am grateful for my family who have had unwavering confidence in me throughout. An enormous thank you to Adam for being my rock (and not to mention chef, cleaner and chauffer whilst writing up). Without you all this PhD would have been impossible.

Declaration

I declare that this thesis is wholly my own work excluding the following figures:

Molecular cloning; Mr Uncaar Boora who sub-cloned JMJD5 constructs, Dr Helen Smith for original JMJD7 cloning, Dr Mathew Coleman for cloning and generating recombinant JMJD5. Cancer bioinformatics presented in Section 2.3.1 was originally performed by Dr Charlotte Eaton. Experimental data presented in Figure 4.4 was performed by Dr Sally Fletcher, Figures 5.26 and 5.27 was performed by Martin Higgs.

Table of Contents

List of figures

List of tables

Abbreviations

2HG	2-hydroxyglutarate
2OG	2-oxoglutarate
AAA$^+$ ATPase	ATPases associated with a variety of cellular activities
APH	Aphidicolin
AR	Androgen receptor
ASD	Autism spectrum disorder
ATM	Ataxia Telangiectasia mutated kinase
ATR	ATM-Rad3-related kinase
ATRIP	ATR-interacting protein
BIR	Break-induced replication
BMP	Bone morphogenic protein
Cdc6	Cell division cycle 6
CDK	Cyclin dependent kinase
Cdt1	Cycle 10-dependent transcript 1
CENPF	Centromere protein F
CFS	Common fragile sites
CHK1	Checkpoint kinase 1
DFRP	DRG family regulatory proteins
DMOG	Dimethyloxaloyglycine
DRG	Developmentally regulated GTP-binding protein
DSB	Double strand break
DSBH	Double-stranded β-helix
EBNA1	Epstein-Barr nuclear antigen-1
EGF	Epidermal growth factor
EIF5A	Eukaryotic translation initiation factor 5A
eRF1	Eukaryotic release factor 1
ESC	Embryonic stem cell
FACT	Facilitates chromatin transactions
FGF	Fibroblast growth factor
FIH	Factor inhibiting HIF
FMRP	Fragile X mental retardation protein
FXS	Fragile X syndrome
GI	Genomic instability
GINS	Go-Ichi-Ni-San
HIF	Hypoxia inducible factor
HSF	Human Splicing Finder
HSPBAP1	Heat Shock Protein-Associated Protein 1
hTERT	Human telomerase
HU	Hydroxyurea
ICM	Inner cell mass
ID	Intellectual disability
IDH	Isocitrate dehydrogenase
IP	Immunoprecipitation
iPSC	Induced pluripotent stem cells
IVTT	*In vitro* transcription/translation
JmjC	Jumonji-C domain

JMJD7	Jumonji domain containing protein 7
JMJD5	Jumonji domain containing protein 5
KDM	Lysine demethylase
MAP2AB	Microtubule-associated protein-2
MCM	Minichromosome maintenance
MGS	Meier-Gorlin syndrome
MiDAS	Mitotic DNA synthesis
Miz-1	Myc-interacting zinc-finger protein 1
MS	Mass spectrometry
mTORC1	Mammalian target of rapamycin complex 1
NE	Neuroectoderm
NLS	Nuclear localisation signal
NOG	N-oxalylglycine
O-GlcNAcylation	*O*-linked β-*N*-acetylglucosaminylation
ORC	Origin recognition complex
PARP	Poly ADP-ribose polymerase
PCNA	Proliferating cell nuclear antigen
PD	Primordial dwarfism
PHD	Prolyl-hydroxylase domain
PIKK	Phosphoinositide 3-kinase related protein kinase
PLA2G4B	Phospholipase A2 beta
Pre-RC	Pre-replicative complex
PTEN	Phosphatase and tensin homolog
PTM	Post-translational modification
qPCR	quantitative PCR
RCC	Regulator of chromosome condensation
RCCD1	Regulator of chromosome condensation 1 domain containing protein
RPA	Replication protein A
RPS6	Ribosome protein S6
RS	DNA replication stress
SAG	Smoothened agonist
SC	Stem cell
SHH	Sonic hedgehog
shRNA	Short hairpin RNA
siRNA	Small interfering RNA
SR	Arginine-serine splice factors
ssDNA	Single stranded DNA
TET	Ten-eleven translocation
TGFβ	Transforming growth factor β
TSC	Tuberous Sclerosis Complex
UFB	Ultrafine DNA anaphase bridge
VHL	von Hippel-Lindau protein
WES	Whole exome sequencing

1 Introduction

In this thesis we investigated Jumonji Domain Containing protein 7 and 5 (JMJD7 and JMJD5), two members of the 2-oxoglutarate oxygenase family of hydroxylase enzymes. To date both are largely uncharacterised but are implicated in human developmental disorders and disease. Consequently, this introduction will give an overview of hydroxylation as a post-translational modification, including its catalysis by the family of 2-oxoglutarate oxygenase enzymes and their roles in disease, with a specific focus on JMJD7, JMJD5, and their confirmed or candidate hydroxylation substrates.

1.1 Post-translational modifications

Post-translational modification (PTM) predominantly involves the addition of a chemical moiety onto a protein during or after its translation. Consequently, PTMs enable complexity of the proteome to extend beyond what is possible by the genome alone (Spoel, 2018). The most common PTMs are phosphorylation, acetylation, N- or O-linked glycosylation, amidation, methylation and ubiquitination (Khoury et al., 2011). Each of these PTMs function independently or in crosstalk with each other to facilitate a variety of protein functions including; folding, localisation, degradation, enzymatic activation and substrate specificity (Knorre et al., 2009, Duan and Walther, 2015, Csizmok and Forman-Kay, 2018). PTMs are commonly dynamic, with their addition and removal being catalysed by specific enzyme classes (e.g. kinases/phosphatases). Moreover, the ability of downstream proteins to detect and respond to PTMs often forms the basis of fundamental signalling pathways, that when dysregulated are associated with disease (Deribe et al., 2010).

1.2 Hydroxylation and the 2-oxoglutarate oxygenase family

Hydroxylation is a relatively poorly characterised PTM that involves covalent addition of an oxygen atom to a C-H bond to generate an alcohol (hydroxyl) group. The hydroxyl group can increase amino acid polarity and act as a donor or acceptor during the formation of hydrogen bonds (Loenarz and Schofield, 2011). The largest family of enzymes that catalyse hydroxylation are 2-oxoglutarate (2-OG) oxygenases. The first 2OG oxygenases were identified while investigating the presence of hydroxyl-proline and hydroxy-lysine in collagen (Kivirikko and Prockop, 1967) and for several decades after hydroxylation was deemed to be a rare PTM (Loenarz and Schofield, 2011). However, the discovery of hydroxylases involved in hypoxia signalling (Ivan et al., 2001, Jaakkola et al., 2001, Lando et al., 2002) inspired further study of this PTM, and since then numerous other 2OG oxygenases have been discovered and characterised. The importance of the 2OG oxygenase family is demonstrated by their evolutionary conservation, their fundamental role in a diverse range of cellular processes and their association with a variety of diseases (Ploumakis and Coleman, 2015).

1.2.1   The 2-oxoglutarate oxygenase family members

2OG oxygenases can be identified by the presence of a catalytic fold consisting of a double-stranded β-helix (DSBH), also referred to as the cupin (barrel-like) or 'jelly-roll' fold (Roach et al., 1995, Loenarz and Schofield, 2011). This DSBH is made up of eight anti-parallel β-strands which fold into the barrel-like structure (Figure 1.1). This fold is fundamental for positioning essential catalytic residues for the hydroxylation reaction, as discussed in Section 1.2.2 (Chen et al., 2006, McDonough et al., 2010, Ploumakis and Coleman, 2015).
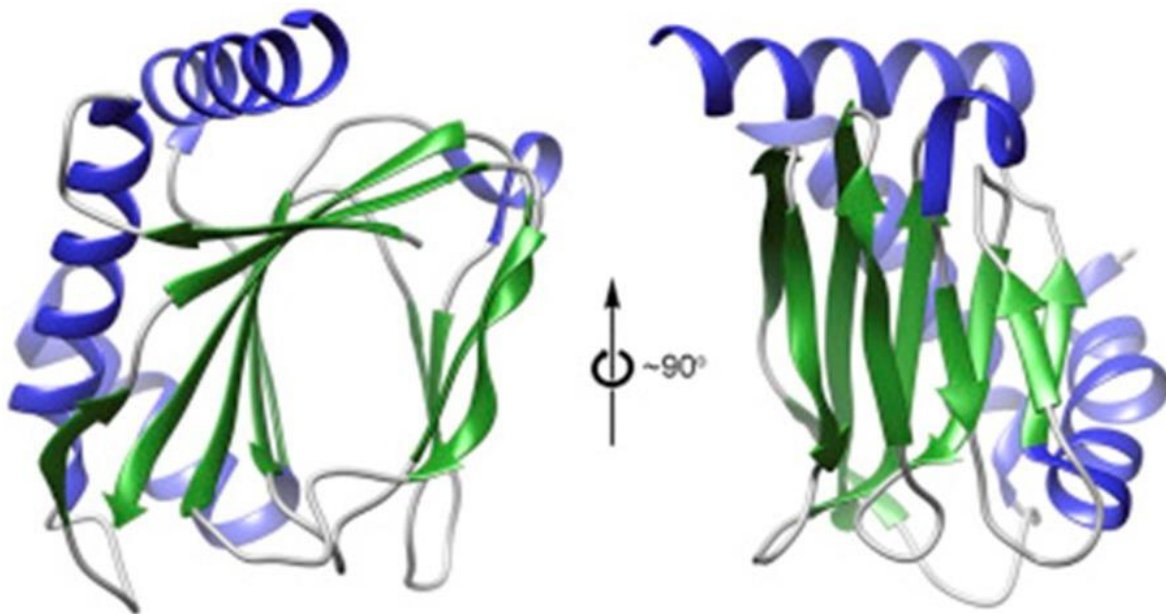
Figure 1.1 Structure of the double stranded β-helix in the 2OG oxygenase catalytic domain
Figure demonstrating the double-stranded β-helix (DSBH) domain common for 2OG oxygenase catalytic sites. The DSBH forms a barrel-like structure (green) that orientates catalytic residues for substrate binding. Left image is from the front view, right image is from the side view. Adapted from Ploumakis and Coleman (2015).

The 2-OG oxygenase family can be divided into sub-families based on similarities in their sequence and structure as well as presence of any additional functional domains acquired throughout evolution (Balciunas and Ronne, 2000, Klose et al., 2006). By doing this, the 2-OG oxygenases can be crudely segregated into three main groups (Figure 1.2). Two of these groups contain a DSBH with homology to that present in the protein 'Jumonji' and are thus referred to as Jumonji-C (JmjC) domain enzymes (Takeuchi et al., 1995, Clissold and Ponting, 2001). This JmjC domain is present in over thirty 2OG oxygenases and is conserved throughout archaea, bacteria and eukaryotes (Balciunas and Ronne, 2000). JmjC enzymes can be sub-divided into the JmjC-only hydroxylases (boxed in red, Figure 1.2) and the JmjC-containing lysine demethylases (KDM, boxed in blue, Figure 1.2).
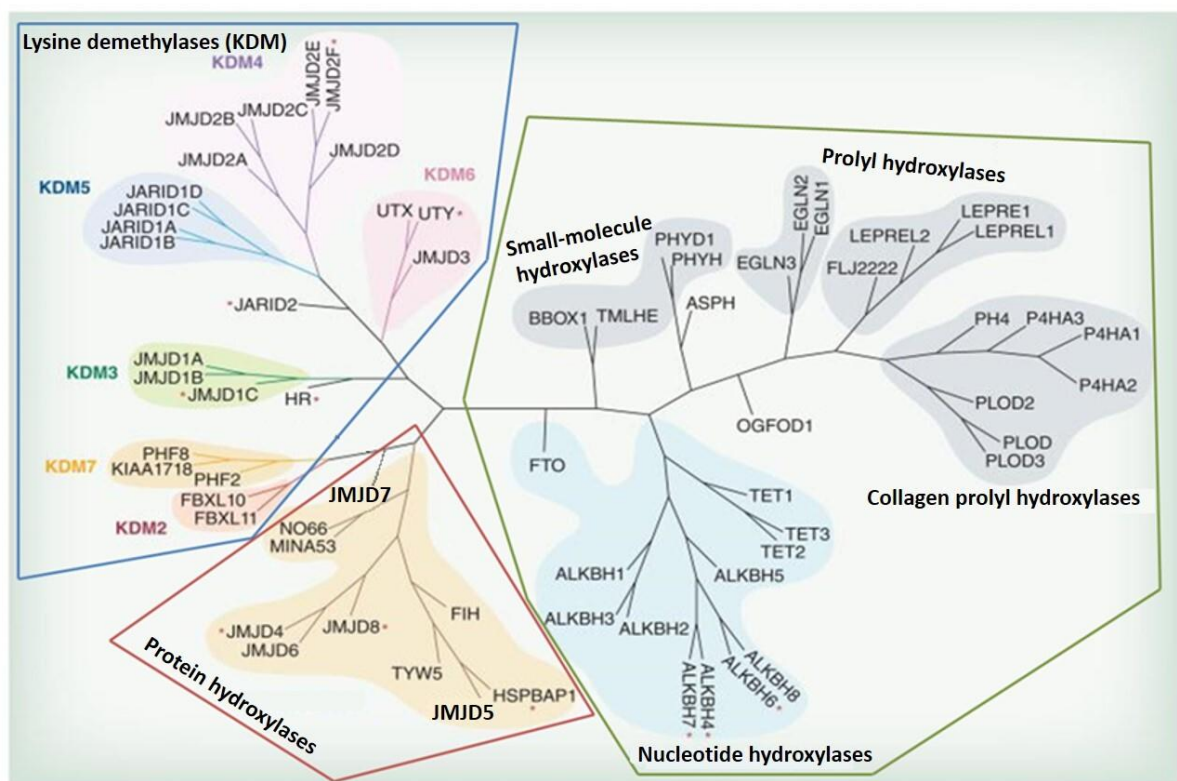
Figure 1.2 Classification of the 2-oxoglutarate oxygenase enzymes into sub-families
2OG oxygenases can be separated into three broad sub-families based on the homology of the DSBH catalytic domain to the Jumonji protein (JmjC domain). Enzymes containing the JmjC domain boxed in red and blue, enzymes with a non-JmjC DSBH boxed in green. Enzymes are then separated further based on substrate specificity including lysine demethylases (KDM), protein, nucleotide, prolyl, collagen and small molecule hydroxylases. Figure adapted from Johansson et al. (2014).

Within these broad sub-families, the enzymes can be further divided based on homology and substrate specificity (Figure 1.2). Although their substrates are diverse (including proteins, nucleic acids and lipids) the reaction mechanism involved is largely conserved (Loenarz and Schofield, 2011) and is discussed below.

1.2.2 Catalytic mechanism

All 2-OG oxygenases use molecular oxygen to catalyse a decarboxylation reaction that involves the hydrolysis of 2-OG and the production of succinate, CO_2, and the hydroxylated prime substrate (Ploumakis and Coleman, 2015). During the reaction both atoms of molecular oxygen are incorporated into the products (one into the substrate, the other into succinate) making the enzymes dioxygenases (McNeill et al., 2002, Welford et al., 2005, Ploumakis and Coleman, 2015). This reaction mechanism is dependent on a highly conserved 'two histidine one carboxylate motif' (HxD...H), which forms a facial triad that binds a reactive Fe(II) ion (Clifton et al., 2006, McDonough et al., 2010). The DSBH orientates the HxD...H motif towards the opening of this substrate binding pocket to solvent expose the Fe(II) ion as the site for the hydroxylation reaction (Clifton et al., 2006).

Once bound into the HxD...H motif, the Fe(II) ion has three remaining coordination sites, two of which are occupied by the bidentate ligand 2-OG. The prime substrate binds to the enzyme and as it does so water molecules are displaced from the active site. This enables molecular oxygen to bind which then initiates the decarboxylation reaction, summarised in Figure 1.3A (Zhou et al., 1998).

One sub-family of 2OG oxygenases mediate this decarboxylation reaction for the demethylation of lysine residues on histone tails (lysine demethylases (KDMs), identified by a blue box in Figure 1.2). In these demethylation reactions the hydroxylated methyl-lysine fragments into formaldehyde and a demethylated lysine residue (Figure 1.3B) (Loenarz and Schofield, 2011). The importance of this reaction in the epigenetics field is discussed below (Section 1.2.3.1).
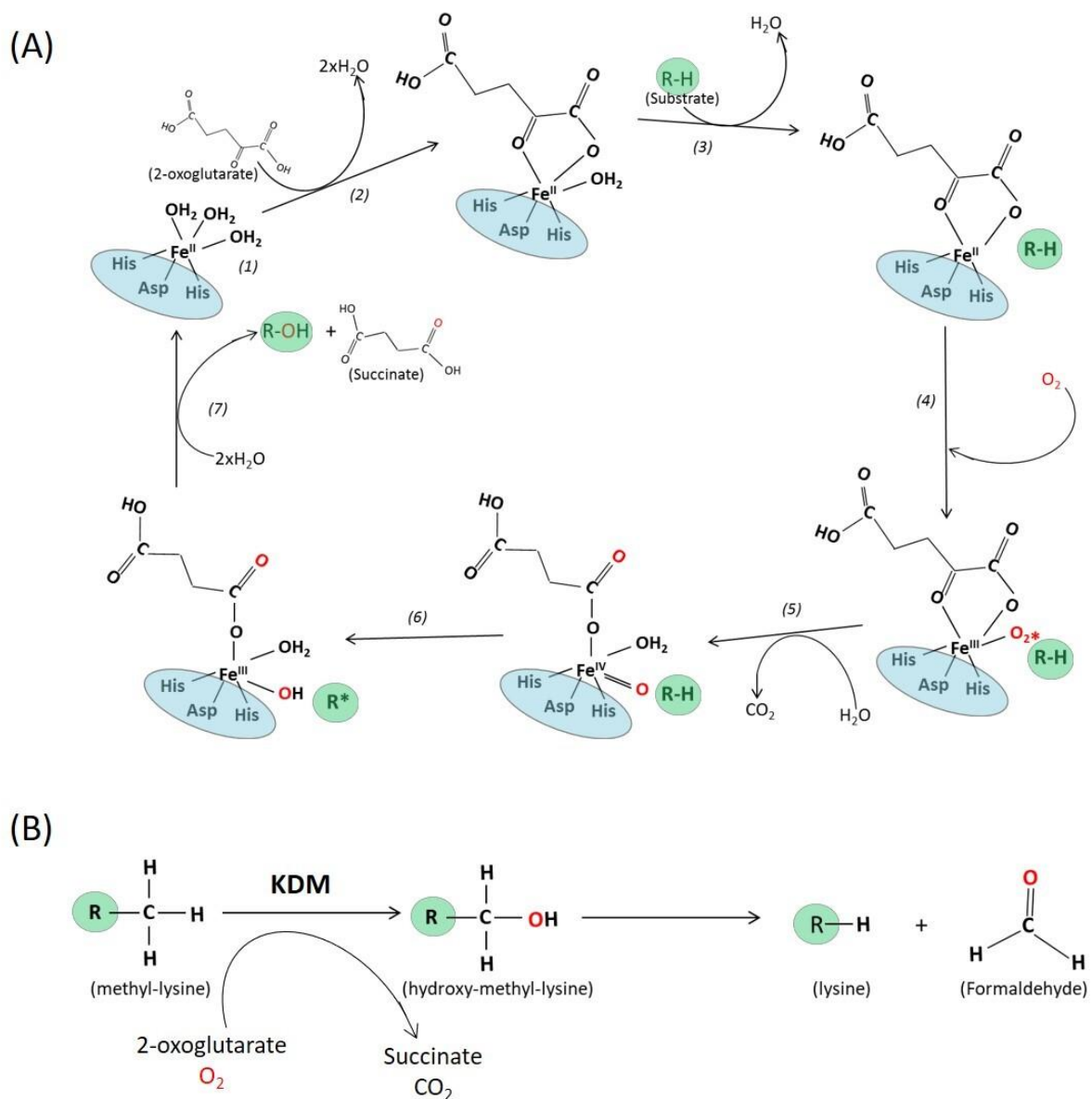
Figure 1.3 The 2-oxyglutarate oxygenase hydroxylation reaction
(A) (1) The HxD…H facial triad of the active site (circled in blue) binds to ferrous ions (Fe^{2+}). (2) 2-oxoglutarate (2OG) binds to the Fe^2 ion. (3) This initiates the binding of the prime substrate (circled in green) into the active site of the enzyme. (4) This displaces a water molecule and enables coordination of molecular oxygen (red molecule) with Fe^{2+}. (5/6) This generates a reactive Fe(IV) complex that is unstable and undergoes a two-step oxidative decarboxylation reaction. (7) In this reaction, the oxygen molecule is incorporated into the by-product of the reaction, succinate, and the prime substrate as a hydroxyl group. The enzyme then regenerates its ferrous ion, though some enzymes require ascorbate to facilitate this. **(B)** Hydroxylation of methylated lysine creates an unstable intermediate that fragments resulting in an unmethylated lysine residue and formaldehyde as a by-product.

1.2.3   2-Oxoglutarate oxygenase family members in disease

The functional significance of hydroxylation reactions depends on the context (e.g. stable hydroxylation versus demethylation) and function of the substrate. However, as mentioned above, an emerging theme is that 2OG oxygenases and their substrates play essential roles in fundamental cellular processes. As a consequence, 2OG oxygenases are commonly implicated in disease. We briefly discuss the role of 2OG oxygenases in disease below, with a specific focus on JmjC-containing 2OG oxygenases, which form the focus of this thesis.

1.2.3.1   JmjC-containing lysine demethylases in disease

One sub-family of JmjC containing 2OG oxygenases are the lysine demethylases (KDMs, identified by a blue box in Figure 1.2). KDMs have been widely implicated in diseases, including developmental disorders and cancer, due to the fundamental nature of their role in epigenetic regulation.

With regards to development, JMJD3 (KDM6B) and UTX (KDM6A) which demethylate histone H3 on lysine 27 that is di- or tri-methylated (H3K27me2/3) have both been implicated in human development. For example, JMJD3 activity promotes neural differentiation and when dysregulated can contribute to neurodegenerative disorders, including Parkinson's and Alzheimer's disease (Fonseca et al., 2012, Park et al., 2014, Tang et al., 2014, Burchfield et al., 2015). Consistent with a fundamental role, deletion or mutation of UTX is associated with a rare developmental disorder called Kabuki syndrome where patients present with intellectual disability plus a range of other developmental defects (Lederer et al., 2012, Miyake et al., 2013, Lederer et al., 2014, Banka et al., 2015). Interestingly, other JmjC-containing KDMs are also implicated in cognitive impairment associated disorders, demonstrating the importance

of their role during neural development (Kim et al., 2017). For example, KIAA1718 (KDM7A) targets methylated lysine 9 and 27 on histone H3 (H3K9/27me) for demethylation, and its expression is predominantly localised to the developing brain. Here it promotes neural differentiation by regulation of 'fibroblast growth factor' 4 (Huang et al., 2010). PHF8 (KDM7B), that demethylates histone H4K20me1, is also essential during brain development and consequently dysregulation is associated with intellectual disability as well as other birth defects such as cleft lip/palate (Laumonnier et al., 2005, Abidi et al., 2007, Koivisto et al., 2007, Chen et al., 2018, Qiao et al., 2008). Similarly, mutations in JARID1C (KDM5C), that demethylates H3K4me2/3, is associated with X-linked intellectual disability disorders prevalent in males (Jensen et al., 2005, Tahiliani et al., 2007, Adegbola et al., 2008, Brookes et al., 2015).

Further demonstrating the importance KDMs in development, FBXL10 (KDM2B) and FBXL11 (KDM2A) can be used as accessory factors to facilitate generation of induced pluripotent stem cells *in vitro* (Wang et al., 2011, Liang et al., 2012). Furthermore, both enzymes have been implicated in cancer (Frescas et al., 2008, Tzatsos et al., 2013, Yan et al., 2018, Lu et al., 2019). This association of KDMs with fundamental roles in both development and cancer appears to be a common theme. For example, many KDMs activate the Androgen Receptor (AR) and regulate metabolic genes during development (Yamane et al., 2006, Okada et al., 2007, Shin and Janknecht, 2007, Wissmann et al., 2007, Wolf et al., 2007, Coffey et al., 2013). Therefore, many KDMs have also been implicated in prostate cancer due to its dependence on AR signalling. As such, KDMs have been proposed as prognostic markers and drug targets in this and other cancers (Suikki et al., 2010, Crea et al., 2012).

Further examples of KDMs with links to tumourigenesis include JARID1A (KDM5A) and JARID1B (KDM5B) which are both demethylases targeting H3K4. JARID1A was originally named 'retinoblastoma binding protein 2' as it contains a phospho-retinoblastoma protein binding motif. As retinoblastoma protein is a major tumour suppressor gene, with critical roles in cell cycle control, it is perhaps unsurprising that JARID1A is important for regulating the cell cycle and is commonly dysregulated in cancer (Klose et al., 2007). On the other hand, the role of JARID1B in cancer relates to epithelial-to-mesenchymal transition, where it inhibits the expression of tumour suppressor miR-200 (Enkhbaatar et al., 2013). Overall, there is a large body of evidence demonstrating the fundamental nature of KDMs and their association with major human diseases, reviewed by Takeuchi et al. (2006).

1.2.3.2 JmjC-containing protein hydroxylases in disease

The JmjC-only sub-family of 2OG oxygenases are largely characterised as protein hydroxylases (identified by a red box in Figure 1.2). This family includes JMJD5 and JMJD7 which are the focus of this PhD and will be discussed in more detail in separate sections that follow below. First, we briefly discuss other members of the JmjC-only sub-family, describing their fundamental cellular roles and association with disease.

A well characterised member of this sub-family is Factor Inhibiting HIF (FIH). FIH prevents binding of 'hypoxia inducible factor' (HIF) to its co-activator protein p300 by hydroxylating an asparagine residue in the C-terminal transactivation domain of the HIFα subunit (Mahon et al., 2001, Lando et al., 2002). Further regulation of HIF is mediated by Prolyl-hydroxylase Domain (PHD) enzymes (a.k.a EGLN1-3), which hydroxylate HIF to promote its interaction with the E3 ubiquitin ligase von Hippel-Lindau (VHL) protein. This targets HIF for proteasomal

degradation (Jaakkola et al., 2001, Ivan et al., 2001, Yu et al., 2001). Under hypoxic conditions the level of oxygen is decreased and correspondingly the extent of HIFα hydroxylation is decreased. This results in the translocation of the HIFα subunit to the nucleus, hetero-dimerisation to the HIFβ subunit, and interaction with p300 to promote gene expression that upregulates a cellular response to hypoxia, reviewed by (Schofield and Ratcliffe, 2004).

In addition to this role FIH also targets residues in ankyrin repeat proteins for hydroxylation (Cockman et al., 2006, Coleman et al., 2007, Cockman et al., 2009, Yang et al., 2011). One most recent example of this activity is towards the E3 ubiquitin ligase HACE1. This hydroxylation event disrupted interaction between HACE1 and Rac1, a protein important in cell motility (Kim et al., 2019). Consequently, due to these fundamental roles FIH has been identified as a tumour suppressor gene. It is commonly dysregulated in many cancers and thus could be used as a prognostic biomarker (Kroeze et al., 2010, Wang et al., 2014a, Chen et al., 2015b, Kang et al., 2018, Kim et al., 2019).

Other JmjC-only family members, MINA and NO66, are also implicated in cancer. Both target ribosomal subunits for histidine hydroxylation: MINA has specificity towards Rpl27a and NO66 targets Rpl8 (Ge et al., 2012). One might expect that, since cell growth is directly associated with protein translation (Rudra and Warner, 2004), these proteins would support tumourigenesis. However, although this may be the case for NO66 (Pires-Luis et al., 2015, Nishizawa et al., 2017, Sinha et al., 2019), MINA may have paradoxical roles in cancer, as it has been implicated as both a tumour suppressor gene and an oncogene in different contexts (Yu et al., 2014, Bundred et al., 2018). Interestingly, MINA and NO66 are also implicated in other physiological processes. For example, NO66 is involved in bone development as it negatively

regulates the osteoblast transcription factor Osterix (Sinha et al., 2010, Chen et al., 2015a). MINA is important for regulating T-cell differentiation and was subsequently associated with allergic response and asthma (Okamoto et al., 2009, Chen et al., 2011b, Mori et al., 2013).

Another JmjC-only oxygenase important for protein translation is JMJD4. Its hydroxylation of 'eukaryotic release factor 1' (eRF1) is essential for optimal translation termination (Feng et al., 2014). Perhaps unsurprisingly JMJD4 is upregulated in cancer (Ploumakis and Coleman, 2015, Ho et al., 2018) but interestingly is dispensable in normal development (Yoo et al., 2016). Another JmjC-only oxygenase implicated in translation is TYW5, which is unusual within this sub-family because it targets an RNA rather than protein substrate. TYW5 is part of the enzymatic cascade to produce the hypermodified base, hydroxywybutosine, in the phenylalanine tRNA (Noma et al., 2010, Kato et al., 2011). The functional significance of TYW5 is unclear, but a role in translation might suggest that TYW5 also supports tumourigenesis, like many other members of this family.

Other, less well characterised JmjC-only subfamily members have also been implicated in disease. For example, JMJD6, is a lysyl-hydroxylase that is reported to target serine-arginine rich proteins, histones, VHL protein and splicing factor U2AF65 (Webby et al., 2009, Unoki et al., 2013, Heim et al., 2014, Alahari et al., 2015), though whether JMJD6 targets all of these substrates is controversial (Bottger et al., 2015, Islam et al., 2019). These activities have been linked to multiple tumourigenic pathways, which might explain why JMJD6 expression is associated with poor prognosis (Boeckel et al., 2011, Lee et al., 2012, Shen et al., 2018, Liu et al., 2019, Wan et al., 2019, Wong et al., 2019). Interestingly, JMJD6 has also been associated

with eye development in *Xenopus laevis* and for adipogenesis (Reyes-Gutierrez et al., 2019, Shin et al., 2019).

Similarly, although JMJD8 is a largely uncharacterised JmjC-only family member, with no substrates yet assigned, it is suggested to localise to the endoplasmic reticulum to facilitate protein folding (Yeo et al., 2017). It has also been implicated in angiogenesis (Boeckel et al., 2016) and has been proposed as a therapeutic target to enhance efficacy of chemotherapy and radiotherapy (Su and Wang, 2019, Wang et al., 2019b). Likewise, the activity of 'Heat Shock Protein-Associated Protein 1' (HSPBAP1) is largely unknown. However, its function has been associated with maturation of macrophages (Fagone et al., 2012), brain development due to over-expression in epileptic patients (Xi et al., 2007), and cancer via interaction with the AR (Saeed et al., 2015, Yang et al., 2015). Overall, the JmjC-only family have diverse substrates, play essential roles in fundamental cellular processes, and are receiving increasing attention for their potential importance in disease, reviewed by Oh et al. (2019).

1.2.3.3 Additional mechanisms for 2OG oxygenase dysregulation in disease

As 2OG oxygenase activity is dependent on the presence of oxygen, iron and 2-OG, these enzymes can be sensitive to changes in cell metabolism and microenvironment (Schofield and Ratcliffe, 2005). This could be another mechanism that the 2OG oxygenases contribute to disease. For example, mutations in isocitrate dehydrogenases alter its usual function from converting isocitrate to 2-OG and instead produces '2-hydroxyglutarate' (2-HG) (Ye et al., 2013). This occurs at such a rate that the enzymes that oxidise this unwanted product are overwhelmed, and thus the levels of 2-HG increase (Xu et al., 2011c, Losman and Kaelin, 2013). As 2-HG is structurally similar to 2-OG it acts as a competitive inhibitor of some 2-OG

oxygenases, including those with tumour suppressor function (Xu et al., 2011b). Therefore, 2-HG is referred to as an oncometabolite (Losman and Kaelin, 2013, Zou et al., 2013). Other oncometabolites that competitively inhibit 2OG oxygenases include fumarate and succinate (Yang et al., 2012, Sciacovelli and Frezza, 2016, Tretter et al., 2016, Collins et al., 2017, Eijkelenkamp et al., 2019).

Due to the dependence on molecular oxygen, the activity of many of these enzymes can also be inhibited by hypoxia. This is the case for the HIF hydroxylases mentioned previously, though the oxygen affinity of FIH suggests it is less sensitive to hypoxia than the PHD enzymes (Koivunen et al., 2004, Tian et al., 2011). That being said, FIH has been proposed as a therapeutic target for disorders associated with hypoxia such as anaemia and stroke (Yeo et al., 2006, Locatelli et al., 2017, Gupta and Wish, 2017, Davis et al., 2019). Other examples include some KDM 2OG oxygenases whose activity are also directly associated with hypoxia (Cascella and Mirica, 2012, Sánchez-Fernández et al., 2013, Hancock et al., 2017, Chakraborty et al., 2019), whereas others indirectly respond to hypoxia due to HIF regulated expression (Pollard et al., 2008, Batie et al., 2017). Moreover, the DNA demethylase activity of 'ten-eleven translocation' (TET) enzymes was found to be directly affected by low oxygen levels in tumour hypoxic conditions. This results in hypermethylation of tumour suppressive genes to promote tumourigenesis (Thienpont et al., 2016). Interestingly, JMJD6 has also been attributed with oxygen sensing properties in the placenta and could be a biomarker of preeclampsia (Alahari et al., 2015, Farrell et al., 2019).

Overall, there is a lot of evidence to demonstrate the fundamental importance of the 2OG oxygenase family and how their dysregulation can result in human developmental disorders and disease. However, several members of the family remain either very poorly characterised or their biological and substrate specificity is controversial. As there is potential merit in the therapeutic targeting of these enzymes (Rose et al., 2011), this means that basic characterisation of these enzymes is warranted. To this end, we investigated the disease-related roles of two poorly characterised members of the JmjC-only sub-family, JMJD7 and JMJD5. As such we provided a focussed introduction to these enzymes in the sections that follow.

1.3 JMJD7

The first 2OG oxygenase investigated in this thesis was a member of the JmjC-only sub-family called JMJD7. Although two hydroxylation substrates have been assigned, the cellular role that JMJD7 and its downstream pathway play is largely uncharacterised.

1.3.1 The JMJD7 hydroxylation substrates DRG1 and DRG2

JMJD7 was recently proposed to have endopeptidase activity to cleave histone tails (Liu et al., 2017, Liu et al., 2018a), a branch of nucleosome proteolysis predominantly important for epigenetic regulation (Dhaenens et al., 2015). However, this activity was not supported by structural and biochemical evidence demonstrating that JMJD7 acts as a protein hydroxylase (Markolovic et al., 2018). Furthermore, two hydroxylation substrates of JMJD7 have been identified as the 'Developmentally Regulated GTPases' (DRG) 1 and 2 (Markolovic et al., 2018). They are both members of the OBG sub-family of 'translation factor' (TRAFAC) GTPases that are highly conserved in archaea and eukaryotes (Leipe et al., 2002). JMJD7 targets lysine

residues for hydroxylation, at position 22 in DRG1 and position 21 in DRG2 (Markolovic et al., 2018), which are located at the apex of a functionally important helix-turn-helix motif (Figure 1.4) (Francis et al., 2012). However, the consequence of this hydroxylation is unknown.
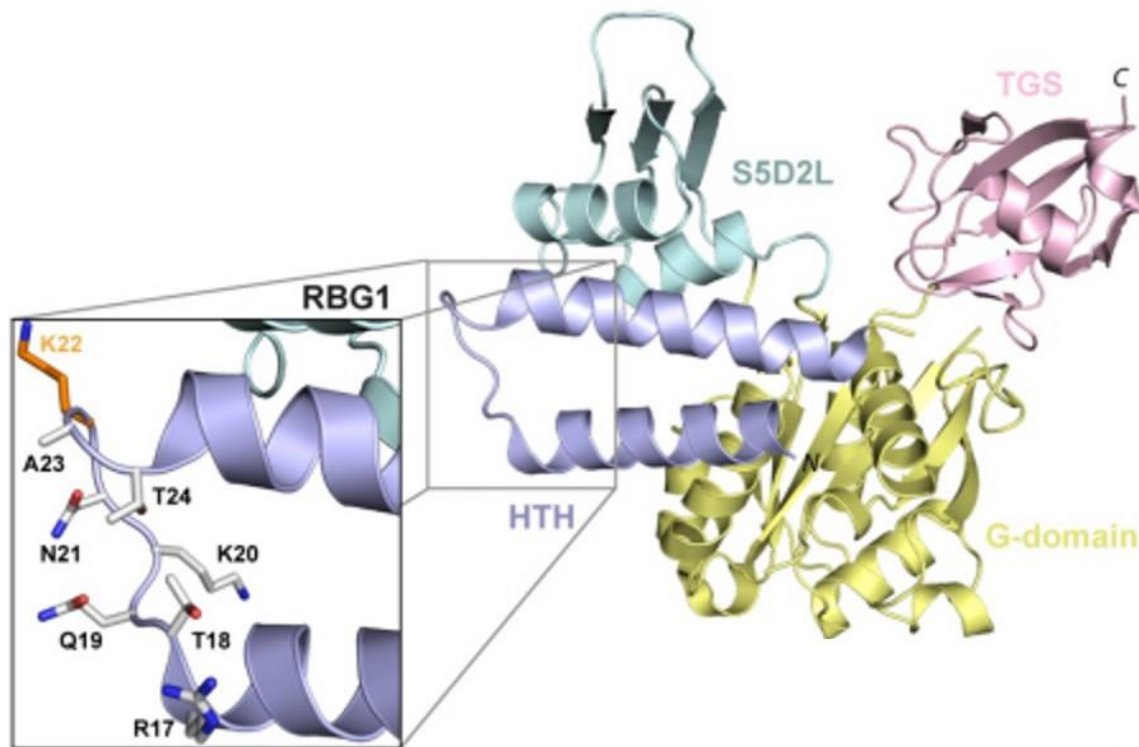
Figure 1.4 Structure of yeast DRG1 (RBG1) to demonstrate the JMJD7 mediated hydroxylation site
The *yeast* orthologue of DRG1, Ribosome-interacting GTPase 1 (RBG1) has 66% sequence identity to human DRG1 (structure PDB ID: 4A9A). RBG1 is comprised of four domains; a highly conserved G-domain responsible for GTPase activity, a TGS (ThrRS, GTPase and SpoT) domain thought to mediate interaction with DFRPs, the S5D2L (ribosomal protein S5 2-like) and helix-turn-helix (HTH) domains both essential for RBG1 function (Francis et al., 2012). A lysine within this HTH domain is targeted for hydroxylation by JMJD7, K22 in human DRG1 and K21 in human DRG2 (Markolovic et al., 2018). The hydroxylated residue is shown in this figure as an orange stick on K22. Figure adapted from Markolovic et al. (2018).

The available literature demonstrates that DRG1 and 2 expression is regulated during development (Kumar et al., 1992, Sazuka et al., 1992, Kumar et al., 1993, Etheridge et al., 1999). They have also been shown to play roles in proliferation (Schenker et al., 1994, Ko et al., 2004, Song et al., 2004, Bower and Johnston, 2010, Ishikawa et al., 2013, Jang et al., 2016),

endosome function (Mani et al., 2016, Mani et al., 2017), microtubule stability (Schellhaus et al., 2017) and protein translation (Ishikawa et al., 2009, Wout et al., 2009, Daugeron et al., 2011, Francis et al., 2012). However, the molecular mechanisms involving DRG1/2 in these processes remain unclear making investigation into the consequence of JMJD7 hydroxylation complicated.

That being said, recent proteomic characterisation, performed by the Coleman lab, has helped to assign potentially specific functions of DRG1 and DRG2. For example, DRG2, consistent with a role in translation, interacts with deoxyhypusine synthase (Dr Qinqin Zhuang). This is the enzyme that catalyses hypusination of eukaryotic initiation factor 5A, which is essential for its role in mRNA translation (Nishimura et al., 2012, Park and Wolff, 2018). Interestingly, an interaction between DRG2 and RNA was also identified which was found to be reduced after JMJD7 knockdown or DRG2 hydroxylation site mutation (Markolovic et al., 2018). Unlike DRG2, the current proteomic data suggests that DRG1 plays a role in transcription as it co-immunoprecipitates with subunits of the 'facilitates chromatin transactions' (FACT) complex (Dr Qinqin Zhuang and Mr Christian Westrip). Therefore, although the DRGs are highly conserved and are highly related in protein sequence (Li and Trueb, 2000), they are likely to have individual roles. In addition, the activities mediated by DRG1 and DRG2 are likely to be facilitated by the 'DRG family regulatory proteins' (DFRP) 1 and 2, which promote the stability and activity of their respective DRG binding partners (Ishikawa et al., 2005, Ishikawa et al., 2009).

1.3.2 JMJD7 and disease

Although there is very little known regarding the functional role of JMJD7, there is evidence of its potential importance in human disease. For example, JMJD7 is implicated in cancer where, paradoxically, it has been identified as both a tumour suppressor gene and oncogene (Zhu et al., 2016, Liu et al., 2017) (Charlotte Eaton, Coleman lab). Consistent with a potential role in supporting tumourigenesis, JMJD7 knockdown reduces cell proliferation (Zhu et al., 2016, Liu et al., 2017, Markolovic et al., 2018).

JMJD7 mutations have also been found in patients with autism spectrum disorder (ASD) (Matsunami et al., 2014) and intellectual disability (ID) (de Ligt et al., 2012) implying that JMJD7 may also have an important role in development (ASD and neural differentiation discussed in greater depth in Chapter 2). Consistent with this the DRG hydroxylation substrates have also been implicated in developmental disorders. For example, the DRG2 gene is localised within a chromosomal region implicated with the ID-associated Smith-Magenis syndrome, and both DRG1 and DRG2 mutations are identified in patients with ASD (Vlangos et al., 2000, Lucas et al., 2001, Bi et al., 2002, Nakamine et al., 2008, de Krom et al., 2009). Interestingly, similarly to NO66 (see above), JMJD7 is also reported to play a role in osteoclast differentiation (Liu et al., 2018b).

Another link between JMJD7 and disease may be related to its rather unique transcriptional regulation. This occurs after transcriptional 'readthrough' from the *JMJD7* gene into the neighbouring *phospholipase A2 beta* (*PLA2G4B*) gene, creating a 'readthrough' transcript that includes the N-terminus and partial JmjC domain of *JMJD7* and the full *PLA2G4B* gene sequences (Figure 1.5) (Cheng et al., 2017). Due to the incomplete JmjC domain the

readthrough protein is unlikely to support DRG hydroxylase activity. Although the exact

regulation and function of this readthrough transcript is unknown, it has been implicated in

cancer and ASD (Matsunami et al., 2014, Su et al., 2016, Ito et al., 2016, Cheng et al., 2017).
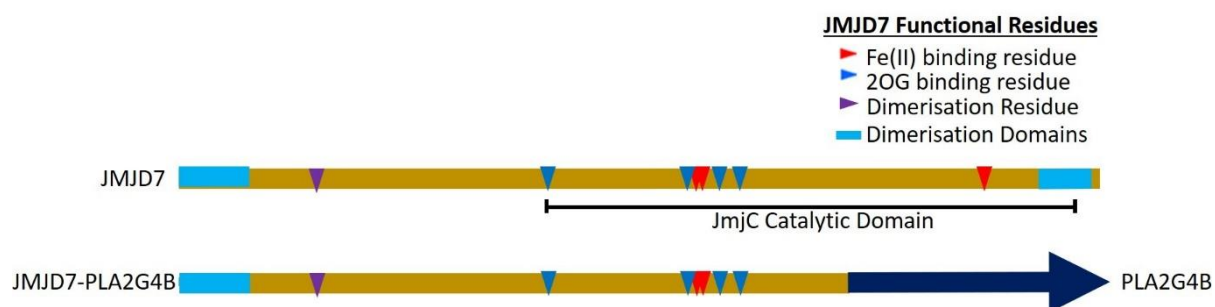
Figure 1.5 Domains present in JMJD7 and the JMJD7-PLAG2B readthrough transcript
The JMJD7 protein sequence labelled with functional domains, including the JmjC domain plus catalytic residues and dimerisation domains. The readthrough transcript includes the N-terminal and partial JmjC catalytic domain from the JMJD7 coding sequence into the neighbouring PLA2G4B gene. Currently the prevalence and function of this readthrough protein is unknown.

Overall, there is a growing body of evidence suggesting the importance of the JMJD7 pathway

in disease. However, the molecular mechanisms responsible are undefined.

1.4 JMJD5

The second 2OG oxygenase investigated in this thesis was JMJD5. Although there is a large

body of literature demonstrating a variety of JMJD5 functions, its enzymatic activity has been

controversial. Below we discuss the literature regarding JMJD5 and then review evidence

supporting that JMJD5 acts as a protein hydroxylase. We then briefly introduce two candidate

hydroxylation substrates of JMJD5, that we provide experimental evidence for later in this

thesis (Chapter 4).

1.4.1 JMJD5 cellular activity

The majority of the current literature surrounding the cellular function of JMJD5 comes from studying its role in cancer, where it has been implicated as having tumour suppressive and oncogenic properties. JMJD5 was originally predicted to be a tumour suppressor gene following a retroviral insertion screen in mice deficient for the BLM DNA helicase (Suzuki et al., 2006). Consistent with a potential tumour suppressor function, JMJD5 expression is downregulated in cancer patients associated with a poor prognosis (Suzuki et al., 2006, Wang et al., 2012, Wu et al., 2016b, Wilkins et al., 2017). Conversely, increased JMJD5 expression is correlated with late stage tumours, increased metastasis and poor overall survival (Hsia et al., 2010, Huang et al., 2015, Lee et al., 2015, Zhang et al., 2015, Zhao et al., 2015, Wu et al., 2016a, Wang et al., 2019a, Yao et al., 2019). The fundamental role of JMJD5 is further highlighted by mouse models, whereby JMJD5 knockout mice were embryonic lethal due to severe growth retardation. Although JMJD5 knockdown mice were viable, they continued to present with growth defects (Ishimura et al., 2012, Oh and Janknecht, 2012, Ishimura et al., 2016).

There are various molecular mechanisms attributed to JMJD5 function that could contribute to this impaired cellular proliferation phenotype (summarised in Figure 1.6). For example, JMJD5 has been linked to the progression of the cell cycle through its regulation of *CCN1A* (Cyclin A1) expression (Hsia et al., 2010, Huang et al., 2013). JMJD5 has also been shown to regulate the p53/p21 pathway, which is functionally implicated in both cancer (Huang et al., 2015, Wu et al., 2016a, Yao et al., 2019) as well as the growth defect of JMJD5 loss of function mouse models (Ishimura et al., 2012, Ishimura et al., 2016). In addition, JMJD5 has also been implicated in promoting microtubule stability for promoting the metastasis of cancer cells and during mitosis (He et al., 2016b, Wu et al., 2016b, Wu et al., 2017). This microtubule stability

role is thought to be facilitated by the binding partner of JMJD5 called 'Regulator of Chromosome Condensation 1 domain containing protein' (RCCD1) (Marcon et al., 2014, Wu et al., 2017). RCCD1 is a member of the 'Regulator of Chromosome Condensation' (RCC) super family and is important for microtubule stability which is oncogenic in breast and ovarian cancer (Marcon et al., 2014, Hoffman et al., 2017, Kar et al., 2016, Wu et al., 2017).

JMJD5 has been also associated with cancer by alternative pathways. For example, it facilitates resistance to chemotherapeutic agents by promoting survival of prostate cancer cell lines via interaction with Pyruvate Kinase M2 and the AR (Wang et al., 2014b, Chen et al., 2019, Wang et al., 2019a). JMJD5 has also been implicated in the epithelial-mesenchymal transition of endothelial cells (Yao et al., 2019). JMJD5 is also associated with proper homologous recombination during double-strand DNA break repair in *C. elegans* (Amendola et al., 2017). Interestingly, JMJD5 has also been linked with the DNA mismatch repair pathway (Suzuki et al., 2006). Perhaps consistent with this, JMJD5 expression and activity are regulated in response to cellular stress and DNA damaging agents (Huang et al., 2015, Shen et al., 2017). Impaired activity of JMJD5 could therefore promote tumourigenesis by increasing genomic instability, a well-established hallmark of cancer (Negrini et al., 2010, Hanahan and Weinberg, 2011). Although the cellular mechanism is yet to be fully established, the importance of JMJD5 in tumourigenesis is highlighted by its proposal as a therapeutic target in cancer (Raynal et al., 2017, Wang et al., 2018).

Independent of a role in cancer, JMJD5 has also been implicated in regulating cell proliferation in other contexts. For example, Myc-interacting zinc-finger protein 1 (Miz-1) was found to negatively regulate JMJD5 in order to promote the cell cycle exit that is essential for Schwann

cell differentiation (Fuhrmann et al., 2018). Other evidence suggests JMJD5 regulation of p21 is important for stem cell differentiation (Zhu et al., 2014). A role for JMJD5 in development is further supported by its association with promoting the differentiation of osteoblasts and osteoclasts (Youn et al., 2012, Munehira et al., 2017).

Finally, JMJD5 was found to bind and facilitate the activity of Hepatitis B virus X protein (Kouwaki et al., 2016), which is a protein essential for viral replication and pathogenesis in hepatocellular carcinoma (Benhenda et al., 2009). Moreover, completely distinct to its previously discussed roles, JMJD5 has also been found to regulate circadian rhythm (Jones et al., 2010, Jones and Harmer, 2011, Shen et al., 2016, Shalaby et al., 2018, Saran et al., 2018, Jones et al., 2019).

Overall, there is strong evidence demonstrating a fundamental role for JMJD5 (summarised in Figure 1.6). However, the specific cellular activity of JMJD5 remains unclear. The identification of JMJD5 hydroxylation substrates will likely help to piece together the direct and specific cellular activities of JMJD5. However, as discussed below, the catalytic activity of JMJD5 is highly controversial.
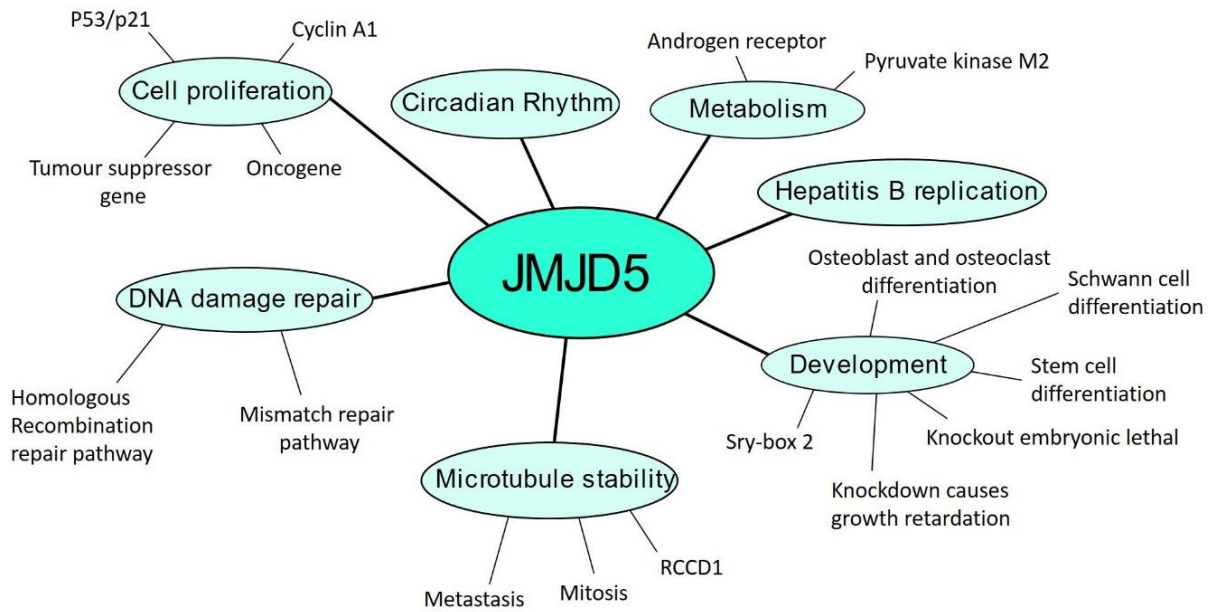
Figure 1.6 Summary of cellular functions attributed to JMJD5
Cellular functions currently assigned to JMJD5 as described in the literature. The molecular mechanism behind how JMJD5 might play a role in these activities is largely uncharacterised. However, the importance of JMJD5 activity is apparent as it is implicated in disease, including cancer.

1.4.2 JMJD5 catalytic activity

The assignment of the catalytic activity of JMJD5 has been highly controversial and therefore a complete understanding of its enzymatic role remains elusive.

Similarly to JMJD7, recent enzymatic activity attributed to JMJD5 was as an endopeptidase for histone tail clipping (Liu et al., 2017, Shen et al., 2017, Liu et al., 2018a). Liu et al. (2017) proposed JMJD5 to have both endopeptidase activity, for an initial cleavage event at histone H3R2me2, and exopeptidase activity to remove one residue after another along the histone tail. Independently, JMJD5 was assigned endopeptidase activity targeted to monomethyl-lysine on histone H3.3 in response to DNA damage and cellular stress (Shen et al., 2017). Although the two groups contradicted each other with regards to the specific histone substrate of JMJD5, both demonstrated that Fe^{2+} and JMJD5 catalytic residues were essential for these clipping events (Liu et al., 2017, Shen et al., 2017).

A more historical function assigned to JMJD5 was as a KDM targeting H3K36me2 (Hsia et al., 2010). This function was found to require both the catalytic activity and nuclear localisation of JMJD5 (Huang et al., 2013) and was thought to be important for cell cycle progression (Hsia et al., 2010, Ishimura et al., 2012, Fuhrmann et al., 2018) and homologous recombination (Amendola et al., 2017). However, there is mounting structural, sequence and biochemical evidence suggesting that JMJD5 cannot act as a KDM or endopeptidase but instead is more similar to other protein hydroxylases of the JmjC-only family members, as reviewed below.

Firstly, the H3K36me2 KDM and histone H3 endopeptidase activities of JMJD5 were not successfully reproduced by other studies (Del Rizzo et al., 2012, Youn et al., 2012, Wang et al., 2013, Williams et al., 2014, Wilkins et al., 2018, Jones et al., 2019). Importantly, the proposed KDM activity of JMJD5 was also not replicated by *in vivo* mouse or *Drosophila* models (Oh and Janknecht, 2012, Shalaby et al., 2017).

Secondly, JMJD5 sequence and structure is more closely related to other JmjC-only protein hydroxylases than with JmjC containing KDMs (Del Rizzo et al., 2012, Wang et al., 2013, Wilkins et al., 2018). For example, the JMJD5 catalytic site contains residues conserved in other JmjC-only family members, but does not contain residues in KDMs that are essential for binding methylated lysine (Del Rizzo et al., 2012). JMJD5 was even found to contain residues in its catalytic site that might block binding to methylated lysine (e.g. W414 which is conserved in FIH) (Elkins et al., 2003, Wang et al., 2013). Moreover, the narrower entrance into the JMJD5 active site compared to KDMs is predicted to block the binding of a methylated lysine (Wang et al., 2013). Consistent with the proposed absence of KDM activity, the JMJD5 sequence does not include other functional domains known to support KDM function, such as histone binding

domains (Markolovic et al., 2016, Wilkins et al., 2018). However, it should be noted that the binding partner of JMJD5, RCCD1, is likely to directly interact with nucleosomes (Marcon et al., 2010). Therefore, RCCD1 could be responsible for the localisation of JMJD5 to chromatin, an important hypothesis to be addressed in the future.

Finally, there is evidence to indicate that JMJD5 acts as a protein hydroxylase. Wilkins et al. (2018) identified that JMJD5 can hydroxylate a specific arginine residue in a synthetic peptide from both 'ribosome protein S6' (RPS6) and RCCD1 *in vitro*. However, the authors could not provide evidence of RPS6 or RCCD1 hydroxylation in cells, suggesting that JMJD5 may still be an orphan protein hydroxylase (Wilkins et al., 2018). We addressed this hypothesis later in this thesis and in doing so identified two novel candidate hydroxylation substrates of JMJD5 as the 'minichromosome maintenance complex' (MCM) subunits 3 and 5 (Chapter 4). As such we next provide a detailed overview of the MCM complex.

1.4.3   JMJD5 candidate substrates, MCM3 and MCM5

A fundamental step of cell proliferation is the complete and accurate replication of the cell genome. This results in two identical copies of the genome that are segregated between the daughter cells at mitosis. In Chapter 4 of this thesis, we propose MCM subunits 3 and 5 as candidate JMJD5 substrates which, as discussed below, act in an essential helicase during DNA replication. Here we provide an overview of the stages and regulation of eukaryote DNA replication, with particular reference to the role of the MCM complex, reviewed by Riera et al. (2017).

1.4.3.1 The minichromosome maintenance complex subunits

The MCM complex was initially discovered in a yeast genetics screen that identified mutants deficient at replicating plasmids called minichromosomes (Maine et al., 1984). Since then evolutionary conserved MCM subunits have been identified in archaea and in all eukaryotes (Bochman and Schwacha, 2009).

The eukaryotic MCM complex is a hetero-hexamer composed of the subunits MCM2-7. These subunits are members of the ATPases associated with a variety of cellular activities (AAA$^+$ ATPase) family. Each subunit shares a conserved MCM domain containing the ATPase catalytic motifs (Koonin, 1993). Also common to each MCM subunit is the presence of a zinc finger important for stabilising the N-terminus of the MCM structure and coordinating ATP hydrolysis between subunits (Poplawski et al., 2001). Outside of these common domains the subunits have individual functional domains. For example, MCM2 and MCM3 subunits have nuclear localisation signals (Young et al., 1997, Takei and Tsujimoto, 1998, Pasion and Forsburg, 1999, Ishimi et al., 2001, Liku et al., 2005), and most MCM4 subunits have conserved motifs targeted by cyclin-dependent kinases (Hendrickson et al., 1996, Forsburg, 2004). The structural domains of the MCM subunits are displayed in Figure 1.7A.
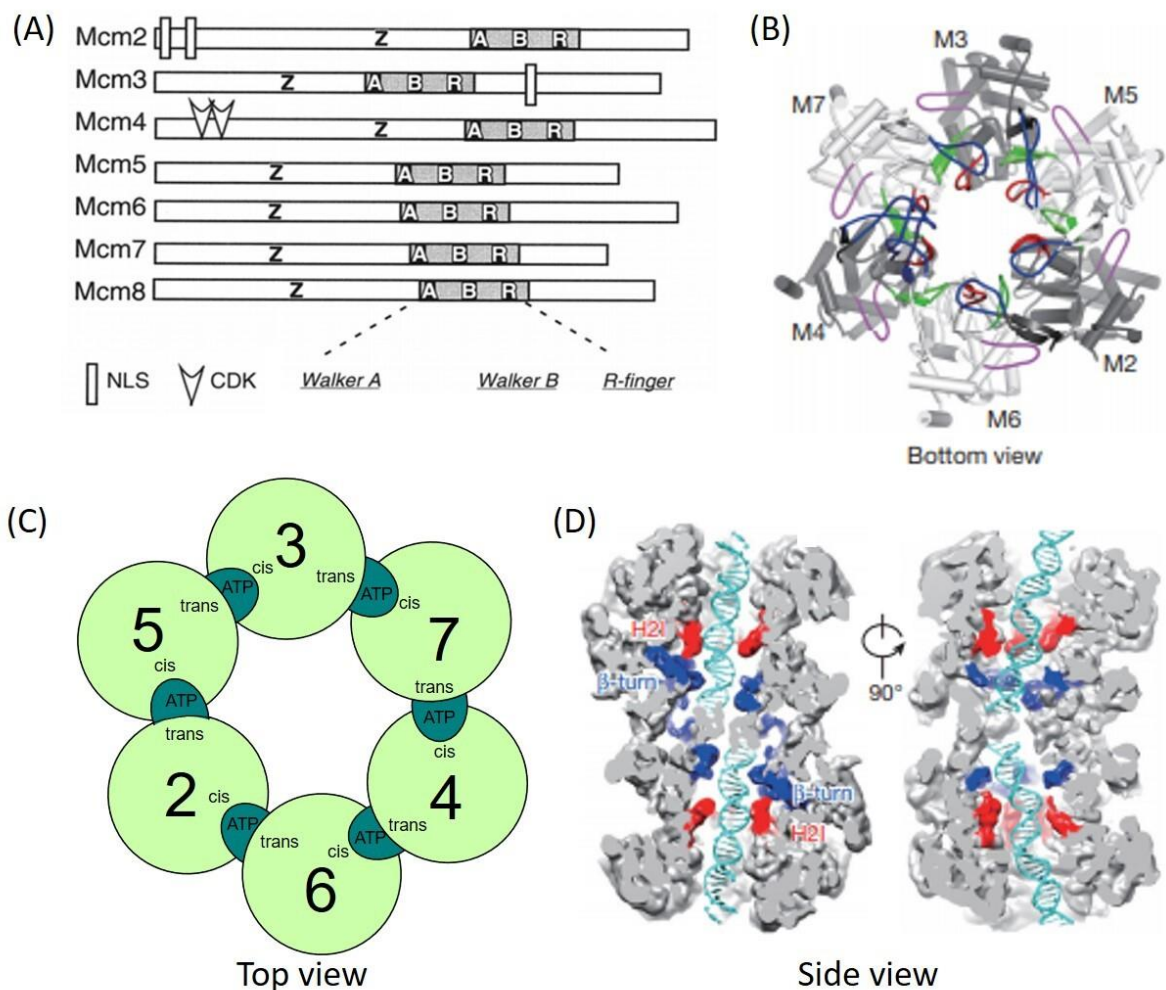
Figure 1.7 MCM subunit functional motifs and assembly into the MCM complex

(A) The MCM subunits share a conserved MCM domain composed of ATPase motifs. These are identified as cis-elements (ATP binding motifs called Walker A and Walker B motifs) and trans-elements (arginine finger that binds the γ-phosphate of ATP). All MCM subunits also contain a zinc finger domain. MCM2 and MCM3 subunits have nuclear localisation signals (NLS) and MCM4 subunits have cyclin-dependent kinase (CDK) target sequences. Figure adapted from Forsburg (2004). **(B)** The heterohexamer MCM complex assembles its subunits into a ring structure and into the centre are β-hairpins (blue coloured loop). Figure adapted from Li et al. (2015). **(C)** Once assembled the MCM complex forms functional ATPase domains between adjacent subunits. One subunit provides the cis-elements and the other trans-elements and ATP is coordinated between the subunits. **(D)** The MCM complex is shown from the side view and cut away to show DNA binding in the central channel. Figure adapted from Li et al. (2015).

The MCM subunits form a heterohexamer complex as a ring-shaped structure (Figure 1.7B) (Pape et al., 2003). Once assembled, two adjacent subunits form a complete ATPase catalytic site at the interface between them, which is essential for ATPase activity (Figure 1.7C) (Davey et al., 2003, Erzberger and Berger, 2006). Two other contacts form between subunits, one via hairpin structures between adjacent subunits and the other between zinc finger domains (Li et al., 2015). The central cavity of the complex is of optimal width and charge to encircle double stranded DNA (Figure 1.7D) (Li et al., 2015). Positioned into this cavity are β-hairpin loops from each subunit that are likely to couple ATPase activity with helicase activity to facilitate movement of DNA through the complex (Figure 1.7B) (Gai et al., 2004, Brewster and Chen, 2010).

1.4.3.2   The role of MCMs during DNA replication

DNA replication is initiated simultaneously from multiple sites termed origins of replication that are located along the length of chromosomes. It is at these origins that multiprotein complexes assemble to facilitate the initiation of bi-directional DNA replication. The first of these protein complexes to assemble at the origin is the pre-replicative complex (pre-RC) in G1 phase (Gillespie et al., 2001). The major role of the pre-RC is the loading of the MCM complex onto DNA origins prior to entry into S phase. Briefly, the origin recognition complex (ORC), facilitated by cell division cycle 6 (Cdc6), binds to origin DNA (Mizushima et al., 2000, Speck and Stillman, 2007). Loading of the MCM complex is mediated by cell division cycle 10-dependent transcript 1 (Cdt1) which binds to the MCM complex and holds it in a confirmation that enables binding onto origin DNA but prevents ATPase activity (Frigola et al., 2017). The loading of one MCM complex results in the sequential loading of another MCM complex

(Remus et al., 2009, Gambus et al., 2011, Fernandez-Cid et al., 2013, Evrin et al., 2013, Ticau et al., 2015). This is essential for bi-directional DNA replication and is depicted in Figure 1.8A.

Before DNA replication can initiate in S phase the assembly of further proteins is required to form the 'replisome'. For example, Cdc45 and the GINS (Go-Ichi-Ni-San) complex are recruited to each MCM complex to form the CMG helicase, which is responsible for DNA unwinding ahead of the replication fork (Gambus et al., 2006, Moyer et al., 2006). The formation of the CMG helicase is facilitated by MCM10, which also aids loading of DNA polymerases and stability of the replisome (Zhu et al., 2007, Chadha et al., 2016). Other essential components in the replisome include the DNA polymerase enzyme processivity factor, 'proliferating cell nuclear antigen' (PCNA) (Moldovan et al., 2007), 'replication protein A' (RPA) that binds to and stabilises single-stranded DNA (Zou et al., 2006), and the fork protection complex and the clamp loader 'replication factor C' (RFC) that together help coordinate DNA polymerase and helicase activity (Podust et al., 1995, Unsal-Kacmaz et al., 2007, Leman and Noguchi, 2012). Other protein complexes support replication ahead of the fork, such as topoisomerases which act to reduce torsional stress (Champoux, 2001), and the histone chaperone FACT complex (Tan et al., 2006, Han et al., 2010). A simplified DNA replication fork structure is depicted in Figure 1.8B.

When two DNA replication forks converge the replication proteins from each fork dissociate. As the CMG complex forms an enclosed ring around the DNA it requires more active removal (Figure 1.8C). Experiments in *Xenopus leavis* demonstrated that removal of the MCM complex from chromatin was dependent on K48-linked poly-ubiquitination of MCM7 which signals for extraction from chromatin (Moreno et al., 2014, Sonneville et al., 2017).
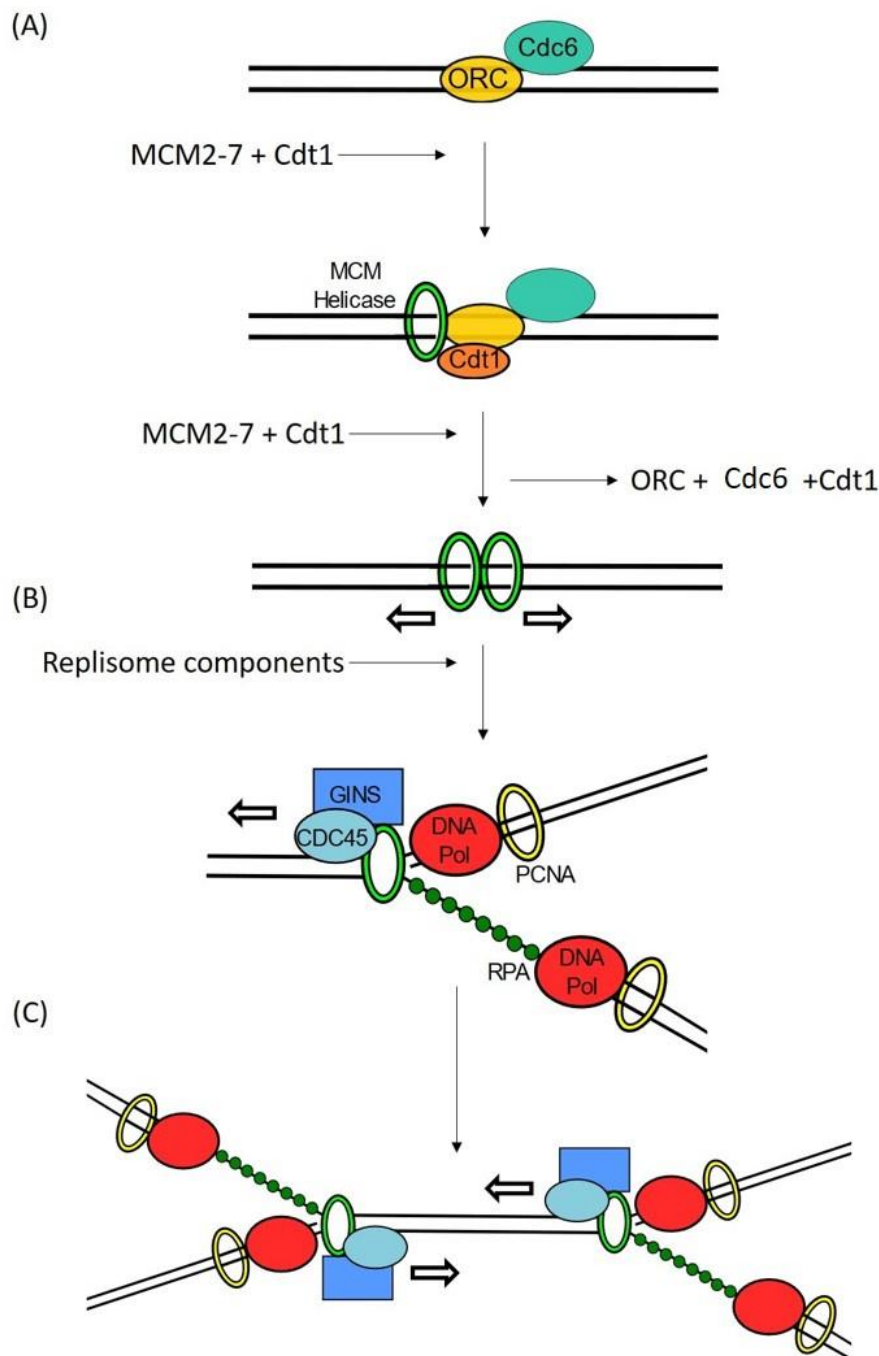
Figure 1.8 A summary of the DNA replication mechanism

(A) Formation of the pre-replicative complex composed of ORC, Cdc6, Cdt1 and the MCM complex are loaded onto origins of DNA replication. (B) Upon loading of two MCM complexes the pre-RC components are no longer required. Instead replisome components bind, a simplistic replication fork is shown here including GINS and Cdc45 to make the CMG with the MCM complex, DNA polymerases and processivity factor PCNA and single-stranded DNA binding protein RPA. There are many more proteins not included, that act ahead and within the replisome essential for progression of the replication fork. (C) When two replication forks converge DNA replication is terminated and the replisome disassembles. Active removal of the MCM complex is required as it encircles the DNA molecule. Included in this diagram are arrows to demonstrate directionality of protein movement along the DNA molecule.

1.4.3.3   Regulation of the MCM complex by post-translational modifications

Proper regulation of DNA replication is essential to maintain genomic stability. Due to the

essential nature of the MCM complex, in the DNA replication process, it is highly regulated.

This can be indirect, such as regulating essential proteins responsible for loading or activation

of the MCM complex. For example, Cdt1 expression levels are cyclic to prevent improper

loading of new MCM complexes. This is mediated by its inhibitor geminin as well as proteolytic

degradation regulated by phosphorylation by 'cyclin dependent kinases' (CDKs) or by

interaction with PCNA (Pozo and Cook, 2016). In addition, MCM regulation can be direct, via

PTM of the MCM subunits. Due to the focus of this project and our hypothesis that the

MCM3/5 subunits could be hydroxylated (Chapter 4), the regulation of the MCM complex by

PTM is summarised below and in Figure 1.9.

The best characterised MCM PTM is phosphorylation, mediated by CDKs and cell division cycle

7-related protein kinase, which facilitate MCM complex formation and regulate loading and

unloading of the complex on chromatin. For example, loading of MCM3 onto chromatin is

dependent on CDK1 phosphorylation of MCM3 at serine 112 and threonine 722 (Schumann et

al., 2018). The phosphorylation on S112 was also found to promote MCM3 incorporation into

the MCM complex (Lin et al., 2008). The complex can also be phosphorylated in response to

DNA damage or 'replication stress' (defined in Chapter 5) (Cortez et al., 2004).

As mentioned above, ubiquitination of the MCM complex is important during termination of

DNA replication for the disassembly of the complex (Moreno et al., 2014, Sonneville et al.,

2017). Interestingly, TRAIP mediated MCM7-ubiquitination and complex unloading has also

been identified as an important step in the repair of replication stalled forks (Priego Moreno

et al., 2019, Wu et al., 2019). The MCM complex is also potentially targeted for a ubiquitin-like modification called UFMylation on subunits 3 and 7, though the consequence of this is currently unknown (Merbl et al., 2013, Pirone et al., 2017).

MCM subunits can also be targeted for SUMOylation when the complex is bound to chromatin (Golebiowski et al., 2009, Elrouby and Coupland, 2010). Levels are highest in G1 phase, but upon entry into S phase, when MCM phosphorylation peaks, the SUMOylation of MCM subunits decreases (Wei and Zhao, 2016). This is important because prevalence of SUMOylation in G1 prevents DNA replication initiation by reducing the formation of the CMG complex (Wei and Zhao, 2016). This PTM has also been implicated in negatively regulating DNA replication in order to maintain genomic stability (Golebiowski et al., 2009, Cremona et al., 2012).

Other PTMs include *O*-linked β-*N*-acetylglucosaminylation (*O*-GlcNAcylation), which is reported to increase affinity between MCM subunits (Leturcq et al., 2018). However, depletion of *O*-GlcNAc transferase had no effect on replication speed, suggesting that this modification could be targeted to dormant origins in response to DNA damage or replication stress (Leturcq et al., 2018). Finally, the PTM acetylation has been implicated in regulating initiation of DNA replication by targeting MCM10 (Fatoba et al., 2013) or MCM3 (Takei et al., 2001).

Overall, tight regulation of MCM function is mediated by an array of PTMs that coordinate activity throughout the cell cycle, reviewed by Li and Xu (2019).
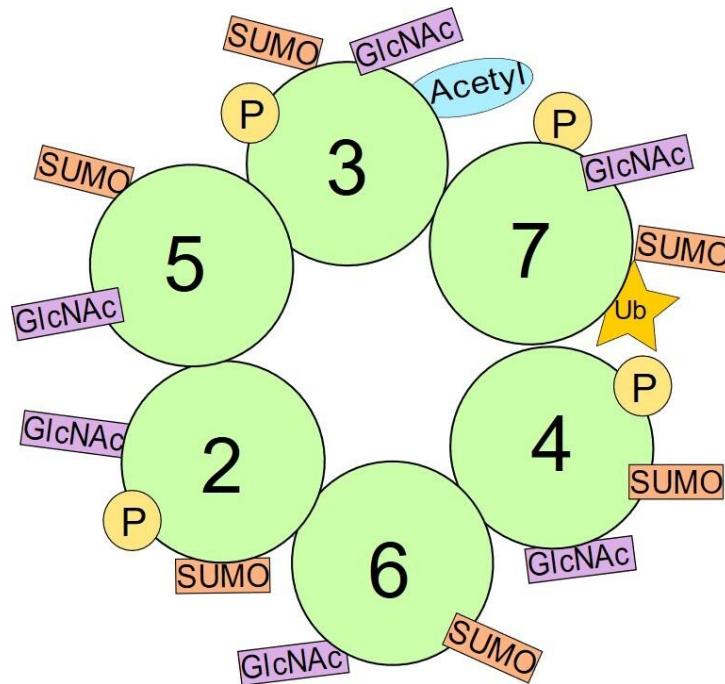
Figure 1.9 A summary of MCM complex PTMs for regulation of DNA replication
This figure summarises some of the PTMs important for regulating the function of the MCM complex during DNA replication. MCM complex assembly can be facilitated by phosphorylation (P) and *O*-GlcNAcylation (GlcNAc). Loading of the complex onto chromatin can be regulated by phosphorylation, and DNA initiation can be regulated by MCM complex SUMOylation (SUMO) and acetylation (Acetyl). Removal of the complex from chromatin is facilitated by ubiquitination (Ub) of MCM7. These subunits can also be regulated by PTM in response to cellular stress, such as DNA damage or replication stress.

1.5 Aims of the study

It is clear from the evidence presented in this introduction that the 2OG oxygenase family of enzymes are important in fundamental cellular processes. Moreover, when dysregulated they can play important roles in the aetiology and progression of human diseases, particularly developmental disorders and cancer. Despite this knowledge, there are many 2OG oxygenase family members that remain poorly characterised. Investigating the role of these enzymes in disease could help to progress our understanding of their cellular and enzymatic functions.

JMJD7 has been implicated in cancer and developmental disorders associated with ID and ASD. Although the hydroxylation substrates of JMJD7 have been assigned, their cellular activities remain largely uncharacterised and the consequence of hydroxylation is unknown. How JMJD7-dependent DRG1 and/or DRG2 hydroxylation might regulate neural differentiation and proliferation has not yet been investigated. Therefore, in this study we aim to analyse the potential role of the JMJD7 hydroxylation pathway in neural differentiation and ASD. Specifically, we aim to generate cellular models of neural differentiation and function in embryonic stem cell, induced pluripotent stem cell and SHSY5Y neuron-like cell lines that could be characterised for future analysis (Chapter 2).

JMJD5 has been associated with many cellular processes, including those linked to the progression of cancer and developmental defects in mouse models. Whether JMJD5 mutation is associated with human developmental disorders is not known. Furthermore, the role of JMJD5 hydroxylase activity in disease is unclear and it is likely that the *bona fide* substrate(s) of JMJD5 have yet to be identified. To address these uncertainties, we aim to characterise the pathogenicity of two JMJD5 mutations identified in patients affected with a novel developmental disorder. We first aim to determine the mRNA products of these *JMJD5* mutations and to characterise their effect on JMJD5 protein expression, stability and activity (Chapter 3). Secondly, we aim to phenotype fibroblast cell lines generated from an affected patient to identify and characterise JMJD5 hydroxylation substrates (Chapter 4). Finally, we aim to investigate the effects of JMJD5 activity on associated cellular processes and the potential pathogenicity of these JMJD5 mutations towards the developmental disorder phenotypes (Chapter 5).

2 Characterisation of the JMJD7 pathway in neurodevelopmental disorders

In this PhD project we aimed to investigate the role of JmjC-only family members in developmental disorders. As discussed in Chapter 1 there are many links between the function of 2-OG oxygenase family members and disease. One JmjC-only sub-family member, JMJD7, has been implicated in cancer (Dr Charlotte Eaton) (Zhu et al., 2016, Liu et al., 2017) and developmental disorders, including intellectual disability (ID) and Autism Spectrum Disorder (ASD) (de Ligt et al., 2012, Matsunami et al., 2014). Unfortunately, the role JMJD7 might play in the aetiology of these disorders is largely limited by the lack of understanding regarding its cellular function (discussed in Chapter 1). However, two JMJD7 hydroxylation substrates were recently identified as the Developmentally Regulated GTPases (DRG) 1 and 2 (Markolovic et al., 2018). Interestingly, these two hydroxylation substrates have also been implicated in ID developmental disorders and ASD (Vlangos et al., 2000, Lucas et al., 2001, Bi et al., 2002, Nakamine et al., 2008, de Krom et al., 2009). This evidence suggests that the JMJD7 hydroxylation pathway could be important for normal brain development or function. However, apart from these observations no attempt has been made in the literature to characterise how this JMJD7 pathway might contribute to neuron differentiation, function and the pathology of ID and ASD. Consequently, in this chapter we aimed to contribute to this by performing a preliminary characterisation of the JMJD7 hydroxylation pathway in neuronal cell models.

In order to do this, two cellular models were established. We developed the first cell model in the 'Centre for Neural Engineering' at the University of Melbourne under the supervision of Assistant Professor Mirella Dottori. This model used embryonic stem cells (ESCs) and ASD patient-derived induced pluripotent stem cells (iPSCs) directed along two neural differentiation pathways. The second cellular model involved JMJD7 loss of function models generated in the neuronal-like cell line SHSY5Y, established at the University of Birmingham. However, due to time constraints at the University of Melbourne complete analysis was not possible. Therefore, the data presented in this chapter focusses on the work performed to generate these cellular models and the pilot data derived from their preliminary characterisation. Consequently, in the following sections we provide a detailed introduction to ESC and iPSC models, SHSY5Y cell lines and an overview of ASD, which was the major focus of the work performed in Melbourne.

2.1 Introduction

2.1.1 Autism Spectrum Disorder (ASD)

ASD affects around 1 in 100 people in the UK (Baird et al., 2006), with a clinical diagnosis that covers a variety of different complex behavioural defects such as language communication, compromised social skills, and restrictive or repetitive behaviours. As autism is a spectrum disorder this has made understanding it from a biological perspective complicated and the specific causes are still ambiguous. Investigation of ASD-associated disorders, such as Fragile X Syndrome, as well as rare single gene mutation cases of ASD have been invaluable to make strides in understanding this disorder at the biological and systems level (Brooks-Kayal, 2010). However, the complete aetiology of ASD is far from being uncovered and the spectral nature of ASD highlights the potential importance of combined environmental and genetic influence

(Lyall et al., 2017). However, as patients can be diagnosed as early as 18 months old (Zwaigenbaum et al., 2016), it is widely appreciated that ASD is associated with impaired prenatal development and postnatal maturation of the brain. The study of this has been established *in vitro* using ESCs and patient-derived iPSCs cellular models, which are introduced in more detail below. In this chapter we aimed to employ these cellular models to characterise the JMJD7 pathway in neuronal cells in order to improve our understanding of its potential role in neural differentiation, maturation, and ASD.

2.1.2   Pluripotent stem cells as models for ASD research

In this chapter, we began characterising the biological role of JMJD7 in neural development using embryonic stem cell (ESC) and ASD patient-derived induced pluripotent stem cell (iPSC) lines. Stem cells (SCs) are able to self-renew and are defined by their differentiation potential.

ESCs are derived from the inner cell mass (ICM, a.k.a embryoblast) of a blastocyst (Figure 2.1B). The ICM can be classified into two types of cell, the hypoblast which will develop into extra-embryonic endoderm, and the epiblast that are pluripotent SCs able to differentiate into all cells of the embryo. It is these epiblast cells, purified from *in vitro* fertilisation blastocycts, that ESC lines are derived for culture *in vitro* (Figure 2.1B). In this project SC populations were maintained on a vitronectin substrate combined with Essential 8™ medium (derived from the original recipe by Chen et al. (2011a)). The ESC line utilised in this project were the H9 line, which was one of the first human ESC lines to be established (Thomson et al., 1998).

As there are many ethical complications associated with using ESCs, therefore, other methods have also been developed to generate pluripotent SCs *in vitro*. One method, somatic cell nuclear transfer, imitated fertilisation by transferring somatic DNA from an adult skin cell into

enucleated oocytes (Briggs and King, 1952). However, this method was still surrounded by ethical complications and poorly efficient. Therefore, this was superseded by induced pluripotent stem cells (iPSCs) created by nuclear reprogramming (Figure 2.1A). In this method fully differentiated somatic cells are reprogrammed using four critical genes required for SC pluripotency: Oct3/4, c-Myc, Klf4 and Sox2 (Takahashi and Yamanaka, 2006, Takahashi et al., 2007). These factors are responsible for reactivating endogenous pluripotency genes and inactivating differentiation promoting genes to revert somatic cells into having ESC characteristics (Sohn et al., 2012).
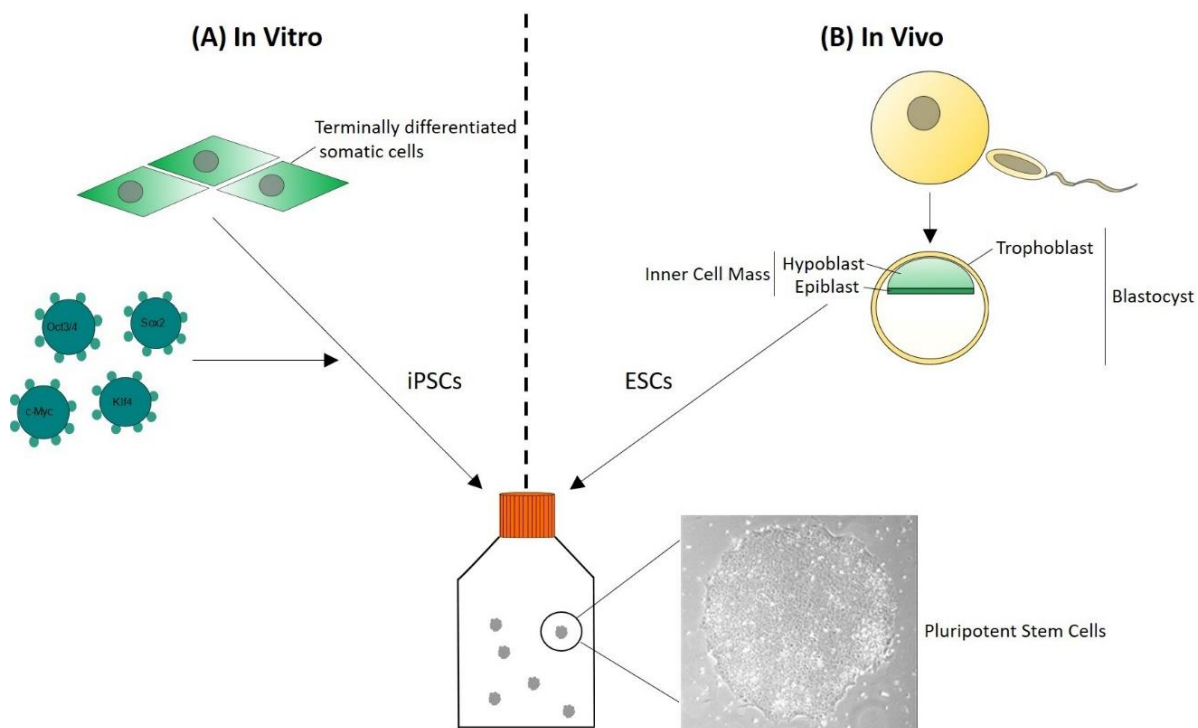
Figure 2.1 Pluripotent stem cells *in vitro*, isolation from blastocysts or generation from differentiated somatic cells

Pluripotent stem cells have the potential to differentiate into all cells of the developing embryo and thus when cultured *in vitro* provide an invaluable model to study development. They can be derived by two methods depicted here. **(A)** Reprogramming of terminally differentiated somatic cells by introduction of four pluripotency factors, Oct3/4, Sox2, c-Myc, Klf4 (the historical method of viral infection is shown in this figure). The product of this *in vitro* manipulation are colonies of cells called induced pluripotent stem cells (iPSCs). **(B)** *In vivo* pluripotent cells are naturally formed after fertilisation and blastulation. The resulting blastocyst is composed of the trophoblast and inner cell mass (ICM). Epiblast cells of the ICM are pluripotent and can be isolated for culture *in vitro*. Human blastocysts are commonly sourced from *in vitro* fertilisation procedures. However, they are ethically controversial and therefore iPSCs are becoming more commonplace.

The delivery of these pluripotency factors can be performed by viral transduction, however, these methods have been deemed unsafe for potential downstream clinical applications due to the risk of cancer (Okita et al., 2007). In this project, reprogramming of ASD patient derived fibroblasts was performed by Ms Tejal Kalkarni and Dr Giovanna D'Abaco using electroporation of reprogramming genes Oct4, Sox2, Lin28, L-Myc and Klf4. A dominant negative p53 was included to improve reprogramming efficiency (Zhao et al., 2008, Utikal et al., 2009, Hong et al., 2009). Epstein-Barr nuclear antigen-1 (EBNA1) was included to contribute towards the inhibition of p53 (Saridakis et al., 2005), facilitate the direction and retention of the reprogramming plasmids into the nucleus, and drive expression of the reprogramming genes downstream of oriP sites (Leight and Sugden, 2000).

This reprogramming of terminally differentiated human cells into iPSCs was a ground-breaking scientific discovery. However, there is debate regarding how similar iPSCs are to the naturally occurring ESCs. Some suggest there are no distinguishable differences between them (Guenther et al., 2010), whereas others demonstrate that iPSCs have changes in differentiation potential, epigenetics and gene expression compared to ESCs (Chin et al., 2009, Bock et al., 2011, Lister et al., 2011, Koyanagi-Aoi et al., 2013). However, these differences could be a result of the reprogramming method, passage number, tissue culture environment, tissue origin of the reprogrammed cells, or due to lines not being isogenic (Baker et al., 2007, Newman and Cooper, 2010, Kim et al., 2011a, Kajiwara et al., 2012, Churko et al., 2017). Despite this, iPSCs remain a widely used tool as the major benefit they provide is the ability to generate disease relevant SC lines and overcome limitations of post-mortem samples or animal models.

2.1.3 *In vitro* versus *in vivo* neural differentiation

Due to the pluripotent nature of ESCs and iPCS they can be induced along any lineage of the developing embryo. This can be achieved using different combinations of small molecule agonists and antagonists as well as growth factors supplemented into the culture media. This means that ESCs and iPSCs, differentiated along multiple neural lineages, enable study of neural differentiation, function and neurodevelopmental disorders *in vitro.*

In this chapter, we utilised *in vitro* methods to generate glutamatergic projection neurons (excitatory, dorsal forebrain neurons) and GABAergic interneurons (inhibitory, ventral forebrain neurons) from SCs. This is because they are the two major neuron types identified within the cerebral cortex, which is the region of the brain that mediates information processing and commonly where improper development relating to ASD is identified (Ha et al., 2015). Consequently, in this chapter we were interested to explore whether the JMJD7 hydroxylation pathway may contribute to the ASD phenotype by investigating whether the pathway was important during development of cerebral cortex (cortical) neurons. The process of forebrain neural differentiation *in vivo,* and how our methods aimed to replicate this *in vitro,* are explained below and depicted in Figure 2.2.

In vivo, the first important lineage decision facing epiblast pluripotent SCs is which of the three germ layers to become. The ectoderm layer is the site for future neural and epidermis lineages (Figure 2.2A). Many studies have shown that neural differentiation is the default fate for these ectoderm cells and that active signalling is required to promote epidermal fate (Stern, 2006). In this model, transforming growth factor β (TGFβ) morphogens expressed in the ectoderm such as bone morphogenic proteins (BMP), activin and nodal, facilitate internal cellular

signalling to promote epidermal fate (Zhou et al., 1993, Jones et al., 1996, Pera et al., 2004, Vallier et al., 2004). Consequently, inhibition of TGF-β signalling is required for neuroectoderm (NE) specification. *In vivo*, these inhibitors are produced by a group of cells responsible for directing neural fate called the 'Spemann organiser' which restricts NE specification to the dorsal side of the embryo (Spemann and Mangold, 1924, Hemmati-Brivanlou et al., 1994, Piccolo et al., 1996, Zimmerman et al., 1996, Stottmann et al., 2006). This process can be replicated *in vitro* by incubating SC colonies with TGF-β small molecule inhibitors LDN/ Noggin and SB431542 to promote NE specification (Figure 2.2B). These cells are grown on a laminin substrate as this has been found to promote the growth, survival and differentiation of neural SCs (Hall et al., 2008).

Following this NE specification event *in vivo* cells migrate and organise into the neural tube which becomes the site for future brain and spinal cord development (Figure 2.2C). NE cells in the neural tube are given rostral-caudal (axis from the front to the back of the brain) and dorsal-ventral identity (axis from the top to the bottom of the brain) which in turn defines the cell's specific terminal differentiation identity. The most rostral region of the neural tube develops into the forebrain (Figure 2.2F), as the site for generatating neurons that will populate the future cerebral cortex (Campbell, 2003) This is the default positional identity of NE cells, meaning that *in vitro* specification can be directed towards glutamatergic (dorsal) or GABAergic (ventral) neurons by giving NE cells a dorsal-ventral identity (Gaspard et al., 2008). *In vivo* this dorsal-ventral identity is defined by a gradient of sonic hedgehog (SHH) signalling (Li et al., 2009) that originates from the notochord (Figure 2.2C). *In vitro* the specification of ventral neurons is promoted by incubating cells with a SHH agonist called SAG (smoothened agonist) (Figure 2.2C).

Following NE specification, the population is expanded by formation of neural progenitors and neurons, which later require further morphological and synaptic maturation. These events take an extended period of time in primates compared to other species (Rakic, 2009), and is thought to be essential for the complexity of the primate cortex (Smart et al., 2002, Hansen et al., 2010, Petanjek et al., 2011, Reillo and Borrell, 2011). Therefore, to mimic this process *in vitro,* NE populations are expanded in fibroblast growth factor (FGF) for 1 week in 2D culture, then in FGF and epidermal growth factor (EGF) for 2 weeks in 3D culture as neurospheres. Developing neurons are then allowed to mature for a further 2 weeks in 2D culture (Figure 2.2F) on Poly-D-lysine and Laminin substrates, as these were reported to promote *in vitro* neuron survival and extension of neurites (Kim et al., 2011b).

During these expansion and maturation stages the *in vitro* models form intrinsically organised polarised structures that are reminiscent of the organisation found *in vivo*. In 2D culture the NE cells form rosette structures with apical and basal polarity (Figure 2.2D). As *in vivo* these structures have mitotic NE cells facing the apical (inner) side and neuron fated NE cells towards the basal (outer) side (Li et al., 2005, Elkabetz et al., 2008). When grown in 3D as neurospheres this cell polarity replicates the *in vivo* organisation of dorsal cortical layers (Eiraku et al., 2008, Nasu et al., 2013). Briefly, NE cells generate neural progenitor cells called radial glia that divide asymmetrically to generate neurons directly, or indirectly via formation of intermediate progenitor cells (called basal progenitors or outer radial progenitors) in the sub-ventricular zone (Noctor et al., 2004). These neurons then migrate into the cortical layers depending on the time of their synthesis, i.e. early neurons migrate to deep cortical layers and later neurons migrate to upper cortical layers (Figure 2.2E). To note, *in vivo* the generation of GABAergic neurons is thought occur predominantly on the ventral side and neurons then migrate into

the dorsal side (Nadarajah and Parnavelas, 2002, Campbell, 2003). However, the organisation of the neural rosette and neurosphere structures are sufficient to facilitate both glutamatergic and GABAergic neural differentiation *in vitro* (Suzuki and Vanderhaeghen, 2015).

Importantly, cells taken at different stages of *in vitro* neural differentiation, also express markers representing key developmental stages identified *in vivo*. For example, pluripotent cells found in SC colonies *in vitro* and the ICM *in vivo* are positive for Oct4 and Nanog (Loh et al., 2006, Lee et al., 2010). Cells after one week of neural induction (early rosettes) stain positive for Sox2, a marker of neural SCs (Ellis et al., 2004, Cavallaro et al., 2008). After the second week of neural induction (late rosettes) cells are positive for Pax6, which can also be found expressed in NE cells and neural progenitors in the developing forebrain *in vivo* (Zhang et al., 2010). A further two weeks of differentiation in 3D culture results in neurospheres positive for TBR2, a marker of basal progenitor cells (Arnold et al., 2008, Sessa et al., 2008), and βIII-tubulin is an established marker of early neurons (Memberg and Hall, 1995). After two weeks of neural maturation *in vitro* cells become positive for microtubule-associated protein-2 (MAP2AB), which is a well-established marker of mature neural dendrites (neural extensions that receive neurotransmitter signals) (Izant and McIntosh, 1980, Huber and Matus, 1984).

Unfortunately, these models are limited as they cannot replicate the extensive *in vivo* maturation and organisation of the cerebral cortex, that continues for months and years postnatally (Dehay et al., 2015). However, they allow researchers to mirror important cellular events found during early neural differentiation *in vivo*. Therefore, in this chapter we aimed to adopt the methods described above to explore the JMJD7 hydroxylation pathway in early stages of neural development, including using cells derived from healthy and ASD patients.
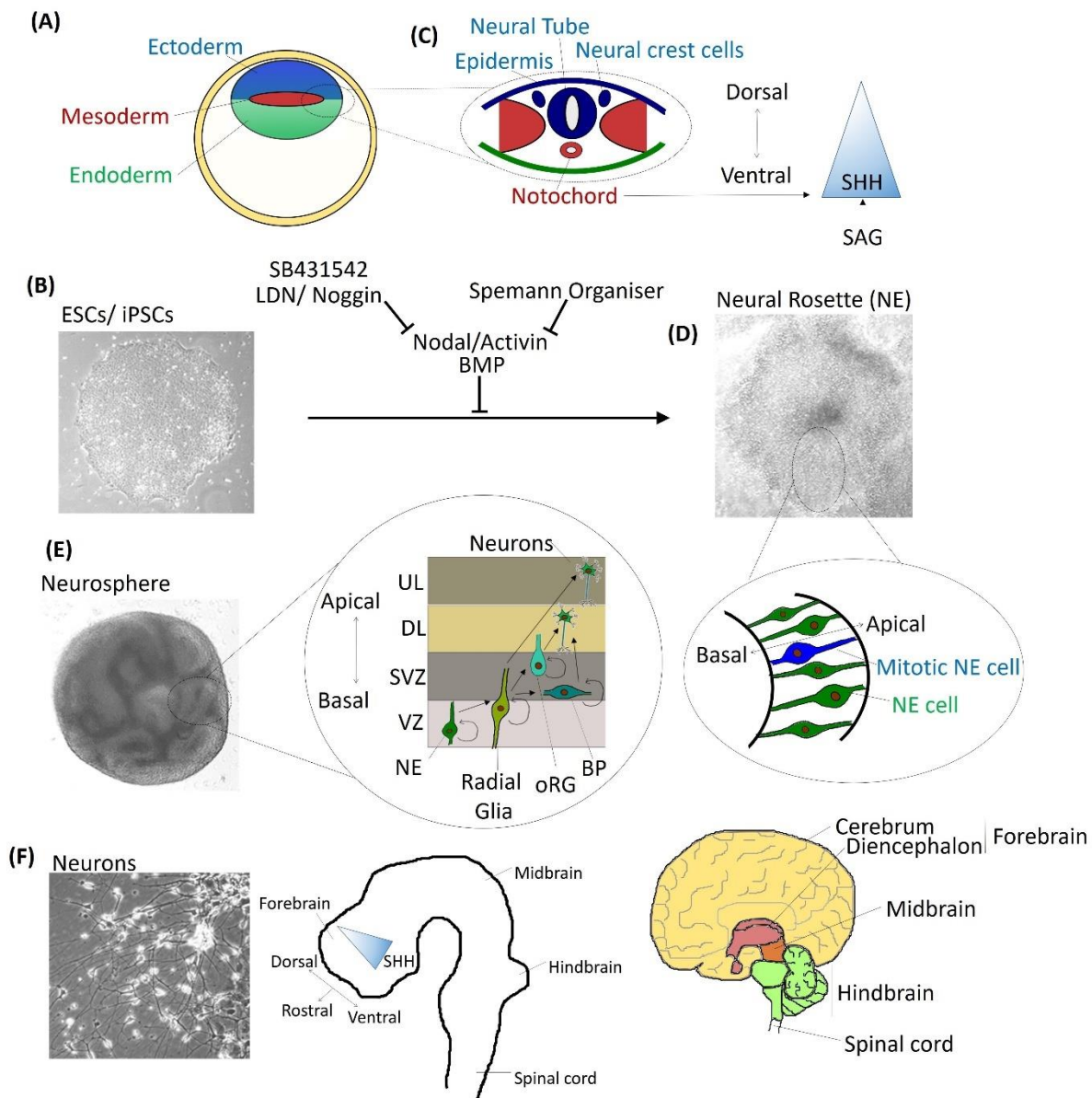
Figure 2.2 Forebrain neural differentiation *in vitro* versus *in vivo*

(A) The future central and peripheral nervous system plus the epidermis are formed from the ectoderm layer. **(B)** Differentiation fate is induced by local cellular signalling and morphogen gradients. For example, the Spemann Organiser promotes neural fate by releasing inhibitors for TGF-β ligands. *In vitro* stem cells are incubated with BMP inhibitor (SB431542) and nodal/activin inhibitor (LDN/Noggin). **(C)** Neural fated cells organise into the neural tube. This is given dorsal-ventral patterning by sonic hedgehog (SHH) signalling from the notochord or *in vitro* using SHH agonist (SAG). **(D)** *In vitro* the cells self-organise into a rosette structure which mirrors that seen in the early neural tube *in vivo*. At the basal side neural stem cells rapidly divide, at the apical side cells acquire a neural fate (neuroectoderm, NE). **(E)** In the forebrain NE cells asymmetrically divide to produce neural progenitors or early neurons that migrate into the cortical layers which can be reproduced *in vitro* as neurospheres. Basal progenitors (BP), outer radial glia progenitors (oRG), ventricular zone (VZ), sub-ventricular zone (SVZ), cortical deep layer (DL), cortical upper layer (UL). **(F)** *In vitro* neural progenitor and early neurons are released from neurospheres to enable maturation of neurons. *In vivo* these forebrain cortical neurons form the cerebral cortex and other regions of the neural tube generate the structures of the brain.

2.1.4 SHSY5Y cellular models

In addition to using SC models described above, we also used the neural-like cell line, SHSY5Y, to characterise the JMJD7 pathway. As SHSY5Y and SC models have distinct strengths and limitations, we proposed that using both in parallel would be advantageous for studying the JMJD7 hydroxylation pathway in the following work presented in this chapter.

Neuronal-like cell lines, such as SHSY5Y, provide a model that overcomes some of the limitations associated with studying SC models. For example, although the knockdown of proteins in SCs is possible by viral (Zaehres et al., 2005) or transfection methods (Ma et al., 2010), these can be technically challenging and have low efficiency compared to SHSY5Y cells. Another benefit is that the generation of neurons from SHSY5Y cells is relatively inexpensive, less technical and time consuming compared to using SCs (Kovalevich and Langford, 2013). As SHSY5Y cells are transformed human cell lines they also provide major benefits over studying rodent primary neurons that are terminally differentiated and therefore cannot be propagated for extended periods of time (Kovalevich and Langford, 2013).

The parental line, SK-N-SH, were derived from a bone marrow biopsy taken from a patient with metastatic neuroblastoma, and the SHSY5Y line was sub-cloned based on their neuron-like morphology and differentiation capabilities (Biedler et al., 1978). Studies have demonstrated the presence of both adherent and non-adherent SHSY5Y cell types (Ross et al., 1983). The significance of these two populations has not been established, however, some suggest they have different neuron differentiation potentials (Encinas et al., 2000).

SHSY5Y cells can differentiate into cholinergic, adrenergic or dopaminergic neuron types by treating them with different stimuli (Xie et al., 2010, Dwane et al., 2013). After differentiation

SHSY5Y cells form neurites and express neuron-specific proteins to form functional synapses (Encinas et al., 2000, Lopez-Carballo et al., 2002, Cheung et al., 2009). The ability to induce SHSY5Y cells into a more mature neuron-like cell types has made them valuable *in vitro* models of neuronal development and disease (Presgraves et al., 2004, Lopes et al., 2010, Xie et al., 2010).

This cell line is also valuable in the undifferentiated state for studying neural characteristics (Cheung et al., 2009). Undifferentiated SHSY5Y cells are neuron-like but more reminiscent of immature neuron-like progenitors (Pahlman et al., 1984, Lopes et al., 2010). For this reason, we utilised undifferentiated adherent SHSY5Y cells in this chapter for our initial work to generate JMJD7 loss of function models.

2.2 Investigation of the JMJD7 pathway in stem cell models

2.2.1 JMJD7 hydroxylation pathway expression in stem cells

Due to reported mutations of JMJD7, and its hydroxylation substrates, in ID and ASD, we were interested in understanding how the JMJD7 pathway might play a role in the aetiology of such conditions. As both disorders are associated with defects in neuronal development, we were first interested to investigate when expression of JMJD7 pathway components could be identified during neuronal development.

The first lineage of cells established during development that can be studied *in vitro* are pluripotent SCs, normally localised within the ICM of the blastocyst, and called embryonic stem cells (ESCs) (described in Section 2.1.2). We were therefore interested to investigate whether components of the JMJD7 hydroxylation pathway were expressed at this early developmental stage. To undertake this analysis ESCs were grown on vitronectin coated

coverslips prior to harvesting for immunofluorescence staining to analyse expression of JMJD7 and its substrates DRG1 and DRG2, plus their obligate binding partners DFRP1 and DFRP2.

Due to positive staining, we hypothesised that all components of this JMJD7 hydroxylation pathway were expressed in ESC colonies (Figure 2.3). Interestingly, the staining patterns of all pathway components were concentrated to the periphery of the colony (Figure 2.3). As mentioned in Section 2.1.3, the default pathway adopted by pluripotent SC colonies is towards rostral neural fates, which has been validated experimentally (Rosowski et al., 2015). Therefore, the potential expression of JMJD7 hydroxylation pathway components in differentiating cells at the periphery of the ESC colonies, led us to hypothesise that the pathway might be regulated during neural differentiation.
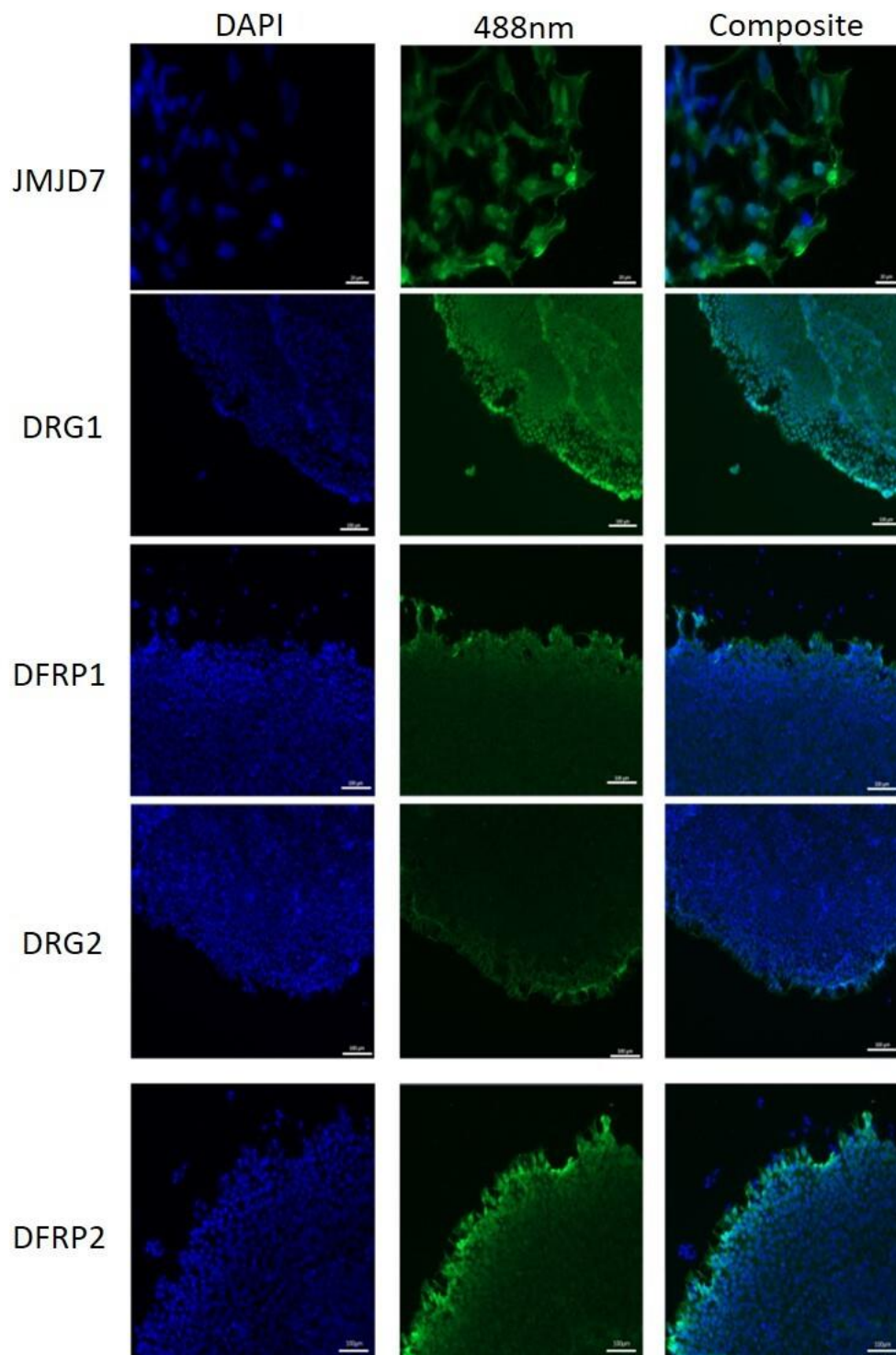
Figure 2.3 JMJD7 hydroxylation pathway protein expression in embryonic stem cell colonies
Embryonic stem cell line, H9, were grown as stem cell colonies on vitronectin coated coverslips before immunofluorescence staining for proteins of the JMJD7 hydroxylation pathway (detected using 488nm Alexa Flour® secondary antibodies). The apparent difference in morphology for the JMJD7 immunofluorescence stained ESC colony is due to the magnification used for this analysis (JMJD7 images scale bar= 20 µm, all other images scale bar= 100 µm). DAPI was used as a nuclear marker. This is representative of an n=1 biological repeat for JMJD7 and n=2 biological repeat for all other pathway components.

2.2.2 Induction of neural lineages from ESCs

To explore the hypothesis that the JMJD7 pathway might be regulated during neural differentiation, we utilised an *in vitro* model to generate two types of cortical neurons from SCs.

As outlined in the introduction to this chapter, well-established protocols have been developed to make use of the pluripotent nature of ESCs. For our investigation, we were most interested in studying two neural lineages, excitatory glutamatergic neurons generated in the dorsal portion of the forebrain, and inhibitory GABAergic neurons generated within the ventral region of the forebrain. The reason for this was that these neuron types form the majority of cells localised within the cerebral cortex, the region of the brain where improper development associated with ASD is most commonly identified (discussed in detail in Section 2.1.3).

In order to differentiate ESCs into these two cortical neuron types *in vitro,* we adopted an already established method that mirrors *in vivo* neural differentiation (summarised in Figure 2.2). Briefly, ESCs are incubated with the activin inhibitor (SB431524) and BMP inhibitor (LDN/ Noggin) for one week to promote neural specification. In order to give the differentiating neurons a ventral identity, the sonic hedgehog agonist SAG was used. This intervention promoted NE formation which could be identified by the self-organisation of the cells into rosette structures. These NE cells were then expanded and allowed to continue differentiation as 2D and 3D colonies to generate neurons, which were then further matured for 2 weeks in 2D culture.

Before analysis of the JMJD7 pathway could be performed, we first wanted to validate whether these neural induction treatments of our ESC colonies had successfully generated populations of glutamatergic or GABAergic neurons. This was determined by immunofluorescence staining of neurons for the expression of GAD67, the enzyme that mediates the decarboxylation of glutamate into the neurotransmitter GABA and is produced exclusively by GABAergic neurons (Chattopadhyaya et al., 2007). MAP2AB co-staining was also used to identify whether the neurons were mature (Section 2.1.3). Importantly, the results presented in Figure 2.4 confirmed the specificity of our induction methods, as only the ESCs treated with SAG during NE specification were positive for GAD67 staining (identified as GABAergic neurons), all others were negative for GAD67 staining (identified as glutamatergic neurons).
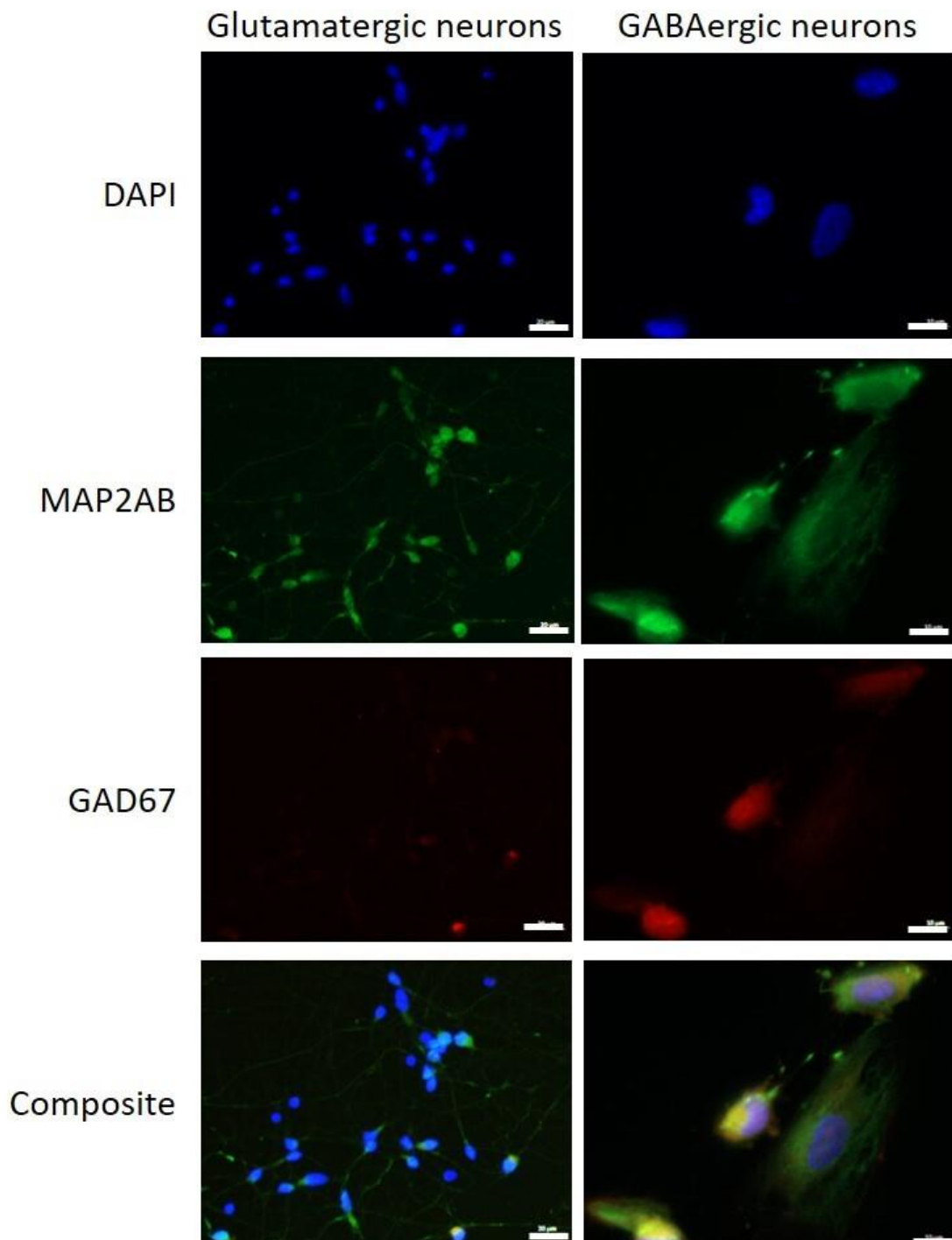
Figure 2.4 Validation of *in vitro* differentiation of stem cells into two different cortical neuron types
Well-established protocols were applied to H9 ESC colonies to promote the differentiation of either glutamatergic or GABAergic neurons. Neurons from each differentiation pathway were matured for two weeks on coverslips before immunofluorescence staining. MAP2AB staining was used to test whether neurons had matured. GAD67 staining was used as a marker of GABAergic neurons. This demonstrated the specificity of each neural differentiation protocol. DAPI was used as a nuclear marker. Glutamatergic neurons scale bar= 20 µm, GABAergic neurons scale bar= 10 µm. This is representative of an n=1 biological repeat.

2.2.3 mRNA expression of JMJD7 pathway components in differentiated neurons

The work presented above gave us confidence that these neural induction methods could be utilised for characterisation of the JMJD7 hydroxylation pathway. As discussed in Section 2.1.3, both glutamatergic and GABAergic cortical neurons have been associated with defects implicated in the aetiology of ASD. Therefore, we first aimed to identify whether components of the JMJD7 hydroxylation pathway were expressed in these two populations of cortical neurons. In order to do this, cDNA was purified from ESCs and matured GABAergic or glutamatergic neuron populations, then transcript abundances were measured by quantitative PCR (qPCR). Analysed transcripts included *JMJD7* and the hydroxylation pathway components *DRG1*, *DRG2*, *DFRP1*, *DFRP2* plus the *JMJD7 read-through* transcript. As detailed in Chapter 1, the *JMJD7* gene can undergo transcriptional readthrough into the neighbouring *PLA2G4B* phospholipase gene to generate fusion proteins. Although this readthrough protein is very poorly characterised it has been implicated in disease, including cancer and ASD (Matsunami et al., 2014, Ito et al., 2016, Su et al., 2016, Cheng et al., 2017). Therefore, we aimed to investigate this *readthrough* transcript in parallel with *JMJD7* to establish differences or similarities between them.

By performing this analysis, we identified a general trend that all transcripts had increased mRNA expression in mature cortical neuron populations compared to ESCs (Figure 2.5). When comparing the two cortical neuron types we found that there was no obvious difference in *DRG* or *DFRP* mRNA expression (Figure 2.5). However, *JMJD7* and the *readthrough* transcript were found to have increased mRNA expression in glutamatergic neurons compared to GABAergic neurons and ESCs (Figure 2.5). Consequently, we hypothesised that JMJD7 might play a more prominent role in glutamatergic differentiation or function.
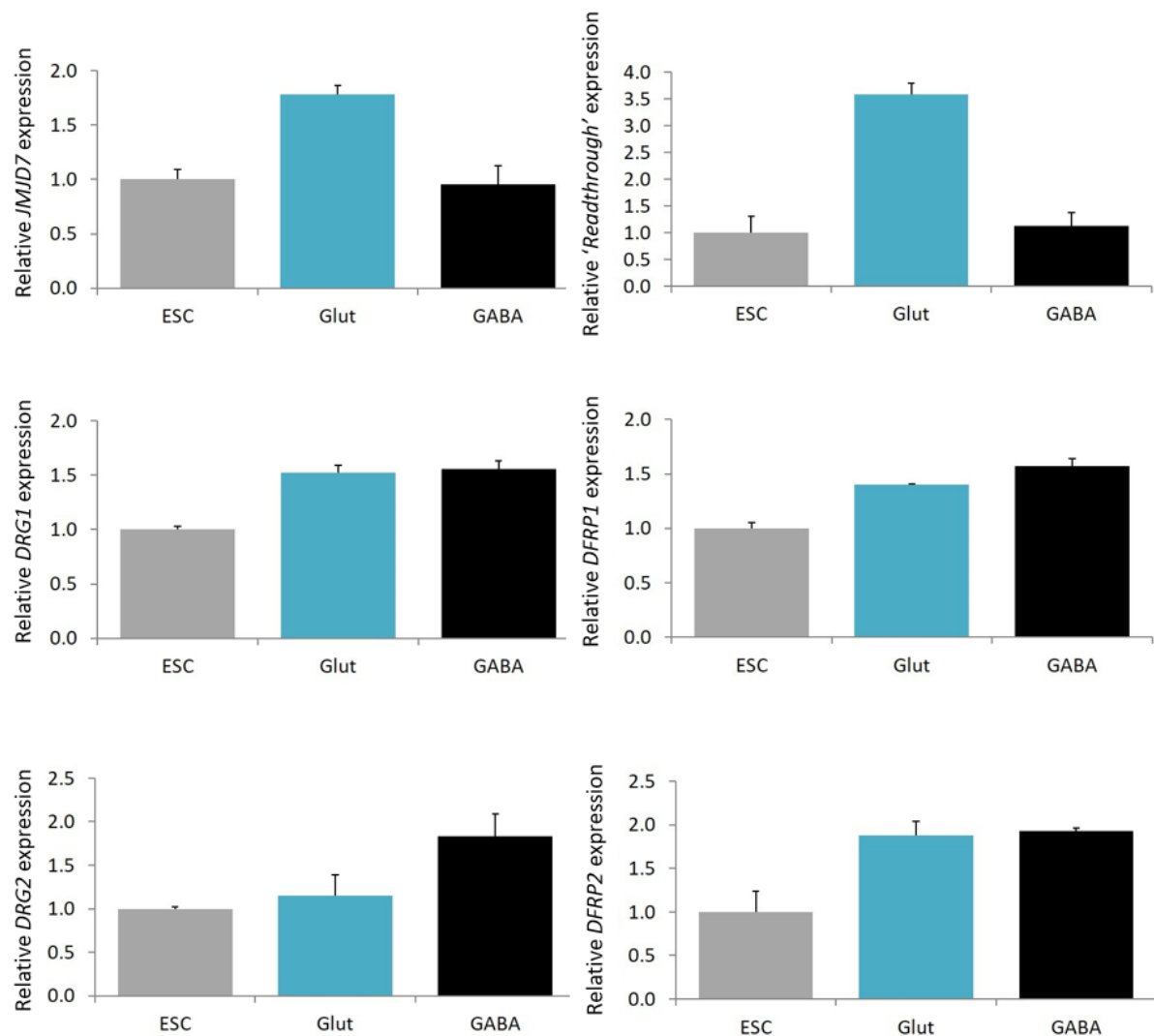
Figure 2.5 mRNA expression of the JMJD7 hydroxylation pathway in ESCs and cortical neurons

cDNA was purified from the embryonic stem cell line H9 (ESC), GABAergic (GABA) neurons and glutamatergic (Glut) neurons presented in Figure 2.4. Quantitative PCR was then performed to determine the mRNA expression of the JMJD7 hydroxylation pathway components, and readthrough transcript, relative to housekeeping gene *β-actin*, and normalised to the ESC sample. This is representative of an n=1 biological repeat, with quadruplicate technical repeats.

2.2.4 JMJD7 hydroxylation pathway proteins in glutamatergic neural populations

One limitation of the mRNA analysis presented above (Figure 2.5) was that it measured expression across a pooled population of cells. Due to the potential presence of neural progenitors and glia in this pool, we were therefore unable to conclude that expression was specific to mature glutamatergic neurons. To address this, we performed immunofluorescence analysis of mature glutamatergic neuron populations. Alongside staining for the JMJD7 hydroxylation pathway components, we also co-stained for MAP2AB to specifically identify mature neurons within the population of cells (Section 2.1.3). We found that all components of the JMJD7 hydroxylation pathway were expressed in MAP2AB positive cells suggesting that the JMJD7 pathway is likely to be active in mature glutamatergic neurons (Figure 2.6).

The added benefit of this immunofluorescence method was that sub-cellular localisation could also be examined. We found that JMJD7, DRG2 and DFRP2 were co-localised with MAP2AB in the cell body and along MAP2AB-positive dendrites. We hypothesised that they were also expressed in axons because staining was observed in neuron extensions that were negative for MAP2AB (example identified by a red arrow, Figure 2.6). DRG1 and DFRP1 were also expressed in the cell body of MAP2AB positive neurons. Interestingly, although they were excluded from MAP2AB-positive dendrites they were expressed in MAP2AB negatively stained axons (Figure 2.6). This differential sub-cellular localisation of the two JMJD7 hydroxylation substrates might suggest that they have non-redundant roles in glutamatergic neurons which will be interesting to explore in the future.
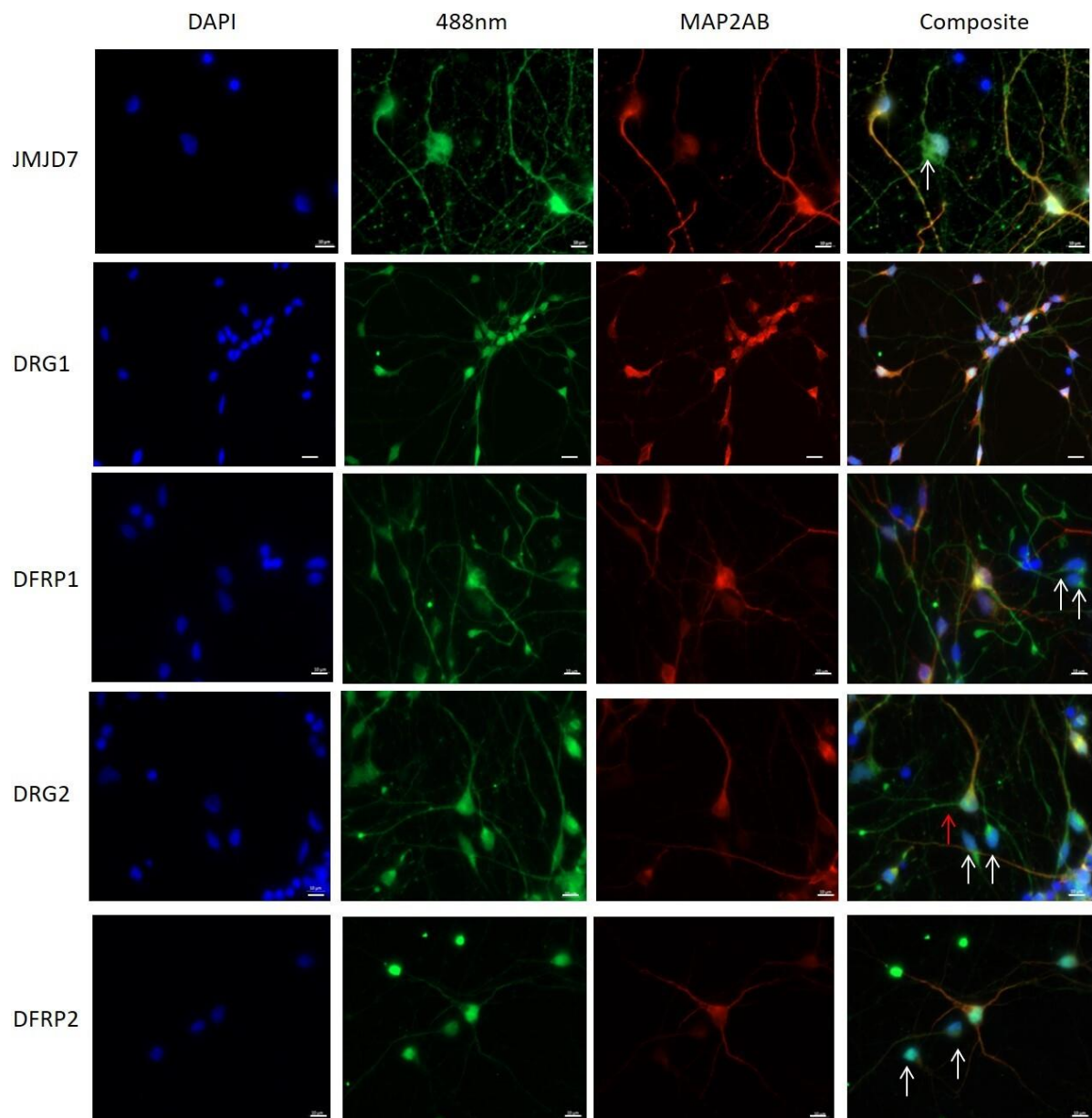
Figure 2.6 Expression of JMJD7 hydroxylation pathway in mature glutamatergic neurons
Glutamatergic neurons were differentiated from ESC line H9 and matured on coverslips for two weeks. Immunofluorescence was then used to determine the expression and sub-cellular localisation of the JMJD7 hydroxylation pathway components. MAP2AB was used as a marker of mature neurons that stains cell bodies and dendrites. DAPI was used as a nuclear marker. White arrows mark MAP2AB negatively stained cells. The red arrow marks an example of a MAP2AB negatively stained axon that stained positive for a component of the JMJD7 pathway (DRG2). All scale bars= 10 μm. This is representative of an n=1 biological repeat for JMJD7 staining and n=2 biological repeat for all other pathway components.

In addition to MAP2AB positive cells, JMJD7 protein and other components of the hydroxylation pathway, were also detected in MAP2AB negative cells (white arrows, Figure 2.6). This suggests that JMJD7 hydroxylation pathway components are not only expressed in neurons, but also other cell types within a population of mature glutamatergic neurons. In order to investigate this further, immunofluorescence staining was performed using different co-staining antibodies to investigate the identity of these cells.

We hypothesised that other cell types in our population of mature neurons, that stained negative for MAP2AB, could either be cells at a different stage of neurogenesis (i.e. immature neurons or neural progenitor cells) or they could be a glial cell type. In order to distinguish between these possibilities, we utilised immunofluorescence co-staining with either β3-tubulin as a marker of early neurons (Section 2.1.3), or s100β to stain mature glia (Raponi et al., 2007).

We found that both hydroxylation substrates and their binding partners were co-localised with β3-tubulin, indicative of their expression in early neurons (Figure 2.7). Also, all components were expressed in s100β positive cells suggesting that all are expressed in glial cells (Figure 2.8). Unfortunately, due to constraints with resources, we were unable to continue this analysis or investigate expression of JMJD7 in these cell types.
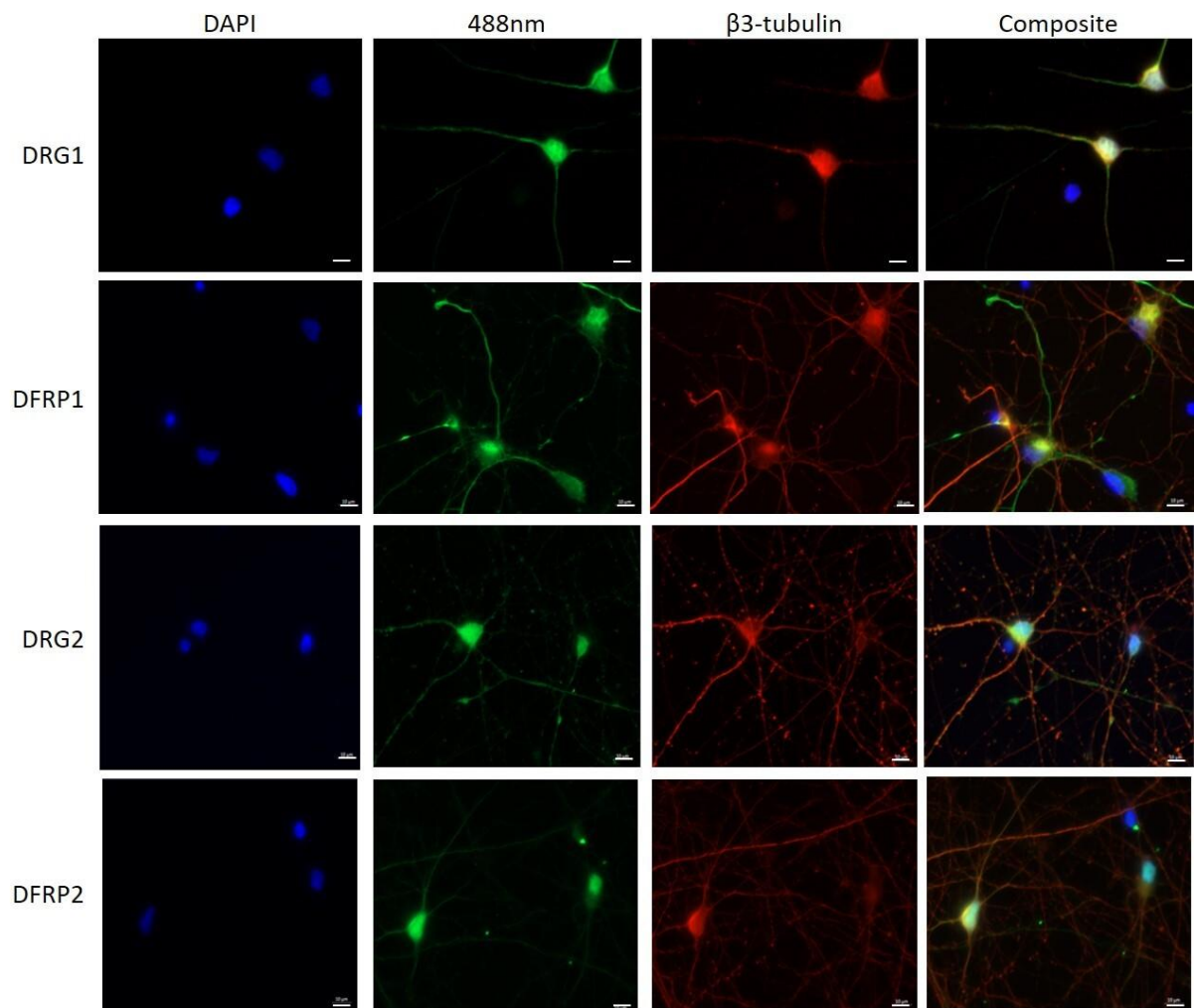
Figure 2.7 Expression of JMJD7 hydroxylation substrates and binding partners in early neurons
Glutamatergic neurons were induced from ESC line H9 and matured on coverslips for two weeks. Immunofluorescence was used to determine the expression and sub-cellular localisation of the JMJD7 hydroxylation substrates and binding partners. βIII-tubulin was used to mark neural progenitor cells. DAPI was used as a nuclear marker. All scale bars= 10 μm. This is representative of n=2.
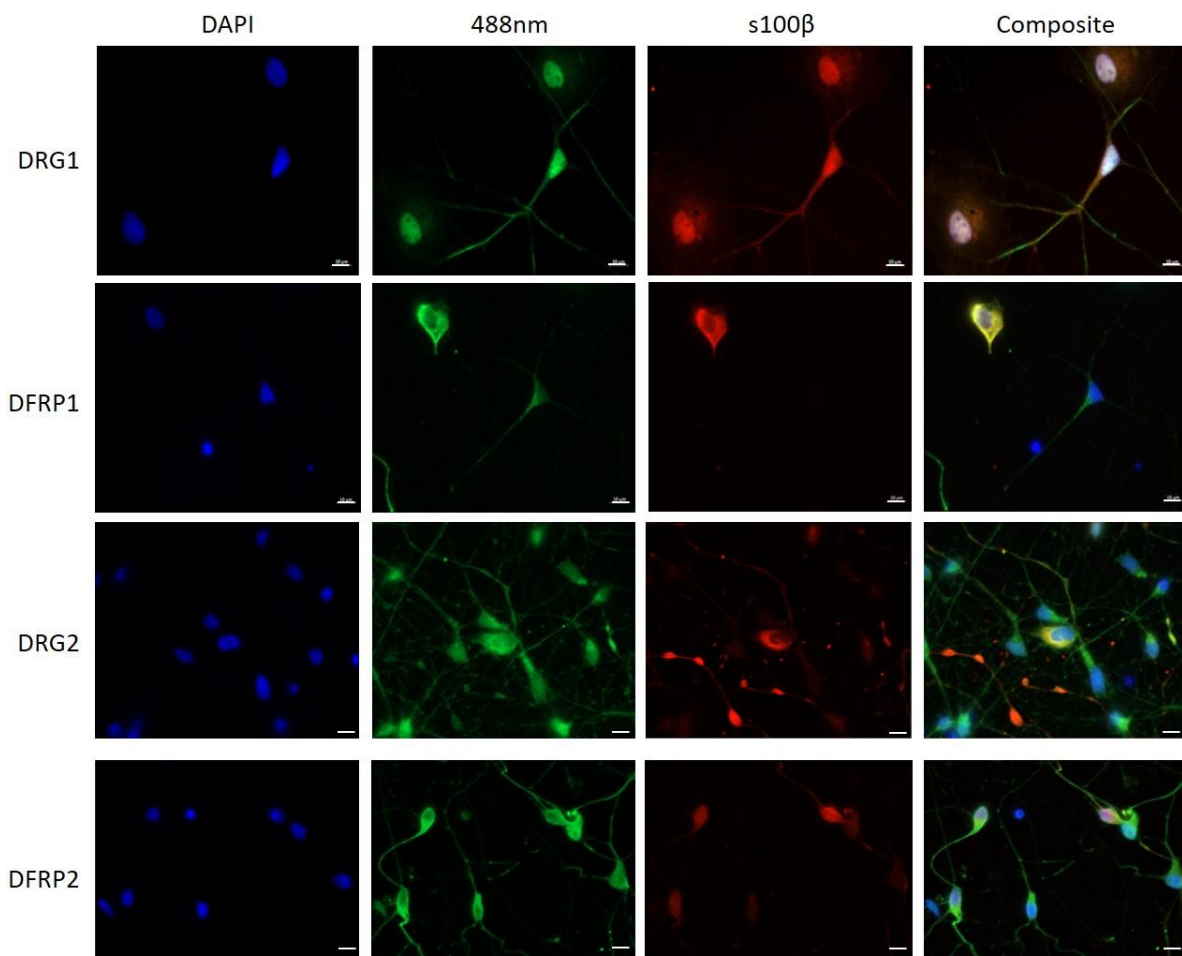
Figure 2.8 Expression of JMJD7 hydroxylation substrates and binding partners in glial cells
Glutamatergic neurons were induced from ESC line H9 and matured on coverslips for two weeks. Immunofluorescence was used to determine the expression and sub-cellular localisation of the JMJD7 hydroxylation substrates and binding partners. S100-β was used to mark glial cells. DAPI used as a nuclear marker. Scale bars= 10 μm. This is representative of n=2.

2.2.5 JMJD7 hydroxylation pathway during glutamatergic neuron differentiation

Currently our data suggested that the expression of the JMJD7 hydroxylation pathway may be upregulated during glutamatergic neural differentiation. In order to investigate this in more detail we aimed to perform further transcript analysis by purifying cDNA for qPCR analysis from ESCs and key stages of glutamatergic neuron differentiation. This included two-week-old neural induction samples (2D neural rosettes), 4-week-old neural induction samples (3D neurospheres), and 2-week matured neuron populations.

We observed a general trend that mRNA expression of JMJD7 hydroxylation pathway components increased during glutamatergic neuron differentiation and peaked at the neurosphere stage (Figure 2.9). In contrast the *readthrough* transcript reduced expression in the 2-week-old neural induction, compared to ESCs, but then peaked in mature neuron populations. This could indicate that the readthrough transcript and JMJD7 have different roles regarding glutamatergic neuron differentiation and function, which should be followed up by future investigation.
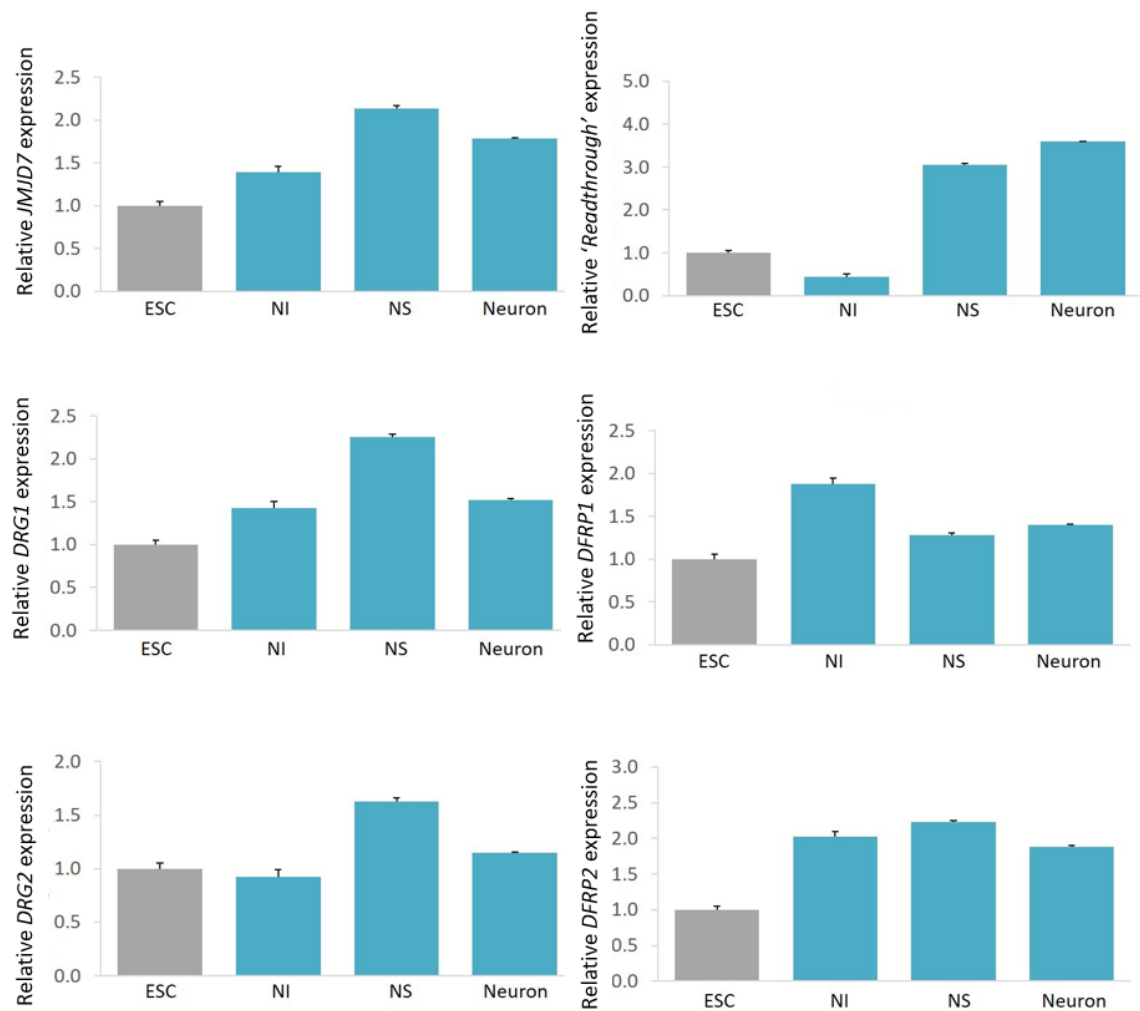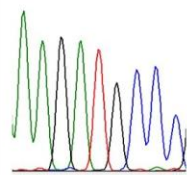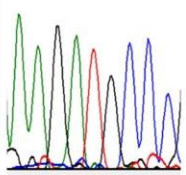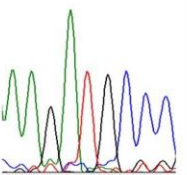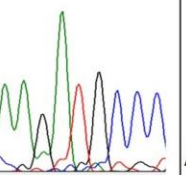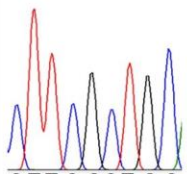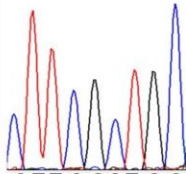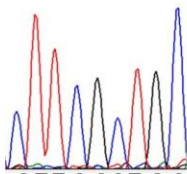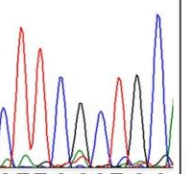
Figure 2.9 mRNA expression of the JMJD7 pathway during glutamatergic neuron differentiation
Glutamatergic neurons were induced from ESC line H9 and cDNA samples taken at different stages including, stem cells (ESC), 2 weeks of neural induction (NI), 2-week-old neurospheres (NS), and neurons. Expression was determined by qPCR, relative to *β-actin*, and normalised to the ESC sample. This is representative of an n=1 biological repeat, with quadruplicate technical repeats.

2.2.6 JMJD7 hydroxylation pathway proteins in ASD neurons

Overall, the data presented above suggested that components of the JMJD7 hydroxylation pathway are upregulated during the differentiation of glutamatergic neurons, a cell type that has been heavily implicated in the aetiology of neurodevelopmental disorders, including ASD (Section 2.1.3). As such, our findings motivated us to directly investigate the expression of JMJD7 pathway components in cells derived from ASD patients.

To do this, we utilised induced pluripotent stem cells (iPSCs) sourced from a control individual (007) and three different ASD patients (119, 125, 147). As JMJD7 is reported to be mutated in ASD and ID (de Ligt et al., 2012, Matsunami et al., 2014), we first aimed to determine the *JMJD7* genotype of the iPSCs so that this could be considered when interpreting future data. cDNA was purified from all iPSCs at the SC colony stage and PCR used to amplify the *JMJD7* cDNA sequence for Sanger sequencing. The *JMJD7* sequencing chromatograms for each cell line were analysed to determine whether the patients carried any mutations, including the known ID and ASD associated *JMJD7* mutations, M160V and R260C (de Ligt et al., 2012, Matsunami et al., 2014). However, all cell lines were found to express the wildtype *JMJD7* mRNA sequence (Table 2.1). With this in mind we continued characterisation of the iPSC lines.

Table 2.1 Chromatograms of JMJD7 cDNA genotyping of control and ASD patient derived iPSC lines
cDNA was purified from stem cells from control iPSC line 007 and three ASD patient derived iPSC lines 119, 125 and 147. The JMJD7 cDNA sequence was amplified using PCR and analysed by Sanger sequencing. Chromatograms were compared to the wildtype JMJD7 sequence NM_001114632.2 and analysed for mutations. Chromatogram sequences covering ID associated mutation M160V (de Ligt et al., 2012) and ASD associated mutation R260C are presented (Matsunami et al., 2014).

ASD Mutation	iPSC Line				ASD/ID Patient
	007	119	125	147	
M160V	A AG AT G C C C Lys Met Pro	A AG AT G C C C Lys Met Pro	A AG AT G C C C Lys Met Pro	A AG AT G C C C Lys Met Pro	de Ligt *et al*, 2012 AAG A/GTG CCC Lys Met/ Pro Val
R260C	C T T C G C T G C Leu Arg Cys	C T T C G C T G C Leu Arg Cys	C T T C G C T G C Leu Arg Cys	C T T C G C T G C Leu Arg Cys	Matsunami *et al*, 2014 CT T C/TGC T G C Leu Arg/ Cys Cys

We first aimed to investigate any differences of JMJD7 pathway component mRNA expression in the iPSC lines. To do this we induced the iPSC lines along the glutamatergic neuron differentiation pathway and purified cDNA at the neurosphere stage (as this stage correlated with the peak of JMJD7 pathway mRNA expression observed previously, Figure 2.9). We observed that mRNA expression of JMJD7 pathway components were increased for two ASD patients (119 and 147) and decreased in another ASD patient (125) compared to the 007 control line (Figure 2.10). Interestingly, expression of the *readthrough* transcript was reduced across all three ASD patient lines compared to the 007 control line (Figure 2.10). Although the patient-derived cells analysed above were obtained from independent families, and are therefore likely to be genetically heterogenous, our preliminary data suggests that further work to explore potential dysregulation of this pathway in ASD is warranted.
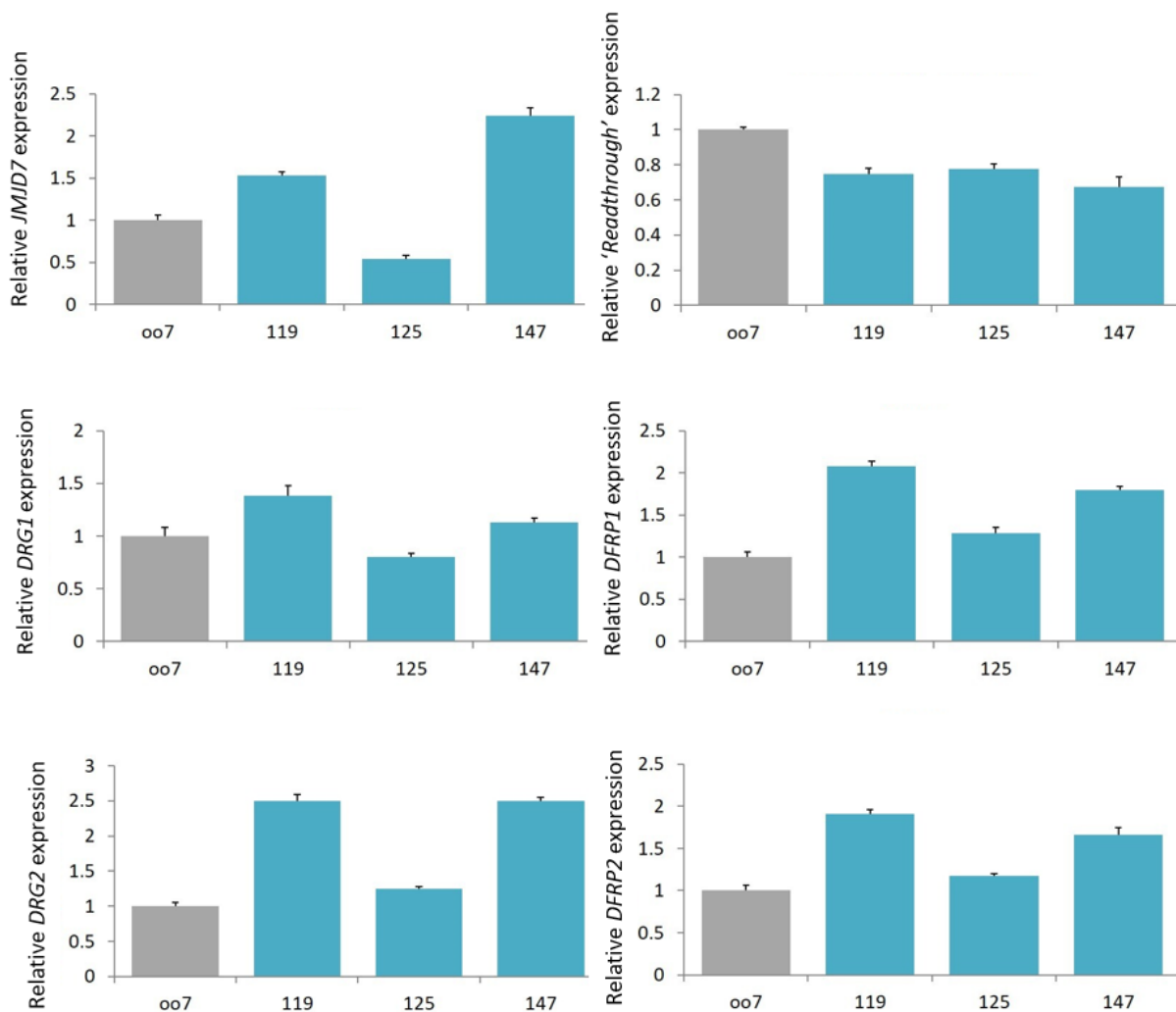
Figure 2.10 mRNA expression of the JMJD7 hydroxylation pathway in control and ASD patient iPSCs
cDNA was purified from the 007 control and ASD-derived 119, 125 and 147 iPSC lines at the neurosphere stage of differentiation towards glutamatergic neurons. Expression of JMJD7 pathway components and the readthrough transcript were determined by qPCR relative to housekeeping gene β-actin and normalised to the 007 iPSC control line. This is representative of an n=1 biological repeat, with quadruplicate technical repeats.

2.3 Development of a JMJD7 loss of function SHSY5Y cell model

The preliminary data above suggested that the JMJD7 pathway is expressed in neurons, and that its levels may be upregulated during glutamatergic neurogenesis. These observations might be consistent with a functionally important role for this pathway during neuronal differentiation and/or function which when dysregulated could contribute to ASD. Consequently, we were next interested to model JMJD7 dysregulation by establishing SHSY5Y cell lines. To this end, we first undertook bioinformatic analysis to determine the potential functional consequences of existing ASD and ID JMJD7 mutations (Section 2.3.1). We then developed a JMJD7 shRNA knockdown model in SHSY5Y cells (Section 2.3.2).

2.3.1 Bioinformatic analysis of JMJD7 ASD and ID mutations

Although two mutations of JMJD7 have been previously described in ID and ASD patients, M160V and R260C respectively (de Ligt et al., 2012, Matsunami et al., 2014), no functional or bioinformatic characterisation of either mutant had been reported. Therefore, we first performed bioinformatic analysis to determine whether these mutations were likely to be pathogenic.

To do this we used two online software tools called SIFT and PolyPhen-2. These tools are able to generate a score that predicts how detrimental a mutation at a certain residue within a protein is likely to be considering sequence conservation (Adzhubei et al., 2010, Sim et al., 2012). The SIFT score is the probability that a change will be tolerated, therefore the lower the score the more deleterious the mutation is predicted to be (≤ 0.05 substitutions are deemed deleterious). PolyPhen-2 scores the probability that the amino acid substitution will

be damaging, therefore, the higher the score the more confident the prediction that the mutation will be deleterious.

For the JMJD7 ID mutation (M160V), SIFT gave a score of 0.23 and PolyPhen-2 generated a score of 0.129, meaning that both software tools predicted the M160V mutation would be tolerated. This is perhaps unsurprising when considering the similar properties of the two amino acids involved in this substitution (Betts and Russell, 2003). Consistent with this, M160 was found to be functionally conserved as a hydrophobic amino acid among JMJD7 orthologues, by the presence of a methionine or leucine at this residue (Figure 2.11).

The JMJD7 ASD R260C mutation was also predicted to be tolerated, as SIFT gave a score of 0.06 and PolyPhen-2 gave a score of 0.011. However, the SIFT score, based on both sequence homology and amino acid properties, was close to the threshold. Therefore, in view of the amino acid substitution that this mutation infers we predicted that the R260C mutation was likely to be damaging to JMJD7 (Betts and Russell, 2003). Consistent with this, the R260 residue was found to be functionally conserved in JMJD7 orthologues as a positively charged amino acid as an arginine or histidine (Figure 2.11).

Interestingly, the R260C mutation was also identified, by analysis performed by Charlotte Eaton (Coleman group), in a patient with endometrial cancer and localised within a hotspot of cancer patient mutations (Figure 2.12). Therefore, this further implied that the R260C mutation was likely to be pathogenic.

Figure 2.11 Sequence alignment for JMJD7 ASD and ID mutations between different species
JMJD7 sequences across a range of species were aligned using Clustal Omega online software to determine the conservation of the two patient JMJD7 mutations M160V and R260C (sequences as Table 7.11).

Previous analysis performed by Charlotte Eaton (Coleman group) also identified that the M160 and R260 residues were localised in the catalytic domain of JMJD7. We further interpreted this analysis to establish how these mutations might affect the JMJD7 protein (Figure 2.12). We observed that both amino acids were positioned in β-strand structures (Figure 2.12B). M160 was found in a β-strand N-terminal to a DSBH fold and R260 was localised within the βV strand of the DSBH catalytic domain (Markolovic et al., 2018). Considering that both amino acids appear to be solvent exposed, it is possible that they are important for mediating protein-protein interactions (discussed in Section 2.4.3).

Figure 2.12 Location of ASD patient mutations M160V and R260C on the JMJD7 protein sequence
(A) Mapped onto the sequence of JMJD7 are two JMJD7 ASD patient mutation residues (M160 and R260), cancer mutations sourced from cBioportal and COSMIC that were recurrent or localised in hotspots, cofactor binding residues and dimerisation domains. **(B)** Mapped onto the crystal structure of JMJD7 (5NFN) are cofactor binding residues and two JMJD7 ASD patient mutation residues (M160 and R260). Front orientation (with catalytic site facing outwards) demonstrates the location of M160 (magenta), reverse orientation (with catalytic site facing towards the back) demonstrates the location of R260 (green). Figure generated using Chimera software.

2.3.2   JMJD7 knockdown system

Bioinformatic analysis of the ASD patient R260C mutation above suggested that it was likely to be deleterious to JMJD7. Therefore, we next aimed to model JMJD7 loss of function in a neuronal cell line.

We first attempted this with RNA interference, using a transient transfection approach in SHSY5Y cells. To this end, we tested three JMJD7 targeted siRNA sequences and two transfection reagents in SHSY5Y cells. The positive control for transfection efficiency was a previously validated JMJD7 siRNA transfection protocol, performed in HEK-293T cells using Oligofectamine™ (Dr Charlotte Eaton). Alongside this a positive control siRNA, targeting an unrelated protein (eRF1) was used. Western blotting confirmed that the transfection was successful, as we observed reduced eRF1 protein levels compared to the siRNA control in HEK-293T cells (Figure 2.13). It also confirmed that two of the three JMJD7 targeted siRNA sequences showed JMJD7 knockdown in HEK-293T cells (#6 and #8, Figure 2.13). Unfortunately, we were unable to observe any eRF1 or JMJD7 knockdown in the SHSY5Y cells using either Oligofectamine™ or INTERFERin® (Figure 2.13).
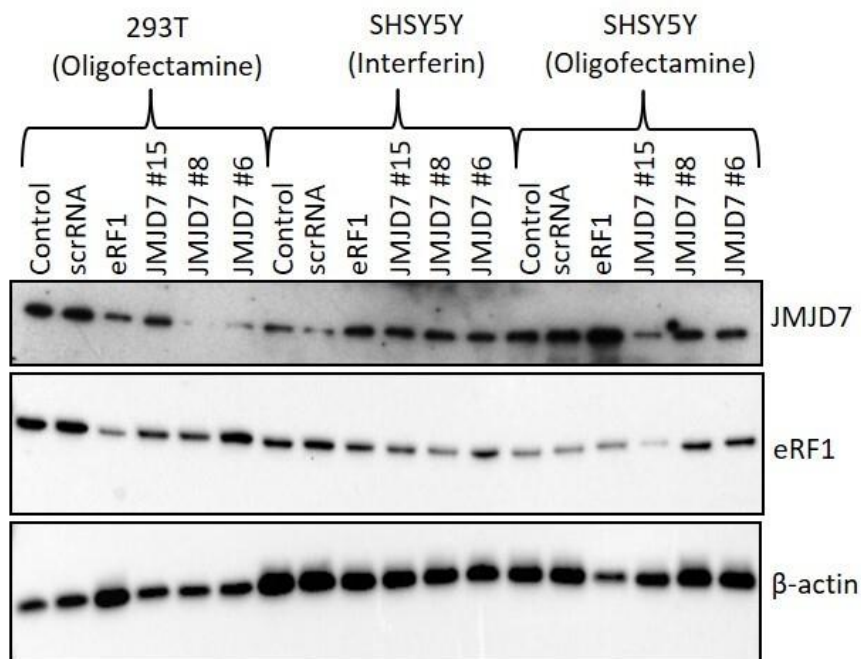
Figure 2.13 Testing siRNA transfection protocols in HEK-293T cells and SHSY5Y cells
Transfection of a scrambled control RNA (scrRNA), positive control siRNA targeting eRF1, or three siRNA sequences targeting JMJD7 (#15, #8, #6) were transfected into HEK-293T cells using Oligofectamine™. The same siRNA sequences were transfected into SHSY5Y cells using Oligofectamine™ and INTERFERin®. 'Control' denotes an un-transfected sample. Protein expression analysed using Western blotting, β-actin was used as a loading control. JMJD7 (36 kDa), eRF1 (49 kDa), β-actin (42 kDa). This is representative of an n=2 biological repeat.

As the siRNA sequences #6 and #8 were able to reduce JMJD7 protein levels in HEK-293T cells, we speculated that the lack of knockdown observed in SHSY5Y cells was due to poor transfection efficiency. This hypothesis was supported by the lack of eRF1 knockdown using either transfection reagent tested in SHSY5Y cells. To improve transfection efficiency, we tested the ability of a panel of transfection reagents to introduce an RNA transfection control into SHSY5Y cells. This control RNA contained an Alexa Fluor® 555 nm label meaning that detection of successfully transfected SHSY5Y cells could be monitored in live cells using an EVOS microscope. However, successful transfection was not achieved using any of the reagents tested (Figure 2.14). Overall, we concluded that transient siRNA transfection was unlikely to be an efficient method for JMJD7 knockdown in SHSY5Y cells.
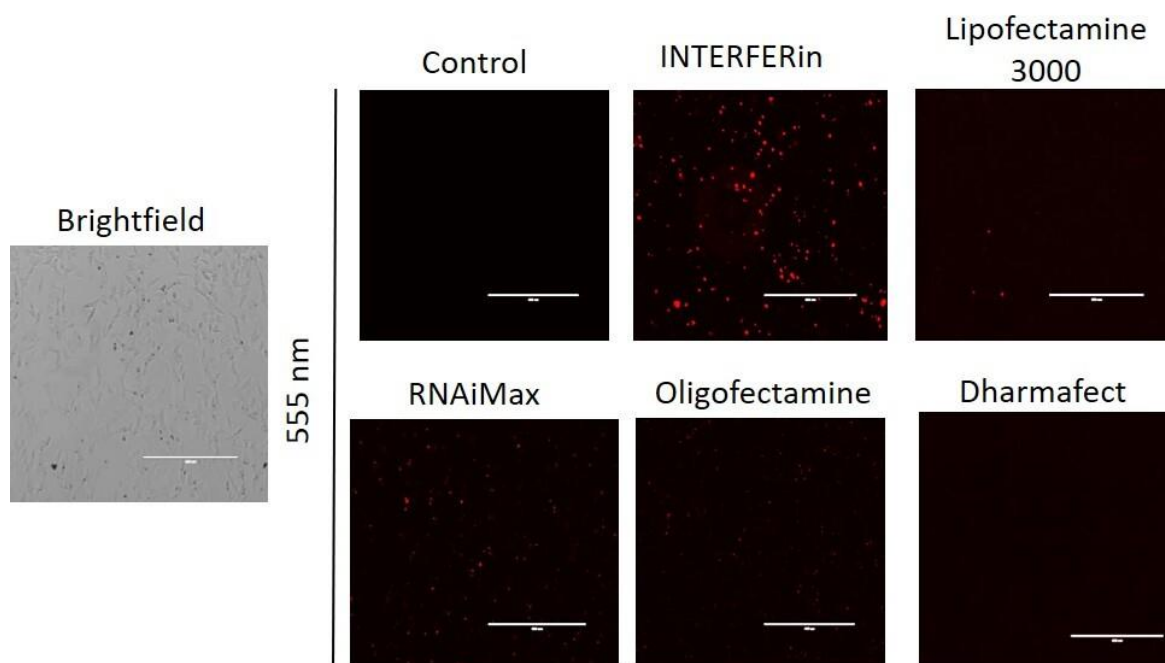
Figure 2.14 Optimisation of RNA transfection into SHSY5Y cells
Five transfection reagents were used to transfect a 555 nm Alexa Fluor® labelled control RNA sequence into SHSY5Y cells. Successful transfection was monitored in live cells using an EVOS microscope, however, only transfection reagent conjugates were detectable as punctate red spots outside of the cells. Scale bars= 400 μm.

Considering these technical difficulties, we next explored alternative means of performing RNA interference in SHSY5Y cells. To avoid transient transfection, we next aimed to develop a JMJD7 shRNA knockdown model in SHSY5Y cells based on a viral delivery system. We first tested JMJD7 shRNA sequence expression vectors (Sigma) which were introduced into SHSY5Y cells by lentiviral infection. As these shRNA sequences were expressed from an IPTG inducible promoter we incubated the SHSY5Y cells with 0.5 µg/mL IPTG for 48 hours prior to harvesting cDNA to analyse *JMJD7* knockdown using qPCR. We found that both shRNA sequences induced *JMJD7* knockdown compared to the control shRNA control (Figure 2.15). However, the maximum level of mRNA knockdown was only 60% for shRNA #501 which was unlikely to be sufficient, based on previous experience within the Coleman group. Furthermore, partial *JMJD7* knockdown was also observed with shRNA #136 in the absence of IPTG, which might indicate 'leaky' shRNA expression (Figure 2.15).
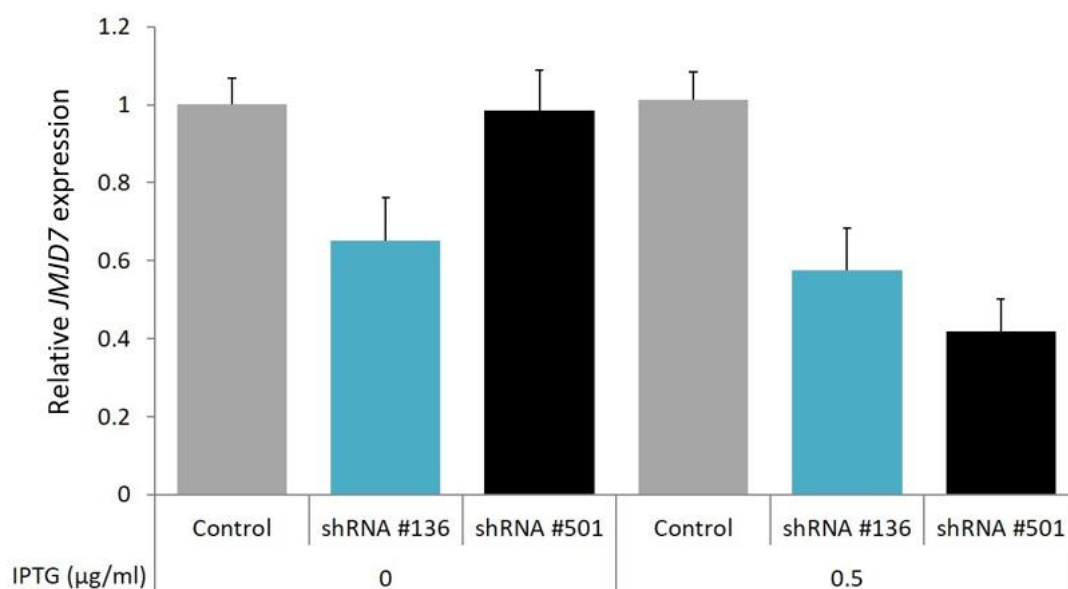
Figure 2.15 IPTG inducible JMJD7 shRNA sequences in SHSY5Y stable expression cell lines
IPTG (0.5 µg/mL) was used for 48 hours to induce the expression of shRNA constructs in SHSY5Y stable expression cell lines. These included a shRNA control and two shRNA sequences targeting JMJD7. Successful knockdown was determined using qPCR relative to *β-actin* and normalised to the control shRNA sequence minus IPTG sample. This is representative of an n=1 biological repeat, with quadruplicate technical repeats.

Overall, because the IPTG-inducible shRNA sequences were not optimal for future analysis, we decided to test a different lentiviral shRNA system. These new shRNA sequences were expressed alongside a GFP cDNA 'marker' under the control of a doxycycline inducible promoter (transOMIC). This meant that shRNA expression could be controlled using doxycycline treatment and monitored using an EVOS microscope by the presence of GFP-expressing cells. As before, we performed lentiviral infection into SHSY5Y cells with the shRNA vectors. We next performed a doxycycline time course to determine the kinetics of GFP (and consequently shRNA) expression from the lentiviral vectors. We concluded that the plasmids responded to doxycycline optimally after 48-72 hours of treatment (Figure 2.16).
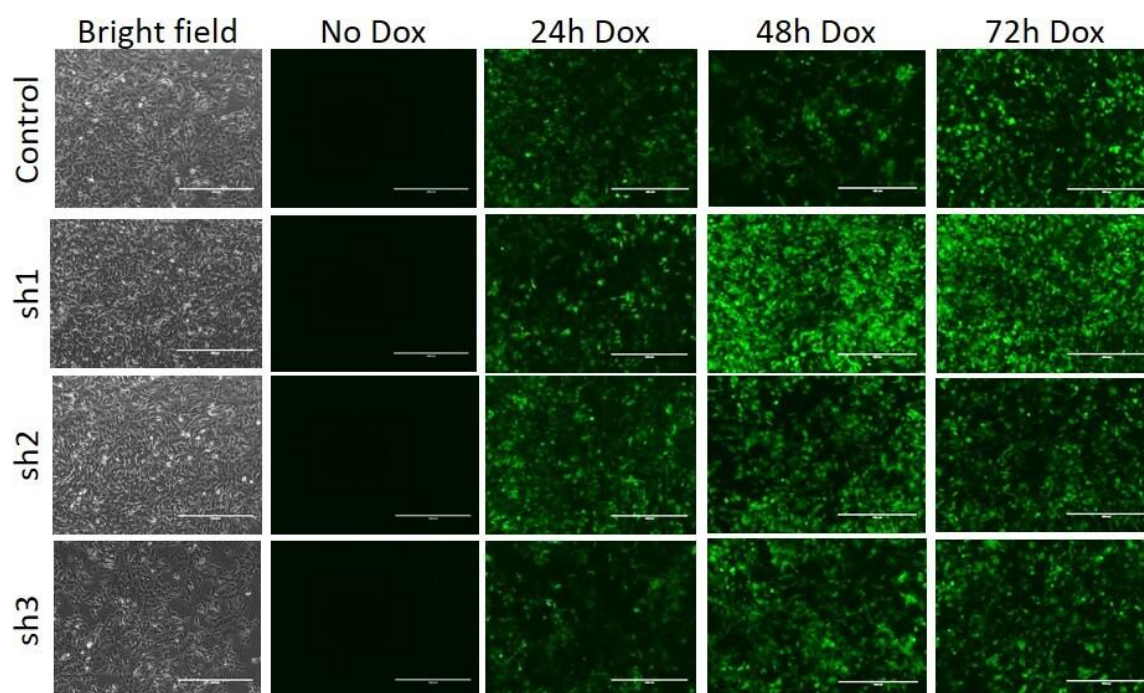
Figure 2.16 Validation of construct expression from SHSY5Y doxycycline inducible shRNA cell lines
Doxycycline (1 μg/mL) was used to induce the expression of shRNA sequences targeting JMJD7 and a shRNA control from SHSY5Y stable expression cell lines. Upstream of the shRNA sequences was a GFP gene, also doxycycline inducible. To validate that the SHSY5Y cell lines responded to doxycycline GFP protein expression was monitored after a doxycycline time course using an EVOS microscope. Scale bars= 400 μm.

Next, we aimed to determine whether JMJD7 knockdown could be identified at the mRNA and protein levels following doxycycline treatment for 48 or 72 hours. We observed that two shRNA sequences (#2 and #3) were able to knockdown *JMJD7* mRNA expression to 20-30% of that detected in shRNA controls (Figure 2.17A). As one of these shRNA sequences (#2) could theoretically also target the JMJD7 *readthrough* transcript, we also investigated whether *readthrough* mRNA expression was altered after doxycycline treatment of these SHSY5Y cells. However, we found that the shRNA knockdown appeared to be specific to *JMJD7* (Figure 2.17B). This was important to ensure that later analysis of these knockdown cells could be used to specifically characterise JMJD7 dependent activities. Western blot analysis of protein samples, generated in parallel, confirmed that the *JMJD7* mRNA knockdown observed for shRNA sequences #2 and #3 (Figure 2.17A) resulted in a significant decrease in JMJD7 protein expression (Figure 2.17C).
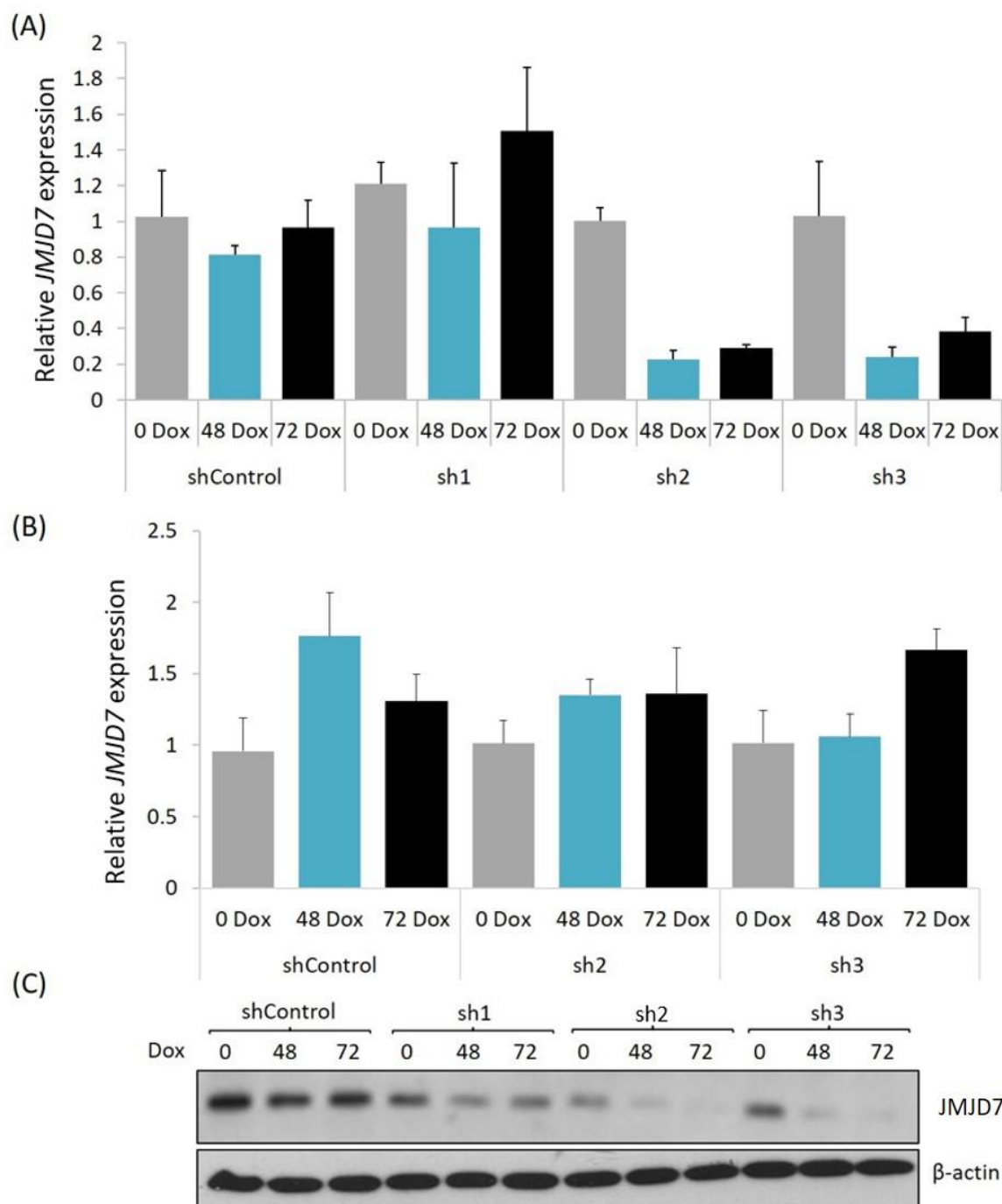
Figure 2.17 Validation of JMJD7 mRNA and protein knockdown in SHSY5Y shRNA cell lines

Stable expression SHSY5Y cell lines for an shRNA control or three shRNA sequences targeting JMJD7 were incubated in 1µg/mL doxycycline for 48 or 72 hours before determining the level of JMJD7 specific knockdown. This involved monitoring the mRNA expression by qPCR for JMJD7 **(A)** and readthrough transcript mRNA **(B)**. This is representative of an n=1 biological repeat with four quadruplicate technical repeats. **(C)** JMJD7 protein knockdown was determined by analysing whole cell extract using Western blotting. This is representative of n=2 biological repeats.

Overall, we concluded that shRNA sequences #2 and #3 were efficient at knocking down JMJD7 expression to a suitable level for future loss of function experiments in SHSY5Y cells. Therefore, we next aimed to apply these cell models to study the potential consequences following loss of JMJD7 expression. Due to current evidence in the literature (discussed in Chapter 1), we first aimed to investigate whether JMJD7 knockdown resulted in a cell proliferation defect. To undertake this analysis, we performed an MTS assay to monitor cell proliferation of SHSY5Y cell lines following JMJD7 knockdown. The MTS assay utilises the ability of live and viable cells to metabolise a colourless MTS substrate into a coloured formazan product, which can be measured by absorbance at 490 nm. From this we identified that SHSY5Y cells had reduced cellular proliferation compared to the control, following JMJD7 knockdown with either shRNA sequences (Figure 2.18). This observation was additionally interesting as the clinical phenotypes of some ASD patients have been linked to deficient cellular proliferation during development (discussed in Section 2.4 below). Therefore, we propose that future investigation of the JMJD7 hydroxylation pathway in the aetiology of ASD is warranted.
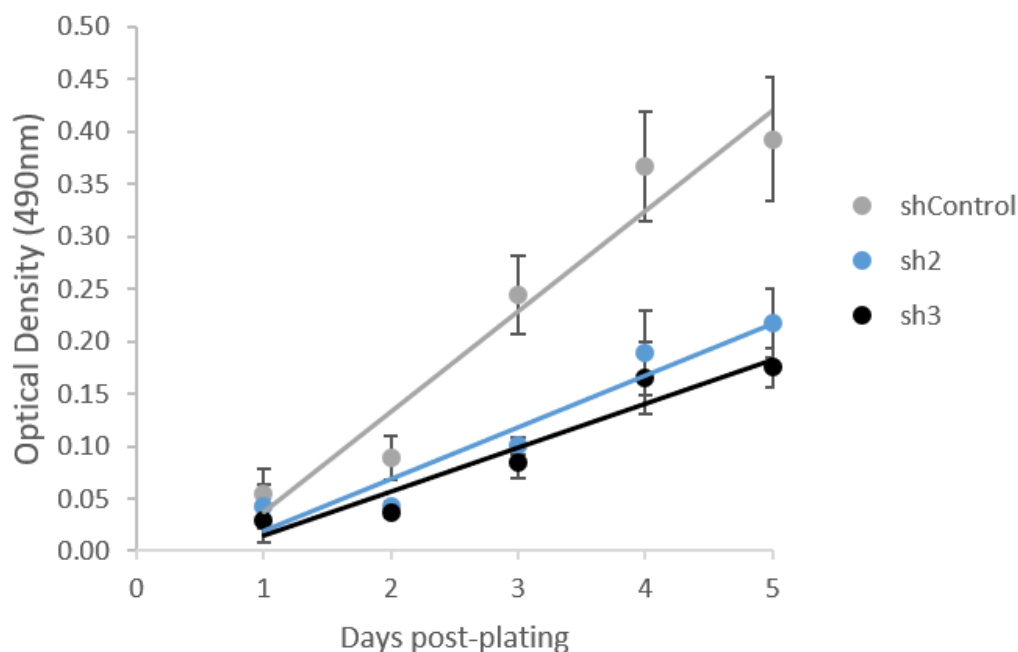
Figure 2.18 Knockdown of JMJD7 in SHSY5Y cell lines correlates with reduced cell proliferation
SHSY5Y cells were induced with 1 μg/mL doxycycline for 48 hours to express an shRNA control or two shRNA sequences targeting JMJD7. Cell proliferation was monitored using the MTS assay (CellTiter 96® Aqueous One Solution Cell Proliferation Assay, Promega) which demonstrated that JMJD7 knockdown resulted in reduced cell proliferation. This is representative of an n=1 biological repeat, with quadruplicate technical repeats.

2.4 Discussion

In this chapter we aimed to explore the cellular function of the JMJD7 hydroxylation pathway by investigating its dysregulation in human disease, specifically focussed on ASD and ID. Prior to our investigation the only knowledge regarding this was the observation that JMJD7 and its hydroxylation substrates, DRG1 and DRG2, were implicated in developmental disorders associated with ID and ASD (Vlangos et al., 2000, Lucas et al., 2001, Bi et al., 2002, Nakamine et al., 2008, de Krom et al., 2009, de Ligt et al., 2012, Matsunami et al., 2014). Consequently, we proposed that characterisation of the JMJD7 pathway in development would help to not only decipher the currently understudied cellular role of this pathway but could also to help further the understanding regarding the aetiology of neural developmental disorders.

Therefore, in this chapter we aimed to develop cellular models to be used in parallel for future investigation. Firstly, we successfully differentiated stem cells into glutamatergic and GABAergic neurons. We then initiated the characterisation of the JMJD7 hydroxylation pathway with regards to mRNA expression levels and protein sub-cellular localisation at different stages along the glutamatergic neural differentiation pathway. This analysis was then progressed to explore the pathway in ASD patient-derived iPSCs. In an independent neuronal-like cell line, SHSY5Y, we then generated a JMJD7 loss of function system to model potential dysregulation of JMJD7 in ASD.

Unfortunately, as mentioned above, the JMJD7 project was prematurely concluded during my PhD due to time restrictions at the University of Melbourne. This meant that only preliminary data was obtained, which will require future repeats and optimisation of experimental limitations. However, we were able to generate some hypotheses regarding the potential function of JMJD7 in neural differentiation and function. These are discussed below with reference to the potential functional consequence they might have with regards to the aetiology of ASD.

2.4.1 A potential role of the JMJD7 pathway during early neural differentiation

In this chapter we presented evidence suggesting the importance of the JMJD7 hydroxylation pathway during neural differentiation. This is discussed below with reference to the potential role of JMJD7 in ASD.

We first observed that all components were expressed at the ESC stage as mRNA (Figure 2.5) and protein (Figure 2.3). Interestingly, immunofluorescence staining of stem cell colonies demonstrated the JMJD7 pathway components were not expressed in the centre but were

concentrated to the periphery of the colonies (Figure 2.3). It is well characterised that stem cells congregate to the centre of colonies, whilst the periphery of these colonies is composed of cells initiating differentiation (Smukler et al., 2006, Rosowski et al., 2015). This implies that the JMJD7 pathway may not be important for pluripotency but instead could be important for promoting differentiation. However, future work in order to make this observation more reliable should include co-staining ESC colonies with stem cell markers such as SOX2, Oct4 and Nanog. This will confirm whether the pattern of JMJD7 hydroxylation pathway expression was real and not an artefact of antibody staining.

The strongest evidence, consistent with our hypothesis that the JMJD7 pathway is likely to be important for neural differentiation, was that all components were found to have increasing levels of mRNA expression during glutamatergic neural differentiation (Figure 2.9). We propose that this mRNA analysis should be complimented in the future with protein expression analysis, as mRNA expression is not always linear with protein expression. However, if increasing expression can infer potential functional importance, then this suggested that JMJD7 pathway might be increasingly important during neural differentiation.

The peak of mRNA expression for JMJD7 pathway components was identified at the neurosphere stage (Figure 2.9). These *in vitro* neurospheres represent the organised structures identified in the *in vivo* developing forebrain that are essential for neural progenitor expansion and early differentiation of neurons. Consequently, neurospheres contain TBR2 expressing basal progenitor cells and βIII-tubulin expressing immature neurons (discussed in Section 2.1.3). Therefore, the neurosphere structures represent a key proliferative stage during neurogenesis. Consistent with this, neurospheres are grown in the presence of growth

factors for two weeks in order to promote neural progenitor expansion for subsequent dissociation to allow neurons to mature. As mature neurons have reduced proliferative potential this population expansion at the neurosphere stage is essential.

Interestingly, we demonstrated that knockdown of JMJD7 resulted in reduced SHSY5Y cell proliferation (Figure 2.18). It should be noted that as this MTS assay is an indirect readout of proliferation, future analysis should aim to confirm this observation using more direct cell proliferation assays. However, our observations (Figure 2.18) are in line with the current literature (Dr Charlotte Eaton) (Zhu et al., 2016, Liu et al., 2017). Moreover, consistent with our hypothesis, the hydroxylation substrates of JMJD7, DRG1 and DRG2, have also previously been implicated in development and play roles important for cell proliferation (Chapter 1). Consequently, we hypothesise that increased regulation of the JMJD7 pathway could be important for promoting proliferation during early neural development. Therefore, we propose that if the JMJD7 pathway is dysregulated this could contribute to ASD phenotypes.

In support of this there are many ASD phenotypes associated with impaired growth during neural development. For example, there is a prevalence of macrocephaly in ASD patients but also occasional presentation of microcephaly (Davidovitch et al., 1996, Fombonne et al., 1999, Sacco et al., 2015). Alongside this altered cerebral volume is associated with common structural abnormalities found in ASD patients (Sparks et al., 2002, Orekhova et al., 2007, Avino and Hutsler, 2010, Courchesne et al., 2011, Supekar et al., 2013, Valvo et al., 2016). *In vitro* modelling of ASD iPSC-derived organoids also demonstrate altered cellular proliferation and cell cycle progression (Mariani et al., 2015). However, some adolescent ASD patients have accelerated cortical thinning, indicating that an ASD cortical growth defect remains prevalent

but can manifest differently throughout development (Zielinski et al., 2014, Wallace et al., 2015).

Overall, we hypothesise that the JMJD7 pathway could be important for early neural differentiation by promoting proliferation and therefore could contribute to ASD if dysregulated. In order to test this hypothesis JMJD7 knockdown should be attempted in stem cells to decipher how this impacts neural differentiation.

2.4.2   A potential role of the JMJD7 pathway in mature neuron function

We also identified expression of the JMJD7 pathway components in mature neurons (Figure 2.5, 2.6 and 2.9). This was consistent with a report that identified increased JMJD7 expression in adult brain tissues, compared to other tissues, in *Kryptolebias marmoratus* fish (Fellous et al., 2019). This led us to hypothesise that JMJD7 might play a role in mature neurons, potentially in neuron function. Consistent with this we found expression of the JMJD7 pathway in s100β positively stained mature glia (Figure 2.8). These glial cells have been shown to be important for supporting the function of neurons (Petrelli et al., 2016).

The major role of mature neurons in the brain is to respond to activation by the propagation of an action potential. This signal is then passed onto proximal neurons by release of neurotransmitters. Gene transcription and protein translation are two fundamental processes for this activity. They are both directly coupled to synaptic activity (activity-dependent transcription/translation) which is essential for synaptic modification, implicated in plasticity and memory (Hernandez and Abel, 2008, Yap and Greenberg, 2018). This activity-dependent transcription/translation is regulated locally, which is important for spatially organising proteins to generate the polarised structures of neurons. It is also important for specific and

rapid response to synaptic activation (Rangaraju et al., 2017, Yap and Greenberg, 2018). Therefore, proper regulation over localised transcription and translation is essential for individual mature neuron function and more generally for brain connectivity fundamental for memory and learning.

Interestingly, the hydroxylation substrates of JMJD7, DRG1 and DRG2, have been implicated by the Coleman lab to have roles in transcription and translation, respectively (discussed in Chapter 1). These seemingly non-redundant roles of DRG1 and DRG2 could be consistent with our observation that DRG1 and DRG2 have different sub-cellular localisation within mature neurons (Figure 2.6). We found DRG1 was expressed in a similar pattern in βIII-tubulin positively stained early neurons (Figure 2.7) and mature neurons (Figure 2.6). Conversely, we found DRG2 expression in MAP2AB or βIII-tubulin co-stained cells were not comparable (Figure 2.6 and 2.7). This suggests that DRG2 appears to be re-localised from the cell body in early neurons to include neural extensions in mature neurons (Figure 2.6 and 2.7).

In order to investigate whether the JMJD7 pathway is important for neuron function future analysis will be required. This could include investigating neuron activity by performing assays such as 'patch clamp', a classical technique able to detect the generation and propagation of action potentials by measuring changes in voltage across the cell membrane. In addition, investigation into whether the pathway is important for transcription and/or translation for neuron function could be performed. For example, by monitoring localised transcription or translation in different regions of the neuron, as performed previously in the literature, reviewed by Holt et al. (2019). More informative assays could also include characterisation of the activity of downstream DRG1 and DRG2 targets, such as the FACT complex or

deoxyhypusine synthase (as identified by proteomic screening by the Coleman lab). These assays could be followed up by using JMJD7, DRG1 and DRG2 knockdown models or expression of ASD patient mutation models. This could help to identify individual roles of each component and their potential pathogenicity in ASD.

2.4.3 Evidence of dysregulated JMJD7 hydroxylation pathway in ASD

Overall, we have presented evidence to suggest that the JMJD7 pathway could be important for neural differentiation and function. This could help to explain why components of this pathway are mutated in neurodevelopmental disorders (Vlangos et al., 2000, Lucas et al., 2001, Bi et al., 2002, Nakamine et al., 2008, de Krom et al., 2009, de Ligt et al., 2012, Matsunami et al., 2014). Possibly in support of this, we observed different mRNA expression levels for JMJD7 pathway components in ASD patient-derived iPSCs compared to a healthy control (Figure 2.10). However, the caveat of this analysis was the small sample size. Therefore, this pilot experiment should be expanded by increasing the size of the patient derived iPSC cohort. Furthermore, it would be interesting to complement the mRNA data with protein expression analysis and to measure DRG hydroxylation levels to directly assess potential dysregulation of JMJD7 activity in ASD.

Further evidence to support the potential dysregulation of this pathway in ASD was from bioinformatic analysis on patient derived JMJD7 ID and ASD mutations. We were unable to draw conclusions regarding the potential pathogenicity of the ID M160V mutation without performing cellular analysis. However, we were able to hypothesise how the ASD mutation R260C might be pathogenic. Online bioinformatic analysis predicted the R260C mutation could be tolerated. However, the SIFT score, which takes into account amino acid conservation

as well as functionality, was close to the tolerance threshold. Consistent with this the R260 residue was found to be functionally conserved (Figure 2.11) suggesting that mutation to cysteine might be pathogenic. This was further supported by the observation that the R260C mutant was also identified in an endometrial cancer patient and within a hotspot of cancer mutations in the JmjC catalytic domain (Dr Charlotte Eaton, shown in Figure 2.12).

Interestingly, evidence suggests that the R260C mutation does not significantly alter JMJD7 protein folding, as Markolovic et al. (2018) utilised this mutant to generate a higher resolution crystal structure of JMJD7. Due to its solvent exposure we hypothesise that the R260 residue could facilitate the interaction of JMJD7 with another protein such as a kinase during JMJD7 phosphorylation (Dr Charlotte Eaton), or with DRG1/2. It would be interesting to follow this up by investigating the activity of this JMJD7 ASD mutant in SHSY5Y cells and SC lines and how it might affect neuron differentiation and function.

2.4.4   A potential role of the JMJD7 pathway in ASD

Here we present our hypothesis regarding how the JMJD7 pathway might contribute to ASD if dysregulated, considering data and previous discussion points presented in this chapter. We hypothesise that the role of JMJD7 in neural development and function could be to regulate transcription and translation via hydroxylation of DRG1 and DRG2. When dysregulated this could contribute to ASD in two ways. Firstly, as proper transcription and translation are directly associated with cellular proliferation and growth (Rudra and Warner, 2004), we hypothesise that this could impact essential neural progenitor expansion phases during early development. Secondly, due to the fundamental nature of transcription and translation for neuron function (discussed in Section 2.4.2) we hypothesise that when dysregulated this could

contribute to ASD. In support of this hypothesis, dysregulated transcription and translation are frequently described in neurodevelopmental disorders, including ASD (Kelleher and Bear, 2008, Yap and Greenberg, 2018). For example, mice with dysregulated protein translation were found to present with ASD phenotypes which could be rescued upon treatment with rapamycin, an inhibitor of mTORC1 (Ehninger et al., 2008, Meikle et al., 2008, Zhou et al., 2009, Gkogkas et al., 2012, Tsai et al., 2012). Moreover, ASD patient mutations modelled in mice caused dysregulated protein synthesis, which was found to be the molecular basis for ASD synaptic defects (Santini and Klann, 2014). Similarly, dysregulated transcription was found to impact neuron and synapse function as well as cell cycle progression, and consequently has been associated with ASD (Parikshak et al., 2013, Amiri et al., 2018). Furthermore, essential components of activity-dependent transcription/translation are commonly mutated in ASD (Ebert and Greenberg, 2013). Transcription and translation are also critically important for neuron development. For example, inheritance of differentially localised mRNA was proposed to facilitate asymmetric division of radial glial progenitor cells, essential for the generation of neurons (Pilaz and Silver, 2017). Moreover, localised translation in growth cones was found to aid migration of early neurons in response to proximal synaptic activity (Jung et al., 2012).

2.4.5 Chapter conclusions

Overall, we hypothesise that the JMJD7 pathway could be involved in regulating transcription and translation important for neural differentiation and function. Moreover, when dysregulated this could contrite to ASD. In order to test this hypothesis, future investigation will be required, and we propose that the cells lines established in this chapter could be essential for this.

3 Characterisation of JMJD5 mutations in patients with a novel developmental disorder

The second 2OG oxygenase enzyme we aimed to investigate in this thesis was JMJD5 which we begin to address below. In this Chapter we describe a novel human developmental disorder associated with compound heterozygous mutations in the JMJD5 gene. We aimed to utilise this opportunity to further characterise the cellular role of JMJD5, with the hope that this information could help with further diagnosis or care of the affected patients. In order to undertake this investigation, we obtained, then immortalised, primary dermal fibroblasts from affected and unaffected members of the family. This Chapter describes the initial steps taken in order to begin the characterisation of these affected patients. Firstly, we confirmed the patient JMJD5 genotypes and explored the effect of the JMJD5 mutations on mRNA splicing. The mutations were then further characterised to determine their effect on the JMJD5 protein with regards to expression, localisation and function. These immortalised cells then provided a novel model for exploring the enzymatic activity and cellular function of JMJD5 which is addressed in Chapter 4 and 5.

3.1 JMJD5 is mutated in patients with a novel developmental disorder

Two siblings were presented at a paediatric medical clinic in Estonia with unexplained developmental defects. Prenatally, these defects included intrauterine growth retardation and failure to thrive. Postnatally the two affected siblings had developmental delay, various skeletal, defects, brain atrophy, reduced muscle tone, and relative macrocephaly (a smaller body size relative to the head size) (Table 3.1 & Figure 3.1A). In order to explore the genetic

basis for the observed clinical phenotypes whole exome sequencing (WES) was performed on the whole family (Dr Sander Pajusalu and Dr Katrin Ounap in clinic). This identified two heritable mutations in *JMJD5* (Figure 3.1B). The maternal *JMJD5* mutation is a point mutation converting the cysteine at position 123 to a tyrosine (C123Y). The paternal *JMJD5* mutation is an eight-base pair deletion within the intron localised between exons 7 and 8 (referred to as 'InMut'). The patients affected by the developmental disorder were found to be compound heterozygote for these *JMJD5* mutations (Figure 3.1B).
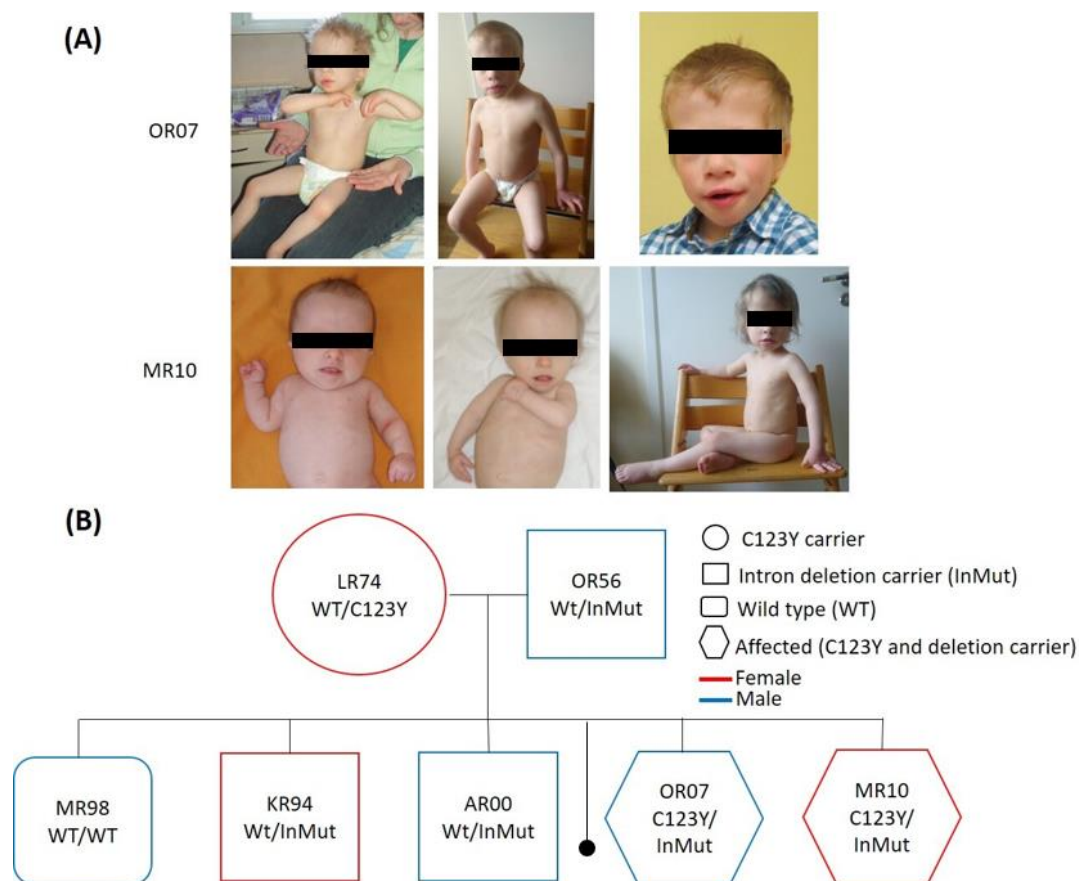
Figure 3.1 Phenotype and *JMJD5* genotypes of a family affected with a novel developmental disorder
(A) Two patients with a novel developmental disorder (images to compliment the clinical evaluation displayed in Table 3.1). We obtained parental consent to include these images. **(B)** The two affected patients are from a family that carry two heritable *JMJD5* mutations; all members of this family are presented here in a family tree diagram. Patient identifications are in bold with *JMJD5* mutation status beneath: wildtype (WT), point mutation converting cysteine at amino acid position 123 to a tyrosine (C123Y), eight-base-pair intronic deletion (InMut). The mother (LR74) carries the C123Y mutation. The father (OR56), KR94 and AR00 carry InMut. Two patients carrying both *JMJD5* mutations (OR07 and MR10) are affected by the developmental disorder. One family member is wildtype for *JMJD5* (MR98). The black dot denotes a miscarriage of unknown *JMJD5* genotype.

Table 3.1 Clinical phenotypes of two patients affected with a novel developmental disorder
Clinical evaluation was performed upon birth and at 10 years of age for patient OR07 or at 7 years of age for patient MR10, by Dr Sander Pajusalu and Dr Katrin Ounap. The patients share similar developmental defects including reduced growth but with a relatively larger head circumference (relative macrocephaly), plus facial and skeletal dysmorphism.

Patient		OR97	MR10
Gender		Male	Female
Prenatal		Intrauterine hypotrophy, oligohydramnion, small placenta	Intrauterine hypotrophy, oligohydramnion
Birth	Weeks	35	40
	Length	43 cm (- 2 SD)	43 cm (-3.5 SD)
	Weight	2360 g (-1 SD)	2386 g (-2.5 SD)
	Head	34 cm (+1 SD)	33.5 cm (-1.5 SD)
Growth	Height	96.5 cm (- 7 SD) at 10 years of age	84.1 cm (-6 SD) at 7 years of age
	Weight	13.1 kg (- 4 SD) at 10 years of age	10.2 kg (-4 SD) at 7 years of age
	Head	52 cm (-1.2 SD) at 10 years of age	51 cm (-0.5 SD) at 7 years of age
Craniofacial	Craniosynostosis	No	No
	Dysmorphism	Triangular face, high forehead, broad nasal bridge, full lips, microretrognathia, high palate, short neck, dysplastic ears	Triangular face, high forehead, deep set eyes, prominent nose, microretrognathia, short neck, dysplastic ears
Nervous system	Development	Moderate intellectual disability	Mild intellectual disability
	Muscular system	Muscular hypotonia	Muscular hypotonia
	EEG	Epileptic activity (generalised myoclonias); no treatment	Mild background abnormalities; no epileptic activity
	MRI	Mild brain atrophy	Mild cortical atrophy and dilated lateral ventricles
Vascular	Cardiac	Foramen ovale apertum	Foramen ovale apertum, mild ventricular septal defect (closed without operation)
Respiratory		Frequent bronchitis in infancy	No
Skeleton		Thoracolumbar scoliosis, sacral dimple	Narrow shoulders, hypoplastic nipples
Limbs	Hands	Single palmar crease	Single palmar crease, F5 clinodactyly
	Feet	Right clubfeet	Sandal gap
Gastrointestinal		Reflux in infancy	No
Genitourinary		Hypospadia, abnormal shape of right kidney (L-shape)	No
Vision		Divergent strabismus	Divergent strabismus
Hair and nails		No	Sparse hair; mild hypoplasia of nails
Immunological		No	No
Lymphatic		No	No
Endocrine	IGF	43.7 µg/L	<25 µg/L
	Thyroid gland	Normal	Hypothyreosis
Growth hormone replacement		Since 2 years 2 months of age, positive efect	Since 4 years of age, positive efect
Other		Hematoma subduralis at 1 month of age (trauma)	No

3.2 Generation of immortalised fibroblast cell lines

In order to perform phenotypic characterisation of the affected patients and their JMJD5 mutations, dermal fibroblasts were obtained as follows. Skin biopsies and fibroblast isolation was performed by Dr Sander Pajusalu and Dr Katrin Ounap (University of Tartu, Estonia) which were then expanded in culture by Professor Grant Stewart (The University of Birmingham).

To then generate long term cellular model systems, for future characterisation experiments, we immortalised the dermal fibroblasts using retroviral transduction of human telomerase (*hTERT*). The *hTERT* gene encodes the catalytic subunit of the telomerase reverse transcriptase enzyme which is responsible for maintaining telomere sequences and is not usually expressed in differentiated cells. Therefore, re-expression of hTERT in our primary fibroblasts would prevent telomere-controlled senescence to overcome the inherent finite lifespan of primary cells, and thus make them immortalised (Lee et al., 2004). This *hTERT* expression vector also contained a hygromycin resistance gene which allowed antibiotic selection of successfully transduced and immortalised cells. A hygromycin dose titration was used to identify the optimal concentration of 70 µg/mL hygromycin for selection and subsequent growth of the immortalised cell lines (Figure 3.2).
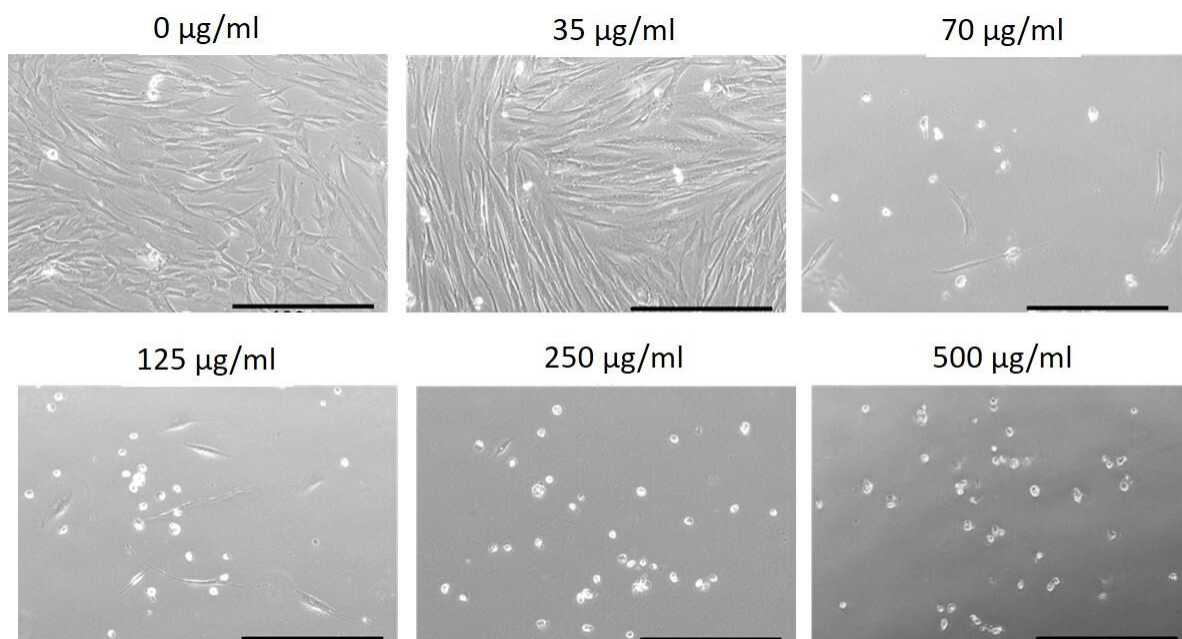
Figure 3.2 Hygromycin dose titration for optimal selection of immortalised fibroblasts
A hygromycin dose titration was performed on primary MR98 fibroblasts for 48 hours before monitoring for cell death using an EVOS microscope. The optimal dose to be subsequently used for selection of successfully immortalised primary fibroblasts was chosen as 70 µg/mL. Scale bars= 400 µm. This is representative of an n=1 biological repeat.

Unfortunately, during the immortalisation process, the primary fibroblasts from one affected patient, MR10, stopped growing. We investigated whether this could be due to entry into senescence by utilising an assay that monitors β-galactosidase activity at pH 6. The principle of the assay is that due to increased numbers of lysosomes in senescent cells there is accumulation of the β-galactosidase enzyme. Consequently, activity of the enzyme is found at the higher than usual pH 6 which can be detected by the hydrolysis of the colourless X-gal substrate into a blue product. Although β-galactosidase activity is not required for senescence it is a well-established biomarker of senescence (Dimri et al., 1995).

We included in our assay an untreated negative control which demonstrated a low level of background staining but were generally healthy and continued to grow throughout the assay until confluent (Figure 3.3A). We also included positive controls, treated with 12.5 μM etoposide or 4% ethanol to induce senescence. These conditions gave us confidence that the assay was optimal for detecting senescence, because cells from both conditions displayed strong blue nuclear staining indicative of active β-galactosidase activity at pH 6 (Figure 3.3C, 3.3C). Consequently, we hypothesised that the MR98 primary fibroblasts had entered senescence, because they had enlarged cellular size and altered morphology, as well as blue β-galactosidase product detectable at pH 6 (Figure 3.3D). This meant that immortalisation and further characterisation of fibroblasts, from this patient, could not be completed.
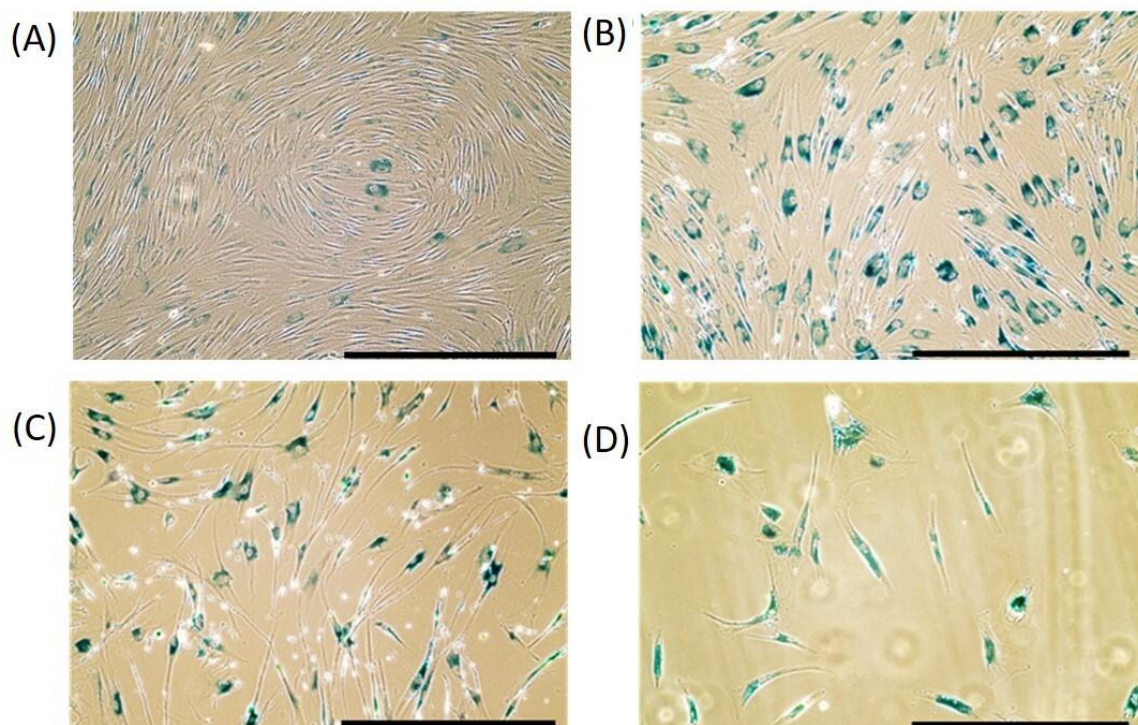
Figure 3.3 Investigating entry into senescence for MR10 primary fibroblasts

MR10 fibroblast entry into senescence was determined using an assay that monitors β-galactosidase activity, at pH 6, by the presence of a blue X-gal product observed using an EVOS microscope. **(A)** Untreated MR98 fibroblasts as a negative control for the assay. MR98 cells as positive controls were treated with **(B)** 12.5μM etoposide for 24 hours, or **(C)** 4% ethanol for 2 hours repeated for three consecutive days. Both (B/C) treatments were followed by a five-day recovery before performing the assay. **(D)** MR10 cells stained clearly for blue β-galactosidase product, had significant growth arrest and morphology change compared to negative control in (A) all indicative of senescence. Scale bars= 400 μm. Negative and positive controls are representative of n=2 biological repeats, MR10 image is representative of an n=1 biological repeat.

3.3 Confirmation of patient genotypes
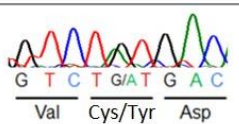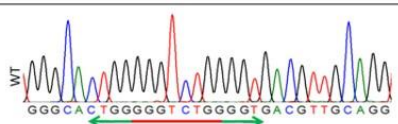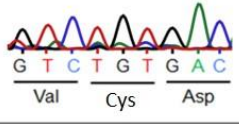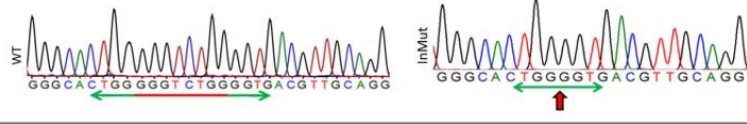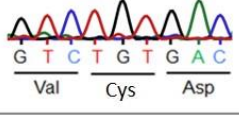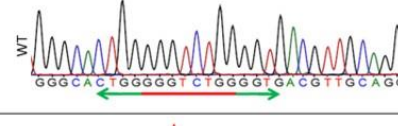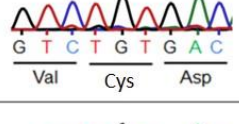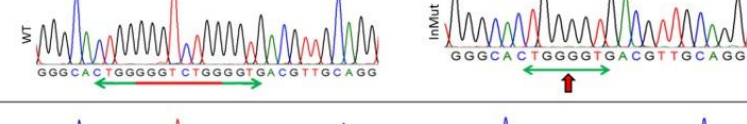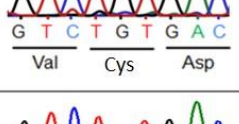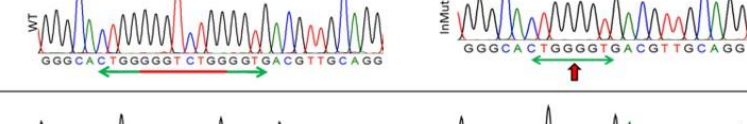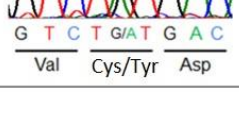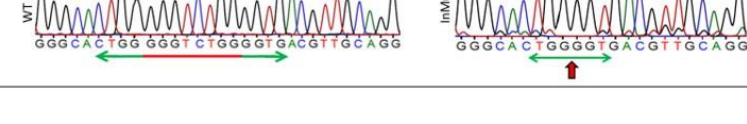
For the successfully immortalised patient fibroblasts, we next aimed to confirm the *JMJD5* genotypes originally identified in clinic by WES (Figure 3.1). To do this, genomic DNA was purified from the fibroblast lines and gene regions surrounding each *JMJD5* mutation were amplified by PCR before analysis using Sanger sequencing (Table 3.2). The presence of the C123Y point mutation was identified on the sequencing chromatograms by the overlap of a black peak corresponding to guanine (to encode cysteine), with a green peak corresponding to adenine (to encode cysteine) at the C123 codon. From this we confirmed that the C123Y point mutation allele was carried only by the mother (LR74) and affected patient (OR07) whereas all other patients were wildtype for this mutation on both alleles (Table 3.2).

Similarly, the presence of the InMut deletion mutation could be identified on the sequencing chromatograms by the loss of eight-base-pairs from the intron, located between exons 7 and 8. To demonstrate this, the sequence missing from the InMut is underlined in red on the wildtype allele chromatogram and the location of these missing nucleotides is shown by a red arrow on the InMut allele chromatogram (Table 3.2). This confirmed that the InMut allele was carried by the father (OR56), InMut carrier children (KR94 and AR00), as well as the affected child (OR07), whereas the mother (LR74) and wildtype sibling (MR98) were wildtype for this mutation on both alleles (Table 3.2).

With the genotype of the immortalised fibroblast cell lines confirmed, we next aimed to determine the effect that each mutation might have on the downstream JMJD5 mRNA and protein products.

Table 3.2 Confirming the patient genomic DNA genotypes of the immortalised fibroblast cell lines
Genomic DNA from successfully immortalised fibroblasts was harvested, PCR used to amplify regions of interest on the *JMJD5* gene for analysis by Sanger sequencing. One locus analysed included the cysteine, at position 123, that is converted to a tyrosine by a point mutation in C123Y carrier patients. The second locus analysed included the eight base pair deletion, within the intron between *JMJD5* exons 7 and 8, identified in InMut carrier patients. Red underlined sequence in the wildtype (WT) allele chromatogram marked the eight-base pairs lost from the InMut. The location of these missing base pairs is shown by a red arrow on the InMut allele chromatogram. Green underlined sequence is common between both WT and InMut.

3.4 InMut results in alternative splicing

The paternal mutation is an eight-base pair deletion at the 5' end of the intron located between exons 7 and 8. Due to the position of the InMut we hypothesised that normal *JMJD5* mRNA splicing could be affected, our rationale is discussed below.

Splicing is an essential stage of processing mRNA into exon-containing sequences for subsequent protein translation. Splicing is mediated by a multi-protein complex called the spliceosome which assembles onto splice sites by complementary base pairing. Introns contain these splice sites at the extreme 5' and 3' ends, termed donor and acceptor splice sites respectively, that are essential for directing the spliceosome to the correct region of the mRNA. Often the presence of enhancer and silencer sequences, localised within the surrounding exons or within the intron sequences themselves, are required to facilitate spliceosome loading and activity, reviewed by Wang and Burge (2008). Some of these splice sequences are depicted in Figure 3.4.
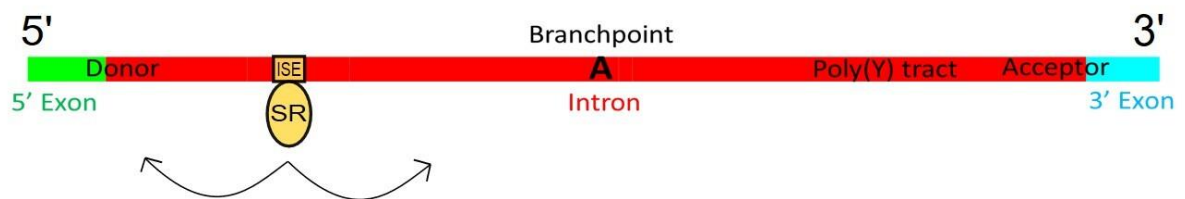
Figure 3.4 The location and function of splice sequences

mRNA splicing is mediated through base pairing between intron and exon sequences with spliceosome subunits. The donor splice site marks the 5' intron-exon boundary and the acceptor splice site marks the 3' intron-exon boundary. The acceptor sequence is composed of the acceptor splice site (located on the extreme 3' end of the intron), a poly pyrimidine (Y) tract important for facilitating splicing, and a branch point whereby an adenine mediates the first nucleophilic attack in the two-step splicing reaction. Other sequences located in the intron or adjacent exons can promote or inhibit splicing. One such element is depicted here, an intron splice enhancer (ISE) that binds to arginine-serine-rich (SR) splicing factors to facilitate nearby splice sites.

Once loaded onto the mRNA sequence the spliceosome catalyses two transesterification reactions that results in the ligation of two exons together and the removal of the intron sequence (Will and Lührmann, 2011). Importantly, the sequence of all splice motifs is essential as they mediate spliceosome recruitment by base pairing. Therefore, mutation of a single splice site sequence could impact normal splicing of an exon and result in an alternative protein product. Consequently, we hypothesised that the InMut deletion might affect splice sites within the intron sequence between exons 7 and 8.

In order to begin investigating this the wildtype and InMut *JMJD5* gene sequences were analysed using 'The Human Splicing Finder' (HSF) (Table 7.12). This is an online bioinformatics tool that is able to predict the presence of splice donor, acceptor, branch sites and auxiliary enhancer or silencer motifs on a sequence (Desmet et al., 2009). The HSF combines 'position weight matrices' and 'maximum entropy principle' algorithms to predict splicing sequences. These algorithms determine the importance of each nucleotide in a predicted sequence to generate a consensus value. This value infers confidence to the functional assignment of a sequence. Therefore, the higher the consensus value the more likely that a sequence would be used for the HSF predicted function *in vivo* (Desmet et al., 2009).

The HSF was able to predict a series of donor sites for the wildtype and InMut sequences (Figure 3.5A). Interestingly, one predicted wildtype donor site (boxed in red, Figure 3.5A) was not predicted for the InMut sequence. However, the presence of a higher scoring donor site, predicted for both wildtype and InMut sequences (black arrows, Figure 3.5A,), suggested that lack of the aforementioned donor site for the InMut may be inconsequential. For the same reason we concluded that the InMut was also unlikely to affect the acceptor splice site

sequence (green arrows, Figure 3.5A) or branch point sequence (blue arrows, Figure 3.5A). We therefore concluded that the InMut was not likely to affect the donor or acceptor splice site sequences directly (Figure 3.5B).

The HSF is also able to determine possible effects that mutations might have on auxiliary sequences and whether consequential changes to splicing are probable (Desmet et al., 2009). Interestingly, HSF predicted two potential splice enhancer sequences that would be removed by the InMut deletion (Figure 3.5B). Intron localised enhancer sequences facilitate splicing by interacting with arginine-serine-rich (SR) splicing factors that promote assembly of the spliceosome onto proximal splice sites (Figure 3.4) (Dvinge et al., 2016). Therefore, mutation of an intron enhancer site could affect the specificity or efficiency of splicing at proximal splice sites.

Overall, the HSF analysis predicted that the InMut was likely to negatively impact normal splicing of *JMJD5* mRNA, in this region, due to the removal of an enhancer site within the intron between exons 7 and 8.

(A)

Wildtype			
Splice site type	Motif	Splice site	Consensus value (0-100)
Donor	CAGGTGGGC	CAGgtgggc	88.33
Donor	GGGGTCTGG	GGGgtctgg	77.62
Donor	GGGGTGACG	GGGgtgacg	78.28
Donor	CAGGTTCTC	CAGgttctc	71.68
Acceptor	GTGACGTTGCAGGT	gtggacgttgcagGT	86.65
Acceptor	CTGCCCCTGGAGAT	ctgcccctggacAT	80.43
Acceptor	TGCTTTCTTCAGGT	tgctttcttcagGT	93.94
Branch Point	TCCCCAC	-	89.44
Branch Point	TCTTCAG	-	71.91

InMut			
Splice site type	Motif	Splice site	Consensus value (0-100)
Donor	CAGGTGGGC	CAGgtgggc	88.33
Donor	GGGGTGACG	GGGgtgacg	78.28
Donor	CAGGTTCTC	CAGgttctc	71.68
Acceptor	GTGACGTTGCAGGT	gtggacgttgcagGT	86.65
Acceptor	CTGCCCCTGGAGAT	ctgcccctggacAT	80.43
Acceptor	TGCTTTCTTCAGGT	tgctttcttcagGT	93.94
Branch Point	TCCCCAC	-	89.44
Branch Point	TCTTCAG	-	71.91

(B)

HSF predicted donor — InMut deletion — HSF predicted branchpoint — HSF predicted acceptor

AGCCAGGTGGGCACTGG***GGGTCTGG***GGTGACGTTGCAGGTTCTCCCCACTGCCCCTGGAGATGATGACGTCCTTTGCTTTCTTCAGGTTGAC

Exon 7 — (1= 62.89) (2= 73.38) — Intron 7-8 — Exon 8

Figure 3.5 HSF predicted splice sites in JMJD5 for the intron between exons 7 and 8
(A) Human splice finder (HSF) predicted sequences of 5' donor splice sites and 3' acceptor splice sites for wildtype and InMut JMJD5 genomic sequences between exons 7 and 8. Red box marks a donor site present in the wildtype sequence but missing from the InMut. Arrows mark splice sites with the highest consensus value and therefore most likely to be a real sequence; donor (black), acceptor (green), branch point (blue). Splice sites demonstrated by lower-case lettering intron sequences and upper-case lettering for exon sequences. **(B)** The splice sequences, as predicted by HSF in (A), are labelled onto the JMJD5 intronic sequence between exons 7 and 8. Two intron splice enhancers were predicted by HSF (numbered 1 and 2, underlined in blue and green, with each consensus values indicated) for the region that overlapped with the InMut deletion (sequence crossed through in bold).

Due to predictions made by HSF, we next wanted to determine whether InMut affected *JMJD5* mRNA splicing in a biological context. To do this the complete *JMJD5* coding sequence was PCR amplified, from cDNA purified from the immortalised patient fibroblast lines. PCR products were examined by agarose gel electrophoresis which identified a doublet banding pattern correlating to patients that were carriers of the InMut (Figure 3.6A). The larger (upper) band, identified in all patients, was approximately 1.3 kb in size and corresponded to the predicted size of wildtype *JMJD5*. The smaller (lower) band, only present for patients carrying

the InMut, was approximately 100bp smaller than the upper band. Therefore, we hypothesised this could be indicative of alternative splicing of InMut *JMJD5*. In order to determine the identity of the two PCR products both the upper and lower bands from the OR07 patient were purified from the agarose gel and analysed by Sanger sequencing. As predicted from the PCR product size, the upper band corresponded to the wildtype *JMJD5* sequence (Figure 3.6B). Interestingly, the smaller PCR product (lower band) was completely missing the mRNA sequence encoded by 7, the exon preceding the InMut (Figure 3.6B).
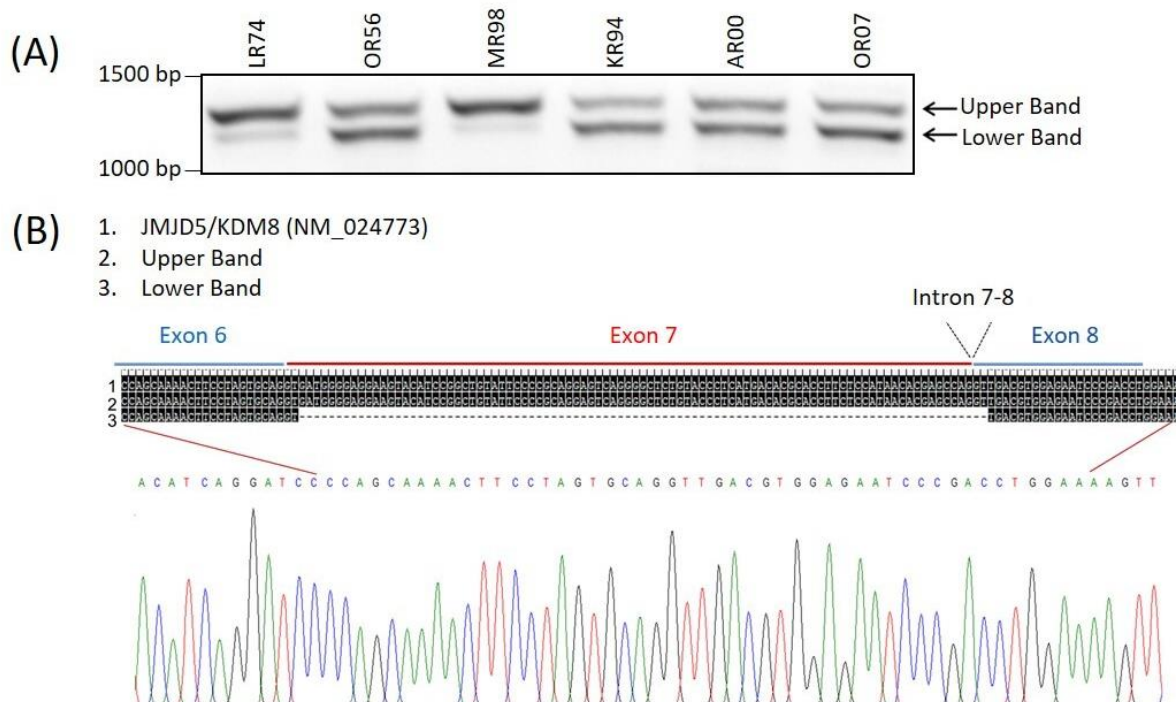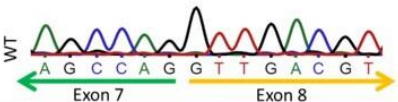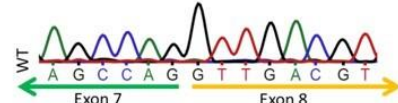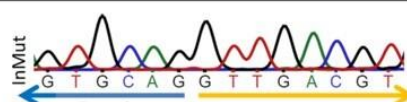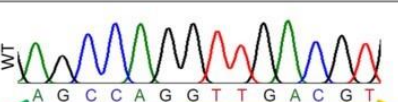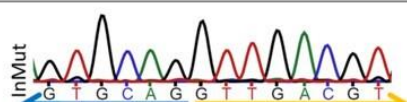
Figure 3.6 Analysis of the InMut demonstrates removal of exon 7 coding sequence from mRNA
PCR amplification of the complete JMJD5 mRNA sequence was performed on cDNA purified from immortalised patient fibroblasts. Patient fibroblast JMJD5 genotypes; MR98 wildtype, LR74 carrier of C123Y, OR56, KR94 and AR00 carriers of InMut, OR07 affected patient carrying C123Y and InMut *JMJD5*. **(A)** PCR products were separated by agarose gel electrophoresis where one band, at approximately 1.3 kb, corresponded to the predicted size for the JMJD5 wildtype gene (upper band). A second band, corresponding to InMut carrier patients, was approximately 100bp smaller than the upper band (lower band). This is representative of n=3 biological repeats. **(B)** Chromatogram for Sanger sequencing performed on the two PCR products purified individually for the affected patient OR07. The larger (upper) band, from the DNA gel, was found to have the same sequence as wildtype JMJD5 (NM_024773). The smaller (lower) band was found to not contain the mRNA sequence for the whole of exon 7 but instead expressed exon 6 directly into exon 8.

Sanger sequencing was then performed on all upper and, where applicable, lower bands from the *JMJD5* PCR reaction products shown in Figure 3.6A. This confirmed that loss of the mRNA sequence encoding exon 7 was consistent for all patients carrying the InMut allele (Table 3.3).

Table 3.3 Removal of exon 7 coding sequence from mRNA consistent for all InMut carrier patients
PCR products separated by gel electrophoresis in Figure 3.6A were purified and analysed by Sanger sequencing. This confirmed that InMut consistently resulted in loss of exon 7 coding sequence from mRNA. Chromatograms underlined in blue mark exon 6 coding sequence, green underling to mark exon 7 coding sequence and yellow underlining to mark exon 8 coding sequence.

With the knowledge that InMut resulted in the removal of the exon 7 coding sequence during *JMJD5* mRNA splicing, we next questioned how this might affect the JMJD5 protein. Exon 7 encodes a large portion of the JmjC catalytic domain for JMJD5 (Figure 3.7A) corresponding to 31 amino acids and 3.59 kDa predicted molecular weight. Examining exon 7 on the crystal

structure of JMJD5 demonstrated that it forms an essential catalytic structural fold, specifically one of the core β-helices, and includes a 2-OG cofactor binding residue (Figure 3.7B). Therefore, we predicted that removal of exon 7 from InMut JMJD5 protein was likely to have a dramatic effect on the structure and stability of JMJD5 but also would impact its catalytic activity. This hypothesis is addressed later in this chapter (Section 3.7).
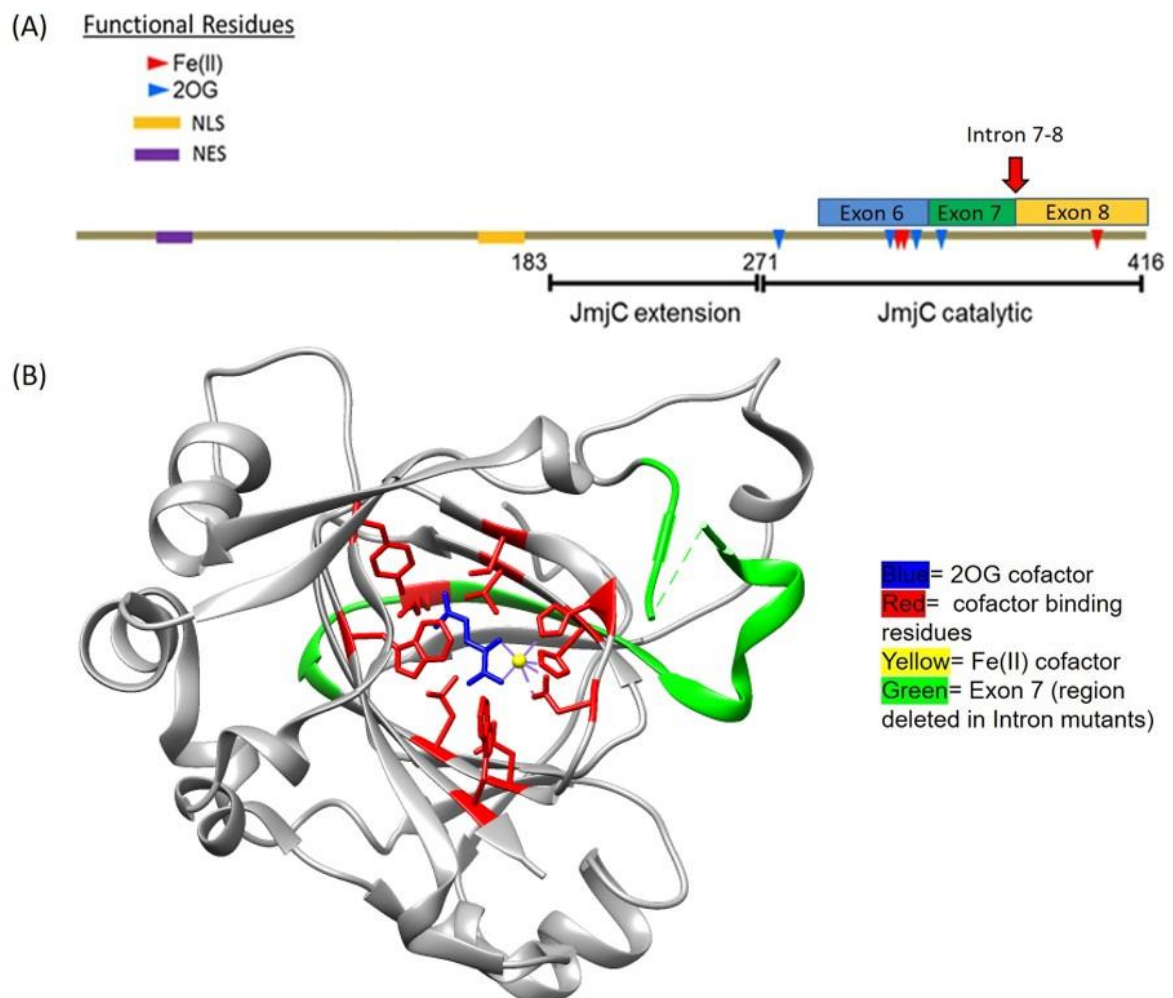
Figure 3.7; Exon 7 mRNA sequence encodes a portion of the JmjC catalytic domain of JMJD5 protein (A) Exon 6, 7 and 8 were mapped onto the protein sequence of JMJD5. Exon 7 constitutes a large portion of the JmjC catalytic domain of JMJD5. Therefore, loss of exon 7 would result in an incomplete JmjC domain and loss of 2-OG cofactor binding residues. **(C)** Mapped onto the 3D crystal structure of JMJD5 (4GAZ) loss of exon 7 sequence removes a large structural fold in the catalytic domain (exon 7 highlighted in green). Figure generated using Chimera software.
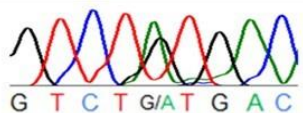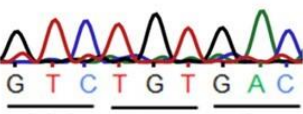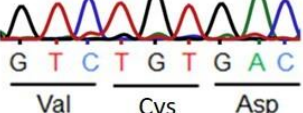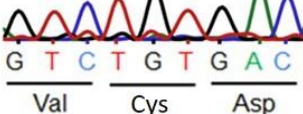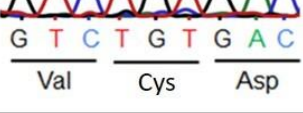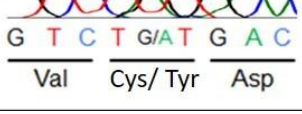
3.5 C123Y is a conserved residue in the N-terminus of JMJD5

The second JMJD5 mutation carried by this family, provided from the maternal allele, was a point mutation converting a cysteine at position 123 to a tyrosine. The presence of this mutation was already confirmed from genomic DNA isolated from the immortalised fibroblasts (Table 3.2). Therefore, we next aimed to investigate whether the mutation was also detected in the corresponding mRNA. The full-length *JMJD5* PCR products, generated and Sanger sequenced above for the InMut analysis (in Section 3.4), were analysed for the presence of the C123Y mutation. As expected, the C123Y mutation was detected only in *JMJD5* cDNA obtained from the mother (LR74) and affected patient (OR07) (Table 3.4).

As the genomic C123Y mutation was present at the mRNA level this raised the question of how this mutation might affect any expressed C123Y mutant JMJD5 protein. Unfortunately, we were unable to utilise the JMJD5 crystal structure to predict the consequences of this mutation because current structures do not include the complete N-terminal domain of JMJD5. Therefore, we used online analysis tools, PolyPhen-2 and SIFT, to determine whether the C123Y mutation was likely to be deleterious to JMJD5. As discussed in Chapter 2, both software tools generate a score to predict whether an amino acid change is likely to be tolerated based on sequence conservation (Adzhubei et al., 2010, Sim et al., 2012). SIFT determines the probably that a change will be tolerated whereas PolyPhen-2 predicts the probability that the change will be damaging. Therefore, a low SIFT score and high PolyPhen-2 score assigned to a mutation implies that a mutation will be detrimental. Interestingly, for the C123Y mutation SIFT gave a score of 0 and PolyPhen-2 gave a score of 1 meaning that both software tools predicted the C123Y amino acid change to be deleterious for JMJD5.

Table 3.4 Confirmation of C123Y mRNA genotype in patient fibroblasts
Chromatogram demonstrating the presence of the guanine to adenine point mutation identified in C123Y JMJD5 mutation carriers. PCR amplification of the complete *JMJD5* mRNA sequence was performed and analysed by Sanger sequencing, samples as used in Figure 3.6 and Table 3.3.

Patient	mRNA Products at C123Y Locus
LR74	
OR56	
MR98	
KR94	
AR00	
OR07	

We complemented this bioinformatic analysis by determining the evolutionary conservation

of the C123 residue in JMJD5 paralogues and orthologues, to predict its potential importance.

We observed that the C123 residue and N-terminus of JMJD5 was not conserved compared to

other human JmjC-only sub-family members (Figure 3.8A). However, C123 was conserved

between diverse JMJD5 orthologs indicative of C123 having an important role specifically

related to JMJD5 function (Figure 3.8B).
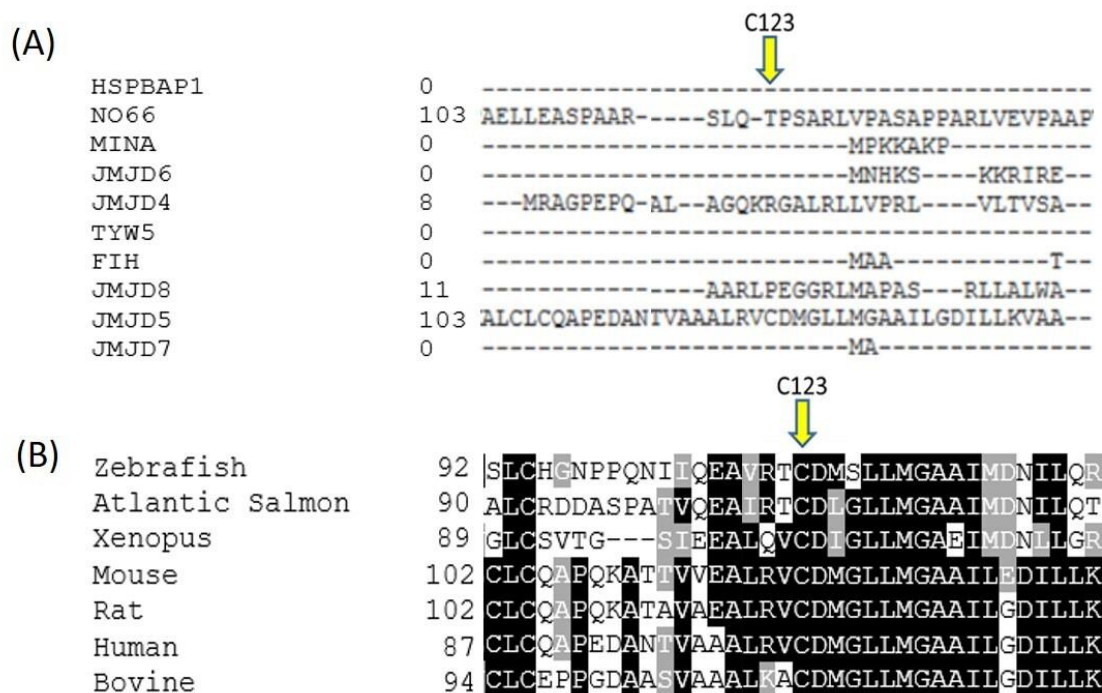
Figure 3.8 Cysteine at amino acid position 123 is highly conserved in JMJD5
Sequence conservation was determined for the C123 residue by protein sequence alignment analysis, performed using Clustal Omega online software, for **(A)** JmjC-only family members in humans and **(B)** JMJD5 across a selection of different species. Protein sequences analysed are outlined in Table 7.11.

Overall, due to the conserved nature of C123 and the dramatic change in amino acid, caused by its substitution to a tyrosine, we hypothesised that the C123Y mutation was likely to have a detrimental effect on JMJD5. This hypothesis is addressed in the following sections.

3.6 JMJD5 mutations affect JMJD5 protein expression and stability

The previous sections confirmed that our immortalised patient fibroblasts carried the expected *JMJD5* mutation genotype, and initial bioinformatics analysis predicted that both of the mutations were likely to negatively affect the JMJD5 protein. Therefore, we next assessed endogenous JMJD5 protein expression across the immortalised fibroblast cell lines. Interestingly, JMJD5 mutation status appeared to correlate with JMJD5 protein expression levels (Figure 3.9A). We found that fibroblasts from patients carrying one JMJD5 mutation had

reduced JMJD5 protein expression compared to the wildtype patient fibroblasts. The fibroblasts from the affected patient (OR07), carrying both JMJD5 mutations, had the lowest JMJD5 protein expression compared to all other fibroblast lines (Figure 3.9A). Interestingly, this difference was not explained by a decrease in *JMJD5* mRNA expression level, as both the wildtype (MR98) and OR07 affected patient fibroblasts expressed similar levels of *JMJD5* mRNA (Figure 3.8B).
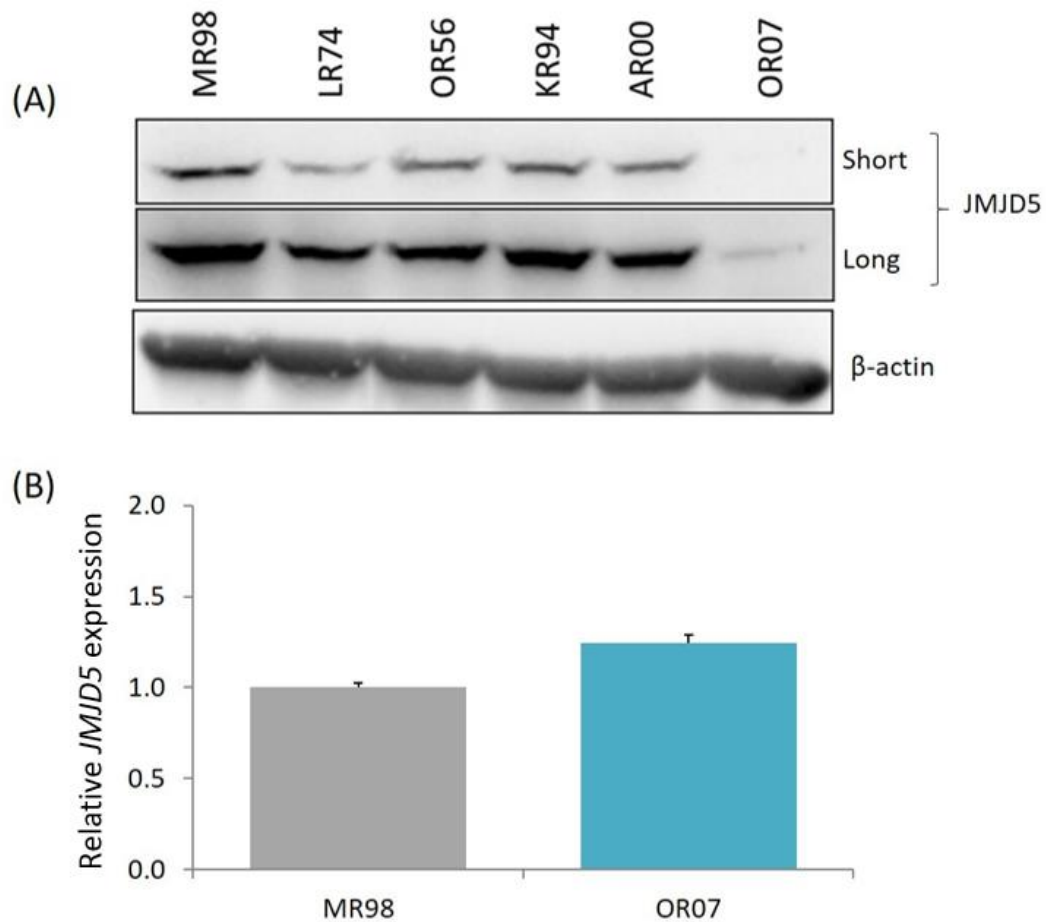
Figure 3.9 JMJD5 mutation correlated with JMJD5 protein expression levels in patient fibroblasts
Patient fibroblast JMJD5 genotypes; MR98 wildtype, LR74 carrier of C123Y, OR56, KR94 and AR00 carriers of InMut, OR07 affected patient carrying C123Y and InMut *JMJD5*. **(A)** JMJD5 protein expression was determined by Western blot analysis of whole cell lysate purified from immortalised patient fibroblasts. β-actin was used as a loading control. This is representative of n=3 biological repeats. 'Short' and 'long' refer to the length of exposure time used to visualise a Western blot signal. JMJD5 (47 kDa), β-actin (42kDa). **(B)** qPCR was used to determine *JMJD5* mRNA expression in wildtype (MR98) and affected (OR07) patient fibroblasts. This is representative of an n=1 biological repeat, with quadruplicate technical repeats.

As a consequence of this result (Figure 3.9), we hypothesised that the reduced JMJD5 protein expression observed for the affected (OR07) patient fibroblasts was likely due to reduced stability of the mutant JMJD5 proteins, rather than reduced transcription from the *JMJD5* gene or increased degradation of the *JMJD5* mRNA.

To address this hypothesis, we investigated the protein expression of each JMJD5 mutation individually (Figure 3.10). To do this wildtype, C123Y and InMut JMJD5 were cloned into expression vectors with an N-terminal HA tag and transfected into HeLa and HEK-293T cells. Western blotting indicated that the C123Y mutant protein expressed less than wildtype, and that InMut protein expression was undetectable (Figure 3.10A and B). A co-transfected plasmid was used as a positive control to demonstrate equal transfection efficiency between samples (Figure 3.10B).

To explore this further the wildtype, C123Y and InMut JMJD5 sequences were sub-cloned into a lentiviral vector with an N-terminal FLAG tag and expressed from a doxycycline inducible promoter. Lentivirus infection of these vectors was performed to generate MR98 patient stable expression fibroblast cell lines (see Section 5.5.1, Chapter 5). Following doxycycline treatment, Western blot analysis confirmed that the C123Y and InMut JMJD5 protein expressed less than wildtype (Figure 3.10C). However, unlike in the transient transfection experiments, in this system the InMut JMJD5 protein was detectable by Western blotting. We found that FLAG-tagged InMut JMJD5 migrated faster than FLAG-tagged wildtype JMJD5 (Figure 3.10C), consistent with predictions that the InMut JMJD5 protein would be approximately 3.6 kDa smaller than wildtype JMJD5 (Section 3.4).
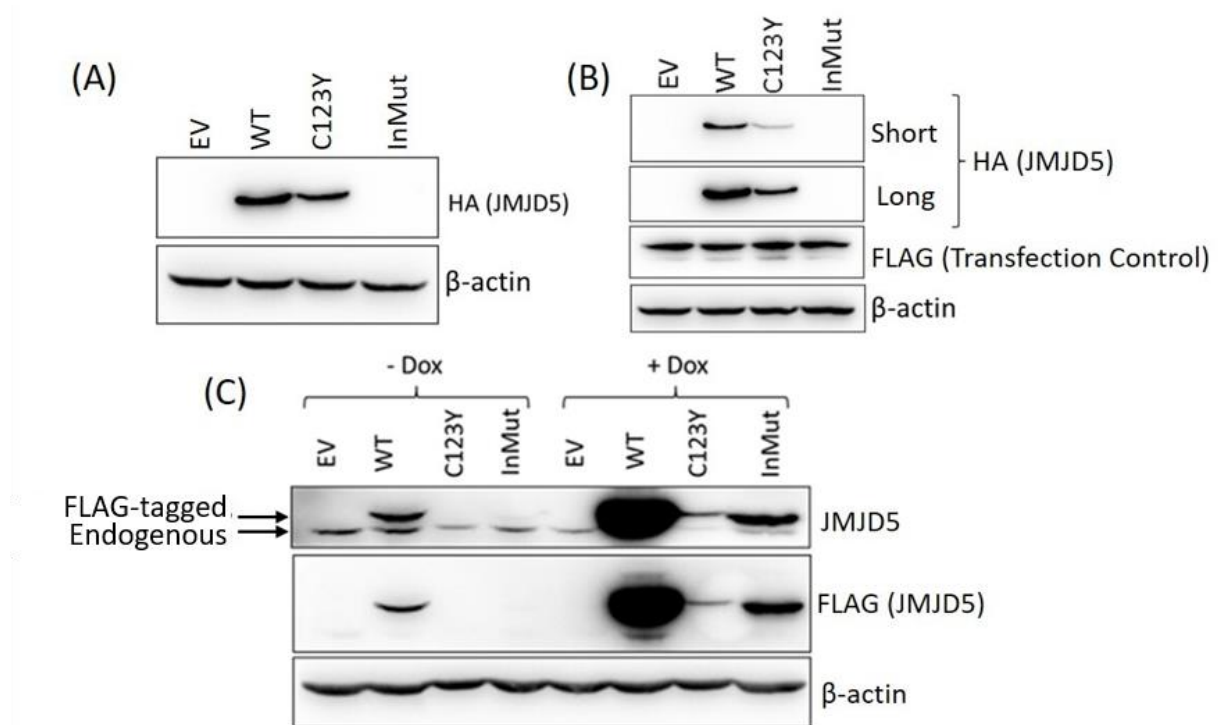
Figure 3.10 C123Y and InMut proteins express less than wildtype JMJD5

N-terminal HA-tagged wildtype, C123Y or InMut JMJD5 expression vectors were transiently transfected into **(A)** HeLa or **(B)** HEK-293T cells. Protein expression analysed by Western blotting. HEK-293T cells were co-transfected with a positive control FLAG-tagged expression vector to establish transfection efficiency. **(C)** MR98 stable expression cell lines were doxycycline treated (1 µg/mL) to express N-terminal FLAG-tagged wildtype, C123Y or InMut JMJD5 for 24 hours. Protein expression was analysed by Western blotting. β-actin was used as a loading control. JMJD5 (47 kDa), β-actin (42kDa). This is representative of n=2 biological repeats.

This evidence was consistent with the hypothesis that the JMJD5 mutants affected JMJD5 protein folding and stability. To test this further we aimed to measure JMJD5 protein turnover using a cycloheximide assay. Cycloheximide interferes with the translocation step of protein translation, thus blocking global protein synthesis, and provides an opportunity to indirectly measure protein stability (Kao et al., 2015). Rapid loss of protein expression following cycloheximide treatment indicates a protein with increased 'turnover'. We applied this assay to monitor the turnover of FLAG-tagged wildtype, C123Y and InMut JMJD5 from the doxycycline inducible MR98 fibroblast cell lines. These cell lines were most suited for this experiment, compared to transient transfection into cancer cell lines, because InMut JMJD5

protein was detectable by Western blotting in this system (Figure 3.10C). From this assay we found that wildtype FLAG-JMJD5 protein expression levels remained stable, even after 10 hours of cycloheximide treatment (Figure 3.11A). In contrast, C123Y and InMut protein expression levels were reduced after only 2 hours of cycloheximide treatment (Figure 3.11A). This result was consistent with both C123Y and InMut reducing the protein stability of JMJD5.

The majority of unstable proteins are degraded in the cell by the proteasome. This proteasomal degradation can be inhibited by MG132 that covalently binds to the catalytic inner rings of the 20S core subunit of the proteasome and consequently inhibits its activity (Adams, 2003). Therefore, application *in vitro* can provide information regarding the degradation pathway a specific protein is targeted for. Therefore, we performed an MG132 assay on our doxycycline inducible MR98 FLAG-JMJD5 expression cell lines to determine whether either JMJD5 mutant were targeted for proteasomal degradation.

We found that JMJD5 wildtype and C123Y were stabilised by proteasome inhibition to a degree, suggesting that the instability of the C123Y mutant is likely mediated by an alternative proteolytic pathway (Figure 3.11B). In contrast, the expression of the InMut JMJD5 was significantly increased by MG132 treatment, suggesting that the InMut is rapidly degraded by the proteasome (Figure 3.11B). Overall, our data indicated that both patient JMJD5 mutations contributed to the reduced overall level of JMJD5 protein expression for the affected patient (Figure 3.8A) due to increased proteolytic degradation because of reduced JMJD5 protein stability (Figure 3.10 and 3.11).
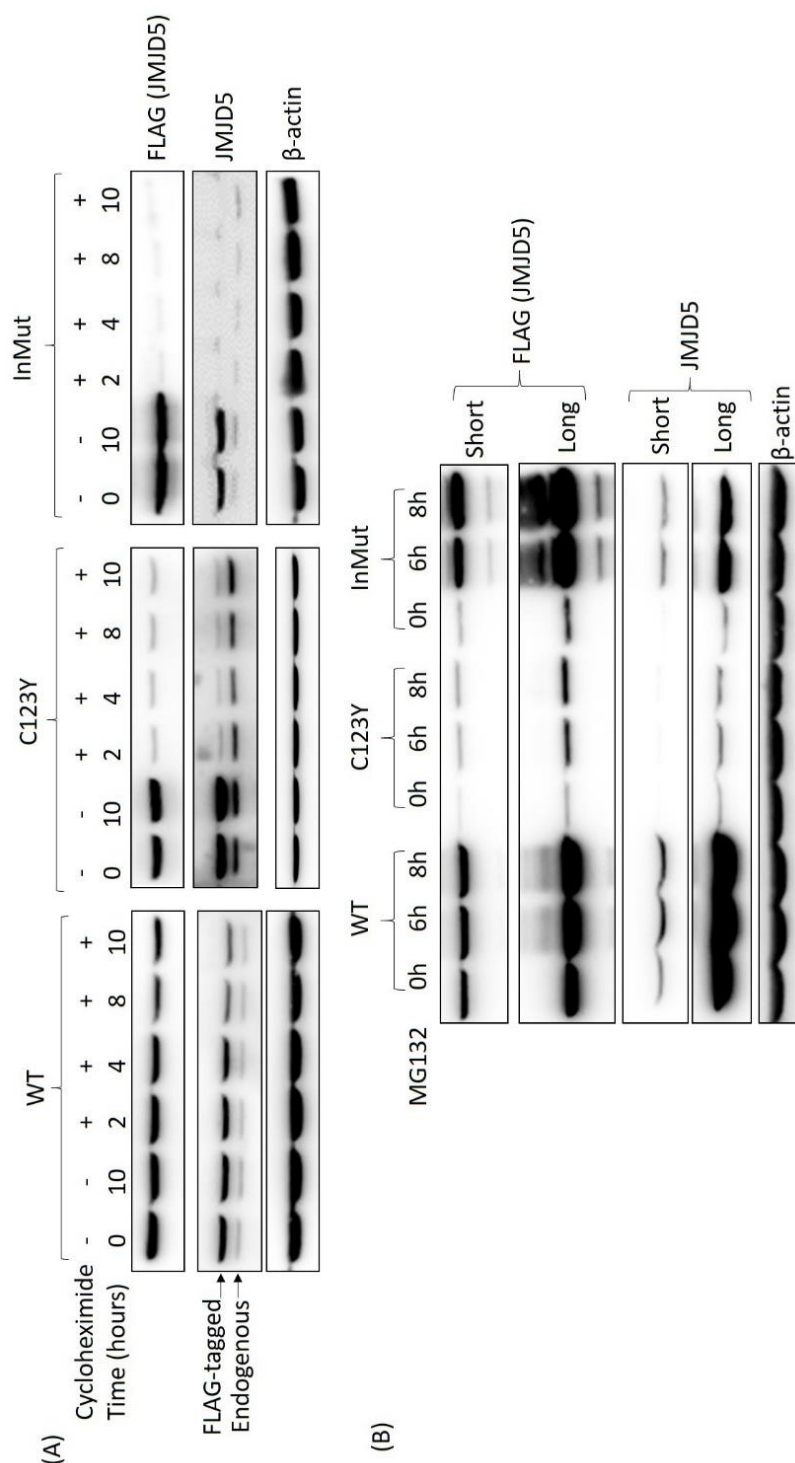
Figure 3.11 C123Y and InMut proteins are less stable than wildtype JMJD5

Stable expression MR98 fibroblast cell lines, doxycycline inducible to express N-terminal FLAG-tagged wildtype, C123Y or InMut JMJD5 were utilised to determine the stability of the JMJD5 mutant proteins. Cells were incubated in doxycycline for 24 hours at 1 µg/mL for C123Y and InMut, or at 10 ng/mL for wildtype JMJD5 cell lines, to ensure more equalised starting protein expression. Cells were then incubated with **(A)** Cycloheximide (50 µg/mL) for 2, 4, 8 and 10 hours, including no treatment controls taken at 0 and 10 hours, then protein expression determined by Western blotting. Arrows on the JMJD5 probed blot identify the larger (upper) band as the FLAG-tagged exogenous version and the smaller (lower) band as the endogenous JMJD5 protein. This is representative of n=2 biological repeats. **(B)** MG132 (10µM) for 6 or 8 hours, with a no treatment control taken at 0 hours, then protein expression determined by Western blotting. This is representative of an n=1 biological repeat. 'Short' and 'long' refer to the length of exposure time used to visualise a Western blot signal. β-actin was used as a loading control. JMJD5 (47 kDa), β-actin (42kDa).

Our data also demonstrated that the InMut had a more deleterious effect to JMJD5 compared to the C123Y mutant (Section 3.5). We therefore hypothesised that any JMJD5 protein expressed in affected patient fibroblasts (Figure 3.9A) would be from the C123Y allele. Consistent with this, the JMJD5 protein expressed in fibroblasts from this patient migrated similarly to the wildtype JMJD5 when separated by SDS-PAGE (Figure 3.9A) and no faster migrating JMJD5, indicative of the smaller InMut protein, was detected (Figure 3.9A). Consequently, we continued to characterise the C123Y mutation to determine what affect it might have on JMJD5 and whether any defective phenotypes might explain the reduced stability of the C123Y mutant JMJD5 protein.

3.7 Characterising the C123Y Mutation

As previously discussed, the cysteine at position 123 is found within the N-terminus of JMJD5, which is not represented in current crystal structures and has been poorly characterised with regards to its function. Investigation of the C123Y mutation was therefore directed by the available literature regarding the JMJD5 N-terminus (Figure 3.12). Specifically, in this section, we investigated the effect of C123Y mutation on JMJD5 nuclear localisation (Section 3.7.1), oligomerisation (Section 3.7.2), interaction with a known N-terminal binding partner (Section 3.7.3), analysis of the proximal protein sequence (Section 3.7.4), and the enzymatic activity of JMJD5 (Section 3.7.5).
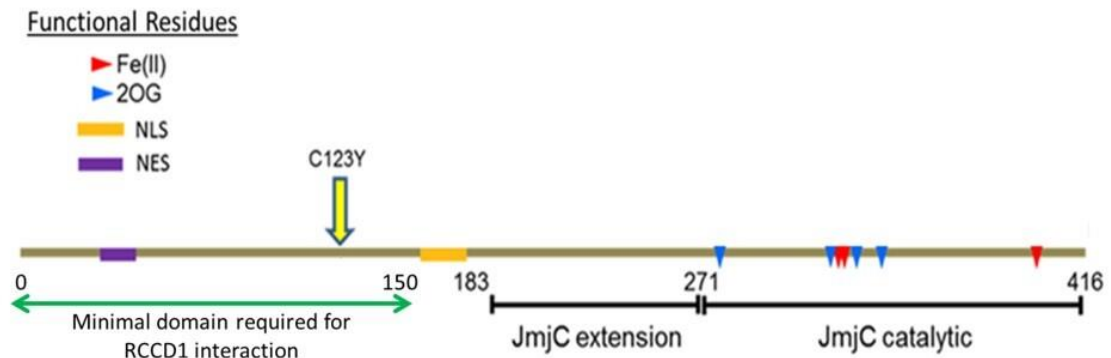
Figure 3.12 The C123Y mutation is located in the N-terminus of JMJD5
Cysteine at position 123, the site of the C123Y point mutation, was mapped onto the JMJD5 protein sequence and found to be localised in the N-terminus. It sits between a nuclear localisation signal (NLS, orange block) and nuclear export signal (NES, purple block) and within a minimal domain identified to interact with binding partner RCCD1 (green arrow). Also included are catalytic domains and residues.

3.7.1   JMJD5 Localisation

JMJD5 is reported in the literature to have a predominantly nuclear localisation (Shen et al., 2017, Huang et al., 2013, Zhu et al., 2014, He et al., 2016a, Kouwaki et al., 2016, Wu et al., 2016b, Shalaby et al., 2018). This may be regulated by its N-terminal domain due to the identification of a nuclear localisation sequence (amino acids 151-170) and a nuclear export sequence (amino acids 30-17) in this region (Huang et al., 2013). Since the C123Y mutation is located between these two signals (Figure 3.12) we investigated how it might affect JMJD5 nuclear localisation. To do this, immunofluorescence analysis was performed in our FLAG-JMJD5 MR98 expression cell lines. Doxycycline treatment was used to over-express FLAG-tagged JMJD5 wildtype or C123Y. An empty vector control was used in parallel which demonstrated no background staining of the FLAG antibody (Figure 3.13).

Consistent with the literature we found the wildtype JMJD5 localised within the nucleus, and this was mirrored by the C123Y mutation (Figure 3.13). Consistent with lower expression levels, as detected previously by Western blotting (Figure 3.10), we observed fewer cells that expressed C123Y JMJD5, at levels detectable by FLAG staining. Overall, this

immunofluorescence analysis demonstrated that C123Y had no negative affect on the nuclear

localisation of JMJD5 and is therefore unlikely to be a contributing factor towards the reduced

C123Y protein stability observed compared to wildtype (Section 3.6).
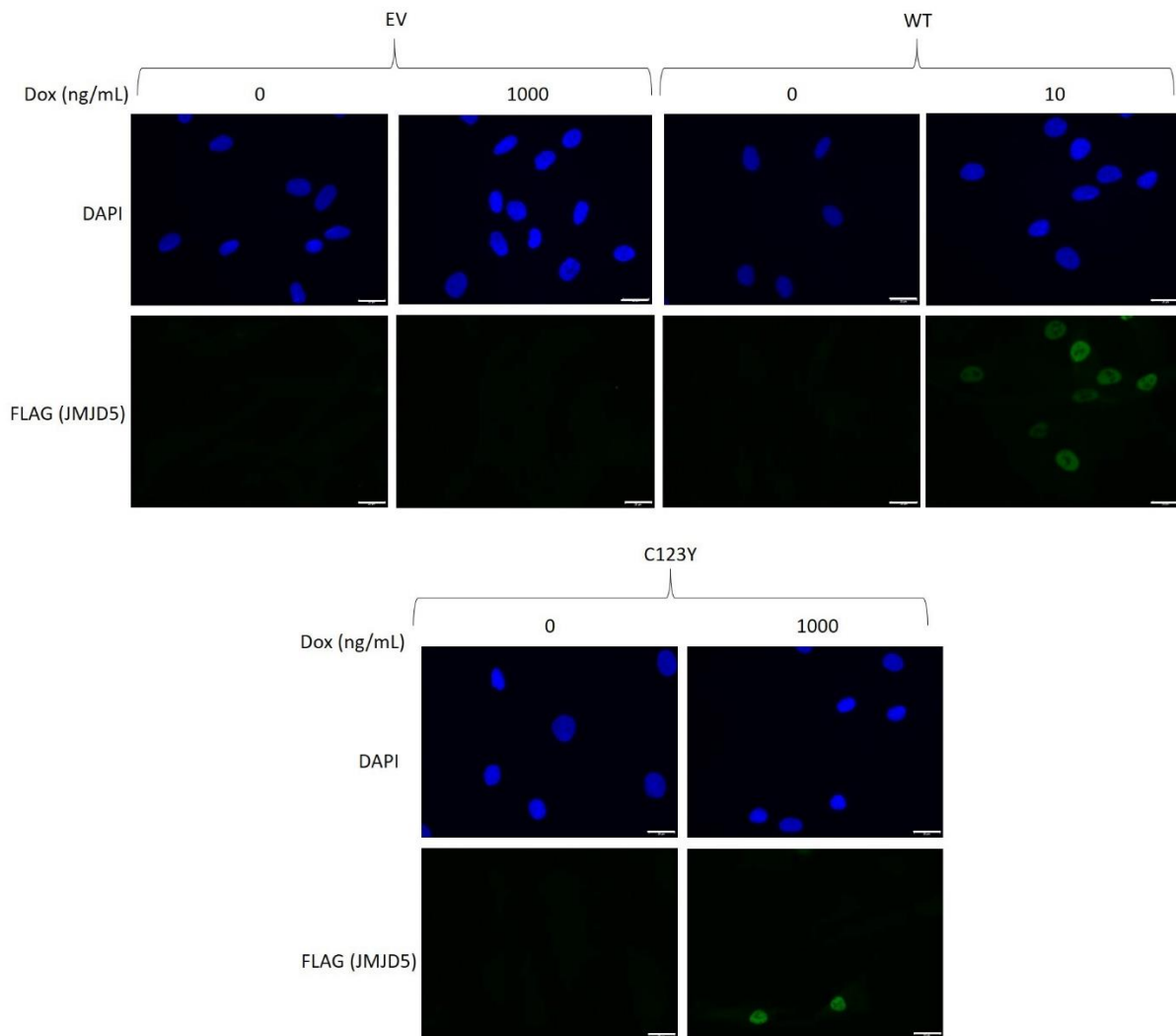
Figure 3.13 C123Y nuclear localisation mirrors that of wildtype JMJD5
Immunofluorescence targeted to FLAG was performed on MR98 stable expression cell lines doxycycline inducible to express N-terminal FLAG-tagged wildtype (WT) or C123Y JMJD5. Doxycycline was used to induce expression of these constructs for 24 hours prior to immunofluorescence staining, at a concentration of 10 ng/mL for wildtype, or 1 μg/mL for C123Y, to ensure more equalised starting protein expression. An empty vector (EV) control was used to confirm the specificity of the FLAG staining. Scale bars= 20 μm. This is representative of n=2 biological repeats.

3.7.2   JMJD5 Oligomerisation

Shen et al. (2017) previously concluded that JMJD5 oligomerised via its C-terminal catalytic domain. However, their data also suggested that the N-terminus of JMJD5 could contribute to this oligomerisation. Alongside this, evidence from other JmjC-only family members suggests that other domains, outside of the catalytic domain, contribute to oligomerisation. For example, the JMJD7 oligomerisation interface includes both N- and C-terminal regions and an extreme N-terminal cysteine residue, which is thought to be important for stabilising the interaction (Markolovic et al., 2018). Consequently, we were next interested to investigate whether the C123Y mutation impacted JMJD5 oligomerisation.

Firstly, we wanted to confirm the finding of Shen et al. (2017) that JMJD5 was able to oligomerise. To test this, HEK-293T cells were co-transfected with wildtype JMJD5 constructs containing two different epitope tags, one with an N-terminal FLAG tag and one an N-terminal HA tag. This was followed by immunoprecipitation (IP) to purify JMJD5 via its FLAG tag. We then used Western blot analysis of immunoprecipitates to detect the co-transfected HA-JMJD5, indicative of oligomerisation between the HA and FLAG-tagged constructs. We successfully observed co-immunoprecipitation of HA-JMJD5 after FLAG-immunoprecipitation confirming that JMJD5 can oligomerise (Figure 3.14A). An empty vector co-transfected with HA-JMJD5 expression vector was also FLAG immunoprecipitated as a negative control and demonstrated no non-specific interaction between HA-JMJD5 and the FLAG beads (Figure 3.14A). This gave confidence to our conclusion that HA-JMJD5 and FLAG-JMJD5 were able to oligomerise.

After confirming that wildtype JMJD5 could oligomerise, and that our assay was reliable, we next investigated whether the C123Y mutant affected JMJD5 oligomerisation. To do this we repeated the same assay but included HA- and FLAG-tagged C123Y JMJD5. In addition, we aimed to extend the previous results by performing the assay in reverse (analysing anti-HA immunoprecipitates for co-purification of co-transfected FLAG-tagged JMJD5).

Firstly, we were able to replicate that wildtype JMJD5 could oligomerise, after both FLAG and HA immunoprecipitation (Figure 3.14B and C). We also found that the C123Y mutant was able to interact with both wildtype and C123Y JMJD5 constructs (Figure 3.14B and C). Therefore, loss of JMJD5 oligomerisation was unlikely to explain the reduced protein stability of the C123Y mutant (Section 3.6).

In addition, we noticed reduced expression of C123Y when co-transfected with empty vector compared to when co-transfected with wildtype JMJD5 (Figure 3.14C). We first hypothesised that this could help to explain the C123Y reduced protein stability. For example, if oligomerisation was important for stability. However, as this observation was only seen for the HA-tagged C123Y construct, we therefore predicted that this was more likely an artefactual observation or a potential Western blot loading issue.
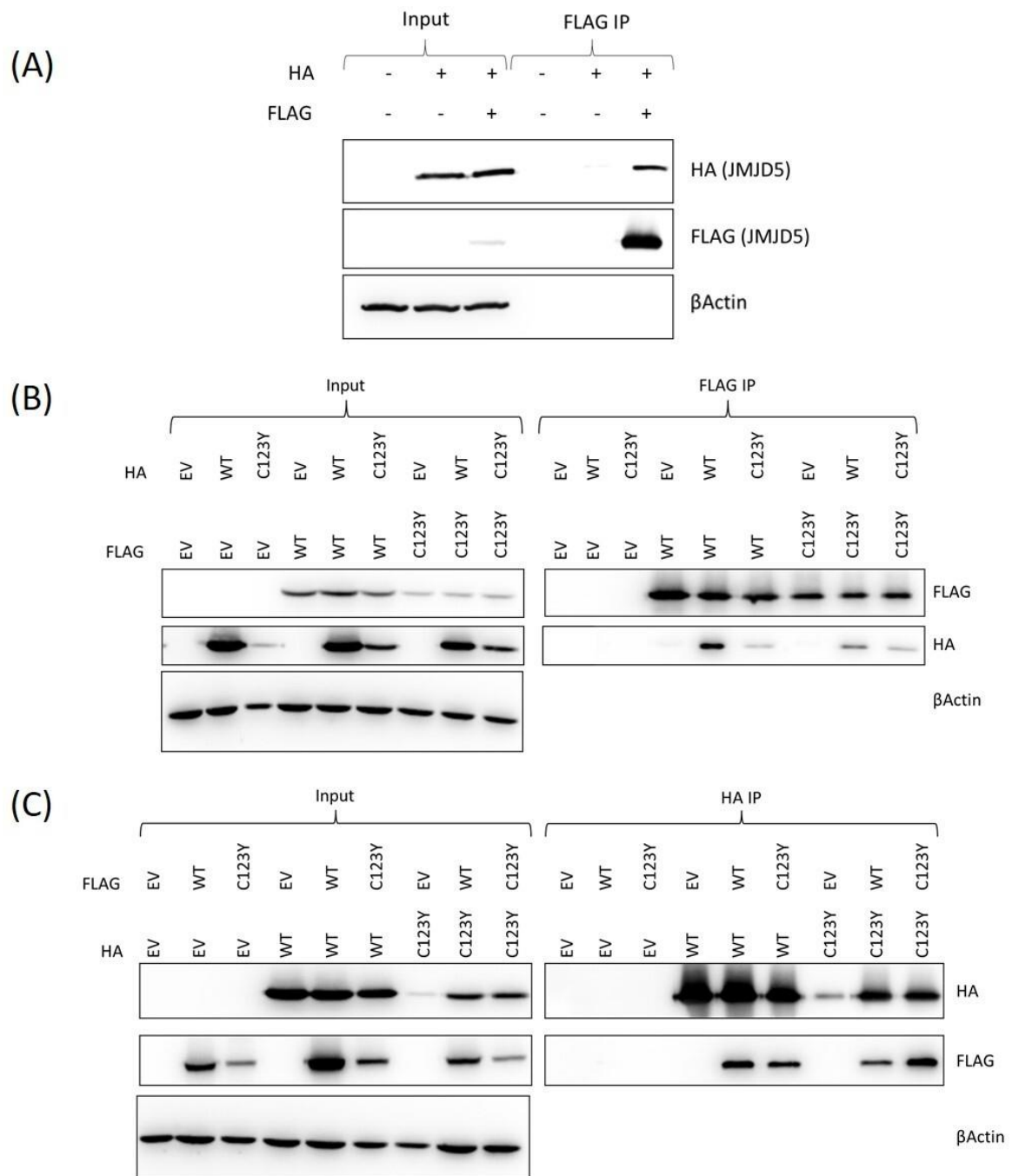
Figure 3.14 JMJD5 wildtype and C123Y can form oligomers

(A) Expression vectors for wildtype JMJD5 with N-terminal HA or FLAG tags were co-transfected into HEK-293T cells. FLAG immunoprecipitates were then analysed by Western blotting to determine presence of the co-transfected HA-tagged construct, indicative of oligomerisation. Empty vector (EV) co-transfected with HA-tagged JMJD5 was used as a negative control. This is representative of an n=1 biological repeat. Expression vectors for N-terminal FLAG-tagged wildtype and C123Y JMJD5 were co-transfected with N-terminal HA-tagged wildtype and C123Y JMJD5. Lysates were then **(B)** FLAG or **(C)** HA immunoprecipitated and analysed by Western blotting. This found that wildtype JMJD5 and C123Y could oligomerise and that C123Y JMJD5 could oligomerise with other C123Y JMJD5 protein. This is representative of n=2 biological repeats. β-actin was used as a loading control. JMJD5 (47 kDa), β-actin (42kDa).

3.7.3 JMJD5 RCCD1 interaction

As discussed in Chapter 1, RCC-domain containing protein 1 (RCCD1) was identified as a binding partner of JMJD5. The interaction domain was mapped to amino acids 1-150 in the N-terminus of JMJD5 (Marcon et al., 2014). As C123 is localised within this domain (Figure 3.11) we next investigated whether the C123Y mutation affected the ability of JMJD5 to interact with RCCD1. To do this we transfected HA-tagged wildtype, catalytic mutant H321A, or C123Y mutant JMJD5 expression vectors into HEK-293T cells. This was followed by HA-immunoprecipitation and Western blotting to determine interaction with endogenous RCCD1.

We found that both JMJD5 wildtype and catalytic mutant H321A were able to interact with RCCD1 (Figure 3.15A). This was expected due to the aforementioned interaction domain being outside of the catalytic domain. We also found that C123Y JMJD5 was able to interact with RCCD1, and the specificity of this was confirmed using an empty vector control (Figure 3.15A). However, our analysis was limited due to the reduced protein expression of C123Y compared to wildtype JMJD5 (Section 3.6). In order to overcome this, we established an *in vitro* pull-down assay. In this assay, HEK-293T whole cell lysate was combined with equalised concentrations of recombinant GST-tagged wildtype or C123Y JMJD5 expressed from *E.coli*. Following this, a GST pull-down was performed and Coomassie staining used to confirm equal loading of the JMJD5 constructs (Figure 3.15B). Endogenous RCCD1 interaction was then determined by Western blotting. We found no difference in RCCD1 interaction between wildtype and C123Y JMJD5 (Figure 3.15B). Consequently, these results suggested that impaired RCCD1 interaction was unlikely to explain the reduced protein stability observed for C123Y (Section 3.6).
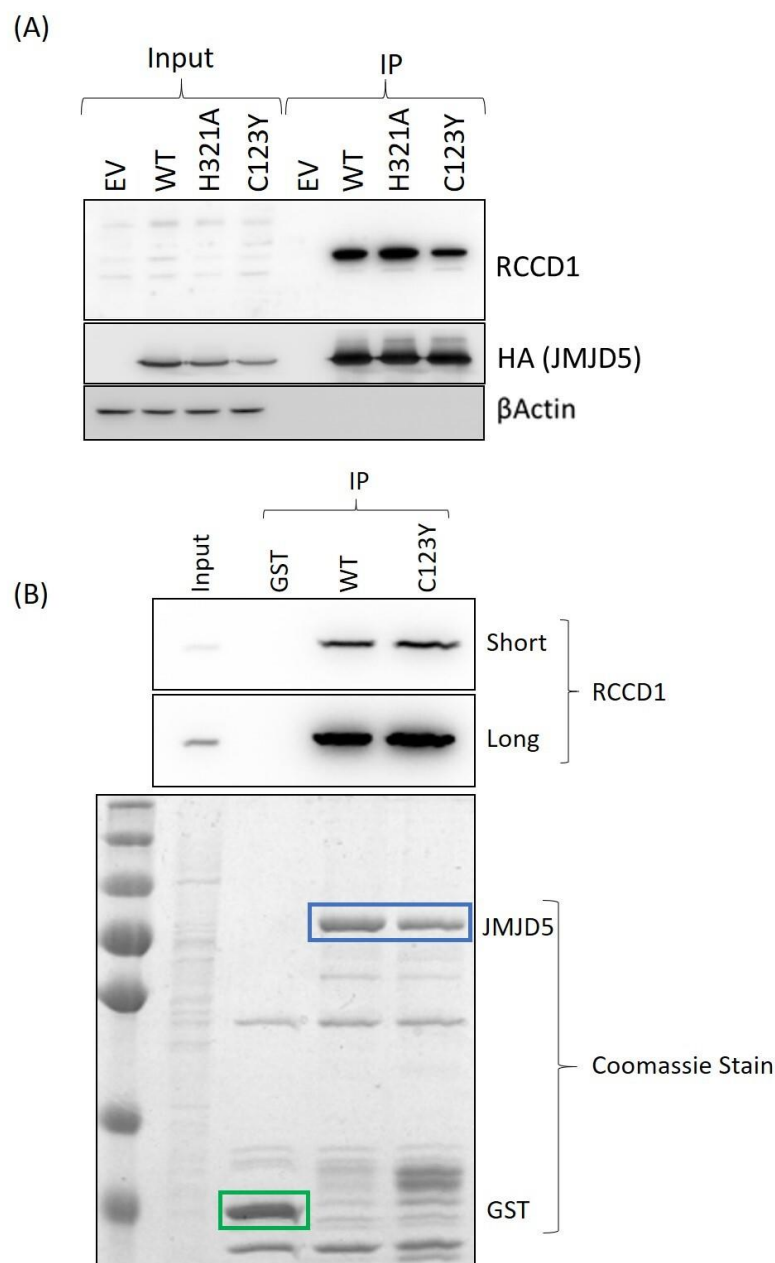
Figure 3.15 JMJD5 binds to RCCD1 independent of catalytic or C123Y mutations

(A) HEK-293T cells were transiently transfected with N-terminal HA-tagged wildtype (WT), C123Y or point mutation H321A expression vectors. HA immunoprecipitation was performed and Western blot analysis used to determine co-immunoprecipitation of endogenous RCCD1. An empty vector (EV) was used as a negative control. β-actin was used as a loading control. This is representative of n=3 biological repeats. **(B)** An *in vitro* interaction was formed between GST-tagged recombinant wildtype (WT) or C123Y JMJD5 with HEK-293T endogenously expressed RCCD1, purified in whole cell lysate. This JMJD5-RCCD1 complex was then purified by GST pull-down using glutathione affinity beads. Coomassie staining was used to demonstrate equal loading of JMJD5 (blue box) or GST epitope tag alone (green box). Western blotting confirmed the interaction between GST-tagged JMJD5 wildtype and C123Y with cell purified endogenous RCCD1. 'Short' and 'long' refer to the length of exposure time used to visualise a Western blot signal. This is representative of an n=1 biological repeat. RCCD1 (40 kDa), β-actin (42kDa).

3.7.4 JMJD5 structure and stability

To further explore the potential mechanisms by which the C123Y mutation destabilises the JMJD5 protein (Section 3.6) we analysed the JMJD5 protein sequence surrounding the C123 residue. We observed three other conserved cysteine residues N-terminal to C123 (Figure 3.16A). As cysteine residues play important structural or functional roles in proteins, due to the presence of a reactive sulphur in its side chain (Betts and Russell, 2003), we predicted C123 could coordinate with the other N-terminal cysteine residues to facilitate JMJD5 folding. To investigate this, we aimed to establish whether these other N-terminal cysteine residues might also be required for JMJD5 protein stability.

To do this each cysteine was mutated individually to a tyrosine (to mimic the C123Y patient mutation) or serine (considered as a conservative substitution). Expression vectors were then transfected into HEK-293T cells and Western blotting used to determine JMJD5 protein expression. We found that C99Y, C105Y and C107Y mutants all had reduced JMJD5 protein expression compared to wildtype, though this was not as significant as the affect observed for C123Y (Figure 3.16B).

Interestingly, C123S mutation also reduced JMJD5 protein expression (Figure 3.16B). This suggests that the reduced C123Y stability is predominantly casued by the loss of cysteine rather than substitution with tyrosine. The only other cysteine to have reduced stability when mutated to a serine was C107 (Figure 3.16B). This observation might be consistent with coordinated activity of C123 and C107 contributing to the JMJD5 stability in this region and could help to explain the loss of stability observed for the C123Y mutant (Section 3.6), a hypothesis to be addressed in the future.
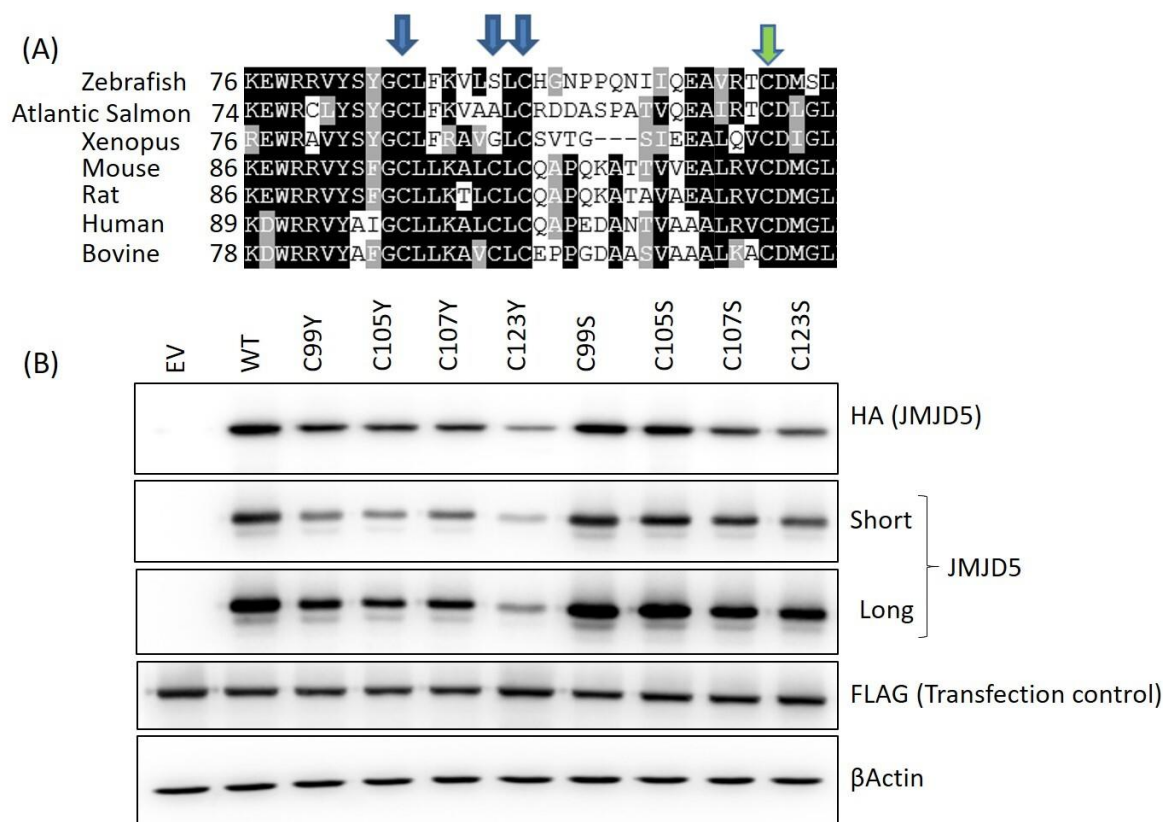
Figure 3.16 Mutation of conserved N-terminal cysteine residues reduces JMJD5 protein expression
(A) Clustal Omega protein sequence alignment between JMJD5 from a variety of species was analysed in the region proximal to C123; the location of the point mutation generating the C123Y mutant. Three other conserved cysteine residues were identified in this region. C123Y marked by green arrow, C99, C105 and C107 marked by blue arrows. Sequences as Table 7.11. **(B)** The four conserved cysteine residues (A) were individually mutated, by site directed mutagenesis, into tyrosine or serine. The expression of these mutant JMNJD5 constructs was then compared to expression of a wildtype JMJD5 construct, by Western blotting, after transient transfection into HEK-293T cells. A FLAG-tagged control was co-transfected to demonstrate transfection efficiency. β-actin was used as a loading control. 'Short' and 'long' refer to the length of exposure time used to visualise a Western blot signal. JMJD5 (47 kDa), β-actin (42kDa). This is representative of an n=1 biological repeat.

3.7.5 JMJD5 enzymatic activity

The JMJD5 literature suggests that its N-terminus may regulate catalytic activity (Hsia et al., 2010). Consistent with this, other regions of JMJD5, outside of the catalytic domain, were found to include residues important for facilitating cofactor binding and mediating substrate release (Wilkins et al., 2018). This evidence raised the possibility that the C123Y mutation might affect JMJD5 enzymatic activity in addition to protein stability (Section 3.6).

In order to investigate this, we optimised an *in vitro* hydroxylation assay. However, as the *bone fide* cellular target of JMJD5 activity is yet to be characterised (discussed in Chapter 1), we made use of a published 'synthetic' peptide substrate consisting of residues 129-144 from the 40S ribosomal protein S6 (RPS6). This peptide has previously been shown to be hydroxylated by JMJD5 *in vitro* (Wilkins et al., 2018). In this assay we incubated equal amounts of recombinant GST-tagged wildtype or C123Y mutant JMJD5 (Figure 3.18A) with cofactors Fe(II), ascorbate and 2-OG plus the RPS6 peptide. We then detected the resulting JMJD5 activity and RPS6 hydroxylation indirectly using the Succinate-Glo™ JmjC Hydroxylase assay kit (Promega). This converts the by-product of the hydroxylation reaction, succinate, into a detectable luminescent signal. This means that the amount of luminescent signal correlates to the amount of succinate produced, which in turn is indicative of the activity level of the 2-OG oxygenase enzyme. We found that the wildtype plus buffer control had increased signal compared to the no enzyme controls (Figure 3.17B), consistent with the JMJD5 literature (Wilkins et al., 2018). This occurs after decarboxylation of 2-OG without the presence of a prime substrate (uncoupled turnover) and is indicative of a functional 2-OG oxygenase (Williams et al., 2014). As expected, the addition of the RPS6 peptide increased the production of succinate by the wildtype JMJD5, consistent with successful hydroxylation (Figure 3.18B). Interestingly, the C123Y JMJD5 mutant had reduced uncoupled turnover suggesting it has lower intrinsic activity compared to wildtype (Figure 2.18B). Consistent with this, activity in response to the addition of the RPS6 peptide was also significantly reduced for the C123Y mutant (Figure 3.17B). However, future investigation will investigate the impurities present in the C123Y recombinant protein preparation (Figure 3.18A), which we cannot rule out might have contributed to the reduced activity detected.
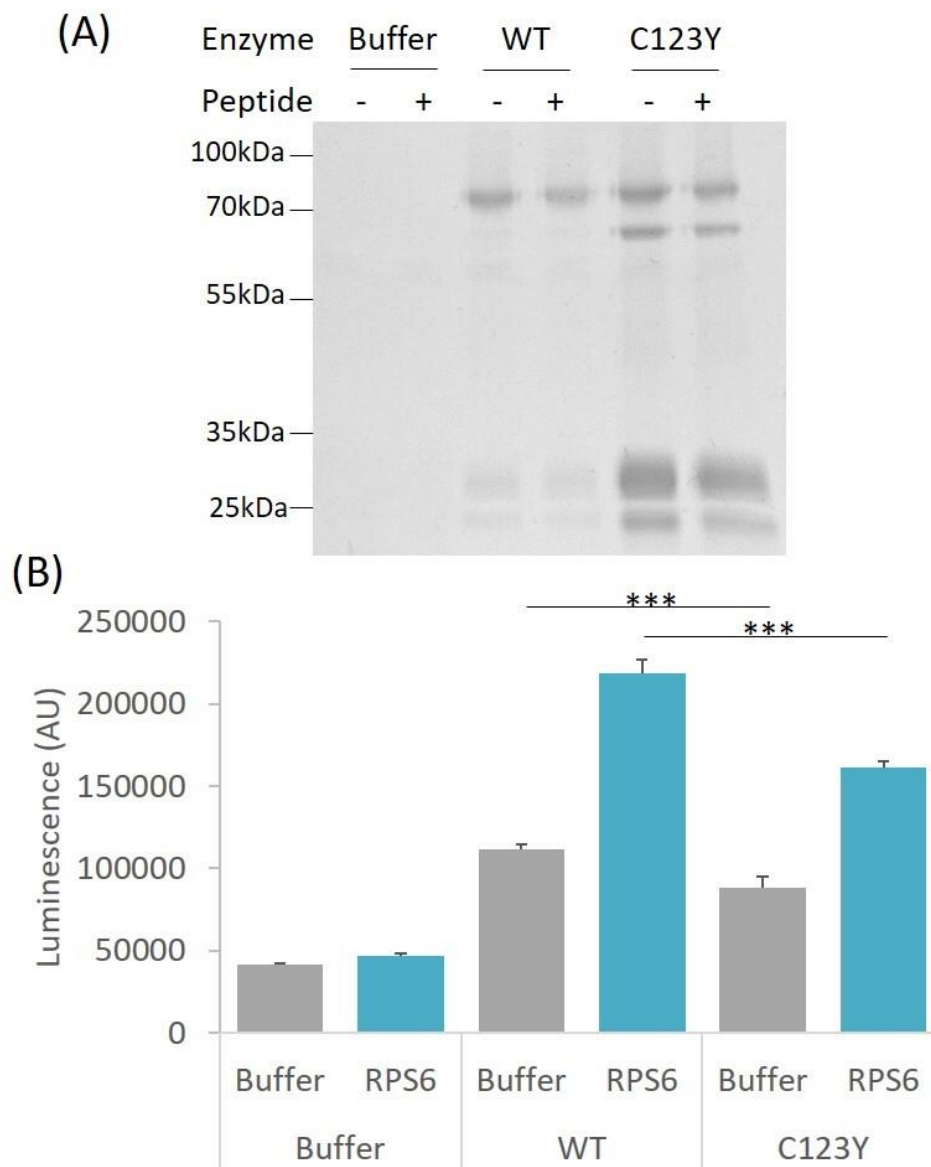
Figure 3.17 The C123Y JMJD5 mutant has decreased hydroxylase activity *in vitro*
GST-tagged recombinant wildtype or C123Y JMJD5 were incubated with Fe^{2+}, ascorbate, 2-OG and a short peptide covering amino acids 129-144 of RPS6; targeted for hydroxylation by JMJD5 in the literature (Wilkins et al., 2018). **(A)** Coomassie staining was used to prove equal loading of the wildtype or C123Y JMJD5 constructs (blue box). **(B)** Successful hydroxylation was determined indirectly using the Succinate-Glo™ JmjC demethylase/hydroxylase Assay, measured by luminescence. This is representative of an n=1 biological repeat, with quadruplicate technical repeats.

Overall, our data suggests that the C123Y mutation may not only affect JMJD5 protein stability but also its activity.

3.8 Discussion

In this Chapter we described work done to characterise two heritable JMJD5 mutations identified in a family affected by a novel developmental disorder. We successfully established immortalised fibroblast cell lines from the family members which we used to confirm the *JMJD5* genotypes. We went on to characterise the JMJD5 mutations with regards to JMJD5 mRNA and protein expression, interactions, stability and enzymatic activity.

3.8.1   Patient derived JMJD5 mutations affect JMJD5 stability and activity

The *JMJD5* mutations carried by the family were an eight-base pair deletion within an intron (InMut) and a point mutation converting an N-terminal cysteine into a tyrosine (C123Y). We identified that all patient derived fibroblasts carrying a JMJD5 mutation were found to have reduced JMJD5 protein expression compared to the wildtype patient (MR98) fibroblasts (Figure 3.8A). The JMJD5 protein expression correlated with the *JMJD5* genotype as it was significantly lower in the affected patient fibroblasts (OR07) that carry both *JMJD5* mutations (Figure 3.8A). Consistent with this both *JMJD5* mutants caused reduced JMJD5 expression which we identified was as a result of reduced protein stability and increased proteolytic degradation (Section 3.7).

During this analysis we found inconsistency for the ability to detect InMut expression between transient transfection and stable expression models (Figure 3.10), which we hypothesise could be due to several reasons. Firstly, the continuous high expression of the InMut protein, driven by maximal doxycycline concentration, could have saturated proteasome degradation (Figure 3.10B). Secondly, the transient transfection system into HEK-293T and HeLa cells may be subjected to a differential rate of protein turnover compared to the patient fibroblasts, for

example, due to the differences in cell proliferation rates (personal observation). It is likely

that a combination of both factors could explain the inconsistency between InMut expression

by the two systems used. However, both models supported the observation that InMut

resulted in reduced JMJD5 protein expression compared to wildtype (Figure 3.10).

3.8.2 Molecular mechanism for InMut reduced JMJD5 stability and activity

The mechanisms by which the C123Y and InMut mutations destabilise JMJD5 protein

expression are likely to be different when considering the difference in nature of the two

mutations. This was confirmed as the InMut mutation was found to have a greater

destabilising effect on the JMJD5 protein compared to the C123Y mutation (Figure 3.10A).

This deletion mutation is located in the intron between exons 7 and 8, which together form a

large proportion of the JmjC catalytic domain of JMJD5 (Figure 3.7A). The mutation was found

to result in the complete loss of mRNA sequence encoding exon 7 (Figure 3.6). We

hypothesised this to be caused by alternative splicing, discussed below.

The online software, HSF, predicted that alternative splicing as a result of the InMut might be

due to loss of enhancer sites from the intron sequence between exons 7 and 8 (Figure 3.5B).

Splicing enhancers, localised within introns or exons, can facilitate spliceosome assembly via

recruitment of arginine-serine (SR) splice factors, whereas splicing silencing sites prevent

splicing at pseudo-exons. Together these regulatory elements help to define splice sites and

boundaries between introns and exons (Wang and Burge, 2008).Therefore, the loss of an

enhancer site within an intron would potentially make intron-exon boundary identification

less optimal (Shen and Green, 2006). The HSF predicted enhancer site for this intron was

proximal to the 5' splice site (Figure 3.5B). Therefore, loss of an enhancer at this location could

render the 5' splice site ineffective and result in alternative splicing. Consequently, we propose

that the InMut results in alternative splicing of mRNA coding sequences linking exon 6 to exon

8 and causing the skipping of exon 7 (model depicted in Figure 3.18).
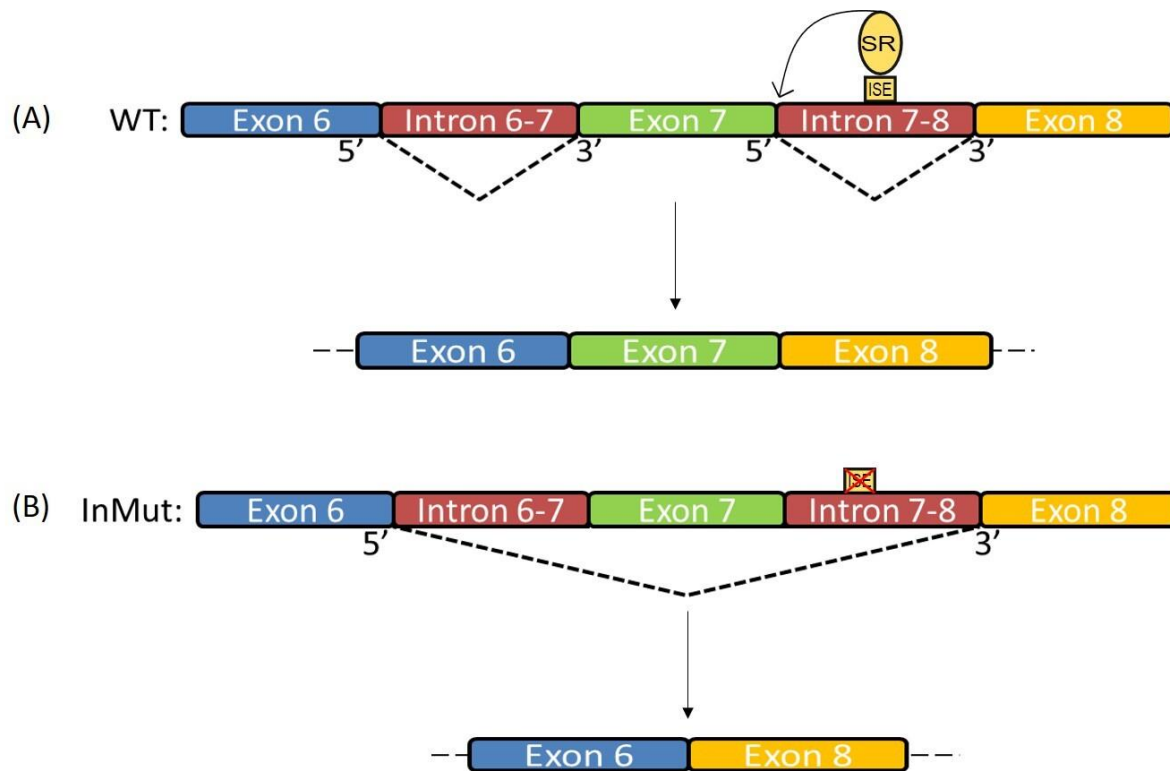
Figure 3.18 Predicted alternative splicing of JMJD5 mRNA as a result of the InMut mutation
This figure represents a hypothetical model of the alternative splicing that might occur due to the InMut. **(A)** Wildtype JMJD5 mRNA sequence is spliced as normal between exons 6, 7 and 8. This is facilitated by the presence of an intron splice enhancer (ISE) located within the intron between exons 7 and 8 (predicted by HSF, Figure 3.5). This ISE is likely to interact with arginine-serine (SR) splicing factors that promote the identity of the 5' splice site at this intron-exon boundary. **(B)** This ISE could be lost due to the eight-base-pair deletion within the intron between exons 7 and 8 (InMut). This could contribute to reduced identification of the 5' splice site by the spliceosome. This is likely to cause splicing between exons 6 and 8, resulting in the skipping of exon 7.

When mapped onto the JMJD5 crystal structure this removal of exon 7 from the protein

sequence causes loss of structural folds essential for folding of the JmjC catalytic domain

(Figure 3.7). In JMJD5, the JmjC domain is formed by amino acids 174 to 416, including the N-

terminal JmjC extension, and forms a topology of helical and β-strands. The core of this is the

DSBH that is supported by α- and 3_{10}-helices (Wilkins et al., 2018). Protein sequence encoded

by exon 7, which is lost from InMut JMJD5, comprises amino acids 331 to 362 (Figure 3.7). This encompasses the C-terminal end of β-strand III, all of β-strand IV, all of helix α6, and the majority of the βIV-βV insert loop which all are incorporated into the DSBH core structure (Wilkins et al., 2018). Since the tertiary folding of this region requires multiple interactions the loss of any section of the DSBH could impact the folding of the remaining JmjC domain, making the observation that InMut causes reduced JMJD5 protein stability unsurprising.

Importantly, loss of protein sequence encoded by exon 7 would also directly inhibit JMJD5 enzymatic activity. Firstly, an important cofactor binding residue (N327) that forms hydrogen bonds with the C_1 carboxylate of 2-OG, localised in the βIII domain, would be lost (Del Rizzo et al., 2012, Wang et al., 2013, Wilkins et al., 2018). Secondly the βIV-βV insert loop, formed by amino acids 342 to 381 would be lost. This domain creates a mobile region which along with the β3-β4 loop of the N-terminal JmjC extension, forms a 'gating' mechanism to facilitate substrate binding and product release during catalysis (Wilkins et al., 2018). In the substrate bound structure the βIV-βV insert loop forms a partial helical confirmation, whilst in the apo-protein it forms a hairpin structure that folds towards the β3-β4 loop to enclose the active site (Wilkins et al., 2018). This flexible βIV-βV insert loop appears to be important for JmjC-only protein hydroxylases, and not for JmjC KDMs, and is therefore likely to be essential for JMJD5 catalytic activity (Wilkins et al., 2018).

Taken together, we predict that the alternatively spliced InMut protein is unable to fold correctly due to the incomplete DSBH domain. This would cause it to be targeted for ubiquitination and rapid turnover by the proteasome (Figure 3.10B), with any residual InMut JMJD5 protein being smaller in size (Figure 3.10C and 3.11B) and catalytically inactive.

3.8.3   Molecular mechanism for C123Y reduced JMJD5 stability and activity

The C123Y mutant protein on the other hand, although less stable than wildtype JMJD5, was significantly more stable than the InMut protein (Figure 3.9 and 3.10A). As the C123 residue was found to be conserved among orthologues of JMJD5 we predicted that this residue might be important for a JMJD5-specific role (Figure 3.8). Consequently, we were interested to investigate whether C123Y JMJD5 had an altered function which could help to explain the reduced stability of this mutant. Unfortunately, the crystal structure of the N-terminus of JMJD5 is unsolved, plus the sequence is not conserved in other JmjC-only family members (Figure 3.8A). Therefore, we used current literature regarding the N-terminus of JMJD5 to investigate the potential properties of the C123Y mutation. However, we observed that the C123Y mutation did not affect JMJD5 nuclear localisation (Section 3.7.1), oligomerisation (Section 3.7.2) or its interaction with RCCD1 (Section 3.7.3). We did observe that the C123Y mutation had reduced catalytic activity when compared to wildtype JMJD5. However, it should be noted that this experiment (Figure 3.17) is a single biological repeat and so attempts to replicate this should be made before reliable conclusions can be drawn. In addition, the sub-optimal activity of C123Y JMJD5 could be explained by the reduced stability of this mutant. To test this hypothesis the assay could be repeated at a lower temperature, where the mutant should be more stable. Overall, the mechanism by which the C123Y mutation affected stability of JMJD5 remained unclear.

To investigate this further we used bioinformatics to assess the potential consequence of the C123Y mutation. Two online software tools, SIFT and PolyPhen-2, predicted that the C123Y mutant would be highly deleterious to JMJD5 (Section 3.5). One significant difference between tyrosine and cysteine is the change in amino acid size. Cysteine is a small amino acid and substitution with a large amino acid, such as tyrosine, could induce steric clashing and impact tertiary folding. Another difference is the change in functional side chains. Cysteine contains a reactive sulphur group, not found in tyrosine, which has important structural or functional roles by forming disulphide bonds or by coordinating metal ions (Betts and Russell, 2003). Taken together we hypothesised that the reduced expression observed for the C123Y mutation could be due to improper folding. We predicted that this folding was likely to be dependent on the activity of the cysteine functional side chain. This is because mutation to a serine, which is a comparable in size to cysteine but lacks the sulphur side chain, still resulted in reduced JMJD5 protein expression (Figure 3.16). A similar result was observed for another conserved N-terminal cysteine residue (at residue 107) when mutated to serine. Considering the properties of cysteine, we hypothesised that these residues could act together to stabilise JMJD5, for example by coordinating a metal ion or forming a disulphide bond. However, it should be noted that due to the lack of conservation for C105 it is unlikely that the four cysteine residues identified in Figure 3.16 establish a zinc finger. Instead cysteine or histidine residues from other regions of the N-terminus, or from other domains in JMJD5, could be involved. Consistent with this hypothesis, zinc fingers between JmjC domains and distal regions of other 2OG oxygenases have been identified to be important for folding (Chen et al., 2006). However, in order to address limitations of our current expression data (Figure 3.16B) future analysis will be required. Firstly, additional repeats should be performed to establish

the reliability of our current observations. Secondly, future experiments will include point mutations of the conserved N-terminal cysteine residues into alanine. This will address whether the cysteine to serine mutations made in our current experiment (Figure 3.16B) infer any other functional change that could implicate structural instability. Finally, acquisition of a crystal structure including the N-terminus of JMJD5 would be hugely beneficial for understanding the implications of the C123Y mutation.

3.8.4 Could the affected patient *JMJD5* genotypes be pathogenic?

Interestingly the growth defect of the affected patients (Table 3.1) was consistent with a JMJD5 mouse model whereby JMJD5 knockdown resulted in growth defects (Oh and Janknecht, 2012, Ishimura et al., 2012, Ishimura et al., 2016). Similar to this mouse model our affected patient fibroblasts were found to have reduced JMJD5 protein expression (Figure 3.8A). This led us to hypothesise that the affected patient *JMJD5* genotype could be pathogenic.

The growth phonotype and lethality of the JMJD5 knockdown mouse model was explained by upregulation of the p53 target gene p21 by JMJD5 (Oh and Janknecht, 2012, Ishimura et al., 2012, Ishimura et al., 2016) which was supported by other evidence in the literature linking JMJD5 and the p53/p21 pathway (Zhu et al., 2014, Wu et al., 2016a). Consequently, we hypothesised that this association between JMJD5 and p53/p21 pathway might help explain cellular phenotypes of the patient fibroblasts. For example, the p53/p21 pathway has been well characterised with regards to senescence (Qian and Chen, 2013). Therefore, the *JMJD5* genotype of the MR10 primary fibroblasts could have made them more susceptible to senescence during the immortalisation process (Figure 3.3). However, this hypothesis is not

supported by other JMJD5 knockdown studies (Ishimura et al., 2012) and the other affected

patient fibroblasts (OR07) which did not demonstrate increased susceptibility to senescence.

This means that the molecular defect that drove MR10 into senescence is not clear. It could

be that MR10 primary fibroblasts entry into senescence was a consequence of the stress of

tissue culture, retroviral infection and the subsequent selection using Hygromycin.

Alternatively, subtle differences in the MR10 patient genetic background could have

exacerbated the cellular response to reduced JMJD5 expression. This will be addressed by

further phenotyping these patient fibroblasts to identify deficient cellular processes that could

explain this senescence.

3.8.5   Affected patients are JMJD5 hypomorphs?

From the evidence in this chapter we hypothesise that the affected patient fibroblasts are

hypomorphic for JMJD5 and thus have partial JMJD5 expression and activity. Consistent with

this JMJD5 protein expression was significantly reduced for the affected compared to

unaffected patient fibroblasts (Figure 3.9). Also, we propose that any JMJD5 protein expressed

in these affected patient fibroblasts would be comprised of the C123Y mutant, due to it being

a similar molecular weight as wildtype JMJD5 and being more stable than the InMut protein

(Figure 3.9, 3.10 and 3.11). In addition, we proposed that this C123Y mutant potentially had

reduced catalytic activity compared to wildtype JMJD5 (Figure 3.17), which might further

support our hypothesis that the affected patients are hypomorphic for JMJD5.

3.8.6 Chapter conclusions

Although mutation of other JmjC domain 2OG-oxygenases has been associated with developmental disorders (discussed in Chapter 1), the family investigated in this chapter represent the first report of a developmental disorder associated with JMJD5 mutations. Therefore, the patient fibroblasts provide a valuable platform to investigate JMJD5 function. Therefore, we next aimed to phenotype fibroblasts isolated from these patients to help clarify and broaden the current literature regarding JMJD5. We also hoped this analysis would provide a more informed clinical diagnosis for the patients. This phenotyping is continued in Chapter 4 by investigating the JMJD5 enzymatic activity and in Chapter 5 by investigating the cellular role of JMJD5.

4 Investigation into the Enzymatic activity of JMJD5

In the previous chapter we began to characterise a novel human developmental disorder associated with two JMJD5 mutations. We propose that further understanding of how JMJD5 might contribute to this developmental disorder could be acquired by investigating the catalytic activity of JMJD5. Therefore, in this chapter we utilised the immortalised patient fibroblast cell lines, as well as other cellular models and *in vitro* assays, to help clarify the catalytic activity of JMJD5.

As discussed in Chapter 1, the literature regarding the catalytic activity of JMJD5 has been highly controversial. Initially JMJD5 was identified as a lysine demethylase targeting H3K36me2 and was thus named KDM8 (Hsia et al., 2010). Since then it was also implicated as an endopeptidase that clipped histone tails (Shen et al., 2017, Liu et al., 2017, Liu et al., 2018a). However, combined biochemical, structural and primary sequence conservation analyses did not support the assignment of these activities (Del Rizzo et al., 2012, Wang et al., 2013, Wilkins et al., 2018). In agreement with this, JMJD5 was characterised as a protein hydroxylase targeting arginine residues (Wilkins et al., 2018). However, no physiologically relevant substrate has yet been identified, therefore, in this chapter we aimed to address this.

We first investigated whether or not the proposed catalytic activities of JMJD5, as described by the current literature, were reproduced in our models. These negative results led us to initiate proteomic screening that aimed to discover a JMJD5 hydroxylation substrate. This approach identified two subunits of the mini-chromosome maintenance (MCM) DNA replication helicase complex (MCM3 and MCM5), that interacted with JMJD5 in a substrate-

like manner. Following this, a series of cellular and *in vitro* assays were used to try and narrow down the position of the putative hydroxylation site within these candidate substrates. Finally, we explored the potential consequences of this hydroxylation event by investigating two cellular disease models that are associated with JMJD5 mutations.

4.1 Investigation into currently proposed JMJD5 substrates

The majority of literature surrounding JMJD5 suggests it functions as a KDM targeting H3K36me2 (discussed in Chapter 1). These studies, relying on overexpression and/or knockdown approaches report global changes in H3K36me2 levels (Hsia et al., 2010, Ishimura et al., 2012, Amendola et al., 2017). Therefore, to begin characterising the enzymatic activity of JMJD5 we first investigated whether we could detect global changes in H3K36me2 levels in our fibroblast models (Chapter 3). Our rationale was that if JMJD5 directly regulated the demethylation of H3K36me2, we would observe an inverse correlation between expression levels of JMJD5 and H3K36me2. To this end, fibroblasts from the JMJD5 wildtype control (MR98), C123Y carrier (LR74), InMut carrier (AR00) and affected patient (OR07) were analysed. We performed sub-cellular fractionation to isolate chromatin and nuclear fractions that were then analysed by Western blotting for H3K36me2 expression levels. This analysis first confirmed our previous observations that the affected patient (OR07) fibroblasts had reduced JMJD5 protein expression compared to unaffected fibroblasts (Figure 4.1A). However, we observed no correlation between JMJD5 and H3K36me2, as levels were not significantly altered across the patient fibroblasts (Figure 4.1A).

To further investigate this, we performed sub-cellular fractionation on our doxycycline inducible MR98 fibroblast cell lines that over-express wildtype or inactive H321A JMJD5

(Section 5.4.1, Chapter 5). The histidine at position 321 is one of the essential residues forming the HxD…H catalytic motif that coordinates the Fe(II) ion (Del Rizzo et al., 2012, Wang et al., 2013, Wilkins et al., 2018). Consequently, point mutation to alanine renders JMJD5 catalytically inactive (Wilkins et al., 2018). Therefore, we used this H321A mutant construct to determine whether any changes to H3K36me2 levels were dependent on JMJD5 catalytic activity. We analysed the samples by Western blotting to explore how over-expression of JMJD5 might affect H3K36me2 levels. We found that H3K36me2 expression levels were comparable between doxycycline treated and untreated, and between JMJD5 wildtype and H321A samples (Figure 4.1B). Therefore, we concluded that H3K36me2 levels were not regulated by JMJD5 or its catalytic activity.

Using the fractionation samples described above, we next investigated whether JMJD5 was able to mediate histone H3 tail clipping in our models. In papers proposing this JMJD5 function they observed a faster migrating band, detected by Western blot using a histone H3 antibody, that they assigned as the clipped form of histone H3 (Shen et al., 2017, Liu et al., 2017, Liu et al., 2018a). Therefore, we investigated whether we could observe this cleavage product in our cell models. We identified a smaller migrating histone H3 band in only one experimental repeat, whilst analysing the MR98 over-expression fibroblast cell lines (arrow Figure 4.1B). However, this band did not correlate with JMJD5 expression or activity in either fibroblast model (Figure 4.1). Therefore, we were unable to detect any evidence of JMJD5-dependent histone H3 tail clipping in our cell models.
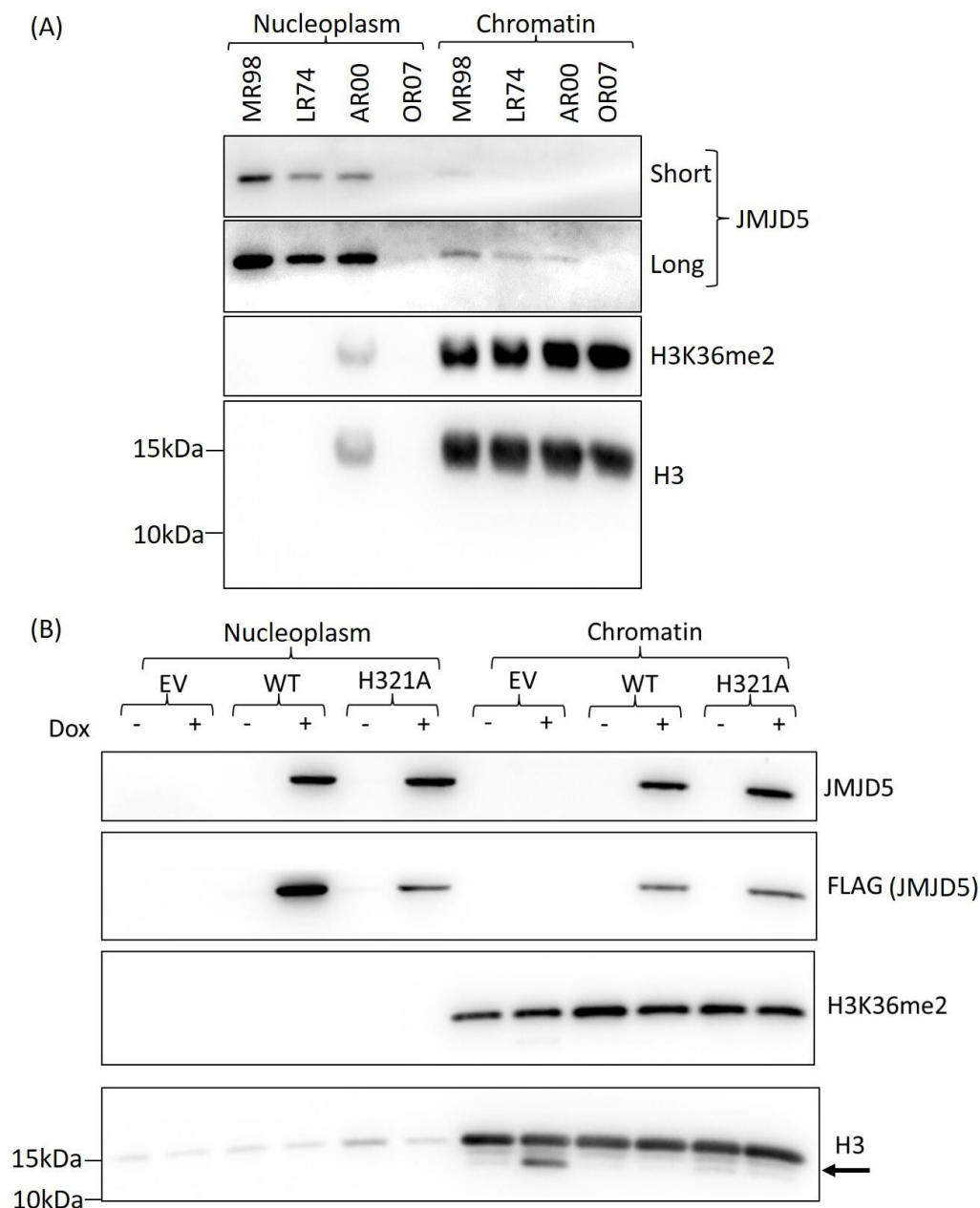
Figure 4.1 Investigating the H3K36me2 demethylation and histone clipping activity of JMJD5
(A) Western blotting analysis of sub-cellular fractionation samples generated from immortalised dermal fibroblasts from patients expressing wildtype JMJD5 (MR98), the C123Y JMJD5 mutation (LR74), the InMut mutation (AR00) or carrying both JMJD5 mutations (OR07). **(B)** Western blot analysis of sub-cellular fractionation performed on MR98 cell lines treated with 1 μg/mL doxycycline for 48 hours to induce expression of FLAG-tagged wildtype JMJD5 or catalytic mutant H321A. Samples analysed for H3K36me2 expression levels and histone H3 clipped product (identified by arrow). Empty vector (EV) used to determine basal levels of H3K36me2 and histone H3 clipped products. Histone H3 (H3) used as a loading control for the chromatin fraction. 'Short' and 'long' refer to the length of exposure time. JMJD5 (47 kDa), H3 (15 kDa), β-actin (42kDa). This figure is representative of n=3 biological repeats for both experiments.

As neither H3K36me2 KDM or histone H3 endopeptidase activities were observed in our models we next investigated whether JMJD5 could interact with the proposed protein hydroxylation substrate ribosomal protein S6 (RPS6) (Wilkins et al., 2018). In this study, Wilkins et al. (2018) demonstrated that JMJD5 could target a synthetic peptide of RPS6 for hydroxylation *in vitro* (we confirmed this in Figure 3.17, Chapter 3). To identify whether RPS6 was a genuine JMJD5 hydroxylation substrate we investigated whether an interaction between RPS6 and JMJD5 occurred in cells. This analysis was performed using our doxycycline-inducible FLAG-tagged JMJD5 MR98 fibroblast cell lines. The presence of endogenous RPS6 was monitored in FLAG immunoprecipitates by Western blotting (methods detailed in Section 7.11.1). Surprisingly, we did not detect endogenous RPS6 interacting with either wildtype or catalytically inactive H321A JMJD5 (Figure 4.2). This was also in spite of incubating cells with DMOG, known to stabilise other 2OG oxygenase complexes with their substrates (discussed below). Therefore, we hypothesised that RPS6 was unlikely to be a true biological hydroxylation substrate of JMJD5 in our cell models.
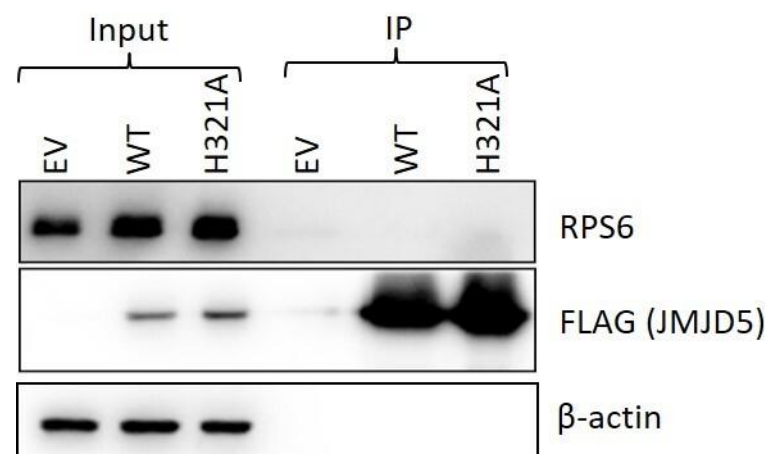
Figure 4.2 Investigating RPS6 interaction with JMJD5 as a potential hydroxylation substrate
MR98 FLAG-tagged JMJD5 wildtype or H321A cell lines were treated with 1 µg/mL doxycycline for 48 hours including 1 mM DMOG for 16 hours before performing FLAG-immunoprecipitation in the presence of 1 mM NOG. Western blotting demonstrated no interaction between JMJD5 endogenous RPS6. β-actin used as a loading control for input samples. Empty vector (EV) used to prove specificity. RPS6 (29 kDa), JMJD5 (47 kDa), β-actin (42kDa). This is representative of n=3 biological repeats.

4.2 Identification of two candidate hydroxylation substrates

We were unable to replicate, in our cell models, any of the proposed JMJD5 substrates currently published in the literature. Therefore, we aimed to explore novel hydroxylation substrate candidates in order to investigate further the catalytic activity of JMJD5. To this end, we carried out a proteomic screen to identify proteins that interacted with JMJD5 in an activity-dependent manner. This approach has been successful for identification of novel hydroxylation substrates of related 2OG oxygenases, such as JMJD4 and JMJD7 (Feng et al., 2014, Markolovic et al., 2018). Briefly, FLAG-tagged wildtype or H321A JMJD5 were constitutively over-expressed in cells before performing FLAG immunoprecipitation (methods detailed in Section 7.11.1). Complexes were eluted with FLAG peptide and proteins identified by Mass Spectrometry (MS). The MS and associated analysis were performed by the Advanced Mass Spectrometry Facility, Oxford University.

A stable enzyme-substrate complex was generated for this MS analysis by incubating the cells and performing subsequent immunoprecipitation reactions in the presence of the pan-inhibitor of 2-oxoglutarate oxygenases, N-oxalylglycine (NOG, the cell soluble derivative is dimethyloxalylglycine, DMOG). This small molecule inhibitor acts as a mimetic of the co-factor 2-OG. However, it is unhydrolysable meaning 2-OG oxygenases remain locked in a substrate-bound intermediate complex (Rose et al., 2011). Consequently, NOG can be used to infer whether an interaction with a 2-OG oxygenase occurs in its catalytic site and in a substrate-like manner.

The top hits identified in the MS screen are shown in Table 4.1. To generate this list, we excluded any proteins present in the empty vector sample, to remove proteins non-specifically interacting with the anti-FLAG beads. We then analysed the data set for proteins whose abundance was significantly reduced in the H321A catalytic mutant sample compared to the wildtype sample. This allowed us to screen for proteins interacting with JMJD5 in an activity-dependent manner. This approach identified two members of the mini-chromosome maintenance complex (MCM) 3 and 5 (Table 4.1). Although these proteins were clearly enriched in the wildtype JMJD5 pulldown, MCM proteins are common contaminants of MS analysis due to their high abundance. Therefore, we aimed to clarify these results by Western blotting samples from independent immunoprecipitates. From this we confirmed that MCM3 and MCM5 co-immunoprecipitated with JMJD5 in an activity-dependent manner (Figure 4.3). This was specific as neither protein was present in the control (empty vector) sample and other MCM subunits, such as MCM7, did not interact with JMJD5 (Figure 4.3). Importantly, RCCD1 bound to JMJD5 independently of enzyme activity, consistent with it not being a substrate (Figure 4.3). The interaction of RCCD1 with both enzymes also confirmed that the lack of MCM3/5 binding to the H321A mutant was not due to an indirect effect, such as improper JMJD5 folding. Other proteins identified by this screen (Table 4.1) were not reproduced in subsequent screens, suggesting that these are false positives (Dr Mathew Coleman).

Table 4.1 Mass spectrometry results of co-immunoprecipitated proteins with wildtype JMJD5
MDA-231 cell lines constitutive to over-express FLAG-tagged JMJD5 wildtype or H321A were treated with 1 mM DMOG for 16 hours prior to FLAG-immunoprecipitation in the presence of 1 mM NOG. Immunoprecipitation samples were analysed by mass spectrometry (MS). Quantitation and analysis of the MS data was undertaken using Progenesis software by the Oxford Advanced Mass Spectrometry facility to identify proteins whose binding was reduced in the H321A sample relative to the wildtype (WT) sample (with correction for the amount of FLAG-JMJD5 'bait' detected). Data was then ranked according to the confidence and probability (Anova test) of the assignment. Filters were applied including a minimal fold change in interaction of 2.5, and a maximum probability of 0.001. This was determined using n=2 technical repeats. Based on the increased number of peptides, confidence, probability and abundance (emPAI score) this predicted MCM3 and MCM5 as substrates of JMJD5.

Protein	Accession	Unique Peptides	Confidence	Anova (p)	emPAI (WT)	Fold change (WT/H321A)
MCM3	Q8N371	35	2868	1.37E-05	4.84(1) 4.29(2)	5.2
MCM5	Q7Z6P5	31	2028	5.03E-05	3.65(1) 3.92(2)	21.8
USP16	Q96AG3	9	611	0.0006	0.49(1) 0.65 (2)	11.9
GNB1L	Q9BYB4	7	573	0.0001	1.48(1) 1.48(2)	5.1
LEMD3	Q9Y2U8	8	512	0.0006	0.53(1) 0.39(2)	4.5
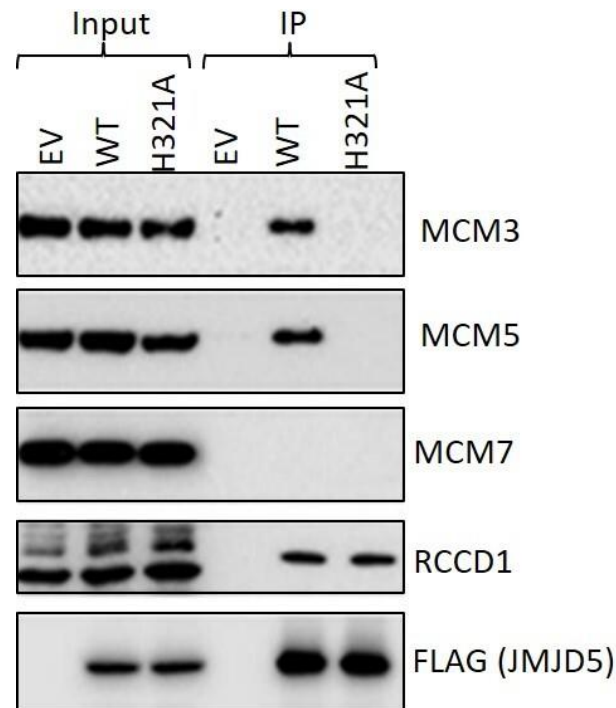
Figure 4.3 MCM3 and MCM5 interact with JMJD5 in a substrate-like manner
MDA-231 cells constitutive to over-express FLAG-tagged JMJD5 wildtype or H321A were treated with 1 mM DMOG for 16 hours prior to FLAG-immunoprecipitation in the presence of 1 mM NOG. Samples were analysed Western blotting to determine interaction of endogenous MCM3, MCM5, MCM7 and RCCD1 with JMJD5. Empty vector (EV) included to prove specificity. MCM3 (91 kDa), MCM5 (82 kDa), MCM7 (81 kDa), RCCD1 (40 kDa), JMJD5 (47 kDa). This is representative of n=3 biological repeats.

To further investigate whether the JMJD5 MCM3/5 interaction was dependent on the catalytic activity of JMJD5 we further interrogated the NOG (DMOG) pan-inhibitor of 2-OG oxygenases. The following experiment was performed by Dr Sally Fletcher (Coleman lab). HA-tagged JMJD5 wildtype and H321A expression vectors were transiently transfected into HEK-293T cells for 24 hours before incubating the cells with or without DMOG for 16 hours. Cell extracts were immunoprecipitated with anti-HA agarose beads and immunoprecipitates analysed by Western blotting (methods as described in Section 7.11.1). We found that as before, endogenous MCM3 and MCM5 interacted with wildtype JMJD5 but not the H321A mutant. Importantly, treating cells with DMOG significantly increased the interaction of MCM3 and MCM5 with only wildtype JMJD5 (Figure 4.4). This result was consistent with our hypothesis that MCM3 and MCM5 bind to JMJD5 in a substrate-like manner.
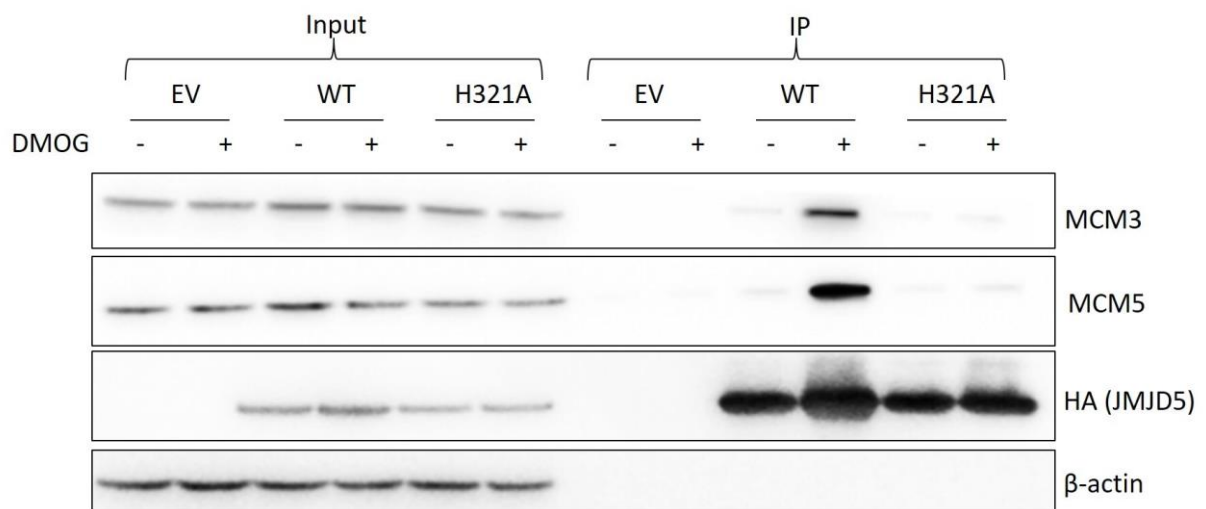
Figure 4.4 MCM3 and MCM5 interaction with wildtype JMJD5 increases in the presence of DMOG
HEK-293T cells transiently transfected with HA-tagged JMJD5 wildtype or H321A expression vectors were treated with or without 1 mM DMOG for 16 hours prior to HA-immunoprecipitation (1 mM NOG included if cells were treated with DMOG prior to immunoprecipitation). Western blotting performed to determine MCM3 and MCM5 interaction with JMJD5. Empty vector (EV) control included to prove specificity. β-actin used as a loading control for input samples. MCM3 (91 kDa), MCM5 (82 kDa), JMJD5 (47 kDa), β-actin (42kDa). This is representative of n=3 biological repeats, performed by Dr Sally Fletcher.

Overall, the results presented above suggest that MCM3 and MCM5 interact with JMJD5 in a substrate-like manner. We were next interested to test whether this interaction could be relevant in our patient fibroblast models (Chapter 3). Therefore, we repeated the co-immunoprecipitation experiment (Section 7.11.1) using our doxycycline inducible JMJD5 over-expression MR98 cell lines. As expected, MCM3 and MCM5 interacted with wildtype JMJD5, but not the H321A catalytic mutant (Figure 4.5).
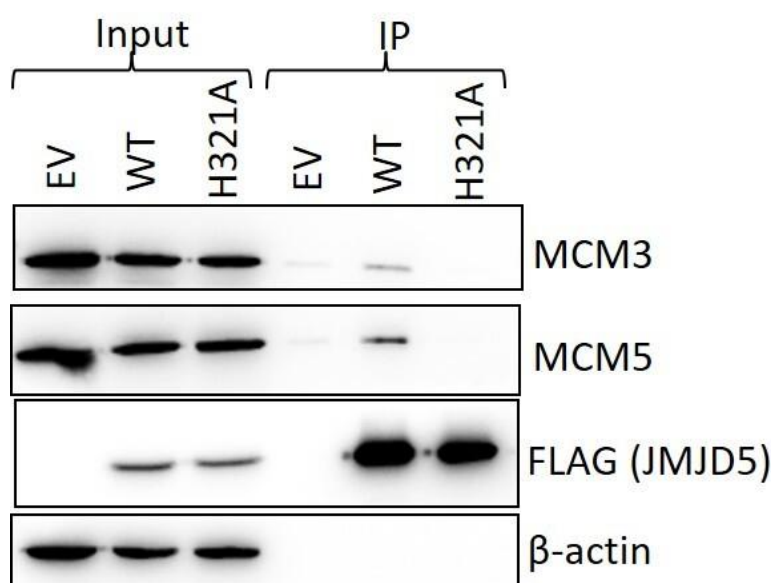
Figure 4.5 MCM3 and MCM5 interact with JMJD5 in fibroblast cellular model
MR98 fibroblast cell lines were treated with 1 µg/mL doxycycline for 48 hours for over-expression of FLAG-tagged JMJD5 wildtype or H321A, then with 1 mM DMOG for 16 hours prior to FLAG-immunoprecipitation in the presence of 1 mM NOG. Western blotting then used to determine endogenous MCM3 and MCM5 interaction with JMJD5. Empty vector (EV) control included to prove specificity. This is representative of n=3 biological repeats. β-actin used as a loading control for input samples. MCM3 (91 kDa), MCM5 (82 kDa), JMJD5 (47 kDa), β-actin (42kDa).

4.3 Assay optimisation to investigate a JMJD5 hydroxylation site

In order to test whether candidate substrates MCM3 and MCM5 were the targets of JMJD5 catalytic activity we endeavoured to identify a hydroxylation site. We predicted that JMJD5 would target arginine residues for hydroxylation in highly basic regions of MCM3/5. Firstly, because Wilkins et al. (2018) demonstrated arginine hydroxylation on a peptide of RPS6.

Secondly, analysis of the JMJD5 crystal structure revealed an acidic substrate binding domain that was predicted to interact with a basic substrate (Del Rizzo et al., 2012, Wang et al., 2013).

Two approaches were adopted to try and identify the hydroxylation site on MCM3 and/or MCM5: 1) cellular models to purify endogenous or exogenous MCM proteins (Section 4.3.1), and 2) *in vitro* assays aimed at identifying minimal interaction domains (Section 4.3.2).

4.3.1 Cellular Models

The aim of our cellular models was to purify sufficient endogenous MCM3 and MCM5 in order to identify a hydroxylation site by MS analysis. First, we attempted to purify the complete endogenous MCM complex from HEK-293T cells using antibodies targeting MCM3, MCM5 and MCM7 subunits, using an anti-FIH antibody as a negative control. The antibodies were bound to protein A agarose beads and incubated with HEK-293T cell extract for immunoprecipitation. These samples were then separated by polyacrylamide gel electrophoresis and successful co-immunoprecipitation analysed by Coomassie staining (Figure 4.6A).

Unfortunately, we found that the MCM3 antibody was not effective at purifying any of the MCM subunits, as no bands were detected by Coomassie staining (Figure 4.6A). However, co-immunoprecipitation using the MCM5 and MCM7 antibodies was more successful (Figure 4.6A). The Coomassie stained bands from these samples were excised and MS used to determine their identity. The three bands in the MCM7 immunoprecipitation were identified as MCM4, MCM6 and MCM7, and band number two in the MCM5 immunoprecipitation was identified as MCM5 (Figure 4.6B and C). Unfortunately, band number one from the MCM5 immunoprecipitate could not be identified by the MS analysis, likely due to a technical problem during MS sample preparation. However, because MCM5 is predicted to exist in a

sub-complex with MCM3 (DaFonseca et al., 2001), we proposed that this was likely the identity of the second band. To test this hypothesis the MCM5 immunoprecipitation reaction was repeated and analysed by Western blotting. We identified that MCM3 was able to co-immunoprecipitate with MCM5 (Figure 4.6C).

Whilst repeating this MCM5 immunoprecipitation, we took this opportunity to also test the ability of an anti-MCM2 antibody to co-immunoprecipitate MCM3 and MCM5 (demonstrated in the datasheet to pulldown the complete MCM complex, Bethyl). Although this antibody was able to pull-down large amounts of MCM2 protein it could not co-purify MCM3 or MCM5 (Figure 4.6C). Overall, we concluded that, the conditions used did not generate sufficient MCM3/5 yield for MS hydroxylation site analysis (estimated at ≤ 100ng).
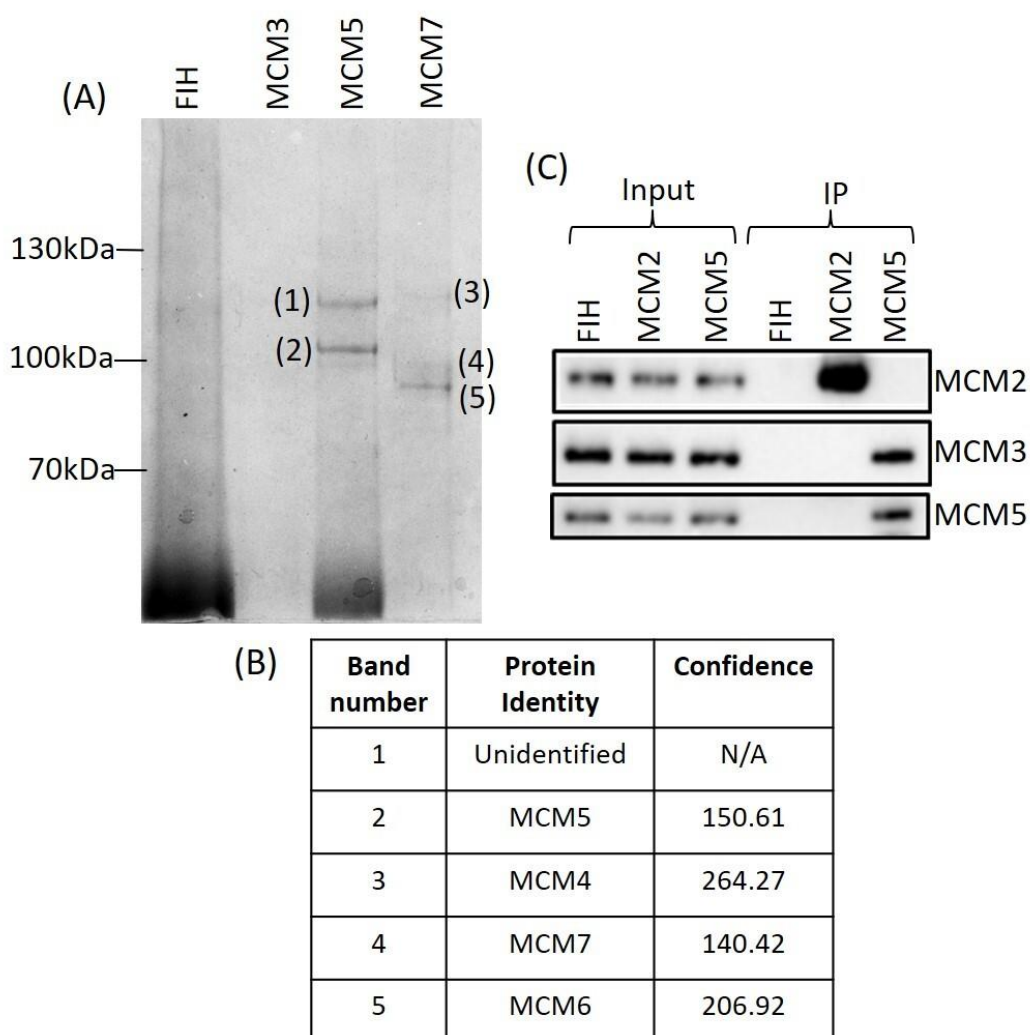
Figure 4.6 Co-immunoprecipitation of endogenous MCM subunit sub-complexes
HEK-293T cell lysates were incubated with protein A agarose beads and antibodies targeting endogenous MCM3, MCM5, MCM7 or negative control FIH for immunoprecipitation. **(A)** Immunoprecipitation samples were separated by poly-acrylamide gel electrophoresis and proteins visualised using Coomassie staining. **(B)** Protein bands from (A) were cut from the poly-acrylamide gel and identified by mass spectrometry (performed by the University of Birmingham Mass Spectrometry Facility). **(C)** Mass spectrometry was unable to identify band 1 (A/B) so the MCM5 immunoprecipitation was repeated, in parallel with testing an MCM2 antibody. Western blotting identified MCM3 co-immunoprecipitation with the MCM5 antibody. This is representative of an n=1 biological repeat. MCM2 (102 kDa), MCM3 (91 kDa), MCM5 (82 kDa).

We noted from the data presented in Figure 4.6C that the MCM2 antibody was more efficient at enriching MCM2 than the other tested antibodies were at purifying their respective targets. Therefore, to optimise our immunoprecipitation conditions, we made several changes to our protocol. Firstly, we quantified HEK-293T lysate concentration prior to immunoprecipitation to ensure lysate to antibody ratios matched those recommended by the manufacturer (Bethyl, A300-191A). In addition, we included nuclease and sonication during lysate preparation in an attempt to improve extraction of the MCM complex from chromatin. Lysates were immunoprecipitated using either anti-MCM2 or anti-FIH (negative control) antibodies. Coomassie staining of eluted samples demonstrated that these conditions improved the yield of MCM2 (estimated at ~2 μg) (Figure 4.7). Methods described in more detail in Section 7.11.3.
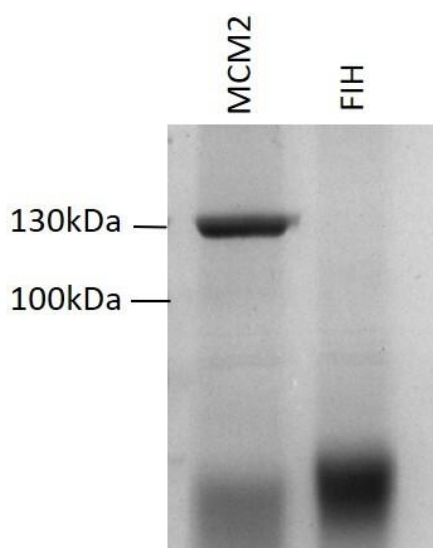
Figure 4.7 Optimisation of endogenous MCM purification
HEK-293T whole cell lysates were sonicated and nuclease treated before quantifying to incubate 3.5 mg of protein with 10 μg antibody targeted to endogenous MCM2 or negative control FIH plus protein A agarose beads. Immunoprecipitated samples were separated by poly-acrylamide gel electrophoresis and proteins visualised using Coomassie blue staining. This is representative of an n=1 biological repeat.

Having identified conditions in which abundant amounts of a single MCM protein could be

purified we next tested four MCM3 and two MCM5 antibodies. This was done in an attempt

to improve immunoprecipitation of these subunits to a similar efficiency as the MCM2

antibody. Lysates from HEK-293T cultures were prepared as above prior to

immunoprecipitation (as for Figure 4.7, described in Section 7.11.3). Abundant MCM2 in

immunoprecipitates confirmed that the assay conditions were optimal and again an FIH

antibody was used as a negative control (Figure 4.8). In this experiment, we identified an

MCM3 antibody successful at purifying endogenous MCM3 (Figure 4.8). Consistent with

previous analysis (Figure 4.6), we confirmed that the Bethyl MCM5 antibody could co-purify

MCM5 and MCM3 (Figure 4.8).
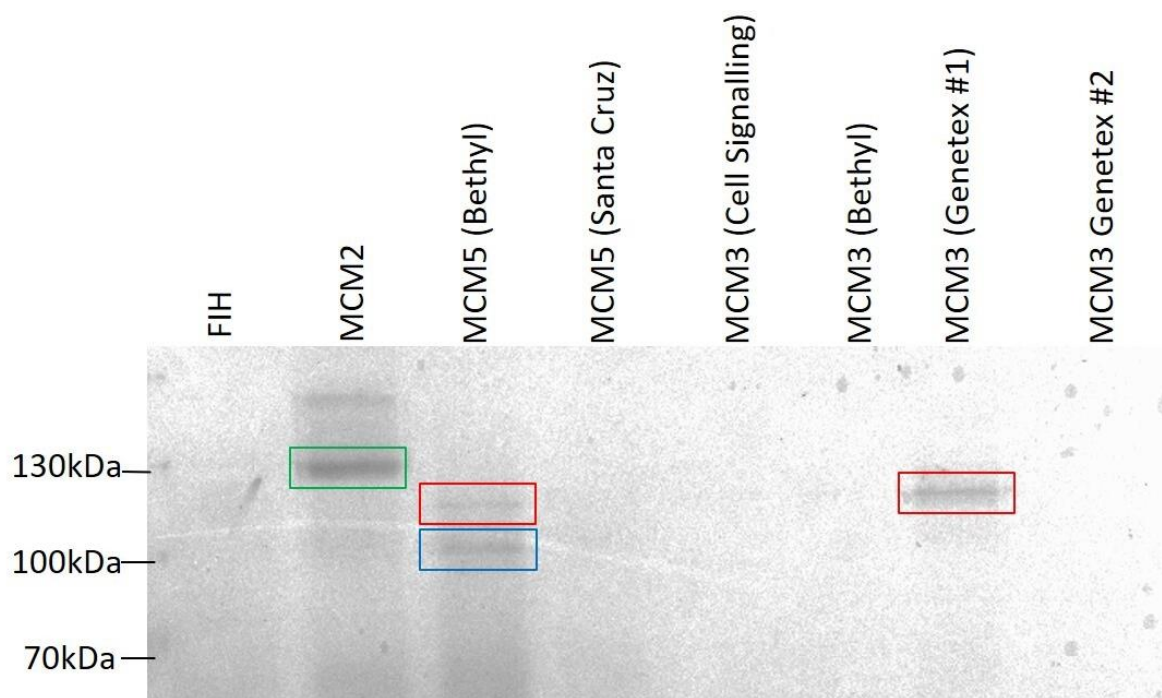
Figure 4.8 Screening MCM3 and MCM5 antibodies for endogenous MCM immunoprecipitation
HEK-293T cell lysates were incubated with protein A agarose beads and antibodies targeting
endogenous MCM2, negative control FIH, or a panel of endogenous MCM3 and MCM5 antibodies.
Immunoprecipitation methods optimised for the MCM2 antibody were used for this experiment (as in
Figure 4.7). The Immunoprecipitates were separated by poly-acrylamide gel electrophoresis and
protein visualised using Coomassie staining. MCM2 (green box), MCM3 (red box), MCM5 (blue box).
This is representative of an n=1 biological repeat.

Having optimised sample preparation conditions and identified successful MCM3 and MCM5

antibodies, we next scaled up the experiment in order to purify higher yields of MCM3 and

MCM5 for MS analysis. A sample of the immunoprecipitates were analysed on a Coomassie

stained gel, which confirmed that the approach had worked successfully (Figure 4.9). The

remainder of each sample (~90%) was submitted for MS analysis in an attempt to identify

potential hydroxylation sites on either of the MCM subunits. Unfortunately, this analysis did

not identify any reliable hydroxylation sites, potentially due to poor sequence coverage.
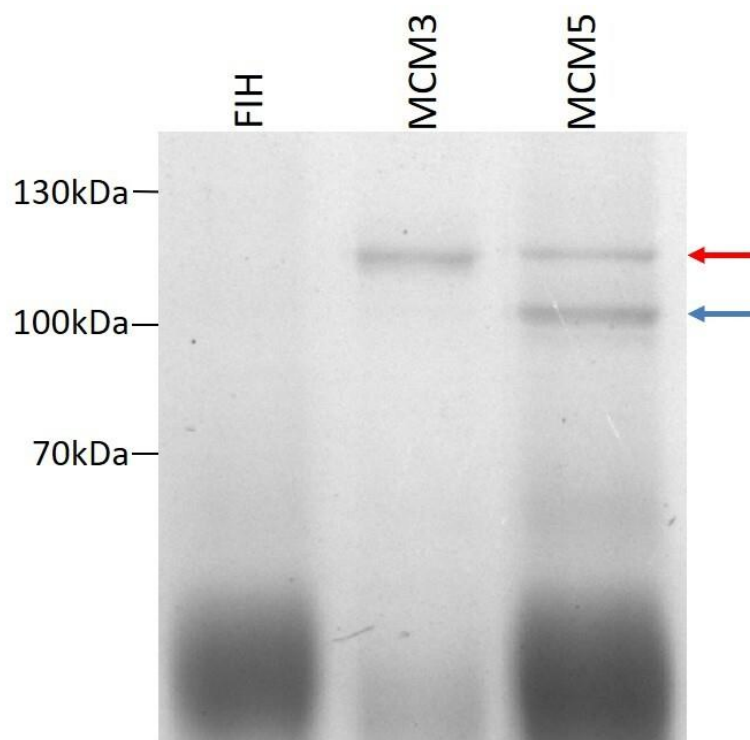
Figure 4.9 Endogenous MCM3 and MCM5 immunoprecipitation for mass spectrometry analysis
HEK-293T cell lysates were incubated with protein A agarose beads and antibodies targeting
endogenous MCM3, MCM5 and negative control FIH for immunoprecipitation. Immunoprecipitation
methods optimised using the MCM2 antibody were used for this experiment (as in Figure 4.7 and 4.8).
Samples were proportionally scaled up to generate more immunoprecipitation sample so that 10%
could be loaded onto poly-acrylamide gel electrophoresis and protein visualised using Coomassie blue
staining. The remainder of the sample was analysed by mass spectrometry. MCM3 (red arrow), MCM5
(blue arrow). This is representative of an n=1 biological repeat.

We predicted that one reason for sub-optimal coverage by MS might be due to low sample yield when purifying endogenous MCM3 and MCM5 by immunoprecipitation. In an attempt to improve this yield, we developed a transient over-expression system to express MCM3 and MCM5 with epitope tags. For this we cloned MCM3 and MCM5, with HA and V5 tags respectively, into mammalian expression vector pcDNA3. The rationale being that high affinity antibodies are available targeting these epitope tags which could therefore improve the MCM3/5 yield after immunoprecipitation.

To perform this assay, the HA-MCM3 expression vector was transfected individually or together with the V5-MCM5 vector into HEK-293T cells followed by HA immunoprecipitation. We co-transfected MCM3/5 because we had consistently co-purified the two subunits (Figure 4.6, 4.8, 4.9), potentially indicative of a known sub-complex of the MCM hexamer (DaFonseca et al., 2001). 10% of the HA-immunoprecipitates were analysed on a Coomassie stained gel, which demonstrated that much higher yields of MCM3 could be obtained using this method (Figure 4.10A). When co-transfected we found that HA immunoprecipitation was sufficient for V5-MCM5 co-purification, indicating that the epitope-tagged over-expressed MCMs were able to interact with each other. However, this was not in a 1:1 ratio as significantly less V5-MCM5 was co-purified (Figure 4.10A). The remainder of the sample (~90%) was analysed by MS. Unfortunately, a reliable hydroxylation PTM was still not detected. Again, we hypothesised this to be due to suboptimal sequence coverage of both MCM3 and MCM5, though this was higher than for endogenously purified MCM3/5.

We considered that the sub-optimal sequence coverage of the co-purified MCM5 might be due to its lower abundance (Figure 4.10A). Therefore, in order to maximise the yield, we transfected HEK-293T cells with expression vectors for either HA-MCM3 or V5-MCM5 followed by immunoprecipitation towards either the HA- or V5-tags. In addition, we co-transfected these cells with or without FLAG-JMJD5 wildtype. Our rationale being that an increased abundance of a particular hydroxylation event, detected by MS in the samples co-transfected with JMJD5, could aid with the detection of a JMJD5-dependent hydroxylation.

Coomassie staining of samples indicated that a MCM3/MCM5 complex could be purified by anti-V5 (MCM5) immunoprecipitation (Figure 4.10B). Anti-HA (MCM3) immunoprecipitation was successful at purifying HA-MCM3 (Figure 4.10B). However, consistent with previous analysis (Figure 4.10A), anti-HA (MCM3) immunoprecipitation was less efficient at co-purifying V5-MCM5.

Samples from this experiment were also analysed by MS but unfortunately, we again failed to observe reliable hydroxylation of MCM3 or MCM5. Overall, we concluded that further technical optimisation to increase sequence coverage, or a greater understanding of the biological context behind the interaction might be required in order to identify the potential MCM3/5 hydroxylation site.
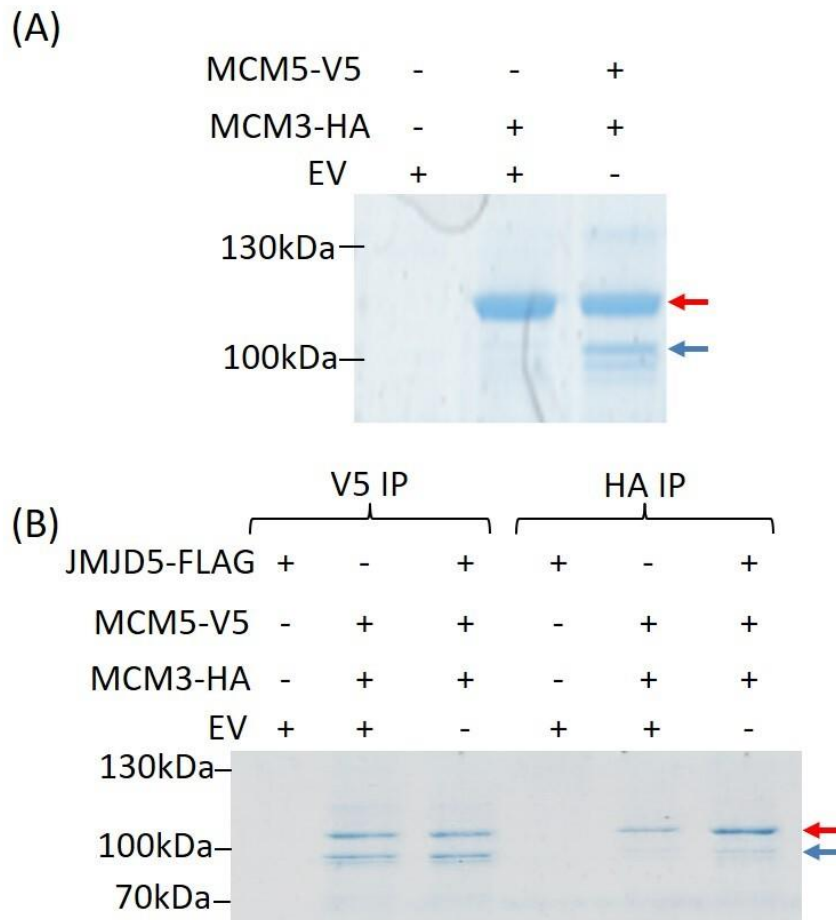
Figure 4.10 Exogenous MCM3 and MCM5 immunoprecipitation for mass spectrometry analysis
(A) HEK-293T cells were transiently transfected with expression vectors for HA-MCM3 with or without co-transfection of V5-MCM5. HA-immunoprecipitation was then used to purify MCM3 (red arrow) and MCM5 (blue arrow) determined by loading 10% of the immunoprecipitation sample onto a poly-acrylamide gel visualised using Coomassie staining. The remainder of the samples were analysed by mass spectrometry. **(B)** HEK-293T cells were transiently co-transfected with HA-MCM3 and V5-MCM5 expression vectors with or without co-transfection of a FLAG-JMJD5 wildtype expression vector. Cell lysates were then HA- or V5-immunoprecipitated to purify MCM3 (red arrow) and MCM5 (blue arrow) determined by loading 10% of the immunoprecipitation sample onto a poly-acrylamide gel, visualised using Coomassie staining. The remainder of the samples were analysed by mass spectrometry. This is representative of an n=1 biological repeat for both experiments.

4.3.2 Models for mapping the JMJD5 interaction domain on MCM3/5

Due to issues faced with cellular models and the dependence of hydroxylation assignment on MS analysis we decided to develop domain mapping as a parallel approach. In the following series of experiments, we aimed to identify regions of MCM3 and/or MCM5 essential for mediating the activity-dependent interaction with JMJD5 (Section 4.2). The rationale being that the putative hydroxylation site would be within a region of MCM3 and/or MCM5 that directly interacts with the catalytic site of JMJD5. If such a region coincided with an area of poor sequence coverage in the MS experiments above it would help rationalise the currently negative data. Moreover, we could then focus future MS efforts on specific regions of MCM3/5. Therefore, we established three assays to help interrogate the JMJD5-MCM3/5 interaction in more detail.

4.3.2.1 *In vitro* MCM3/5 JMJD5 interaction assay

In the first assay we attempted to replicate, *in vitro*, the JMJD5-MCM3/5 interaction identified in Section 4.2. To do this we generated FLAG-tagged JMJD5 from HEK-293Ts which was then incubated with *in vitro* synthesised MCM3 and MCM5 (a schematic of the assay is shown in Figure 4.11A). Our rationale for synthesising MCM3/5 *in vitro* was that it would be unhydroxylated. This could firstly make it a good substrate for JMJD5 and secondly could potentially facilitate identification of a JMJD5-dependent hydroxylation site. To synthesise MCM3 and MCM5 we used a cell-free *in vitro* transcription/translation (IVTT) system. This method enables synthesis of proteins from DNA expression vectors *in vitro* using a rabbit reticulocyte lysate. We established IVTT reactions with the previously cloned HA-MCM3 or V5-MCM5 vectors, or with two newly cloned V5-MCM3 and HA-MCM5 vectors. Successful IVTT was determined by Western blotting for the corresponding epitope tags. Although we

successfully synthesised both HA- and V5-tagged MCM3, only V5-MCM5 could be generated by IVTT (Figure 4.11B). The IVTT reaction was then scaled up to generate HA-MCM3, V5-MCM5 or HA-MCM3/V5-MCM5 to a suitable concentration for subsequent interaction analysis, as validated by Western blotting (Figure 4.11C).

We were next interested to determine whether the IVTT MCM3/5 sample could be used to form an *in vitro* interaction with JMJD5 (as depicted in Figure 4.11A, methods described in more detail in Section 7.11.2). Briefly, HEK-293T cells were transiently transfected with a FLAG-tagged JMJD5 wildtype expression vector. FLAG-immunoprecipitation was then used to purify the FLAG-tagged JMJD5 protein which was then incubated with IVTT MCM3/MCM5 (from Figure 4.11C). Continued FLAG-immunoprecipitation was performed for subsequent analysis by Western blotting. The presence of MCM3/5 in the immunoprecipitates would be indicative of an interaction formed with JMJD5 *in vitro*. Unfortunately, no interaction could be detected (Figure 4.11C). This meant that, at least under the conditions tested, this IVTT pulldown assay was not immediately useful for further analysis of the JMJD5-MCM3/5 interaction.
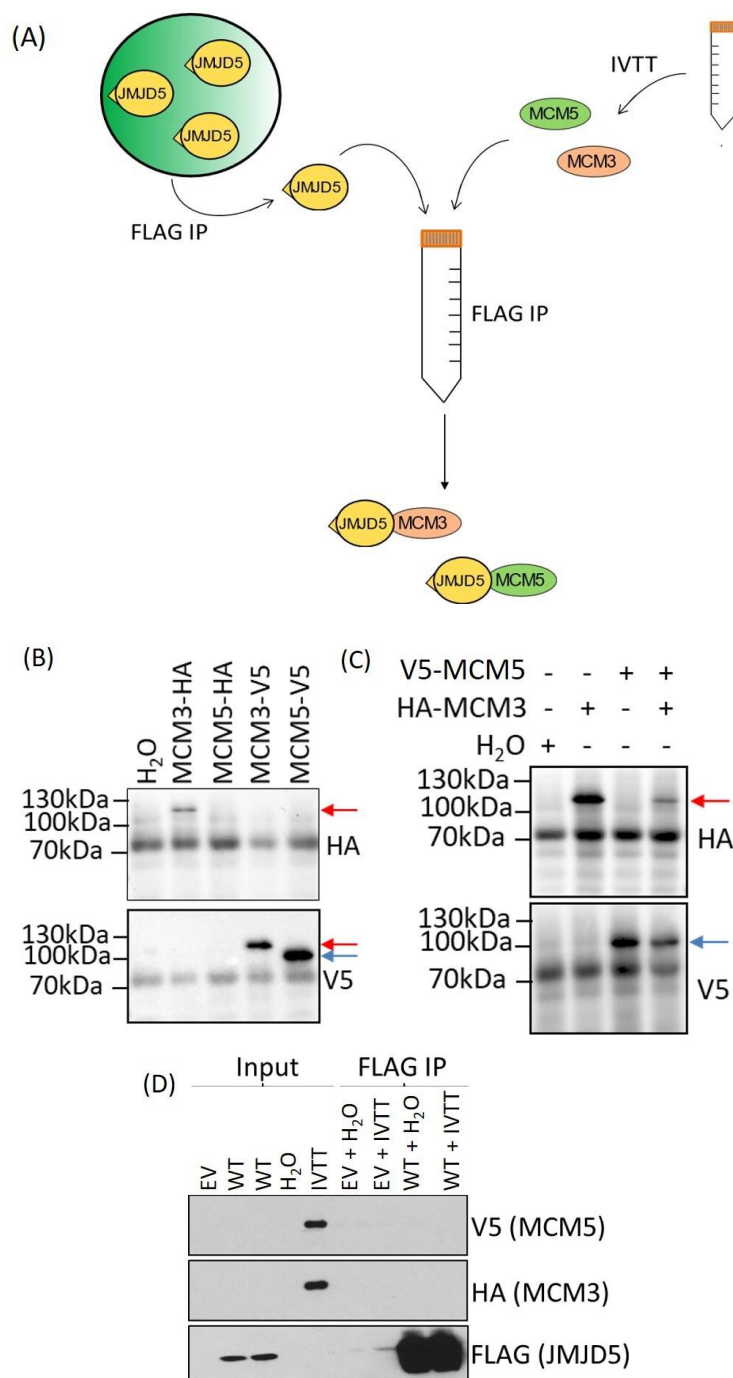
Figure 4.11 Generation and testing of IVTT synthesised MCM3 and MCM5 interaction with JMJD5
(A) Schematic of the *in vitro* interaction assay; FLAG-JMJD5 wildtype (WT) transfected into HEK-293T cells was purified by FLAG immunoprecipitation. HA-MCM3 and/or V5-MCM5, generated by IVTT, were added to the immunoprecipitation and successful interaction detected by Western blotting. **(B)** MCM3 and MCM5 with HA or V5 tags were synthesised by IVTT, samples analysed by Western blotting. MCM3 (red arrow), MCM5 (blue arrow). This is representative of an n=2 biological repeat. **(C)** HA-MCM3 and V5-MCM5 synthesised by IVTT in a relatively scaled-up experiment. 10% of the IVTT sample was analysed by Western blotting. MCM3 (red arrow), MCM5 (blue arrow). **(D)** *In vitro* interaction assay performed as described in (A) using co-synthesised HA-MCM3 and V5-MCM5 IVTT sample from (C) were analysed by Western blotting. Empty vector (EV) included to prove specificity. This is representative of an n=1 biological repeat. MCM5 (82 kDa), MCM3 (91 kDa), JMJD5 (47 kDa).

4.3.2.2 Screening for a minimal domain in MCM3/5 to support JMJD5 interaction

The second assay we established also aimed to identify a minimal domain within MCM3 and MCM5 essential for interaction with JMJD5. This was attempted by screening a series of MCM3 and MCM5 mutants for their ability to interact with JMJD5. The MCM3/5 mutants were chosen based on: 1) regions consistently not covered in the MS analysis, 2) highly basic regions (i.e. with similar properties predicted for a JMJD5 substrate based on JMJD5 structural analyses), 3) functionally important regions, such as the MCM domain, and 4) cancer patient mutations identified from COSMIC and cBioPortal online databases, with a specific focus on arginine residues because of the assignment of JMJD5 as an arginine hydroxylase (Wilkins et al., 2018). These truncations and mutations are described in more detail below and are depicted in Figure 4.12.

Within HA-MCM3 we generated truncation mutants to determine the importance of the MCM domain for mediating JMJD5 interaction. This included the N-terminal region of MCM3 up to amino acid residue 491, to remove an arginine of interest localised within the MCM domain and the C-terminal domain (491*). We also generated a C-terminal deletion up to the end of the MCM domain (N-terminus). We generated cancer patient mutations converting arginine residues at position 664 to a cysteine (R664C) and at position 667 to a glutamine (R667Q) because they were found to be localised within the nuclear localisation signal (NLS) of MCM3 (Takei and Tsujimoto, 1998). The MCM3 NLS was of interest because is a highly basic region poorly covered by previous MS analysis. To further test the importance of this region containing the NLS we generated another C-terminal deletion up to residue 701 (701*).

Within V5-MCM5 we generated truncations to investigate the major regions of MCM5 for interaction with JMJD5. These included the N-terminus up to the end of the MCM domain (N-terminus), a construct containing only the MCM domain (MCM), and a truncation from the start of the MCM domain through to the C-terminus (C-terminus). We also generated a truncation construct up to residue 723 (723*) and a point mutation converting arginine at position 723 to an alanine (R723A). We were interested in investigating this extreme C-terminal domain of MCM5 because it was not covered by previous MS analysis, is recurrently mutated at R723 in cancer and is highly basic.
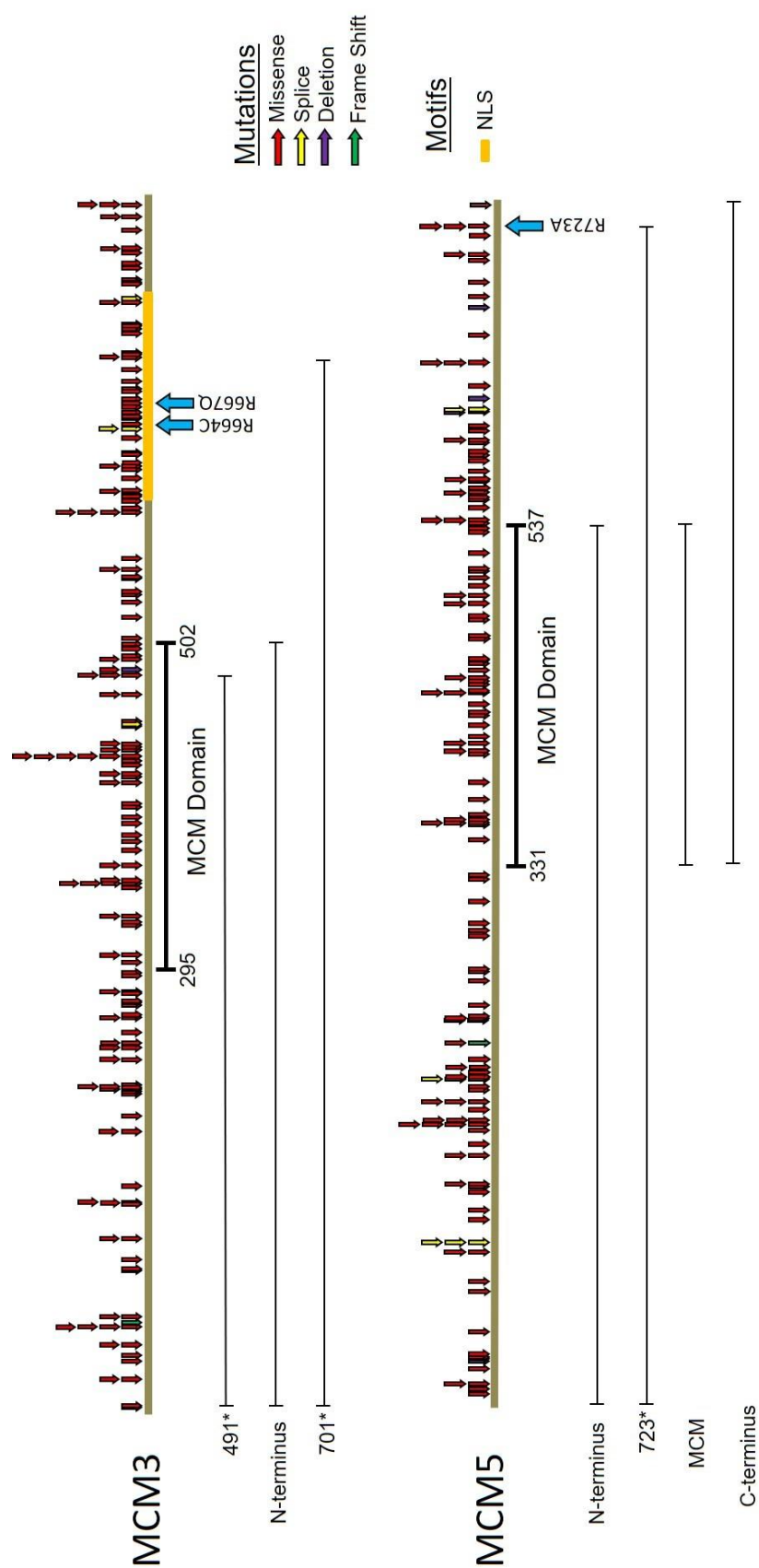
Figure 4.12 MCM3 and MCM5 point mutation and truncations

MCM3 and MCM5 protein sequences annotated with relevant functional motifs including catalytic ATPase MCM domains, and the nuclear localisation signal (NLS) in MCM3 (Takei and Tsujimoto, 1998). Cloning was used to generate truncations in MCM3 (491*, N-terminus, 701* and MCM5 (N-terminus, 723*, MCM, C-terminus), and site directed mutagenesis used to generate point mutations at residues of interest, shown by blue arrows, in MCM3 (R664C, R667Q) and MCM5 (R723A). The cancer mutations identified from COSMIC and cBioPortal are annotated by arrows; missense mutations (red), alternative splice mutations (yellow), deletion mutations (purple) and frameshift mutations (green).

Next, we assessed whether these MCM constructs could be expressed in cells. Each MCM construct was transiently transfected into HEK-293T cells and protein expression determined by Western blotting. In some cases, multiple clones of the same vector were tested, some of which did not express or were incorrect. For example, 491*(1) and 732*(1) did not express. Clone (2) of the MCM5 'C-terminus' construct was not found to migrate at the predicted size by SDS-PAGE and was confirmed by Sanger sequencing to be incorrect. We found that all other MCM3 and MCM5 constructs were able to be expressed as proteins (Figure 4.13A and B).

We were then interested to determine which of these constructs were competent at interacting with JMJD5. We first tested only two MCM5 constructs (R723A and 723*) in a pilot experiment. Briefly, expression vectors for wildtype, R723A, or 723* MCM5 were co-transfected with wildtype or H321A FLAG-tagged JMJD5 into HEK-293T cells. FLAG-JMJD5 was immunoprecipitated prior to Western blotting to determine the presence of MCM proteins in the immunoprecipitates (methods as Section 7.11.1). As expected, wildtype JMJD5 interacted with wildtype V5-MCM5. Wildtype JMJD5 was also able to interact with both R723A and 723* (Figure 4.13C). However, this interaction appeared to no longer be activity-dependent, as an interaction was also observed between V5-MCM5 and FLAG-JMJD5 H321A (Figure 4.13C). Unfortunately, overexpression of MCM3 also led to an activity-independent interaction with JMJD5 (data not shown), suggesting that this approach was unlikely to be suitable for dissecting a minimal activity-dependent interaction domain of MCM3/5.
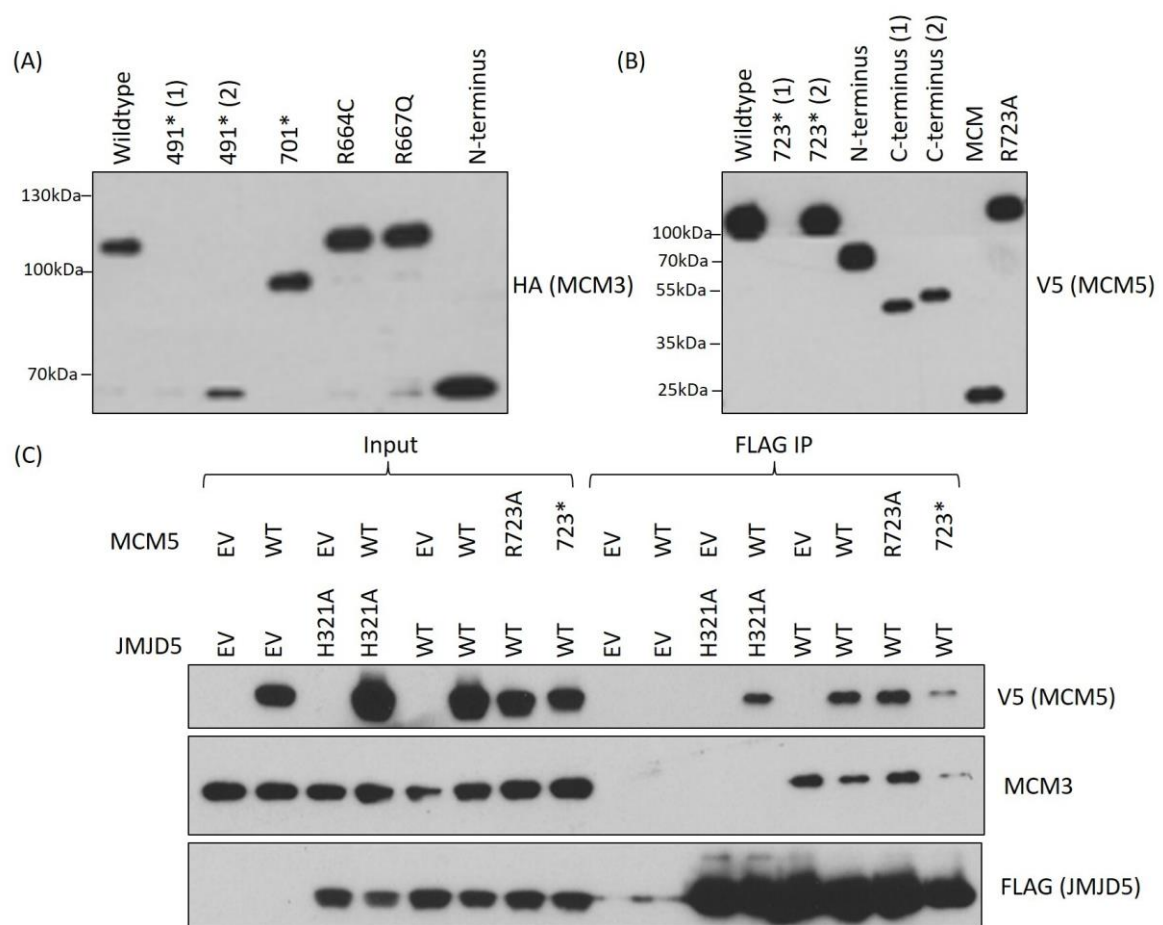
Figure 4.13 Testing expression of MCM3 and MCM5 mutants and their interaction with JMJD5
HEK-293T cells were transiently transfected with expression vectors for **(A)** HA-tagged MCM3 or **(B)** V5-tagged MCM5 truncation and point mutations (Figure 4.12). Expression of the constructs was determined using Western blotting. **(C)** V5-tagged MCM5 expression vectors for wildtype, R723A and 723* truncation were transiently transfected into HEK-293T cells alongside FLAG-tagged JMJD5 wildtype or catalytic mutant H321A expression vectors, then incubated with 1 mM DMOG for 16 hours prior to FLAG-immunoprecipitation in the presence of 1 mM NOG. Immunoprecipitates were then analysed by Western blotting. Empty vector (EV) was used to prove specificity. This is representative of an n=1 biological repeat. MCM3 (91 kDa), MCM5 (82 kDa), JMJD5 (47 kDa).

4.3.2.3 Peptide Competition Assays

A major problem with the previous approach was the loss of activity-dependent binding upon overexpression of epitope-tagged MCM3/5. Therefore, we considered taking advantage of an existing assay in which we observed an activity-dependent interaction, that being the interaction between overexpressed JMJD5 and endogenous MCM3/5 (Section 4.2). In this *in vitro* assay we aimed to compete off endogenously bound MCM3 and/or MCM5 from JMJD5 by using small peptides covering regions of interest within these MCM proteins (depicted in Figure 4.14). Such competition assays could help to narrow down regions within MCM3 and MCM5 that bind JMJD5 catalytic residues, which could then be the focus of future MS hydroxylation site analyses.

To do this wildtype JMJD5-HA was over-expressed in HEK-293T cells after transient transfection. HA-immunoprecipitation was carried out for six hours to purify HA-JMJD5 complexed with endogenous MCM3/5, in the presence of DMOG. Samples were then incubated with a peptide of interest for a further 16 hours to compete off any endogenous MCM3 or MCM5 bound to the JMJD5 enzyme (methods described in more detail in Section 7.11.2). To test the validity of this approach we first used the RPS6 peptide substrate as a positive control. This peptide has previously been shown to interact with the JMJD5 catalytic site, as demonstrated through successful hydroxylation by JMJD5 *in vitro* (Wilkins et al., 2018) (Figure 3.18 in Chapter 3). As an additional positive control, we also included the essential cofactor 2OG in some samples, reasoning that this could compete with the NOG analogue used to trap the MCM3/5 complex on JMJD5 (Figure 4.4).
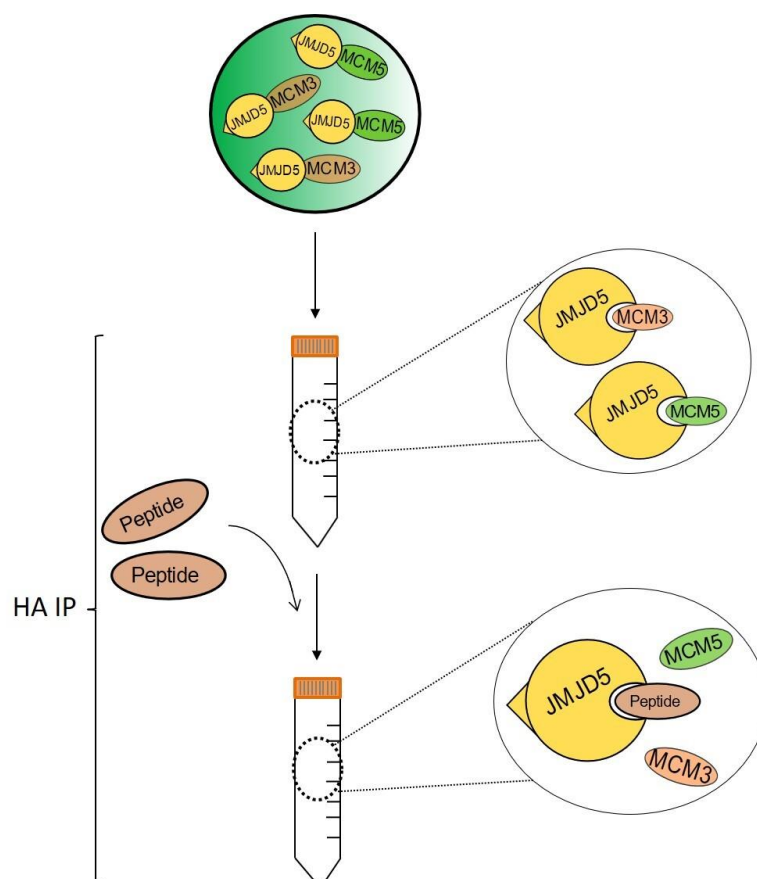
Figure 4.14 Peptide competition assay schematic
HEK-293T cells transfected with HA-JMJD5 and endogenous JMJD5-MCM3/5 complexes purified using HA immunoprecipitation in the presence of 1 mM DMOG/NOG. Incubated in this immunoprecipitation reaction were peptides covering protein sequences of interest. The rationale being that regions of protein that mediate direct interaction with JMJD5 catalytic residues might be able compete off endogenously bound MCM3/5. If successful, this would be detected by Western blotting as reduced MCM3/5 interaction with JMJD5 in the immunoprecipitates.

As expected, we found that endogenous MCM3 and MCM5 co-immunoprecipitated with wildtype JMJD5 (lane 3), but not with the JMJD5 catalytic mutant H321A (lane 2) or in the empty vector control (lane 1) (Figure 4.15). Consistent with our hypothesis, it appeared that addition of 2OG was sufficient to compete with NOG and release MCM3 and MCM5 (comparison between lanes 3 and 5). In addition, the presence of 0.1 or 1 mg/mL RPS6 peptide was also able to compete off MCM3 and MCM5 (comparison of lanes 7 and 8 with lane 3). Both of these observations validated the assay and also provided further evidence supporting that MCM3/5 bind directly in the catalytic pocket of JMJD5.

As initial results obtained from the pilot competition assay suggested it would be suitable for screening candidate MCM3 and MCM5 peptides, we used the methods described above to investigate the ability for a peptide covering the MCM3 NLS (^{658}LEKEKKRKKRSEDE^{671}) to compete with endogenously bound MCM3/5 for JMJD5. As mentioned above the NLS of MCM3 was of interest because it is highly basic and poorly covered by previous MS analysis. Unfortunately, we found that the addition of this peptide was not sufficient at competition with the endogenously bound MCM3 or MCM5. However, we will aim to use this assay for screening other MCM3/5 peptides in the future.
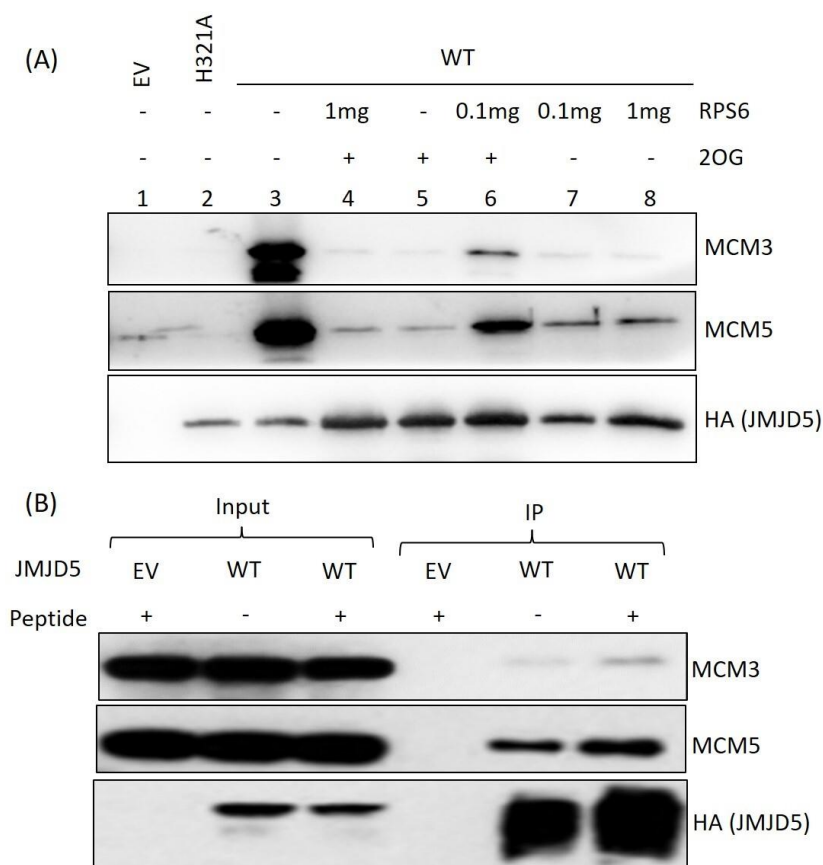
Figure 4.15 Optimisation and testing of the peptide competition assay
Two individual assays were set up in HEK-293T cells as described in Figure 4.14. **(A)** Added into a HA-immunoprecipitation reaction was 0.1 or 1 mg/mL of the RPS6 peptide, an *in vitro* JMJD5 hydroxylation substrate (Wilkins et al., 2018) (Figure 3.17 in Chapter 3), plus or minus cofactor 2-oxoglutatrate (2OG). **(B)** Added into a HA-immunoprecipitation reaction was 1 mg/mL peptide covering the MCM3 nuclear localisation signal. Western blotting was used to determine competition of MCM3/5 from JMJD5. Empty vector (EV) used to prove specificity. This is representative of an n=1 biological repeat. MCM3 (91 kDa), MCM5 (82 kDa), JMJD5 (47 kDa).

4.4 The JMJD5-MCM3/5 Interaction is Disease Relevant

Although further optimisation and investigation of the approaches presented above will be required in order to confidently identify the putative hydroxylation site in MCM3 and/or MCM5, we have presented several lines of evidence that support our hypothesis that MCM3/5 are candidate JMJD5 substrates. Therefore, we were next interested to determine the potential disease relevance of this interaction.

We first aimed to determine whether patients affected by a developmental disorder (Chapter 3) might have an altered MCM3/5 phenotype that correlates with their *JMJD5* genotype. As we predicted the affected patients to be hypomorphic for JMJD5 (Chapter 3) we proposed that this investigation could provide information regarding potential functional consequence of the JMJD5-MCM3/5 interaction.

We first tested whether the protein expression of the MCM3/5 subunits were altered in these fibroblasts. To do this whole cell lysate, generated using RIPA and sonication to purify the chromatin fraction, were analysed by Western blotting. We also investigated the expression of the other MCM complex subunits as literature has suggested that changes to expression of one subunit can alter protein expression in the other subunits (Chuang et al., 2010, Drissi et al., 2018). As expected the affected patient fibroblasts had the lowest JMJD5 protein expression compared with the other patient fibroblasts (Figure 4.20A). It also appeared that MCM subunit protein levels were reduced in this patient compared to the other family members tested (Figure 4.16A). This observation was confirmed by performing densitometry analysis and determining affected patient protein expression relative to the wildtype patient fibroblast protein expression (Figure 4.16B). This demonstrated that MCM protein expression

correlated with reduced JMJD5 protein expression for the affected patient and thus suggested that loss of interaction with JMJD5 could alter the stability of the MCM proteins. This hypothesis will be interesting to investigate in the future once a hydroxylation site in MCM3/5 has been identified.
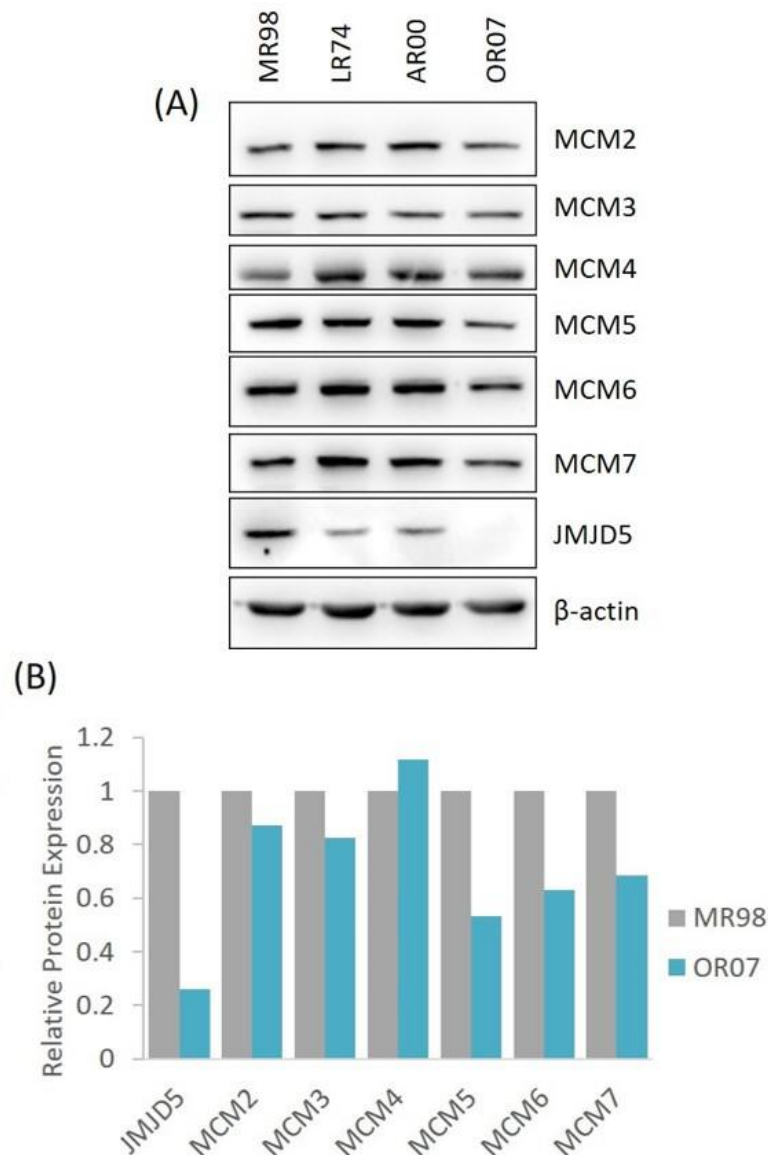
Figure 4.16 Affected patient fibroblasts have reduced MCM protein levels
(A) Whole cell lysate from patient fibroblast cell lines expressing JMJD5 wildtype (MR98), C123Y mutation carrier (LR74), InMut carrier (AR00) and both JMJD5 mutations (OR07) was harvested and analysed by Western blotting for endogenous MCM subunit expression. β-actin used as a loading control. **(B)** The Western blot protein bands from (A) were analysed using densitometry. Protein expression was normalised to loading control β-actin and relative to the wildtype (MR98) fibroblasts. This is representative of an n=1 biological repeat. MCM2 (102 kDa), MCM3 (91 kDa), MCM4 (97 kDa), MCM5 (82 kDa), MCM6 (93 kDa), MCM7 (81 kDa), JMJD5 (47 kDa), β-actin (42kDa).

We were next interested to determine whether the N-terminal JMJD5 missense mutation (C123Y), that we predicted would contribute to the low JMJD5 protein expression in the affected patient fibroblasts (Chapter 3), might affect its interaction with MCM3/5. To test this, we transiently transfected HEK-293T cells with HA-tagged wildtype, H321A or C123Y JMJD5 expression vectors. HA immunoprecipitation was performed and endogenous MCM3 and MCM5 interaction with the JMJD5 constructs was determined by Western blotting. As expected, wildtype JMJD5, but not the H321A catalytic mutant, was able to interact with endogenous MCM3 and MCM5 (Figure 4.17A). We also found that the C123Y mutation was able to interact with endogenous MCM3 and MCM5 (Figure 4.17A). However, our interpretation of the results from this experiment was limited, due to the reduced expression of C123Y compared to wildtype or H321A JMJD5, as expected from prior analysis (Chapter 3).

To overcome this, we used the *in vitro* assay as outlined in Chapter 3 (Section 3.7.3). Briefly, recombinant GST-tagged JMJD5 wildtype and C123Y were incubated with HEK-293T whole cell lysates followed by GST pulldown. Equal loading of the JMJD5 constructs was confirmed by Coomassie staining (Figure 4.17B). Western blotting was used to detect endogenous MCM3 and MCM5 in the immunoprecipitates, indicative of interaction with JMJD5. Using this approach, we observed that the C123Y JMJD5 mutant was able to interact with MCM3 and MCM5 in a similar manner to the wildtype enzyme (Figure 4.17B). However, based on previous analysis potentially implicating that C123Y is less active than wildtype (Section 3.7.5, Chapter 3) this should be addressed once a hydroxylation site in MCM3/5 has been identified.
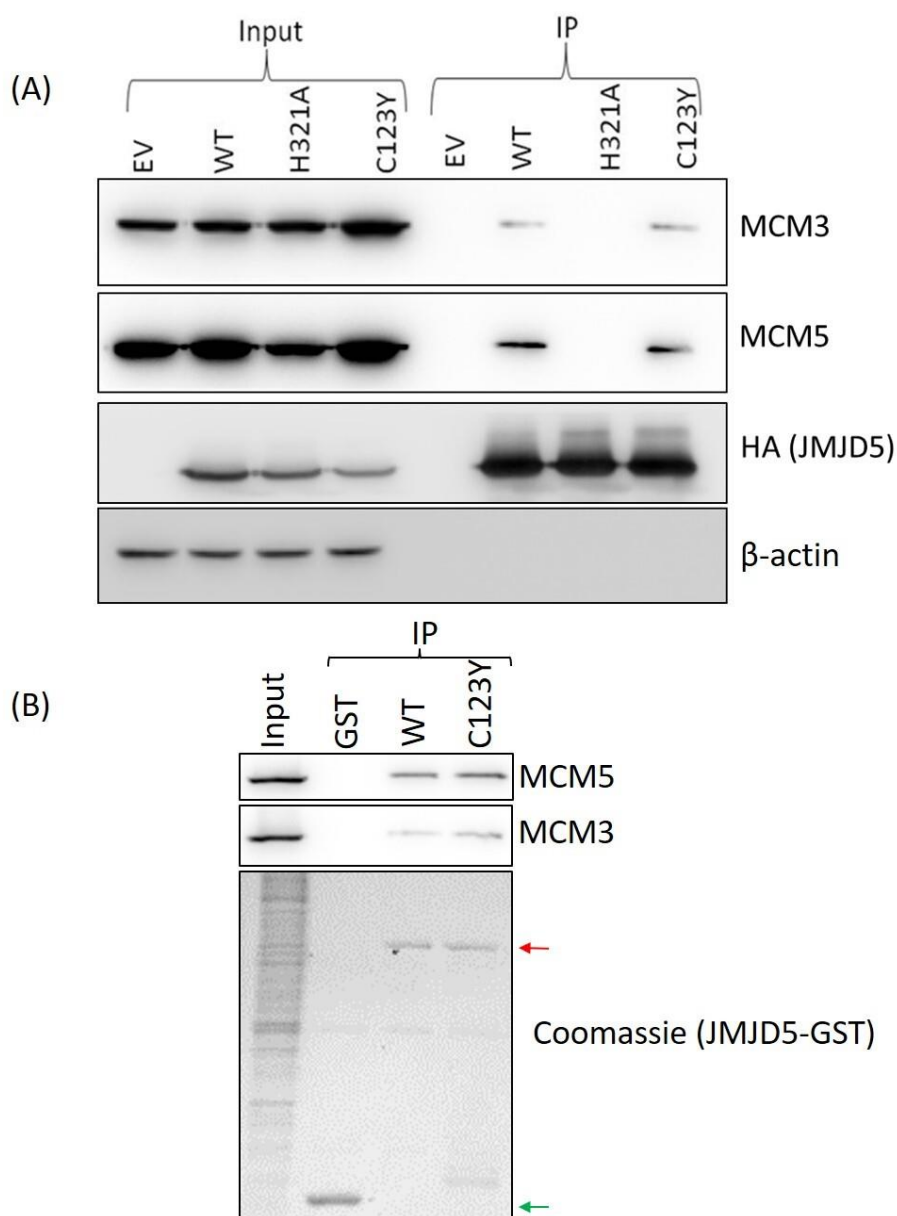
Figure 4.17 C123Y JMJD5 mutant is able to interact with endogenous MCM3 and MCM5
(A) HEK-293T cells were transiently transfected with HA-tagged JMJD5 wildtype or H321A expression vectors, then treated with 1 mM DMOG for 16 hours prior to HA-immunoprecipitation in the presence of 1 mM NOG. Western blotting used to determine endogenous MCM3 and MCM5 interaction with JMJD5. β-actin used as a loading control for input samples. Empty vector (EV) used to prove specificity. This is representative of n=3 biological repeats. **(B)** An *in vitro* interaction was formed between GST-tagged recombinant wildtype (WT) or C123Y JMJD5 with endogenously expressed MCM3 and MCM5 from HEK-293T whole cell lysate. This JMJD5-MCM3/5 complex was then purified by GST pulldown. Samples analysed by Coomassie staining to demonstrate equal loading of JMJD5 (red arrow) or GST epitope tag alone (green arrow). Western blotting confirmed the interaction between GST-tagged JMJD5 with cell purified endogenous MCM3 and MCM5. This is representative of an n=1 biological repeat. MCM3 (91 kDa), MCM5 (82 kDa), JMJD5 (47 kDa), β-actin (42kDa).

To continue this analysis, we next aimed to investigate whether other JMJD5 mutations, associated with human diseases, might alter the interaction with MCM3/5. Specifically, we focussed on cancer, because of the growing evidence that both MCMs (reviewed by Seo and Kang (2018)) and JMJD5 (Chapter 1) play important roles during tumourigenesis. As outlined in Chapter 1, JMJD5 has been implicated as a tumour suppressor gene in some contexts. Since tumour suppressor genes are often inactivated by mutations, we first analysed online cancer mutation databases COSMIC and cBioportal to identify JMJD5 mutations. Interestingly, we found that the majority of mutations, and especially recurrent and hot spot cancer mutations (which imply functional significance), were clustered in the catalytic domain at the C-terminus of JMJD5 (Figure 4.18A). This suggests that JMJD5 catalytic activity is important for its tumour suppressor function and thus these mutations could affect MCM3/5 interaction.

To test this hypothesis, we initially generated three JMJD5 cancer mutations by SDM which were tested for their ability to interact with MCM3 and MCM5. A melanoma mutation, P190L, was chosen as it was a recurrent mutation localised at the extreme N-terminus of the JmjC extension (Figure 4.18A). This N-terminal extension is predicted to stabilise the JmjC catalytic domain and thus could be important for JMJD5 function (Del Rizzo et al., 2012). Another melanoma patient mutation, D323N, was chosen as the residue forms the essential HxD…H motif for coordinating Fe(II) ions in the catalytic domain of JMJD5 (Del Rizzo et al., 2012, Wang et al., 2013, Wilkins et al., 2018). P395Q is a recurrent lung cancer mutation and was chosen because it localises in the C-terminus of the JmjC catalytic domain.

Expression vectors for wildtype, H321A or these JMJD5 mutants were transiently transfected into HEK-293T cells. HA immunoprecipitation was then performed and the presence of endogenous MCM3 and MCM5 in the immunoprecipitates analysed by Western blotting. Interestingly, we found that all three JMJD5 cancer mutations had reduced interaction with MCM3 and MCM5, compared to the wildtype enzyme, and were at a level comparable to the inactive H321A mutant (Figure 4.18B). This suggested that these cancer mutations might affect the catalytic activity of JMJD5, which will be tested in the future using an *in vitro* hydroxylation assay. It would also be interesting to determine how these mutations affect JMJD5 stability, as the P395Q mutation resulted in reduced JMJD5 expression compared to wildtype (Figure 4.18B). Overall, together this analysis suggests that the JMJD5-MCM3/5 interaction might be relevant to disease associated with JMJD5 inactivating mutations.
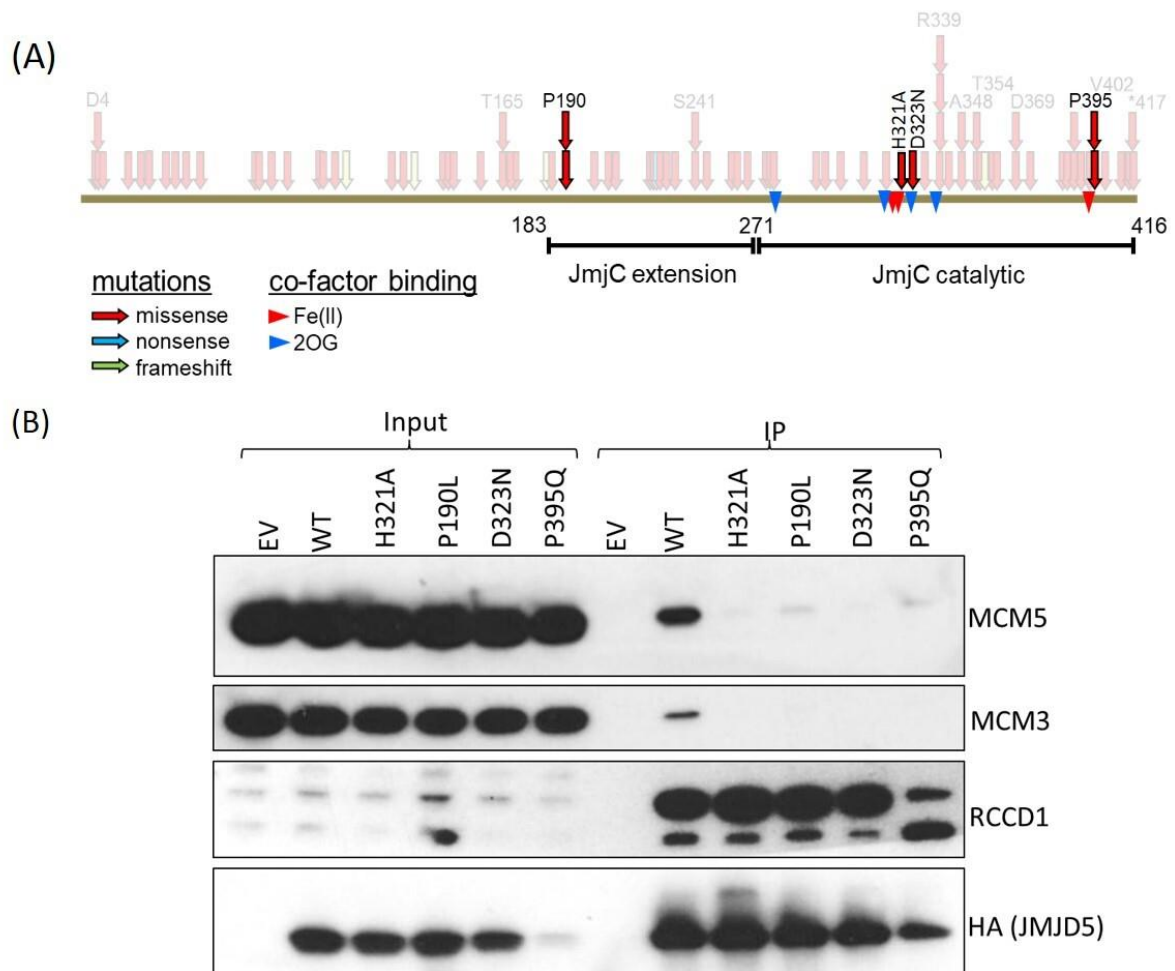
Figure 4.18 Investigation of JMJD5 cancer mutants for their ability to bind MCM3 and MCM5
(A) COSMIC and cBioPortal were used to identify JMJD5 cancer mutations that were annotated onto the protein sequence of JMJD5. Missense (red arrow), nonsense (blue arrow), frameshift (green arrow), cofactor binding residues (red and blue triangles). **(B)** Three JMJD5 cancer mutations of interest were generated by site directed mutagenesis to contain a HA-tag and expression vectors transiently transfected into HEK-293T cells. Cells were then treated with 1 mM DMOG for 16 hours prior to HA-immunoprecipitation in the presence of 1 mM NOG. Western blot analysis used to determine endogenous MCM3, MCM5 and RCCD1 interaction with JMJD5. Empty vector (EV) control used to prove specificity. β-actin used as a loading control. Representative of n=3 biological repeats. MCM5 (82 kDa), MCM3 (91 kDa), RCCD1 (40 kDa), JMJD5 (47 kDa).

4.5 Discussion

In this chapter we aimed to investigate the highly controversial literature surrounding the enzymatic role of JMJD5. To do this we first investigated three hydroxylation substrates of JMJD5 previously proposed in the literature: H3K36me2 for demethylation (Hsia et al., 2010), histone H3 for endopeptidase cleavage (Shen et al., 2017, Liu et al., 2017, Liu et al., 2018b) and ribosomal subunit RPS6 for hydroxylation (Wilkins et al., 2018). However, we were unable to detect JMJD5 activity dependent changes in global H3K36me2 expression or histone H3 cleavage (Figure 4.1). Overall, we concluded that in our models JMJD5 does not act as an endopeptidase or KDM. In support of this, there is a growing body of structural and biochemical evidence in the literature which concludes that JMJD5 cannot support these activities (discussed in detail in Chapter 1). We were also unable to detect an interaction between JMJD5 and RPS6 (Figure 4.2). In addition, we observed that RCCD1 interacted with JMJD5 in a manner that was independent of enzyme activity (Figure 4.3). This supports the literature indicating that RCCD1 binds to the N-terminus of JMJD5 (Marcon et al., 2014). Overall, the current literature and our own data indicated that JMJD5 was an orphan hydroxylase. Therefore, we investigated novel hydroxylation substrates of JMJD5 by performing proteomic screening.

In doing so we successfully identified two candidate substrates, MCM3 and MCM5, that consistently interacted with JMJD5 in an activity-dependent manner (Section 4.2). This was further confirmed by the observations that the NOG-mediated 'trapping' of MCM3/5 on JMJD5 (Figure 4.4) was out-competed by 2OG and an RPS6 peptide *in vitro* substrate (Figure 4.15A). Furthermore, JMJD5 interaction with MCM3/5 was ablated after mutation of JMJD5

residues critical for binding the RPS6 arginine (Wilkins et al., 2018), demonstrated by Dr Sally

Fletcher (Coleman lab). Although the evidence supporting MCM3/5 as a novel JMJD5

substrates is strong, identification of the hydroxylated residue by MS was technically

challenging, as discussed below.

4.5.1   Investigating MCM3/5 hydroxylation

In order to confirm MCM3 and/or MCM5 as true substrates of JMJD5 we endeavoured to

identify a hydroxylation site. To do this we screened endogenous and over-expressed

MCM3/5 purified from cells for hydroxylation (Section 4.3.1). Currently the only reliable

method available for discovering and quantifying hydroxylation is by MS which we adopted in

this thesis. Unfortunately, we were unable to observe a reliable assignment of arginine

hydroxylation, dependent on JMJD5, in any of our samples. However, our attempts were

largely hindered by poor sequence coverage. This could be for multiple reasons discussed

below.

One factor limiting good sequence coverage is the choice of protease used for MS sample

preparation. For example, trypsin, which is one of the most commonly used proteases for MS

analysis and was predominantly used for our own analysis, cuts after arginine and lysine

residues. This means that arginine and/or lysine rich sequences are digested into peptide

fragments too small for analysis. Consequently, such regions are absent from sequence

coverage. Due to their functional role in binding and unwinding DNA, MCM proteins contain

a number of highly charged and basic motifs (Riera et al., 2017). These regions, perhaps

unsurprisingly, were largely missing from our trypsin-based MS analyses. However, these

highly charged and basic regions are also most likely to be targeted by JMJD5 for

hydroxylation, as predicted from JMJD5 structural analyses (Del Rizzo et al., 2012, Wang et al., 2013, Wilkins et al., 2018). In an attempt to address this, we tested an alternative protease, elastase, for sample preparation prior to MS analysis. Elastase has a more degenerate specificity compared to trypsin, which results in more and often overlapping peptide products. Thus, elastase digestion can result in better sequence coverage (previous observation in the Coleman lab). Although, this approach did improve sequence coverage, we again did not identify a hydroxylation site and areas of the MCM3/5 sequence were still absent.

There are also inherent limitations to using MS for identification of a hydroxylation site that could have hindered our analysis. For example, artificial oxidation of a variety of amino acids can occur during sample preparation (Morand et al. (1993) and personal observations). Therefore, biasing analysis to search for specific oxidations can result in false positives. This problem can be exemplified by a recent study where comprehensive MS analysis of alternative PHD candidate substrates were reported to likely be artefacts of prior incorrect MS analyses (Cockman et al., 2019). Overall, our future analysis will require optimisation of sample preparation and MS analysis.

There are additional factors that could have contributed to our lack of hydroxylation site assignment. For example, due to evidence presented in the following chapter there is ambiguity regarding the activity of epitope tagged JMJD5 (Chapter 5). Therefore, reduced activity of epitope tagged JMJD5 could be a potentially contributing factor to the lack of hydroxylation observed in our experiments. To address this, repetition of some experiments performed in this chapter could be done in the presence of un-tagged JMJD5.

In addition, there might be a biological rationale for why MCM3/5 hydroxylation might not have occurred under the conditions tested. This is because although we could consistently identify a JMJD5-MCM3/5 complex from cells, we know very little regarding where, when or how this interaction took place. For example, we do not know whether JMJD5 targets the entire pool of MCM3/5 or a sub-population. Therefore, when analysing a mixed population of MCM3/5 by MS this could result in an undetectable level of hydroxylation. This should be addressed in future experiments, as discussed below.

Firstly, we will aim to characterise the sub-cellular location that the interaction takes place. For example, we observed that only a small portion of JMJD5 localised on chromatin with the majority present in the nucleoplasm (Figure 4.1A), as supported by the literature (Hsia et al., 2010, Youn et al., 2012, Huang et al., 2013, Zhu et al., 2014, Kouwaki et al., 2016, Shen et al., 2017). However, the MCM hexamer has been predominantly characterised as a chromatin bound complex, though some studies have also identified MCMs in the nucleoplasm (Hesketh et al., 2015). Therefore, understanding where JMJD5 and MCM3/5 interact could help to identify optimal conditions for future MS analyses. This could be investigated using imaging approaches such as proximity ligation assays, or genomic approaches such as chromatin immunoprecipitation.

Secondly, we will aim to understand when the JMJD5-MCM3/5 interaction take places. For example, it would be interesting to establish whether this occurs in a specific cell cycle phase. Moreover, it is possible that this interaction could be in response to a biological signal. For example, it is known that MCM localisation, chromatin loading, and activation are highly regulated (Deegan and Diffley, 2016). Furthermore, JMJD5 expression and/or localisation has

been shown to be regulated after cellular stress or induction of DNA damage (Huang et al., 2015, Shen et al., 2017). Therefore, it would be exciting to explore how DNA damage, DNA replication stress or stage of the cell cycle might impact JMJD5 sub-cellular localisation, activity, and its interaction with MCM3/5. This would also be an opportunity to investigate the role of the interaction between RCCD1 and JMJD5. Specifically, to explore the hypothesis that RCCD1 could be responsible for recruiting JMJD5 to chromatin (Chapter 1).

Thirdly, it would be interesting to explore whether JMJD5 is itself regulated by a PTM and whether this needs to be considered when monitoring a hydroxylation event *in vitro*. In addition, MCM proteins are known to be highly modified (Chapter 1). Therefore, it is possible that JMJD5 interacts with an MCM complex with specific PTMs. This could help to explain why no interaction was detected *in vitro* between JMJD5 and IVTT synthesised MCM3 and MCM5 (Figure 4.11). However, this could also be explained by a lack of cofactors present for this interaction which should also be addressed in future *in vitro* assays. In addition, the lack of JMJD5-MCM3/5 interaction associated with this *in vitro* assay (Figure 4.11) could also be explained by inactive MCM3/5 generated by IVTT. For example, if not properly folded or active the MCM3/5 could be prevented from interacting with JMJD5 *in vitro*. Therefore, the IVTT generated MCM3/5 samples used for future *in vitro* experiments should be first analysed for their functionality; including ATP binding, native folding and complex assembly.

In addition to investigating the JMJD5-MCM3/5 interaction in cells, further effort should be put towards mapping the minimal domain in MCM3/5 sufficient for a JMJD5 interaction. Based on current assays this is likely to be most successful using peptide competition assays (Figure 4.15). This approach could also be expanded to test competition of bacterially expressed sub-

domains of MCM3 and MCM5, recently purified by the Coleman lab. Such reagents could also provide an opportunity for direct hydroxylation reactions *in vitro,* using the GST-tagged JMJD5 protein that we demonstrated were active in Chapter 3 (Section 3.7.5).

Future analysis should also address any relevance of our consistent identification of a potential MCM3/5 subcomplex (Section 4.3.1). It is highly likely that our inability to purify the complete MCM hexamer was due to high salt concentrations in our lysis buffers. This would be consistent with the literature which has identified that MCM subunits have different affinities for each other *in vitro* and demonstrate that increasing salt concentrations result in the disruption of the heterohexamer (Prokhorova and Blow, 2000, Crevel et al., 2001). However, our ability to identify MCM3/5 sub-complexes could also infer potential functional importance of the JMJD5 targeted population. Although MCM sub-complexes (MCM3/5 and MCM4/6/7) have consistently been identified and purified in the literature (Prokhorova and Blow, 2000, Lee and Hurwitz, 2001, Davey et al., 2003, Yu et al., 2004), there is debate regarding their potential functional importance. Some evidence suggests that these MCM sub-complexes are identified at different stages of the cell cycle and may be required for loading the complete MCM complex onto chromatin (Coue et al., 1998). Some *in vitro* studies also suggest that the MCM4/6/7 sub-complex is responsible for ATPase and DNA helicase activity (Lee and Hurwitz, 2001, Schwacha and Bell, 2001, Davey et al., 2003). However, others propose the complex must be whole in order for successful nuclear localisation, loading and activation of the MCM complex for DNA replication (Prokhorova and Blow, 2000). Therefore, further investigation into this MCM3/5 sub-population, to establish whether it is functionally important or an artefact of experimental conditions, could be beneficial in optimising future experiments for

MS analysis. This could also help us in the future to infer functional importance of the hydroxylation reaction.

4.5.2 The Potential JMJD5-MCM3/5 Hydroxylation Pathway in Disease

Considering the evidence supporting a role for both MCM proteins and JMJD5 in human disease, we initiated preliminary investigation into potential regulation of the JMJD5-MCM3/5 interaction in this context.

Firstly, we found that the JMJD5-MCM3/5 interaction replicated in the fibroblast background (Figure 4.5). This was important as it constituted a more physiologically relevant model compared to the transformed cancer cell lines used previously (Figure 4.3 and 4.4). Interestingly, the JMJD5 C123Y developmental disorder mutation was found to interact with MCM3 and MCM5 in a similar manner to wildtype (Figure 4.17). This is perhaps unsurprising considering the location of the mutation outside of the catalytic domain. However, in Chapter 3 we demonstrated evidence suggesting that the C123Y mutation might inhibit the activity of JMJD5 (Section 3.7.5). Therefore, after identification of an MCM3/5 hydroxylation site, it would be interesting to test the activity of the C123Y mutant against the relevant synthetic peptide.

Interestingly, our analyses of online cancer databases identified a variety of tumour associated JMJD5 mutations, including hotspot and recurrent mutations, which were enriched in the catalytic domain (Figure 4.18). We hypothesised therefore that these mutations might interfere with JMJD5 function. Consistent with this, we observed that three recurrent cancer mutations reduced the interaction with MCM3 and MCM5 (Figure 4.18). This interaction level was comparable to the catalytic point mutation H321A further suggesting an effect of these

cancer mutations on JMJD5 activity. These preliminary findings have led to the development of a library of >20 JMJD5 cancer mutants, by the Coleman group. The majority of these show reduced MCM3/5 binding in the immunoprecipitation assay developed here (Tristan Kennedy, Coleman lab). In addition, we have acquired three cancer cell lines containing JMJD5 mutations, identified from COSMIC and cBioPortal analysis. These cell lines are KNS-62, derived from a metastatic bronchial squamous cancer patient (Takaki, 1980), which contains the JMJD5 mutation R339Q. Another is LU99A, a cell line derived from a lung cancer patient (Yamada et al., 1985) also containing the R339Q JMJD5 mutation. The final cell line is SKCO1, derived from a metastatic colorectal adenocarcinoma containing the JMJD5 mutation T165I. We have successfully confirmed the *JMJD5* genotype of these cell lines (data not shown) and now aim to characterise the JMJD5 mutations for how they might affect MCM3/5 interaction. Moreover, we propose that phenotypic analysis of these JMJD5 mutant cancer cell lines will help to compliment analysis performed for the affected patient fibroblasts (Chapter 5) and will help to address the disease relevance of JMJD5 in cancer.

Overall, JMJD5 mutations imply that interaction with MCM3/5 could be functionally important in the aetiology of disease. Consistent with this, our preliminary investigation suggested that JMJD5 loss of function in patient fibroblasts, affected by a developmental disorder, correlated with reduced MCM subunit protein expression (Figure 4.16). Interestingly, relatively low changes of MCM expression or cellular distribution were previously found to increase the susceptibility to developmental defects including growth retardation (Chuang et al., 2010). Therefore, further investigation into the potential functional consequence of the JMJD5-MCM3/5 interaction is warranted, as even mild perturbations in MCM regulation can have profound consequences.

4.5.3   Chapter conclusions

Overall, in this chapter we have presented evidence to suggest that MCM3 and MCM5 are novel candidate substrates of JMJD5. However, better understanding regarding the context of this interaction will help to not only understand more about the function of this interaction, but also to optimise *in vitro* and cellular assays to identify a hydroxylation site on MCM3 and/or MCM5. This will be essential for understanding the potential functional consequence of MCM hydroxylation and will help elucidate how JMJD5 dysregulation might be involved in the aetiology of disease.

5 Phenotyping JMJD5 mutations to investigate pathogenicity and cellular function

In Chapter 3 we described two JMJD5 mutations identified in patients with a novel human developmental disorder. We identified that both mutations negatively affected JMJD5 protein stability and enzymatic activity and proposed that the affected patient was hypomorphic for JMJD5 (Chapter 3). Consequently, we hypothesised that the clinical symptoms observed in the affected patients were likely to be as a result of their *JMJD5* genotype. In this chapter we investigated this by performing phenotypic analysis on dermal fibroblast cell lines that were generated from family members affected by this developmental disorder. We hoped that this investigation would give more information regarding origins of the disorder, which could help with future clinical intervention for the affected patients. Moreover, the immortalised dermal fibroblasts obtained from this family provided a novel cellular model to investigate JMJD5. Consequently, we aimed to utilise this model to clarify and broaden the current literature regarding the cellular functions of JMJD5. The direction and rationale for our phenotypic analysis is discussed below.

As mentioned above we hypothesised that the clinical phenotypes of our affected patients were likely to be as a direct result of their *JMJD5* genotypes. This was firstly because the *JMJD5* genotype segregated with clinical symptoms of the patients (Chapter 3). Secondly, because the retarded growth of the affected patients aligned with severe growth defects observed in a JMJD5 knockout mouse model (Ishimura et al., 2012). Interestingly, other developmental disorders, broadly classified into a group termed Primordial Dwarfism (PD), had some overlapping clinical phenotypes with our affected patients. For example, intrauterine growth

restriction that continues to worsen postnatally (Shaheen et al., 2014). PD disorders have heterogeneous genetic causes but are commonly associated with pathways essential for cell survival or proliferation (Klingseisen and Jackson, 2011) . Therefore, when considering how JMJD5 mutations might translate to patient clinical phenotypes, we initially focussed on cellular processes implicated in cell growth, proliferation and survival.

Due to the assignment of the minichromosome maintenance complex (MCM) subunits 3 and 5 as candidate substrates of JMJD5 (Chapter 4), we were particularly interested in exploring whether our affected patients had a phenotype associated with deficient DNA replication. In fact, the association between developmental growth and DNA replication has already been made. For example, Meier-Gorlin Syndrome (MGS) patients are classified with a PD disorder while presenting with pathogenic mutations in components essential for DNA replication licencing and firing. These include pre-RC components ORC1, ORC4, ORC6, Cdt1, Cdc6 (Bicknell et al., 2011a, Bicknell et al., 2011b, Guernsey et al., 2011, Kuo et al., 2012, Shalev et al., 2015), as well as Cdt1 inhibitor Geminin which is important for regulating pre-RC formation (Burrage et al., 2015). Furthermore, MGS patients have also been found to carry mutations in the helicase essential for DNA replication, including MCM5 (Vetro et al., 2017), and Cdc45 of the GINS complex (Fenwick et al., 2016, Ting et al., 2019). Other components of the DNA replisome that have also been found to contribute towards PD disorders are DONSON, which acts as a DNA replication fork protection factor (Reynolds et al., 2017, Karaca et al., 2019), and POLE which encodes the catalytic subunit of DNA polymerase ε (Logan et al., 2018). Perhaps unsurprisingly, many of these PD disorder patients have increased DNA replication stress (defined in Section 5.1.1) as a result of their genotypes (Balasov et al., 2015, Harley et al., 2016, Vetro et al., 2017, Reynolds et al., 2017). This evidence that PD classification of patients

is strongly associated with mutations in replication factors is highly supportive of our hypothesis that JMJD5 mutations in our developmental disorder patients could be associated with deficient DNA replication.

Interestingly, both the MCM complex and JMJD5 have also been linked to increased replication stress and genomic instability. Specifically, the activity of the MCM complex at 'dormant origins', which is an essential mechanism for cells to overcome or deal with periods of DNA replication stress, discussed in more detail in Section 5.1.1.2 (Woodward et al., 2006, Ge et al., 2007, Ibarra et al., 2008). In addition, JMJD5 loss of function has been linked to increased genomic instability, with some speculating that this could be due to a role in DNA damage repair (Suzuki et al., 2006, Amendola et al., 2017, Shen et al., 2017).

Considering the observations outlined above, we hypothesised that the affected patient fibroblasts might show signs of replication stress, as a result of impaired DNA replication. Therefore, in this chapter we aimed to investigate this and hoped that this characterisation would help to shed light on the pathogenicity of the *JMJD5* genotype as well as helping to better define the biological activity of JMJD5. Before presenting the results of this investigation we first provide a more detailed overview of the replication stress field, and the methods used for studying it.

5.1 An introduction to DNA replication stress

DNA replication stress (RS) does not define a single event or refer to a specific DNA damage structure, but rather RS is broadly defined as anything that slows or impedes the progression of the DNA replication fork (Zeman and Cimprich, 2014). It is essential for a cell to restore progression of DNA replication as unresolved RS can result in under-replicated DNA or DNA damage. Therefore, pathways downstream of RS are essential for maintaining genomic stability.

5.1.1 Causes of DNA replication stress

RS can be caused by many endogenous and exogenous sources (summarised in Figure 5.1A). In relation to endogenous sources, there are regions of the genome termed common fragile sites (CFS) that are more susceptible to causing RS than others because of their inherent properties (Glover et al., 1984). For example, difficult to replicate regions such as telomeres and repetitive sequences (Krasilnikova and Mirkin, 2004). In addition, highly transcribed regions have inherent properties increasing their susceptibility to RS, including positive supercoiling of DNA between the transcription and replisome machinery, RNA hybridisation to DNA (R-loops) which can form as the gene is transcribed, and collisions between the transcription machinery and the replisome (Bermejo et al., 2012, Barlow et al., 2013, Garcia-Muse and Aguilera, 2016). Alongside CFS, other endogenous sources of RS include physical obstacles such as sites of DNA damage, repair intermediates or DNA secondary structures (Zeman and Cimprich, 2014, Thys and Wang, 2015). RS can also be caused by improper origin firing and depletion of essential factors, such as nucleotides (Anglana et al., 2003, Toledo et al., 2013, Mejlvang et al., 2014). Exogenous sources of RS imitate or exacerbate these endogenous properties. For example, hydroxyurea inhibits ribonucleotide reductase to

diminish nucleotide production, aphidicolin inhibits DNA polymerases and topoisomerase inhibitors exacerbate topological DNA stress. Other sources include ultraviolet light, ionising radiation and chemotherapeutic compounds, such as cisplatin, which cause DNA damage lesions, reviewed by (Vesela et al., 2017).

RS leads to functional uncoupling of the DNA helicase and replisome (Byun et al., 2005). The product of this is stalled DNA replication forks with long stretches of single stranded DNA (ssDNA) as the helicase continues to unwind DNA ahead of the stalled fork (Figure 5.1B). In fact, the presence of ssDNA at replication forks is considered a hallmark of RS (Magdalou et al., 2014). Overall, there are a multitude of sources of RS that pose a barrier to the completion of DNA replication, consequently the cell is prepared with mechanisms to prevent and respond to RS, discussed in the following section.
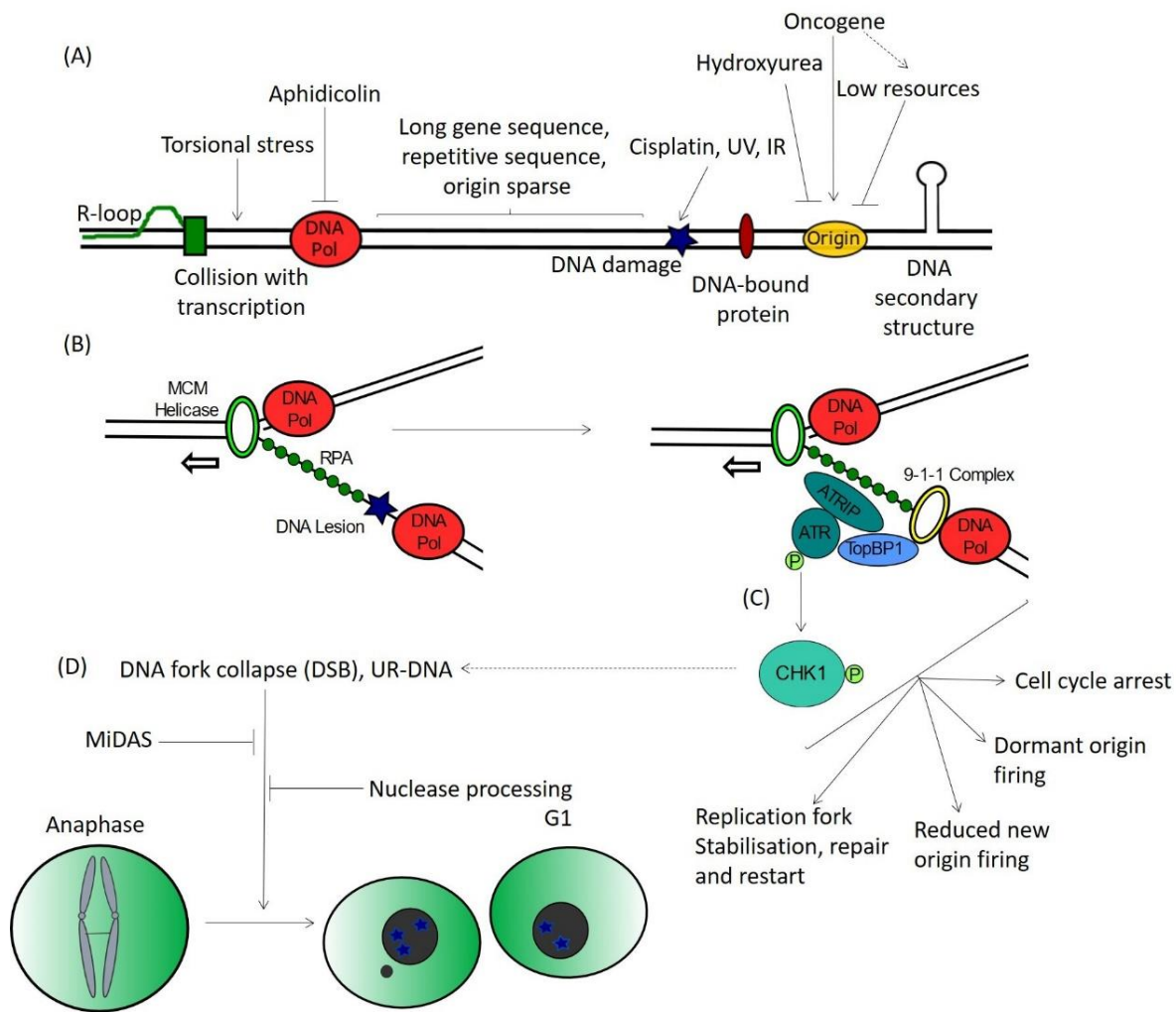
Figure 5.1 Causes, cellular response and consequences of DNA replication stress
(A) Endogenous and exogenous sources of replication stress. Abbreviations: DNA-RNA annealing (R-loop), DNA polymerase (DNA pol), ultraviolet light (UV) and ionising radiation (IR). **(B)** The cellular response to replication stress. Functional uncoupling between the mini-chromosome maintenance complex (MCM) helicase and DNA polymerase due to a lesion (blue star) commonly results in a stalled fork and long stretches of single-stranded DNA. This is bound by RPA, ATRIP-ATR, the 9-1-1 complex and TopBP1 which results in the phosphorylation and activation of ATR followed by activation of CHK1. **(C)** ATR and CHK1 activate the replication stress response pathway that aims to repair the damage before continued DNA replication. **(D)** If unsuccessful, DNA forks collapse resulting in a double strand break (DSB) or under-replicated DNA (UR-DNA). During mitosis mitotic DNA synthesis (MiDAS) aims to prevent anaphase bridges (DNA links between two separating sister chromatids) which are also processed by nucleases. If unsuccessful this can result in chromosome breakage to form micronuclei and/or 53BP1 bodies (blue stars) detectable in G1 phase.

5.1.2 The Cellular response to DNA replication stress

The cellular response to RS is aimed towards restoring the progression of the replication fork to ensure completion of DNA replication (summarised in Figure 5.1B). As discussed above, the major products of RS are stalled DNA replication forks associated with long stretches of ssDNA (Magdalou et al., 2014). This ssDNA is rapidly bound by RPA, which helps to stabilise the ssDNA by preventing nuclease degradation, and signals to activate the RS response pathway (Zou and Elledge, 2003, Fanning et al., 2006). This signal is amplified by a highly conserved phosphoinositide 3-kinase related protein kinase (PIKK) ATM-Rad3-related (ATR) (Cimprich and Cortez, 2008). Another key PIKK in the cell is Ataxia Telangiectasia Mutated (ATM), which is generally activated in response to double strand breaks (DSBs). The recruitment of ATR to sites of RS, is facilitated by ATR-interacting protein (ATRIP) which binds to RPA at sites of ssDNA (Zou and Elledge, 2003, Ball et al., 2007). This is joined by another protein complex, RAD9-RAD1-HUS1 (a.k.a. the 9-1-1 complex), that is loaded onto the 5' ssDNA primer-template junction (Majka et al., 2006). The 9-1-1 complex then recruits TopBP1, via its interaction with RAD9, which mediates activation of ATR (Lee et al., 2007, Mordes et al., 2008).

Once activated, ATR amplifies the signal by phosphorylating the histone variant H2AX resulting in γH2AX (Ward and Chen, 2001). ATR also helps to activate the cellular response to RS by phosphorylating and activating the checkpoint kinase 1 (CHK1) (Lopez-Girona et al., 2001, Capasso et al., 2002). Once activated, phosphorylated CHK1 is released from chromatin in order to phosphorylate substrates that regulate downstream cellular pathways (Smits et al., 2006). Consequently, the ATR and CHK1 kinases act as the central regulators of the RS response (summarised in Figure 5.1C). The combined effort of the activated kinases is to mediate signalling that prevents late origin firing and inhibition of the cell cycle to enable time

for DNA repair and replication fork restart. This activity ensures that the source of the stress is resolved before continued replication occurs. It also preserves essential resources, such as nucleotides, for when DNA replication is re-started. This activity is also essential for preventing fork collapse which can result in single-ended DSBs (Cortez, 2015). The activity of ATR-CHK1 is reviewed by Cimprich and Cortez (2008).

DNA replication can also be continued by the activation of dormant origins, which is especially important when two converging forks stall. The discovery of dormant origins helped to resolve the 'MCM paradox' relating to why there is loading in excess of MCM complexes onto DNA (Das et al., 2014). During unperturbed S phase the majority of MCM complexes are not activated, however, during RS dormant origins can be activated to ensure complete DNA replication of regions surrounding a stalled fork (Woodward et al., 2006, Ge et al., 2007, Ibarra et al., 2008). Although the regulation of these dormant origins was largely thought to be a stochastic event (Ge et al., 2007), recent evidence demonstrates that they are activated proximal to stalled forks by ATR-CHK1 mediated phosphorylation of MCM2 (Cortez et al., 2004, Trenz et al., 2008, Ge and Blow, 2010).

It is essential for cells to repair damage and complete DNA replication in order to maintain genomic stability. If this is not completed successfully in S phase, then cells can attempt to amend this during G2 phase and early mitosis. An essential pathway for this is by mitotic DNA synthesis (MiDAS). The major aim of this pathway is to avoid under-replicated DNA by completing DNA replication before completion of mitosis to prevent chromosome separation defects (summarised in Figure 5.1D). Any remaining lesions can result in the formation of ultrafine DNA anaphase bridges (UFBs) between sister chromatids. These are commonly

associated with CFS and can be removed by nuclease and helicase processing during mitosis for repair by MiDAS (Garribba et al., 2018, Minocherhomji et al., 2015). However, if unsuccessful this can contribute towards loss of genetic material and thus genomic instability (Chan et al., 2009). The importance of these combined pathways to prevent genomic instability is discussed below.

5.1.3 Consequences of DNA replication stress

The consequences of unresolved or persistent RS can be increased genomic instability (GI) and reduced cellular survival. During RS high rates of mutagenesis can occur due to errors generated while repairing RS-induced damage. For example, lesions repaired by the DNA damage tolerance pathway called 'translesion synthesis', where the replication is completed by lesion bypass, commonly result in nucleotide substitution due to the lower fidelity of the DNA polymerases involved (Prakash et al., 2005, McCulloch and Kunkel, 2008). Under-replicated regions of DNA are repaired by break-induced replication (BIR) pathways which utilises invasion into a homologues sequence to generate a replication fork that has low processivity and is highly error-prone (Hastings et al., 2009, Costantino et al., 2014). Also, single-ended DSBs, created after fork collapse, are susceptible to error-prone repair pathways as they do not present the usual template for normal DSB repair mechanisms (Gelot et al., 2015). Furthermore, as introduced above, unresolved RS lesions not repaired before the end of mitosis pose a barrier to proper chromatid separation. This can result in the formation of micronuclei or 53BP1 bodies which are discussed in greater depth in the next section (Figure 5.1D).

Importantly, one result of GI is the accumulation of mutations that can further promote RS, by dysregulating downstream response pathways and cell cycle checkpoints. This positive feedback between increased RS and GI is now recognised as an important driver of tumourigenesis. As a result, RS has been proposed as a hallmark of cancer and consequently a potential therapeutic target (Gaillard et al., 2015, Macheret and Halazonetis, 2015).

RS can also contribute to the aetiology of other human diseases. For example, as discussed above, PD patients that carry mutations in proteins essential for DNA replication commonly present with RS phenotypes (Bicknell et al., 2011b, Balasov et al., 2015, Harley et al., 2016, Reynolds et al., 2017, Vetro et al., 2017). ATR mutations themselves are rare, due to the fundamental nature of the protein (de Klein et al., 2000). However, a PD disorder called 'Seckel syndrome' is caused by mutations in ATR, which results in impaired RS response and clinical growth retardation phenotypes (O'Driscoll et al., 2003). These brief examples help to illustrate how essential the RS response pathway is for normal cellular function and how when mutated the resulting dysregulation can contribute to human disease.

5.1.4 Monitoring DNA replication stress *in vitro*

RS can be detected and studied in many ways *in vitro*. Examples include the detection of ATR-specific phosphorylation events such as phosphorylated serine 33 on RPA or serine 345 on CHK1 (Zeman and Cimprich, 2014). Other markers include phosphorylated H2AX (γH2AX), RPA foci and ssDNA. However, these markers often rely on a strong ATR response and so are not always sensitive enough to detect low level RS (Zeman and Cimprich, 2014). Furthermore, these markers may not detect other sources of RS, such as DNA-protein complexes, which can activate alternative pathways (Zeman and Cimprich, 2014). Moreover, these markers may not

necessarily be specific for RS as many of the downstream targets of the ATM pathway (DSB response) also converge on the ATR pathway (RS response) (Cimprich and Cortez, 2008). For example, γH2AX and formation of RAD51 foci have been found in ATR-deficient cells due to the activity of ATM, which demonstrates that the ATR and ATM pathways can coordinate in their downstream cellular responses in order to prevent GI and maintain cell viability (Jazayeri et al., 2006). Therefore, RS is often studied using multiple methods in parallel and in conjunction with known RS inducing agents.

In this chapter we used three assays in parallel to test our hypothesis that our affected patient fibroblasts could have increased RS. The assays included: 1) counting micronuclei, 2) counting 53BP1 bodies, and 3) monitoring progression of DNA replication by the DNA fibre analysis. These assays are described in detail below.

5.1.4.1   Indirect analysis of replication stress: micronuclei and 53BP1 bodies

If RS is persistent or un-resolved during S phase and before the anaphase stage of mitosis, then RS can be detected in the subsequent daughter cells (Figure 5.1). As discussed above, this is because unresolved RS poses a barrier to proper chromosome separation during mitosis in the form of UFB (Figure 5.1D). If repair is unsuccessful, DNA can be lost from cells after chromosome breakage in the form of micronuclei. Alternatively, the damage may persist and become associated with 53BP1 nuclear bodies that endeavour to resolve the damage to prevent GI. Both micronuclei and 53BP1 bodies can therefore be used *in vitro* to monitor RS in the subsequent daughter cells (Figure 5.2).

Counting micronuclei provides a quicker and cheaper alternative to analysing chromosome abnormalities after metaphase spread. As the counting of micronuclei can be performed simply by using DAPI staining of cells, it also means that the assay can be scaled up to screen larger populations of cells. Micronuclei are composed of whole or fragmented chromosomes not incorporated into daughter nuclei (Fenech et al., 2011). Although they can be caused by errors in the regulation of mitosis, DNA damage or chromosomal rearrangements, they are most common after periods of RS (Fenech et al., 2011). In this thesis we counted micronuclei in the patient fibroblasts as a marker of RS (Figure 5.2).

Nuclear bodies are defined as dynamic protein complexes that are microscopically detectable and localised within sub-nuclear domains (Fernandez-Vidal et al., 2017). The major component of 53BP1 bodies is the protein 53BP1. This has been demonstrated to be important for V(D)J recombination (Manis et al., 2004) and DSB repair, where it can be visualised in small nuclear foci throughout the cell cycle by immunofluorescence (Anderson et al., 2001, Ward et al., 2003). In response to RS 53BP1 forms larger multi-protein complexes called 53BP1 bodies which are distinct structures playing a separate role to 53BP1 foci. These bodies form in the G1 phase of daughter cells following RS that occurred in the mother cell. Their major role is to mediate recruitment repair proteins that facilitate the resolution of the damage (Harrigan et al., 2011, Lukas et al., 2011, Moreno et al., 2016, Fernandez-Vidal et al., 2017, Feng and Jasin, 2018, Her et al., 2018, Spies et al., 2019).. Therefore, the presence of 53BP1 bodies in G1 cells has been adopted as a method to monitor RS, which we used in this chapter to analyse the patient fibroblasts (Figure 5.2).

In these assays we treated the cells with aphidicolin, which causes RS due to its inhibition of B-family DNA polymerases. Its potency is most strongly directed towards DNA polymerase α where it competes with nucleotides binding to the active site (Baranovskiy et al., 2014). Therefore, aphidicolin was used as a positive control for the induction of RS markers.
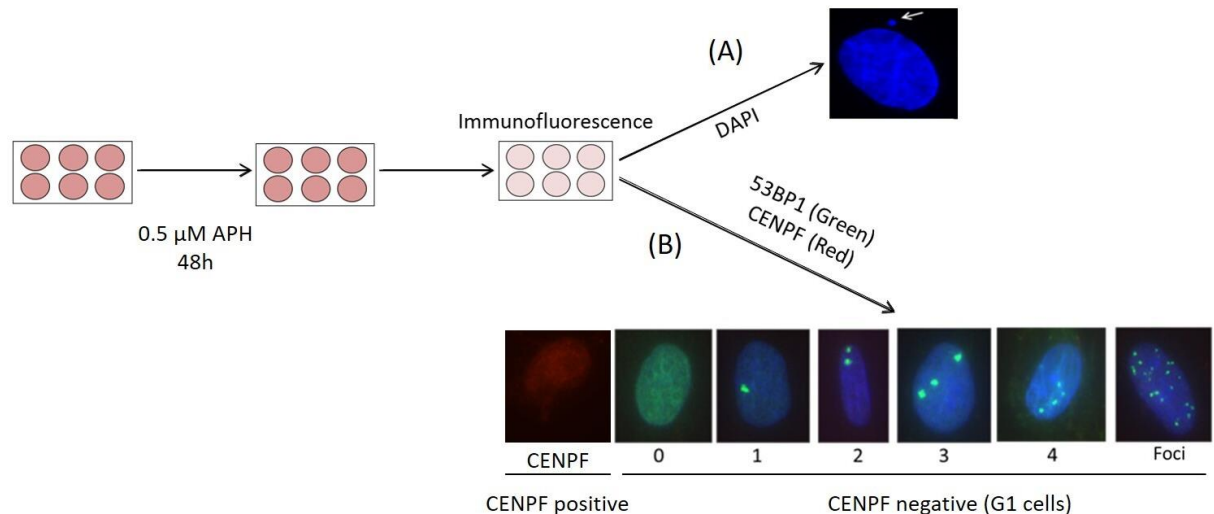
Figure 5.2 Method of monitoring micronuclei and 53BP1 bodies
In this thesis two assays were used to monitor DNA replication stress indirectly by the detection of micronuclei and 53BP1 bodies (present in G1 cells). Fibroblasts were plated onto coverslips and 0.5 μM aphidicolin (APH) treatments performed 48 hours prior to harvesting the cells for immunofluorescence. **(A)** Micronuclei were detected using DAPI staining of DNA. **(B)** 53BP1 bodies were detected by using co-staining for CENPF as a marker of the cell cycle (CENPF negative cells were indicative of G1 phase), and 53BP1 staining to detect bodies. These 53BP1 bodies were distinguished from 53BP1 foci due to their larger size, presence specifically in G1 cells and frequency per cell.

5.1.4.2   Direct analysis of replication stress: DNA fibre analysis

Progression of DNA replication can be monitored *in vitro* using the DNA fibre assay. The basis of the assay is the incorporation of halogenated thymidine nucleotide analogues into actively replicating DNA by replication machinery in the cell. The subsequent detection of these nucleotides by immunofluorescence, gives resolution at the single DNA molecule level, as opposed to the cellular level achieved using BrdU flow cytometry approaches (Nieminuszczy et al., 2016). However, one limitation of the assay is that fibres only encompass a few kilobases

of DNA compared for example to complete chromosomal analysis after metaphase spread (Quinet et al., 2017). However, in this thesis we utilised the DNA fibre assay as a direct and sensitive method of detecting RS to complement micronuclei and 53BP1 bodies analysis in the patient fibroblasts. The DNA fibre method is outlined in more detail below.

Firstly, cells are incubated with a chlorine-labelled thymidine analogue (CldU) for 20 minutes, which is then removed and replaced with an iodine-labelled thymidine analogue (IdU), also incubated for 20 minutes. Each incubation allows incorporation of the analogue into newly synthesised DNA. Cell lysates are then run down the length of a microscope slide to spread DNA fibres. These DNA fibres are then analysed using immunofluorescence to detect each thymidine analogue (methods adapted from Parra and Windle (1993)). In this thesis the first analogue (CldU) was detected using Alexa Fluor® 555 nm (red) secondary antibody and the second analogue (IdU) was detected using Alexa Fluor® 488 nm (green) secondary antibody (Figure 5.3A).

The different staining pattern of DNA fibres allows the identification of different DNA structures (Figure 5.3B) including origin firing, ongoing replication and termination (described in more detail in Section 5.3.3). In this thesis we used these fibre structures to determine the relative abundance of stalled replication forks (Section 5.3.3), asymmetric fork progression (Section 5.3.4), and calculation of replication fork speed (Section 5.3.5).

In these assays we also included treatment of hydroxyurea, incubated for two hours between each thymidine analogue. As hydroxyurea is an inhibitor of ribonucleotide reductase it prevents the synthesis of nucleotides. This causes RS due to the subsequent depletion of the

nucleotide pool available for DNA replication (Singh and Xu, 2016). Therefore, hydroxyurea treatment was used as a positive control for replication fork abnormalities in response to RS.
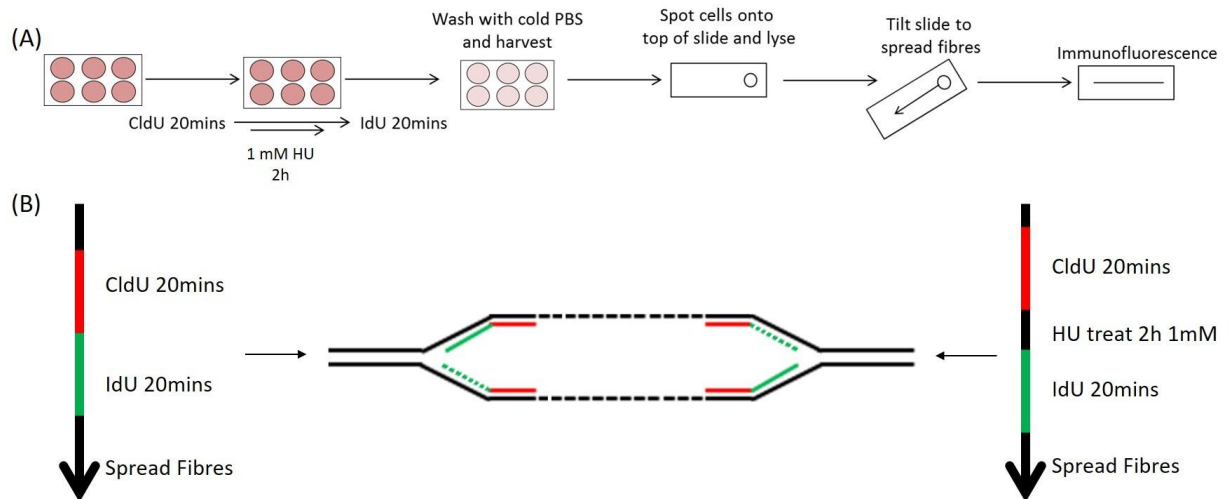
Figure 5.3 The DNA fibre assay method
The progression of DNA replication forks was monitored using the DNA fibre assay. **(A)** Fibroblasts were incubated with a chlorine-labelled thymidine analogue (CldU) for 20 minutes before washing out and incubating the cells with an iodine-labelled thymidine analogue (IdU) for 20 minutes. In between these labels cells could be incubated with 1 mM hydroxyurea (HU) for 2 hours. Cells were then lysed, 'spread' down the length of the microscope slide and fixed. Immunofluorescence staining was then used to distinguish between the chlorine- and iodine-labelled thymidine analogues. **(B)** The first thymidine analogue (CldU) was detected using an Alexa Fluor® 555 nm secondary antibody (red), the second thymidine analogue (IdU) was detected using an Alexa Fluor® 488 nm secondary antibody (green). This enabled identification of different DNA replication structures based on labelling patterns.

5.2 Identification of a JMJD5 associated cellular phenotype

In this chapter we aimed to test our hypothesis that the *JMJD5* genotypes caused the clinical phenotypes of the affected patients by investigating JMJD5-dependent cellular functions.

The most striking clinical phenotype of the affected patients was reduced pre- and postnatal growth (Table 3.1, Chapter 3). Therefore, we were first interested to establish whether this growth phenotype was reproduced *in vitro*. In order to do this, we compared cellular phenotypes of fibroblasts acquired from the affected patient (OR07) with fibroblasts from the

JMJD5 wildtype patient (MR98), the carrier of the C123Y mutation (LR74) and a carrier of the InMut (AR00).

Firstly, we monitored cell cycle progression in an asynchronous population of fibroblasts from each patient using propidium iodide staining and flow cytometry analysis. Propidium iodide binds non-specifically to nucleic acid and can therefore be used to monitor the DNA content of cells, which can in turn be used to determine cell cycle phase. The percentage of cells in each phase of the cell cycle was determined based on the total number of cells analysed. From this we determined that there was no significant difference in the distribution of cells between phases of the cell cycle between our patient fibroblasts (Figure 5.4A). Therefore, the *JMJD5* genotype did not appear to alter cell cycle progression.

Next, we aimed to monitor cell proliferation by performing an MTS assay, which as discussed in Chapter 2 utilises the detection of a coloured formazan product as a readout for the presence of viable cells. When we performed this assay on the patient fibroblasts, we found no correlation between cell proliferation and *JMJD5* genotype (Figure 5.4B). However, because this is an indirect method which assumes that metabolism is comparable between cell lines, we decided to use a more direct cellular proliferation assay. In this assay fibroblasts were plated at a low density and cell numbers were manually counted over six days. However, again we found no difference in cellular proliferation that correlated with *JMJD5* genotype (Figure 5.4C). Overall, these assays indicated that the *JMJD5* genotype in this fibroblast model was not associated with significant changes in cell proliferation.
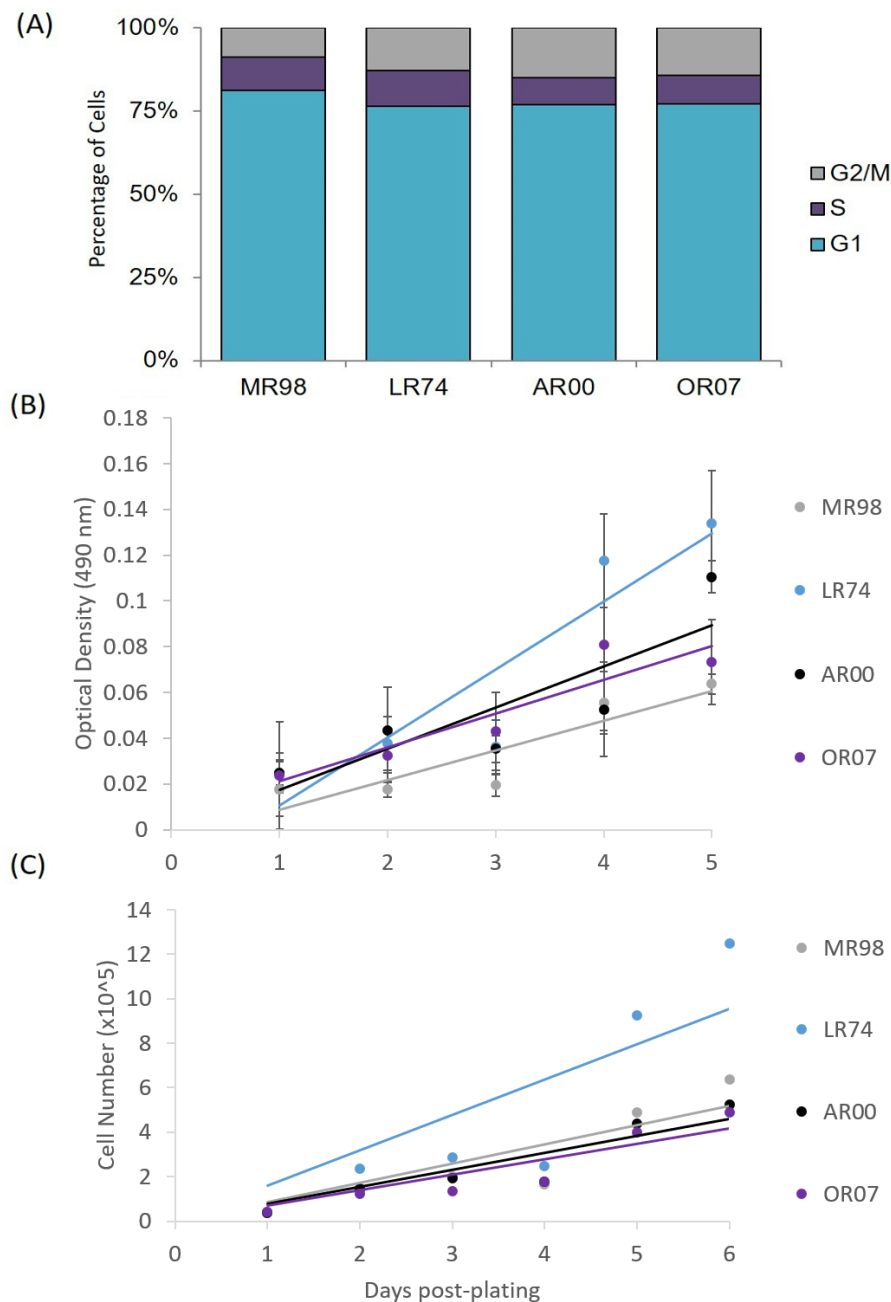
Figure 5.4 Patient fibroblasts have similar cell cycle progression and proliferation rates
Analysis performed on patient fibroblasts from MR98 (JMJD5 wildtype patient), LR74 (C123Y carrier patient), AR00 (InMut carrier patient) and OR07 (affected patient). **(A)** Fibroblasts grown until at 70% confluent then harvested into ethanol. RNAse A was added to remove contaminating RNA, and nucleotides stained using propidium iodide before running samples on a CyanB flow cytometry machine (Beckman Coulter). Live and viable cells were gated, based on their forward and side scatter, then analysed for propidium iodide staining to determine cell cycle phase, presented as a percentage of total cells analysed. This is representative of an n=1 biological repeat. Fibroblasts were plated at low density and cell proliferation monitored by: **(B)** MTS assay performed every day for five days. This is representative of an n=1 biological repeat, with quadruplicate technical repeats. OR **(C)** Manual counting cell numbers daily for six days using a haemocytometer. This is representative of an n=1 biological repeat averaged over quadruplicate technical repeats.

We next aimed to investigate whether exposing the cells to an exogenous stress could precipitate a cellular phenotype in the affected patient fibroblasts. In order to undertake this investigation, we plated the patient fibroblast cell lines at limited density and colonies formed after two weeks were visualised using the non-specific protein stain crystal violet. Colony formation was calculated by counting the number of colonies compared to the number of cells originally plated. This was then plotted relative to the wildtype patient fibroblasts (MR98).

Interestingly, we found that the affected patient fibroblasts had significantly reduced colony formation compared to all other patient fibroblast cells (Figure 5.5). This suggested that the *JMJD5* genotype could be pathogenic. Consequently, we aimed to investigate the phenotype of these cells in more detail.
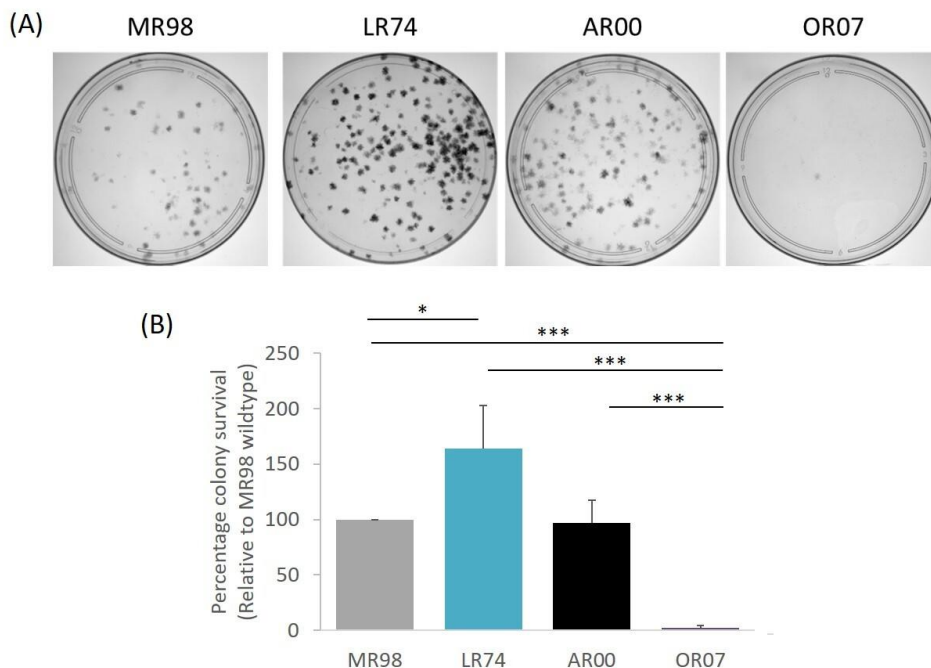
Figure 5.5 The affected patient fibroblasts have reduced colony formation
Patient fibroblasts from MR98 (JMJD5 wildtype patient), LR74 (C123Y carrier patient), AR00 (InMut carrier patient) and OR07 (affected patient) were plated at a limited plating density and grown for two weeks. Colonies were then stained using crystal violet. **(A)** Images representative of n=3 biological repeats. **(B)** Colony formation determined relative to the number of cells plated and expressed as a percentage relative to the wildtype patient (MR98) fibroblasts. Statistical analysis performed using the two-tailed Student's t-test (p-value ≤ 0.05 represented by '*', ≤0.01 represented by '**', ≤0.001 represented by '***'). This is representative of n=3 biological repeats.

5.3 Affected patient fibroblasts have increased DNA replication stress

In order to investigate the molecular mechanism behind the colony formation phenotype of the affected patient fibroblasts we endeavoured to identify a cellular pathway defective in these fibroblasts. As outlined in the introduction to this chapter, we hypothesised that the *JMJD5* genotypes of the affected patients could cause dysregulated DNA replication. Therefore, we aimed to monitor the fibroblasts for endogenous RS, response to RS inducing agents, and whether any phenotype correlated with *JMJD5* genotype.

5.3.1 Affected patient fibroblasts have increased micronuclei

RS was first monitored by counting the percentage of cells with micronuclei. As discussed in Section 5.1.4.1, micronuclei can be detected using DAPI staining as a marker of RS in the previous S phase (Figure 5.6A).

At the basal level, we found that unaffected patient fibroblasts had a low frequency of cells with micronuclei, whereas the affected patient fibroblasts had a significantly higher frequency of cells with micronuclei (Figure 5.6B). We found that all fibroblast lines responded to 48 hours of aphidicolin treatment with increased frequency of micronuclei (Figure 5.6C). Interestingly, the affected patient fibroblasts responded significantly more to aphidicolin treatment than the unaffected cell lines. Overall, we hypothesised that the affected patient fibroblasts had increased levels of basal RS compared to unaffected patient fibroblasts.
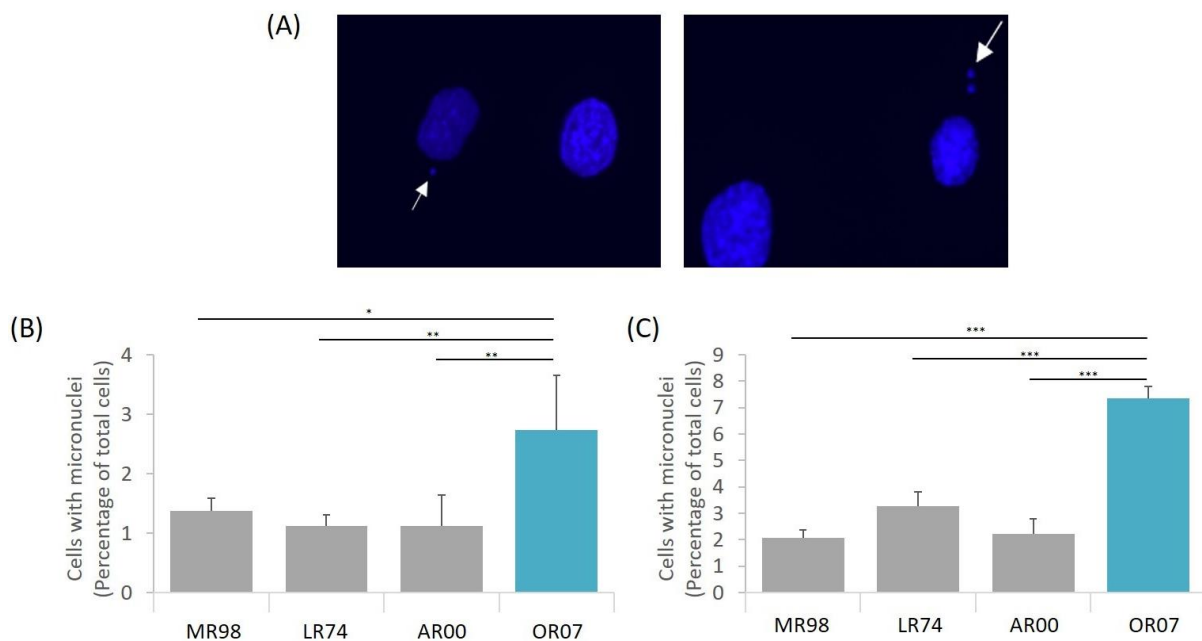
Figure 5.6 The affected patient fibroblasts have increased frequency of micronuclei

Patient fibroblasts from MR98 (JMJD5 wildtype patient), LR74 (C123Y carrier patient), AR00 (InMut carrier patient) and OR07 (affected patient) were analysed by immunofluorescence. **(A)** DAPI staining was performed to detect micronuclei (white arrows). Total number of cells containing micronuclei was determined. Cells containing **(B)** endogenous micronuclei or **(C)** micronuclei after 48 hours of 0.5 μM aphidicolin treatment were counted and expressed as a percentage of total cells counted. Statistical analysis performed using the two-tailed Student's t-test (p-value ≤ 0.05 represented by '*', ≤0.01 represented by '**', ≤0.001 represented by '***'). This is representative of n=6 biological repeats.

5.3.2 Affected patient fibroblasts have increased 53BP1 bodies in G1 cells

In order to confirm whether our micronuclei phenotype correlated with the *JMJD5* genotype, we used an independent readout of RS by counting 53BP1 bodies. As mentioned in Section 5.1.4.1, 53BP1 bodies are a reliable method of detecting unresolved damage from RS from the previous S phase. They are distinct from 53BP1 foci, which are markers of DNA double strand breaks, because of their larger size and their presence specifically in G1 phase of the cell cycle. Immunofluorescence analysis was used to detect 53BP1 bodies, which were counted in G1 cells, as determined by co-staining with centromere protein F (CENPF) (Figure 5.7A). CENPF is a centromere-kinetochore binding protein that is expressed highly in G2 and mitosis, moderately expressed in S phase and not expressed in G1. Therefore, it is used widely as a

marker of cell cycle phase (Liao et al., 1995). In this thesis we counted 53BP1 bodies in CENPF negatively stained cells indicative of cells in G1 phase. We found that cells had a range from zero up to ten 53BP1 bodies per G1 phase cell (Figure 5.7B). However, as the majority of cells contained one to three 53BP1 bodies we totalled cells containing any number of 53BP1 bodies and measured this as a percentage of total cells counted.

We observed that the affected patient fibroblasts had a significantly increased basal frequency of G1 cells with 53BP1 bodies, compared to the unaffected patient fibroblasts (Figure 5.7C). This basal level of RS was exacerbated in response to aphidicolin treatment in all patient fibroblasts, with the greatest response observed in the affected patient fibroblasts (Figure 5.7D). These results are consistent with the micronuclei data, and therefore together indicate that affected patient fibroblasts exhibit elevated RS, consistent with our hypothesis.
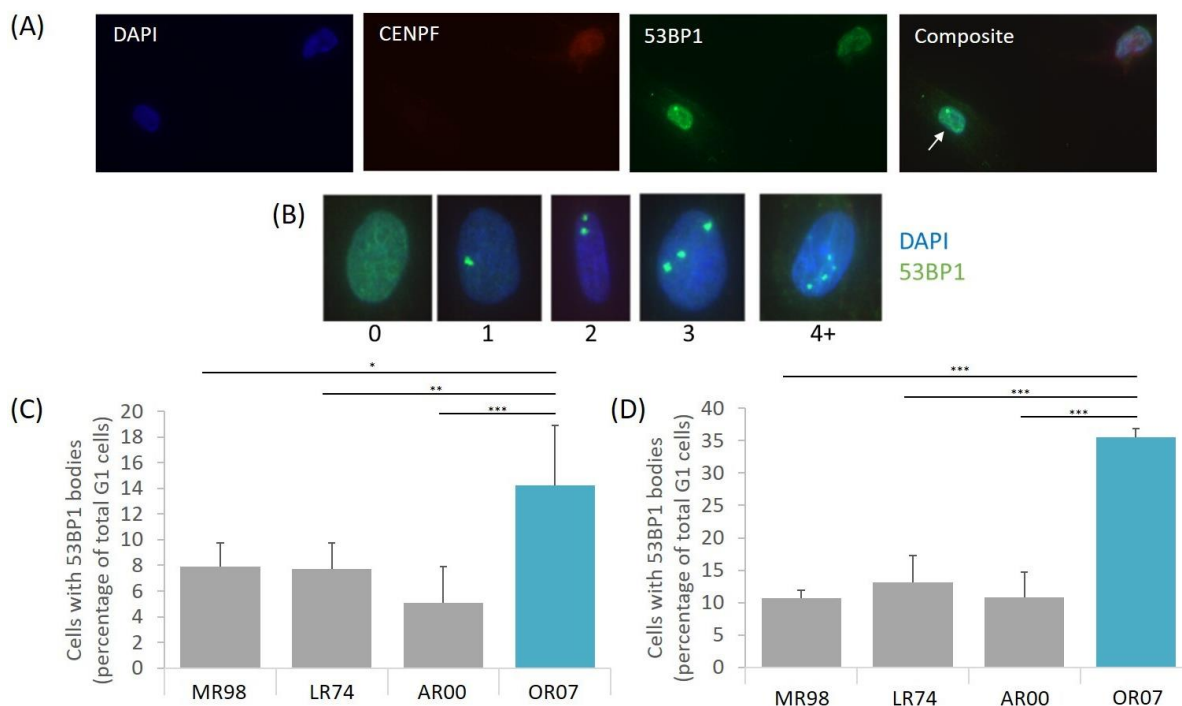
Figure 5.7 The affected patient fibroblasts have increased 53BP1 bodies in G1 cells

Patient fibroblasts from MR98 (JMJD5 wildtype patient), LR74 (C123Y carrier patient), AR00 (InMut carrier patient) and OR07 (affected patient) were plated onto coverslips. Cells were then harvested for immunofluorescence staining. **(A)** DAPI staining of DNA was used as a counterstain for nuclei. CENPF was used to determine the phase of the cell cycle (CENPF negatively stained cells marking G1 cells). In G1 cells 53BP1 bodies were counted using 53BP1 staining (white arrow). **(B)** The total number of G1 cells containing 53BP1 bodies was counted, as **(C)** endogenous 53BP1 bodies or **(D)** 53BP1 bodies after 48 hours of 0.5 μM aphidicolin treatment. This was expressed as a percentage of total G1 cells counted. Statistical analysis performed using the two-tailed Student's t-test (p-value ≤ 0.05 represented by '*', ≤0.01 represented by '**', ≤0.001 represented by '***'). This is representative of n=6 biological repeats.

5.3.3 Affected patient fibroblasts have increased stalled replication forks

Since RS is defined by stalled DNA replication forks (Zeman and Cimprich, 2014), we would expect the affected patient fibroblasts to have an increased frequency of stalled DNA replication forks compared to the unaffected fibroblasts. Therefore, we aimed to monitor this using the DNA fibre assay (described in Section 5.1.4.2). In this assay identification of different DNA structures is made possible as the two thymidine analogues can be distinguished using immunofluorescence.

Lengths of replicating DNA that continue replicating during incubation with each analogue form red-green structures (ongoing fork, Figure 5.8A). Lengths of replicating DNA, where DNA replication origins fired during incubation of the first chlorine-labelled analogue, and then continued DNA replication during the second iodine-labelled analogue, form green-red-green structures (First label origin, Figure 5.8A). DNA replication origins that fired during incubation with the second thymidine-labelled analogue form green only structures (Second label origin, Figure 5.8A). DNA replication forks that replicated during incubation with the first chlorine-labelled analogue but then converged and terminated during the second thymidine-labelled analogue form red-green-red structures (Second label termination, Figure 5.8A). All these DNA replication structures were defined as ongoing DNA replication forks. The presence of red only structures (Figure 5.8A) represented DNA replication forks that either terminated during incubation with the first chlorine-labelled analogue or had stalled. Terminated DNA replication forks have a relatively low frequency that are comparable between unperturbed DNA replication and in times of RS. Therefore, we could conclude that increased frequency of red only DNA fibre structures was representative of stalled forks. We plotted these stalled forks as a percentage of total number of forks counted.

Using this approach, we identified that the affected patient fibroblasts had significantly increased frequency of stalled forks compared to the unaffected patient fibroblasts (Figure 5.8B). To confirm that these were stalled forks we treated the cells with hydroxyurea. As expected, we found that all patient fibroblasts responded to hydroxyurea treatment with increased frequency of stalled forks. However, this was potentiated in the affected patient fibroblasts compared to the unaffected patient fibroblasts (Figure 5.8C). Overall, these results are consistent with our hypothesis that a RS phenotype correlated with *JMJD5* genotype.
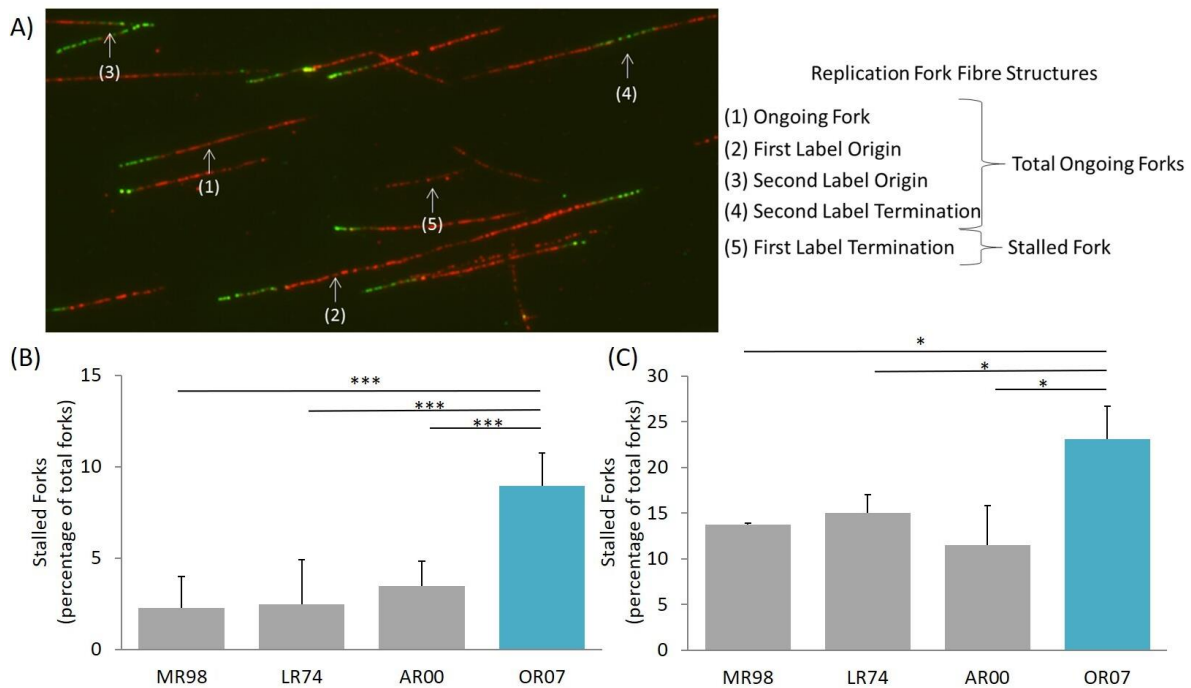
Figure 5.8 The affected patient fibroblasts have increased prevalence of stalled replication forks
The DNA fibre assay was performed on patient fibroblasts from MR98 (JMJD5 wildtype patient), LR74 (C123Y carrier patient), AR00 (InMut carrier patient) and OR07 (affected patient) **(A)** based on the CldU and IdU staining pattern different DNA fibre structures could be identified which corresponded to different DNA replication fork structures. The number of red-only DNA fibre structures (stalled forks) were determined as a percentage of all fork types counted after **(B)** endogenous replication stress, or **(C)** after treatment with 1 mM hydroxyurea for 2 hours between the thymidine analogue incubations. Statistical analysis performed using the two-tailed Student's t-test (p-value ≤ 0.05 represented by '*', ≤0.01 represented by '**', ≤0.001 represented by '***'). This is representative of n=6 biological repeats.

5.3.4 Affected patient fibroblasts have increased replication fork asymmetry

In order to continue to validate our RS phenotype, we performed further analysis on our DNA fibre experiments. As DNA replication occurs bidirectionally, the speed of DNA replication should be comparable between replication forks travelling away from the same origin during unperturbed DNA replication (Conti et al., 2007). Therefore, asymmetry between the progression of replication forks is representative of RS.

In order to monitor this, the length of green tracts were measured on DNA fibre structures from first labelled origins (Figure 5.9A). These structures provided a reliable method of measuring the difference in speed of two replication forks as these green tracts initiated from the same origin. Asymmetry in the progression of these DNA replication forks could then be established by calculating the ratio between the green tract lengths. A ratio near to one is representative of equal green tract lengths, whilst ratios greater than one occur when there is a difference in length between the two green tracts, indicative of fork asymmetry.

We found that, at the basal level, the affected patient fibroblasts had significantly increased DNA replication fork progression asymmetry compared to the unaffected patient fibroblasts (Figure 5.9B). Interestingly, only the affected patient fibroblasts responded to the presence of hydroxyurea with significantly increased replication fork asymmetry (Figure 5.9B). This observation was consistent with a RS phenotype correlating with *JMJD5* genotype.
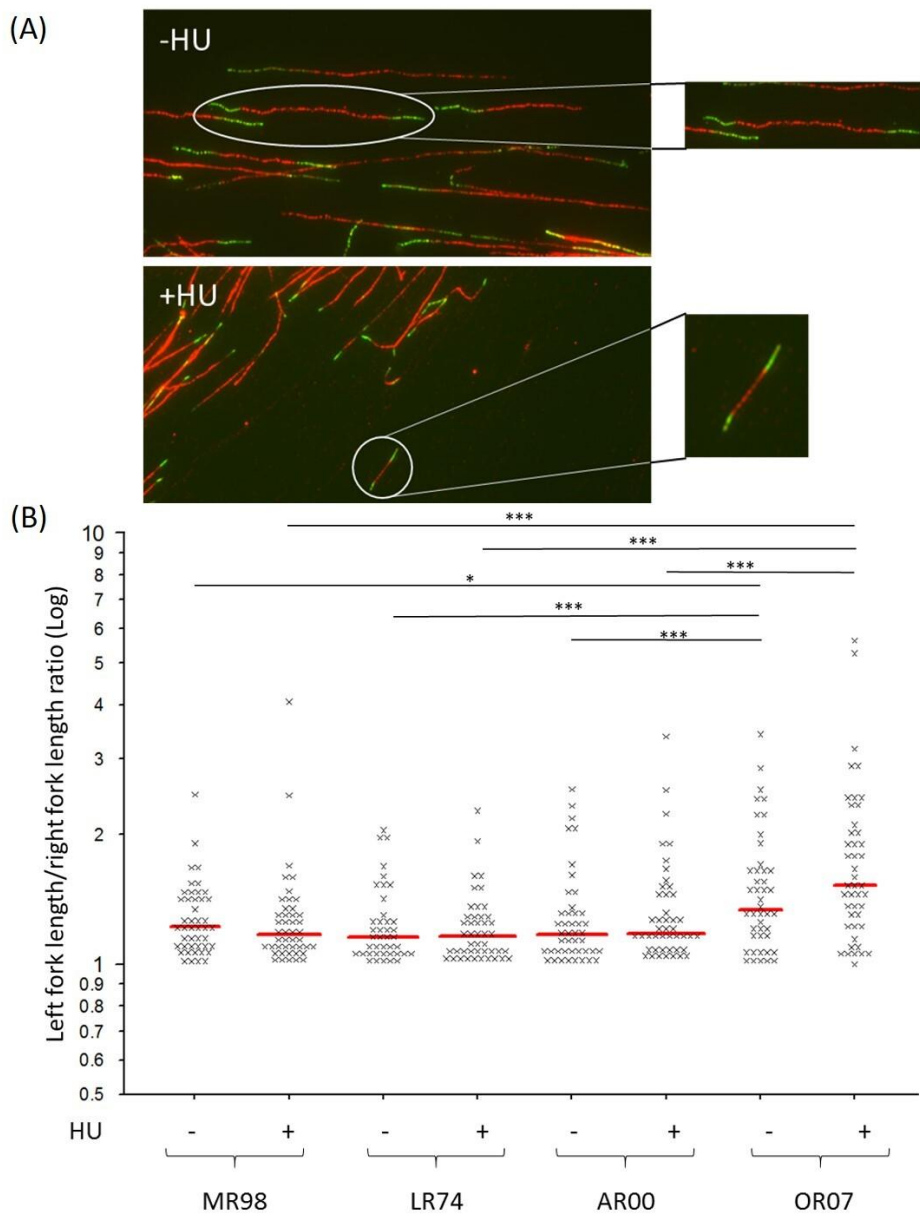
Figure 5.9 The affected patient fibroblasts have increased DNA fork asymmetry

The DNA fibre assay was performed on patient fibroblasts from MR98 (JMJD5 wildtype patient), LR74 (C123Y carrier patient), AR00 (InMut carrier patient) and OR07 (affected patient). The green tracts from first labelled origins (structure 2 in Figure 5.8A) were measured and a ratio determined between them displayed as a logarithmic value. **(A)** Green tracts with a ratio near the value of one were deemed symmetric (-HU example), the higher the value of the ratio the more asymmetric the green tracts (+HU example). **(B)** The affected patient fibroblasts were found to have increased asymmetry between green tracts at the endogenous level and after 1 mM hydroxyurea (HU) treatment for 2 hours between thymidine analogue incubations. Statistical analysis performed using the Mann-Whitney U test (p-value ≤ 0.05 represented by '*', ≤0.01 represented by '**', ≤0.001 represented by '***'). This is representative of n=6 biological repeats.

5.3.5   Patient fibroblasts have comparable replication fork speeds

As a consequence of increased RS and stalling of DNA replication forks, the speed of DNA replication can be compromised. In order to analyse this in our patient fibroblasts we measured the total DNA fibre lengths of ongoing forks (Figure 5.10A). We were then able to determine the total speed of the DNA replication forks (Equation 7.1).

When we performed this analysis, we found that patient fibroblasts had on average a fork speed of 1.56 kb/minute, which is comparable to other values found for immortalised cells (Técher et al., 2013). As expected, all fibroblasts responded to hydroxyurea induced RS with reduced total fork speed (Figure 5.10B). However, this phenotype was not significantly worse in the affected patients (Figure 5.10B), suggesting that replication fork speed is not hindered by the *JMJD5* genotype.

(A)

(B)
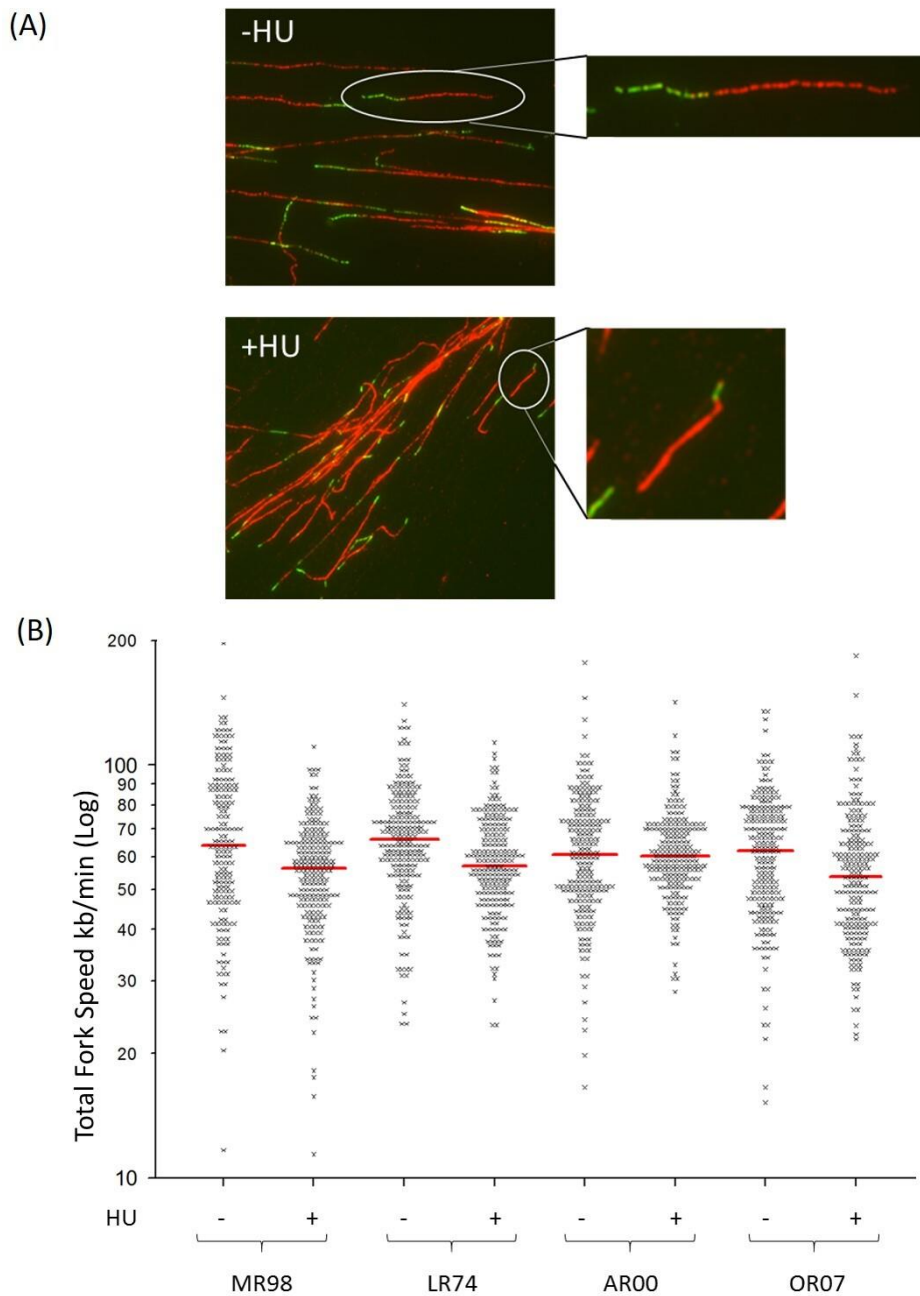
Figure 5.10 The patient fibroblasts have similar DNA replication fork speeds

The DNA fibre assay was performed for patient fibroblasts from MR98 (JMJD5 wildtype patient), LR74 (C123Y carrier patient), AR00 (InMut carrier patient) and OR07 (affected patient). The total length of DNA fibres from ongoing fork structures (structure 1 in Figure 5.8A) was measured using ImageJ and fork speed calculated using equation 5.1 which was displayed as a logarithmic value. **(A)** Shorter fibres were found after HU treatment, relative to endogenous fibre lengths, indicative of replication stress. **(B)** All patient fibroblasts were found to have reduced fork speed after 1 mM hydroxyurea (HU) treatment for 2 hours between thymidine analogue incubations, however, there was no significant difference for the affected patient.

5.4 Re-expression of JMJD5 in affected patient fibroblasts

Our current data demonstrated that the affected patient cells had increased RS and were sensitive to exogenous stress. We were next interested to establish whether the basis of these phenotypes was the *JMJD5* mutant genotype. In order to do this, we aimed to develop a system to re-introduce wildtype JMJD5 protein expression into the affected patient cell lines. If the re-expression of JMJD5 was able to rescue the RS phenotypes, then we could conclude that the affected patient RS phenotypes were caused by the loss of JMJD5 expression or activity. The next sections describe the development and optimisation of this rescue system.

5.4.1 Generation of JMJD5 FLAG-tagged rescue cell lines

In order to mediate the re-expression of JMJD5 we generated stable expression cell lines in fibroblasts from the affected patient (OR07) and wildtype patient (MR98). This was achieved by using lentiviral transduction of expression vectors containing FLAG-tagged JMJD5 wildtype or the H321A point mutation, which renders JMJD5 catalytically inactive (Chapter 4). Both JMJD5 constructs were expressed under a doxycycline inducible promoter. However, prior experience using this vector in related projects have identified that physiological protein re-expression can be achieved without doxycycline treatment, by relying on 'leaky' expression from the promotor. Therefore, we monitored leaky JMJD5 re-expression in these cell lines by Western blot analysis and found there was detectable FLAG-JMJD5 expression without the addition of doxycycline (Figure 5.11).
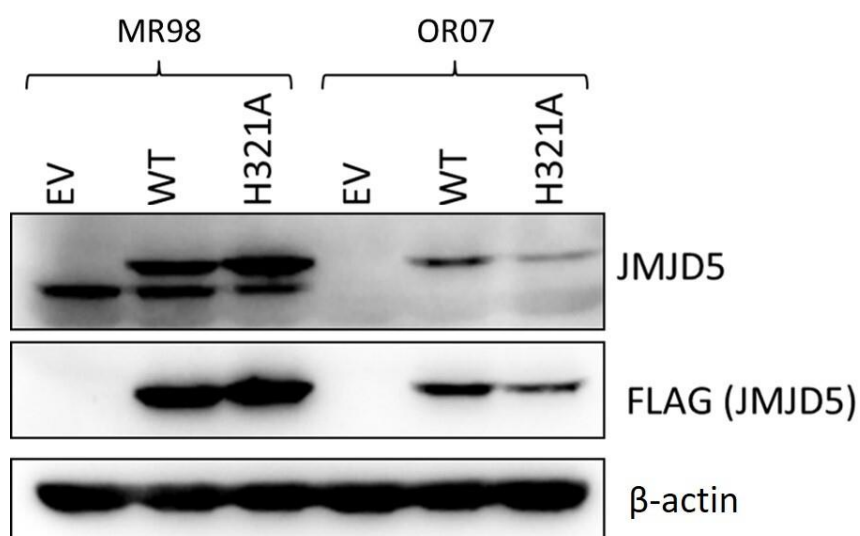
Figure 5.11 FLAG-tagged JMJD5 rescue cell line protein expression
MR98 and OR07 patient fibroblasts were infected with lentivirus to contain a doxycycline inducible expression vector for express FLAG-tagged wildtype or catalytic H321A mutant JMJD5. Minus doxycycline cell samples were analysed by Western blotting to determine 'leaky' vector expression. Empty vector (EV) cell lines used to determine basal endogenous JMJD5 expression in MR98 cells. β-actin used as a loading control. This is representative of n=3 biological repeats. JMJD5 (47 kDa), β-actin (42kDa).

We undertook a pilot experiment to establish whether rescue of the RS phenotype, in the affected patient fibroblasts, could be achieved with these levels of FLAG-JMJD5 re-expression. This was monitored by counting the frequency of endogenous micronuclei and 53BP1 bodies plus and minus aphidicolin in the OR07 rescue cell lines. We found that there was no difference between the empty vector or wildtype JMJD5 OR07 patient rescue cell lines for either assay suggesting that rescue was not achieved (Figure 5.12).
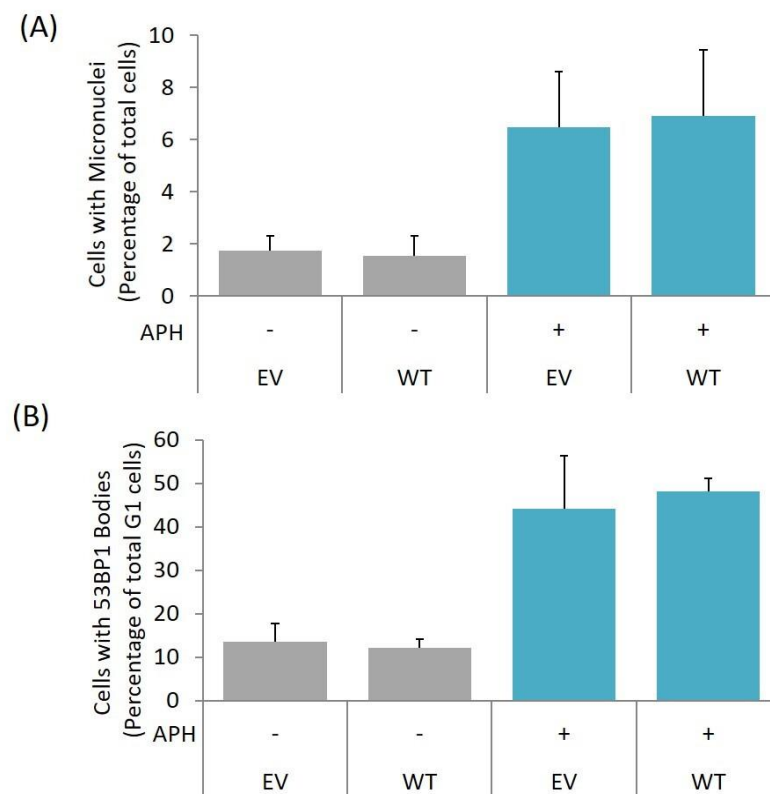
Figure 5.12 Replication stress not rescued by 'leaky' FLAG-JMJD5 re-expression
OR07 affected patient fibroblasts doxycycline inducible to express FLAG-tagged JMJD5 wildtype (WT) were tested for their DNA replication stress phenotype minus doxycycline ('leaky' vector expression). No rescue of endogenous or induced replication stress phenotype (after 48 hours 0.5 µM aphidicolin (APH) treatment), was detected for **(A)** micronuclei, or **(B)** 53BP1 bodies. Empty vector (EV) cell lines used to determine basal levels of replication stress. This is representative of n=3 biological repeats.

We predicted that the lack of rescue in these experiments could be because the leaky re-expression levels of FLAG-JMJD5 in the OR07 patient cell lines were lower than the endogenous JMJD5 levels present in the wildtype patient (MR98) fibroblasts (Figure 5.11). Consequently, we established a doxycycline dose titration to induce higher levels of FLAG-JMJD5 protein re-expression for 48 hours prior to assaying for RS (Figure 5.13A). However, we again found that there was no rescue of the RS phenotype in the affected patient fibroblasts, as monitored by micronuclei, 53BP1 bodies, or DNA replication stalled forks (Figure 5.13B-D).
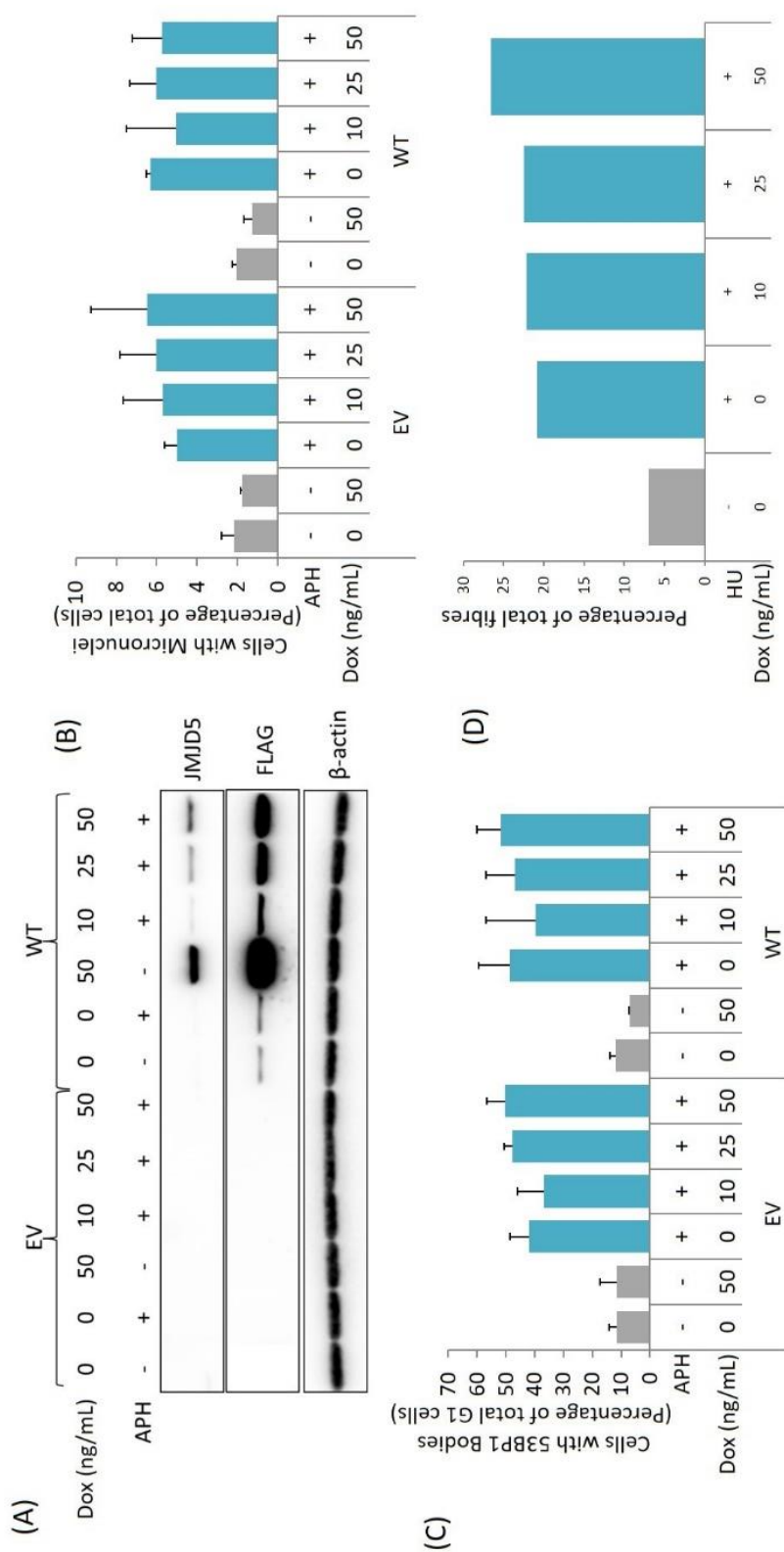
Figure 5.13 No replication stress rescued by low FLAG-JMJD5 re-expression levels

OR07 affected patient fibroblasts doxycycline inducible to express FLAG-tagged JMJD5 wildtype (WT) were treated with a doxycycline dose titration. **(A)** Western blot analysis identified that increased expression vector occurred in a doxycycline inducible manner. β-actin used as a loading control. Cells were treated with doxycycline for 48 hours prior to replication stress analysis. No rescue of the endogenous or induced replication stress phenotype (after 48 hours 0.5 μM aphidicolin (APH) treatment) was found for **(B)** micronuclei, or **(C)** 53BP1 bodies. Empty vector was used to determine basal levels of replication stress. This is representative of n=3 biological repeats. **(D)** No rescue of exogenous DNA replication stalled forks, using the DNA fibre assay, was found after 1 mM hydroxyurea (HU) treatment for 2 hours between thymidine analogue incubations. Empty vector (EV) cell lines were used to determine basal levels of DNA replication stress. This is representative of an n=1 biological repeat. JMJD5 (47 kDa), β-actin (42kDa).

In response to this we hypothesised six reasons why our system may not be supporting a rescue of the affected patient RS phenotype. Firstly, if the re-expression of FLAG-JMJD5 was heterogeneous across the population of cells then it could mask a successful rescue. Secondly, doxycycline could itself induce or exacerbate a RS phenotype. Thirdly, doxycycline treatment could induce supra-physiological expression levels of JMJD5 that could cause a RS phenotype and therefore mask a rescue. Fourth, the period of time fibroblasts had re-expressed JMJD5 for, in our previous attempts, may not have been long enough in order to rescue the RS phenotype. Fifth, the FLAG-tag could be detrimental to the activity of the exogenous JMJD5. Finally, it remained possible that the RS phenotype of these affected patient fibroblasts might not be caused by their *JMJD5* genotype.

5.4.2   Monitoring the heterogeneity of JMJD5 re-expression

Here we attempted to address our first hypothesis regarding the lack of rescue, due to potential heterogeneous re-expression of FLAG-JMJD5. This could occur if a high proportion of the cell population did not express FLAG-JMJD5 and continued to present a RS phenotype.

As Western blotting monitors protein expression from a pooled population of cells, any such heterogeneity in expression would not be apparent from our existing analysis. Therefore, immunofluorescence was performed in order to determine relative FLAG expression in the OR07 fibroblast rescue cell lines after a doxycycline dose titration. In this analysis we used the JMJD5 wildtype rescue cell lines, treated with the highest concentration of doxycycline (1000 ng/mL), in order to decipher the highest level of FLAG expression. In parallel, we used the empty vector rescue cell line to establish any background level of staining. From these two samples we assigned the relative FLAG staining levels as 'none', 'low', or 'high' (Figure 5.14B)

and used this system to assess the relative FLAG-JMJD5 re-expression in each sample, which we expressed as a percentage of the total number of cells counted (Figure 5.14C).

As expected, we observed no FLAG expression for the empty vector rescue cell lines (Figure 5.14C/D). We observed that although some of the wildtype OR07 rescue cell lines expressed low levels of FLAG-JMJD5 at zero and 10 ng/mL doxycycline, the majority of cells did not express detectable FLAG-JMJD5, at least within the limits of this assay (Figure 5.14C/D). At higher concentrations of doxycycline (25, 50, 200, 1000 ng/mL) the proportion of cells expressing FLAG-JMJD5 increased, though there were some differences in re-expression levels i.e. some cells expressed lower or higher protein levels compared to other cells within the same population. However, as the dose of doxycycline increased the degree of heterogeneity in FLAG-JMJD5 expression decreased (Figure 5.14C/D). Consequently, in order to test whether a more homogeneous level of FLAG-JMJD5 re-expression could rescue the RS phenotype, we treated the wildtype JMJD5 OR07 rescue cell lines with 200 ng/mL and 1000 ng/mL of doxycycline. This was performed for 48 hours, in the presence or absence of RS inducing agents, prior to monitoring RS. Unfortunately, we observed no rescue of micronuclei (Figure 5.15B), 53BP1 bodies (Figure 5.15C), or stalled DNA replication forks (Figure 5.15D), at either doxycycline concentration dose tested.

Overall, we concluded that although these higher concentrations of doxycycline ensured a more homogeneous population of cells expressing FLAG-JMJD5 protein, these conditions were still not optimal for a rescue of the RS phenotype.
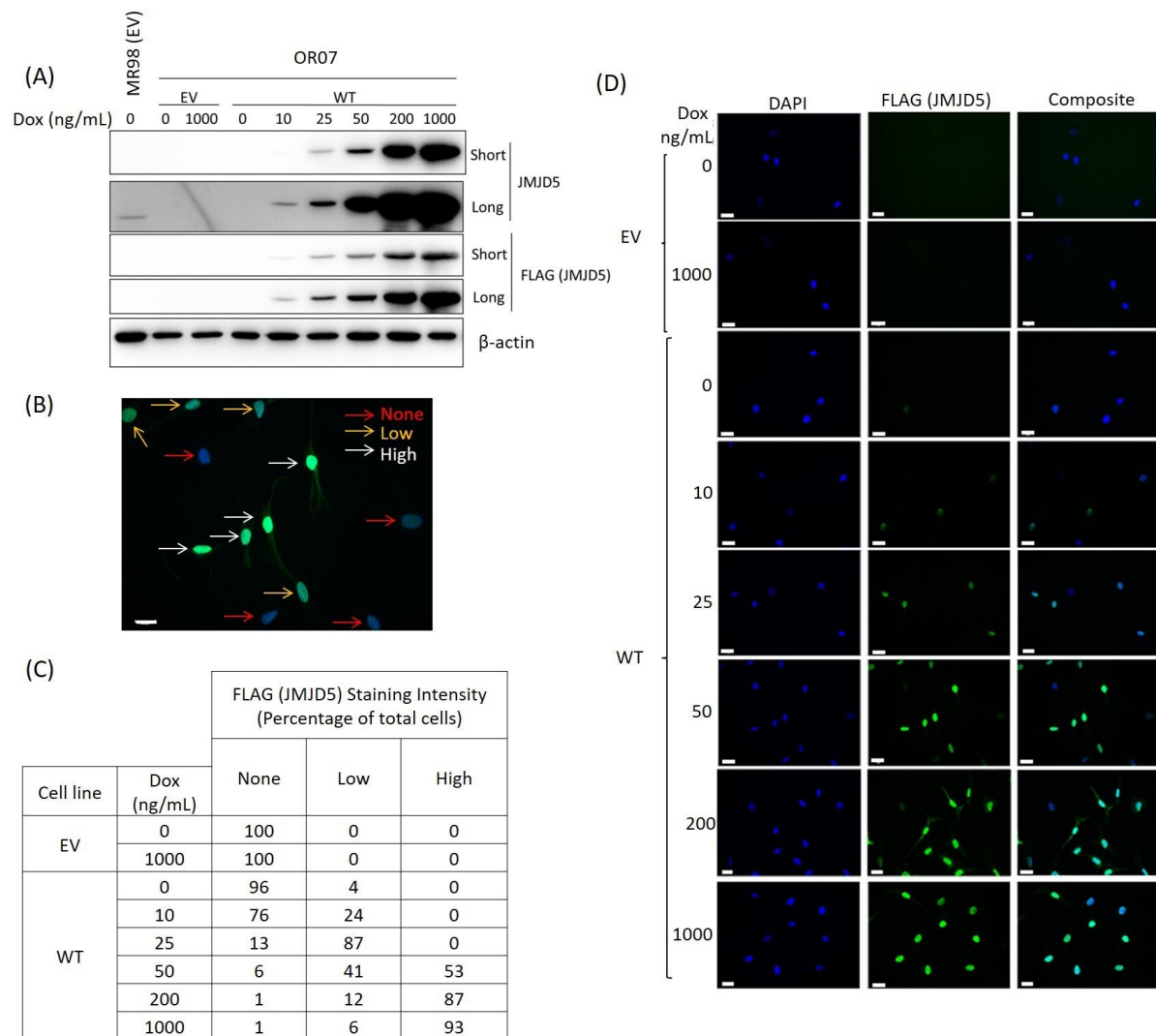
Figure 5.14 Determining the heterogeneity of FLAG-JMJD5 re-expression in OR07 rescue cell lines
OR07 affected patient fibroblasts doxycycline inducible to express FLAG-tagged JMJD5 wildtype (WT) were treated with a doxycycline dose titration. Cells were treated with doxycycline for 48 hours prior analysis. **(A)** Western blot analysis determined that the vectors expression correlated to doxycycline concentration and this was compared to endogenous JMJD5 expression from MR98 stable expression empty vector (EV) cell lines. 'Short' and 'long' refer to the length of exposure time used to visualise the Western blot signal. β-actin used as a loading control. **(B)** The expression of FLAG-JMJD5 was determined as 'high', 'low' or 'none' based on analysis of 1000 ng/mL treated empty vector and wildtype JMJD5 immunofluorescence samples. **(C)** Samples were analysed for their FLAG-tagged JMJD5 re-expression levels using the system developed in (B), this was shown as a percentage of total cells counted. **(D)** Representative immunofluorescence images. Scale bars= 20 µm. DAPI was used as a counterstain for the nucleus. This is representative of an n=1 biological repeat. JMJD5 (47 kDa), β-actin (42kDa).
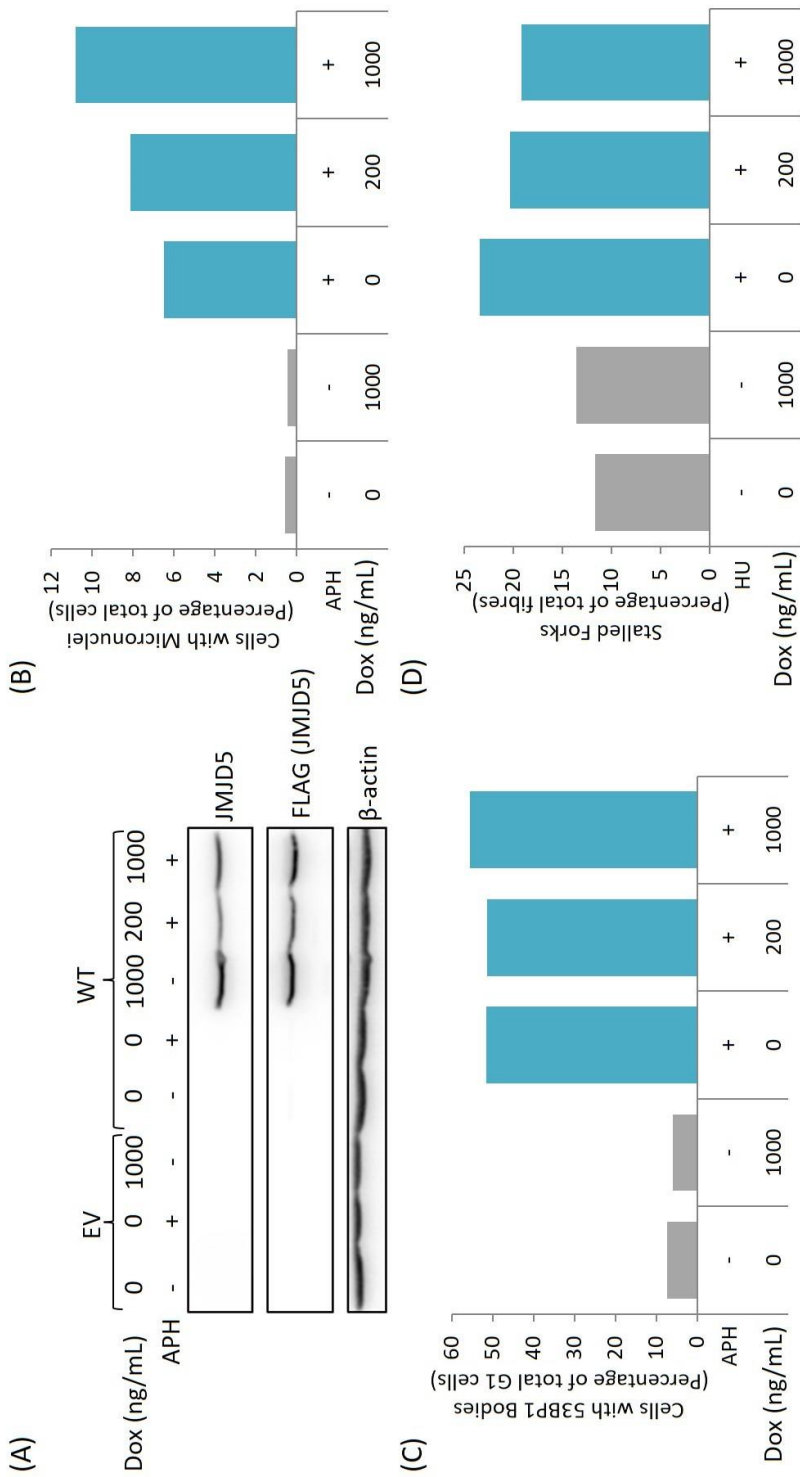
Figure 5.15 No replication stress rescued by high FLAG-JMJD5 re-expression levels

OR07 affected patient fibroblasts doxycycline inducible to express FLAG-tagged JMJD5 wildtype (WT) were treated with 200 or 1000 ng/mL doxycycline for 48 hours prior to analysis. **(A)** Western blot analysis used to determine successful expression of the FLAG-JMJD5 construct. β-actin used as a loading control. There was no rescue of endogenous or induced DNA replication stress (by treatment with 0.5 μM aphidicolin (APH) for 48 hours) identified for **(B)** micronuclei, or **(C)** 53BP1 bodies. **(D)** No rescue of endogenous or induced DNA stalled forks (by treatment with 1 mM hydroxyurea (HU) for 2 hours between thymidine analogue incubations) was identified. Empty vector (EV) cell lines were used to determine the basal level of DNA replication stress. This is representative of an n=1 biological repeat. JMJD5 (47 kDa), β-actin (42kDa).

5.4.3 Monitoring the effect of doxycycline treatment and JMJD5 over-expression

Our next hypotheses to explain an apparent lack of RS rescue in our re-expression model was firstly that doxycycline treatment might exacerbate or induce a RS phenotype. In support of this hypothesis, previous reports have indicated that doxycycline can inhibit DNA repair pathways (Lamb et al., 2015). Secondly, we hypothesised that supra-physiological levels of JMJD5 re-expression (such as those observed in Figure 5.13A) might itself induce RS.

Here we aimed to test both of these hypotheses simultaneously by using MR98 doxycycline inducible cell lines expressing either empty vector or FLAG-JMJD5 wildtype, treated with 1000 ng/mL doxycycline for 48 hours prior to measuring RS. The MR98 cell lines were most suited to this analysis because it enabled us to monitor the effect of doxycycline and JMJD5 over-expression without the added variable of JMJD5 mutations, present in the other fibroblast lines. We monitored RS in these cell lines in the form of micronuclei, 53BP1 bodies and stalled replication forks. This was done in the presence of RS inducing drugs in order to determine whether the presence of doxycycline or high expression of FLAG-JMJD5 exacerbated this phenotype. We found that high concentrations of doxycycline did not significantly exacerbate the RS phenotype of the empty vector MR98 cell line (Figure 5.16). Similarly, over-expression of FLAG-JMJD5 also did not appear to exacerbate the RS of the MR98 cells (Figure 5.16).

Overall, we concluded that the lack of RS phenotype rescue in our model was not likely to be affected by either the doxycycline concentrations used or high levels of FLAG-JMJD5 over-expression.
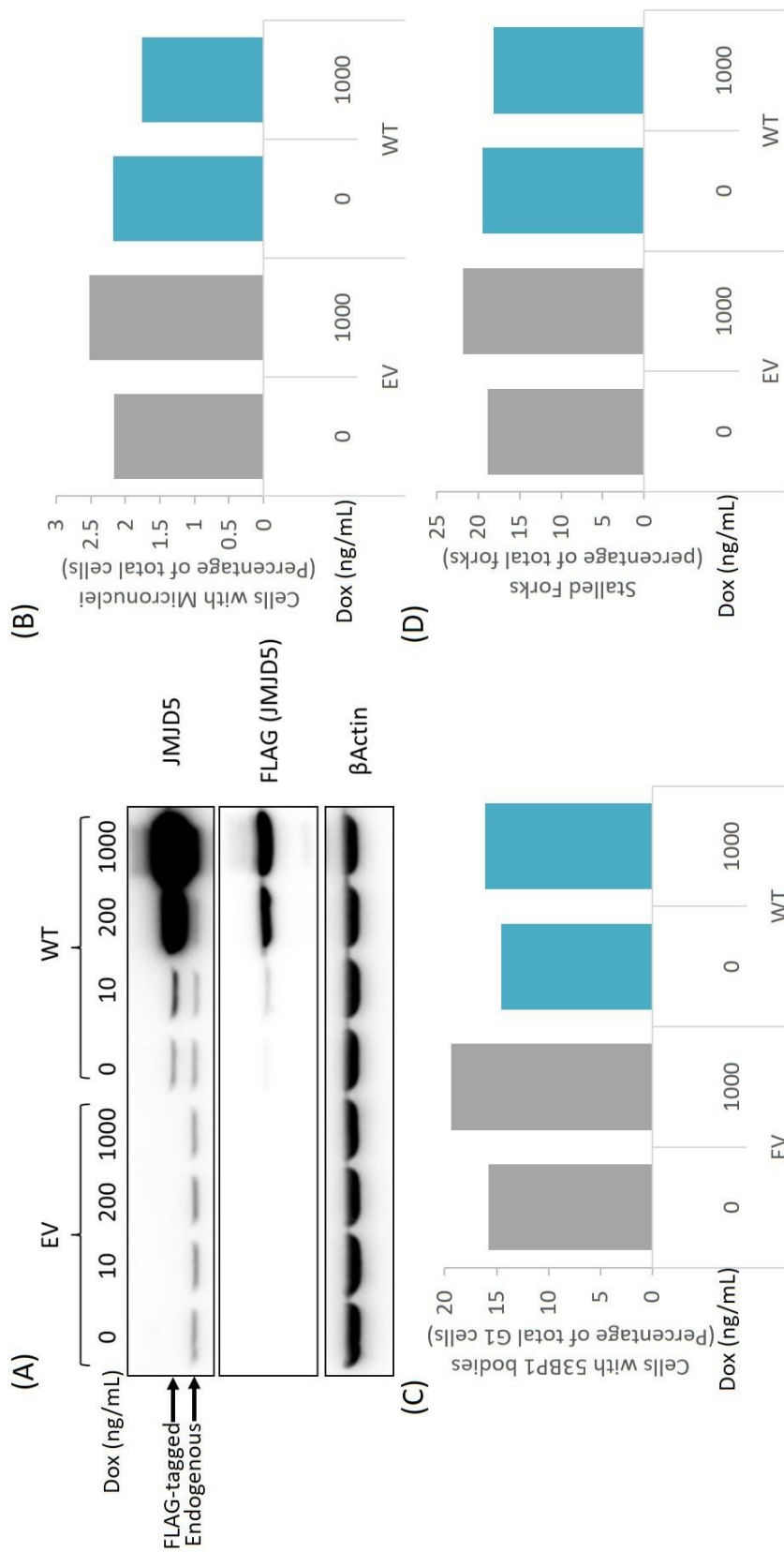
Figure 5.16 High doxycycline or FLAG-JMJD5 expression does not exacerbate DNA replication stress
MR98 patient fibroblasts doxycycline inducible to express FLAG-tagged JMJD5 wildtype (WT)
were treated with 10, 200 or 1000 ng/mL doxycycline for 48 hours prior to analysis. **(A)** Western blot analysis used to determine
successful expression of the FLAG-JMJD5 construct (tagged and endogenous JMJD5 labelled). β-actin used as a loading control.
DNA replication stress was induced by treatment with 0.5 μM aphidicolin for 48 hours. This phenotype was not exacerbated by
treatment of the high doxycycline concentration (1000 ng/mL) or strong expression of JMJD5 wildtype measured by **(B)**
micronuclei or **(C)** 53BP1 bodies. **(D)** DNA replication stalled forks induced by treatment with 1 mM hydroxyurea for 2 hours
between thymidine analogues, was also not exacerbated by treatment of the high doxycycline concentration (1000 ng/mL) or
strong JMJD5 expression. This is representative of an n=1 biological repeat. JMJD5 (47 kDa), β-actin (42kDa).

5.4.4 Monitoring the length of time for JMJD5 re-expression

The next hypothesis regarding the lack of RS rescue was that the cells may require a longer period of FLAG-JMJD5 re-expression. One reason for considering this was the fact that the fibroblast lines grow relatively slowly in culture (personal observation). Moreover, we predicted successful RS might require multiple complete cell cycles. This is because candidate substrates, MCM3 and MCM5, could require turnover or progression through the cell cycle in order to restore hydroxylation and the consequence of this to be visible.

To address this, OR07 patient rescue cell lines were treated with doxycycline for five days to induce FLAG-JMJD5 re-expression (Figure 5.17A) prior to analysing their RS phenotype. We monitored RS by counting the frequency of micronuclei and 53BP1 bodies. We observed that there was a partial rescue of micronuclei after re-expression of wildtype JMJD5 (Figure 5.17B). However, we also noted some variability in the empty vector control samples (Figure 5.17B). Furthermore, although we detected a partial rescue of 53BP1 bodies after re-expression of wildtype JMJD5, this was only detected with a single doxycycline treatment (10 ng/mL) (Figure 5.17C). Therefore, we concluded that re-expression of FLAG-tagged JMJD5 for five days was not sufficient to rescue the RS phenotype of these cells.
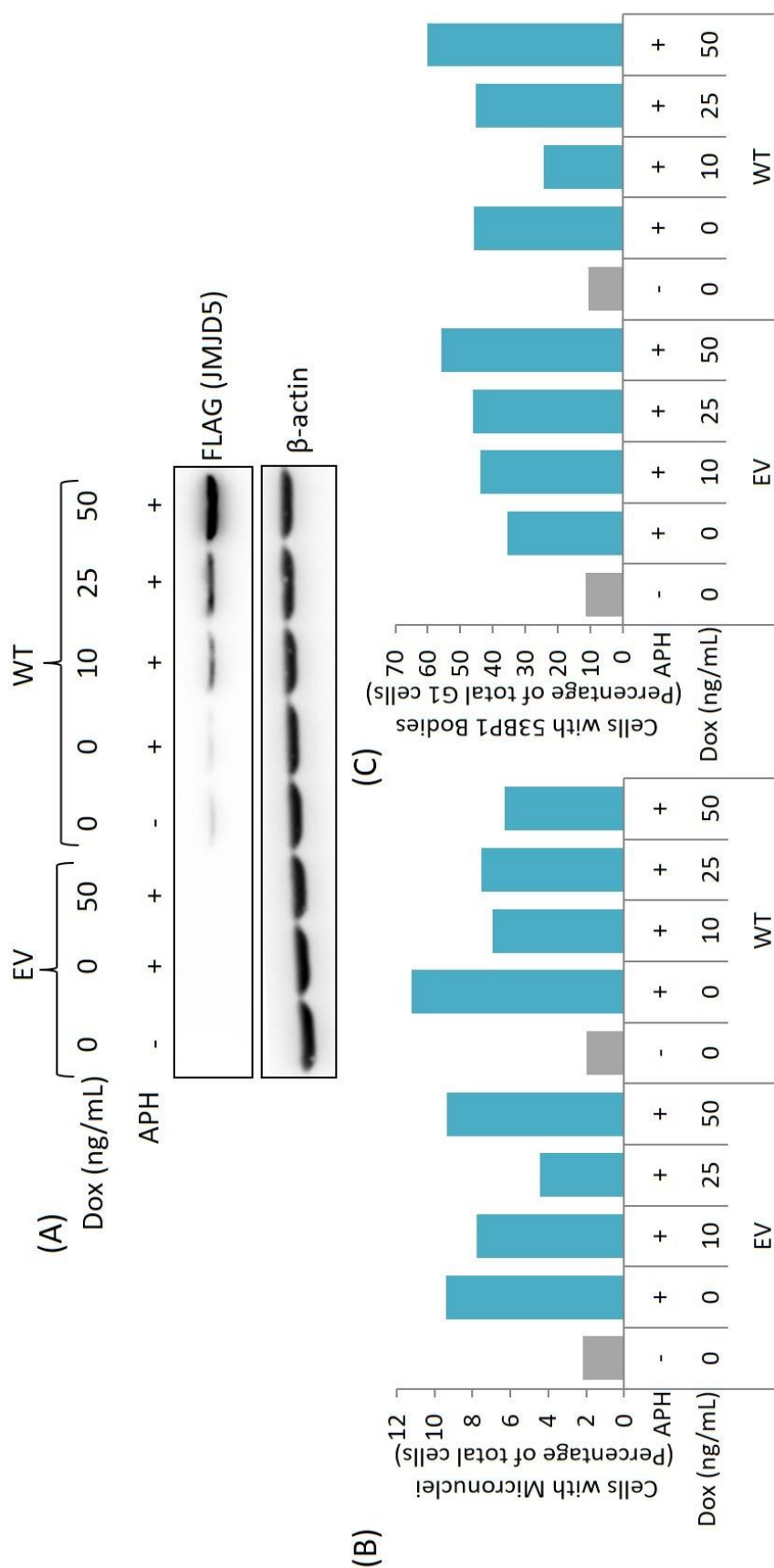
Figure 5.17 No replication stress rescued by increased time of FLAG-JMJD5 re-expression OR07 affected patient fibroblasts doxycycline inducible to express FLAG-tagged JMJD5 wildtype (WT) were treated with 10, 25 or 50 ng/mL doxycycline (Dox) for 48 hours prior to further analysis. **(A)** Western blot analysis was used to determine successful expression of the FLAG-JMJD5 construct. β-actin used as a loading control. No rescue of endogenous or induced DNA replication stress (by treatment with 0.5 µM aphidicolin (APH) for 48 hours) was identified for **(B)** micronuclei, or **(C)** 53BP1 bodies in G1 cells. This is representative of an n=1 biological repeat. JMJD5 (47 kDa), β-actin (42kDa).

5.4.5 Generation of JMJD5 no-tag rescue cell lines

Following the above optimisation, we were concerned that the FLAG-tag could be affecting the activity of the re-expressed JMJD5, and/or the duration of JMJD5 re-expression may still not be long enough. Therefore, we aimed to address these potential limitations in parallel.

We addressed the first hypothesis by cloning wildtype or H321A catalytically inactive mutant JMJD5 into the same doxycycline inducible lentiviral expression vector, but without an epitope tag. Lentiviral infection of these expression vectors was performed to make stable expression cell lines in the affected patient (OR07) fibroblasts. To test no-tag JMJD5 expression the cells were treated with a doxycycline titration and analysed by Western blot analysis. This showed that the lowest doses of doxycycline induced no-tag JMJD5 levels similar to endogenous JMJD5 expression in MR98 cells (Figure 5.18).
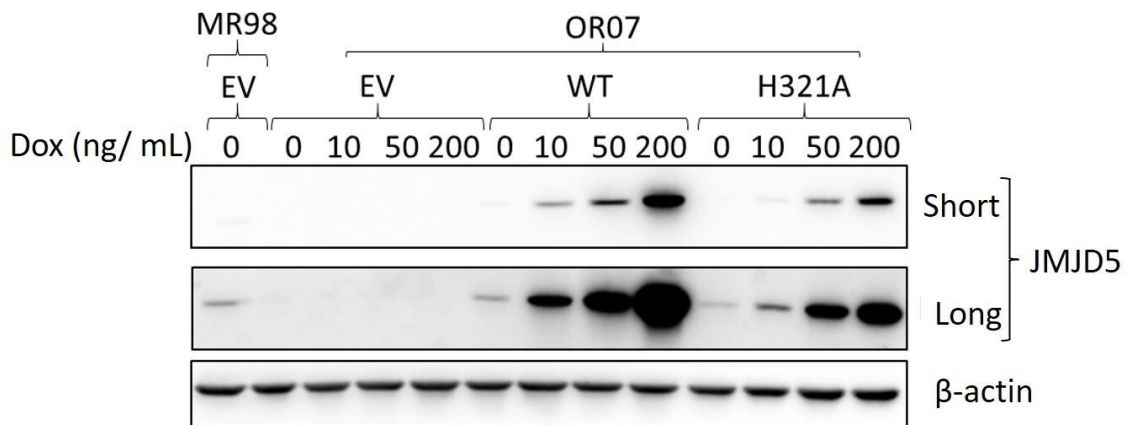
Figure 5.18 No-tag JMJD5 OR07 patient rescue cell line protein expression
OR07 patient fibroblasts were infected with lentivirus to contain an expression vector doxycycline inducible to express a no epitope tag wildtype (WT) or catalytic H321A mutant JMJD5. Cells were treated with a doxycycline dose titration and protein expression determined by Western blotting. 'Short' and 'long' refer to the length of exposure time used to visualise the Western blot signal. Empty vector (EV) cell lines were used to determine basal endogenous JMJD5 expression in MR98 cells. β-actin used as a loading control. This is representative of n=3 biological repeats. JMJD5 (47 kDa), β-actin (42kDa).

In order to address any potential heterogeneity of no-tag JMJD5 re-expression in this cell population we performed immunofluorescence analysis. Prior to this, we first had to identify antibodies that were able to detect un-tagged JMJD5. To do this, MR98 cell lines were treated with 1 µg/mL doxycycline to induce over-expression of FLAG-JMJD5, then fixed using methanol or acetone before co-staining with anti-FLAG antibody and a panel of JMJD5 antibodies. Overlapping FLAG and JMJD5 immunofluorescence staining was used to infer JMJD5 antibody specificity. From this optimisation experiment we identified two JMJD5 antibodies, AB36104 (Abcam) and Abclonal®, that appeared able to detect over-expressed JMJD5 (shown in Figure 5.19). We also concluded that optimal immunofluorescence staining with these antibodies was found after fixing cells with methanol (Figure 5.19).
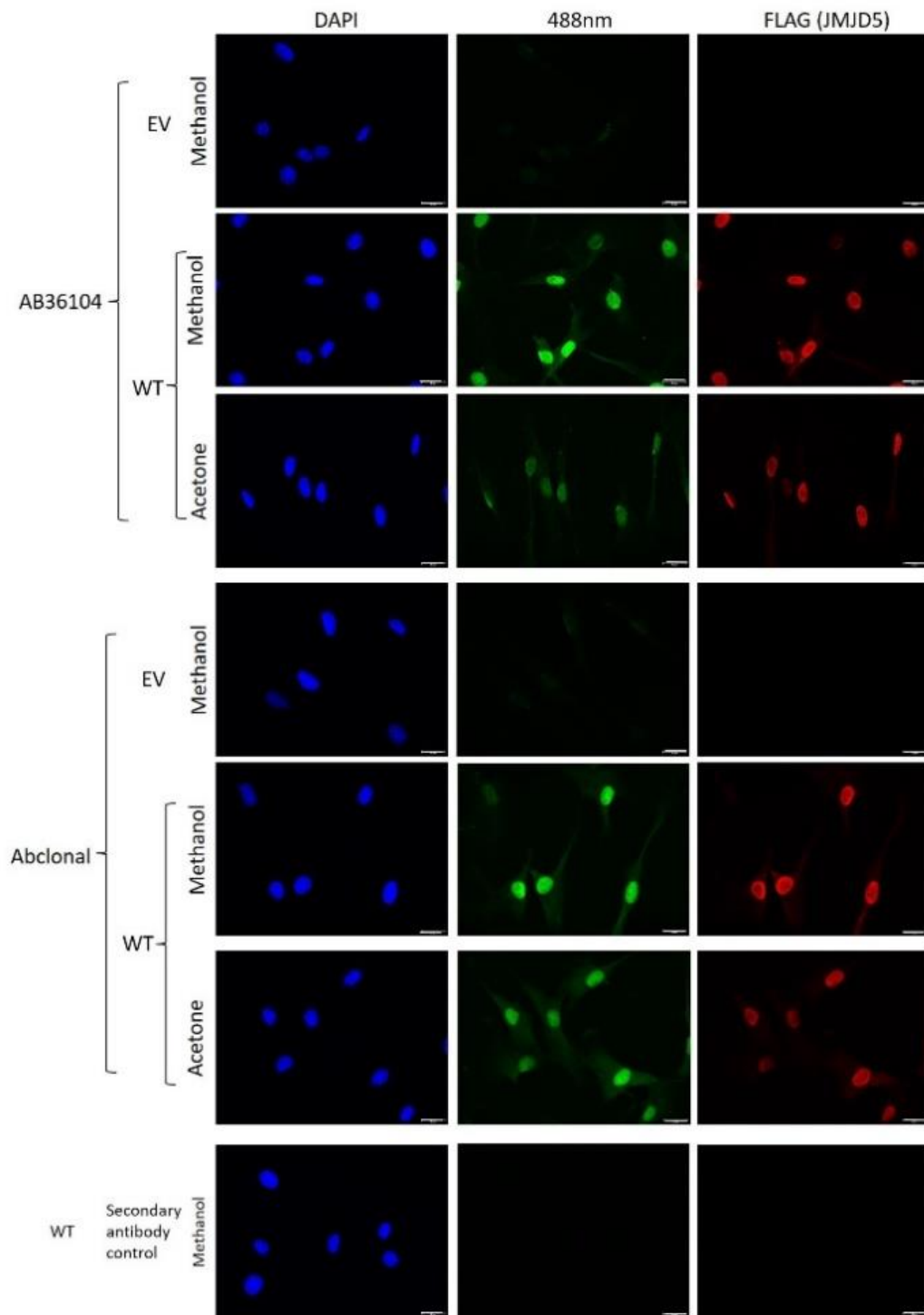
Figure 5.19 Screening of JMJD5 antibodies for use in over-expression immunofluorescence analysis
MR98 cell lines doxycycline inducible to express FLAG-tagged wildtype (WT) JMJD5 were plated onto coverslips and 1 µg/mL doxycycline treated for 48 hours prior to harvesting for immunofluorescence. Cells were fixed using either methanol or acetone incubation for 10 minutes at -20 ˚C. A panel of JMJD5 antibodies were tested using co-staining with FLAG and an empty vector (EV) cell line to determine the specificity of the antibodies. Secondary only antibody control was used to validate all antibodies used in the assay. DAPI was used as a counterstain for nuclei. Scale bars= 20 µm. This is representative of an n=1 biological repeat.

As the lowest doses of doxycycline induced JMJD5 re-expression in our rescue system to a similar level as endogenous JMJD5 (Figure 5.18), we next tested whether our antibodies were capable of detecting endogenous JMJD5. To do this we fixed U2OS cells in methanol and performed immunofluorescence analysis using the AB36104 (Abcam) and Abclonal antibodies at two different concentrations. Staining with the AB36104 (Abcam) antibody resulted in a specific nuclear stain, consistent with the literature (Shen et al., 2017, Huang et al., 2013, Zhu et al., 2014, Kouwaki et al., 2016, Shalaby et al., 2018, Wang et al., 2018) and our over-expression studies (Figure 5.14 and 5.19). In contrast, the Abclonal antibody resulted in non-specific cytoplasmic staining (Figure 5.20). Overall, we decided that the optimal condition for detecting endogenous JMJD5 or physiological re-expression levels of no-tag JMJD5 was to use the AB36104 (Abcam) JMJD5 antibody after methanol fixation.

We then used these optimised immunofluorescence conditions to monitor the heterogeneity of no-tag JMJD5 re-expression in the OR07 rescue cell lines. To do this the OR07 rescue cells were treated for 48 hours with a doxycycline titration before performing immunofluorescence staining, as above. We analysed all samples to determine the percentage of cells expressing relative levels of no-tag JMJD5, similarly to analysis in Section 5.4.2. As expected, we found no detectable JMJD5 expression in the empty vector OR07 cell lines (Figure 5.21). We also found that both wildtype and H321A JMJD5 were expressed relatively homogeneously at all doxycycline concentrations, i.e. the majority of cells in the population had similar expression levels of JMJD5 (Figure 5.21). Consistent with Western blot analysis (Figure 5.18) we found that wildtype no-tag JMJD5 had higher protein expression levels compared to H321A JMJD5 at the same concentration of doxycycline (Figure 5.21).
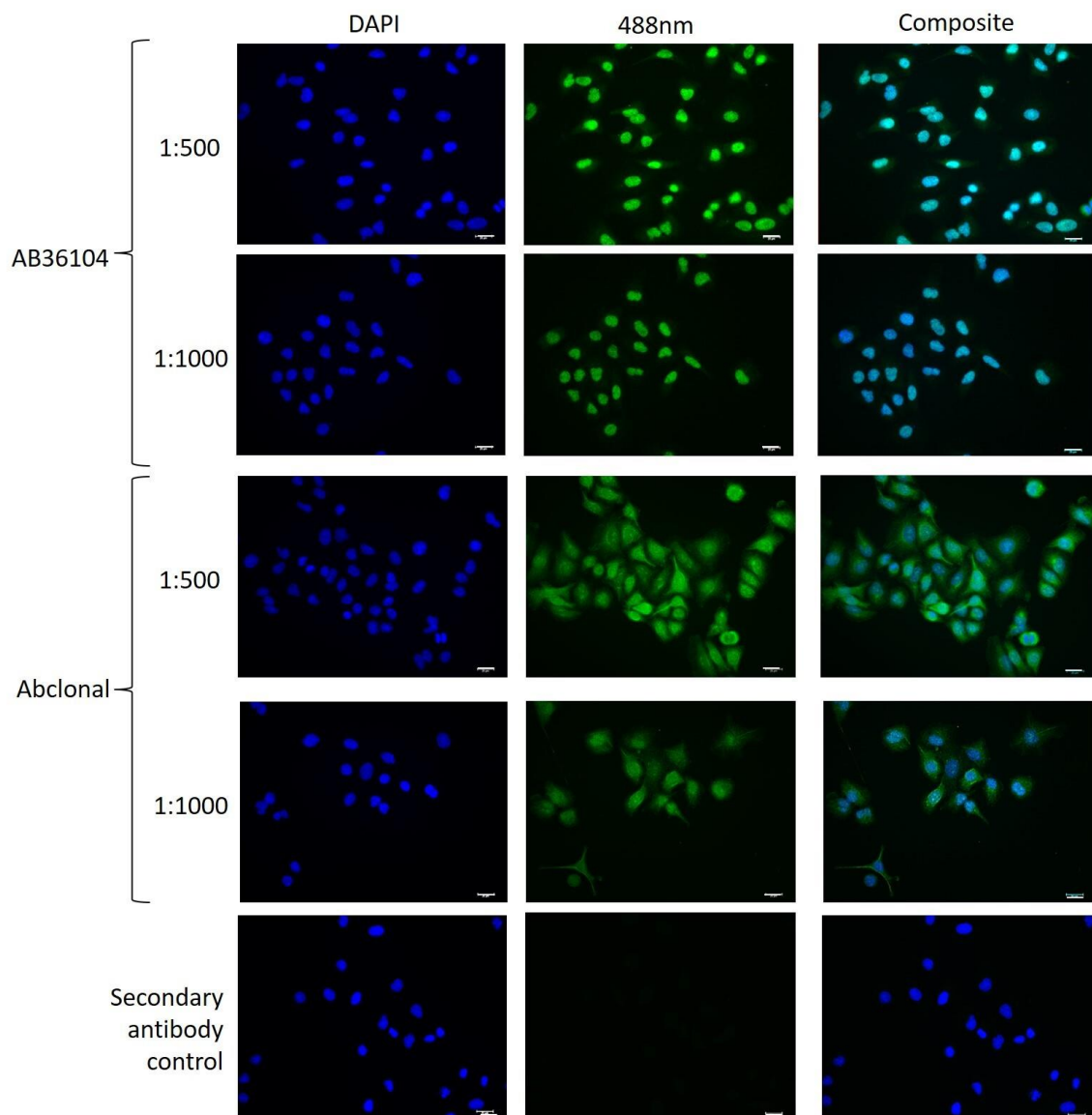
Figure 5.20 Screening of JMJD5 antibodies for endogenous expression immunofluorescence analysis
U2OS cells were plated onto coverslips before harvesting for immunofluroescence analysis by fixing in methanol. Two antibodies previously validated using over-expression of FLAG-JMJD5 (Figure 5.20) were tested against their ability to bind endogenously expressed JMJD5 at 1:500 or 1:1000 antibody diltuons. Secondary only antibody control was used to validate all antibodies used in the assay. DAPI was used as a counterstain for nuclei. Scale bars= 20 μm. This is representative of an n=1 biological repeat.

(A)

(B)

Cell line	Dox (ng/mL)	FLAG (JMJD5) Staining Intensity (Percentage of total cells)		
		None	Low	High
EV	0	100	0	0
	200	100	0	0
WT	0	0	98	2
	10	0	90	10
	50	0	10	90
	200	0	2	98
H321A	0	0	100	0
	10	0	98	2
	50	0	70	30
	200	0	10	90

(C)
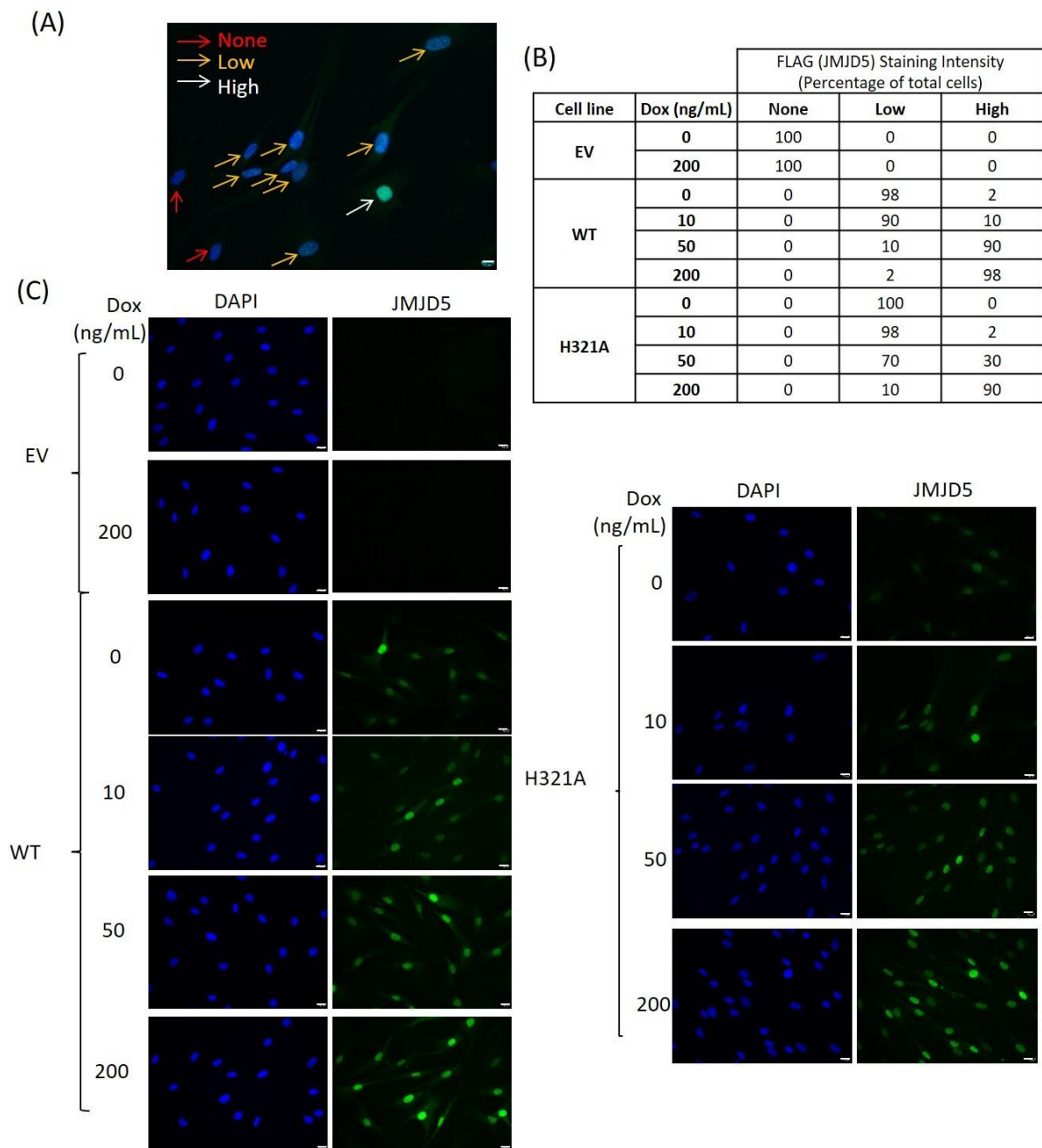
Figure 5.21 Determining the heterogeneity of no-tag JMJD5 re-expression in OR07 rescue cell lines
OR07 affected patient fibroblasts doxycycline inducible to express no-tag JMJD5 wildtype (WT) and H321A catalytic point mutation were treated with a doxycycline dose titration for 48 hours. Immunofluorescence was used to determine JMJD5 expression, using antibodies and immunofluorescence conditions established in Figure 5.19 and 5.20. This was indicative of no-tag JMJD5 re-expression. DAPI was used as a counterstain for the nucleus. **(A)** Samples were analysed for their FLAG-tagged JMJD5 re-expression levels using the system developed in Figure 5.15C. **(B)** This was shown as a percentage of total cells counted. **(C)** Representative images of samples analysed. Scale bars= 10 µm. This is representative of an n=1 biological repeat.

Overall, from the combined Western blot (Figure 5.18) and immunofluorescence analysis (Figure 5.21) we decided to monitor the RS phenotype of these cells after zero and 10 ng/mL doxycycline treatment. This was because both conditions resulted in no-tag JMJD5 re-expression protein levels comparable to endogenous JMJD5 (Figure 5.18) and were relatively homogeneous across the population of cells (Figure 5.21). In order to address whether longer re-expression of JMJD5 might be required to restore a replication defect, we grew the no-tag OR07 patient rescue cell lines for 2 weeks in doxycycline prior to RS analysis. We included in this analysis the H321A catalytically inactive JMJD5 mutant in order to determine whether any potential rescue was activity dependent.

Consistent with previous analyses we found that the OR07 empty vector control rescue cell lines had high endogenous RS, as indicated by monitoring micronuclei, 53BP1 bodies and performing the DNA fibre assay to monitor stalled forks and fork asymmetry (Figure 5.22). Excitingly, we found that, under these experimental conditions, re-expression of wildtype JMJD5 (Figure 5.18) rescued these replication stress phenotypes (Figure 5.22). Interestingly, we found that re-expression of the inactive H321A mutant completely failed to rescue the RS phenotype observed in the affected patient cells (Figure 5.22). This demonstrated that the hydroxylase activity of JMJD5 was essential for the rescue effects observed.
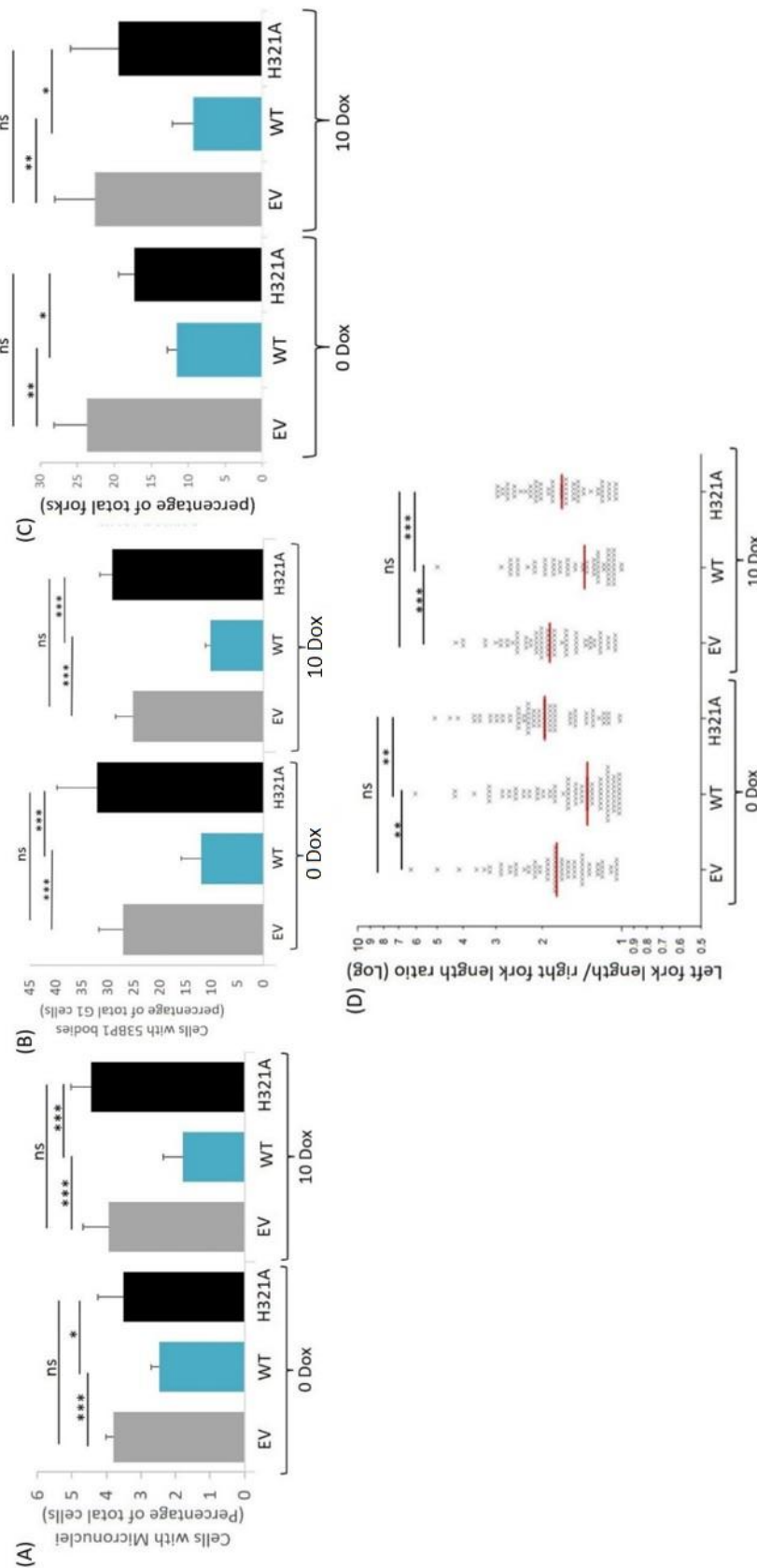
Figure 5.22 Rescue of endogenous replication stress by re-expression of no-tag wildtype JMJD5 No-tag JMJD5 OR07 rescue cell lines were grown for two weeks plus or minus 10 ng/mL doxycycline prior to replication stress analysis. Empty vector cells were included to determine basal levels of DNA replication stress. H321A expression cell lines were used to determine the activity dependence of the rescue. Rescue of endogenous replication stress was found after re-expression of JMJD5 wildtype, measured by **(A)** micronuclei, **(B)** 53BP1 bodies, **(C)** DNA stalled forks, **(D)** DNA fork asymmetry. Statistical analysis for A, B and C performed using the two-tailed Student's t-test. Statistical analysis for D performed using the Mann-Whitney U test. Statistical significance for all was determined by a p-value ≤ 0.05 represented by '*', ≤0.01 represented by '**', ≤0.001 represented by '***', p-value >0.05 not significant represented by 'ns'. Representative protein expression as shown in Figure 5.18. This is representative of n=3 biological repeats.

Having identified experimental conditions suitable for rescuing the RS phenotype of the affected patient fibroblasts, we were next interested to explore whether the colony formation phenotype of these cells could also be rescued. To do this the no-tag OR07 patient rescue cell lines were grown in zero or 10 ng/mL doxycycline for 2 weeks prior to plating at limited density and colony formation monitored after two weeks (with continued doxycycline incubation). As before, we determined the percentage survival based on the number of cells originally plated and plotted this relative to the empty vector control samples.

We observed that 'leaky' re-expression of wildtype JMJD5 was able to increase colony formation of the affected patient fibroblasts (Figure 5.23). With increased re-expression of wildtype JMJD5 (10 ng/mL doxycycline), colony formation was further improved (Figure 5.23). Importantly, this rescue was again activity-dependent, as re-expression of the H321A catalytic mutant JMJD5 completely failed to rescue colony formation (Figure 5.23). In fact, expression of the H321A mutant significantly reduced colony formation compared to both the wildtype and empty vector cell lines (Figure 5.23). Therefore, we hypothesise that under these conditions the H321A mutant could be acting in a dominant negative manner.
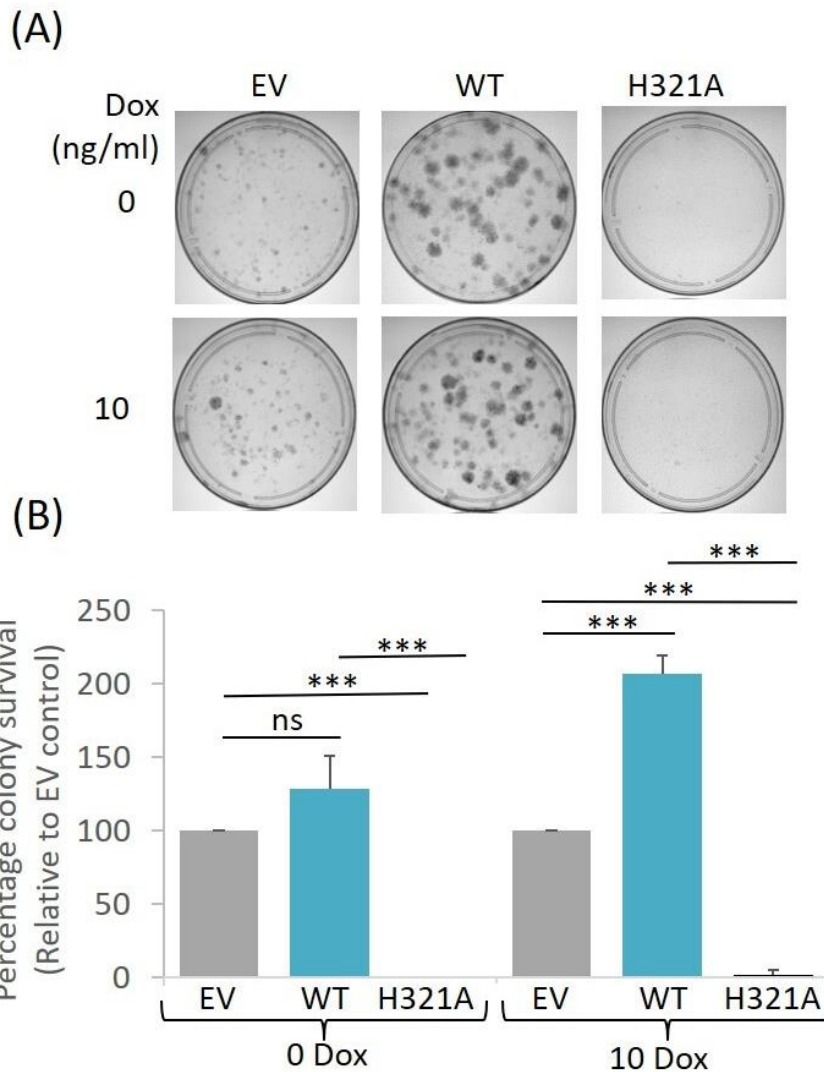
Figure 5.23 Rescue of colony formation phenotype by re-expression of no-tag wildtype JMJD5
No-tag JMJD5 OR07 rescue cell lines were grown for two weeks plus or minus 10 ng/mL doxycycline then plated at a limited plating density. Colonies stained using crystal violet grown after two weeks. **(A)** Images representative of n=3 biological repeats. **(B)** Colony formation was determined relative to the original number of cells plated and expressed as a percentage relative to the empty vector controls. Empty vector cell lines were used to determine the basal number of colonies, H321A expression cell lines used to determine the activity dependence of the rescue. Statistical analysis performed using the two-tailed Student's t-test (p-value ≤ 0.05 represented by '*', ≤0.01 represented by '**', ≤0.001 represented by '***', p-value >0.05 not significant represented by 'ns'). Representative protein expression as shown in Figure 5.18. This is representative of n=3 biological repeats.

Overall, the ability of wildtype JMJD5 re-expression to rescue the phenotypes in the affected

patient fibroblasts confirmed that the *JMJD5* genotype caused the colony formation and RS

phenotypes of these cells.

5.5 A JMJD5 loss of function model has increased replication stress

Overall, in this chapter we identified that a RS phenotype was associated with loss of JMJD5 expression and activity in immortalised patient-derived fibroblasts. As JMJD5 activity has been implicated in other diseases, such as cancer (discussed in Chapter 1), we were next interested to determine whether this JMJD5-associated RS phenotype was reproduced in other contexts.

In order to do this, we aimed to establish a JMJD5 knockdown model in a cancer cell line. First, we tested two constitutively expressed shRNA sequences targeting JMJD5 (Sigma), which were delivered into HeLa cells (human cervical cancer line) using lentivirus infection. Knockdown efficiency was determined using qPCR to measure *JMJD5* mRNA expression levels, which were normalised to a *β-actin* loading control and calculated relative to a control shRNA sequence. We found that only one out of the two shRNA sequences successfully reduced the levels of JMJD5 mRNA expression (Figure 5.24A). However, when growing the cells, we noticed that both sequences resulted in high levels of cell death (Figure 5.24B) which was also apparent in an MTS assay (Figure 5.24C). As this phenotype did not correlate with the *JMJD5* knockdown efficiency, we were concerned about potential off-target effects of this system. Therefore, we explored other approaches for JMJD5 knockdown.
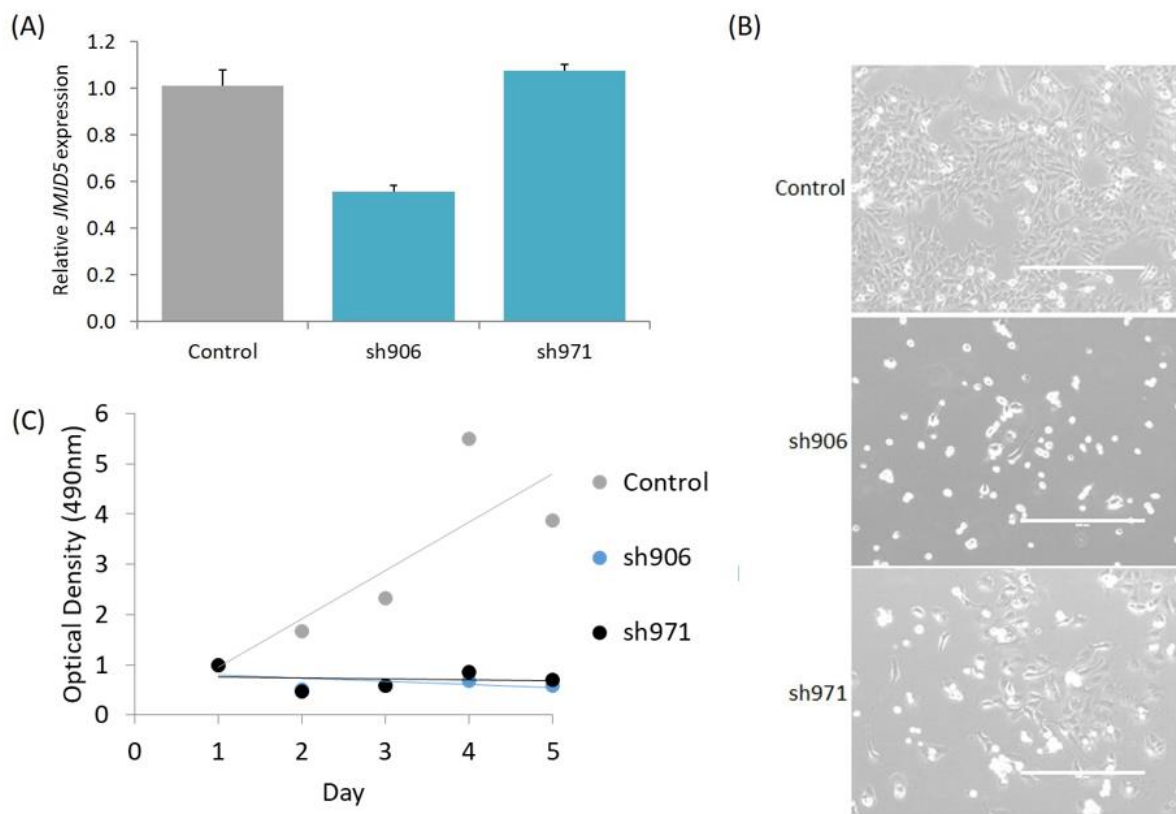
Figure 5.24 Optimisation of constitutively expressed shRNA targeted JMJD5 sequences
HeLa cells were infected with lentivirus to contain constitutively expressed control or JMJD5 targeted JMJD5 shRNA sequences (sh906 and sh971). **(A)** *JMJD5* knockdown was determined at the mRNA level by analysing cDNA by quantitative PCR to measure *JMJD5* expression normalised to the *β-actin* loading control and relative to the control shRNA sequence. This is representative of an n=1 biological repeat with quadruplicate technical repeats. **(B)** EVOS microscope was used to determine the cell health of the cells which found that JMJD5 shRNA expressing cells had increased cell death compared to controls. Scale bars= 400 μm. **(C)** MTS assay confirmed the increased cell death observed for the shRNA expressing cells. This is representative of an n=1 biological repeat.

Considering the severe phenotypes associated with constitutive JMJD5 knockdown, as demonstrated by our patient fibroblasts and JMJD5 mouse models (Oh and Janknecht, 2012, Ishimura et al., 2012, Ishimura et al., 2016), we next decided to explore an inducible JMJD5 knockdown system. Therefore, we tested a doxycycline inducible shRNA system (Dharmacon). These expression vectors encode an RFP gene upstream of the shRNA sequence meaning that successful doxycycline induction and shRNA expression can be monitored by detecting RFP-expressing cells using an EVOS microscope. Following lentiviral delivery of these vectors into

HeLa cells, we found that all shRNA expression vectors were responsive to doxycycline, but there was also 'leaky' expression, as indicated by RFP in the absence of doxycycline (Figure 5.25A). Surprisingly, qPCR analysis of cDNA derived from these cells indicated that none of the shRNA sequences resulted in *JMJD5* knockdown (Figure 5.25B).
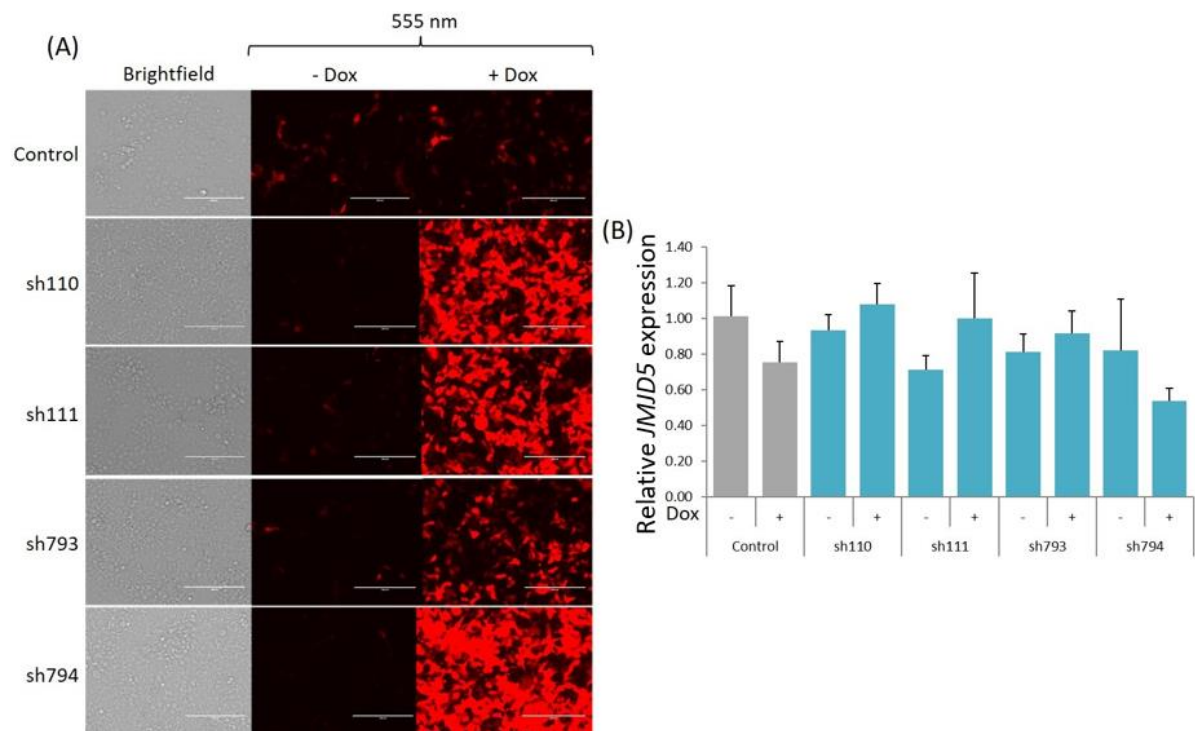
Figure 5.25 Optimisation of doxycycline inducible shRNA targeted JMJD5 sequences
HEK-293T cells were infected with lentivirus to contain doxycycline inducible shRNA expression vectors expressing a control shRNA or four different JMJD5 targeted shRNA sequences (sh110, sh111, sh793 and sh794). Upstream of the shRNA sequences was an RFP gene. Cells were treated with 1 µg/mL doxycycline (Dox) for 48 hours before, **(A)** Successful expression from the vector determined by visualising cells at 555nm on an EVOS microscope. Scale bars= 400 µm. **(B)** Lack of *JMJD5* knockdown determined using qPCR analysis on cDNA, normalised to the *β-actin* loading control and relative to the control shRNA sequence. This is representative of an n=1 biological repeat with quadruplicate technical repeats.

Considering the lack of success using shRNA systems for JMJD5 knockdown we next explored the efficacy of transient knockdown using siRNA transfection (these experiments were undertaken in collaboration with Dr Martin Higgs). We found that a JMJD5 siRNA SMARTpool, transfected into HeLa cells, successfully knocked down *JMJD5* mRNA expression levels (Figure

2.26A). We next monitored the RS phenotype in these cells and found that upon JMJD5 knockdown, cells had increased numbers of endogenous 53BP1 bodies (Figure 5.26B) which was exacerbated when treated with aphidicolin (Figure 2.26C). This RS phenotype was also reproduced in U2OS cells (human osteosarcoma cell line), following siRNA knockdown of JMJD5, measured by endogenous 53BP1 bodies and stalled DNA replication forks (Figure 2.27).
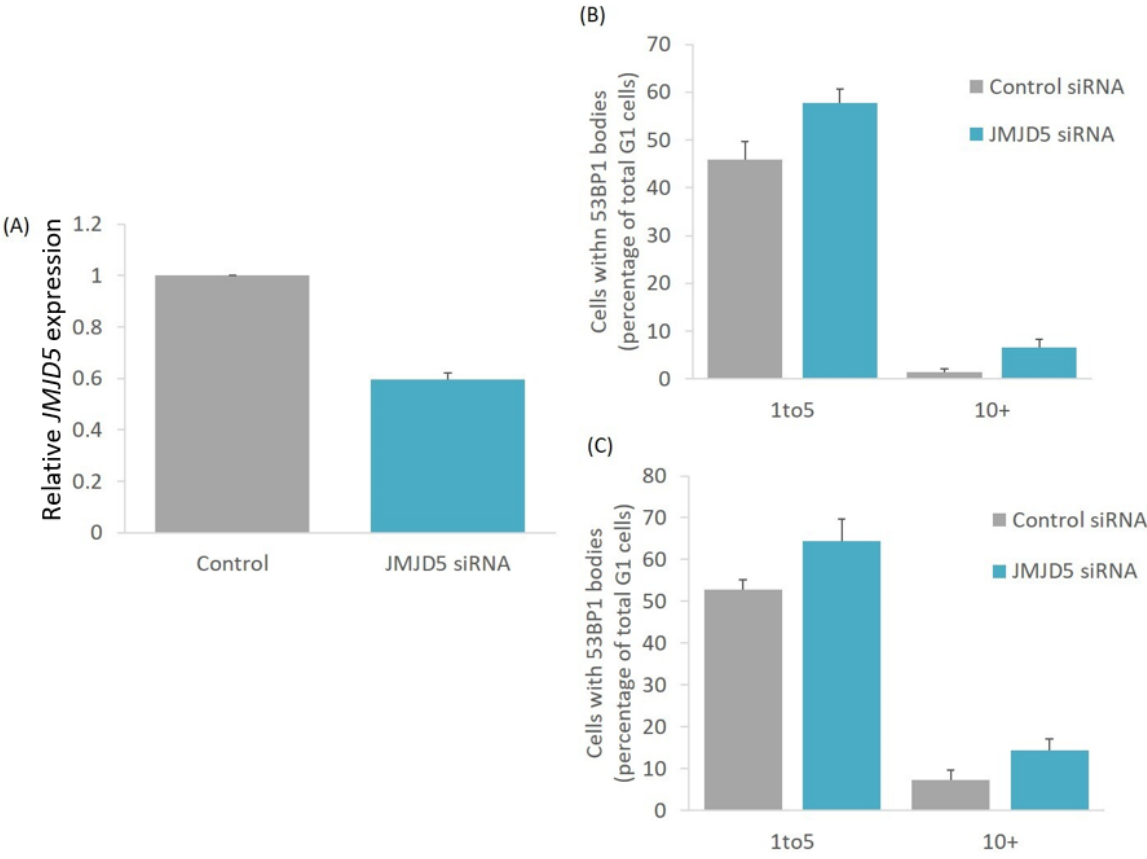
Figure 5.26 JMJD5 siRNA knockdown in HeLa cells results in a DNA replication stress phenotype
SMARTpool siRNA or a control was transiently transfected into HeLa cells using Oligofectamine™ for 48 hours prior to further analysis. **(A)** *JMJD5* knockdown was determined at the mRNA level using quantitative PCR on cDNA purified from the cell lines normalised to the *β-actin* loading control relative to the control shRNA sequence. This is representative of n=2 biological repeats with quadruplicate technical repeats. DNA replication stress was determined by counting 53BP1 bodies in G1 cells **(B)** at the endogenous level, or **(C)** after treatment with 0.5 μM aphidicolin for 48 hours. This is representative of n=2 biological repeats. The DNA replication stress analysis was performed by Dr Martin Higgs.
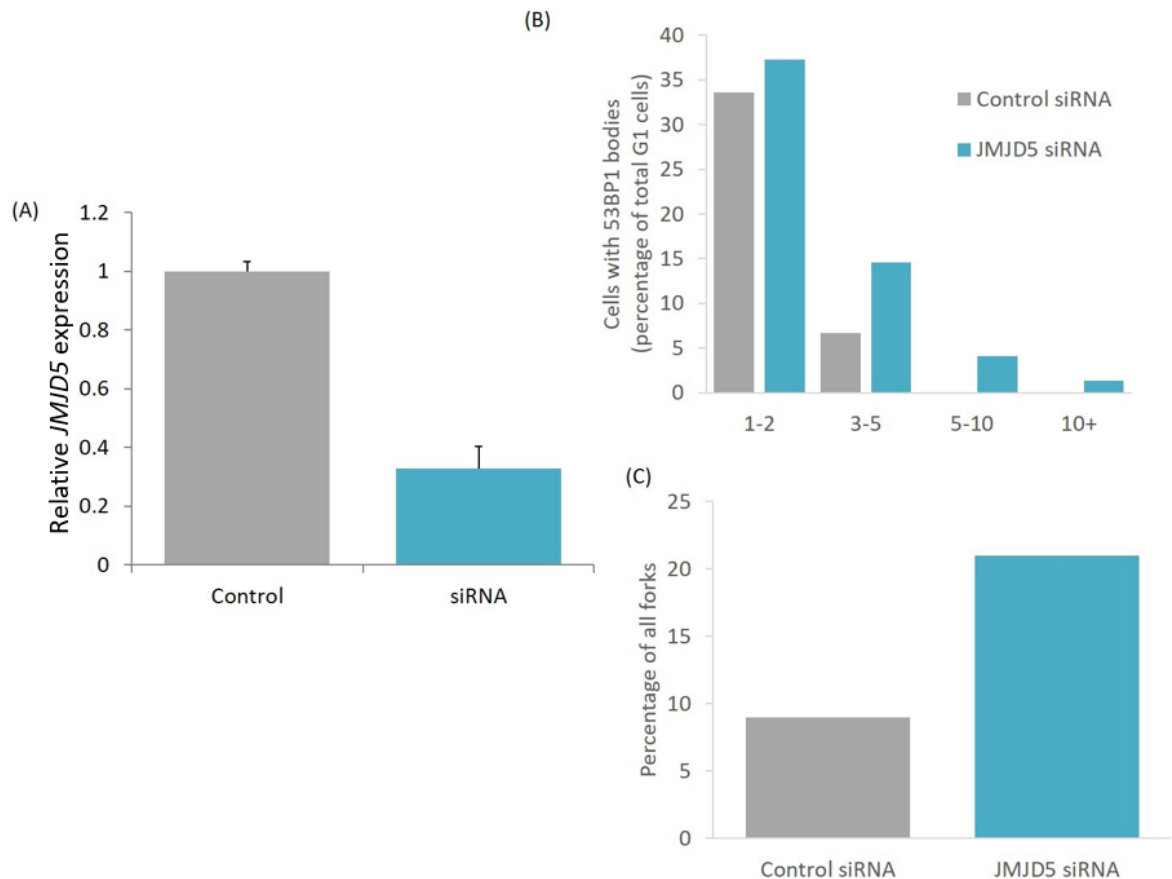
Figure 5.27 JMJD5 siRNA knockdown in U2OS cells results in a DNA replication stress phenotype

SMARTpool siRNA or a control was transiently transfected into U2OS cells using Oligofectamine™ for 48 hours. **(A)** *JMJD5* knockdown was determined at the mRNA level using quantitative PCR on cDNA purified from the cell lines normalised to the *β-actin* loading control relative to the control shRNA sequence. This is representative of an n=1 biological repeat, with quadruplicate technical repeats. DNA replication stress was determined **(B)** by counting endogenous 53BP1 bodies in G1 cells, or **(C)** by the presence of stalled DNA replication forks analysed using the DNA fibre assay. This is representative of an n=1 biological repeat. The DNA replication stress analysis was performed by Dr Martin Higgs.

Overall, this analysis confirmed our previous observation that loss of JMJD5 activity results in a RS phenotype. The ability to reproduce this in two independent cell models suggested that this was not restricted to our patient fibroblasts. Instead, this might be consistent with a ubiquitous role for JMJD5 activity, possibly through promoting an aspect of DNA replication via hydroxylation of the MCM complex (discussed below).

5.6 Discussion

In this chapter we performed phenotypic analysis on fibroblasts taken from a patient affected by a novel developmental disorder, that we hypothesised was hypomorphic for JMJD5 (Chapter 3). By doing this analysis we aimed to identify whether the *JMJD5* genotype of these patients correlated with a cellular phenotype. We then aimed to determine whether the *JMJD5* genotype caused these phenotypes by using re-expression of wildtype JMJD5 into the affected patient fibroblasts. In this chapter we observed a colony formation defect and RS phenotype that were both rescued by re-expression of JMJD5 in an activity-dependent manner. The RS phenotype was reproduced in two independent cell models and therefore we concluded that we had identified a novel cellular function of JMJD5 with regards to RS. This also confirmed that the *JMJD5* genotype of the affected patients was pathogenic. Below we discuss the potential significance of this finding and our hypotheses regarding the molecular mechanisms behind JMJD5-associated RS.

5.6.1 *JMJD5* patient genotypes results in a cell survival phenotype

Interestingly, the retarded growth clinical phenotype of our affected patients was consistent with a JMJD5 knockdown mouse that also displayed severe developmental growth defects (Oh and Janknecht, 2012, Ishimura et al., 2012, Ishimura et al., 2016). In support of this there is a large body of evidence indicating a fundamental role for JMJD5 in cell cycle progression and cellular proliferation in cell models and during development (Ishimura et al., 2012, Zhu et al., 2014, Ishimura et al., 2016, Shalaby et al., 2017, Fuhrmann et al., 2018). However, we did not observe a cell cycle progression or a cellular proliferation defect that correlated with the *JMJD5* genotype of our patient fibroblasts (Figure 5.4). Instead, after plating at limited cell density we identified that the affected patient fibroblasts presented with a colony formation

defect (Figure 5.5). This cell survival phenotype is supported by evidence in the literature whereby the proliferative potential of Caco-2 cells was unchanged, but their colony formation was significantly decreased upon JMJD5 knockdown (Zhang et al., 2015). Overall, it is likely that JMJD5 has a fundamental role in cell proliferation and survival, which may be dependent on the context and growth conditions used.

Rescue of the colony formation phenotype in our affected patient fibroblasts was only possible after re-expression of wildtype JMJD5, and not inactive H321A JMJD5, indicating that JMJD5 activity is required for colony formation (Figure 5.23). Interestingly, we found that re-expression of the H321A catalytic mutant JMJD5 actually worsened the colony formation phenotype (Figure 5.23) suggesting that it might be acting as a dominant negative. This result is consistent with observations in the literature whereby expression of H321A JMJD5 hinders the proliferation of MCF7 cells (Hsia et al., 2010). As JMJD5 has been demonstrated to oligomerise (Shen et al., 2017) (Section 3.7.2 in Chapter 3), we hypothesise that one possible mechanism for H321A acting as a dominant negative is by forming oligomers with wildtype JMJD5 which could inhibit its function. To test this hypothesis, we would first aim to determine any functional importance of JMJD5 oligomerisation.

Overall, we demonstrated that the *JMJD5* genotype of the affected patients caused a cellular survival defect *in vitro*. Evidence from PD patients, presenting with similar clinical growth phenotypes to our patients, indicate that genes involved in processes essential for cellular survival and proliferation can be pathogenic. These include those that directly regulate growth such as insulin-like growth factor 1 production (Savage et al., 2010, Netchine et al., 2011), or cellular pathways that indirectly affect prenatal growth such as mitosis (Rauch et al., 2008, Al-

Dosari et al., 2010, Dauber et al., 2012), DNA damage repair (O'Driscoll et al., 2003, Griffith et al., 2008, Kalay et al., 2011, Ogi et al., 2012, Murray et al., 2015, Harley et al., 2016, Tarnauskaitė et al., 2019), mRNA splicing of a subset of fundamental genes (Edery et al., 2011, He et al., 2011), and DNA replication (as discussed in in the introduction to this chapter). Overall, the genotype and subsequent deficient cellular phenotypes of PD patients causes impaired cellular proliferation and/or survival resulting in reduced cell numbers. This contributes to the growth retardation clinical phenotypes presented by the patients, reviewed by Klingseisen and Jackson (2011). Therefore, we hypothesised that the *JMJD5* genotype of our affected patent fibroblasts could result in a molecular deficiency that translates into reduced cell survival and clinical growth retardation.

5.6.2 *JMJD5* patient genotypes result in a replication stress phenotype

To explore potential consequences of the JMJD5 mutations identified in our affected patients, we first investigated whether DNA replication was altered by assaying for RS. Our rationale for this was that essential components of the MCM replicative helicase were proposed as candidate substrates of JMJD5 in Chapter 4. Also as discussed in the introduction to this chapter, similar disorders associated with growth retardation symptoms can result from pathogenic mutations in essential DNA replication proteins.

We observed that the affected patient fibroblasts had increased RS compared to the unaffected patient fibroblasts (Figure 5.6 to 5.9). By re-expressing wildtype JMJD5 we confirmed that this was caused by their loss of function JMJD5 mutations (Figure 5.22). Interestingly, this RS phenotype could be reproduced in two independent cancer cell lines after JMJD5 knockdown (Figure 5.26 and 5.27).

The RS phenotype that we identified in the affected patient fibroblasts was demonstrated by increased frequency of micronuclei and 53BP1 bodies, which was further exacerbated after incubation with aphidicolin (Figure 5.6, 5.7 and 5.22). These are both relatively indirect RS markers as they identify previous S phase stress in subsequent daughter cells (Section 5.1.4.1). However, the ability to detect micronuclei and 53BP1 bodies suggests that the RS source was persistent and/or strong enough to bypass repair pathways in S phase and mitosis. Therefore, it raises the possibility that JMJD5 could be responsible for causing RS that is strong, persistent or difficult to repair. Alternatively, it could indicate that JMJD5 is required for signalling or facilitating repair of DNA damage caused by RS in either S phase or mitosis. In order to distinguish between these possibilities more detailed analysis could be performed in the future. For example, it would be interesting to identify the sub-class of micronuclei induced by JMJD5 knockdown. For example, those that contain γH2AX are directly caused by RS (Xu et al., 2011a). Mechanistic insights into their origins can also be determined by exploring whether the micronuclei contain centromeres (Fenech et al., 2011). A more detailed insight into chromosome aberrations and genomic instability in our affected patient fibroblasts could also be achieved by analysing chromosomes after metaphase spreading.

Future analysis will also aim to determine whether the RS pathway is properly activated in the affected patient fibroblasts. For example, we will aim to monitor markers of ATR-CHK1 activity, including phosphorylation of ATR, CHK1, RAD51 and H2AX. Interestingly, pan-nuclear staining of γH2AX was recently found to be indicative of cell death after lethal RS, and therefore this can be used as a more specific marker of RS (Moeglin et al., 2019). We will also aim to investigate the lesions generated by JMJD5-associated RS, for example, by investigating formation of ssDNA and RPA foci. More detailed analysis could also involve screening RS

inducing drugs that have different mechanisms of action, to identify those that sensitise cells with reduced JMJD5 expression to RS.

In this chapter, we also demonstrated the JMJD5-associated RS phenotype using DNA fibre analysis. We found JMJD5 activity was essential for progression of the replication fork, by monitoring the prevalence of DNA replication stalled forks (Figure 5.8 and 5.22) and asymmetric progression of replication forks (Figure 5.9 and 5.22). However, we found that no significant difference in replication fork speed was found for the affected patient fibroblasts (Figure 5.10). The reason for this is unclear but could be due to limitations of the assay as it is only able to monitor global fork speed. For example, reduced fork speed at CFS, which would be most likely to demonstrate a difference in speed during RS (as discussed in Section 5.1.1), would not be apparent with the resolution of this assay. However, it could also be that the fork speeds appear unchanged in the OR07 patient fibroblasts due to the activation of dormant origins. As demonstrated by Rodriguez-Acebes et al. (2018), fork speed and origin activity are influenced by each other and so are difficult to distinguish using DNA fibre assays.

However, consistent with our observations, others have also demonstrated that global fork speed can remain unchanged during RS, despite fork stalling and asymmetry (Reynolds et al., 2017). Therefore, the manifestation of our affected patient fibroblast RS phenotype could be investigated further to help infer a mechanistic role regarding JMJD5-associated RS. For example, JMJD5 probably does not alter nucleotide availability because it has been well documented that fork progression is reduced when nucleotide pools are depleted (Anglana et al., 2003, Beck et al., 2012, Poli et al., 2012). Instead, it could be that JMJD5-associated RS activates the intra-S phase checkpoint to inhibit new DNA origin firing rather than slowing

replication forks (Iyer and Rhind, 2017, Mutreja et al., 2018). Consistent with this, our data suggest that JMJD5-associated RS causes fork stalling (Figure 5.8 and 5.9). Moreover, if the RS in our cell lines was caused by or resulted in fork slowing, then we would expect DNA forks to have remained symmetrical in progression but fork speed to have reduced (Nieminuszczy et al., 2016).

Although, further experimental investigation will be essential in order to decipher how JMJD5 activity might impact DNA replication and thus cause RS, we next propose our hypothesis for this.

5.6.3 Hypotheses for the JMJD5-associated replication stress molecular mechanism

As discussed in Chapter 1, there are various cellular functions attributed to JMJD5 (summarised in Figure 1.6) that could theoretically contribute to RS if deficient. For example, aberrant cell cycle progression due to reduced cyclin A1 expression or dysregulation of the p53/p21 pathway could contribute to RS (Hsia et al., 2010, Huang et al., 2015, Wu et al., 2016a, Shalaby et al., 2017). Consistent with this, improper regulation of cell proliferation is common in cancer cells and can be a source of RS due to the inevitable depletion of essential resources (Dominguez-Sola et al., 2007, Halazonetis et al., 2008, Burrell et al., 2013, Hills and Diffley, 2014, Kotsantis et al., 2018). Also, the proper response of pathways involved in regulating cell cycle progression and cellular proliferation is essential as they are commonly targeted by ATR/CHK1 in response to RS (Zeman and Cimprich, 2014). Moreover, JMJD5 could also exacerbate RS due to deficient chromosome segregation via its proposed role in mitotic spindle assembly and stabilisation (Marcon et al., 2014, He et al., 2016b).

JMJD5 could also be implicated in RS via its proposed roles in DNA repair. For example, JMJD5 was predicted to be involved in mismatch repair (Suzuki et al., 2006), a pathway important for correcting DNA polymerase errors and crucial for maintaining genomic stability (Kunkel and Erie, 2015). JMJD5 was also implicated in facilitating efficient homologous recombination (Amendola et al., 2017). The importance of homologous recombination-based repair and restart of stalled forks is demonstrated by the fact that targets of ATR phosphorylation include the Bloom's helicase (Li et al., 2004), BRCA1 (Tibbetts et al., 2000) and the Werner's syndrome protein (Pichierri et al., 2003). Also, during MiDAS, homologous recombination-based BIR pathways ensure complete DNA replication occurs (as discussed in the introduction to this chapter).

Our current analysis is not detailed enough to disregard any of these possible ways that JMJD5 could contribute to or respond to RS. However, it is also possible that these JMJD5 functions are in fact an indirect consequence of JMJD5-associated RS.

We demonstrated in this chapter that prevention of RS by JMJD5 is dependent on its catalytic activity (Figure 5.22). Consequently, we propose that inhibition of a cellular process, which is directly regulated by a JMJD5 hydroxylation substrate, would be responsible for the RS observed upon depletion of JMJD5 activity. The currently proposed hydroxylation substrates of JMJD5 are H3K36me2 (Hsia et al., 2010), p53 (Huang et al., 2015), NFATC1 (Youn et al., 2012), PKM2 (Wang et al., 2014b), RCCD1 (Marcon et al., 2014) and RPS6 (Wilkins et al., 2018). Interestingly, Wilkins et al. (2018) found no evidence that JMJD5 hydroxylates H3K36me2, p53, NFATC1, or PKM2. However, they did identify some activity towards RCCD1 and RPS6 peptides, though this was only found *in vitro*. In this thesis we provided further evidence

suggesting that H3K36me2, RPS6 and RCCD1 are unlikely to be physiologically relevant JMJD5 substrates (Chapter 4). Instead, we identified two novel candidate substrates as MCM3 and/or MCM5 subunits of the DNA replicative helicase (Chapter 4). Consequently, we propose that the molecular mechanism underlying JMJD5-associated RS is likely to be mediated by hydroxylation of MCM3 and/or MCM5.

In support of this hypothesis, the MCM complex is essential for DNA replication (Chapter 1). Importantly, the MCM complex is also known to play an important role in preventing RS in the form of dormant origins. These dormant origins are activated proximal to stalled replication forks to promote complete replication of DNA (as discussed in the introduction to this chapter). Furthermore, there is evidence to suggest that proper regulation of origin firing is important for preventing RS. For example, over-firing of origins in cancer cells results in exhaustion of resources essential for DNA replication and can also result in re-replication. Conversely, under-firing of origins can also result in RS, as replication forks must travel longer distances thus increasing the chance of fork stalling. The resulting under-replicated regions of DNA then pose a barrier to proper chromosome segregation at mitosis and can be a source for loss of genetic material (Taylor and Lindsay, 2016). Interestingly, the MCM complex has also been directly implicated in the RS response. For example, MCM7 has been associated with facilitating the recruitment of ATR onto sites of DNA damage to stimulate the S phase checkpoint (Tsao et al., 2004). Additionally, studies have demonstrated that the MCM subunits are direct targets of ATR and ATM in response to DNA damage or RS (Cortez et al., 2004).

The importance of MCM function has also been established *in vivo*. For example, a mouse model of an MCM4 mutation (D573H), that assembles into and inactivates the MCM complex,

is associated with chromosomal instability and the development of T cell lymphoblastic leukaemia/lymphoma (Bagley et al., 2012). Likewise, an independent MCM4 mutation (F391I) causes reduced licencing of dormant origins, increased DNA replication fork stalling, fork asymmetry and mammary adenocarcinomas as well as increased sensitivity to RS-inducing agents (Shima et al., 2007). Furthermore, knockdown of MCM proteins in cell models results in increased genomic instability and susceptibility to replication stress inducing agents (Ge et al., 2007, Shima et al., 2007, Kunnev et al., 2010).

Other evidence demonstrating the importance of MCM complex function comes from evidence in human disease. For example, an MGS patient carrying mutations in MCM5 presented with a growth defect and cells derived from this patient had increased RS (Vetro et al., 2017). Consistent with this, MCM5 knockdown results in retarded growth in zebrafish (Ryu et al., 2005). Furthermore, patients with pathogenic MCM4 mutations present with retarded growth phenotypes (Hughes et al., 2012). Moreover, susceptibility to retarded growth during development was found to be increased after relatively low changes to MCM expression levels or localisation, which was attributed to reduced firing of dormant origins (Chuang et al., 2010). Potentially consistent with this, our preliminary data found an association between reduced protein expression levels of JMJD5 and MCM subunits (Chapter 4).

Overall, we hypothesise that JMJD5 promotes the normal function of MCM3/5, and that loss of this regulation results in defective DNA replication resulting in RS. However, identification of the putative MCM3/5 hydroxylation site will be hugely beneficial for future testing of this hypothesis.

5.6.4 Chapter Conclusions

Overall, in this chapter we performed phenotypic analysis on affected patient fibroblasts to confirm that their *JMJD5* genotypes were pathogenic. In doing so we also identified a novel cellular role for JMJD5 with regards to RS. We hypothesised that this increased RS in affected patient fibroblasts could be responsible for the reduced colony formation *in vitro* and could contribute to the clinical growth phenotypes of the affected patients *in vivo*. This is consistent with PD classified disorders that have mutations in proteins essential for DNA replication, demonstrate RS and present with clinical growth defects. This information provides potentially useful information for clinicians that we hope will aid with the clinical diagnosis and future care of the affected patients. Furthermore, our findings potentially strengthen the assignment of MCM3 and/or MCM5 as candidate JMJD5 substrates. It could also imply why JMJD5 has been implicated in diverse cellular processes and as such warrants further investigation.

6 **Final discussion**

The overall aim of this thesis was to investigate the potential role of two JmjC-only 2OG oxygenase sub-family members, JMJD7 and JMJD5, in human developmental disorders to further characterise their cellular and enzymatic functions.

6.1 JMJD7

JMJD7 has been assigned two hydroxylation substrates, DRG1 and DRG2 (Markolovic et al., 2018). However, the functional consequences of this are currently unclear due to poor characterisation regarding both the enzyme and its substrates (Chapter 1). Interestingly, components of the JMJD7 hydroxylation pathway have been implicated in neurodevelopmental disorders associated with ASD and ID (Vlangos et al., 2000, Lucas et al., 2001, Bi et al., 2002, Nakamine et al., 2008, de Krom et al., 2009, de Ligt et al., 2012, Matsunami et al., 2014). Therefore, we developed cellular models in ESCs, iPSCs and SHSY5Y cell lines to characterise this pathway during cortical neuron differentiation, in order to help clarify the role of this pathway in neurodevelopmental disorders.

Our findings suggest that expression of the JMJD7 pathway is upregulated during highly proliferative stages of neural differentiation. Consistent with this we found that JMJD7 knockdown resulted in reduced proliferation in SHSY5Y neuronal-like cells. In addition, our data suggest that the JMJD7 pathway could be important for neuron function. Together with our expression analyses of pathway components in ASD patient-derived iPSCs, and bioinformatic analysis of the ASD-associated JMJD7 R260C mutation, our findings are consistent with a previously unexplored role of this novel pathway in neuronal differentiation,

function, and ASD. However, the exact molecular mechanisms involved remain unclear. As such, future work will aim to extend the preliminary observations presented here in order to address this.

Firstly, mass spectrometry of DRG1 and DRG2 hydroxylation could be performed at key stages of neural differentiation. This could help to determine whether changes in JMJD7 mRNA levels that we observed result in altered JMJD7 protein activity during neural differentiation and neuron function. Such analysis could also be applied to ASD patient-derived iPSCs. However, the cohort size should be significantly increased if further analysis of this pathway is undertaken in using this model (only 3 lines were available at the time of this study).

Targeted genetic analyses could also be undertaken to determine how frequently this pathway is dysregulated in ASD (and other neurodevelopmental disorders), including screening for additional patient mutations in JMJD7, DRG1, DRG2, DFRP1, DFRP2 and candidate downstream targets (discussed further below). Functional analyses of newly identified mutants could be undertaken in SHSY5Y cells or ESCs to identify how they might impact neural differentiation and/or function.

The potential importance of JMJD7 in neurodevelopmental disorders could also extend beyond that suggested by its mutation frequency alone. For example, wildtype JMJD7 function could be altered in neurons by the microenvironment and the availability of critical cofactors such as oxygen. As discussed in Chapter 1, there is emerging evidence for direct (inhibition of catalytic activity due to decreased oxygen levels) and indirect regulation (expression regulated by the HIF pathway) of 2OG oxygenases in response to hypoxia. Interestingly, hypoxia, caused by a multitude of pre- and postnatal complications, has also been implicated in the aetiology

of ASD (Burstyn et al., 2011, Karimi et al., 2017). Moreover, hypoxia caused by perinatal complications could be used as an early method of identifying children for future ASD screening or intervention (Getahun et al., 2017). Although no investigation to date has been performed regarding how JMJD7 might be affected by hypoxia, it could be interesting to explore this in relation to its potential role in ASD.

Any future investigation into the role of the JMJD7 pathway should address activity in transcription and translation, in light of recent work by the Coleman lab that assigns these processes as potential targets of DRG1/DFRP1 and DRG2/DFRP2 activity. Moreover, as discussed in Chapter 2, it has been well established that transcription and translation are important for neuron differentiation and function and can contribute to ASD (Kelleher and Bear, 2008, Yap and Greenberg, 2018).

The hypothesis that DRG1/DFRP1 might regulate transcription followed the proteomic assignment of its interaction with the FACT complex (Coleman lab). The current working model is that dysregulated JMJD7-DRG1/DFRP1 could impair the activity of transcriptional regulators, which could result in 'transcription stress' (impaired progression of RNA polymerase and transcription elongation, Ljungman (2007)) and subsequent DNA damage and GI. Due to the fundamental nature of this assignment, we hypothesise that impaired function of DRG1 and DFRP1 might also play a role in other neurodevelopmental disorders and cancer. Interestingly, several families affected by a novel developmental disorder that is associated with loss-of-function DRG1 mutations have recently been identified (Coleman lab). Furthermore, bioinformatics analyses of cancer mutation and patient survival databases implicated DRG1 and DFRP1 as tumour suppressors (Charlotte Eaton, Coleman lab).

Similarly, the hypothesis that DRG2/DFRP2 might regulate translation followed the identification of its interaction with critical enzymes involved in regulating the eukaryotic translation initiation factor 5A (EIF5A) (Coleman lab). These enzymes promote the activity of EIF5A by catalysing the addition of a PTM, unique to EIF5A, called hypusine (hydroxyputrescine and lysine) (Turpaev, 2018). Therefore, it is possible that altered JMJD7-DRG2/DFRP2 activity could dysregulate EIF5A activity which in turn could interfere with translation and affect normal neuronal differentiation and/or function. Consistent with the importance of the EIF5A pathway in development, mutations in a critical regulator of this pathway were recently identified in a novel developmental disorder associated with developmental delay and seizures (Ganapathi et al., 2019). Furthermore, the EIF5A pathway has been widely implicated in tumourigenesis (Mathews and Hershey, 2015).

Consistent with our hypothesis that JMJD7 regulation of DRG1/2 could be relevant in cancer, the association of common transcription and translation pathways in cancer and neurodevelopmental disorders have already been described. One example is MeCP2, which is a methyl-CpG binding protein that can be activating or inhibitory towards gene expression (Chahrour et al., 2008). Therefore, dependent on context MeCP2 is a tumour suppressor or oncogene associated with multiple cancer types (Müller et al., 2003, Zhao et al., 2013, Zhang et al., 2017, Qin et al., 2017). In addition, MeCP2 is dysregulated in Rett's syndrome, a neurodevelopmental disorder where all patients present with ASD (Wen et al., 2017, Kelleher and Bear, 2008).

Interestingly, defects in protein translation are also common in both cancer and neurodevelopmental disorders such as ASD. One example is the fragile X mental retardation

protein (FMRP), which regulates the transport and translation of mRNA in the brain and loss

of FMRP results in the neurodevelopmental disorder, fragile X syndrome (FXS), where 15-30%

of patients present with ASD (Wang, 2015). FMRP directly regulates the translation of multiple

genes important for plasma membrane plasticity (Zalfa et al., 2017), which is essential for

synaptic plasticity and development in the brain (Pfeiffer and Huber, 2007). Interestingly FXS

patients with low FMRP levels, have decreased risk of cancer (Schultz-Pedersen et al., 2001),

whilst high levels of FMRP expression are identified in multiple cancer types (Luca et al., 2013).

It is hypothesised that this elevated FMRP activity at the leading edge of cancer cells can

facilitate metastasis (Luca et al., 2013, Zalfa et al., 2017).

Furthermore, the Tuberous Sclerosis Complex (TSC) proteins TSC1 and TSC2 regulate protein

translation by inhibiting mammalian target of rapamycin complex (mTORC1) (Tee et al., 2003).

Inactivating mutations in either TSC1 or 2 cause up-regulation of mTORC and protein

synthesis, which results in the TSC disorder where patients have a 25-60% prevalence of ASD

(Wiznitzer, 2004). Interestingly, TSC1 and TSC2 are also tumour suppressor genes (Mieulet and

Lamb, 2010). Similarly, inactivating mutations in proteins upstream of mTOR regulation, such

as phosphatase and tensin homolog (PTEN), are also common in cancer (Lee et al., 2019).

Interestingly, PTEN mutations also cause the neurodevelopmental disorder 'PTEN hamartoma

syndrome' which is associated with ASD and macrocephaly (Butler et al., 2005, Kwon et al.,

2006).Overall, these brief examples highlight the importance of common pathways regulating

transcription and translation that are implicated in the aetiology of both neurodevelopmental

disorders (associated with ASD) and cancer. By analogy with these examples, we propose the

JMJD7-DRG1/2 pathway and its regulation of transcription and translation are worthy of

further investigation.

6.2 JMJD5

The second aim of this thesis was to investigate the role of the JmjC-only sub-family member JMJD5. Although this enzyme has many potential cellular functions attributed to it, its precise role in the cell was controversial due to a variety of misassigned substrates (Chapter 1). In order to address this, we aimed to characterise the pathogenicity of two JMJD5 mutations identified in patients with a novel developmental disorder. We first identified that both JMJD5 mutations affected the stability and potentially reduced the catalytic activity of JMJD5. Consequently, we hypothesised that the affected patients were hypomorphic for JMJD5(Chapter 3). Therefore, fibroblasts isolated from this family represented a novel platform for characterising the enzymatic and cellular activity of JMJD5. We first identified that none of the currently proposed hydroxylation substrates of JMJD5 were related to either JMJD5 activity or the genotype of our fibroblast models. Instead we identified two novel candidate JMJD5 substrates as the minichromosome maintenance complex subunits MCM3 and/or MCM5 (Chapter 4). Furthermore, investigation into the pathogenicity of the *JMJD5* genotype led us to identify a novel role for JMJD5 activity in RS (Chapter 5).

Considering all of the evidence presented in this thesis, we propose that loss of function JMJD5 mutations interfere with normal DNA replication, resulting in RS. We believe that JMJD5 facilitates DNA replication *via* its candidate substrates MCM3 and/or MCM5. However, future work will be required to identify whether MCM3/5 are *bone fide* hydroxylation substrates of JMJD5. Such work will require further understanding regarding the nature, regulation and context of the JMJD5-MCM3/5 interaction. One way to address this would be to perform the MS screen and JMJD5-MCM3/5 interaction assays, established in Chapter 4, in the presence

of ATM, ATR or checkpoint kinase inhibitors in order to interrogate the nature of this interaction and potential hydroxylation event. Once the hydroxylation site has been identified, we will then aim to characterise the functional consequences of this hydroxylation event on the biology of the target MCM, as well as how it affects the MCM complex, DNA replication, and how this causes RS when dysregulated.

The pathogenicity of JMJD5 with regards to RS was demonstrated by rescue experiments performed in the developmental disorder affected patient fibroblasts. However, considering the fundamental nature of DNA replication, we hypothesise that the impact of defects associated with this pathway are likely to extend beyond development. As discussed in Chapter 1, JMJD5 has been implicated in cancer where, dependent on context, it acts as either a tumour suppressor gene or oncogene. However, the mechanisms behind this paradox are unknown. In Chapter 4 we provided evidence that some JMJD5 cancer patient mutations impaired MCM3/5 interaction. We hypothesise that these mutations are likely to be tumour suppressor mutations, considering the phenotype observed after JMJD5 loss of function in affected patient fibroblasts and by siRNA knockdown in cancer cell lines (Chapter 5). This means that loss of function JMJD5 cancer mutations could promote tumourigenesis by increasing RS and GI, which are well-established hallmarks of cancer (Gaillard et al., 2015, Macheret and Halazonetis, 2015). Therefore, the interaction between JMJD5 and MCM3/5 could be functionally important in preventing tumourigenesis. To test this hypothesis in the future, we will perform phenotypic analysis on cancer cell lines carrying JMJD5 mutations (Chapter 4) to determine their RS phenotypes and whether this is caused by their *JMJD5* genotypes.

As discussed for JMJD7 above, potential effects of dysregulated JMJD5 activity could also be independent of genetic mutation and be regulated by hypoxia. Similar to JMJD7, there have been no studies to date investigating JMJD5 regulation in hypoxia. In spite of this, we propose that hypoxia could be an interesting future avenue to investigate with regards to the tumour suppressor function of JMJD5. This is because under severe hypoxic conditions ($\leq 0.1\%$ oxygen levels) the progression of DNA replication is impaired (Hammond et al., 2002, Bencokova et al., 2009, Pires et al., 2010, Foskolou et al., 2016). The molecular mechanism behind this hypoxia-induced RS is reviewed by Ng et al. (2018) and the cellular consequences are largely dependent on the period of hypoxia (Pires et al., 2010). For example, after chronic periods of hypoxia (>12 hours) cells arrest and are unable to undergo fork restart. This may be due to inhibition and disassembly of MCM subunits, which once removed cannot be reloaded during S phase (Pires et al., 2010, Hammond et al., 2006). Interestingly, we provided evidence in the affected patient fibroblasts model suggesting that impaired JMJD5 function correlated with reduced expression of MCM subunits (Figure 4.16, Chapter 4). However, further repeats will be required to determine the reliability of this observation as this is currently a single biological repeat. To explore this observation further it could be investigated in the rescue cell lines established in Chapter 5. These experiments will aim to determine whether re-introduction of JMJD5 is sufficient to rescue any reduced MCM expression in the affected patient fibroblasts. In summary, it would be interesting to determine whether JMJD5 activity is abrogated by hypoxia and what role this might play in MCM dysregulation and RS during chronic hypoxia. Moreover, it would be interesting to investigate whether JMJD5 inhibitors could sensitise hypoxic tumours to chemo- or radiotherapy, as has been demonstrated previously for ATR inhibitors (Pires et al., 2012, Leszczynska et al., 2016).

Another potentially interesting avenue of investigation is the effect oncometabolites might have on JMJD5 function. As discussed in Chapter 1, generation and accumulation of oncometabolites can result in the inhibition of 2OG oxygenases, which has been linked to tumourigenesis. Interestingly, there is evidence suggesting that inhibition of 2OG oxygenases by oncometabolites can disrupt DNA damage repair pathways, which can promote GI. For example, two enantiomers of the oncometabolite 2HG were shown to result in deficient homologous recombination via inhibition of JMJD2A (KDM4A) and JMJD2B (KDM4B) (Sulkowski et al., 2017). Therefore, it could be worthwhile investigating the role of JMJD5 inhibition in relation to oncometabolite-mediated RS, DNA damage and GI.

Finally, JMJD5 loss of function has recently been found to render cells sensitive to Poly ADP-ribose Polymerase (PARP) inhibition (Zimmermann et al., 2018) (Sally Fletcher, Coleman lab). PARPs mediate 'poly ADP-ribosylation', a PTM commonly involved in DNA synthesis and repair. Thus, cells that are dependent on PARP associated pathways for survival are particularly sensitive to PARP inhibition (Morales et al., 2014). A reason for PARP inhibitor sensitivity in JMJD5 loss of function cells could be due to the associated increase in RS. This is because PARP can be activated at stalled replication forks to promote fork restart and repair (Sugimura et al., 2008, Bryant et al., 2009). If the effect of JMJD5 on PARP inhibitor sensitivity is activity-dependent, it would support JMJD5 as a potential therapeutic target. For example, JMJD5 inhibitors could be used to promote catastrophic RS and DNA damage in hypoxic tumours, and to increase the efficacy of PARP inhibitors.

6.3 Final conclusion

In summary, we successfully performed preliminary characterisation of two JmjC-only protein hydroxylases by studying their role in human developmental disorders. By doing so we have provided evidence that further strengthens the importance of 2OG oxygenases in regulating fundamental cellular pathways, that when dysregulated contribute to disease. This supports growing interest in 2OG oxygenases as valid therapeutic targets or biomarkers in disease. Moreover, we propose that this greater understanding of 2OG oxygenase family members could potentially provide essential information to expand clinical diagnoses and support future patient care.

7 Methods

7.1 Cell culture

7.1.1 Cancer and patient cell lines

All cells were cultured at 37˚C, in a humidified atmosphere, with 5% CO_2 and media supplemented with 1% Penicillin and Streptomycin (Gibco). Mycoplasma tests were carried out regularly. Upon 70-80% confluency, cells were removed from culture flasks using TripLE express trypsin (ThermoFisher Scientific). Trypsin was inactivated using culture media before re-seeding cells into culture flasks. Alternatively, cells to be plated for experiments were first counted using an automated counter (Invitrogen™ Countess II™) or manually by haemocytometer. Cells were generally plated for 60% confluency the following day, any differences to this are indicated.

HEK-293T cells, HeLa and MDA-231 purchased from the ATCC. Cells grown in DMEM (Gibco) plus 10% foetal bovine serum (FBS, Sigma-Aldrich®). U2OS, kindly supplied by Dr Martin Higgs, cultured in McCoy's 5A Medium (Gibco) plus 10% FBS. SHSY5Y (European Collection of Cell Cultures) cultured in 50% HAM F12 (ThermoFisher Scientific), 50% Minimum Essential Medium Eagle (Sigma-Aldrich®), 15% FBS, 2 mM Glutamine (Gibco). KNS-62 and LU99A purchased from JCRB, SKCO1 purchased from the ATCC. KNS-62 cells and SKCO1 grown in MEME (Sigma-Aldrich®) plus 20% FBS. LU99A cells grown in RPMI-1640 (Thermo) and 10% FBS. Primary patient fibroblasts and hTERT immortalised cells were grown in DMEM plus 20% FBS (Sigma-Aldrich®). Formal patient consent was obtained by Dr Sander Pajusalu and Dr Katrin Ounap (University of Tartu, Estonia) prior to skin biopsies and isolation of dermal fibroblasts.

7.1.2   Stem cell culture

The human Embryonic Stem Cell line (ESC) H9 was derived by The WiCell Institute, University of Melbourne, from donated *in vitro* fertilisation embryos. Human induced pluripotent stem cell lines (iPSC) were 007 as a healthy control (provided by A/Prof Alice Pebay), and three lines were derived from ASD patients, 119, 125, 147. Fibroblasts for 119, 125 and 147 were donated by Dr Philip Schwartz at the Children's Hospital of Orange County Research Institute, California. These fibroblasts were reprogrammed by Ms Tejal Kalkarni and Dr Giovanna D'Abaco supervised by Prof Mirella Dottori using non-viral episomal vectors (Life Technologies, Epi5™ Episomal iPSC Reprogramming Kit) using Nucleofector™ kit (Lonza). Approval to utilise these cells was obtained by Prof Mirella Dottori from The University of Melbourne (Approval number: 0605017).

All cell lines were maintained as stem cells on 10 µg/mL Vitronectin substrate (Stem Cell Technologies) diluted in CellAdhere™ Dilution Buffer (Stem Cell Technologies). Cells were maintained as 'bulk culture' in T25 flasks using Essential 8 media (ThemoFisher Scientific). Each day the media was changed and cells monitored for differentiation (stem cells observed as uniform cells growing in colonies with defined borders, Figure 7.1A. Spontaneous differentiation identified by colonies with broken borders, Figure 7.1B). When at 60-70% confluent colonies were passaged by washing twice with 1X PBS, incubated with 0.5 mM EDTA at 37°C for 4 minutes. Once cells began to detach the EDTA was removed and cells washed off gently using E8 media. Cells were gently mixed to prevent complete disruption of colonies and re-seeded onto fresh Vitronectin or plated for induction as required.

7.2 Neural induction of stem cells

The following process is summarised in Figure 7.1. For neural induction stem cells were passaged, as above, then plated onto 10 µg/mL Laminin substrate (Invitrogen™). Stem cells were grown in N2B27 media (50% Neurobasal Medium, 50% DMEM/F12, 1X N-2 supplement, 1X B-27 supplement, 1X ITS-A, 2mM total concentration L-Glutaine/ Glutamax, 50 units/mL Penicillin/ Streptomycin, 0.3% w/v Glucose). For differentiation into dorsal forebrain neurons (Glutamatergic excitatory neurons) N2B27 media was supplemented with 10 µM Activin inhibitor SB431524 (Tocris) and 500 ng/mL BMP inhibitor LDN/ Noggin (PeproTech) for 1 week. Ventral forebrain neuron differentiation (GABAergic inhibitory neurons) required supplementing N2B27 media as above but also including 400 nM sonic hedgehog agonist (smoothened agonist (SAG), Merck). After 1 week treated with small molecule inhibitors cells were expanded using N2B27 media plus 20 ng/mL FGF (Miltenyi Biotec) for 1 week. Neural fated colonies were identified by the presence of rosette structures (Figure 7.1C and D). These rosettes were cut away from other non-differentiated or inappropriately differentiated cells and into pieces using a 21-gauge needle (Figure 7.1E). These pieces were pated into one well of 96-well U-bottomed plate in Neurobasal Media (NBM, Neurobasal Medium, 1X N-2 supplement, 1X B-27 supplement, 1X ITS-A, 2 mM L-Glutamine/ Glutamax, 50 units/mL Penicillin/ Streptomycin). The NBM media included 20 ng/mL FGF and EGF (PeproTech) for culture of neurospheres (Figure 7.1F). After 2 weeks Neurospheres were dissociated manually by pipetting then plated onto 10 µg/mL Poly-D-Lysine (Sigma-Aldrich®) plus Laminin substrates and neurons matured for 2 weeks in NBM (Figure 7.1G and H).
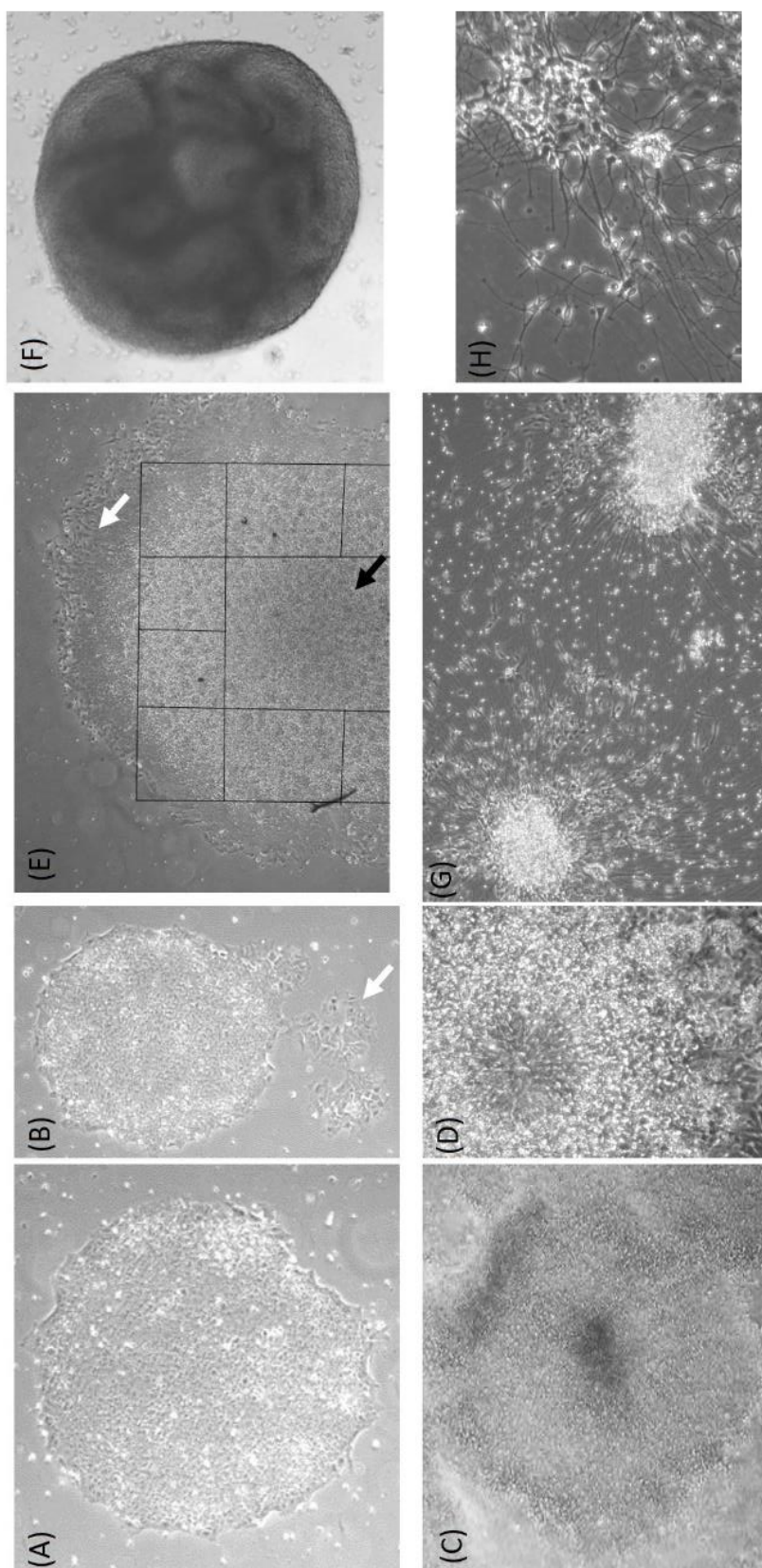
Figure 7.1 Brightfield images of the *in vitro* neural induction pathway

(**A**) Stem cell colonies grow as uniform cells in rounded colonies with defined borders. (**B**) Broken borders of stem cell colonies demonstrate cell differentiation (white arrow). The health and level of spontaneous differentiation was monitored regularly for the ESC colonies in culture. (**C**) After induction of stem cell colonies towards neural lineages cells self-organised into rosette structures. (**D**) Zoomed in image to demonstrate the rosette structures. (**E**) After two weeks in culture the neural differentiating cells were cut from the stem cells in the centre of the colony (black arrow) and any inappropriately differentiating cells at the periphery of the colony (white arrow). (**F**) Sheets of neural differentiating cells cut from rosettes were grown in 3D culture as neurospheres. (**G**) Neurospheres were dissociated gently for neuron maturation. (**H**) Zoomed in image demonstrating the neuron morphology of a cell body and neural extensions protruding to form connections with other cells.

7.3 DNA transfection

Transfection of plasmid DNA was carried out using FuGENE® (Promega) according to the manufacturer's protocol. Briefly, a ratio of 1 µg plasmid DNA was mixed with 3 µl FuGENE® in Optimem, vortexed to mix then added to cells at 60% confluency. Cells were left to incubate for 48 hours before further use. Where required expression of plasmids was induced 24 hours after initial transfection using doxycycline (Sigma). The concentration and duration of doxycycline incubation is indicated for each experiment.

7.4 Viral transduction

Stable expression cell lines were generated by transduction with either retrovirus or lentivirus. Retrovirus infection was used to generate the immortalised fibroblast cell lines using human telomerase (*hTERT*, generously supplied by Professor Grant Stewart). Lentivirus was used to generate all other stable expression cell lines.

All HEK-293T transfections were performed with FuGENE® as described above. HEK-293Ts were plated at $5x10^5$cells/well into 6-well plates and 24 hours later transfected with the plasmid of interest making up 50% of the total DNA concentration (i.e. 500 ng for one well of a 6-well plate, vectors described in Section 7.22.1). Control cells, not infected with virus, were also plated with the relevant selection antibiotic to monitor cell death and successful infection. Once virus infected recipient fibroblasts had selected, they were expanded for use.

7.4.1 Retroviral transduction

For generation of retroviral particles, HEK-293T cells were transfected with the retroviral vector plus packaging vectors (pCMV-Gag-Pol provided by Professor Grant Stewart, and pMD2.G), each at 25% of the total DNA concentration (i.e. 250 ng for 1 well of a 6-well plate). The following day recipient fibroblasts were plated into 6-well plates. 48 hours after HEK-293T transfection, virus containing media was removed and filtered (0.45 μm pore size). Before adding retrovirus medium to recipient fibroblasts, 4 μg/mL Polybrene (generously supplied by Professor Grant Stewart) was added, to improve transduction efficiency. 24 hours later a second transduction of recipient fibroblasts was carried out. 24 hours after this second transduction, the medium on recipient fibroblasts was changed to include 70 μg/mL Hygromycin selection antibiotic (ThermoFisher Scientific).

7.4.2 Lentiviral transduction

For generation of lentiviral particles, HEK-293T cells were transfected with 35% final concentration of packaging vector psPAX2 (i.e. 350 ng for one well of a 6-well plate) and 15% final concentration envelope vector pMD2.G (150 ng for one well of a for a 6-well plate). The following day recipient cells were plated, into 6-well plates, at a suitable density for the cell type to be at 70% confluency. 48 hours post HEK-293T transfection, virus containing medium was removed, filtered (0.45 μm pore size) and lentiviral medium diluted 1:1 in recipient cell culture medium. Lentiviral containing medium was added to recipient cells. 48 hours post transduction recipient cells were selected using 1 μg/mL Puromycin (Invitrogen™).

7.5 Knockdown

7.5.1 shRNA knockdown

Stable expression short hairprin RNA (shRNA) cell lines were generated using lentiviral transduction as detailed in Section 7.4.2 (sequences provided in Table 7.1, vector maps in Figure 7.2). Where appropriate, doxycycline or IPTG was used to induce expression of shRNA plasmids. Knockdown efficiency for all cell lines was determined by harvesting cells for quantitative PCR and/or Western blotting.

Table 7.1 shRNA sequences

shRNA	Sequence (5' to 3')
JMJD7 sh136 (IPTG inducible, Sigma)	CCGGGATCTTGGAATGTGGTCATAACTCGAGTTATGACCACATTC CAAGATCTTTTTG
JMJD7 sh501 (IPTG inducible, Sigma)	CCGGGGGCTGCATCGCAGTGAATTTCTCGAGAAATTCACTGCGAT GCAGCCCTTTTTG
JMJD7 sh1 (transOMIC)	GGCAACCTACCAGCTAACTGA
JMJD7 sh2 (transOMIC)	CGCCGGCAACCTACCAGCTAA
JMJD7 sh3 (transOMIC)	GCGGGCCGGTGAGATGCTCTA
JMJD5 sh906 (Sigma)	CCGGGCATCAGAAAGCCGAATGTTTCTCGAGAAACATTCGGCTTT CTGATGCTTTTTTG
JMJD5 sh971 (Sigma)	CCGGCCTGTTCATCCCGGTGAAATACTCGAGTATTTCACCGGGAT GAACAGGTTTTTTG
JMJD5 sh110 (Dharmacon)	TAGTGAACAGATGAATGCT
JMJD5 sh111 (Dharmacon)	TACAGAAAGCATAGAGCCT
JMJD5 sh793 (Dharmacon)	TTTTCTAACTTCACATCTG
JMJD5 sh794 (Dharmacon)	TTTTTCTAACTTCACATCT
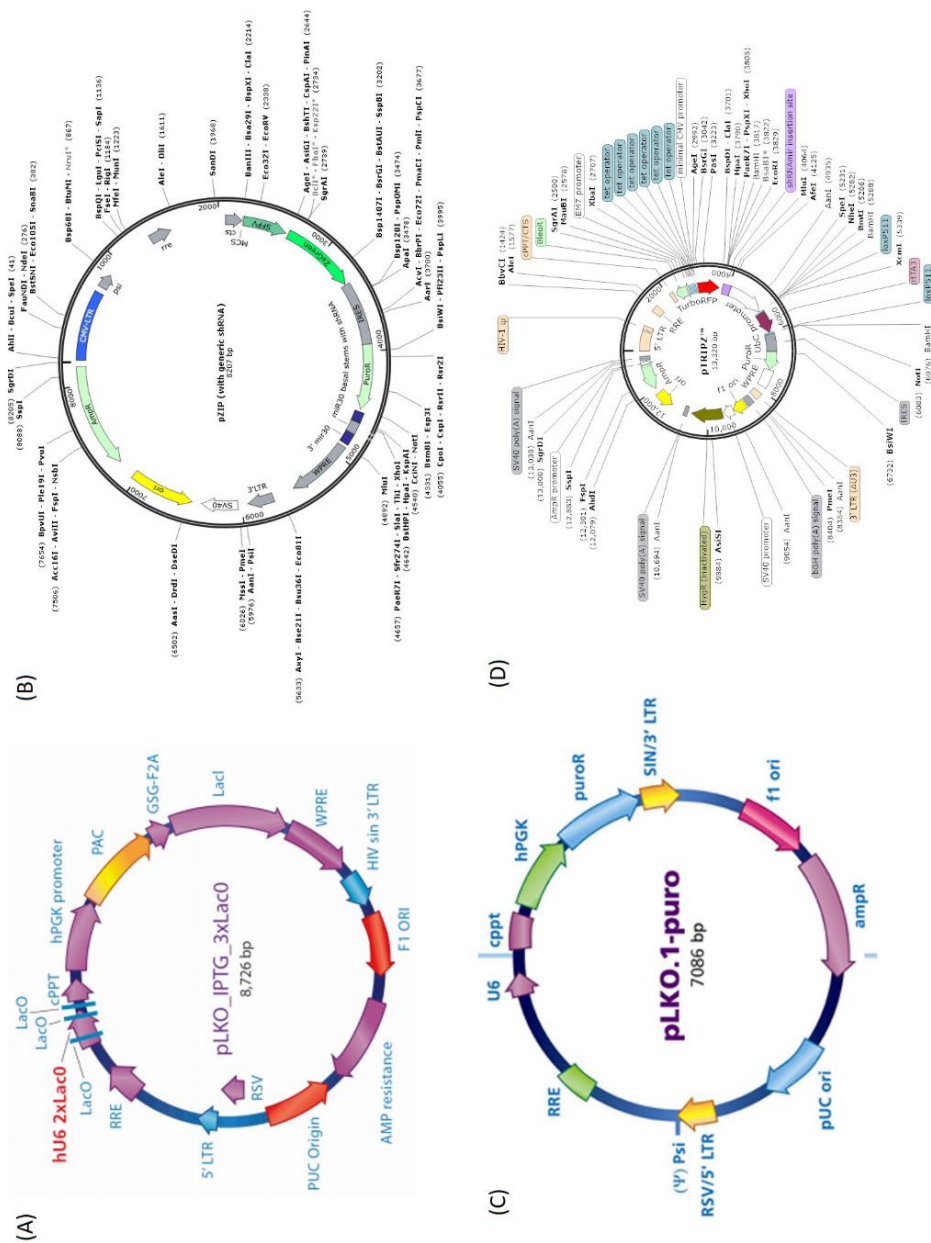
Figure 7.2 shRNA vector maps

(A) Vector map used for IPTG inducible JMJD7 shRNA. Vector is pLKO (Sigma), figure from Sigma-Aldrich®. (B) Vector map used for doxycycline inducible JMJD7 shRNA. Vector is shERWOOD-UltramiR (transOMIC). Figure from transOMIC technologies™. (C) Vector map used for the constitutive JMJD5 shRNA sequences. Vector is pLKO.1 (Sigma), figure from Sigma-Aldrich®. (D) Vector map for Dharmacon JMJD5 shRNA vector (derived from pTRIPZ™). Figure from SnapGene™.

7.5.2 siRNA transfection

Small interfering RNA (siRNA) transfection was performed using Oligofectamine™ (Invitrogen™), according to the manufacturer's protocol. siRNA was transiently transfected twice over two consecutive days, at a final concentration of 50 nM. A non-targeting control (MISSION® siRNA Universal Negative control #1) and a positive control siRNA for eRF1 (MISSION® siRNA) were used where applicable (sequences provided in Table 7.2). Knockdown efficiency was determined by harvesting cells for quantitative PCR and Western blotting.

Table 7.2 siRNA sequences

siRNA	Sequence (5' to 3')
JMJD7 (Dharmacon)	#6 sequence unknown
	#8 sequence unknown
	#15 sequence unknown
JMJD5 (SMARTpool)	Sigma-Aldrich® 82891: CTGACATGCAGACAGCATT
	Sigma-Aldrich® 82890: GTCAACGAGTTCATCAGCA
	Sigma-Aldrich® 82888: CCCTCATGACGGTCAACGA
	Sigma-Aldrich® 82889: GACAGCATTCATCTGTTCA

Optimisation of JMJD7 siRNA transfection was performed using 20 nM BLOCK-iT™ 555 nm Alexa Fluor® labelled RNA (ThermoFischer Scientific) transfected with INTERFERin® (Polyplus), Lipofectamine™ 3000 (ThermoFisher Scientific), RNAiMax (ThermoFisher Scientific), Oliofectamine™ or DharmaFECT (Dharmacon), all according to the manufacturer's protocols.

7.6 Cell proliferation and viability assays

7.6.1 MTS assay

Cell proliferation/viability was measured using the MTS assay (CellTiter 96® Aqueous One Solution Cell Proliferation Assay, Promega). Cell treatments were performed prior to seeding cells into a 96-well plate (cancer cell lines at 1000 cells/well or 2000 cells/well for SHSY5Y cells or patient fibroblasts). Cell growth was monitored every 24 hours for a minimum of five days.

CellTiter 96 Aqueous MTS reagent (Promega) and Phenazine methosulfate (PMS, Sigma-Aldrich®) were dissolved in 1X PBS according to the manufacturer's protocol. MTS working reagent was made by combining 1 mL MTS with 50 µl PMS. Cell growth/viability was monitored by incubating 20 µl MTS working reagent in each well for 1 hour at 37˚C 5% CO_2, protected from light, then absorbance measured at 490 nm using an EnSpire™ Multimode plate reader (Perkin Elmer).

7.6.2 Manual counting proliferation assay

The cellular proliferation of patient fibroblasts was monitored by manual counting. Cells were plated into 6-well plates at 0.5 $x10^5$ cells/well then cell counts were made every day for six days using a haemocytometer. To do this, cells were harvested by trypsinisation into a final volume of 200 µl and a 10 µl sample of this loaded into the haemocytometer for counting. Wells were counted in duplicate and an average cell count made using all four 0.25 x 0.25 mm gridded areas of the haemocytometer.

7.6.3 Colony formation assay

Colony formation of fibroblasts and rescue fibroblast cell lines was performed using a limited dilution assay. Cells were harvested by trypsinisation, counted and diluted to 1x10^5 cells/mL. Cells were serial diluted and 10^4 cells plated into 10cm plates. 2 weeks after seeding for parental fibroblasts or rescue fibroblasts, colonies were washed in 1X PBS, then fixed and stained using 0.1% crystal violet (Fluka) in 50% methanol. Colony formation was calculated by determining total colony numbers relative to original cell number plated.

7.6.4   Senescence assay

Senescence of the primary patient fibroblast cell line MR10 was monitored using Senescence β-Galactosidase Staining kit (Cell Signalling Technology), according to the manufacturer's recommendations. Wildtype patient fibroblasts (MR98) were used as negative and positive controls for the assay. The negative control remained untreated and left to grow confluent. Positive controls for senescence were induced by two methods; (1) treatment with 4% ethanol for 2 hours repeated for three days, or (2) treatment with 12.5 µM etoposide (Sigma-Aldrich®) for 24 hours. After treatment, both positive control conditions were left to recover for five days before performing the senescence assay. Control and MR10 cells were monitored for β-Galactosidase activity, at pH 6 against the substrate X-gal, by the presence of blue product using an EVOS microscope. The principle being that senescent cells have increased numbers of lysosomes and therefore activity of the β-galactosidase enzyme is found at the higher that usual pH 6.

7.7 Flow cytometry

Patient fibroblasts were grown to 70% confluency, harvested by trypsinisation, fixed in ice-cold 70% ethanol before treating with 100 µg/mL RNase A (Thermo). Cells were stained with 20 µg/mL propidium iodide (PI, Sigma) then run on a CyanB flow cytometry machine (Beckman Coulter) before cell cycle analysis was performed using Summit v4.3 software (Beckman Coulter). Firstly, viable cells were gated using forward and side scatter. Secondly, PI staining was used to determine cell cycle stage which was measured at 695 nm. This was then expressed as a percentage of total cells analysed.

7.8 Whole cell extracts

To prepare whole cell extracts, cells were lysed using JIES (100 mM NaCl, 20 mM Tris-HCl pH 7.4, 5 mM $MgCl_2$, 0.5% v/v NP-40), or RIPA (150 mM NaCl, 25 mM Tris pH 8, 1% v/v NP40, 0.5% v/v Sodium deoxycholate, 0.1% v/v SDS) supplemented with 1X SIGMAFAST protease inhibitor cocktail (PIC, Sigma-Aldrich®). Cells were washed in 1X PBS and scraped, followed by centrifugation at 1500 rpm for 5 minutes (34 cm rotor). Cell pellets were lysed on ice, in a suitable volume of JIES or RIPA for the cell type and pellet size. Cells lysed with RIPA were sonicated (5 μm Amplitude) twice for 20 seconds, incubating on ice between each round of sonication. All cell lysates were centrifuged at 14000 rpm for 10 minutes at 4˚C (16 cm rotor) and supernatant collected. All protein samples were quantified, equalised and prepared for Western blot in 1X sample buffer (Laemmli buffer: 125 mM Tris pH 6.8, 6% w/v SDS, 50% v/v glycerol, 225 mM DTT, 0.1% w/v bromphenol blue).

7.9 Sub-cellular fractionation

Cells were separated into cytoplasm, nucleoplasm and chromatin fractions using a combination of two lysis buffers, both supplemented with 1X SIGMAFAST protease inhibitor. Cells were washed with 1X PBS, collected by scraping into 1X PBS, then pelleted by centrifugation at 1500 rpm for 5 minutes (34 cm rotor). Cell pellets were lysed in Buffer I (10 mM Hepes pH7.9, 100 mM KCl, 1.5 mM $MgCl_2$, 0.34 M sucrose, 10% glycerol, 1 mM DTT). Lysates were mixed by pipette and incubated on ice for 5 minutes before centrifugation at 3500 rpm (16 cm rotor) for 5 minutes. This supernatant was collected, centrifuged at 13000 rpm (16 cm rotor) for 15 minutes and the resulting supernatant used as the cytoplasm fraction. The previous pellet was resuspended in Buffer II (3 mM EDTA, 1 mM DTT) and

incubated mixing at full speed on a Thermomix at 4˚C for 15 minutes before centrifugation at 4000 rpm (16 cm rotor) for 5 minutes. Supernatant was collected as the nucleoplasm fraction. The previous pellet was resuspended in Buffer I, sonicated (5 μm Amplitude) and centrifuged at 13000 rpm (16 cm rotor) for 5 minutes. The supernatant was collected as the chromatin fraction. All protein samples were quantified, equalised across the different cellular fractions and prepared for Western blot in 20% glycerol (v/v) and sample buffer (1X).

7.10   Protein stability assays

Protein stability was monitored using MG132 and cycloheximide assays. Epitope-tagged protein over-expression was induced from stable expression cell lines 24 hours after seeding in 10 cm plates using 1 μg/mL doxycycline for 16 hours. Following this, cells were treated with 50 μg/mL cycloheximide (Sigma-Aldrich®) and samples taken after 0, 2, 4, 8 and 10 hours. Alternatively, cells were treated with 10 μM MG132 (BioVision) and samples taken after 0, 6 or 8 hours. Samples were quantified, equalised and prepared for Western blot in sample buffer (1X).

7.11   Immunoprecipitation

Whole cell extracts were collected from 10 or 15 cm plates in a suitable volume of JIES or RIPA supplemented with 1X protease inhibitor cocktail, as above. An input sample was taken in 1X sample buffer. The remainder of the supernatant was incubated mixing with immunoprecipitation beads at 4 ˚C in 15 cm tubes; bead types and immunoprecipitation times are indicated for each experiment in the sub-sections below.

Once immunoprecipitation incubations were complete, beads were washed repeatedly with lysis buffer as follows. Agarose beads were collected by centrifugation at 800 rpm for one

minute (16 cm rotor), whilst magnetic beads were collected using a MagnaRack (Invitrogen™). Beads were then washed with 1 mL fresh JIES + 1X PIC, vortexed to mix and beads collected as above. These wash steps were repeated a total of six times before collecting beads a final time and removing residual supernatant. Proteins were eluted from beads by adding 2X sample buffer to the beads and boiling on a heat block at 100 ˚C for 5 minutes. For peptide elution, TBS (20 mM Tris pH 8, 100 mM NaCl) plus 100 µg/mL HA, V5 (ThermoFisher Scientific) or FLAG (Sigma-Aldrich®) peptide was added to the beads and incubated for 20 minutes at 20 ˚C mixing at full speed on a ThermoMix. Where appropriate the eluate was removed from the beads before preparing samples for Western blotting in sample buffer (1X). Alternatively, immunoprecipitates were analysed by mass spectrometry (Section 7.12).

7.11.1 Enzyme-substrate interaction assay

To investigate enzyme-substrate interactions, cells were treated with 1 mM DMOG (Cayman Chemical) 16 hours prior to harvesting, and 1 mM NOG (Cayman Chemical) added to the lysis buffer and wash steps in order to maintain the enzyme-substrate complex. These supernatants were incubated with anti-FLAG magnetic agarose beads, anti-HA agarose beads or anti-V5 agarose beads (Sigma-Aldrich®) for 16 hours.

7.11.2 IVTT or peptide competition assay

For IVTT or peptide competition assays, whole cell extract samples were left to immunoprecipitate for 6 hours in order to purify tagged-JMJD5 enzyme before mixing with IVTT reaction products or peptide (0.1 or 1 mg/mL) and leaving to incubate overnight rotating at 4 ˚C. Peptides included MCM3 NLS ([658]LEKEKKRKKRSEDE[671]) or RPS6 ([129]VPRRLGPKRASRIRKL[144]).

7.11.3 Purification of endogenous protein

Purification of endogenous MCM proteins was carried out by first preparing a whole cell lysate sample, as follows. Cells lysed in JIES were sonicated (5 μm Amplitude) twice for 20 seconds and treated with 100 units/mL Benzonase®(Sigma) for 1 hour at 4°C with mixing. Protein samples were centrifuged (Section 7.8) before mixing 3.5 mg of protein with 10 μg antibody (Table 7.3) and 30 μl Protein A agarose beads (Millipore). Immunoprecipitation took place at 4°C for 16 hours with mixing.

Table 7.3 Antibodies for endogenous immunoprecipitation

Target	Antibody
FIH	Sanata Cruz, sc-48813
MCM2	Bethyl, A300-191A
MCM5	Bethyl, A300-195A
MCM5	Sanat Cruz, sc-22780
MCM3	Cell Signalling, 4012S
MCM3	Bethyl, A300-192A
MCM3	Genetex #1 (GTX110241) and #2 (GTX111102)

7.12   Mass Spectrometry

Immunoprecipitates, generated in Section 7.11, for mass spectrometry analysis were submitted to the Advanced Mass Spectrometry Facility (Target Discovery Institute, University of Oxford). Briefly, proteins were purified from eluants by methanol/chloroform extraction and digested with the indicated proteases prior to peptide purification and MSMS sequencing analyses on an Orbitrap Fusion Lumos (ThermoFisher). Data was processed by PEAKS 8.5 software (Bioinformatics Solutions Inc) and searched for fixed modifications (carbamidomethyl (cysteine)) and variable modifications (including DKNPR hydroxylation and methionine oxidation). Analysis of potential hydroxylation was undertaken with the assistance of Dr Mathew Coleman using PEAKS software.

7.13   Protein quantification assay

The concentration of protein extracts was determined using the Pierce protein assay reagent (ThermoFisher Scientific), according to the manufacturer's recommendations, by measuring optical density at 660 nm on a EnSpire™ Multimode plate reader (Perkin Elmer). BSA (Sigma-Aldrich®) of known dilutions was used as a protein standard.

7.14   Western blotting

Protein samples prepared in sample buffer (1X) were boiled for 5 minutes at 100 ˚C then separated on a 12% polyacrylamide gel, made in-house, or Criterion TGX pre-cast gels (BioRad Laboratories) at 150 V in a Tris/ glycine/ SDS Running Buffer (Geneflow). For coomassie staining gels were washed in water and incubated rocking in InstantBlue™ (Sigma-Aldrich®) before washing again in water and imaged using a Vilber Lourmat Fusion Fx imager. Western blotting required the transfer of gels onto 0.45 µm methanol activated PVDF membrane (GE Healthcare). This was performed at 320 mA for 25 minutes per gel in a Tris/glycine Transfer Buffer (Geneflow) plus 40% methanol. Membranes were blocked in PBST-M (5% milk powder, 1X PBS-T, 0.1 % Tween-20) for 1 hour rocking at room temperature then incubated in primary antibody (Table 7.4) for 1 hour mixing at room temperature or overnight at 4 ˚C. After incubation, membranes were washed 3 times in PBS-T (1X PBS, 0.1 % Tween-20) shaking for 15 minutes at room temperature before incubating for 1 hour at room temperature in HRP-labelled secondary antibody diluted in PBST-M (Table 7.4). Membranes were washed as before then imaged using a Fusion FX Vilber Imager. Visualisation of bands was performed using 1:1 dilution of Clarity (BioRad) or Femto ECL (BioRad). Densitometric quantification of bands was performed using Fusion FX Vilber software.

Table 7.4 Primary and secondary antibodies for Western blotting

Target	Antibody
β-Actin	HRP-tagged, Abcam AB49900
JMJD5	Collaborators Matsuura Yoshiharu Lab, Japan
JMJD7	Novus, St John's Laboratory
HA	HRP-tagged Sigma-Aldrich®, (12013819001)
FLAG	HRP-tagged Sigma-Aldrich®, A8592
P53	Calbiochem, OP43
α-Goat-HRP	DAKO, P0449
α-Rabbit-HRP	Cell Signalling Technology 7074S
α-Mouse-HRP	Cell Signalling Technology 7076S
RCCD1	Santa Cruz Biotechnology sc240810
Histone 3	Abcam AB1791
H3K36me2	Abcam AB9049
eRF1	SantaCruz (365686)
DRG1	Protein Tech (13190-1)
DRG2	Protein Tech (14743-1)
DFRP1	Sigma-Aldrich® (HP031099)
DFRP2	GeneTex (GTX120331)
MCM2	Bethyl Laboratories A300-191A
MCM3	Bethyl Laboratories A300-192A
MCM4	GeneTex GTX109740
MCM5	Bethyl Laboratories A300-195A
MCM6	GeneTex GTX129216
MCM7	Cell Signalling Technology 3735S
RPS6	Cell Signalling Technology 2217
V5	BioRad MCA1360P

7.15   RNA purification

Cell pellets were collected by scraping cells into 1X PBS followed by centrifugation at 1500 rpm for 5 minutes (34 cm rotor). Fibroblast and cancer cell line pellets were lysed and RNA purified using the GenElute™ Mammalian Total RNA Miniprep kit, following the manufacturer's protocol. Neural RNA was purified and eluted using PureLink™ RNA Kit (ThermoFisher Scientific) according to the manufacturer's protocol. Nanodrop was used to determine the concentration and purity of RNA (determined by 260/ 280 values). Samples stored at -80 ˚C.

7.16   cDNA synthesis

cDNA was generated from RNA, diluted to 1 µg/mL in a 10 µl volume, using the High Capacity

cDNA reverse transcription kit (Applied Biosystems) according to the manufacturer's protocol

for fibroblasts and cancer cell lines. Neuron cDNA was generated using Sensifast cDNA

Synthesis Kit (Bioline) according to manufacturer's protocol. All cDNA samples stored at -80˚C.

7.17   Quantitative PCR (qPCR)

qPCR was performed using the PCR Master Mix (Applied Biosystems) according to the

manufacturer's protocol. Transcript abundance was measured using gene-specific TaqMan

probes (ThermoFisher), including an internal loading control (VIC-labelled *ACTB* probe) and a

FAM-labelled probe for the cDNA of interest (Table 7.5). qPCR was performed on an Applied

Biosystems 7500 Real Time PCR System (at 50 ˚C 2 minutes, 95 ˚C 10 minutes, 95 ˚C 15 seconds

repeated forty times then held at 60 ˚C for 1 minute). The comparative 2-ΔΔCt method was

used for quantification of gene expression (Livak and Schmittgen., 2001).

Table 7.5 Primers used for qPCR

qPCR Primer	Sequence (5' to 3')
JMJD7	Hs00979972_g1
JMJD7 read through transcript	Hs00979965_m1
DRG1	Hs02563393_s1
DRG2	Hs00954099_m1
DFRP1	Hs00218440_m1
DFRP2	Hs01086104_g1
JMJD5	Hs00227070_m1
ACTB	4326315E

7.18   Genomic DNA purification

Genomic DNA was purified and eluted from immortalised fibroblast cell pellets using the

Invitrogen™ K1820-01 kit, according to manufacturer's instructions. Samples stored at -80 ˚C.

7.19   Sanger sequencing of endogenous transcripts

PCR reactions were performed using custom primers (Table 7.6) on template cDNA or genomic DNA. PCR products were purified (GenElute™) and prepped for Sanger sequencing (Source Bioscience or Australian Genome Research Facility). PCR products were also analysed by separating samples using a 1% agarose gel made in TBE (Geneflow).

In order to analyse the InMut locus at both alleles, genomic DNA was purified (Section 7.18) and the InMut region PCR amplified, as described above. The PCR products were then cloned using a TOPO cloning method (described by manufacturer, ThermoFisher) and transformed into DH5α competent *E.coli* (NEB). Colonies were then screened by purifying DNA and analysed by Sanger sequencing (Source Bioscience), methods as described in Section 7.23.3.

Table 7.6 Primers for cell line sequencing

Primer	Sequence (5' to 3')
C123Y (cDNA)	Forward: CACATGGCAGGACGTAGACAA
	Reverse: GCCTCTTTCCAGGGAGGTGT
C123Y (gDNA)	Forward: CACATGGCAGGACGTAGACAA
	Reverse: GCCTCTTTCCAGGGAGGTGT
InMut (cDNA)	Forward: TCCAGCATTTCAGGGAGCAG
	Reverse: ATGTCAGGCCCTTTCAGCTC
InMut (gDNA)	Forward: CTGTATTCCCCGCAGGAGTC
	Reverse: CAGGAGACAGGATGCAGGAC
JMJD7 (007 and ASD iPSC lines)	Forward: TGACGCAGCCATGGCGGA
	Reverse: GCGTGCTTGGTGGTGTTCA
JMJD5 (Cancer cell lines)	Forward: CAGCCCAAAGGCGACTCG
	Reverse: CTTGTCTCTATAGATTCC

7.20 DNA fibre assay

Progression of DNA synthesis was monitored with the DNA Fibre Assay using halogenated thymidine analogues CldU and IdU (Sigma-Aldrich®). An IdU solution was equilibrated at 37 ˚C 5% CO_2 for a minimum of 1 hour prior to use. Fibroblasts were plated into 6-well plates at $3x10^5$ cells/well to ensure a confluency that cells would continue proliferation (rescue experiments were plated into the relevant concentrations of doxycycline). The following day cells were incubated with 250 μM CldU for 20 minutes at 37 ˚C before washing with media and incubating with 1 mM Hydroxyurea (Sigma-Aldrich®) for 2 hours at 37 ˚C. Cells were washed in media before incubating with 250 μM pre-equilibrated IdU for 20 minutes at 37 ˚C. Control cells not drug treated were incubated sequentially with each analogue for 20 minutes at 37 ˚C. Following incubation, IdU was washed off using ice-cold 1X PBS and cells were harvested by trypsinisation then collected in 10% FBS in 1X PBS on ice. Cell suspension was diluted to $5x10^5$ cells/mL in 1X PBS. 2 μl of cell suspension was spotted at the top of a microscope slide and left to dry for 4 minutes. 7 μl of spreading buffer (200 mM Tris pH 7.4, 50 mM EDTA, 0.5% SDS) was mixed with the drying cell sample on the microscope slide and incubated for 2 minutes before tilting slides to allow the sample to slowly run down the length of the slide. This was left to dry for 2 minutes before fixing in 3:1 methanol to acetic acid for 10 minutes. Slides were allowed to dry for 10 minutes before storing at 4 ˚C or staining. To stain DNA fibres, microscope slides were washed twice with H_2O, then once with 2.5 M HCl before incubating in HCl for 1 hour 15 minutes to denature the DNA. Slides were washed twice in 1X PBS, twice with blocking solution (1% BSA Fraction V, Roche), 0.1% Tween-20 in 1X PBS) and incubated in blocking solution for 30 minutes. Slides were incubated for 1 hour with primary antibodies Rat α-BrdU (BioRad) and Mouse α-BrdU (Becton Dickinson) diluted in

blocking solution. Primary antibodies were removed and the slides washed three times in 1X

PBS before fixing with 4% paraformaldehyde (PFA, 40% w/v PFA in 1X PBS, pH 6.9) for 10

minutes. Slides were washed three times in 1X PBS and three times in blocking solution before

incubating, for 1.5 hours, with Alexa Fluor® secondary antibody α-Rat 555 nm and α-Mouse

488 nm diluted 1:500 in blocking solution. Following secondary antibody incubation, slides

were washed twice with 1X PBS, three times in blocking solution, and twice again in 1X PBS

before mounting (Sigma-Aldrich®). Fibres were imaged using a fluorescence microscope

(Nikon E600) then analysed using ImageJ to count DNA fibre structures (discussed in Section

5.3.3), the measurement of replication fork asymmetry (discussed in Section 5.3.4), or the

measurement of replication fork speeds (discussed in Section 5.3.5, using equation 7.1).

$$\frac{\left(\frac{total\ fibre\ length\ in\ \mu m}{9.55\ pixels}\right) \times 2.59}{40\ minutes} = Replication\ fork\ speed\ (kb/minute)$$

Equation 7.1 The equation used to determine the speed of DNA replication forks
Total fibre length of ongoing fork structures was measured in pixels using ImageJ. As 1 μm equals 9.55
pixels (for the microscope camera used) this measurement could be converted into total fibre length
(μm). This value was multiplied by 2.59 to convert the total fibre length into kilobases (kb), considering
that 1 μm equals 2.59 kb of DNA (Jackson and Pombo, 1998). This value was divided by 40 minutes, as
the total time cells were incubated with the two thymidine analogues, to determine the total
replication fork speed as kb/minute.

7.21   Immunofluorescence

7.21.1 ESCs and neurons

Confluent stem cell colonies were passaged (Section 7.1.2) and plated onto coverslips coated

with 10 μg/mL Vitronectin substrate (Stem Cell Technologies). Alternatively, 2-week-old

excitatory neurospheres (Section 7.2) were dissociated and plated onto coverslips coated with

10 μg/mL Poly-D-Lysine (Sigma-Aldrich®) and 10 μg/mL Laminin substrate (Invitrogen™).

Neurons were matured on these coverslips for 2 weeks (Section 7.2). Cells were washed three

times with 1X PBS before fixing with 4% PFA for 15 minutes. After washing 3 times in 1X PBS, cells were permeabilised with 0.2% Triton-X-100 for 15 minutes. Cells were washed three times with 1X PBS then blocked for 1 hour in 10% FCS (ThermoFisher Scientific) diluted in 1X PBS before incubating overnight at 4 ˚C with primary antibodies (Table 7.7), diluted in 10% FCS. Cells were washed in 1X PBS as before then incubated for 1 hour at room temperature with secondary antibodies (Table 7.7) diluted 1:1000 in 10% FCS. Cells were washed 3 times with 1X PBS then incubated with 1 µg/mL DAPI (Sigma-Aldrich®) diluted in 1X PBS for 5 minutes at room temperature. Cells were washed in 1X PBS as before then once in H_2O before mounting onto slides using Moviol (Milipore). Immunofluorescence imaging and analysis was done using Zeis microscope and Zen Pro software.

7.21.2 Detection of replication stress markers in patient-derived fibroblasts

Fibroblasts were plated onto coverslips (22 mm x 22 mm, Leica) in 6-well plates, at $3x10^5$ cells/well. For 53BP1 bodies and micronuclei assays cells were treated with +/- 0.5 µM Aphidicolin (Sigma-Aldrich®) for 48 hours (+/- doxycycline for rescue experiments). Subsequently cells were fixed with 4% PFA cells then washed in 1X PBS. For 53BP1 bodies and micronuclei assays cells were then incubated in nuclear extraction buffer (20 mM NaCl, 3 mM MgCl, 300 mM Sucrose, 10 mM PIPES, 0.5% Triton-x-100) on ice for 5 minutes. For all methods cells were washed twice in 1X PBS then permeabilised using 0.1% Triton-x-100 for 10 minutes. Coverslips were then stained for immunofluorescence. Other experiments required alternative methods to fix cells, including methanol or acetone treatment for 10 minutes at -20 ˚C, before washing with 1X PBS and immunofluorescence staining. To stain, cells were washed three times in 1X PBS before blocking in 1% BSA (Sigma-Aldrich®, A7906) in 1X PBS for 1 hour. Coverslips were incubated with primary antibody (Table 7.7), diluted in blocking

solution, for 1 hour at room temperature. Coverslips were washed three times in blocking

solution before incubating with secondary antibody (Table 7.7), diluted 1:1000 in blocking

solution, for 1 hour at room temperature. Coverslips were washed three times in blocking

solution then incubated with DAPI (Invitrogen™) diluted in 1X PBS for 10 minutes at room

temperature. Cells were washed three times in 1X PBS and mounted (ProLong® Gold, Cell

Signalling). 53BP1 bodies were counted in G1 cells (determined by negative CENPF counter

staining) and micronuclei counted using DAPI staining on a Nikon E600 microscope. Images of

immunofluorescence staining were taken using a Leica microscope.

Table 7.7 Primary and secondary antibodies for immunofluorescence

Target	Antibody
JMJD7	Novus, NBP1-91110
DRG1	Proteintech, 13190-1-AP
DRG2	Proteintech, 14743-1-AP
DFRP1	ATLAS, HPA031099
DFRP2	GeneTex, GTX120331
vGlut1	Abcam, 72311
GABA	Sigma-Aldrich®, A2052
MAP2AB	Sigma-Aldrich®, M1406
βIII-Tubulin	Millipore, MAB1637
S100β	Sigma-Aldrich®, S2532
FLAG	Sigma-Aldrich®, F1804
HA	BioLenged, 901501
CENPF	BD Biosciences, 610768
53BP1	Bio-Techne, NB100-904V
MCM3	Bethyl Laboratories, A300-192A
MCM5	Bethyl Laboratories, A300-195A
JMJD5	Abclonal, A11606
	Abcam ab36104
	Abcam, AB28883
	DSHB, PCRP-KDM8-1A2
	Collaborators Matsuura Yoshiharu Lab, Japan
Mouse 555nm	Life technologies, A31570
Mouse 488nm	Life technologies A10684
Rabbit 488nm	Life technologies, A11070
Rabbit 555nm	Life technologies, A21430

7.22   *In vitro* assays

7.22.1 Generation of GST tagged JMJD5

Methods described below were performed by Dr Mathew Coleman. Human *JMJD5* cDNA sequence was cloned into pGEX-4T-1 (Amersham), as described below (Section 7.22). pGEX-4T-1 JMJD5 was transformed into BL21(DE3) competent cells (Promega). Overnight cultures were grown in 2X Luria-Bertani (LB) broth plus 50 μg/mL ampicillin and then back diluted 1:100 in 1 L of room temperature 2X LB plus 50 μg/mL ampicillin. Cultures were incubated at 37 ˚C and 200 rpm until reaching an absorbance of OD_{600nm} of 0.6. Cultures were then chilled to 18 ˚C before inducing protein expression with 0.5 mM IPTG for 16 hours. Cultures were spun at 6000g for 10 minutes to pellet bacteria. Pellets were resuspended in 100 mL of lysis buffer (50 mM Tris pH 8.0, 300 mM NaCl, 0.5 mM TCEP (tris(2-carboxyethyl)phosphine) reducing agent (Sigma), 1X PIC, 20 U/ml TurboNuclease (Sigma), 0.5 mg/ml lysozyme (Sigma) and 0.1% v/v Triton-X-100) and allowed to rotate for 1 hour at 4 ˚C. Samples were centrifuged at 18000 rpm (34cm rotor) for 15 minutes at 4 ˚C. Supernatants were incubated with 1 mL Glutathione Sepharose beads (GST, GE Healthcare) at 4 ˚C overnight with mixing. Beads were washed 6 times with 10 mL wash buffer (50 mM Tris pH 8.0, 300 mM NaCl, 0.5 mM TCEP, and 0.1% v/v Triton-X-100) before eluting GST-tagged JMJD5 with 10 mM glutathione (Sigma), 50 mM Tris pH 8.0, 300 mM NaCl, and 0.5 mM TCEP. Three sequential 1 mL elutions were performed at room temperature for 10 minutes with rotation. Samples were analysed by SDS-PAGE and Coomassie staining before combining relevant fractions and dialysing in a 7K molecular weight cut off Slide-A-Lyzer dialysis cassette (Pierce) against 50 mM Tris pH 8.0, 300 mM NaCl, and 0.5 mM TCEP overnight at 4 ˚C with mixing. Dialysed samples were concentrated to 2 mg/mL

using a 6 mL protein concentrator fitted with a 10K molecular weight cut off polyethersulfone membrane (Pierce).

7.22.2 *In vitro* interaction assay

Glutathione Sepharose beads (GST) beads were pre-blocked with 5% BSA (Sigma-Aldrich®) for 2 hours rotating at 4 ˚C. Blocked beads were washed in JIES buffer and incubated with HEK-293T whole cell lysate (lysed in JIES) and either 6 μg GST, GST-tagged JMJD5 wildtype or GST-tagged C123Y (Section 7.21.1) for 2 hours rotating at 4 ˚C. Beads were washed 6 times in JIES before boiling in 2X Laemlli buffer for 5 minutes. Samples were analysed by Western blotting and Coomassie staining.

7.22.3 *In vitro* hydroxylation reaction

RPS6 peptide (^{129}VPRRLGPKRASRIRKL^{144}) was solubilised to 400 μM in substrate buffer (50 mM Tris-HCl pH 7.5, 150 mM NaCl, 1 mM DTT). Stock $(NH_4)_2Fe(SO_4)_2$ was prepared in 20 mM HCl to a concentration of 500 mM and then diluted to 10 mM with MilliQ water prior to use. A 2X master mix of buffers and co-factors was prepared as follows; 50 mM HEPES pH 7.5, 200 μM Fe(II), 1 mM ascorbate, and 400 μM 2-oxoglutarate. Reactions consisted of 10 μL 2X co-factor mix plus 5 μL control buffer (50 mM Tris pH 8.0, 300 mM NaCl, and 0.5 mM TCEP), 5 μL GST-tagged 2 mg/mL wildtype or C123Y JMJD5, and 5 μL of substrate buffer or RPS6 peptide (total volume 20 μl). The reaction was mixed at 1000 rpm and 37 ˚C for 15 seconds before incubating at 37 ˚C for 2 hours. Reaction sample was diluted 1:10 in H_2O before analysis using the *in vitro* hydroxylation assay.

7.22.4 *In vitro* hydroxylation assay

The following protocol was used for the Succinate-Glo™ JmjC demethylase/ hydroxylase Assay (Promega). 5 µL of diluted hydroxylation reaction plus 5 µL of Succinate-Glo™ detection reagent I was placed into one well of a white walled clear bottom 384-well plate, in triplicate. The plate was sealed with parafilm before mixing on a thermomix at 1000 rpm for 15 seconds and incubating at room temperature for 1 hour. 10 µL Succinate-Glo™ detection reagent II was then added to the wells before re-sealing and mixing the plate as before, with subsequent incubation at room temperature for 10 minutes. Reactions were analysed for luminescence using a PerkinElmer Enspire plate reader. Presence of a luminescent signal was an indirect indication of a successful hydroxylation reaction, as succinate was processed by enzymes in the kit to generate a luminescent signal.

7.23   Molecular biology

7.23.1 Vectors and plasmids

Five vectors and their derivatives were used in this thesis. These included modified forms of the Dharmacon lentiviral vectors pTRIPZ[TM] (Figure 7.3A), termed 'pTIPZ' (the pTRIPZ™ vector minus the RFP gene, a gift from Dr Tencho Tenev, Institute of Cancer Research, London) and 'pIPZ' (the pTIPZ vector minus the RFP gene and doxycycline inducible promoter). The remaining vectors were pGEX-4T-1 (Figure 7.3B), pcDNA3 (Figure 7.3C) and pEF6 (generous gift from Prof Richard Marais).
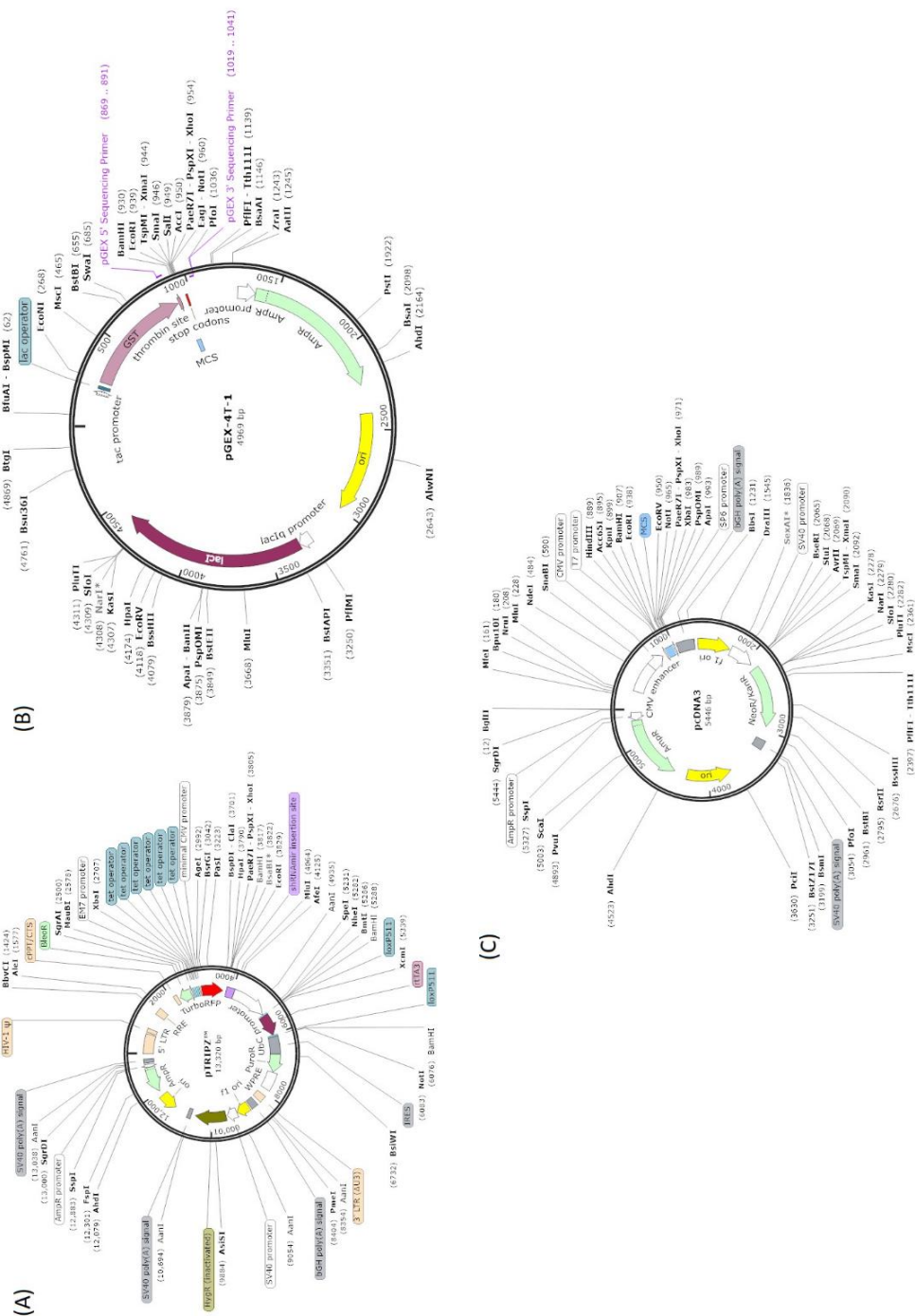
Figure 7.3 Cloning plasmid maps

(A) Vector map for Dharmacon™ pTRIPZ™ vector. In place of the shRNA sequences we cloned our sequences of interest. The pTIPZ derivative was minus the RFP gene, and the pIPZ derivative was minus both the RFP gene and doxycycline inducible promoter. (B) Vector map for pGEX-4T-1. (C) Vector map for pcDNA3. All vector maps generated by SnapGene®.

7.23.2 Cloning protocol

A PCR was carried out using the protocol supplied by Phusion High Fidelity DNA Polymerase (NEB) and custom primers (Table 7.8). PCR templates were either cDNA purified from HeLa cells or plasmid DNA from previously cloned constructs.

Table 7.8 Cloning primers

Primer	Sequence (5' to 3')
MCM3-HA	Forward:GTCATTAAGCTTATGGATTACCCATACGATGT TCCAGATTACGCTGCGGGTACCGTGGTGCTG
	Reverse: AATGACCTCGAGTCAGATGAGGAAGATGAT
MCM5-V5	Forward:GTCATTAAGCTTATGGGTAAGCCTATCCCTA ACCCTCTCCTCGGTCTCGATTCTACGTCGGGATTCGACGATCCT
	Reverse: AATGACGCGGCCGCTCACTTGAGGCGGTAGAG
MCM3 N-terminal domain	Forward: GTCATTAAGCTTATGGATTACCCATACGATGTTCC
	Reverse: AATGACCTCGAGAAGGACATGGTCTGAGATC
MCM5 R731*	Forward:GTCATTAAGCTTATGGGTAAGCCTATCCCTAACC CTCTCCTCGGTCTCGATTCTACGTCGGGATTCGACGATCCT
	Reverse: AATGACGCGGCCGCTCACTTGCGCTGCATGCG
MCM5 R731A	Forward:GTCATTAAGCTTATGGGTAAGCCTATCCCTAACC CTCTCCTCGGTCTCGATTCTACGTCGGGATTCGACGATCCT
	Reverse: AATGACGCGGCCGCTCACTTGAGGGCGTAGAG
MCM5 MCM domain	Forward:GTCATTAAGCTTATGGGTAAGCCTATCCCTAACCCT CTCCTCGGTCTCGATTCTACGGTCTATGAGGTCATCTCC
	Reverse: AATGACGCGGCCGCGATGACATGCTTGGCCAG
MCM5 C-terminal domain	Forward:GTCATTAAGCTTATGGGTAAGCCTATCCCTAACCCT CTCCTCGGTCTCGATTCTACGGTCTATGAGGTCATCTCC
	Reverse: AATGACGCGGCCGCTCACTTGAGGCGGTAGAG
MCM5 N-terminal domain	Forward:GTCATTAAGCTTATGGGTAAGCCTATCCCTAACCCTC TCCTCGGTCTCGATTCTACGTCGGGATTCGACGATCCT
	Reverse: AATGACGCGGCCGCGATGACATGCTTGGCCAG

To generate sticky ends for ligation, PCR products were purified using GenElute™ PCR clean-up kit (Sigma-Aldrich®) and digested, alongside the appropriate vector, using ThermoFisher Scientific FastDigest™ restriction enzymes, according to the manufacturer's instructions (Table 7.9).

Table 7.9 Restriction enzymes used for cloning

Substrate	Restriction enzyme
MCM3 pcDNA3	HindIII and XhoI
MCM5 pcDNA3	HindIII and NotI
InMut PEF6	EcoRI and SalI

Digested inserts and vectors were recovered using a GenElute™ gel purification kit (Sigma-Aldrich®) after electrophoresis on a 1% agarose gel. To prevent self-ligation, digested vectors were treated with calf intestinal phosphatase (BioLabs) for 30 minutes at 37 ˚C before purification using the GenElute™ PCR clean-up kit. Vectors and inserts were ligated together using T4 ligase (NEB) for 10 minutes at room temperature. To improve ligation efficiency, T4 ligase was inactivated at 65 ˚C for 10 minutes. The amount of insert required in each ligation reaction was determined using the equation 7.2.

$$\frac{Mass\ of\ Vector\ (ng) \times Size\ of\ Insert\ (kb)}{Size\ of\ Vector\ (kb)} \times Vector\ (M):Insert\ Ratio$$

Equation 7.2 Equation to determine ligation ratios for cloning

7.23.3 Bacterial transformation

2.5 μL of ligation products were incubated with 25 μL DH5α competent *E.coli* (NEB) on ice for 30 minutes before a heat shock at 42 ˚C for 30 seconds. Samples were mixed with SOC media and incubated for 1 hour shaking at 37 ˚C. Samples were spread onto 50 μg/mL Ampicillin LB Agar plates and incubated at 37 ˚C overnight. Colonies were collected and grown in LB containing 50 μg/mL Ampicillin overnight before purifying DNA according to the manufacturer's protocol for the GenElute™ Plasmid Miniprep. kit Successful cloning was verified by Sanger sequencing (Source BioScience).

7.23.4 Site directed mutagenesis (SDM)

Two SDM protocols were used in this thesis (primers details are provided in Table 7.10). The first SDM method used short overlapping primers and the manufacturer suggested PCR reaction conditions for Phusion® High Fidelity DNA Polymerase (NEB). This method was used to generate HA-MCM3 point mutations and HA-JMJD5 cancer mutations P190L, D323N and P395Q. The second SDM method was based on non-overlapping HPLC purified primers, phosphorylated with T4 polynucleotide kinase, according to the instructions provided with the corresponding kit (ThermoFisher Scientific). PCR reactions were performed according to the manufacturer's protocol for the ThermoFisher Scientific Phusion SDM kit. This SDM method was used for generating the HA-JMJD5 C123Y point mutation. PCR products from both methods were DpnI digested (ThermoFisher Scientific) to remove the PCR template (methylated bacterial DNA), then PCR purified (GenElute™). Samples were transformed into DH5α high competency *E.coli* (NEB) as in Section 7.22.3. Successful mutagenesis was verified by screening plasmid DNA isolated from colonies by Sanger sequencing (Source BioScience).

Table 7.10 SDM primers

Primer	Sequence (5' to 3')
MCM3 701*	Forward: AagActCgcCagCcaGatGccAaaGatGggGatTgaTacGac
	Reverse: tgTgtCacTgaAgtCatAggGgtCgtAtcAatCccCatCttT
MCM3 491*	Forward: TtcAtcAtgCtgGatCagAtgGatCctTagCagGatCggGag
	Reverse: gaCatGgtCtgAgaTctCccGatCctGctAagGatCcaTctG
MCM3 R664C	Forward: GAAGGAGAAGAAATGTAAGAAGCGAAGTGAGGATGAATCAGAG
	Reverse: CACTTCGCTTCTTACATTTCTTCTCCTTCTCCAGAACCTTCTTAAAG
MCM3 R667Q	Forward: AAACGTAAGAAGCAAAGTGAGGATGAATCAGAGACAGAAGATG
	Reverse: GATTCATCCTCACTTTGCTTCTTACGTTTCTTCTCCTTCTCCAG
JMJD5 P190L	Forward: GAAAAAACAGTCCCCCGGCTGCACCGTCTGTCCCTCCAGCAT
	Reverse: AAACTGCTCCCTGAAATGCTGGAGGGACAGACGGTGCAGCCG
JMJD5 D323N	Forward: CCACTACATCAGAATCCCCAGCAAAACTTCCTAGTGCAGGTG
	Reverse: GTTTTGCTGGGGATTCTGATGTAGTGGGGAGATGGTTCCCTG
JMJD5 P395Q	Forward: CTGTCTCCTGGAGAGATCCTGTTCATCCAGGTGAAATACTGG
	Reverse: AGCCCGCACGTAATGCCAGTATTTCAGCTGGATGAACAGGAT
JMJD5 C123Y	Forward: GCGGGTCTATGACATGGGC
	Reverse: AGGGCTGCGGCCACA

7.24   *In vitro* transcription and translation (IVTT)

HA-MCM3 and V5-MCM5 were generated by IVTT by incubating 1 μg MCM3 or MCM5 wildtype or SDM plasmid constructs with Promega TnT® T7 Quick Coupled Transcription/ Translation System mastermix and 20 μM methionine. Samples were incubated at 30 ˚C for 1 hour before analysis by Western blot or use in immunoprecipitation assays (Section 7.11).

7.25 Bioinformatics analysis

7.25.1 Cancer mutations

COSMIC and cBioPortal databases were utilised to identify and compile cancer patient mutations. These databases were searched for 'KDM8' or 'JMJD7' individually, all cancer patient and cancer cell line mutations were compiled, and duplicates removed (datasets as of July 2016). These mutations were then aligned along the human JMJD5 or JMJD7 sequence (Table 7.11).

Table 7.11 Amino acid sequences used for bioinformatic analysis

Protein	Species	Amino Acid Sequence Code (NCBI)
JMJD5	Human	NP_001138820.1
	Zebrafish	A8E534
	Atlantic Salmon	B5XF11
	Xenopus	B2GUS6
	Mouse	Q9CXT6
	Rat	Q497B8
	Bovine	Q1JP61
JMJD7	Human	NP_001108104.1
	Zebrafish	NP_001017615.1
	Atlantic Salmon	XP_014049567.1
	Xenopus	NP_001011279.1
	Mouse	NP_001108109.1
	Rat	NP_001108128.1
	Bovine	NP_001108130.1
HSBP1	Human	NP_001528.1
TYW5		NP_001034782.1
FIH		NP_060372.2
JMJD8		AAI37101.1
JMJD6		NP_001074930.1
JMJD4		NP_075383.2
NO66		NP_078920.2
MINA53		NP_001035998.1

7.25.2 Sequence alignment

Sequence alignment was used to establish conservation (sequences as Table 7.11) using the online multiple sequence alignment tool Clustal Omega.

7.25.3 Mutation analysis

To predict the effect of point mutations on protein structure or function, two online bioinformatic software tools were utilised, SIFT and PolyPhen-2. Both calculate the probability that an amino acid substitution will be tolerated at a specific residue based on sequence conservation. The SIFT score is the probability that a change will be tolerated, whereas, PolyPhen-2 scores the probability that the amino acid substitution will be damaging (Adzhubei et al., 2010, Sim et al., 2012). The major difference in analysis being that SIFT also accounts for changes in amino acid properties.

7.25.4 Human Splice Finder

To predict the effect of the eight-base-pair intron mutation deletion Human Splice Finder (HSF) version 3.1 was utilised. This bioinformatics tool uses 'position weight matrices' and 'maximum entropy principle' algorithms (Desmet et al., 2009) in order to predict splice site motifs within a given DNA sequence. The wildtype and intron deletion mutation sequences analysed are shown in Table 7.12.

Table 7.12 Amino acid sequences analysed by human splice finder

JMJD5	Sequence
Wildtype	GTGATGGGGAGGAAGTACATCCGGCTGTATTCCCCGCAGGAGTCAGGGGCTCTGTACCCTCATGAC ACGCACCTTCTCCATAACACGAGCCAGGTGGGCACTGGGGGTCTGGGGTGACGTTGCAGGTTCTCC CCACTGCCCCTGGAGATGATGACGTCCTTTGCTTTCTTCAGGTTGACGTGGAGAATCCCGACCTGGA AAAGTTCCCCAAGTTTGCCAAGGCCCCATTCCTGTCCTGCATCCTGTCTCCTGGAGAGATCCTGTTCA TCCCGGTGAAATACTGGCATTACGTGCGGGCTCTGGATTTGAGCTTCTCGGTCAGCTTCTGGTGGTC GTAG
InMut	GTGATGGGGAGGAAGTACATCCGGCTGTATTCCCCGCAGGAGTCAGGGGCTCTGTACCCTCATGAC ACGCACCTTCTCCATAACACGAGCCAGGTGGGCACTGGGGTGACGTTGCAGGTTCTCCCCACTGCC CCTGGAGATGATGACGTCCTTTGCTTTCTTCAGGTTGACGTGGAGAATCCCGACCTGGAAAAGTTCC CCAAGTTTGCCAAGGCCCCATTCCTGTCCTGCATCCTGTCTCCTGGAGAGATCCTGTTCATCCCGGTG AAATACTGGCATTACGTGCGGGCTCTGGATTTGAGCTTCTCGGTCAGCTTCTGGTGGTCGTAG

7.25.5 Predicting molecular weight and isoelectric point of proteins

The molecular weight and isoelectric point of wildtype and InMut JMJD5 sequences were analysed using the online software ExPASy. Human wildtype JMJD5 as Table 7.11.

7.25.6 Crystal structure analysis

The crystal structure of JMJD5 PDB: 4GAZ (Wang et al., 2013) and JMJD7 PDB: 5NFN (Markolovic et al., 2018) were visualised and annotated using UCSF Chimera.

7.26   Statistical analysis

Statistics were performed on experiments with at least three independent biological repeats and the statistical test used is indicated for each experiment. Microsoft Excel® was used to perform the 'two-tailed Student's t-test', and Sigmaplot (Systat Software Inc) was used to perform the 'Mann-Whitney U test'. A p-value ≤0.05 (represented by '*'), ≤0.01 (represented by '**'), or ≤0.001 (represented by '***') was considered statistically significant. All histograms include standard deviation, calculated using Microsoft Excel®, and displayed as error bars.

8 References

ABIDI, F. E., MIANO, M. G., MURRAY, J. C. & SCHWARTZ, C. E. 2007. A novel mutation in the PHF8 gene is associated with X-linked mental retardation with cleft lip/cleft palate. *Clinical genetics,* 72, 19-22.

ADAMS, J. 2003. The proteasome: structure, function, and role in the cell. *Cancer Treatment Reviews,* 29, 3-9.

ADEGBOLA, A., GAO, H., SOMMER, S. & BROWNING, M. 2008. A novel mutation in JARID1C/SMCX in a patient with autism spectrum disorder (ASD). *Am J Med Genet A,* 146a, 505-11.

ADZHUBEI, I. A., SCHMIDT, S., PESHKIN, L., RAMENSKY, V. E., GERASIMOVA, A., BORK, P., KONDRASHOV, A. S. & SUNYAEV, S. R. 2010. A method and server for predicting damaging missense mutations. *Nat Methods,* 7, 248-9.

AL-DOSARI, M. S., SHAHEEN, R., COLAK, D. & ALKURAYA, F. S. 2010. Novel CENPJ mutation causes Seckel syndrome. *J Med Genet,* 47, 411-4.

ALAHARI, S., POST, M. & CANIGGIA, I. 2015. Jumonji Domain Containing Protein 6: A Novel Oxygen Sensor in the Human Placenta. *Endocrinology,* 156, 3012-25.

AMENDOLA, P. G., ZAGHET, N., RAMALHO, J. J., VILSTRUP JOHANSEN, J., BOXEM, M. & SALCINI, A. E. 2017. JMJD-5/KDM8 regulates H3K36me2 and is required for late steps of homologous recombination and genome integrity. *PLoS Genet,* 13, e1006632.

AMIRI, A., COPPOLA, G., SCUDERI, S., WU, F., ROYCHOWDHURY, T., LIU, F., POCHAREDDY, S., SHIN, Y., SAFI, A., SONG, L., ZHU, Y., SOUSA, A. M. M., PSYCH, E. C., GERSTEIN, M., CRAWFORD, G. E., SESTAN, N., ABYZOV, A. & VACCARINO, F. M. 2018. Transcriptome and epigenome landscape of human cortical development modeled in organoids. *Science (New York, N.Y.),* 362, eaat6720.

ANDERSON, L., HENDERSON, C. & ADACHI, Y. 2001. Phosphorylation and rapid relocalization of 53BP1 to nuclear foci upon DNA damage. *Mol Cell Biol,* 21, 1719-29.

ANGLANA, M., APIOU, F., BENSIMON, A. & DEBATISSE, M. 2003. Dynamics of DNA replication in mammalian somatic cells: nucleotide pool modulates origin choice and interorigin spacing. *Cell,* 114, 385-94.

ARNOLD, S. J., HUANG, G. J., CHEUNG, A. F., ERA, T., NISHIKAWA, S., BIKOFF, E. K., MOLNAR, Z., ROBERTSON, E. J. & GROSZER, M. 2008. The T-box transcription factor Eomes/Tbr2 regulates neurogenesis in the cortical subventricular zone. *Genes Dev,* 22, 2479-84.

AVINO, T. A. & HUTSLER, J. J. 2010. Abnormal cell patterning at the cortical gray–white matter boundary in autism spectrum disorders. *Brain Research,* 1360, 138-146.

BAGLEY, B. N., KEANE, T. M., MAKLAKOVA, V. I., MARSHALL, J. G., LESTER, R. A., CANCEL, M. M., PAULSEN, A. R., BENDZICK, L. E., BEEN, R. A., KOGAN, S. C., CORMIER, R. T., KENDZIORSKI, C., ADAMS, D. J. & COLLIER, L. S. 2012. A Dominantly Acting Murine Allele of Mcm4 Causes Chromosomal Abnormalities and Promotes Tumorigenesis. *PLOS Genetics,* 8, e1003034.

BAIRD, G., SIMONOFF, E., PICKLES, A., CHANDLER, S., LOUCAS, T., MELDRUM, D. & CHARMAN, T. 2006. Prevalence of disorders of the autism spectrum in a population cohort of children in South Thames: the Special Needs and Autism Project (SNAP). *Lancet,* 368, 210-5.

BAKER, D. E., HARRISON, N. J., MALTBY, E., SMITH, K., MOORE, H. D., SHAW, P. J., HEATH, P. R., HOLDEN, H. & ANDREWS, P. W. 2007. Adaptation to culture of human embryonic stem cells and oncogenesis in vivo. *Nat Biotechnol,* 25, 207-15.

BALASOV, M., AKHMETOVA, K. & CHESNOKOV, I. 2015. Drosophila model of Meier-Gorlin syndrome based on the mutation in a conserved C-Terminal domain of Orc6. *Am J Med Genet A,* 167a, 2533-40.

BALCIUNAS, D. & RONNE, H. 2000. Evidence of domain swapping within the jumonji family of transcription factors. *Trends in Biochemical Sciences,* 25, 274-276.

BALL, H. L., EHRHARDT, M. R., MORDES, D. A., GLICK, G. G., CHAZIN, W. J. & CORTEZ, D. 2007. Function of a conserved checkpoint recruitment domain in ATRIP proteins. *Mol Cell Biol,* 27, 3367-77.

BANKA, S., LEDERER, D., BENOIT, V., JENKINS, E., HOWARD, E., BUNSTONE, S., KERR, B., MCKEE, S., LLOYD, I. C., SHEARS, D., STEWART, H., WHITE, S. M., SAVARIRAYAN, R., MANCINI, G. M., BEYSEN, D., COHN, R. D., GRISART, B., MAYSTADT, I. & DONNAI, D. 2015. Novel KDM6A (UTX) mutations and a clinical and molecular review of the X-linked Kabuki syndrome (KS2). *Clin Genet,* 87, 252-8.

BARANOVSKIY, A. G., BABAYEVA, N. D., SUWA, Y., GU, J., PAVLOV, Y. I. & TAHIROV, T. H. 2014. Structural basis for inhibition of DNA replication by aphidicolin. *Nucleic acids research,* 42, 14013-14021.

BARLOW, J. H., FARYABI, R. B., CALLEN, E., WONG, N., MALHOWSKI, A., CHEN, H. T., GUTIERREZ-CRUZ, G., SUN, H. W., MCKINNON, P., WRIGHT, G., CASELLAS, R., ROBBIANI, D. F., STAUDT, L., FERNANDEZ-CAPETILLO, O. &

NUSSENZWEIG, A. 2013. Identification of early replicating fragile sites that contribute to genome instability. *Cell,* 152, 620-32.

BATIE, M., DRUKER, J., D'IGNAZIO, L. & ROCHA, S. 2017. KDM2 Family Members are Regulated by HIF-1 in Hypoxia. *Cells,* 6.

BECK, H., NÄHSE-KUMPF, V., LARSEN, M. S. Y., O'HANLON, K. A., PATZKE, S., HOLMBERG, C., MEJLVANG, J., GROTH, A., NIELSEN, O., SYLJUÅSEN, R. G. & SØRENSEN, C. S. 2012. Cyclin-dependent kinase suppression by WEE1 kinase protects the genome through control of replication initiation and nucleotide consumption. *Molecular and cellular biology,* 32, 4226-4236.

BENCOKOVA, Z., KAUFMANN, M. R., PIRES, I. M., LECANE, P. S., GIACCIA, A. J. & HAMMOND, E. M. 2009. ATM Activation and Signaling under Hypoxic Conditions. *Molecular and Cellular Biology,* 29, 526.

BENHENDA, S., COUGOT, D., BUENDIA, M. A. & NEUVEUT, C. 2009. Hepatitis B virus X protein molecular functions and its role in virus life cycle and pathogenesis. *Adv Cancer Res,* 103, 75-109.

BERMEJO, R., LAI, M. S. & FOIANI, M. 2012. Preventing replication stress to maintain genome stability: resolving conflicts between replication and transcription. *Mol Cell,* 45, 710-8.

BETTS, M. & RUSSELL, R. 2003. Amino Acid Properties and Consequences of Substitutions.

BI, W., YAN, J., STANKIEWICZ, P., PARK, S. S., WALZ, K., BOERKOEL, C. F., POTOCKI, L., SHAFFER, L. G., DEVRIENDT, K., NOWACZYK, M. J., INOUE, K. & LUPSKI, J. R. 2002. Genes in a refined Smith-Magenis syndrome critical deletion interval on chromosome 17p11.2 and the syntenic region of the mouse. *Genome Res,* 12, 713-28.

BICKNELL, L. S., BONGERS, E. M. H. F., LEITCH, A., BROWN, S., SCHOOTS, J., HARLEY, M. E., AFTIMOS, S., AL-AAMA, J. Y., BOBER, M., BROWN, P. A. J., VAN BOKHOVEN, H., DEAN, J., EDREES, A. Y., FEINGOLD, M., FRYER, A., HOEFSLOOT, L. H., KAU, N., KNOERS, N. V. A. M., MACKENZIE, J., OPITZ, J. M., SARDA, P., ROSS, A., TEMPLE, I. K., TOUTAIN, A., WISE, C. A., WRIGHT, M. & JACKSON, A. P. 2011a. Mutations in the pre-replication complex cause Meier-Gorlin syndrome. *Nature Genetics,* 43, 356-359.

BICKNELL, L. S., WALKER, S., KLINGSEISEN, A., STIFF, T., LEITCH, A., KERZENDORFER, C., MARTIN, C.-A., YEYATI, P., AL SANNA, N., BOBER, M., JOHNSON, D., WISE, C., JACKSON, A. P., O'DRISCOLL, M. & JEGGO, P. A. 2011b. Mutations in ORC1, encoding the largest subunit of the origin recognition complex, cause microcephalic primordial dwarfism resembling Meier-Gorlin syndrome. *Nature Genetics,* 43, 350-355.

BIEDLER, J. L., ROFFLER-TARLOV, S., SCHACHNER, M. & FREEDMAN, L. S. 1978. Multiple neurotransmitter synthesis by human neuroblastoma cell lines and clones. *Cancer Res,* 38, 3751-7.

BOCHMAN, M. L. & SCHWACHA, A. 2009. The Mcm complex: unwinding the mechanism of a replicative helicase. *Microbiology and molecular biology reviews : MMBR,* 73, 652-683.

BOCK, C., KISKINIS, E., VERSTAPPEN, G., GU, H., BOULTING, G., SMITH, Z. D., ZILLER, M., CROFT, G. F., AMOROSO, M. W., OAKLEY, D. H., GNIRKE, A., EGGAN, K. & MEISSNER, A. 2011. Reference Maps of human ES and iPS cell variation enable high-throughput characterization of pluripotent cell lines. *Cell,* 144, 439-52.

BOECKEL, J. N., DERLET, A., GLASER, S. F., LUCZAK, A., LUCAS, T., HEUMULLER, A. W., KRUGER, M., ZEHENDNER, C. M., KALUZA, D., DODDABALLAPUR, A., OHTANI, K., TREGUER, K. & DIMMELER, S. 2016. JMJD8 Regulates Angiogenic Sprouting and Cellular Metabolism by Interacting With Pyruvate Kinase M2 in Endothelial Cells. *Arterioscler Thromb Vasc Biol,* 36, 1425-33.

BOECKEL, J. N., GUARANI, V., KOYANAGI, M., ROEXE, T., LENGELING, A., SCHERMULY, R. T., GELLERT, P., BRAUN, T., ZEIHER, A. & DIMMELER, S. 2011. Jumonji domain-containing protein 6 (Jmjd6) is required for angiogenic sprouting and regulates splicing of VEGF-receptor 1. *Proc Natl Acad Sci U S A,* 108, 3276-81.

BOTTGER, A., ISLAM, M. S., CHOWDHURY, R., SCHOFIELD, C. J. & WOLF, A. 2015. The oxygenase Jmjd6--a case study in conflicting assignments. *Biochem J,* 468, 191-202.

BOWER, N. I. & JOHNSTON, I. A. 2010. Discovery and characterization of nutritionally regulated genes associated with muscle growth in Atlantic salmon. *Physiol Genomics,* 42a, 114-30.

BREWSTER, A. S. & CHEN, X. S. 2010. Insights into the MCM functional mechanism: lessons learned from the archaeal MCM complex. *Critical reviews in biochemistry and molecular biology,* 45, 243-256.

BRIGGS, R. & KING, T. J. 1952. Transplantation of Living Nuclei From Blastula Cells into Enucleated Frogs' Eggs. *Proceedings of the National Academy of Sciences of the United States of America,* 38, 455-463.

BROOKES, E., LAURENT, B., OUNAP, K., CARROLL, R., MOESCHLER, J. B., FIELD, M., SCHWARTZ, C. E., GECZ, J. & SHI, Y. 2015. Mutations in the intellectual disability gene KDM5C reduce protein stability and demethylase activity. *Hum Mol Genet,* 24, 2861-72.

BROOKS-KAYAL, A. 2010. Epilepsy and autism spectrum disorders: Are there common developmental mechanisms? *Brain and Development,* 32, 731-738.

BRYANT, H. E., PETERMANN, E., SCHULTZ, N., JEMTH, A. S., LOSEVA, O., ISSAEVA, N., JOHANSSON, F., FERNANDEZ, S., MCGLYNN, P. & HELLEDAY, T. 2009. PARP is activated at stalled forks to mediate Mre11-dependent replication restart and recombination. *Embo j,* 28**,** 2601-15.

BUNDRED, J. R., HENDRIX, E. & COLEMAN, M. L. 2018. The emerging roles of ribosomal histidyl hydroxylases in cell biology, physiology and disease. *Cell Mol Life Sci,* 75**,** 4093-4105.

BURCHFIELD, J. S., LI, Q., WANG, H. Y. & WANG, R.-F. 2015. JMJD3 as an epigenetic regulator in development and disease. *The international journal of biochemistry & cell biology,* 67**,** 148-157.

BURRAGE, L. C., CHARNG, W.-L., ELDOMERY, M. K., WILLER, J. R., DAVIS, E. E., LUGTENBERG, D., ZHU, W., LEDUC, M. S., AKDEMIR, Z. C., AZAMIAN, M., ZAPATA, G., HERNANDEZ, P. P., SCHOOTS, J., DE MUNNIK, S. A., ROEPMAN, R., PEARRING, J. N., JHANGIANI, S., KATSANIS, N., VISSERS, L. E. L. M., BRUNNER, H. G., BEAUDET, A. L., ROSENFELD, J. A., MUZNY, D. M., GIBBS, R. A., ENG, C. M., XIA, F., LALANI, S. R., LUPSKI, J. R., BONGERS, E. M. H. F. & YANG, Y. 2015. De Novo GMNN Mutations Cause Autosomal-Dominant Primordial Dwarfism Associated with Meier-Gorlin Syndrome. *American journal of human genetics,* 97**,** 904-913.

BURRELL, R. A., MCCLELLAND, S. E., ENDESFELDER, D., GROTH, P., WELLER, M. C., SHAIKH, N., DOMINGO, E., KANU, N., DEWHURST, S. M., GRONROOS, E., CHEW, S. K., ROWAN, A. J., SCHENK, A., SHEFFER, M., HOWELL, M., KSCHISCHO, M., BEHRENS, A., HELLEDAY, T., BARTEK, J., TOMLINSON, I. P. & SWANTON, C. 2013. Replication stress links structural and numerical cancer chromosomal instability. *Nature,* 494**,** 492-496.

BURSTYN, I., WANG, X., YASUI, Y., SITHOLE, F. & ZWAIGENBAUM, L. 2011. Autism spectrum disorders and fetal hypoxia in a population-based cohort: accounting for missing exposures via Estimation-Maximization algorithm. *BMC medical research methodology,* 11**,** 2-2.

BUTLER, M. G., DASOUKI, M. J., ZHOU, X. P., TALEBIZADEH, Z., BROWN, M., TAKAHASHI, T. N., MILES, J. H., WANG, C. H., STRATTON, R., PILARSKI, R. & ENG, C. 2005. Subset of individuals with autism spectrum disorders and extreme macrocephaly associated with germline PTEN tumour suppressor gene mutations. *J Med Genet,* 42**,** 318-21.

BYUN, T. S., PACEK, M., YEE, M. C., WALTER, J. C. & CIMPRICH, K. A. 2005. Functional uncoupling of MCM helicase and DNA polymerase activities activates the ATR-dependent checkpoint. *Genes Dev,* 19**,** 1040-52.

CAMPBELL, K. 2003. Dorsal-ventral patterning in the mammalian telencephalon. *Curr Opin Neurobiol,* 13**,** 50-6.

CAPASSO, H., PALERMO, C., WAN, S., RAO, H., JOHN, U. P., CONNELL, M. J. & WALWORTH, N. C. 2002. Phosphorylation activates Chk1 and is required for checkpoint-mediated cell cycle arrest. *Journal of Cell Science,* 115**,** 4555.

CASCELLA, B. & MIRICA, L. M. 2012. Kinetic Analysis of Iron-Dependent Histone Demethylases: α-Ketoglutarate Substrate Inhibition and Potential Relevance to the Regulation of Histone Demethylation in Cancer Cells. *Biochemistry,* 51**,** 8699-8701.

CAVALLARO, M., MARIANI, J., LANCINI, C., LATORRE, E., CACCIA, R., GULLO, F., VALOTTA, M., DEBIASI, S., SPINARDI, L., RONCHI, A., WANKE, E., BRUNELLI, S., FAVARO, R., OTTOLENGHI, S. & NICOLIS, S. K. 2008. Impaired generation of mature neurons by neural stem cells from hypomorphic Sox2 mutants. *Development,* 135**,** 541.

CHADHA, G. S., GAMBUS, A., GILLESPIE, P. J. & BLOW, J. J. 2016. Xenopus Mcm10 is a CDK-substrate required for replication fork stability. *Cell Cycle,* 15**,** 2183-2195.

CHAHROUR, M., JUNG, S. Y., SHAW, C., ZHOU, X., WONG, S. T. C., QIN, J. & ZOGHBI, H. Y. 2008. MeCP2, a Key Contributor to Neurological Disease, Activates and Represses Transcription. *Science,* 320**,** 1224.

CHAKRABORTY, A. A., LAUKKA, T., MYLLYKOSKI, M., RINGEL, A. E., BOOKER, M. A., TOLSTORUKOV, M. Y., MENG, Y. J., MEIER, S. R., JENNINGS, R. B., CREECH, A. L., HERBERT, Z. T., MCBRAYER, S. K., OLENCHOCK, B. A., JAFFE, J. D., HAIGIS, M. C., BEROUKHIM, R., SIGNORETTI, S., KOIVUNEN, P. & KAELIN, W. G. 2019. Histone demethylase KDM6A directly senses oxygen to control chromatin and cell fate. *Science,* 363**,** 1217.

CHAMPOUX, J. J. 2001. DNA topoisomerases: structure, function, and mechanism. *Annu Rev Biochem,* 70**,** 369-413.

CHAN, K. L., PALMAI-PALLAG, T., YING, S. & HICKSON, I. D. 2009. Replication stress induces sister-chromatid bridging at fragile site loci in mitosis. *Nature Cell Biology,* 11**,** 753-760.

CHATTOPADHYAYA, B., DI CRISTO, G., WU, C. Z., KNOTT, G., KUHLMAN, S., FU, Y., PALMITER, R. D. & HUANG, Z. J. 2007. GAD67-mediated GABA synthesis and signaling regulate inhibitory synaptic innervation in the visual cortex. *Neuron,* 54**,** 889-903.

CHEN, G., GULBRANSON, D. R., HOU, Z., BOLIN, J. M., RUOTTI, V., PROBASCO, M. D., SMUGA-OTTO, K., HOWDEN, S. E., DIOL, N. R., PROPSON, N. E., WAGNER, R., LEE, G. O., ANTOSIEWICZ-BOURGET, J., TENG, J. M. C. &

THOMSON, J. A. 2011a. Chemically defined conditions for human iPSC derivation and culture. *Nature methods,* 8, 424-429.

CHEN, Q., SINHA, K., DENG, J. M., YASUDA, H., KRAHE, R., BEHRINGER, R. R. & DE CROMBRUGGHE, B. 2015a. Mesenchymal Deletion of Histone Demethylase NO66 in Mice Promotes Bone Formation. *J Bone Miner Res,* 30, 1608-17.

CHEN, T., REN, Z., YE, L. C., ZHOU, P. H., XU, J. M., SHI, Q., YAO, L. Q. & ZHONG, Y. S. 2015b. Factor inhibiting HIF1alpha (FIH-1) functions as a tumor suppressor in human colorectal cancer by repressing HIF1alpha pathway. *Cancer Biol Ther,* 16, 244-52.

CHEN, T. J., WANG, H. J., LIU, J. S., CHENG, H. H., HSU, S. C., WU, M. C., LU, C. H., WU, Y. F., WU, J. W., LIU, Y. Y., KUNG, H. J. & WANG, W. C. 2019. Mutations in the PKM2 exon-10 region are associated with reduced allostery and increased nuclear translocation. *Commun Biol,* 2, 105.

CHEN, X., WANG, S., ZHOU, Y., HAN, Y., LI, S., XU, Q., XU, L., ZHU, Z., DENG, Y., YU, L., SONG, L., CHEN, A. P., SONG, J., TAKAHASHI, E., HE, G., HE, L., LI, W. & CHEN, C. D. 2018. Phf8 histone demethylase deficiency causes cognitive impairments through the mTOR pathway. *Nature Communications,* 9, 114.

CHEN, Y., YANG, X., HUANG, Y., LIU, E. & WANG, L. 2011b. Associations of the Single-Nucleotide Polymorphisms of the Mina Gene with the Development of Asthma in Chinese Han Children: A Case–Control Study. *Genetic Testing and Molecular Biomarkers,* 15, 531-536.

CHEN, Z., ZANG, J., WHETSTINE, J., HONG, X., DAVRAZOU, F., KUTATELADZE, T. G., SIMPSON, M., MAO, Q., PAN, C.-H., DAI, S., HAGMAN, J., HANSEN, K., SHI, Y. & ZHANG, G. 2006. Structural Insights into Histone Demethylation by JMJD2 Family Members. *Cell,* 125, 691-702.

CHENG, Y., WANG, Y., LI, J., CHANG, I. & WANG, C.-Y. 2017. A novel read-through transcript JMJD7-PLA2G4B regulates head and neck squamous cell carcinoma cell proliferation and survival. *Oncotarget,* 8, 1972-1982.

CHEUNG, Y. T., LAU, W. K., YU, M. S., LAI, C. S., YEUNG, S. C., SO, K. F. & CHANG, R. C. 2009. Effects of all-trans-retinoic acid on human SH-SY5Y neuroblastoma as in vitro model in neurotoxicity research. *Neurotoxicology,* 30, 127-35.

CHIN, M. H., MASON, M. J., XIE, W., VOLINIA, S., SINGER, M., PETERSON, C., AMBARTSUMYAN, G., AIMIUWU, O., RICHTER, L., ZHANG, J., KHVOROSTOV, I., OTT, V., GRUNSTEIN, M., LAVON, N., BENVENISTY, N., CROCE, C. M., CLARK, A. T., BAXTER, T., PYLE, A. D., TEITELL, M. A., PELEGRINI, M., PLATH, K. & LOWRY, W. E. 2009. Induced pluripotent stem cells and embryonic stem cells are distinguished by gene expression signatures. *Cell Stem Cell,* 5, 111-23.

CHUANG, C. H., WALLACE, M. D., ABRATTE, C., SOUTHARD, T. & SCHIMENTI, J. C. 2010. Incremental genetic perturbations to MCM2-7 expression and subcellular distribution reveal exquisite sensitivity of mice to DNA replication stress. *PLoS Genet,* 6, e1001110.

CHURKO, J. M., LEE, J., AMEEN, M., GU, M., VENKATASUBRAMANIAN, M., DIECKE, S., SALLAM, K., IM, H., WANG, G., GOLD, J. D., SALOMONIS, N., SNYDER, M. P. & WU, J. C. 2017. Transcriptomic and epigenomic differences in human induced pluripotent stem cells generated from six reprogramming methods. *Nature Biomedical Engineering,* 1, 826-837.

CIMPRICH, K. A. & CORTEZ, D. 2008. ATR: an essential regulator of genome integrity. *Nat Rev Mol Cell Biol,* 9, 616-27.

CLIFTON, I. J., MCDONOUGH, M. A., EHRISMANN, D., KERSHAW, N. J., GRANATINO, N. & SCHOFIELD, C. J. 2006. Structural studies on 2-oxoglutarate oxygenases and related double-stranded β-helix fold proteins. *Journal of Inorganic Biochemistry,* 100, 644-669.

CLISSOLD, P. M. & PONTING, C. P. 2001. JmjC: cupin metalloenzyme-like domains in jumonji, hairless and phospholipase A2β. *Trends in Biochemical Sciences,* 26, 7-9.

COCKMAN, M. E., LANCASTER, D. E., STOLZE, I. P., HEWITSON, K. S., MCDONOUGH, M. A., COLEMAN, M. L., COLES, C. H., YU, X., HAY, R. T., LEY, S. C., PUGH, C. W., OLDHAM, N. J., MASSON, N., SCHOFIELD, C. J. & RATCLIFFE, P. J. 2006. Posttranslational hydroxylation of ankyrin repeats in IkappaB proteins by the hypoxia-inducible factor (HIF) asparaginyl hydroxylase, factor inhibiting HIF (FIH). *Proc Natl Acad Sci U S A,* 103, 14767-72.

COCKMAN, M. E., LIPPL, K., TIAN, Y.-M., PEGG, H. B., FIGG, W. D. J., ABBOUD, M. I., HEILIG, R., FISCHER, R., MYLLYHARJU, J., SCHOFIELD, C. J. & RATCLIFFE, P. J. 2019. Lack of activity of recombinant HIF prolyl hydroxylases (PHDs) on reported non-HIF substrates. *eLife,* 8, e46490.

COCKMAN, M. E., WEBB, J. D. & RATCLIFFE, P. J. 2009. FIH-dependent asparaginyl hydroxylation of ankyrin repeat domain-containing proteins. *Ann N Y Acad Sci,* 1177, 9-18.

COFFEY, K., ROGERSON, L., RYAN-MUNDEN, C., ALKHARAIF, D., STOCKLEY, J., HEER, R., SAHADEVAN, K., O'NEILL, D., JONES, D., DARBY, S., STALLER, P., MANTILLA, A., GAUGHAN, L. & ROBSON, C. N. 2013. The lysine demethylase, KDM4B, is a key molecule in androgen receptor signalling and turnover. *Nucleic Acids Res,* 41**,** 4433-46.

COLEMAN, M. L., MCDONOUGH, M. A., HEWITSON, K. S., COLES, C., MECINOVIC, J., EDELMANN, M., COOK, K. M., COCKMAN, M. E., LANCASTER, D. E., KESSLER, B. M., OLDHAM, N. J., RATCLIFFE, P. J. & SCHOFIELD, C. J. 2007. Asparaginyl hydroxylation of the Notch ankyrin repeat domain by factor inhibiting hypoxia-inducible factor. *J Biol Chem,* 282, 24027-38.

COLLINS, R. R. J., PATEL, K., PUTNAM, W. C., KAPUR, P. & RAKHEJA, D. 2017. Oncometabolites: A New Paradigm for Oncology, Metabolism, and the Clinical Laboratory. *Clinical Chemistry,* 63**,** 1812.

CONTI, C., SACCÀ, B., HERRICK, J., LALOU, C., POMMIER, Y. & BENSIMON, A. 2007. Replication fork velocities at adjacent replication origins are coordinately modified during DNA replication in human cells. *Molecular biology of the cell,* 18**,** 3059-3067.

CORTEZ, D. 2015. Preventing replication fork collapse to maintain genome integrity. *DNA Repair (Amst),* 32**,** 149-157.

CORTEZ, D., GLICK, G. & ELLEDGE, S. J. 2004. Minichromosome maintenance proteins are direct targets of the ATM and ATR checkpoint kinases. *Proceedings of the National Academy of Sciences of the United States of America,* 101**,** 10078-10083.

COSTANTINO, L., SOTIRIOU, S. K., RANTALA, J. K., MAGIN, S., MLADENOV, E., HELLEDAY, T., HABER, J. E., ILIAKIS, G., KALLIONIEMI, O. P. & HALAZONETIS, T. D. 2014. Break-induced replication repair of damaged forks induces genomic duplications in human cells. *Science,* 343**,** 88-91.

COUE, M., AMARIGLIO, F., MAIORANO, D., BOCQUET, S. & MECHALI, M. 1998. Evidence for different MCM subcomplexes with differential binding to chromatin in Xenopus. *Exp Cell Res,* 245**,** 282-9.

COURCHESNE, E., MOUTON, P. R., CALHOUN, M. E., SEMENDEFERI, K., AHRENS-BARBEAU, C., HALLET, M. J., BARNES, C. C. & PIERCE, K. 2011. Neuron Number and Size in Prefrontal Cortex of Children With Autism. *JAMA,* 306**,** 2001-2010.

CREA, F., SUN, L., MAI, A., CHIANG, Y. T., FARRAR, W. L., DANESI, R. & HELGASON, C. D. 2012. The emerging role of histone lysine demethylases in prostate cancer. *Mol Cancer,* 11**,** 52.

CREMONA, C. A., SARANGI, P., YANG, Y., HANG, L. E., RAHMAN, S. & ZHAO, X. 2012. Extensive DNA damage-induced sumoylation contributes to replication and repair and acts in addition to the mec1 checkpoint. *Molecular cell,* 45**,** 422-432.

CREVEL, G., IVETIC, A., OHNO, K., YAMAGUCHI, M. & COTTERILL, S. 2001. Nearest neighbour analysis of MCM protein complexes in Drosophila melanogaster. *Nucleic Acids Res,* 29**,** 4834-42.

CSIZMOK, V. & FORMAN-KAY, J. D. 2018. Complex regulatory mechanisms mediated by the interplay of multiple post-translational modifications. *Current Opinion in Structural Biology,* 48**,** 58-67.

DAFONSECA, C. J., SHU, F. & ZHANG, J. J. 2001. Identification of two residues in MCM5 critical for the assembly of MCM complexes and Stat1-mediated transcription activation in response to IFN-gamma. *Proc Natl Acad Sci U S A,* 98**,** 3034-9.

DAS, M., SINGH, S., PRADHAN, S. & NARAYAN, G. 2014. MCM Paradox: Abundance of Eukaryotic Replicative Helicases and Genomic Integrity. *Mol Biol Int,* 2014**,** 574850.

DAUBER, A., LAFRANCHI, S. H., MALIGA, Z., LUI, J. C., MOON, J. E., MCDEED, C., HENKE, K., ZONANA, J., KINGMAN, G. A., PERS, T. H., BARON, J., ROSENFELD, R. G., HIRSCHHORN, J. N., HARRIS, M. P. & HWA, V. 2012. Novel microcephalic primordial dwarfism disorder associated with variants in the centrosomal protein ninein. *J Clin Endocrinol Metab,* 97**,** E2140-51.

DAUGERON, M. C., PROUTEAU, M., LACROUTE, F. & SERAPHIN, B. 2011. The highly conserved eukaryotic DRG factors are required for efficient translation in a manner redundant with the putative RNA helicase Slh1. *Nucleic Acids Res,* 39**,** 2221-33.

DAVEY, M. J., INDIANI, C. & O'DONNELL, M. 2003. Reconstitution of the Mcm2-7p heterohexamer, subunit arrangement, and ATP site architecture. *J Biol Chem,* 278**,** 4491-9.

DAVIDOVITCH, M., PATTERSON, B. & GARTSIDE, P. 1996. Head Circumference Measurements in Children With Autism. *Journal of Child Neurology,* 11**,** 389-393.

DAVIS, C. K., JAIN, S. A., BAE, O.-N., MAJID, A. & RAJANIKANT, G. K. 2019. Hypoxia Mimetic Agents for Ischemic Stroke. 6.

DE KLEIN, A., MUIJTJENS, M., VAN OS, R., VERHOEVEN, Y., SMIT, B., CARR, A. M., LEHMANN, A. R. & HOEIJMAKERS, J. H. 2000. Targeted disruption of the cell-cycle checkpoint gene ATR leads to early embryonic lethality in mice. *Curr Biol,* 10**,** 479-82.

DE KROM, M., STAAL, W. G., OPHOFF, R. A., HENDRIKS, J., BUITELAAR, J., FRANKE, B., DE JONGE, M. V., BOLTON, P., COLLIER, D., CURRAN, S., VAN ENGELAND, H. & VAN REE, J. M. 2009. A Common Variant in DRD3 Receptor Is Associated with Autism Spectrum Disorder. *Biological Psychiatry,* 65**,** 625-630.

DE LIGT, J., WILLEMSEN, M. H., VAN BON, B. W., KLEEFSTRA, T., YNTEMA, H. G., KROES, T., VULTO-VAN SILFHOUT, A. T., KOOLEN, D. A., DE VRIES, P., GILISSEN, C., DEL ROSARIO, M., HOISCHEN, A., SCHEFFER, H., DE VRIES, B. B., BRUNNER, H. G., VELTMAN, J. A. & VISSERS, L. E. 2012. Diagnostic exome sequencing in persons with severe intellectual disability. *N Engl J Med,* 367**,** 1921-9.

DEEGAN, T. D. & DIFFLEY, J. F. 2016. MCM: one ring to rule them all. *Curr Opin Struct Biol,* 37**,** 145-51.

DEHAY, C., KENNEDY, H. & KOSIK, KENNETH S. 2015. The Outer Subventricular Zone and Primate-Specific Cortical Complexification. *Neuron,* 85**,** 683-694.

DEL RIZZO, P. A., KRISHNAN, S. & TRIEVEL, R. C. 2012. Crystal structure and functional analysis of JMJD5 indicate an alternate specificity and function. *Mol Cell Biol,* 32**,** 4044-52.

DERIBE, Y. L., PAWSON, T. & DIKIC, I. 2010. Post-translational modifications in signal integration. *Nat Struct Mol Biol,* 17**,** 666-72.

DESMET, F.-O., HAMROUN, D., LALANDE, M., COLLOD-BÉROUD, G., CLAUSTRES, M. & BÉROUD, C. 2009. Human Splicing Finder: an online bioinformatics tool to predict splicing signals. *Nucleic acids research,* 37**,** e67-e67.

DHAENENS, M., GLIBERT, P., MEERT, P., VOSSAERT, L. & DEFORCE, D. 2015. Histone proteolysis: a proposal for categorization into 'clipping' and 'degradation'. *BioEssays : news and reviews in molecular, cellular and developmental biology,* 37**,** 70-79.

DIMRI, G. P., LEE, X., BASILE, G., ACOSTA, M., SCOTT, G., ROSKELLEY, C., MEDRANO, E. E., LINSKENS, M., RUBELJ, I. & PEREIRA-SMITH, O. 1995. A biomarker that identifies senescent human cells in culture and in aging skin in vivo. *Proceedings of the National Academy of Sciences of the United States of America,* 92**,** 9363-9367.

DOMINGUEZ-SOLA, D., YING, C. Y., GRANDORI, C., RUGGIERO, L., CHEN, B., LI, M., GALLOWAY, D. A., GU, W., GAUTIER, J. & DALLA-FAVERA, R. 2007. Non-transcriptional control of DNA replication by c-Myc. *Nature,* 448**,** 445-51.

DRISSI, R., CHAUVIN, A., MCKENNA, A., LÉVESQUE, D., BLAIS-BROCHU, S., JEAN, D. & BOISVERT, F.-M. 2018. Destabilization of the MiniChromosome Maintenance (MCM) complex modulates the cellular response to DNA double strand breaks. *Cell cycle (Georgetown, Tex.),* 17**,** 2593-2609.

DUAN, G. & WALTHER, D. 2015. The roles of post-translational modifications in the context of protein interaction networks. *PLoS Comput Biol,* 11**,** e1004049.

DVINGE, H., KIM, E., ABDEL-WAHAB, O. & BRADLEY, R. K. 2016. RNA splicing factors as oncoproteins and tumour suppressors. *Nat Rev Cancer,* 16**,** 413-30.

DWANE, S., DURACK, E. & KIELY, P. A. 2013. Optimising parameters for the differentiation of SH-SY5Y cells to study cell adhesion and cell migration. *BMC Research Notes,* 6**,** 366.

EBERT, D. H. & GREENBERG, M. E. 2013. Activity-dependent neuronal signalling and autism spectrum disorder. *Nature,* 493**,** 327-37.

EDERY, P., MARCAILLOU, C., SAHBATOU, M., LABALME, A., CHASTANG, J., TOURAINE, R., TUBACHER, E., SENNI, F., BOBER, M. B., NAMPOOTHIRI, S., JOUK, P. S., STEICHEN, E., BERLAND, S., TOUTAIN, A., WISE, C. A., SANLAVILLE, D., ROUSSEAU, F., CLERGET-DARPOUX, F. & LEUTENEGGER, A. L. 2011. Association of TALS developmental disorder with defect in minor splicing component U4atac snRNA. *Science,* 332**,** 240-3.

EHNINGER, D., HAN, S., SHILYANSKY, C., ZHOU, Y., LI, W., KWIATKOWSKI, D. J., RAMESH, V. & SILVA, A. J. 2008. Reversal of learning deficits in a Tsc2+/– mouse model of tuberous sclerosis. *Nature Medicine,* 14**,** 843-848.

EIJKELENKAMP, K., OSINGA, T. E., LINKS, T. P. & VAN DER HORST-SCHRIVERS, A. N. A. 2019. Clinical implications of the oncometabolite succinate in SDHx-mutation carriers. *Clinical Genetics,* 0.

EIRAKU, M., WATANABE, K., MATSUO-TAKASAKI, M., KAWADA, M., YONEMURA, S., MATSUMURA, M., WATAYA, T., NISHIYAMA, A., MUGURUMA, K. & SASAI, Y. 2008. Self-organized formation of polarized cortical tissues from ESCs and its active manipulation by extrinsic signals. *Cell Stem Cell,* 3**,** 519-32.

ELKABETZ, Y., PANAGIOTAKOS, G., AL SHAMY, G., SOCCI, N. D., TABAR, V. & STUDER, L. 2008. Human ES cell-derived neural rosettes reveal a functionally distinct early neural stem cell stage. *Genes Dev,* 22, 152-65.

ELKINS, J. M., HEWITSON, K. S., MCNEILL, L. A., SEIBEL, J. F., SCHLEMMINGER, I., PUGH, C. W., RATCLIFFE, P. J. & SCHOFIELD, C. J. 2003. Structure of Factor-inhibiting Hypoxia-inducible Factor (HIF) Reveals Mechanism of Oxidative Modification of HIF-1α. 278, 1802-1806.

ELLIS, P., FAGAN, B. M., MAGNESS, S. T., HUTTON, S., TARANOVA, O., HAYASHI, S., MCMAHON, A., RAO, M. & PEVNY, L. 2004. SOX2, a persistent marker for multipotential neural stem cells derived from embryonic stem cells, the embryo or the adult. *Dev Neurosci,* 26, 148-65.

ELROUBY, N. & COUPLAND, G. 2010. Proteome-wide screens for small ubiquitin-like modifier (SUMO) substrates identify Arabidopsis proteins implicated in diverse biological processes. *Proceedings of the National Academy of Sciences of the United States of America,* 107, 17415-17420.

ENCINAS, M., IGLESIAS, M., LIU, Y., WANG, H., MUHAISEN, A., CENA, V., GALLEGO, C. & COMELLA, J. X. 2000. Sequential treatment of SH-SY5Y cells with retinoic acid and brain-derived neurotrophic factor gives rise to fully differentiated, neurotrophic factor-dependent, human neuron-like cells. *J Neurochem,* 75, 991-1003.

ENKHBAATAR, Z., TERASHIMA, M., OKTYABRI, D., TANGE, S., ISHIMURA, A., YANO, S. & SUZUKI, T. 2013. KDM5B histone demethylase controls epithelial-mesenchymal transition of cancer cells by regulating the expression of the microRNA-200 family. *Cell Cycle,* 12, 2100-12.

ERZBERGER, J. P. & BERGER, J. M. 2006. Evolutionary relationships and structural mechanisms of AAA+ proteins. *Annu Rev Biophys Biomol Struct,* 35, 93-114.

ETHERIDGE, N., TRUSOV, Y., VERBELEN, J. P. & BOTELLA, J. R. 1999. Characterization of ATDRG1, a member of a new class of GTP-binding proteins in plants. *Plant Mol Biol,* 39, 1113-26.

EVRIN, C., FERNANDEZ-CID, A., ZECH, J., HERRERA, M. C., RIERA, A., CLARKE, P., BRILL, S., LURZ, R. & SPECK, C. 2013. In the absence of ATPase activity, pre-RC formation is blocked prior to MCM2-7 hexamer dimerization. *Nucleic Acids Res,* 41, 3162-72.

FAGONE, P., DI ROSA, M., PALUMBO, M., DE GREGORIO, C., NICOLETTI, F. & MALAGUARNERA, L. 2012. Modulation of heat shock proteins during macrophage differentiation. *Inflamm Res,* 61, 1131-9.

FANNING, E., KLIMOVICH, V. & NAGER, A. R. 2006. A dynamic model for replication protein A (RPA) function in DNA processing pathways. *Nucleic Acids Res,* 34, 4126-37.

FARRELL, A., ALAHARI, S., ERMINI, L., TAGLIAFERRO, A., LITVACK, M., POST, M. & CANIGGIA, I. 2019. Faulty oxygen sensing disrupts angiomotin function in trophoblast cell migration and predisposes to preeclampsia. *JCI Insight,* 4.

FATOBA, S. T., TOGNETTI, S., BERTO, M., LEO, E., MULVEY, C. M., GODOVAC-ZIMMERMANN, J., POMMIER, Y. & OKOROKOV, A. L. 2013. Human SIRT1 regulates DNA binding and stability of the Mcm10 DNA replication factor via deacetylation. *Nucleic Acids Res,* 41, 4065-79.

FELLOUS, A., EARLEY, R. L. & SILVESTRE, F. 2019. The Kdm/Kmt gene families in the self-fertilizing mangrove rivulus fish, Kryptolebias marmoratus, suggest involvement of histone methylation machinery in development and reproduction. *Gene,* 687, 173-187.

FENECH, M., KIRSCH-VOLDERS, M., NATARAJAN, A. T., SURRALLES, J., CROTT, J. W., PARRY, J., NORPPA, H., EASTMOND, D. A., TUCKER, J. D. & THOMAS, P. 2011. Molecular mechanisms of micronucleus, nucleoplasmic bridge and nuclear bud formation in mammalian and human cells. *Mutagenesis,* 26, 125-32.

FENG, T., YAMAMOTO, A., WILKINS, S. E., SOKOLOVA, E., YATES, L. A., MUNZEL, M., SINGH, P., HOPKINSON, R. J., FISCHER, R., COCKMAN, M. E., SHELLEY, J., TRUDGIAN, D. C., SCHODEL, J., MCCULLAGH, J. S., GE, W., KESSLER, B. M., GILBERT, R. J., FROLOVA, L. Y., ALKALAEVA, E., RATCLIFFE, P. J., SCHOFIELD, C. J. & COLEMAN, M. L. 2014. Optimal translational termination requires C4 lysyl hydroxylation of eRF1. *Mol Cell,* 53, 645-54.

FENG, W. & JASIN, M. 2018. 53BP1 nuclear body-marked replication stress in a human mammary cell model of BRCA2 deficiency. *bioRxiv,* 462119.

FENWICK, AIMEE L., KLISZCZAK, M., COOPER, F., MURRAY, J., SANCHEZ-PULIDO, L., TWIGG, STEPHEN R. F., GORIELY, A., MCGOWAN, SIMON J., MILLER, KERRY A., TAYLOR, INDIRA B., LOGAN, C., BOZDOGAN, S., DANDA, S., DIXON, J., ELSAYED, SOLAF M., ELSOBKY, E., GARDHAM, A., HOFFER, MARIETTE J. V., KOOPMANS, M., MCDONALD-MCGINN, DONNA M., SANTEN, GIJS W. E., SAVARIRAYAN, R., DE SILVA, D., VANAKKER, O., WALL, STEVEN A., WILSON, LOUISE C., YUREGIR, OZGE O., ZACKAI, ELAINE H., PONTING, CHRIS P., JACKSON, ANDREW P., WILKIE, ANDREW O. M., NIEDZWIEDZ, W. & BICKNELL, LOUISE S. 2016. Mutations in CDC45, Encoding an Essential Component of the Pre-initiation Complex, Cause Meier-Gorlin Syndrome and Craniosynostosis. *The American Journal of Human Genetics,* 99, 125-138.

FERNANDEZ-CID, A., RIERA, A., TOGNETTI, S., HERRERA, M. C., SAMEL, S., EVRIN, C., WINKLER, C., GARDENAL, E., UHLE, S. & SPECK, C. 2013. An ORC/Cdc6/MCM2-7 complex is formed in a multistep reaction to serve as a platform for MCM double-hexamer assembly. *Mol Cell,* 50, 577-88.

FERNANDEZ-VIDAL, A., VIGNARD, J. & MIREY, G. 2017. Around and beyond 53BP1 Nuclear Bodies. *International journal of molecular sciences,* 18, 2611.

FOMBONNE, E., ROGE, B., CLAVERIE, J., COURTY, S. & FREMOLLE, J. 1999. Microcephaly and macrocephaly in autism. *J Autism Dev Disord,* 29, 113-9.

FONSECA, M. B., NUNES, A. F., MORGADO, A. L., SOLÁ, S. & RODRIGUES, C. M. P. 2012. TAp63γ Demethylation Regulates Protein Stability and Cellular Distribution during Neural Stem Cell Differentiation. *PLOS ONE,* 7, e52417.

FORSBURG, S. L. 2004. Eukaryotic MCM proteins: beyond replication initiation. *Microbiology and molecular biology reviews : MMBR,* 68, 109-131.

FOSKOLOU, I. P., BIASOLI, D., OLCINA, M. M. & HAMMOND, E. M. Measuring DNA Replication in Hypoxic Conditions. *In:* KOUMENIS, C., COUSSENS, L. M., GIACCIA, A. & HAMMOND, E., eds. Tumor Microenvironment, 2016// 2016 Cham. Springer International Publishing, 11-25.

FRANCIS, S. M., GAS, M. E., DAUGERON, M. C., BRAVO, J. & SERAPHIN, B. 2012. Rbg1-Tma46 dimer structure reveals new functional domains and their role in polysome recruitment. *Nucleic Acids Res,* 40, 11100-14.

FRESCAS, D., GUARDAVACCARO, D., KUCHAY, S. M., KATO, H., POLESHKO, A., BASRUR, V., ELENITOBA-JOHNSON, K. S., KATZ, R. A. & PAGANO, M. 2008. KDM2A represses transcription of centromeric satellite repeats and maintains the heterochromatic state. *Cell Cycle,* 7, 3539-47.

FRIGOLA, J., HE, J., KINKELIN, K., PYE, V. E., RENAULT, L., DOUGLAS, M. E., REMUS, D., CHEREPANOV, P., COSTA, A. & DIFFLEY, J. F. X. 2017. Cdt1 stabilizes an open MCM ring for helicase loading. *Nature communications,* 8, 15720-15720.

FUHRMANN, D., MERNBERGER, M., NIST, A., STIEWE, T. & ELSASSER, H. P. 2018. Miz1 Controls Schwann Cell Proliferation via H3K36(me2) Demethylase Kdm8 to Prevent Peripheral Nerve Demyelination. *J Neurosci,* 38, 858-877.

GAI, D., ZHAO, R., LI, D., FINKIELSTEIN, C. V. & CHEN, X. S. 2004. Mechanisms of conformational change for a replicative hexameric helicase of SV40 large tumor antigen. *Cell,* 119, 47-60.

GAILLARD, H., GARCÍA-MUSE, T. & AGUILERA, A. 2015. Replication stress and cancer. *Nature Reviews Cancer,* 15, 276.

GAMBUS, A., JONES, R. C., SANCHEZ-DIAZ, A., KANEMAKI, M., VAN DEURSEN, F., EDMONDSON, R. D. & LABIB, K. 2006. GINS maintains association of Cdc45 with MCM in replisome progression complexes at eukaryotic DNA replication forks. *Nature Cell Biology,* 8, 358-366.

GAMBUS, A., KHOUDOLI, G. A., JONES, R. C. & BLOW, J. J. 2011. MCM2-7 form double hexamers at licensed origins in Xenopus egg extract. *J Biol Chem,* 286, 11855-64.

GANAPATHI, M., PADGETT, L. R., YAMADA, K., DEVINSKY, O., WILLAERT, R., PERSON, R., AU, P. B., TAGOE, J., MCDONALD, M., KARLOWICZ, D., WOLF, B., LEE, J., SHEN, Y., OKUR, V., DENG, L., LEDUC, C. A., WANG, J., HANNER, A., MIRMIRA, R. G., PARK, M. H., MASTRACCI, T. L. & CHUNG, W. K. 2019. Recessive Rare Variants in Deoxyhypusine Synthase, an Enzyme Involved in the Synthesis of Hypusine, Are Associated with a Neurodevelopmental Disorder. *Am J Hum Genet,* 104, 287-298.

GARCIA-MUSE, T. & AGUILERA, A. 2016. Transcription-replication conflicts: how they occur and how they are resolved. *Nat Rev Mol Cell Biol,* 17, 553-63.

GARRIBBA, L., WU, W., OZER, O., BHOWMICK, R., HICKSON, I. D. & LIU, Y. 2018. Inducing and Detecting Mitotic DNA Synthesis at Difficult-to-Replicate Loci. *Methods Enzymol,* 601, 45-58.

GASPARD, N., BOUSCHET, T., HOUREZ, R., DIMIDSCHSTEIN, J., NAEIJE, G., VAN DEN AMEELE, J., ESPUNY-CAMACHO, I., HERPOEL, A., PASSANTE, L., SCHIFFMANN, S. N., GAILLARD, A. & VANDERHAEGHEN, P. 2008. An intrinsic mechanism of corticogenesis from embryonic stem cells. *Nature,* 455, 351-357.

GE, W., WOLF, A., FENG, T., HO, C.-H., SEKIRNIK, R., ZAYER, A., GRANATINO, N., COCKMAN, M. E., LOENARZ, C., LOIK, N. D., HARDY, A. P., CLARIDGE, T. D. W., HAMED, R. B., CHOWDHURY, R., GONG, L., ROBINSON, C. V., TRUDGIAN, D. C., JIANG, M., MACKEEN, M. M., MCCULLAGH, J. S., GORDIYENKO, Y., THALHAMMER, A., YAMAMOTO, A., YANG, M., LIU-YI, P., ZHANG, Z., SCHMIDT-ZACHMANN, M., KESSLER, B. M., RATCLIFFE, P. J., PRESTON, G. M., COLEMAN, M. L. & SCHOFIELD, C. J. 2012. Oxygenase-catalyzed ribosome hydroxylation occurs in prokaryotes and humans. *Nature chemical biology,* 8, 960-962.

GE, X. Q. & BLOW, J. J. 2010. Chk1 inhibits replication factory activation but allows dormant origin firing in existing factories. *The Journal of cell biology,* 191, 1285-1297.

GE, X. Q., JACKSON, D. A. & BLOW, J. J. 2007. Dormant origins licensed by excess Mcm2-7 are required for human cells to survive replicative stress. *Genes Dev,* 21, 3331-41.

GELOT, C., MAGDALOU, I. & LOPEZ, B. 2015. Replication Stress in Mammalian Cells and Its Consequences for Mitosis. *Genes,* 6, 267-298.

GETAHUN, D., FASSETT, M. J., PELTIER, M. R., WING, D. A., XIANG, A. H., CHIU, V. & JACOBSEN, S. J. 2017. Association of Perinatal Risk Factors with Autism Spectrum Disorder. *Amer J Perinatol,* 07, 295-304.

GILLESPIE, P. J., LI, A. & BLOW, J. J. 2001. Reconstitution of licensed replication origins on Xenopus sperm nuclei using purified proteins. *BMC Biochem,* 2, 15.

GKOGKAS, C. G., KHOUTORSKY, A., RAN, I., RAMPAKAKIS, E., NEVARKO, T., WEATHERILL, D. B., VASUTA, C., YEE, S., TRUITT, M., DALLAIRE, P., MAJOR, F., LASKO, P., RUGGERO, D., NADER, K., LACAILLE, J.-C. & SONENBERG, N. 2012. Autism-related deficits via dysregulated eIF4E-dependent translational control. *Nature,* 493, 371.

GLOVER, T. W., BERGER, C., COYLE, J. & ECHO, B. 1984. DNA polymerase α inhibition by aphidicolin induces gaps and breaks at common fragile sites in human chromosomes. *Human Genetics,* 67, 136-142.

GOLEBIOWSKI, F., MATIC, I., TATHAM, M. H., COLE, C., YIN, Y., NAKAMURA, A., COX, J., BARTON, G. J., MANN, M. & HAY, R. T. 2009. System-Wide Changes to SUMO Modifications in Response to Heat Shock. *Science Signaling,* 2, ra24.

GRIFFITH, E., WALKER, S., MARTIN, C. A., VAGNARELLI, P., STIFF, T., VERNAY, B., AL SANNA, N., SAGGAR, A., HAMEL, B., EARNSHAW, W. C., JEGGO, P. A., JACKSON, A. P. & O'DRISCOLL, M. 2008. Mutations in pericentrin cause Seckel syndrome with defective ATR-dependent DNA damage signaling. *Nat Genet,* 40, 232-6.

GUENTHER, M. G., FRAMPTON, G. M., SOLDNER, F., HOCKEMEYER, D., MITALIPOVA, M., JAENISCH, R. & YOUNG, R. A. 2010. Chromatin structure and gene expression programs of human embryonic and induced pluripotent stem cells. *Cell Stem Cell,* 7, 249-57.

GUERNSEY, D. L., MATSUOKA, M., JIANG, H., EVANS, S., MACGILLIVRAY, C., NIGHTINGALE, M., PERRY, S., FERGUSON, M., LEBLANC, M., PAQUETTE, J., PATRY, L., RIDEOUT, A. L., THOMAS, A., ORR, A., MCMASTER, C. R., MICHAUD, J. L., DEAL, C., LANGLOIS, S., SUPERNEAU, D. W., PARKASH, S., LUDMAN, M., SKIDMORE, D. L. & SAMUELS, M. E. 2011. Mutations in origin recognition complex gene ORC4 cause Meier-Gorlin syndrome. *Nat Genet,* 43, 360-4.

GUPTA, N. & WISH, J. B. 2017. Hypoxia-Inducible Factor Prolyl Hydroxylase Inhibitors: A Potential New Treatment for Anemia in Patients With CKD. *American Journal of Kidney Diseases,* 69, 815-826.

HA, S., SOHN, I.-J., KIM, N., SIM, H. J. & CHEON, K.-A. 2015. Characteristics of Brains in Autism Spectrum Disorder: Structure, Function and Connectivity across the Lifespan. *Experimental neurobiology,* 24, 273-284.

HALAZONETIS, T. D., GORGOULIS, V. G. & BARTEK, J. 2008. An Oncogene-Induced DNA Damage Model for Cancer Development. *Science,* 319, 1352.

HALL, P. E., LATHIA, J. D., CALDWELL, M. A. & FFRENCH-CONSTANT, C. 2008. Laminin enhances the growth of human neural stem cells in defined culture media. *BMC neuroscience,* 9, 71-71.

HAMMOND, E. M., DENKO, N. C., DORIE, M. J., ABRAHAM, R. T. & GIACCIA, A. J. 2002. Hypoxia Links ATR and p53 through Replication Arrest. *Molecular and Cellular Biology,* 22, 1834.

HAMMOND, E. M., MANDELL, D. J., SALIM, A., KRIEG, A. J., JOHNSON, T. M., SHIRAZI, H. A., ATTARDI, L. D. & GIACCIA, A. J. 2006. Genome-Wide Analysis of p53 under Hypoxic Conditions. *Molecular and Cellular Biology,* 26, 3492.

HAN, J., LI, Q., MCCULLOUGH, L., KETTELKAMP, C., FORMOSA, T. & ZHANG, Z. 2010. Ubiquitylation of FACT by the cullin-E3 ligase Rtt101 connects FACT to DNA replication. *Genes Dev,* 24, 1485-90.

HANAHAN, D. & WEINBERG, ROBERT A. 2011. Hallmarks of Cancer: The Next Generation. *Cell,* 144, 646-674.

HANCOCK, R. L., MASSON, N., DUNNE, K., FLASHMAN, E. & KAWAMURA, A. 2017. The Activity of JmjC Histone Lysine Demethylase KDM4A is Highly Sensitive to Oxygen Concentrations. *ACS Chemical Biology,* 12, 1011-1019.

HANSEN, D. V., LUI, J. H., PARKER, P. R. L. & KRIEGSTEIN, A. R. 2010. Neurogenic radial glia in the outer subventricular zone of human neocortex. *Nature,* 464, 554-561.

HARLEY, M. E., MURINA, O., LEITCH, A., HIGGS, M. R., BICKNELL, L. S., YIGIT, G., BLACKFORD, A. N., ZLATANOU, A., MACKENZIE, K. J., REDDY, K., HALACHEV, M., MCGLASSON, S., REIJNS, M. A. M., FLUTEAU, A., MARTIN, C. A., SABBIONEDA, S., ELCIOGLU, N. H., ALTMULLER, J., THIELE, H., GREENHALGH, L., CHESSA, L., MAGHNIE, M., SALIM, M., BOBER, M. B., NURNBERG, P., JACKSON, S. P., HURLES, M. E., WOLLNIK, B., STEWART, G. S. & JACKSON, A. P. 2016. TRAIP promotes DNA damage response during genome replication and is mutated in primordial dwarfism. *Nat Genet,* 48, 36-43.

HARRIGAN, J. A., BELOTSERKOVSKAYA, R., COATES, J., DIMITROVA, D. S., POLO, S. E., BRADSHAW, C. R., FRASER, P. & JACKSON, S. P. 2011. Replication stress induces 53BP1-containing OPT domains in G1 cells. *J Cell Biol,* 193**,** 97-108.

HASTINGS, P. J., IRA, G. & LUPSKI, J. R. 2009. A Microhomology-Mediated Break-Induced Replication Model for the Origin of Human Copy Number Variation. *PLOS Genetics,* 5**,** e1000327.

HE, H., LIYANARACHCHI, S., AKAGI, K., NAGY, R., LI, J., DIETRICH, R. C., LI, W., SEBASTIAN, N., WEN, B., XIN, B., SINGH, J., YAN, P., ALDER, H., HAAN, E., WIECZOREK, D., ALBRECHT, B., PUFFENBERGER, E., WANG, H., WESTMAN, J. A., PADGETT, R. A., SYMER, D. E. & DE LA CHAPELLE, A. 2011. Mutations in U4atac snRNA, a component of the minor spliceosome, in the developmental disorder MOPD I. *Science,* 332**,** 238-40.

HE, Z., WU, J., SU, X., ZHANG, Y., PAN, L., WEI, H., FANG, Q., LI, H., WANG, D.-L. & SUN, F.-L. 2016a. JMJD5 (Jumonji Domain-containing 5) Associates with Spindle Microtubules and Is Required for Proper Mitosis. 291**,** 4684-4697.

HE, Z., WU, J., SU, X., ZHANG, Y., PAN, L., WEI, H., FANG, Q., LI, H., WANG, D. L. & SUN, F. L. 2016b. JMJD5 (Jumonji Domain-containing 5) Associates with Spindle Microtubules and Is Required for Proper Mitosis. *J Biol Chem,* 291**,** 4684-97.

HEIM, A., GRIMM, C., MÜLLER, U., HÄUßLER, S., MACKEEN, M. M., MERL, J., HAUCK, S. M., KESSLER, B. M., SCHOFIELD, C. J., WOLF, A. & BÖTTGER, A. 2014. Jumonji domain containing protein 6 (Jmjd6) modulates splicing and specifically interacts with arginine–serine-rich (RS) domains of SR- and SR-like proteins. *Nucleic Acids Research,* 42**,** 7833-7850.

HEMMATI-BRIVANLOU, A., KELLY, O. G. & MELTON, D. A. 1994. Follistatin, an antagonist of activin, is expressed in the Spemann organizer and displays direct neuralizing activity. *Cell,* 77**,** 283-295.

HENDRICKSON, M., MADINE, M., DALTON, S. & GAUTIER, J. 1996. Phosphorylation of MCM4 by cdc2 protein kinase inhibits the activity of the minichromosome maintenance complex. *Proc Natl Acad Sci U S A,* 93**,** 12223-8.

HER, J., RAY, C., ALTSHULER, J., ZHENG, H. & BUNTING, S. F. 2018. 53BP1 Mediates ATR-Chk1 Signaling and Protects Replication Forks under Conditions of Replication Stress. *Molecular and Cellular Biology,* 38**,** e00472-17.

HERNANDEZ, P. J. & ABEL, T. 2008. The role of protein synthesis in memory consolidation: Progress amid decades of debate. *Neurobiology of Learning and Memory,* 89**,** 293-311.

HESKETH, E. L., KNIGHT, J. R., WILSON, R. H., CHONG, J. P. & COVERLEY, D. 2015. Transient association of MCM complex proteins with the nuclear matrix during initiation of mammalian DNA replication. *Cell Cycle,* 14**,** 333-41.

HILLS, STEPHANIE A. & DIFFLEY, JOHN F. X. 2014. DNA Replication and Oncogene-Induced Replicative Stress. *Current Biology,* 24**,** R435-R444.

HO, Y. J., SHIH, C. P., YEH, K. T., SHI, B., GONG, Z., LIN, Y. M. & LU, J. W. 2018. Correlation between high expression levels of jumonji domain-containing 4 and short survival in cases of colon adenocarcinoma. *Biochem Biophys Res Commun,* 503**,** 1442-1449.

HOFFMAN, J. D., GRAFF, R. E., EMAMI, N. C., TAI, C. G., PASSARELLI, M. N., HU, D., HUNTSMAN, S., HADLEY, D., LEONG, L., MAJUMDAR, A., ZAITLEN, N., ZIV, E. & WITTE, J. S. 2017. Cis-eQTL-based trans-ethnic meta-analysis reveals novel genes associated with breast cancer risk. *PLoS Genet,* 13**,** e1006690.

HOLT, C. E., MARTIN, K. C. & SCHUMAN, E. M. 2019. Local translation in neurons: visualization and function. *Nature Structural & Molecular Biology,* 26**,** 557-566.

HONG, H., TAKAHASHI, K., ICHISAKA, T., AOI, T., KANAGAWA, O., NAKAGAWA, M., OKITA, K. & YAMANAKA, S. 2009. Suppression of induced pluripotent stem cell generation by the p53-p21 pathway. *Nature,* 460**,** 1132-1135.

HSIA, D. A., TEPPER, C. G., POCHAMPALLI, M. R., HSIA, E. Y., IZUMIYA, C., HUERTA, S. B., WRIGHT, M. E., CHEN, H. W., KUNG, H. J. & IZUMIYA, Y. 2010. KDM8, a H3K36me2 histone demethylase that acts in the cyclin A1 coding region to regulate cancer cell proliferation. *Proc Natl Acad Sci U S A,* 107**,** 9671-6.

HUANG, C., XIANG, Y., WANG, Y., LI, X., XU, L., ZHU, Z., ZHANG, T., ZHU, Q., ZHANG, K., JING, N. & CHEN, C. D. 2010. Dual-specificity histone demethylase KIAA1718 (KDM7A) regulates neural differentiation through FGF4. *Cell Res,* 20**,** 154-65.

HUANG, X., ZHANG, L., QI, H., SHAO, J. & SHEN, J. 2013. Identification and functional implication of nuclear localization signals in the N-terminal domain of JMJD5. *Biochimie,* 95**,** 2114-22.

HUANG, X., ZHANG, S., QI, H., WANG, Z., CHEN, H. W., SHAO, J. & SHEN, J. 2015. JMJD5 interacts with p53 and negatively regulates p53 function in control of cell cycle and proliferation. *Biochim Biophys Acta,* 1853**,** 2286-95.

HUBER, G. & MATUS, A. 1984. Differences in the cellular distributions of two microtubule-associated proteins, MAP1 and MAP2, in rat brain. *J Neurosci,* 4**,** 151-60.

HUGHES, C. R., GUASTI, L., MEIMARIDOU, E., CHUANG, C.-H., SCHIMENTI, J. C., KING, P. J., COSTIGAN, C., CLARK, A. J. L. & METHERELL, L. A. 2012. MCM4 mutation causes adrenal failure, short stature, and natural killer cell deficiency in humans. *The Journal of Clinical Investigation,* 122**,** 814-820.

IBARRA, A., SCHWOB, E. & MENDEZ, J. 2008. Excess MCM proteins protect human cells from replicative stress by licensing backup origins of replication. *Proc Natl Acad Sci U S A,* 105**,** 8956-61.

ISHIKAWA, K., AKIYAMA, T., ITO, K., SEMBA, K. & INOUE, J. 2009. Independent stabilizations of polysomal Drg1/Dfrp1 complex and non-polysomal Drg2/Dfrp2 complex in mammalian cells. *Biochem Biophys Res Commun,* 390**,** 552-6.

ISHIKAWA, K., AZUMA, S., IKAWA, S., SEMBA, K. & INOUE, J. 2005. Identification of DRG family regulatory proteins (DFRPs): specific regulation of DRG1 and DRG2. *Genes Cells,* 10**,** 139-50.

ISHIKAWA, K., ITO, K., INOUE, J. & SEMBA, K. 2013. Cell growth control by stable Rbg2/Gir2 complex formation under amino acid starvation. *Genes Cells,* 18**,** 859-72.

ISHIMI, Y., KOMAMURA-KOHNO, Y., ARAI, K.-I. & MASAI, H. 2001. Biochemical Activities Associated with Mouse Mcm2 Protein. *Journal of Biological Chemistry,* 276**,** 42744-42752.

ISHIMURA, A., MINEHATA, K., TERASHIMA, M., KONDOH, G., HARA, T. & SUZUKI, T. 2012. Jmjd5, an H3K36me2 histone demethylase, modulates embryonic cell proliferation through the regulation of Cdkn1a expression. *Development,* 139**,** 749-59.

ISHIMURA, A., TERASHIMA, M., TANGE, S. & SUZUKI, T. 2016. Jmjd5 functions as a regulator of p53 signaling during mouse embryogenesis. *Cell Tissue Res,* 363**,** 723-33.

ISLAM, M. S., MCDONOUGH, M. A., CHOWDHURY, R., GAULT, J., KHAN, A., PIRES, E. & SCHOFIELD, C. J. 2019. Biochemical and structural investigations clarify the substrate selectivity of the 2-oxoglutarate oxygenase JMJD6. *J Biol Chem,* 294**,** 11637-11652.

ITO, T., MATSUBARA, D., TANAKA, I., MAKIYA, K., TANEI, Z.-I., KUMAGAI, Y., SHIU, S.-J., NAKAOKA, H. J., ISHIKAWA, S., ISAGAWA, T., MORIKAWA, T., SHINOZAKI-USHIKU, A., GOTO, Y., NAKANO, T., TSUCHIYA, T., TSUBOCHI, H., KOMURA, D., ABURATANI, H., DOBASHI, Y., NAKAJIMA, J., ENDO, S., FUKAYAMA, M., SEKIDO, Y., NIKI, T. & MURAKAMI, Y. 2016. Loss of YAP1 defines neuroendocrine differentiation of lung tumors. *Cancer science,* 107**,** 1527-1538.

IVAN, M., KONDO, K., YANG, H., KIM, W., VALIANDO, J., OHH, M., SALIC, A., ASARA, J. M., LANE, W. S. & KAELIN, W. G., JR. 2001. HIFalpha targeted for VHL-mediated destruction by proline hydroxylation: implications for O2 sensing. *Science,* 292**,** 464-8.

IYER, D. R. & RHIND, N. 2017. Replication fork slowing and stalling are distinct, checkpoint-independent consequences of replicating damaged DNA. *PLoS Genet,* 13**,** e1006958.

IZANT, J. G. & MCINTOSH, J. R. 1980. Microtubule-associated proteins: a monoclonal antibody to MAP2 binds to differentiated neurons. *Proc Natl Acad Sci U S A,* 77**,** 4741-5.

JAAKKOLA, P., MOLE, D. R., TIAN, Y. M., WILSON, M. I., GIELBERT, J., GASKELL, S. J., VON KRIEGSHEIM, A., HEBESTREIT, H. F., MUKHERJI, M., SCHOFIELD, C. J., MAXWELL, P. H., PUGH, C. W. & RATCLIFFE, P. J. 2001. Targeting of HIF-alpha to the von Hippel-Lindau ubiquitylation complex by O2-regulated prolyl hydroxylation. *Science,* 292**,** 468-72.

JACKSON, D. A. & POMBO, A. 1998. Replicon clusters are stable units of chromosome structure: evidence that nuclear organization contributes to the efficient activation and propagation of S phase in human cells. *The Journal of cell biology,* 140**,** 1285-1295.

JANG, S. H., KIM, A. R., PARK, N. H., PARK, J. W. & HAN, I. S. 2016. DRG2 Regulates G2/M Progression via the Cyclin B1-Cdk1 Complex. *Mol Cells,* 39**,** 699-704.

JAZAYERI, A., FALCK, J., LUKAS, C., BARTEK, J., SMITH, G. C., LUKAS, J. & JACKSON, S. P. 2006. ATM- and cell cycle-dependent regulation of ATR in response to DNA double-strand breaks. *Nat Cell Biol,* 8**,** 37-45.

JENSEN, L. R., AMENDE, M., GUROK, U., MOSER, B., GIMMEL, V., TZSCHACH, A., JANECKE, A. R., TARIVERDIAN, G., CHELLY, J., FRYNS, J. P., VAN ESCH, H., KLEEFSTRA, T., HAMEL, B., MORAINE, C., GECZ, J., TURNER, G., REINHARDT, R., KALSCHEUER, V. M., ROPERS, H. H. & LENZNER, S. 2005. Mutations in the JARID1C gene, which is involved in transcriptional regulation and chromatin remodeling, cause X-linked mental retardation. *Am J Hum Genet,* 76**,** 227-36.

JOHANSSON, C., TUMBER, A., CHE, K., CAIN, P., NOWAK, R., GILEADI, C. & OPPERMANN, U. 2014. The roles of Jumonji-type oxygenases in human disease. *Epigenomics,* 6**,** 89-120.

JONES, C. M., DALE, L., HOGAN, B. L., WRIGHT, C. V. & SMITH, J. C. 1996. Bone morphogenetic protein-4 (BMP-4) acts during gastrula stages to cause ventralization of Xenopus embryos. *Development,* 122, 1545.

JONES, M. A., COVINGTON, M. F., DITACCHIO, L., VOLLMERS, C., PANDA, S. & HARMER, S. L. 2010. Jumonji domain protein JMJD5 functions in both the plant and human circadian systems. *Proc Natl Acad Sci U S A,* 107, 21623-8.

JONES, M. A. & HARMER, S. 2011. JMJD5 Functions in concert with TOC1 in the arabidopsis circadian system. *Plant Signal Behav,* 6, 445-8.

JONES, M. A., MOROHASHI, K., GROTEWOLD, E. & HARMER, S. L. 2019. Arabidopsis JMJD5/JMJ30 Acts Independently of LUX ARRHYTHMO Within the Plant Circadian Clock to Enable Temperature Compensation. *Front Plant Sci,* 10, 57.

JUNG, H., YOON, B. C. & HOLT, C. E. 2012. Axonal mRNA localization and local protein synthesis in nervous system assembly, maintenance and repair. *Nat Rev Neurosci,* 13, 308-24.

KAJIWARA, M., AOI, T., OKITA, K., TAKAHASHI, R., INOUE, H., TAKAYAMA, N., ENDO, H., ETO, K., TOGUCHIDA, J., UEMOTO, S. & YAMANAKA, S. 2012. Donor-dependent variations in hepatic differentiation from human-induced pluripotent stem cells. *Proc Natl Acad Sci U S A,* 109, 12538-43.

KALAY, E., YIGIT, G., ASLAN, Y., BROWN, K. E., POHL, E., BICKNELL, L. S., KAYSERILI, H., LI, Y., TUYSUZ, B., NURNBERG, G., KIESS, W., KOEGL, M., BAESSMANN, I., BURUK, K., TORAMAN, B., KAYIPMAZ, S., KUL, S., IKBAL, M., TURNER, D. J., TAYLOR, M. S., AERTS, J., SCOTT, C., MILSTEIN, K., DOLLFUS, H., WIECZOREK, D., BRUNNER, H. G., HURLES, M., JACKSON, A. P., RAUCH, A., NURNBERG, P., KARAGUZEL, A. & WOLLNIK, B. 2011. CEP152 is a genome maintenance protein disrupted in Seckel syndrome. *Nat Genet,* 43, 23-6.

KANG, J., SHIN, S. H., YOON, H., HUH, J., SHIN, H. W., CHUN, Y. S. & PARK, J. W. 2018. FIH Is an Oxygen Sensor in Ovarian Cancer for G9a/GLP-Driven Epigenetic Regulation of Metastasis-Related Genes. *Cancer Res,* 78, 1184-1199.

KAO, S.-H., WANG, W.-L., CHEN, C.-Y., CHANG, Y.-L., WU, Y.-Y., WANG, Y.-T., WANG, S.-P., NESVIZHSKII, A. I., CHEN, Y.-J., HONG, T.-M. & YANG, P.-C. 2015. Analysis of Protein Stability by the Cycloheximide Chase Assay. *Bio-protocol,* 5, e1374.

KAR, S. P., BEESLEY, J., AMIN AL OLAMA, A., MICHAILIDOU, K., TYRER, J., KOTE-JARAI, Z., LAWRENSON, K., LINDSTROM, S., RAMUS, S. J., THOMPSON, D. J., KIBEL, A. S., DANSONKA-MIESZKOWSKA, A., MICHAEL, A., DIEFFENBACH, A. K., GENTRY-MAHARAJ, A., WHITTEMORE, A. S., WOLK, A., MONTEIRO, A., PEIXOTO, A., KIERZEK, A., COX, A., RUDOLPH, A., GONZALEZ-NEIRA, A., WU, A. H., LINDBLOM, A., SWERDLOW, A., ZIOGAS, A., EKICI, A. B., BURWINKEL, B., KARLAN, B. Y., NORDESTGAARD, B. G., BLOMQVIST, C., PHELAN, C., MCLEAN, C., PEARCE, C. L., VACHON, C., CYBULSKI, C., SLAVOV, C., STEGMAIER, C., MAIER, C., AMBROSONE, C. B., HOGDALL, C. K., TEERLINK, C. C., KANG, D., TESSIER, D. C., SCHAID, D. J., STRAM, D. O., CRAMER, D. W., NEAL, D. E., ECCLES, D., FLESCH-JANYS, D., EDWARDS, D. R., WOKOZORCZYK, D., LEVINE, D. A., YANNOUKAKOS, D., SAWYER, E. J., BANDERA, E. V., POOLE, E. M., GOODE, E. L., KHUSNUTDINOVA, E., HOGDALL, E., SONG, F., BRUINSMA, F., HEITZ, F., MODUGNO, F., HAMDY, F. C., WIKLUND, F., GILES, G. G., OLSSON, H., WILDIERS, H., ULMER, H. U., PANDHA, H., RISCH, H. A., DARABI, H., SALVESEN, H. B., NEVANLINNA, H., GRONBERG, H., BRENNER, H., BRAUCH, H., ANTON-CULVER, H., SONG, H., LIM, H. Y., MCNEISH, I., CAMPBELL, I., VERGOTE, I., GRONWALD, J., LUBINSKI, J., STANFORD, J. L., BENITEZ, J., DOHERTY, J. A., PERMUTH, J. B., CHANG-CLAUDE, J., DONOVAN, J. L., DENNIS, J., SCHILDKRAUT, J. M., SCHLEUTKER, J., HOPPER, J. L., KUPRYJANCZYK, J., PARK, J. Y., FIGUEROA, J., et al. 2016. Genome-Wide Meta-Analyses of Breast, Ovarian, and Prostate Cancer Association Studies Identify Multiple New Susceptibility Loci Shared by at Least Two Cancer Types. *Cancer Discov,* 6, 1052-67.

KARACA, E., POSEY, J. E., BOSTWICK, B., LIU, P., GEZDIRICI, A., YESIL, G., COBAN AKDEMIR, Z., BAYRAM, Y., HARMS, F. L., MEINECKE, P., ALAWI, M., BACINO, C. A., SUTTON, V. R., KORTUM, F. & LUPSKI, J. R. 2019. Biallelic and De Novo Variants in DONSON Reveal a Clinical Spectrum of Cell Cycle-opathies with Microcephaly, Dwarfism and Skeletal Abnormalities. *Am J Med Genet A,* 179, 2056-2066.

KARIMI, P., KAMALI, E., MOUSAVI, S. M. & KARAHMADI, M. 2017. Environmental factors influencing the risk of autism. *Journal of research in medical sciences : the official journal of Isfahan University of Medical Sciences,* 22, 27-27.

KATO, M., ARAISO, Y., NOMA, A., NAGAO, A., SUZUKI, T., ISHITANI, R. & NUREKI, O. 2011. Crystal structure of a novel JmjC-domain-containing protein, TYW5, involved in tRNA modification. *Nucleic Acids Res,* 39, 1576-85.

KELLEHER, R. J. & BEAR, M. F. 2008. The Autistic Neuron: Troubled Translation? *Cell,* 135, 401-406.

KHOURY, G. A., BALIBAN, R. C. & FLOUDAS, C. A. 2011. Proteome-wide post-translational modification statistics: frequency analysis and curation of the swiss-prot database. *Scientific Reports,* 1, 90.

KIM, I., SHIN, S. H., LEE, J. E. & PARK, J. W. 2019. Oxygen sensor FIH inhibits HACE1-dependent ubiquitination of Rac1 to enhance metastatic potential in breast cancer cells. *Oncogene,* 38, 3651-3666.

KIM, J. H., LEE, J. H., LEE, I. S., LEE, S. B. & CHO, K. S. 2017. Histone Lysine Methylation and Neurodevelopmental Disorders. *Int J Mol Sci,* 18.

KIM, K., ZHAO, R., DOI, A., NG, K., UNTERNAEHRER, J., CAHAN, P., HUO, H., LOH, Y. H., ARYEE, M. J., LENSCH, M. W., LI, H., COLLINS, J. J., FEINBERG, A. P. & DALEY, G. Q. 2011a. Donor cell type can influence the epigenome and differentiation potential of human induced pluripotent stem cells. *Nat Biotechnol,* 29, 1117-9.

KIM, Y. H., BAEK, N. S., HAN, Y. H., CHUNG, M. A. & JUNG, S. D. 2011b. Enhancement of neuronal cell adhesion by covalent binding of poly-D-lysine. *J Neurosci Methods,* 202, 38-44.

KIVIRIKKO, K. I. & PROCKOP, D. J. 1967. Enzymatic hydroxylation of proline and lysine in protocollagen. *Proceedings of the National Academy of Sciences of the United States of America,* 57, 782-789.

KLINGSEISEN, A. & JACKSON, A. P. 2011. Mechanisms and pathways of growth failure in primordial dwarfism. *Genes Dev,* 25, 2011-24.

KLOSE, R. J., KALLIN, E. M. & ZHANG, Y. 2006. JmjC-domain-containing proteins and histone demethylation. *Nature Reviews Genetics,* 7, 715-727.

KLOSE, R. J., YAN, Q., TOTHOVA, Z., YAMANE, K., ERDJUMENT-BROMAGE, H., TEMPST, P., GILLILAND, D. G., ZHANG, Y. & KAELIN, W. G., JR. 2007. The retinoblastoma binding protein RBP2 is an H3K4 demethylase. *Cell,* 128, 889-900.

KNORRE, D. G., KUDRYASHOVA, N. V. & GODOVIKOVA, T. S. 2009. Chemical and functional aspects of posttranslational modification of proteins. *Acta naturae,* 1, 29-51.

KO, M. S., LEE, U. H., KIM, S. I., KIM, H. J., PARK, J. J., CHA, S. J., KIM, S. B., SONG, H., CHUNG, D. K., HAN, I. S., KWACK, K. & PARK, J. W. 2004. Overexpression of DRG2 suppresses the growth of Jurkat T cells but does not induce apoptosis. *Arch Biochem Biophys,* 422, 137-44.

KOIVISTO, A. M., ALA-MELLO, S., LEMMELA, S., KOMU, H. A., RAUTIO, J. & JARVELA, I. 2007. Screening of mutations in the PHF8 gene and identification of a novel mutation in a Finnish family with XLMR and cleft lip/cleft palate. *Clin Genet,* 72, 145-9.

KOIVUNEN, P., HIRSILÄ, M., GÜNZLER, V., KIVIRIKKO, K. I. & MYLLYHARJU, J. 2004. Catalytic Properties of the Asparaginyl Hydroxylase (FIH) in the Oxygen Sensing Pathway Are Distinct from Those of Its Prolyl 4-Hydroxylases. 279, 9899-9904.

KOONIN, E. V. 1993. A common set of conserved motifs in a vast variety of putative nucleic acid-dependent ATPases including MCM proteins involved in the initiation of eukaryotic DNA replication. *Nucleic Acids Res,* 21, 2541-7.

KOTSANTIS, P., PETERMANN, E. & BOULTON, S. J. 2018. Mechanisms of Oncogene-Induced Replication Stress: Jigsaw Falling into Place. *Cancer discovery,* 8, 537-555.

KOUWAKI, T., OKAMOTO, T., ITO, A., SUGIYAMA, Y., YAMASHITA, K., SUZUKI, T., KUSAKABE, S., HIRANO, J., FUKUHARA, T., YAMASHITA, A., SAITO, K., OKUZAKI, D., WATASHI, K., SUGIYAMA, M., YOSHIO, S., STANDLEY, D. M., KANTO, T., MIZOKAMI, M., MORIISHI, K. & MATSUURA, Y. 2016. Hepatocyte Factor JMJD5 Regulates Hepatitis B Virus Replication through Interaction with HBx. *J Virol,* 90, 3530-42.

KOVALEVICH, J. & LANGFORD, D. 2013. Considerations for the use of SH-SY5Y neuroblastoma cells in neurobiology. *Methods Mol Biol,* 1078, 9-21.

KOYANAGI-AOI, M., OHNUKI, M., TAKAHASHI, K., OKITA, K., NOMA, H., SAWAMURA, Y., TERAMOTO, I., NARITA, M., SATO, Y., ICHISAKA, T., AMANO, N., WATANABE, A., MORIZANE, A., YAMADA, Y., SATO, T., TAKAHASHI, J. & YAMANAKA, S. 2013. Differentiation-defective phenotypes revealed by large-scale analyses of human pluripotent stem cells. *Proc Natl Acad Sci U S A,* 110, 20569-74.

KRASILNIKOVA, M. M. & MIRKIN, S. M. 2004. Replication stalling at Friedreich's ataxia (GAA)n repeats in vivo. *Mol Cell Biol,* 24, 2286-95.

KROEZE, S. G., VERMAAT, J. S., VAN BRUSSEL, A., VAN MELICK, H. H., VOEST, E. E., JONGES, T. G., VAN DIEST, P. J., HINRICHS, J., BOSCH, J. L. & JANS, J. J. 2010. Expression of nuclear FIH independently predicts overall survival of clear cell renal cell carcinoma patients. *Eur J Cancer,* 46, 3375-82.

KUMAR, S., IWAO, M., YAMAGISHI, T., NODA, M. & ASASHIMA, M. 1993. Expression of GTP-binding protein gene drg during Xenopus laevis development. *Int J Dev Biol,* 37, 539-46.

KUMAR, S., TOMOOKA, Y. & NODA, M. 1992. Identification of a set of genes with developmentally down-regulated expression in the mouse brain. *Biochem Biophys Res Commun,* 185**,** 1155-61.

KUNKEL, T. A. & ERIE, D. A. 2015. Eukaryotic Mismatch Repair in Relation to DNA Replication. *Annual Review of Genetics,* 49**,** 291-313.

KUNNEV, D., RUSINIAK, M. E., KUDLA, A., FREELAND, A., CADY, G. K. & PRUITT, S. C. 2010. DNA damage response and tumorigenesis in Mcm2-deficient mice. *Oncogene,* 29, 3630-3638.

KUO, A. J., SONG, J., CHEUNG, P., ISHIBE-MURAKAMI, S., YAMAZOE, S., CHEN, J. K., PATEL, D. J. & GOZANI, O. 2012. The BAH domain of ORC1 links H4K20me2 to DNA replication licensing and Meier-Gorlin syndrome. *Nature,* 484**,** 115-9.

KWON, C. H., LUIKART, B. W., POWELL, C. M., ZHOU, J., MATHENY, S. A., ZHANG, W., LI, Y., BAKER, S. J. & PARADA, L. F. 2006. Pten Regulates Neuronal Arborization and Social Interaction in Mice. *Neuron,* 50**,** 377-388.

LAMB, R., FIORILLO, M., CHADWICK, A., OZSVARI, B., REEVES, K. J., SMITH, D. L., CLARKE, R. B., HOWELL, S. J., CAPPELLO, A. R., MARTINEZ-OUTSCHOORN, U. E., PEIRIS-PAGÈS, M., SOTGIA, F. & LISANTI, M. P. 2015. Doxycycline down-regulates DNA-PK and radiosensitizes tumor initiating cells: Implications for more effective radiation therapy. *Oncotarget,* 6**,** 14005-14025.

LANDO, D., PEET, D. J., GORMAN, J. J., WHELAN, D. A., WHITELAW, M. L. & BRUICK, R. K. 2002. FIH-1 is an asparaginyl hydroxylase enzyme that regulates the transcriptional activity of hypoxia-inducible factor. *Genes Dev,* 16**,** 1466-71.

LAUMONNIER, F., HOLBERT, S., RONCE, N., FARAVELLI, F., LENZNER, S., SCHWARTZ, C. E., LESPINASSE, J., VAN ESCH, H., LACOMBE, D., GOIZET, C., PHAN-DINH TUY, F., VAN BOKHOVEN, H., FRYNS, J. P., CHELLY, J., ROPERS, H. H., MORAINE, C., HAMEL, B. C. & BRIAULT, S. 2005. Mutations in PHF8 are associated with X linked mental retardation and cleft lip/cleft palate. *J Med Genet,* 42**,** 780-6.

LEDERER, D., GRISART, B., DIGILIO, M. C., BENOIT, V., CRESPIN, M., GHARIANI, S. C., MAYSTADT, I., DALLAPICCOLA, B. & VERELLEN-DUMOULIN, C. 2012. Deletion of KDM6A, a histone demethylase interacting with MLL2, in three patients with Kabuki syndrome. *Am J Hum Genet,* 90**,** 119-24.

LEDERER, D., SHEARS, D., BENOIT, V., VERELLEN-DUMOULIN, C. & MAYSTADT, I. 2014. A three generation X-linked family with Kabuki syndrome phenotype and a frameshift mutation in KDM6A. *Am J Med Genet A,* 164a**,** 1289-92.

LEE, J.-K. & HURWITZ, J. 2001. Processive DNA helicase activity of the minichromosome maintenance proteins 4, 6, and 7 complex requires forked DNA structures. *Proceedings of the National Academy of Sciences,* 98**,** 54.

LEE, J., KUMAGAI, A. & DUNPHY, W. G. 2007. The Rad9-Hus1-Rad1 checkpoint clamp regulates interaction of TopBP1 with ATR. *J Biol Chem,* 282**,** 28036-44.

LEE, K. M., CHOI, K. H. & OUELLETTE, M. M. 2004. Use of exogenous hTERT to immortalize primary human cells. *Cytotechnology,* 45**,** 33-8.

LEE, S.-H., JEYAPALAN, J. N., APPLEBY, V., MOHAMED NOOR, D. A., SOTTILE, V. & SCOTTING, P. J. 2010. Dynamic methylation and expression of Oct4 in early neural stem cells. *Journal of anatomy,* 217**,** 203-213.

LEE, S. H., LEE, E. H., LEE, S. H., LEE, Y. M., KIM, H. D. & KIM, Y. Z. 2015. Epigenetic Role of Histone 3 Lysine Methyltransferase and Demethylase in Regulating Apoptosis Predicting the Recurrence of Atypical Meningioma. *J Korean Med Sci,* 30**,** 1157-66.

LEE, Y.-R., CHEN, M., LEE, J. D., ZHANG, J., LIN, S.-Y., FU, T.-M., CHEN, H., ISHIKAWA, T., CHIANG, S.-Y., KATON, J., ZHANG, Y., SHULGA, Y. V., BESTER, A. C., FUNG, J., MONTELEONE, E., WAN, L., SHEN, C., HSU, C.-H., PAPA, A., CLOHESSY, J. G., TERUYA-FELDSTEIN, J., JAIN, S., WU, H., MATESIC, L., CHEN, R.-H., WEI, W. & PANDOLFI, P. P. 2019. Reactivation of PTEN tumor suppressor for cancer treatment through inhibition of a MYC-WWP1 inhibitory pathway. *Science,* 364**,** eaau0159.

LEE, Y. F., MILLER, L. D., CHAN, X. B., BLACK, M. A., PANG, B., ONG, C. W., SALTO-TELLEZ, M., LIU, E. T. & DESAI, K. V. 2012. JMJD6 is a driver of cellular proliferation and motility and a marker of poor prognosis in breast cancer. *Breast Cancer Research,* 14**,** 3001.

LEIGHT, E. R. & SUGDEN, B. 2000. EBNA-1: a protein pivotal to latent infection by Epstein-Barr virus. *Rev Med Virol,* 10**,** 83-100.

LEIPE, D. D., WOLF, Y. I., KOONIN, E. V. & ARAVIND, L. 2002. Classification and evolution of P-loop GTPases and related ATPases. *J Mol Biol,* 317**,** 41-72.

LEMAN, A. R. & NOGUCHI, E. 2012. Local and global functions of Timeless and Tipin in replication fork protection. *Cell Cycle,* 11**,** 3945-55.

LESZCZYNSKA, K. B., DOBRYNIN, G., LESLIE, R. E., IENT, J., BOUMELHA, A. J., SENRA, J. M., HAWKINS, M. A., MAUGHAN, T., MUKHERJEE, S. & HAMMOND, E. M. 2016. Preclinical testing of an ATR inhibitor demonstrates improved response to standard therapies for esophageal cancer. *Radiotherapy and Oncology,* 121**,** 232-238.

LETURCQ, M., MORTUAIRE, M., HARDIVILLE, S., SCHULZ, C., LEFEBVRE, T. & VERCOUTTER-EDOUART, A. S. 2018. O-GlcNAc transferase associates with the MCM2-7 complex and its silencing destabilizes MCM-MCM interactions. *Cell Mol Life Sci,* 75**,** 4321-4339.

LI, B. & TRUEB, B. 2000. DRG represents a family of two closely related GTP-binding proteins. *Biochim Biophys Acta,* 1491**,** 196-204.

LI, N., ZHAI, Y., ZHANG, Y., LI, W., YANG, M., LEI, J., TYE, B.-K. & GAO, N. 2015. Structure of the eukaryotic MCM complex at 3.8 Å. *Nature,* 524**,** 186.

LI, W., KIM, S. M., LEE, J. & DUNPHY, W. G. 2004. Absence of BLM leads to accumulation of chromosomal DNA breaks during both unperturbed and disrupted S phases. *J Cell Biol,* 165**,** 801-12.

LI, X.-J., DU, Z.-W., ZARNOWSKA, E. D., PANKRATZ, M., HANSEN, L. O., PEARCE, R. A. & ZHANG, S.-C. 2005. Specification of motoneurons from human embryonic stem cells. *Nature Biotechnology,* 23**,** 215-221.

LI, X.-J., ZHANG, X., JOHNSON, M. A., WANG, Z.-B., LAVAUTE, T. & ZHANG, S.-C. 2009. Coordination of sonic hedgehog and Wnt signaling determines ventral and dorsal telencephalic neuron types from human embryonic stem cells. *Development,* 136**,** 4055.

LI, Z. & XU, X. 2019. Post-Translational Modifications of the Mini-Chromosome Maintenance Proteins in DNA Replication. *Genes,* 10**,** 331.

LIANG, G., HE, J. & ZHANG, Y. 2012. Kdm2b promotes induced pluripotent stem cell generation by facilitating gene activation early in reprogramming. *Nature cell biology,* 14**,** 457-466.

LIAO, H., WINKFEIN, R. J., MACK, G., RATTNER, J. B. & YEN, T. J. 1995. CENP-F is a protein of the nuclear matrix that assembles onto kinetochores at late G2 and is rapidly degraded after mitosis. *J Cell Biol,* 130**,** 507-18.

LIKU, M. E., NGUYEN, V. Q., ROSALES, A. W., IRIE, K. & LI, J. J. 2005. CDK phosphorylation of a novel NLS-NES module distributed between two subunits of the Mcm2-7 complex prevents chromosomal rereplication. *Molecular biology of the cell,* 16**,** 5026-5039.

LIN, D. I., AGGARWAL, P. & DIEHL, J. A. 2008. Phosphorylation of MCM3 on Ser-112 regulates its incorporation into the MCM2-7 complex. *Proceedings of the National Academy of Sciences of the United States of America,* 105**,** 8079-8084.

LISTER, R., PELIZZOLA, M., KIDA, Y. S., HAWKINS, R. D., NERY, J. R., HON, G., ANTOSIEWICZ-BOURGET, J., O'MALLEY, R., CASTANON, R., KLUGMAN, S., DOWNES, M., YU, R., STEWART, R., REN, B., THOMSON, J. A., EVANS, R. M. & ECKER, J. R. 2011. Hotspots of aberrant epigenomic reprogramming in human induced pluripotent stem cells. *Nature,* 471**,** 68-73.

LIU, H., WANG, C., LEE, S., DENG, Y., WITHER, M., OH, S., NING, F., DEGE, C., ZHANG, Q., LIU, X., JOHNSON, A. M., ZANG, J., CHEN, Z., JANKNECHT, R., HANSEN, K., MARRACK, P., LI, C. Y., KAPPLER, J. W., HAGMAN, J. & ZHANG, G. 2017. Clipping of arginine-methylated histone tails by JMJD5 and JMJD7. *Proc Natl Acad Sci U S A,* 114**,** E7717-e7726.

LIU, H., WANG, C., LEE, S., NING, F., WANG, Y., ZHANG, Q., CHEN, Z., ZANG, J., NIX, J., DAI, S., MARRACK, P., HAGMAN, J., KAPPLER, J. & ZHANG, G. 2018a. Specific Recognition of Arginine Methylated Histone Tails by JMJD5 and JMJD7. *Sci Rep,* 8**,** 3275.

LIU, Y., ARAI, A., KIM, T., KIM, S., PARK, N. H. & KIM, R. H. 2018b. Histone Demethylase Jmjd7 Negatively Regulates Differentiation of Osteoclast. *Chin J Dent Res,* 21**,** 113-118.

LIU, Y., LONG, Y. H., WANG, S. Q., ZHANG, Y. Y., LI, Y. F., MI, J. S., YU, C. H., LI, D. Y., ZHANG, J. H. & ZHANG, X. J. 2019. JMJD6 regulates histone H2A.X phosphorylation and promotes autophagy in triple-negative breast cancer cells via a novel tyrosine kinase activity. *Oncogene,* 38**,** 980-997.

LIVAK, K. J., Schmittgen, T.D. 2001. Analysis of relative gene expression data using real-time quantitative PCR and the 2(-Delta Delta C(T)) Method. *Methods*, 25 (4), 402-408

LJUNGMAN, M. 2007. The transcription stress response. *Cell Cycle,* 6**,** 2252-7.

LOCATELLI, F., FISHBANE, S., BLOCK, G. A. & MACDOUGALL, I. C. 2017. Targeting Hypoxia-Inducible Factors for the Treatment of Anemia in Chronic Kidney Disease Patients. *American Journal of Nephrology,* 45**,** 187-199.

LOENARZ, C. & SCHOFIELD, C. J. 2011. Physiological and biochemical aspects of hydroxylations and demethylations catalyzed by human 2-oxoglutarate oxygenases. *Trends in Biochemical Sciences,* 36**,** 7-18.

LOGAN, C. V., MURRAY, J. E., PARRY, D. A., ROBERTSON, A., BELLELLI, R., TARNAUSKAITĖ, Ž., CHALLIS, R., CLEAL, L., BOREL, V., FLUTEAU, A., SANTOYO-LOPEZ, J., CONSORTIUM, S. G. P., AITMAN, T., BARROSO, I., BASEL, D.,

BICKNELL, L. S., GOEL, H., HU, H., HUFF, C., HUTCHISON, M., JOYCE, C., KNOX, R., LACROIX, A. E., LANGLOIS, S., MCCANDLESS, S., MCCARRIER, J., METCALFE, K. A., MORRISSEY, R., MURPHY, N., NETCHINE, I., O'CONNELL, S. M., OLNEY, A. H., PARIA, N., ROSENFELD, J. A., SHERLOCK, M., SYVERSON, E., WHITE, P. C., WISE, C., YU, Y., ZACHARIN, M., BANERJEE, I., REIJNS, M., BOBER, M. B., SEMPLE, R. K., BOULTON, S. J., RIOS, J. J. & JACKSON, A. P. 2018. DNA Polymerase Epsilon Deficiency Causes IMAGe Syndrome with Variable Immunodeficiency. *American journal of human genetics,* 103, 1038-1044.

LOH, Y.-H., WU, Q., CHEW, J.-L., VEGA, V. B., ZHANG, W., CHEN, X., BOURQUE, G., GEORGE, J., LEONG, B., LIU, J., WONG, K.-Y., SUNG, K. W., LEE, C. W. H., ZHAO, X.-D., CHIU, K.-P., LIPOVICH, L., KUZNETSOV, V. A., ROBSON, P., STANTON, L. W., WEI, C.-L., RUAN, Y., LIM, B. & NG, H.-H. 2006. The Oct4 and Nanog transcription network regulates pluripotency in mouse embryonic stem cells. *Nature Genetics,* 38, 431-440.

LOPES, F. M., SCHRODER, R., DA FROTA, M. L., JR., ZANOTTO-FILHO, A., MULLER, C. B., PIRES, A. S., MEURER, R. T., COLPO, G. D., GELAIN, D. P., KAPCZINSKI, F., MOREIRA, J. C., FERNANDES MDA, C. & KLAMT, F. 2010. Comparison between proliferative and neuron-like SH-SY5Y cells as an in vitro model for Parkinson disease studies. *Brain Res,* 1337, 85-94.

LOPEZ-CARBALLO, G., MORENO, L., MASIA, S., PEREZ, P. & BARETTINO, D. 2002. Activation of the phosphatidylinositol 3-kinase/Akt signaling pathway by retinoic acid is required for neural differentiation of SH-SY5Y human neuroblastoma cells. *J Biol Chem,* 277, 25297-304.

LOPEZ-GIRONA, A., TANAKA, K., CHEN, X. B., BABER, B. A., MCGOWAN, C. H. & RUSSELL, P. 2001. Serine-345 is required for Rad3-dependent phosphorylation and function of checkpoint kinase Chk1 in fission yeast. *Proc Natl Acad Sci U S A,* 98, 11289-94.

LOSMAN, J.-A. & KAELIN, W. G., JR. 2013. What a difference a hydroxyl makes: mutant IDH, (R)-2-hydroxyglutarate, and cancer. *Genes & development,* 27, 836-852.

LU, D. H., YANG, J., GAO, L. K., MIN, J., TANG, J. M., HU, M., LI, Y., LI, S. T., CHEN, J. & HONG, L. 2019. Lysine demethylase 2A promotes the progression of ovarian cancer by regulating the PI3K pathway and reversing epithelialmesenchymal transition. *Oncol Rep,* 41, 917-927.

LUCA, R., AVERNA, M., ZALFA, F., VECCHI, M., BIANCHI, F., LA FATA, G., DEL NONNO, F., NARDACCI, R., BIANCHI, M., NUCIFORO, P., MUNCK, S., PARRELLA, P., MOURA, R., SIGNORI, E., ALSTON, R., KUCHNIO, A., FARACE, M. G., FAZIO, V. M., PIACENTINI, M., DE STROOPER, B., ACHSEL, T., NERI, G., NEVEN, P., EVANS, D. G., CARMELIET, P., MAZZONE, M. & BAGNI, C. 2013. The fragile X protein binds mRNAs involved in cancer progression and modulates metastasis formation. *EMBO Mol Med,* 5, 1523-36.

LUCAS, R. E., VLANGOS, C. N., DAS, P., PATEL, P. I. & ELSEA, S. H. 2001. Genomic organisation of the ∼1.5 Mb Smith-Magenis syndrome critical interval: Transcription map, genomic contig, and candidate gene analysis. *European Journal of Human Genetics,* 9, 892-902.

LUKAS, C., SAVIC, V., BEKKER-JENSEN, S., DOIL, C., NEUMANN, B., PEDERSEN, R. S., GROFTE, M., CHAN, K. L., HICKSON, I. D., BARTEK, J. & LUKAS, J. 2011. 53BP1 nuclear bodies form around DNA lesions generated by mitotic transmission of chromosomes under replication stress. *Nat Cell Biol,* 13, 243-53.

LYALL, K., CROEN, L., DANIELS, J., FALLIN, M. D., LADD-ACOSTA, C., LEE, B. K., PARK, B. Y., SNYDER, N. W., SCHENDEL, D., VOLK, H., WINDHAM, G. C. & NEWSCHAFFER, C. 2017. The Changing Epidemiology of Autism Spectrum Disorders. *Annual review of public health,* 38, 81-102.

MA, Y., JIN, J., DONG, C., CHENG, E.-C., LIN, H., HUANG, Y. & QIU, C. 2010. High-efficiency siRNA-based gene knockdown in human embryonic stem cells. *RNA (New York, N.Y.),* 16, 2564-2569.

MACHERET, M. & HALAZONETIS, T. D. 2015. DNA Replication Stress as a Hallmark of Cancer. *Annual Review of Pathology: Mechanisms of Disease,* 10, 425-448.

MAGDALOU, I., LOPEZ, B. S., PASERO, P. & LAMBERT, S. A. E. 2014. The causes of replication stress and their consequences on genome stability and cell fate. *Seminars in Cell & Developmental Biology,* 30, 154-164.

MAHON, P. C., HIROTA, K. & SEMENZA, G. L. 2001. FIH-1: a novel protein that interacts with HIF-1alpha and VHL to mediate repression of HIF-1 transcriptional activity. *Genes & development,* 15, 2675-2686.

MAINE, G. T., SINHA, P. & TYE, B. K. 1984. Mutants of S. cerevisiae defective in the maintenance of minichromosomes. *Genetics,* 106, 365-85.

MAJKA, J., BINZ, S. K., WOLD, M. S. & BURGERS, P. M. 2006. Replication protein A directs loading of the DNA damage checkpoint clamp to 5'-DNA junctions. *J Biol Chem,* 281, 27855-61.

MANI, M., LEE, U. H., YOON, N. A., KIM, H. J., KO, M. S., SEOL, W., JOE, Y., CHUNG, H. T., LEE, B. J., MOON, C. H., CHO, W. J. & PARK, J. W. 2016. Developmentally regulated GTP-binding protein 2 coordinates Rab5 activity and transferrin recycling. *Mol Biol Cell,* 27, 334-48.

MANI, M., LEE, U. H., YOON, N. A., YOON, E. H., LEE, B. J., CHO, W. J. & PARK, J. W. 2017. Developmentally regulated GTP-binding protein 2 is required for stabilization of Rac1-positive membrane tubules. *Biochem Biophys Res Commun,* 493, 758-764.

MANIS, J. P., MORALES, J. C., XIA, Z., KUTOK, J. L., ALT, F. W. & CARPENTER, P. B. 2004. 53BP1 links DNA damage-response pathways to immunoglobulin heavy chain class-switch recombination. *Nature Immunology,* 5, 481-487.

MARCON, E., NI, Z., PU, S., TURINSKY, A. L., TRIMBLE, S. S., OLSEN, J. B., SILVERMAN-GAVRILA, R., SILVERMAN-GAVRILA, L., PHANSE, S., GUO, H., ZHONG, G., GUO, X., YOUNG, P., BAILEY, S., ROUDEVA, D., ZHAO, D., HEWEL, J., LI, J., GRASLUND, S., PADUCH, M., KOSSIAKOFF, A. A., LUPIEN, M., EMILI, A., WODAK, S. J. & GREENBLATT, J. 2014. Human-chromatin-related protein interactions identify a demethylase complex required for chromosome segregation. *Cell Rep,* 8, 297-310.

MARIANI, J., COPPOLA, G., ZHANG, P., ABYZOV, A., PROVINI, L., TOMASINI, L., AMENDUNI, M., SZEKELY, A., PALEJEV, D., WILSON, M., GERSTEIN, M., GRIGORENKO, E. L., CHAWARSKA, K., PELPHREY, K. A., HOWE, J. R. & VACCARINO, F. M. 2015. FOXG1-Dependent Dysregulation of GABA/Glutamate Neuron Differentiation in Autism Spectrum Disorders. *Cell,* 162, 375-390.

MARKOLOVIC, S., LEISSING, T. M., CHOWDHURY, R., WILKINS, S. E., LU, X. & SCHOFIELD, C. J. 2016. Structure—function relationships of human JmjC oxygenases—demethylases versus hydroxylases. *Current Opinion in Structural Biology,* 41, 62-72.

MARKOLOVIC, S., ZHUANG, Q., WILKINS, S. E., EATON, C. D., ABBOUD, M. I., KATZ, M. J., MCNEIL, H. E., LESNIAK, R. K., HALL, C., STRUWE, W. B., KONIETZNY, R., DAVIS, S., YANG, M., GE, W., BENESCH, J. L. P., KESSLER, B. M., RATCLIFFE, P. J., COCKMAN, M. E., FISCHER, R., WAPPNER, P., CHOWDHURY, R., COLEMAN, M. L. & SCHOFIELD, C. J. 2018. The Jumonji-C oxygenase JMJD7 catalyzes (3S)-lysyl hydroxylation of TRAFAC GTPases. *Nat Chem Biol,* 14, 688-695.

MATHEWS, M. B. & HERSHEY, J. W. 2015. The translation factor eIF5A and human cancer. *Biochim Biophys Acta,* 1849, 836-44.

MATSUNAMI, N., HENSEL, C. H., BAIRD, L., STEVENS, J., OTTERUD, B., LEPPERT, T., VARVIL, T., HADLEY, D., GLESSNER, J. T., PELLEGRINO, R., KIM, C., THOMAS, K., WANG, F., OTIENO, F. G., HO, K., CHRISTENSEN, G. B., LI, D., PREKERIS, R., LAMBERT, C. G., HAKONARSON, H. & LEPPERT, M. F. 2014. Identification of rare DNA sequence variants in high-risk autism families and their prevalence in a large case/control population. *Molecular Autism,* 5, 5.

MCCULLOCH, S. D. & KUNKEL, T. A. 2008. The fidelity of DNA synthesis by eukaryotic replicative and translesion synthesis polymerases. *Cell Res,* 18, 148-61.

MCDONOUGH, M. A., LOENARZ, C., CHOWDHURY, R., CLIFTON, I. J. & SCHOFIELD, C. J. 2010. Structural studies on human 2-oxoglutarate dependent oxygenases. *Current Opinion in Structural Biology,* 20, 659-672.

MCNEILL, L. A., HEWITSON, K. S., GLEADLE, J. M., HORSFALL, L. E., OLDHAM, N. J., MAXWELL, P. H., PUGH, C. W., RATCLIFFE, P. J. & SCHOFIELD, C. J. 2002. The use of dioxygen by HIF prolyl hydroxylase (PHD1). *Bioorg Med Chem Lett,* 12, 1547-50.

MEIKLE, L., POLLIZZI, K., EGNOR, A., KRAMVIS, I., LANE, H., SAHIN, M. & KWIATKOWSKI, D. J. 2008. Response of a Neuronal Model of Tuberous Sclerosis to Mammalian Target of Rapamycin (mTOR) Inhibitors: Effects on mTORC1 and Akt Signaling Lead to Improved Survival and Function. *The Journal of Neuroscience,* 28, 5422.

MEJLVANG, J., FENG, Y., ALABERT, C., NEELSEN, K. J., JASENCAKOVA, Z., ZHAO, X., LEES, M., SANDELIN, A., PASERO, P., LOPES, M. & GROTH, A. 2014. New histone supply regulates replication fork speed and PCNA unloading. *The Journal of Cell Biology,* 204, 29.

MEMBERG, S. P. & HALL, A. K. 1995. Dividing neuron precursors express neuron-specific tubulin. *J Neurobiol,* 27, 26-43.

MERBL, Y., REFOUR, P., PATEL, H., SPRINGER, M. & KIRSCHNER, M. W. 2013. Profiling of ubiquitin-like modifications reveals features of mitotic control. *Cell,* 152, 1160-72.

MIEULET, V. & LAMB, R. F. 2010. Tuberous sclerosis complex: linking cancer to metabolism. *Trends in Molecular Medicine,* 16, 329-335.

MINOCHERHOMJI, S., YING, S., BJERREGAARD, V. A., BURSOMANNO, S., ALELIUNAITE, A., WU, W., MANKOURI, H. W., SHEN, H., LIU, Y. & HICKSON, I. D. 2015. Replication stress activates DNA repair synthesis in mitosis. *Nature,* 528, 286-90.

MIYAKE, N., MIZUNO, S., OKAMOTO, N., OHASHI, H., SHIINA, M., OGATA, K., TSURUSAKI, Y., NAKASHIMA, M., SAITSU, H., NIIKAWA, N. & MATSUMOTO, N. 2013. KDM6A Point Mutations Cause Kabuki Syndrome. *Human Mutation,* 34, 108-110.

MIZUSHIMA, T., TAKAHASHI, N. & STILLMAN, B. 2000. Cdc6p modulates the structure and DNA binding activity of the origin recognition complex in vitro. *Genes & development,* 14, 1631-1641.

MOEGLIN, E., DESPLANCQ, D., CONIC, S., OULAD-ABDELGHANI, M., STOESSEL, A., CHIPER, M., VIGNERON, M., DIDIER, P., TORA, L. & WEISS, E. 2019. Uniform Widespread Nuclear Phosphorylation of Histone H2AX Is an Indicator of Lethal DNA Replication Stress. *Cancers (Basel),* 11.

MOLDOVAN, G. L., PFANDER, B. & JENTSCH, S. 2007. PCNA, the maestro of the replication fork. *Cell,* 129, 665-79.

MORALES, J., LI, L., FATTAH, F. J., DONG, Y., BEY, E. A., PATEL, M., GAO, J. & BOOTHMAN, D. A. 2014. Review of poly (ADP-ribose) polymerase (PARP) mechanisms of action and rationale for targeting in cancer and other diseases. *Crit Rev Eukaryot Gene Expr,* 24, 15-28.

MORAND, K., TALBO, G. & MANN, M. 1993. Oxidation of peptides during electrospray ionization. *Rapid Communications in Mass Spectrometry,* 7, 738-743.

MORDES, D. A., GLICK, G. G., ZHAO, R. & CORTEZ, D. 2008. TopBP1 activates ATR through ATRIP and a PIKK regulatory domain. *Genes Dev,* 22, 1478-89.

MORENO, A., CARRINGTON, J. T., ALBERGANTE, L., AL MAMUN, M., HAAGENSEN, E. J., KOMSELI, E.-S., GORGOULIS, V. G., NEWMAN, T. J. & BLOW, J. J. 2016. Unreplicated DNA remaining from unperturbed S phases passes through mitosis for resolution in daughter cells. *Proceedings of the National Academy of Sciences,* 113, E5757.

MORENO, S. P., BAILEY, R., CAMPION, N., HERRON, S. & GAMBUS, A. 2014. Polyubiquitylation drives replisome disassembly at the termination of DNA replication. *Science,* 346, 477-81.

MORI, T., OKAMOTO, K., TANAKA, Y., TEYE, K., UMATA, T., OHNEDA, K., TOKUYAMA, K., OKABE, M. & TSUNEOKA, M. 2013. Ablation of Mina53 in Mice Reduces Allergic Response in the Airways. *Cell Structure and Function,* 38, 155-167.

MOYER, S. E., LEWIS, P. W. & BOTCHAN, M. R. 2006. Isolation of the Cdc45/Mcm2-7/GINS (CMG) complex, a candidate for the eukaryotic DNA replication fork helicase. *Proc Natl Acad Sci U S A,* 103, 10236-10241.

MÜLLER, H. M., FIEGL, H., GOEBEL, G., HUBALEK, M. M., WIDSCHWENDTER, A., MÜLLER-HOLZNER, E., MARTH, C. & WIDSCHWENDTER, M. 2003. MeCP2 and MBD2 expression in human neoplastic and non-neoplastic breast tissue and its association with oestrogen receptor status. *British journal of cancer,* 89, 1934-1939.

MUNEHIRA, Y., YANG, Z. & GOZANI, O. 2017. Systematic Analysis of Known and Candidate Lysine Demethylases in the Regulation of Myoblast Differentiation. *J Mol Biol,* 429, 2055-2065.

MURRAY, JENNIE E., VAN DER BURG, M., IJSPEERT, H., CARROLL, P., WU, Q., OCHI, T., LEITCH, A., MILLER, EDWARD S., KYSELA, B., JAWAD, A., BOTTANI, A., BRANCATI, F., CAPPA, M., CORMIER-DAIRE, V., DESHPANDE, C., FAQEIH, EISSA A., GRAHAM, GAIL E., RANZA, E., BLUNDELL, TOM L., JACKSON, ANDREW P., STEWART, GRANT S. & BICKNELL, LOUISE S. 2015. Mutations in the NHEJ Component XRCC4 Cause Primordial Dwarfism. *The American Journal of Human Genetics,* 96, 412-424.

MUTREJA, K., KRIETSCH, J., HESS, J., URSICH, S., BERTI, M., ROESSLER, F. K., ZELLWEGER, R., PATRA, M., GASSER, G. & LOPES, M. 2018. ATR-Mediated Global Fork Slowing and Reversal Assist Fork Traverse and Prevent Chromosomal Breakage at DNA Interstrand Cross-Links. *Cell Rep,* 24, 2629-2642.e5.

NADARAJAH, B. & PARNAVELAS, J. G. 2002. Modes of neuronal migration in the developing cerebral cortex. *Nat Rev Neurosci,* 3, 423-32.

NAKAMINE, A., OUCHANOV, L., JIMENEZ, P., MANGHI, E. R., ESQUIVEL, M., MONGE, S., FALLAS, M., BURTON, B. K., SZOMJU, B., ELSEA, S. H., MARSHALL, C. R., SCHERER, S. W. & MCINNES, L. A. 2008. Duplication of 17(p11.2p11.2) in a male child with autism and severe language delay. *Am J Med Genet A,* 146a, 636-43.

NASU, M., TAKATA, N., DANJO, T., SAKAGUCHI, H., KADOSHIMA, T., FUTAKI, S., SEKIGUCHI, K., EIRAKU, M. & SASAI, Y. 2013. Robust Formation and Maintenance of Continuous Stratified Cortical Neuroepithelium by Laminin-Containing Matrix in Mouse ES Cell Culture. *PLOS ONE,* 7, e53024.

NEGRINI, S., GORGOULIS, V. G. & HALAZONETIS, T. D. 2010. Genomic instability — an evolving hallmark of cancer. *Nature Reviews Molecular Cell Biology,* 11, 220-228.

NETCHINE, I., AZZI, S., LE BOUC, Y. & SAVAGE, M. O. 2011. IGF1 molecular anomalies demonstrate its critical role in fetal, postnatal growth and brain development. *Best Pract Res Clin Endocrinol Metab,* 25, 181-90.

NEWMAN, A. M. & COOPER, J. B. 2010. Lab-specific gene expression signatures in pluripotent stem cells. *Cell Stem Cell,* 7, 258-62.

NG, N., PURSHOUSE, K., FOSKOLOU, I. P., OLCINA, M. M. & HAMMOND, E. M. 2018. Challenges to DNA replication in hypoxic conditions. *The FEBS Journal,* 285, 1563-1571.

NIEMINUSZCZY, J., SCHWAB, R. A. & NIEDZWIEDZ, W. 2016. The DNA fibre technique - tracking helicases at work. *Methods,* 108, 92-8.

NISHIMURA, K., LEE, S. B., PARK, J. H. & PARK, M. H. 2012. Essential role of eIF5A-1 and deoxyhypusine synthase in mouse embryonic development. *Amino Acids,* 42**,** 703-10.

NISHIZAWA, Y., NISHIDA, N., KONNO, M., KAWAMOTO, K., ASAI, A., KOSEKI, J., TAKAHASHI, H., HARAGUCHI, N., NISHIMURA, J., HATA, T., MATSUDA, C., MIZUSHIMA, T., SATOH, T., DOKI, Y., MORI, M. & ISHII, H. 2017. Clinical Significance of Histone Demethylase NO66 in Invasive Colorectal Cancer. *Annals of Surgical Oncology,* 24**,** 841-849.

NOCTOR, S. C., MARTÍNEZ-CERDEÑO, V., IVIC, L. & KRIEGSTEIN, A. R. 2004. Cortical neurons arise in symmetric and asymmetric division zones and migrate through specific phases. *Nature Neuroscience,* 7**,** 136-144.

NOMA, A., ISHITANI, R., KATO, M., NAGAO, A., NUREKI, O. & SUZUKI, T. 2010. Expanding role of the jumonji C domain as an RNA hydroxylase. *J Biol Chem,* 285**,** 34503-7.

O'DRISCOLL, M., RUIZ-PEREZ, V. L., WOODS, C. G., JEGGO, P. A. & GOODSHIP, J. A. 2003. A splicing mutation affecting expression of ataxia-telangiectasia and Rad3-related protein (ATR) results in Seckel syndrome. *Nat Genet,* 33**,** 497-501.

OGI, T., WALKER, S., STIFF, T., HOBSON, E., LIMSIRICHAIKUL, S., CARPENTER, G., PRESCOTT, K., SURI, M., BYRD, P. J., MATSUSE, M., MITSUTAKE, N., NAKAZAWA, Y., VASUDEVAN, P., BARROW, M., STEWART, G. S., TAYLOR, A. M. R., O'DRISCOLL, M. & JEGGO, P. A. 2012. Identification of the First ATRIP–Deficient Patient and Novel Mutations in ATR Define a Clinical Spectrum for ATR–ATRIP Seckel Syndrome. *PLOS Genetics,* 8**,** e1002945.

OH, S. & JANKNECHT, R. 2012. Histone demethylase JMJD5 is essential for embryonic development. *Biochem Biophys Res Commun,* 420**,** 61-5.

OH, S., SHIN, S. & JANKNECHT, R. 2019. The small members of the JMJD protein family: Enzymatic jewels or jinxes? *Biochim Biophys Acta Rev Cancer,* 1871**,** 406-418.

OKADA, Y., SCOTT, G., RAY, M. K., MISHINA, Y. & ZHANG, Y. 2007. Histone demethylase JHDM2A is critical for Tnp1 and Prm1 transcription and spermatogenesis. *Nature,* 450**,** 119-23.

OKAMOTO, M., VAN STRY, M., CHUNG, L., KOYANAGI, M., SUN, X., SUZUKI, Y., OHARA, O., KITAMURA, H., HIJIKATA, A., KUBO, M. & BIX, M. 2009. Mina, an Il4 repressor, controls T helper type 2 bias. *Nature Immunology,* 10**,** 872.

OKITA, K., ICHISAKA, T. & YAMANAKA, S. 2007. Generation of germline-competent induced pluripotent stem cells. *Nature,* 448**,** 313-7.

OREKHOVA, E. V., STROGANOVA, T. A., NYGREN, G., TSETLIN, M. M., POSIKERA, I. N., GILLBERG, C. & ELAM, M. 2007. Excess of high frequency electroencephalogram oscillations in boys with autism. *Biol Psychiatry,* 62**,** 1022-9.

PAHLMAN, S., RUUSALA, A. I., ABRAHAMSSON, L., MATTSSON, M. E. & ESSCHER, T. 1984. Retinoic acid-induced differentiation of cultured human neuroblastoma cells: a comparison with phorbolester-induced differentiation. *Cell Differ,* 14**,** 135-44.

PAPE, T., MEKA, H., CHEN, S., VICENTINI, G., VAN HEEL, M. & ONESTI, S. 2003. Hexameric ring structure of the full-length archaeal MCM protein complex. *EMBO Rep,* 4**,** 1079-83.

PARIKSHAK, N. N., LUO, R., ZHANG, A., WON, H., LOWE, J. K., CHANDRAN, V., HORVATH, S. & GESCHWIND, D. H. 2013. Integrative functional genomic analyses implicate specific molecular pathways and circuits in autism. *Cell,* 155**,** 1008-21.

PARK, D. H., HONG, S. J., SALINAS, R. D., LIU, S. J., SUN, S. W., SGUALDINO, J., TESTA, G., MATZUK, M. M., IWAMORI, N. & LIM, D. A. 2014. Activation of neuronal gene expression by the JMJD3 demethylase is required for postnatal and adult brain neurogenesis. *Cell Rep,* 8**,** 1290-9.

PARK, M. H. & WOLFF, E. C. 2018. Hypusine, a polyamine-derived amino acid critical for eukaryotic translation. *J Biol Chem,* 293**,** 18710-18718.

PARRA, I. & WINDLE, B. 1993. High resolution visual mapping of stretched DNA by fluorescent hybridization. *Nature Genetics,* 5**,** 17-21.

PASION, S. G. & FORSBURG, S. L. 1999. Nuclear Localization of Schizosaccharomyces pombeMcm2/Cdc19p Requires MCM Complex Assembly. *Molecular Biology of the Cell,* 10**,** 4043-4057.

PERA, M. F., ANDRADE, J., HOUSSAMI, S., REUBINOFF, B., TROUNSON, A., STANLEY, E. G., OOSTWAARD, D. W.-V. & MUMMERY, C. 2004. Regulation of human embryonic stem cell differentiation by BMP-2 and its antagonist noggin. *Journal of Cell Science,* 117**,** 1269.

PETANJEK, Z., JUDAŠ, M., ŠIMIĆ, G., RAŠIN, M. R., UYLINGS, H. B. M., RAKIC, P. & KOSTOVIĆ, I. 2011. Extraordinary neoteny of synaptic spines in the human prefrontal cortex. *Proceedings of the National Academy of Sciences,* 108**,** 13281.

PETRELLI, F., PUCCI, L. & BEZZI, P. 2016. Astrocytes and Microglia and Their Potential Link with Autism Spectrum Disorders. 10.

PFEIFFER, B. E. & HUBER, K. M. 2007. Fragile X mental retardation protein induces synapse loss through acute postsynaptic translational regulation. *J Neurosci,* 27**,** 3120-30.

PICCOLO, S., SASAI, Y., LU, B. & DE ROBERTIS, E. M. 1996. Dorsoventral patterning in Xenopus: inhibition of ventral signals by direct binding of chordin to BMP-4. *Cell,* 86**,** 589-98.

PICHIERRI, P., ROSSELLI, F. & FRANCHITTO, A. 2003. Werner's syndrome protein is phosphorylated in an ATR/ATM-dependent manner following replication arrest and DNA damage induced during the S phase of the cell cycle. *Oncogene,* 22**,** 1491-500.

PILAZ, L. J. & SILVER, D. L. 2017. Moving messages in the developing brain-emerging roles for mRNA transport and local translation in neural stem cells. *FEBS Lett,* 591**,** 1526-1539.

PIRES-LUIS, A. S., VIEIRA-COIMBRA, M., VIEIRA, F. Q., COSTA-PINHEIRO, P., SILVA-SANTOS, R., DIAS, P. C., ANTUNES, L., LOBO, F., OLIVEIRA, J., GONCALVES, C. S., COSTA, B. M., HENRIQUE, R. & JERONIMO, C. 2015. Expression of histone methyltransferases as novel biomarkers for renal cell tumor diagnosis and prognostication. *Epigenetics,* 10**,** 1033-43.

PIRES, I. M., BENCOKOVA, Z., MILANI, M., FOLKES, L. K., LI, J. L., STRATFORD, M. R., HARRIS, A. L. & HAMMOND, E. M. 2010. Effects of acute versus chronic hypoxia on DNA damage responses and genomic instability. *Cancer Res,* 70**,** 925-35.

PIRES, I. M., OLCINA, M. M., ANBALAGAN, S., POLLARD, J. R., REAPER, P. M., CHARLTON, P. A., MCKENNA, W. G. & HAMMOND, E. M. 2012. Targeting radiation-resistant hypoxic tumour cells through ATR inhibition. *British Journal Of Cancer,* 107**,** 291.

PIRONE, L., XOLALPA, W., SIGURETHSSON, J. O., RAMIREZ, J., PEREZ, C., GONZALEZ, M., DE SABANDO, A. R., ELORTZA, F., RODRIGUEZ, M. S., MAYOR, U., OLSEN, J. V., BARRIO, R. & SUTHERLAND, J. D. 2017. A comprehensive platform for the analysis of ubiquitin-like protein modifications using in vivo biotinylation. *Sci Rep,* 7**,** 40756.

PLOUMAKIS, A. & COLEMAN, M. L. 2015. OH, the Places You'll Go! Hydroxylation, Gene Expression, and Cancer. *Mol Cell,* 58**,** 729-41.

PODUST, L. M., PODUST, V. N., SOGO, J. M. & HUBSCHER, U. 1995. Mammalian DNA polymerase auxiliary proteins: analysis of replication factor C-catalyzed proliferating cell nuclear antigen loading onto circular double-stranded DNA. *Mol Cell Biol,* 15**,** 3072-81.

POLI, J., TSAPONINA, O., CRABBE, L., KESZTHELYI, A., PANTESCO, V., CHABES, A., LENGRONNE, A. & PASERO, P. 2012. dNTP pools determine fork progression and origin usage under replication stress. *Embo j,* 31**,** 883-94.

POLLARD, P. J., LOENARZ, C., MOLE, D. R., MCDONOUGH, M. A., GLEADLE, J. M., SCHOFIELD, C. J. & RATCLIFFE, P. J. 2008. Regulation of Jumonji-domain-containing histone demethylases by hypoxia-inducible factor (HIF)-1alpha. *Biochem J,* 416**,** 387-94.

POPLAWSKI, A., GRABOWSKI, B., LONG, S. E. & KELMAN, Z. 2001. The Zinc Finger Domain of the Archaeal Minichromosome Maintenance Protein Is Required for Helicase Activity. *Journal of Biological Chemistry,* 276**,** 49371-49377.

POZO, P. N. & COOK, J. G. 2016. Regulation and Function of Cdt1; A Key Factor in Cell Proliferation and Genome Stability. *Genes,* 8**,** 2.

PRAKASH, S., JOHNSON, R. E. & PRAKASH, L. 2005. Eukaryotic translesion synthesis DNA polymerases: specificity of structure and function. *Annu Rev Biochem,* 74**,** 317-53.

PRESGRAVES, S. P., AHMED, T., BORWEGE, S. & JOYCE, J. N. 2004. Terminally differentiated SH-SY5Y cells provide a model system for studying neuroprotective effects of dopamine agonists. *Neurotox Res,* 5**,** 579-98.

PRIEGO MORENO, S., JONES, R. M., POOVATHUMKADAVIL, D., SCARAMUZZA, S. & GAMBUS, A. 2019. Mitotic replisome disassembly depends on TRAIP ubiquitin ligase activity. *Life science alliance,* 2**,** e201900390.

PROKHOROVA, T. A. & BLOW, J. J. 2000. Sequential MCM/P1 Subcomplex Assembly Is Required to Form a Heterohexamer with Replication Licensing Activity. 275**,** 2491-2498.

QIAN, Y. & CHEN, X. 2013. Senescence regulation by the p53 protein family. *Methods Mol Biol,* 965**,** 37-61.

QIAO, Y., LIU, X., HARVARD, C., HILDEBRAND, M. J., RAJCAN-SEPAROVIC, E., HOLDEN, J. J. & LEWIS, M. E. 2008. Autism-associated familial microdeletion of Xp11.22. *Clin Genet,* 74**,** 134-44.

QIN, Y., ZHAO, L., WANG, X., TONG, D., HOOVER, C., WU, F., LIU, Y., WANG, L., LIU, L., NI, L., SONG, T. & HUANG, C. 2017. MeCP2 regulated glycogenes contribute to proliferation and apoptosis of gastric cancer cells. *Glycobiology,* 27**,** 306-317.

QUINET, A., CARVAJAL-MALDONADO, D., LEMACON, D. & VINDIGNI, A. 2017. Chapter Three - DNA Fiber Analysis: Mind the Gap! *In:* EICHMAN, B. F. (ed.) *Methods in Enzymology.* Academic Press.

RAKIC, P. 2009. Evolution of the neocortex: a perspective from developmental biology. *Nature Reviews Neuroscience,* 10**,** 724-735.

RANGARAJU, V., TOM DIECK, S. & SCHUMAN, E. 2017. Local translation in neuronal compartments: how local is local? *EMBO reports,* 18.

RAPONI, E., AGENES, F., DELPHIN, C., ASSARD, N., BAUDIER, J., LEGRAVEREND, C. & DELOULME, J. C. 2007. S100B expression defines a state in which GFAP-expressing cells lose their neural stem cell potential and acquire a more mature developmental stage. *Glia,* 55**,** 165-77.

RAUCH, A., THIEL, C. T., SCHINDLER, D., WICK, U., CROW, Y. J., EKICI, A. B., VAN ESSEN, A. J., GOECKE, T. O., AL-GAZALI, L., CHRZANOWSKA, K. H., ZWEIER, C., BRUNNER, H. G., BECKER, K., CURRY, C. J., DALLAPICCOLA, B., DEVRIENDT, K., DORFLER, A., KINNING, E., MEGARBANE, A., MEINECKE, P., SEMPLE, R. K., SPRANGER, S., TOUTAIN, A., TREMBATH, R. C., VOSS, E., WILSON, L., HENNEKAM, R., DE ZEGHER, F., DORR, H. G. & REIS, A. 2008. Mutations in the pericentrin (PCNT) gene cause primordial dwarfism. *Science,* 319**,** 816-9.

RAYNAL, N. J., DA COSTA, E. M., LEE, J. T., GHARIBYAN, V., AHMED, S., ZHANG, H., SATO, T., MALOUF, G. G. & ISSA, J. J. 2017. Repositioning FDA-Approved Drugs in Combination with Epigenetic Drugs to Reprogram Colon Cancer Epigenome. *Mol Cancer Ther,* 16**,** 397-407.

REILLO, I. & BORRELL, V. 2011. Germinal Zones in the Developing Cerebral Cortex of Ferret: Ontogeny, Cell Cycle Kinetics, and Diversity of Progenitors. *Cerebral Cortex,* 22**,** 2039-2054.

REMUS, D., BEURON, F., TOLUN, G., GRIFFITH, J. D., MORRIS, E. P. & DIFFLEY, J. F. 2009. Concerted loading of Mcm2-7 double hexamers around DNA during DNA replication origin licensing. *Cell,* 139**,** 719-30.

REYES-GUTIERREZ, P., CARRASQUILLO-RODRIGUEZ, J. W. & IMBALZANO, A. N. 2019. Promotion of adipogenesis by JMJD6 requires the AT hook-like domain and is independent of its catalytic function. *PLoS One,* 14**,** e0216015.

REYNOLDS, J. J., BICKNELL, L. S., CARROLL, P., HIGGS, M. R., SHAHEEN, R., MURRAY, J. E., PAPADOPOULOS, D. K., LEITCH, A., MURINA, O., TARNAUSKAITE, Z., WESSEL, S. R., ZLATANOU, A., VERNET, A., VON KRIEGSHEIM, A., MOTTRAM, R. M., LOGAN, C. V., BYE, H., LI, Y., BREAN, A., MADDIREVULA, S., CHALLIS, R. C., SKOULOUDAKI, K., ALMOISHEER, A., ALSAIF, H. S., AMAR, A., PRESCOTT, N. J., BOBER, M. B., DUKER, A., FAQEIH, E., SEIDAHMED, M. Z., AL TALA, S., ALSWAID, A., AHMED, S., AL-AAMA, J. Y., ALTMULLER, J., AL BALWI, M., BRADY, A. F., CHESSA, L., COX, H., FISCHETTO, R., HELLER, R., HENDERSON, B. D., HOBSON, E., NURNBERG, P., PERCIN, E. F., PERON, A., SPACCINI, L., QUIGLEY, A. J., THAKUR, S., WISE, C. A., YOON, G., ALNEMER, M., TOMANCAK, P., YIGIT, G., TAYLOR, A. M., REIJNS, M. A., SIMPSON, M. A., CORTEZ, D., ALKURAYA, F. S., MATHEW, C. G., JACKSON, A. P. & STEWART, G. S. 2017. Mutations in DONSON disrupt replication fork stability and cause microcephalic dwarfism. *Nat Genet,* 49**,** 537-549.

RIERA, A., BARBON, M., NOGUCHI, Y., REUTER, L. M., SCHNEIDER, S. & SPECK, C. 2017. From structure to mechanism-understanding initiation of DNA replication. *Genes & development,* 31**,** 1073-1088.

ROACH, P. L., CLIFTON, I. J., FULOP, V., HARLOS, K., BARTON, G. J., HAJDU, J., ANDERSSON, I., SCHOFIELD, C. J. & BALDWIN, J. E. 1995. Crystal structure of isopenicillin N synthase is the first from a new structural family of enzymes. *Nature,* 375**,** 700-4.

RODRIGUEZ-ACEBES, S., MOURÓN, S. & MÉNDEZ, J. 2018. Uncoupling fork speed and origin activity to identify the primary cause of replicative stress phenotypes. *The Journal of biological chemistry,* 293**,** 12855-12861.

ROSE, N. R., MCDONOUGH, M. A., KING, O. N. F., KAWAMURA, A. & SCHOFIELD, C. J. 2011. Inhibition of 2-oxoglutarate dependent oxygenases. *Chemical Society Reviews,* 40**,** 4364-4397.

ROSOWSKI, K. A., MERTZ, A. F., NORCROSS, S., DUFRESNE, E. R. & HORSLEY, V. 2015. Edges of human embryonic stem cell colonies display distinct mechanical properties and differentiation potential. *Scientific reports,* 5**,** 14218-14218.

ROSS, R. A., SPENGLER, B. A. & BIEDLER, J. L. 1983. Coordinate morphological and biochemical interconversion of human neuroblastoma cells. *J Natl Cancer Inst,* 71**,** 741-7.

RUDRA, D. & WARNER, J. R. 2004. What better measure than ribosome synthesis? *Genes Dev,* 18**,** 2431-6.

RYU, S., HOLZSCHUH, J., ERHARDT, S., ETTL, A.-K. & DRIEVER, W. 2005. Depletion of minichromosome maintenance protein 5 in the zebrafish retina causes cell-cycle defect and apoptosis. *Proceedings of the National Academy of Sciences of the United States of America,* 102**,** 18467-18472.

SACCO, R., GABRIELE, S. & PERSICO, A. M. 2015. Head circumference and brain size in autism spectrum disorder: A systematic review and meta-analysis. *Psychiatry Res,* 234**,** 239-51.

SAEED, K., OSTLING, P., BJORKMAN, M., MIRTTI, T., ALANEN, K., VESTERINEN, T., SANKILA, A., LUNDIN, J., LUNDIN, M., RANNIKKO, A., NORDLING, S., MPINDI, J. P., KOHONEN, P., ILJIN, K., KALLIONIEMI, O. & RANTALA, J. K. 2015. Androgen receptor-interacting protein HSPBAP1 facilitates growth of prostate cancer cells in androgen-deficient conditions. *Int J Cancer,* 136, 2535-45.

SÁNCHEZ-FERNÁNDEZ, ELENA M., TARHONSKAYA, H., AL-QAHTANI, K., HOPKINSON, RICHARD J., MCCULLAGH, JAMES S. O., SCHOFIELD, CHRISTOPHER J. & FLASHMAN, E. 2013. Investigations on the oxygen dependence of a 2-oxoglutarate histone demethylase. *Biochemical Journal,* 449, 491.

SANTINI, E. & KLANN, E. 2014. Reciprocal signaling between translational control pathways and synaptic proteins in autism spectrum disorders. *Science Signaling,* 7, re10.

SARAN, A. R., KALINOWSKA, D., OH, S., JANKNECHT, R. & DITACCHIO, L. 2018. JMJD5 links CRY1 function and proteasomal degradation. *PLOS Biology,* 16, e2006145.

SARIDAKIS, V., SHENG, Y., SARKARI, F., HOLOWATY, M. N., SHIRE, K., NGUYEN, T., ZHANG, R. G., LIAO, J., LEE, W., EDWARDS, A. M., ARROWSMITH, C. H. & FRAPPIER, L. 2005. Structure of the p53 binding domain of HAUSP/USP7 bound to Epstein-Barr nuclear antigen 1 implications for EBV-mediated immortalization. *Mol Cell,* 18, 25-36.

SAVAGE, M. O., BURREN, C. P. & ROSENFELD, R. G. 2010. The continuum of growth hormone-IGF-I axis defects causing short stature: diagnostic and therapeutic challenges. *Clin Endocrinol (Oxf),* 72, 721-8.

SAZUKA, T., KINOSHITA, M., TOMOOKA, Y., IKAWA, Y., NODA, M. & KUMAR, S. 1992. Expression of DRG during murine embryonic development. *Biochem Biophys Res Commun,* 189, 371-7.

SCHELLHAUS, A. K., MORENO-ANDRÉS, D., CHUGH, M., YOKOYAMA, H., MOSCHOPOULOU, A., DE, S., BONO, F., HIPP, K., SCHÄFFER, E. & ANTONIN, W. 2017. Developmentally Regulated GTP binding protein 1 (DRG1) controls microtubule dynamics. *Scientific Reports,* 7, 9996.

SCHENKER, T., LACH, C., KESSLER, B., CALDERARA, S. & TRUEB, B. 1994. A novel GTP-binding protein which is selectively repressed in SV40 transformed fibroblasts. *J Biol Chem,* 269, 25447-53.

SCHOFIELD, C. J. & RATCLIFFE, P. J. 2004. Oxygen sensing by HIF hydroxylases. *Nature Reviews Molecular Cell Biology,* 5, 343-354.

SCHOFIELD, C. J. & RATCLIFFE, P. J. 2005. Signalling hypoxia by HIF hydroxylases. *Biochemical and Biophysical Research Communications,* 338, 617-626.

SCHULTZ-PEDERSEN, S., HASLE, H., OLSEN, J. H. & FRIEDRICH, U. 2001. Evidence of decreased risk of cancer in individuals with fragile X. *Am J Med Genet,* 103, 226-30.

SCHUMANN, M., MALESEVIC, M., HINZE, E., MATHEA, S., MELESHIN, M., SCHUTKOWSKI, M., HAEHNEL, W. & SCHIENE-FISCHER, C. 2018. Regulation of the Minichromosome Maintenance Protein 3 (MCM3) Chromatin Binding by the Prolyl Isomerase Pin1. *J Mol Biol,* 430, 5169-5181.

SCHWACHA, A. & BELL, S. P. 2001. Interactions between two catalytically distinct MCM subgroups are essential for coordinated ATP hydrolysis and DNA replication. *Mol Cell,* 8, 1093-104.

SCIACOVELLI, M. & FREZZA, C. 2016. Oncometabolites: Unconventional triggers of oncogenic signalling cascades. *Free Radical Biology and Medicine,* 100, 175-181.

SEO, Y.-S. & KANG, Y.-H. 2018. The Human Replicative Helicase, the CMG Complex, as a Target for Anti-cancer Therapy. 5.

SESSA, A., MAO, C.-A., HADJANTONAKIS, A.-K., KLEIN, W. H. & BROCCOLI, V. 2008. Tbr2 Directs Conversion of Radial Glia into Basal Precursors and Guides Neuronal Amplification by Indirect Neurogenesis in the Developing Neocortex. *Neuron,* 60, 56-69.

SHAHEEN, R., FAQEIH, E., ANSARI, S., ABDEL-SALAM, G., AL-HASSNAN, Z. N., AL-SHIDI, T., ALOMAR, R., SOGATY, S. & ALKURAYA, F. S. 2014. Genomic analysis of primordial dwarfism reveals novel disease genes. *Genome research,* 24, 291-299.

SHALABY, N. A., PINZON, J. H., NARAYANAN, A. S., JIN, E. J., RITZ, M. P., DOVE, R. J., WOLFENBERG, H., RODAN, A. R., BUSZCZAK, M. & ROTHENFLUH, A. 2018. JmjC domain proteins modulate circadian behaviors and sleep in Drosophila. *Scientific Reports,* 8, 815.

SHALABY, N. A., SAYED, R., ZHANG, Q., SCOGGIN, S., ELIAZER, S., ROTHENFLUH, A. & BUSZCZAK, M. 2017. Systematic discovery of genetic modulation by Jumonji histone demethylases in Drosophila. *Scientific Reports,* 7, 5240.

SHALEV, S. A., KHAYAT, M., ETTY, D. S. & ELPELEG, O. 2015. Further insight into the phenotype associated with a mutation in the ORC6 gene, causing Meier-Gorlin syndrome 3. *Am J Med Genet A,* 167a, 607-11.

SHEN, C., QUAN, Q., YANG, C., WEN, Y. & LI, H. 2018. Histone demethylase JMJD6 regulates cellular migration and proliferation in adipose-derived mesenchymal stem cells. *Stem Cell Res Ther,* 9, 212.

SHEN, H. & GREEN, M. R. 2006. RS domains contact splicing signals and promote splicing by a common mechanism in yeast through humans. *Genes & development,* 20**,** 1755-1765.

SHEN, J., XIANG, X., CHEN, L., WANG, H., WU, L., SUN, Y., MA, L., GU, X., LIU, H., WANG, L., YU, Y. N., SHAO, J., HUANG, C. & CHIN, Y. E. 2017. JMJD5 cleaves monomethylated histone H3 N-tail under DNA damaging stress. *EMBO Rep,* 18**,** 2131-2143.

SHEN, Y., WU, X., LIU, D., SONG, S., LIU, D. & WANG, H. 2016. Cold-dependent alternative splicing of a Jumonji C domain-containing gene MtJMJC5 in Medicago truncatula. *Biochem Biophys Res Commun,* 474**,** 271-276.

SHIMA, N., ALCARAZ, A., LIACHKO, I., BUSKE, T. R., ANDREWS, C. A., MUNROE, R. J., HARTFORD, S. A., TYE, B. K. & SCHIMENTI, J. C. 2007. A viable allele of Mcm4 causes chromosome instability and mammary adenocarcinomas in mice. *Nat Genet,* 39**,** 93-8.

SHIN, J. Y., SON, J., KIM, W. S., GWAK, J. & JU, B. G. 2019. Jmjd6a regulates GSK3beta RNA splicing in Xenopus laevis eye development. *PLoS One,* 14**,** e0219800.

SHIN, S. & JANKNECHT, R. 2007. Activation of androgen receptor by histone demethylases JMJD2A and JMJD2D. *Biochem Biophys Res Commun,* 359**,** 742-6.

SIM, N.-L., KUMAR, P., HU, J., HENIKOFF, S., SCHNEIDER, G. & NG, P. C. 2012. SIFT web server: predicting effects of amino acid substitutions on proteins. *Nucleic acids research,* 40**,** W452-W457.

SINGH, A. & XU, Y. J. 2016. The Cell Killing Mechanisms of Hydroxyurea. *Genes (Basel),* 7.

SINHA, K. M., BAGHERI-YARMAND, R., LAHIRI, S., LU, Y., ZHANG, M., AMRA, S., RIZVI, Y., WAN, X., NAVONE, N., OZPOLAT, B., LOGOTHETIS, C., GAGEL, R. F. & HUARD, J. 2019. Oncogenic and osteolytic functions of histone demethylase NO66 in castration-resistant prostate cancer. *Oncogene,* 38**,** 5038-5049.

SINHA, K. M., YASUDA, H., COOMBES, M. M., DENT, S. Y. & DE CROMBRUGGHE, B. 2010. Regulation of the osteoblast-specific transcription factor Osterix by NO66, a Jumonji family histone demethylase. *Embo j,* 29**,** 68-79.

SMART, I. H. M., DEHAY, C., GIROUD, P., BERLAND, M. & KENNEDY, H. 2002. Unique Morphological Features of the Proliferative Zones and Postmitotic Compartments of the Neural Epithelium Giving Rise to Striate and Extrastriate Cortex in the Monkey. *Cerebral Cortex,* 12**,** 37-53.

SMITS, V. A. J., REAPER, P. M. & JACKSON, S. P. 2006. Rapid PIKK-Dependent Release of Chk1 from Chromatin Promotes the DNA-Damage Checkpoint Response. *Current Biology,* 16**,** 150-159.

SMUKLER, S. R., RUNCIMAN, S. B., XU, S. & VAN DER KOOY, D. 2006. Embryonic stem cells assume a primitive neural stem cell fate in the absence of extrinsic influences. *The Journal of Cell Biology,* 172**,** 79.

SOHN, Y. D., HAN, J. W. & YOON, Y. S. 2012. Generation of induced pluripotent stem cells from somatic cells. *Prog Mol Biol Transl Sci,* 111**,** 1-26.

SONG, H., KIM, S. I., KO, M. S., KIM, H. J., HEO, J. C., LEE, H. J., LEE, H. S., HAN, I. S., KWACK, K. & PARK, J. W. 2004. Overexpression of DRG2 increases G2/M phase cells and decreases sensitivity to nocodazole-induced apoptosis. *J Biochem,* 135**,** 331-5.

SONNEVILLE, R., MORENO, S. P., KNEBEL, A., JOHNSON, C., HASTIE, C. J., GARTNER, A., GAMBUS, A. & LABIB, K. 2017. CUL-2LRR-1 and UBXN-3 drive replisome disassembly during DNA replication termination and mitosis. *Nature Cell Biology,* 19**,** 468.

SPARKS, B. F., FRIEDMAN, S. D., SHAW, D. W., AYLWARD, E. H., ECHELARD, D., ARTRU, A. A., MARAVILLA, K. R., GIEDD, J. N., MUNSON, J., DAWSON, G. & DAGER, S. R. 2002. Brain structural abnormalities in young children with autism spectrum disorder. *Neurology,* 59**,** 184.

SPECK, C. & STILLMAN, B. 2007. Cdc6 ATPase activity regulates ORC x Cdc6 stability and the selection of specific DNA sequences as origins of DNA replication. *The Journal of biological chemistry,* 282**,** 11705-11714.

SPEMANN, H. & MANGOLD, H. 1924. Induction of embryonic primordia by implantation of organizers from a different species. 1923. *Int J Dev Biol,* 45**,** 13-38.

SPIES, J., LUKAS, C., SOMYAJIT, K., RASK, M.-B., LUKAS, J. & NEELSEN, K. J. 2019. 53BP1 nuclear bodies enforce replication timing at under-replicated DNA to limit heritable DNA damage. *Nature Cell Biology,* 21**,** 487-497.

SPOEL, S. H. 2018. Orchestrating the proteome with post-translational modifications. *Journal of experimental botany,* 69**,** 4499-4503.

STERN, C. D. 2006. Neural induction: 10 years on since the 'default model'. *Curr Opin Cell Biol,* 18**,** 692-7.

STOTTMANN, R. W., BERRONG, M., MATTA, K., CHOI, M. & KLINGENSMITH, J. 2006. The BMP antagonist Noggin promotes cranial and spinal neurulation by distinct mechanisms. *Developmental Biology,* 295**,** 647-663.

SU, P., WEN, S., ZHANG, Y., LI, Y., XU, Y., ZHU, Y., LV, H., ZHANG, F., WANG, M. & TIAN, Z. 2016. Identification of the Key Genes and Pathways in Esophageal Carcinoma. *Gastroenterology research and practice,* 2016**,** 2968106-2968106.

SU, Y. & WANG, J. 2019. JmjC domain-containing protein 8 (JMJD8) represses Ku70/Ku80 expression via attenuating AKT/NF-kappaB/COX-2 signaling. *Biochim Biophys Acta Mol Cell Res,* 1866**,** 118541.

SUGIMURA, K., TAKEBAYASHI, S., TAGUCHI, H., TAKEDA, S. & OKUMURA, K. 2008. PARP-1 ensures regulation of replication fork progression by homologous recombination on damaged DNA. *J Cell Biol,* 183**,** 1203-12.

SUIKKI, H. E., KUJALA, P. M., TAMMELA, T. L., VAN WEERDEN, W. M., VESSELLA, R. L. & VISAKORPI, T. 2010. Genetic alterations and changes in expression of histone demethylases in prostate cancer. *Prostate,* 70**,** 889-98.

SULKOWSKI, P. L., CORSO, C. D., ROBINSON, N. D., SCANLON, S. E., PURSHOUSE, K. R., BAI, H., LIU, Y., SUNDARAM, R. K., HEGAN, D. C., FONS, N. R., BREUER, G. A., SONG, Y., MISHRA-GORUR, K., DE FEYTER, H. M., DE GRAAF, R. A., SUROVTSEVA, Y. V., KACHMAN, M., HALENE, S., GUNEL, M., GLAZER, P. M. & BINDRA, R. S. 2017. 2-Hydroxyglutarate produced by neomorphic IDH mutations suppresses homologous recombination and induces PARP inhibitor sensitivity. *Sci Transl Med,* 9.

SUPEKAR, K., UDDIN, L. Q., KHOUZAM, A., PHILLIPS, J., GAILLARD, W. D., KENWORTHY, L. E., YERYS, B. E., VAIDYA, C. J. & MENON, V. 2013. Brain hyperconnectivity in children with autism and its links to social deficits. *Cell Rep,* 5**,** 738-47.

SUZUKI, I. K. & VANDERHAEGHEN, P. 2015. Is this a brain which I see before me? Modeling human neural development with pluripotent stem cells. *Development,* 142**,** 3138-50.

SUZUKI, T., MINEHATA, K.-I., AKAGI, K., JENKINS, N. A. & COPELAND, N. G. 2006. Tumor suppressor gene identification using retroviral insertional mutagenesis in Blm-deficient mice. *The EMBO Journal,* 25**,** 3422-3431.

TAHILIANI, M., MEI, P., FANG, R., LEONOR, T., RUTENBERG, M., SHIMIZU, F., LI, J., RAO, A. & SHI, Y. 2007. The histone H3K4 demethylase SMCX links REST target genes to X-linked mental retardation. *Nature,* 447**,** 601-5.

TAKAHASHI, K., TANABE, K., OHNUKI, M., NARITA, M., ICHISAKA, T., TOMODA, K. & YAMANAKA, S. 2007. Induction of Pluripotent Stem Cells from Adult Human Fibroblasts by Defined Factors. *Cell,* 131**,** 861-872.

TAKAHASHI, K. & YAMANAKA, S. 2006. Induction of pluripotent stem cells from mouse embryonic and adult fibroblast cultures by defined factors. *Cell,* 126**,** 663-76.

TAKAKI, T. 1980. An epithelial cell line (KNS-62) derived from a brain metastasis of bronchial squamous cell carcinoma. *J Cancer Res Clin Oncol,* 96**,** 27-33.

TAKEI, Y., SWIETLIK, M., TANOUE, A., TSUJIMOTO, G., KOUZARIDES, T. & LASKEY, R. 2001. MCM3AP, a novel acetyltransferase that acetylates replication protein MCM3. *EMBO Rep,* 2**,** 119-23.

TAKEI, Y. & TSUJIMOTO, G. 1998. Identification of a Novel MCM3-associated Protein that Facilitates MCM3 Nuclear Localization. *Journal of Biological Chemistry,* 273**,** 22177-22180.

TAKEUCHI, T., WATANABE, Y., TAKANO-SHIMIZU, T. & KONDO, S. 2006. Roles of jumonji and jumonji family genes in chromatin regulation and development. *Dev Dyn,* 235**,** 2449-59.

TAKEUCHI, T., YAMAZAKI, Y., KATOH-FUKUI, Y., TSUCHIYA, R., KONDO, S., MOTOYAMA, J. & HIGASHINAKAGAWA, T. 1995. Gene trap capture of a novel mouse gene, jumonji, required for neural tube formation. *Genes Dev,* 9**,** 1211-22.

TAN, B. C., CHIEN, C. T., HIROSE, S. & LEE, S. C. 2006. Functional cooperation between FACT and MCM helicase facilitates initiation of chromatin DNA replication. *Embo j,* 25**,** 3975-85.

TANG, Y., LI, T., LI, J., YANG, J., LIU, H., ZHANG, X. J. & LE, W. 2014. Jmjd3 is essential for the epigenetic modulation of microglia phenotypes in the immune pathogenesis of Parkinson's disease. *Cell Death Differ,* 21**,** 369-80.

TARNAUSKAITĖ, Ž., BICKNELL, L. S., MARSH, J. A., MURRAY, J. E., PARRY, D. A., LOGAN, C. V., BOBER, M. B., DE SILVA, D. C., DUKER, A. L., SILLENCE, D., WISE, C., JACKSON, A. P., MURINA, O. & REIJNS, M. A. M. 2019. Biallelic variants in DNA2 cause microcephalic primordial dwarfism. *Human Mutation,* 40**,** 1063-1070.

TAYLOR, E. M. & LINDSAY, H. D. 2016. DNA replication stress and cancer: cause or cure? *Future Oncol,* 12**,** 221-37.

TÉCHER, H., KOUNDRIOUKOFF, S., AZAR, D., WILHELM, T., CARIGNON, S., BRISON, O., DEBATISSE, M. & LE TALLEC, B. 2013. Replication Dynamics: Biases and Robustness of DNA Fiber Analysis. *Journal of Molecular Biology,* 425**,** 4845-4855.

TEE, A. R., MANNING, B. D., ROUX, P. P., CANTLEY, L. C. & BLENIS, J. 2003. Tuberous sclerosis complex gene products, Tuberin and Hamartin, control mTOR signaling by acting as a GTPase-activating protein complex toward Rheb. *Curr Biol,* 13**,** 1259-68.

THIENPONT, B., STEINBACHER, J., ZHAO, H., D'ANNA, F., KUCHNIO, A., PLOUMAKIS, A., GHESQUIERE, B., VAN DYCK, L., BOECKX, B., SCHOONJANS, L., HERMANS, E., AMANT, F., KRISTENSEN, V. N., PENG KOH, K., MAZZONE, M., COLEMAN, M., CARELL, T., CARMELIET, P. & LAMBRECHTS, D. 2016. Tumour hypoxia causes DNA hypermethylation by reducing TET activity. *Nature,* 537**,** 63-68.

THOMSON, J. A., ITSKOVITZ-ELDOR, J., SHAPIRO, S. S., WAKNITZ, M. A., SWIERGIEL, J. J., MARSHALL, V. S. & JONES, J. M. 1998. Embryonic stem cell lines derived from human blastocysts. *Science,* 282**,** 1145-7.

THYS, R. G. & WANG, Y. H. 2015. DNA Replication Dynamics of the GGGGCC Repeat of the C9orf72 Gene. *J Biol Chem,* 290**,** 28953-62.

TIAN, Y.-M., YEOH, K. K., LEE, M. K., ERIKSSON, T., KESSLER, B. M., KRAMER, H. B., EDELMANN, M. J., WILLAM, C., PUGH, C. W., SCHOFIELD, C. J. & RATCLIFFE, P. J. 2011. Differential Sensitivity of Hypoxia Inducible Factor Hydroxylation Sites to Hypoxia and Hydroxylase Inhibitors. 286**,** 13041-13051.

TIBBETTS, R. S., CORTEZ, D., BRUMBAUGH, K. M., SCULLY, R., LIVINGSTON, D., ELLEDGE, S. J. & ABRAHAM, R. T. 2000. Functional interactions between BRCA1 and the checkpoint kinase ATR during genotoxic stress. *Genes Dev,* 14**,** 2989-3002.

TICAU, S., FRIEDMAN, L. J., IVICA, N. A., GELLES, J. & BELL, S. P. 2015. Single-molecule studies of origin licensing reveal mechanisms ensuring bidirectional helicase loading. *Cell,* 161**,** 513-525.

TING, C. Y., BHATIA, N. S., LIM, J. Y., GOH, C. J., VASANWALA, R. F., ONG, C. C., SEOW, W. T., YEOW, V. K., TING, T. W., NG, I. S. & JAMUAR, S. S. 2019. Further delineation of CDC45-related Meier-Gorlin syndrome with craniosynostosis and review of literature. *Eur J Med Genet.*

TOLEDO, L. I., ALTMEYER, M., RASK, M. B., LUKAS, C., LARSEN, D. H., POVLSEN, L. K., BEKKER-JENSEN, S., MAILAND, N., BARTEK, J. & LUKAS, J. 2013. ATR prohibits replication catastrophe by preventing global exhaustion of RPA. *Cell,* 155**,** 1088-103.

TRENZ, K., ERRICO, A. & COSTANZO, V. 2008. Plx1 is required for chromosomal DNA replication under stressful conditions. *Embo j,* 27**,** 876-85.

TRETTER, L., PATOCS, A. & CHINOPOULOS, C. 2016. Succinate, an intermediate in metabolism, signal transduction, ROS, hypoxia, and tumorigenesis. *Biochimica et Biophysica Acta (BBA) - Bioenergetics,* 1857**,** 1086-1101.

TROPEPE, V., HITOSHI, S., SIRARD, C., MAK, T. W., ROSSANT, J. & VAN DER KOOY, D. 2001. Direct Neural Fate Specification from Embryonic Stem Cells: A Primitive Mammalian Neural Stem Cell Stage Acquired through a Default Mechanism. *Neuron,* 30**,** 65-78.

TSAI, P. T., HULL, C., CHU, Y., GREENE-COLOZZI, E., SADOWSKI, A. R., LEECH, J. M., STEINBERG, J., CRAWLEY, J. N., REGEHR, W. G. & SAHIN, M. 2012. Autistic-like behaviour and cerebellar dysfunction in Purkinje cell Tsc1 mutant mice. *Nature,* 488**,** 647-651.

TSAO, C. C., GEISEN, C. & ABRAHAM, R. T. 2004. Interaction between human MCM7 and Rad17 proteins is required for replication checkpoint signaling. *Embo j,* 23**,** 4660-9.

TURPAEV, K. T. 2018. Translation Factor eIF5A, Modification with Hypusine and Role in Regulation of Gene Expression. eIF5A as a Target for Pharmacological Interventions. *Biochemistry (Mosc),* 83**,** 863-873.

TZATSOS, A., PASKALEVA, P., FERRARI, F., DESHPANDE, V., STOYKOVA, S., CONTINO, G., WONG, K.-K., LAN, F., TROJER, P., PARK, P. J. & BARDEESY, N. 2013. KDM2B promotes pancreatic cancer via Polycomb-dependent and -independent transcriptional programs. *The Journal of clinical investigation,* 123**,** 727-739.

UNOKI, M., MASUDA, A., DOHMAE, N., ARITA, K., YOSHIMATSU, M., IWAI, Y., FUKUI, Y., UEDA, K., HAMAMOTO, R., SHIRAKAWA, M., SASAKI, H. & NAKAMURA, Y. 2013. Lysyl 5-hydroxylation, a novel histone modification, by Jumonji domain containing 6 (JMJD6). *J Biol Chem,* 288**,** 6053-62.

UNSAL-KACMAZ, K., CHASTAIN, P. D., QU, P. P., MINOO, P., CORDEIRO-STONE, M., SANCAR, A. & KAUFMANN, W. K. 2007. The human Tim/Tipin complex coordinates an Intra-S checkpoint response to UV that slows replication fork displacement. *Mol Cell Biol,* 27**,** 3131-42.

UTIKAL, J., POLO, J. M., STADTFELD, M., MAHERALI, N., KULALERT, W., WALSH, R. M., KHALIL, A., RHEINWALD, J. G. & HOCHEDLINGER, K. 2009. Immortalization eliminates a roadblock during cellular reprogramming into iPS cells. *Nature,* 460**,** 1145-1148.

VALLIER, L., REYNOLDS, D. & PEDERSEN, R. A. 2004. Nodal inhibits differentiation of human embryonic stem cells along the neuroectodermal default pathway. *Developmental Biology,* 275**,** 403-421.

VALVO, G., BALDINI, S., RETICO, A., ROSSI, G., TANCREDI, R., FERRARI, A. R., CALDERONI, S., APICELLA, F., MURATORI, F., SANTORELLI, F. M. & SICCA, F. 2016. Temporal lobe connects regression and macrocephaly to autism spectrum disorders. *European Child & Adolescent Psychiatry,* 25**,** 421-429.

VESELA, E., CHROMA, K., TURI, Z. & MISTRIK, M. 2017. Common Chemical Inductors of Replication Stress: Focus on Cell-Based Studies. *Biomolecules,* 7**,** 19.

VETRO, A., SAVASTA, S., RUSSO RAUCCI, A., CERQUA, C., SARTORI, G., LIMONGELLI, I., FORLINO, A., MARUELLI, S., PERUCCA, P., VERGANI, D., MAZZINI, G., MATTEVI, A., STIVALA, L. A., SALVIATI, L. & ZUFFARDI, O. 2017. MCM5: a new actor in the link between DNA replication and Meier-Gorlin syndrome. *European Journal of Human Genetics,* 25**,** 646-650.

VLANGOS, C. N., DAS, P., PATEL, P. I. & ELSEA, S. H. 2000. Assignment of developmentally regulated GTP-binding protein (DRG2) to human chromosome band 17p11.2 with somatic cell hybrids and localization to the Smith-Magenis syndrome critical interval. *Cytogenet Cell Genet,* 88**,** 283-5.

WALLACE, G. L., EISENBERG, I. W., ROBUSTELLI, B., DANKNER, N., KENWORTHY, L., GIEDD, J. N. & MARTIN, A. 2015. Longitudinal cortical development during adolescence and young adulthood in autism spectrum disorder: increased cortical thinning but comparable surface area changes. *Journal of the American Academy of Child and Adolescent Psychiatry,* 54**,** 464-469.

WAN, J., LIU, H., YANG, L., MA, L., LIU, J. & MING, L. 2019. JMJD6 promotes hepatocellular carcinoma carcinogenesis by targeting CDK4. *Int J Cancer,* 144**,** 2489-2500.

WANG, E., ZHANG, C., POLAVARAM, N., LIU, F., WU, G., SCHROEDER, M. A., LAU, J. S., MUKHOPADHYAY, D., JIANG, S.-W., O'NEILL, B. P., DATTA, K. & LI, J. 2014a. The Role of Factor Inhibiting HIF (FIH-1) in Inhibiting HIF-1 Transcriptional Activity in Glioblastoma Multiforme. *PLOS ONE,* 9**,** e86102.

WANG, H. 2015. Fragile X mental retardation protein: from autism to neurodegenerative disease. *Frontiers in cellular neuroscience,* 9**,** 43-43.

WANG, H., ZHOU, X., WU, M., WANG, C., ZHANG, X., TAO, Y., CHEN, N. & ZANG, J. 2013. Structure of the JmjC-domain-containing protein JMJD5. *Acta Crystallogr D Biol Crystallogr,* 69**,** 1911-20.

WANG, H. J., HSIEH, Y. J., CHENG, W. C., LIN, C. P., LIN, Y. S., YANG, S. F., CHEN, C. C., IZUMIYA, Y., YU, J. S., KUNG, H. J. & WANG, W. C. 2014b. JMJD5 regulates PKM2 nuclear translocation and reprograms HIF-1alpha-mediated glucose metabolism. *Proc Natl Acad Sci U S A,* 111**,** 279-84.

WANG, H. J., POCHAMPALLI, M., WANG, L. Y., ZOU, J. X., LI, P. S., HSU, S. C., WANG, B. J., HUANG, S. H., YANG, P., YANG, J. C., CHU, C. Y., HSIEH, C. L., SUNG, S. Y., LI, C. F., TEPPER, C. G., ANN, D. K., GAO, A. C., EVANS, C. P., IZUMIYA, Y., CHUU, C. P., WANG, W. C., CHEN, H. W. & KUNG, H. J. 2019a. KDM8/JMJD5 as a dual coactivator of AR and PKM2 integrates AR/EZH2 network and tumor metabolism in CRPC. *Oncogene,* 38**,** 17-32.

WANG, L., JIANG, F., MA, F. & ZHANG, B. 2019b. MiR-873-5p suppresses cell proliferation and epithelial-mesenchymal transition via directly targeting Jumonji domain-containing protein 8 through the NF-kappaB pathway in colorectal cancer. *J Cell Commun Signal.*

WANG, T., CHEN, K., ZENG, X., YANG, J., WU, Y., SHI, X., QIN, B., ZENG, L., ESTEBAN, M. A., PAN, G. & PEI, D. 2011. The histone demethylases Jhdm1a/1b enhance somatic cell reprogramming in a vitamin-C-dependent manner. *Cell Stem Cell,* 9**,** 575-87.

WANG, Y., LIU, L., JI, F., JIANG, J., YU, Y., SHENG, S. & LI, H. 2018. Soybean (Glycine max) prevents the progression of breast cancer cells by downregulating the level of histone demethylase JMJD5. *J Cancer Res Ther,* 14**,** S609-s615.

WANG, Z. & BURGE, C. B. 2008. Splicing regulation: from a parts list of regulatory elements to an integrated splicing code. *Rna,* 14**,** 802-13.

WANG, Z., WANG, C., HUANG, X., SHEN, Y., SHEN, J. & YING, K. 2012. Differential proteome profiling of pleural effusions from lung cancer and benign inflammatory disease patients. *Biochim Biophys Acta,* 1824**,** 692-700.

WARD, I. M. & CHEN, J. 2001. Histone H2AX is phosphorylated in an ATR-dependent manner in response to replicational stress. *J Biol Chem,* 276**,** 47759-62.

WARD, I. M., MINN, K., VAN DEURSEN, J. & CHEN, J. 2003. p53 Binding protein 53BP1 is required for DNA damage responses and tumor suppression in mice. *Mol Cell Biol,* 23**,** 2556-63.

WEBBY, C. J., WOLF, A., GROMAK, N., DREGER, M., KRAMER, H., KESSLER, B., NIELSEN, M. L., SCHMITZ, C., BUTLER, D. S., YATES, J. R., DELAHUNTY, C. M., HAHN, P., LENGELING, A., MANN, M., PROUDFOOT, N. J., SCHOFIELD, C. J. & BÖTTGER, A. 2009. Jmjd6 Catalyses Lysyl-Hydroxylation of U2AF65, a Protein Associated with RNA Splicing. *Science,* 325**,** 90.

WEI, L. & ZHAO, X. 2016. A new MCM modification cycle regulates DNA replication initiation. *Nature structural & molecular biology,* 23**,** 209-216.

WELFORD, R. W. D., KIRKPATRICK, J. M., MCNEILL, L. A., PURI, M., OLDHAM, N. J. & SCHOFIELD, C. J. 2005. Incorporation of oxygen into the succinate co-product of iron(II) and 2-oxoglutarate dependent oxygenases from bacteria, plants and humans. *FEBS Letters,* 579, 5170-5174.

WEN, Z., CHENG, T.-L., LI, G.-Z., SUN, S.-B., YU, S.-Y., ZHANG, Y., DU, Y.-S. & QIU, Z. 2017. Identification of autism-related MECP2 mutations by whole-exome sequencing and functional validation. *Molecular Autism,* 8, 43.

WILKINS, O. M., TITUS, A. J., GUI, J., ELIOT, M., BUTLER, R. A., STURGIS, E. M., LI, G., KELSEY, K. T. & CHRISTENSEN, B. C. 2017. Genome-scale identification of microRNA-related SNPs associated with risk of head and neck squamous cell carcinoma. *Carcinogenesis,* 38, 986-993.

WILKINS, S. E., ISLAM, M. S., GANNON, J. M., MARKOLOVIC, S., HOPKINSON, R. J., GE, W., SCHOFIELD, C. J. & CHOWDHURY, R. 2018. JMJD5 is a human arginyl C-3 hydroxylase. *Nat Commun,* 9, 1180.

WILL, C. L. & LÜHRMANN, R. 2011. Spliceosome structure and function. *Cold Spring Harbor perspectives in biology,* 3, a003707.

WILLIAMS, S. T., WALPORT, L. J., HOPKINSON, R. J., MADDEN, S. K., CHOWDHURY, R., SCHOFIELD, C. J. & KAWAMURA, A. 2014. Studies on the catalytic domains of multiple JmjC oxygenases using peptide substrates. *Epigenetics,* 9, 1596-1603.

WISSMANN, M., YIN, N., MULLER, J. M., GRESCHIK, H., FODOR, B. D., JENUWEIN, T., VOGLER, C., SCHNEIDER, R., GUNTHER, T., BUETTNER, R., METZGER, E. & SCHULE, R. 2007. Cooperative demethylation by JMJD2C and LSD1 promotes androgen receptor-dependent gene expression. *Nat Cell Biol,* 9, 347-53.

WIZNITZER, M. 2004. Autism and tuberous sclerosis. *J Child Neurol,* 19, 675-9.

WOLF, S. S., PATCHEV, V. K. & OBENDORF, M. 2007. A novel variant of the putative demethylase gene, s-JMJD1C, is a coactivator of the AR. *Arch Biochem Biophys,* 460, 56-66.

WONG, M., SUN, Y., XI, Z., MILAZZO, G., POULOS, R. C., BARTENHAGEN, C., BELL, J. L., MAYOH, C., HO, N., TEE, A. E., CHEN, X., LI, Y., CIACCIO, R., LIU, P. Y., JIANG, C. C., LAN, Q., JAYATILLEKE, N., CHEUNG, B. B., HABER, M., NORRIS, M. D., ZHANG, X. D., MARSHALL, G. M., WANG, J. Y., HUTTELMAIER, S., FISCHER, M., WONG, J. W. H., XU, H., PERINI, G., DONG, Q., GEORGE, R. E. & LIU, T. 2019. JMJD6 is a tumorigenic factor and therapeutic target in neuroblastoma. *Nat Commun,* 10, 3319.

WOODWARD, A. M., GÖHLER, T., LUCIANI, M. G., OEHLMANN, M., GE, X., GARTNER, A., JACKSON, D. A. & BLOW, J. J. 2006. Excess Mcm2–7 license dormant origins of replication that can be used under conditions of replicative stress. *The Journal of Cell Biology,* 173, 673.

WOUT, P. K., SATTLEGGER, E., SULLIVAN, S. M. & MADDOCK, J. R. 2009. Saccharomyces cerevisiae Rbg1 protein and its binding partner Gir2 interact on Polyribosomes with Gcn1. *Eukaryot Cell,* 8, 1061-71.

WU, B. H., CHEN, H., CAI, C. M., FANG, J. Z., WU, C. C., HUANG, L. Y., WANG, L. & HAN, Z. G. 2016a. Epigenetic silencing of JMJD5 promotes the proliferation of hepatocellular carcinoma cells by down-regulating the transcription of CDKN1A 686. *Oncotarget,* 7, 6847-63.

WU, J., HE, Z., WANG, D. L. & SUN, F. L. 2016b. Depletion of JMJD5 sensitizes tumor cells to microtubule-destabilizing agents by altering microtubule stability. *Cell Cycle,* 15, 2980-2991.

WU, J., HE, Z., YANG, X. M., LI, K. L., WANG, D. L. & SUN, F. L. 2017. RCCD1 depletion attenuates TGF-beta-induced EMT and cell migration by stabilizing cytoskeletal microtubules in NSCLC cells. *Cancer Lett,* 400, 18-29.

WU, R. A., SEMLOW, D. R., KAMIMAE-LANNING, A. N., KOCHENOVA, O. V., CHISTOL, G., HODSKINSON, M. R., AMUNUGAMA, R., SPARKS, J. L., WANG, M., DENG, L., MIMOSO, C. A., LOW, E., PATEL, K. J. & WALTER, J. C. 2019. TRAIP is a master regulator of DNA interstrand crosslink repair. *Nature,* 567, 267-272.

XI, Z. Q., SUN, J. J., WANG, X. F., LI, M. W., LIU, X. Z., WANG, L. Y., ZHU, X., XIAO, F., LI, J. M., GONG, Y. & GUAN, L. F. 2007. HSPBAP1 is found extensively in the anterior temporal neocortex of patients with intractable epilepsy. *Synapse,* 61, 741-7.

XIE, H. R., HU, L. S. & LI, G. Y. 2010. SH-SY5Y human neuroblastoma cell line: in vitro cell model of dopaminergic neurons in Parkinson's disease. *Chin Med J (Engl),* 123, 1086-92.

XU, B., SUN, Z., LIU, Z., GUO, H., LIU, Q., JIANG, H., ZOU, Y., GONG, Y., TISCHFIELD, J. A. & SHAO, C. 2011a. Replication stress induces micronuclei comprising of aggregated DNA double-strand breaks. *PloS one,* 6, e18618-e18618.

XU, W., YANG, H., LIU, Y., YANG, Y., WANG, P., KIM, S.-H., ITO, S., YANG, C., WANG, P., XIAO, M.-T., LIU, L.-X., JIANG, W.-Q., LIU, J., ZHANG, J.-Y., WANG, B., FRYE, S., ZHANG, Y., XU, Y.-H., LEI, Q.-Y., GUAN, K.-L., ZHAO, S.-M. & XIONG, Y. 2011b. Oncometabolite 2-Hydroxyglutarate Is a Competitive Inhibitor of α-Ketoglutarate-Dependent Dioxygenases. *Cancer Cell,* 19, 17-30.

XU, W., YANG, H., LIU, Y., YANG, Y., WANG, P., KIM, S. H., ITO, S., YANG, C., WANG, P., XIAO, M. T., LIU, L. X., JIANG, W. Q., LIU, J., ZHANG, J. Y., WANG, B., FRYE, S., ZHANG, Y., XU, Y. H., LEI, Q. Y., GUAN, K. L., ZHAO, S. M. & XIONG, Y. 2011c. Oncometabolite 2-hydroxyglutarate is a competitive inhibitor of alpha-ketoglutarate-dependent dioxygenases. *Cancer Cell,* 19**,** 17-30.

YAMADA, T., HIROHASHI, S., SHIMOSATO, Y., KODAMA, T., HAYASHI, S., OGURA, T., GAMOU, S. & SHIMIZU, N. 1985. Giant cell carcinomas of the lung producing colony-stimulating factor in vitro and in vivo. *Jpn J Cancer Res,* 76**,** 967-76.

YAMANE, K., TOUMAZOU, C., TSUKADA, Y., ERDJUMENT-BROMAGE, H., TEMPST, P., WONG, J. & ZHANG, Y. 2006. JHDM2A, a JmjC-containing H3K9 demethylase, facilitates transcription activation by androgen receptor. *Cell,* 125**,** 483-95.

YAN, M., YANG, X., SHEN, R., WU, C., WANG, H., YE, Q., YANG, P., ZHANG, L., CHEN, M., WAN, B., ZHANG, Q., XIA, S., LU, X., SHAO, G., ZHOU, X., YU, J. & SHAO, Q. 2018. miR-146b promotes cell proliferation and increases chemosensitivity, but attenuates cell migration and invasion via FBXL10 in ovarian cancer. *Cell Death Dis,* 9, 1123.

YANG, M., CHOWDHURY, R., GE, W., HAMED, R. B., MCDONOUGH, M. A., CLARIDGE, T. D., KESSLER, B. M., COCKMAN, M. E., RATCLIFFE, P. J. & SCHOFIELD, C. J. 2011. Factor-inhibiting hypoxia-inducible factor (FIH) catalyses the post-translational hydroxylation of histidinyl residues within ankyrin repeat domains. *Febs j,* 278**,** 1086-97.

YANG, M., SOGA, T., POLLARD, P. J. & ADAM, J. 2012. The emerging role of fumarate as an oncometabolite. *Front Oncol,* 2**,** 85.

YANG, Z., ZHUANG, L., SZATMARY, P., WEN, L., SUN, H., LU, Y., XU, Q. & CHEN, X. 2015. Upregulation of heat shock proteins (HSPA12A, HSP90B1, HSPA4, HSPA5 and HSPA6) in tumour tissues is associated with poor outcomes from HBV-related early-stage hepatocellular carcinoma. *Int J Med Sci,* 12**,** 256-63.

YAO, J., WU, X., ZHANG, D., WANG, L., ZHANG, L., REYNOLDS, E. X., HERNANDEZ, C., BOSTROM, K. I. & YAO, Y. 2019. Elevated endothelial Sox2 causes lumen disruption and cerebral arteriovenous malformations. *J Clin Invest,* 129, 3121-3133.

YAP, E. L. & GREENBERG, M. E. 2018. Activity-Regulated Transcription: Bridging the Gap between Neural Activity and Behavior. *Neuron,* 100**,** 330-348.

YE, D., MA, S., XIONG, Y. & GUAN, K.-L. 2013. R-2-hydroxyglutarate as the key effector of IDH mutations promoting oncogenesis. *Cancer cell,* 23**,** 274-276.

YEO, E. J., RYU, J. H., CHO, Y. S., CHUN, Y. S., HUANG, L. E., KIM, M. S. & PARK, J. W. 2006. Amphotericin B blunts erythropoietin response to hypoxia by reinforcing FIH-mediated repression of HIF-1. *Blood,* 107**,** 916-23.

YEO, K. S., TAN, M. C., LIM, Y.-Y. & EA, C.-K. 2017. JMJD8 is a novel endoplasmic reticulum protein with a JmjC domain. *Scientific Reports,* 7**,** 15407.

YOO, H., SON, D., LEE, Y. J. & HONG, K. 2016. Mouse JMJD4 is dispensable for embryogenesis. *Mol Reprod Dev,* 83**,** 588-93.

YOUN, M. Y., YOKOYAMA, A., FUJIYAMA-NAKAMURA, S., OHTAKE, F., MINEHATA, K., YASUDA, H., SUZUKI, T., KATO, S. & IMAI, Y. 2012. JMJD5, a Jumonji C (JmjC) domain-containing protein, negatively regulates osteoclastogenesis by facilitating NFATc1 protein degradation. *J Biol Chem,* 287**,** 12994-3004.

YOUNG, M. R., SUZUKI, K., YAN, H., GIBSON, S. & TYE, B. K. 1997. Nuclear accumulation of Saccharomyces cerevisiae Mcm3 is dependent on its nuclear localization sequence. *Genes Cells,* 2**,** 631-43.

YU, F., WHITE, S. B., ZHAO, Q. & LEE, F. S. 2001. HIF-1alpha binding to VHL is regulated by stimulus-sensitive proline hydroxylation. *Proc Natl Acad Sci U S A,* 98**,** 9630-5.

YU, M., SUN, J., THAKUR, C., CHEN, B., LU, Y., ZHAO, H. & CHEN, F. 2014. Paradoxical Roles of Mineral Dust Induced Gene on Cell Proliferation and Migration/Invasion. *PLOS ONE,* 9, e87998.

YU, Z., FENG, D. & LIANG, C. 2004. Pairwise Interactions of the Six Human MCM Protein Subunits. *Journal of Molecular Biology,* 340**,** 1197-1206.

ZAEHRES, H., LENSCH, M. W., DAHERON, L., STEWART, S. A., ITSKOVITZ-ELDOR, J. & DALEY, G. Q. 2005. High-efficiency RNA interference in human embryonic stem cells. *Stem Cells,* 23**,** 299-305.

ZALFA, F., PANASITI, V., CAROTTI, S., ZINGARIELLO, M., PERRONE, G., SANCILLO, L., PACINI, L., LUCIANI, F., ROBERTI, V., D'AMICO, S., COPPOLA, R., ABATE, S. O., RANA, R. A., DE LUCA, A., FIERS, M., MELOCCHI, V., BIANCHI, F., FARACE, M. G., ACHSEL, T., MARINE, J.-C., MORINI, S. & BAGNI, C. 2017. The fragile X mental retardation protein regulates tumor invasiveness-related pathways in melanoma cells. *Cell death & disease,* 8, e3169-e3169.

ZEMAN, M. K. & CIMPRICH, K. A. 2014. Causes and consequences of replication stress. *Nat Cell Biol,* 16, 2-9.

ZHANG, J., ZHAO, J., GAO, N., WANG, Y., CHEN, Y. & HAN, J. 2017. MECP2 expression in gastric cancer and its correlation with clinical pathological parameters. 96, e7691.

ZHANG, R., HUANG, Q., LI, Y., SONG, Y. & LI, Y. 2015. JMJD5 is a potential oncogene for colon carcinogenesis. *Int J Clin Exp Pathol,* 8, 6482-9.

ZHANG, X., HUANG, C. T., CHEN, J., PANKRATZ, M. T., XI, J., LI, J., YANG, Y., LAVAUTE, T. M., LI, X.-J., AYALA, M., BONDARENKO, G. I., DU, Z.-W., JIN, Y., GOLOS, T. G. & ZHANG, S.-C. 2010. Pax6 Is a Human Neuroectoderm Cell Fate Determinant. *Cell Stem Cell,* 7, 90-100.

ZHAO, L. Y., ZHANG, J., GUO, B., YANG, J., HAN, J., ZHAO, X. G., WANG, X. F., LIU, L. Y., LI, Z. F., SONG, T. S. & HUANG, C. 2013. MECP2 promotes cell proliferation by activating ERK1/2 and inhibiting p38 activity in human hepatocellular carcinoma HEPG2 cells. *Cell Mol Biol (Noisy-le-grand),* Suppl 59, Ol1876-81.

ZHAO, Y., YIN, X., QIN, H., ZHU, F., LIU, H., YANG, W., ZHANG, Q., XIANG, C., HOU, P., SONG, Z., LIU, Y., YONG, J., ZHANG, P., CAI, J., LIU, M., LI, H., LI, Y., QU, X., CUI, K., ZHANG, W., XIANG, T., WU, Y., ZHAO, Y., LIU, C., YU, C., YUAN, K., LOU, J., DING, M. & DENG, H. 2008. Two Supporting Factors Greatly Improve the Efficiency of Human iPSC Generation. *Cell Stem Cell,* 3, 475-479.

ZHAO, Z., SUN, C., LI, F., HAN, J., LI, X. & SONG, Z. 2015. Overexpression of histone demethylase JMJD5 promotes metastasis and indicates a poor prognosis in breast cancer. *Int J Clin Exp Pathol,* 8, 10325-34.

ZHOU, J., BLUNDELL, J., OGAWA, S., KWON, C.-H., ZHANG, W., SINTON, C., POWELL, C. M. & PARADA, L. F. 2009. Pharmacological Inhibition of mTORC1 Suppresses Anatomical, Cellular, and Behavioral Abnormalities in Neural-Specific Pten Knock-Out Mice. *The Journal of Neuroscience,* 29, 1773.

ZHOU, J., GUNSIOR, M., BACHMANN, B. O., TOWNSEND, C. A. & SOLOMON, E. I. 1998. Substrate Binding to the α-Ketoglutarate-Dependent Non-Heme Iron Enzyme Clavaminate Synthase 2: Coupling Mechanism of Oxidative Decarboxylation and Hydroxylation. *Journal of the American Chemical Society,* 120, 13539-13540.

ZHOU, X., SASAKI, H., LOWE, L., HOGAN, B. L. & KUEHN, M. R. 1993. Nodal is a novel TGF-beta-like gene expressed in the mouse node during gastrulation. *Nature,* 361, 543-7.

ZHU, H., HU, S. & BAKER, J. 2014. JMJD5 regulates cell cycle and pluripotency in human embryonic stem cells. *Stem Cells,* 32, 2098-110.

ZHU, S., XU, Y., SONG, M., CHEN, G., WANG, H., ZHAO, Y., WANG, Z. & LI, F. 2016. PRDM16 is associated with evasion of apoptosis by prostatic cancer cells according to RNA interference screening. *Mol Med Rep,* 14, 3357-61.

ZHU, W., UKOMADU, C., JHA, S., SENGA, T., DHAR, S. K., WOHLSCHLEGEL, J. A., NUTT, L. K., KORNBLUTH, S. & DUTTA, A. 2007. Mcm10 and And-1/CTF4 recruit DNA polymerase alpha to chromatin for initiation of DNA replication. *Genes & development,* 21, 2288-2299.

ZIELINSKI, B. A., PRIGGE, M. B., NIELSEN, J. A., FROEHLICH, A. L., ABILDSKOV, T. J., ANDERSON, J. S., FLETCHER, P. T., ZYGMUNT, K. M., TRAVERS, B. G., LANGE, N., ALEXANDER, A. L., BIGLER, E. D. & LAINHART, J. E. 2014. Longitudinal changes in cortical thickness in autism and typical development. *Brain,* 137, 1799-812.

ZIMMERMAN, L. B., DE JESUS-ESCOBAR, J. M. & HARLAND, R. M. 1996. The Spemann organizer signal noggin binds and inactivates bone morphogenetic protein 4. *Cell,* 86, 599-606.

ZIMMERMANN, M., MURINA, O., REIJNS, M. A. M., AGATHANGGELOU, A., CHALLIS, R., TARNAUSKAITĖ, Ž., MUIR, M., FLUTEAU, A., AREGGER, M., MCEWAN, A., YUAN, W., CLARKE, M., LAMBROS, M. B., PANEESHA, S., MOSS, P., CHANDRASHEKHAR, M., ANGERS, S., MOFFAT, J., BRUNTON, V. G., HART, T., DE BONO, J., STANKOVIC, T., JACKSON, A. P. & DUROCHER, D. 2018. CRISPR screens identify genomic ribonucleotides as a source of PARP-trapping lesions. *Nature,* 559, 285-289.

ZOU, L. & ELLEDGE, S. J. 2003. Sensing DNA damage through ATRIP recognition of RPA-ssDNA complexes. *Science,* 300, 1542-8.

ZOU, P., XU, H., CHEN, P., YAN, Q., ZHAO, L., ZHAO, P. & GU, A. 2013. IDH1/IDH2 Mutations Define the Prognosis and Molecular Profiles of Patients with Gliomas: A Meta-Analysis. *PLOS ONE,* 8, e68782.

ZOU, Y., LIU, Y., WU, X. & SHELL, S. M. 2006. Functions of human replication protein A (RPA): from DNA replication to DNA damage and stress responses. *J Cell Physiol,* 208, 267-73.

ZWAIGENBAUM, L., BRYSON, S. E., BRIAN, J., SMITH, I. M., ROBERTS, W., SZATMARI, P., RONCADIN, C., GARON, N. & VAILLANCOURT, T. 2016. Stability of diagnostic assessment for autism spectrum disorder between 18 and 36 months in a high-risk cohort. *Autism Res,* 9, 790-800.